K-FELDSPAR THERMOCHRONOLOGY OF PROTEROZOIC BASEMENT ROCKS: RECONCILING REGIONAL TECTONISM, FLUID ALTERATION, AND ARGON TRANSPORT IN MICROTEXTURALLY COMPLEX FELDSPAR

by
Robert E. Sanders

Submitted as partial fulfillment of the
Requirements for the Degree of
Doctor of Philosophy in Earth and Environmental Science
with Dissertation in Geology
December 19, 2008

Department of Earth and Environmental Science
New Mexico Institute of Mining and Technology
Socorro, New Mexico

ABSTRACT

Three linked, but stand-alone studies use K-feldspar thermochronology to reconstruct tectonic and fluid histories while simultaneously evaluating the underpinnings of the method. Primary conclusions are: (Chapter 1) disparate thermal histories across the Ancestral Rocky Mountain and Laramide-age Montezuma fault, New Mexico, demonstrate that this fault has a Precambrian ancestry and was reactivated by these younger tectonic events. Major basement denudation leading to the formation of the Great Unconformity occurred post-Grenville (1.1 to 0.8 Ga) as a result of intracratonic lithospheric deformation related to the assembly and insipient rifting of Laurentia; (Chapter 2) Coupled Precambrian brittle deformation and fluid infiltration in the Pecos area, New Mexico, is revealed by dating of secondary metasomatic K-feldspar, and, in a broader scope, indicates intermittent fluid pulses throughout the Neoproterozoic and Early Paleozoic related to basin development and circulation of evolved crustal fluids. Microsampling discrete areas of secondary K-feldspar in primary perthitic microcline demonstrates that K-feldspar have the potential to record both a regional thermal/cooling signature and the timing of fluid alteration at the sub-grain scale; (Chapter 3) new understanding revealed by microsampling, experimental diffusion studies, and $^{40}Ar/^{39}Ar$ dating of complex alkali feldspar populations from the Klokken syenite, Greenland, partly negate previous challenges to the fundamental assumptions of K-feldspar

thermochronology. Specifically, these experiments demonstrate that both $^{40}Ar^*$ and ^{39}Ar behave similarly during laboratory degassing, and that $^{40}Ar^*$ loss under laboratory conditions does occur in a manner analogous to loss in nature.

Chapter 1 is an effort to characterize the basement thermal history of the southern Sangre de Cristo Range, New Mexico, and to evaluate the Precambrian ancestry of several prominent faults known to be active in the Phanerozoic. A suite of K-feldspar, mica, and hornblende was sampled and analyzed by the $^{40}Ar/^{39}Ar$ method. Overall, mafic mineral data and modeled K-feldspar thermal histories from the Sangre de Cristo mountains indicates Grenville-age (ca. 1.1 Ga) initiation of basement cooling and exhumation to shallow crustal depths (<200°C) by ca. 800 Ma, following mid-crustal metamorphism at ca. 1.4 Ga. To the east and across the Montezuma fault zone in the Las Vegas basin, K-feldspar record younger apparent ages and modeled thermal histories indicating this basement segment was not exhumed until later between 750 and 600 Ma. Contrasts in these MDD thermal models suggest there were two episodes of faulting and differential displacement of structural blocks in the Neoproterozoic followed by reactivation during the Ancestral Rocky Mountain and Laramide orogens. No differences in K-feldspar thermal histories were observed from samples on opposing sides of the Picuris-Pecos fault zone suggesting that no significant vertical offset occurred on this fault in the Neoproterozoic. The two documented episodes of faulting and exhumation recorded by basement K-feldspars are inferred to be associated with regional tectonism related to the intracratonic contractional effects of the Grenville orogen and the subsequent extension related to rifting of Laurentia. The application of the MDD model to this particular study demonstrates that differences in modeled thermal histories for K-

feldspar can be reasonably resolved by a complex geologic history and recurrent movement on a Proterozoic structure.

Chapter 2 focuses on the occurrence of secondary, metasomatic K-feldspar in fractures and in primary plagioclase in the Pecos River valley that was identified during a regional investigation of the Sangre de Cristo Range. $^{40}Ar/^{39}Ar$ analyses of replacement feldspars are used to date the timing of fluid infiltration and feldspar precipitation in fractures and localized breccia zones to constrain when deformation occurred. Analyses yielded a wide range of total gas ages including young Neoproterozoic and Paleozoic ages that can only be explained in the context of the known regional exhumation history as mineral growth ages for feldspars that formed below the $^{40}Ar^*$ closure temperature.

Microsampling, imaging, and $^{40}Ar/^{39}Ar$ analyses of film perthite and patch perthite microtextures demonstrates that discrete age populations of secondary K-feldspar are preserved in the primary pegmatitic microcline, and that at the sub-grain scale, unaltered microcline record total gas ages similar to other primary K-feldspar in the Sangre de Cristo Range. With an improved understanding of the K-feldspar mineralogy and argon data, and utilization of other techniques including U-Pb epidote geochronology, fluid inclusion microthermometry, and gas analyses, a complex geologic history is revealed. Multiple metasomatic episodes and coeval brittle deformation related to regional tectonic activity are evident in the Pecos region. Together, chapters 1 and 2 suggest that the Pecos area experienced a rich tectonic history and low-temperature (~280°C) hydrothermal activity throughout the Neoproterozoic. Likely, fluid circulation is associated with tectonic activity related to Grenville compression and Neoproterozoic extension.

Chapter 3 revisits alkali feldspars from the Precambrian Klokken syenite intrusion, Greenland, that historically provided evidence to question the laboratory diffusive behavior of argon in feldspar and whether the behavior is analogous to diffusion in nature (cf. Parsons et al., 1988; 1999). Pristine cryptoperthites yield $^{40}Ar/^{39}Ar$ total gas ages similar to the intrusion age, but deuterically altered sub-grains of patch-perthite have much younger and more complex age spectra. Unlike the Pecos situation where young patch perthite ages can be explained by fluid events long after crystallization or metamorphism, Klokken patch perthite has been convincingly interpreted to have formed shortly after syenite intrusion. Initial progress in understanding the complex Klokken data came from microsampling of patch and braid perthite sub-grains that showed a bimodal distribution of ages that could be directly correlated to a textural feature. Within a predominantly patch-perthite grain, braid perthite sub-domains preserve ages are similar to the emplacement age, while patch perthites record Paleozoic ages. While this shows that with careful microsampling meaningful age information can be recovered from otherwise complex bulk data, it does not fully explain the mechanism responsible for young ages in the context of the published thermal history. An investigation into the diffusion behavior of the contrasting microtextural varieties was conducted to evaluate and recognize laboratory and natural causes that might explain the young patch perthite ages. Samples were subjected to a series of isothermal heating experiments prior to irradiation (650, 700, 900, 1000, 1100°C). Comparison of the resulting measured age spectra with MDD model spectra predicted from the degassing behavior of ^{39}Ar and known laboratory thermal history show an overall good correlation between ^{39}Ar and $^{40}Ar^*$ diffusive behavior in all samples heated to 650 and 700°C. This correlation is less

robust once 900°C is reached and changes in argon retentivities are also observed. While this has implications for the MDD method and accurate recovery of kinetic information, the lower temperature data strongly argue that the young Klokken patch perthite ages do not reflect anomalously low argon retention in nature that is then obscured by laboratory artifacts. Here it is proposed that the Klokken history is more complex than published and a mechanism yet to be fully identified in the Klokken patch perthite has caused $^{40}Ar^*$ loss. A working model is that the highly permeable syenite units contain microporous patch perthite that has undergone fluid modification that facilitated $^{40}Ar^*$ loss. Thus, the abundant turbidity of the patch perthite provides microporosity for low-temperature fluid infiltration, in this case during the Paleozoic, and satisfies both the kinetic parameters and a plausible geologic history.

Collectively, the three studies in this dissertation substantiate the validity of the MDD model and demonstrate the utility of linking it with microtextural characterization to determine accurate geologic histories recorded in complex data. The implication that discrete fluid events can modify primary feldspar microtextures, facilitate K-feldspar-K-feldspar replacement reactions, and go under-recognized questions how common this phenomenon is. As a whole, many feldspar studies report good correlation with independent geologic or geochronology information despite varied thermal, tectonic, and presumably hydrologic histories. Research presented here lays the foundation for continued efforts to recover the intricacies of the relationship between microtexture and argon transport. Advances in microanalytical techniques will clarify processes that have been developed here incipiently. Furthermore, this work identifies avenues to propel

investigations of the fundamental assumptions behind the MDD technique so that the interpretations inferred from the method are geologically meaningful and accurate.

TABLE OF CONTENTS

LIST OF FIGURES

LIST OF TABLES

LIST OF APPENDICES

This dissertation is accepted on behalf of the
Faculty of the Institute by the following committee:

6-18-08

Advisor

Andrew R Campbell

Karl E Kalstrom 6-5-08

William C [illegible] 6-17-08

[illegible] 6/26/08

Date

I release this document to the New Mexico Institute of Mining and Technology.

6/30/08

Student's Signature Date

CHAPTER 1: $^{40}AR/^{39}AR$ THERMOCHRONOLOGY CONSTRAINTS ON THE TIMING OF PROTEROZOIC BASEMENT EXHUMATION AND FAULT ANCESTRY, SOUTHERN SANGRE DE CRISTO RANGE, NEW MEXICO

1.1 Abstract

Proterozoic ancestry is increasingly proposed for both Ancestral Rocky Mountain (Pennsylvanian-Permian) and Laramide-age (late Cretaceous-Early Tertiary) faults in the southwestern U.S. We test this hypothesis using $^{40}Ar/^{39}Ar$ thermochronology of Proterozoic basement rocks in the southern Sangre de Cristo Range, New Mexico. Hornblende and mica samples yield ages consistent with basement rocks cooling below ~500°C after ca. 1.4 Ga regional metamorphism, followed by protracted basement residence at temperatures between 300 and 400°C until the Neoproterozoic. K-feldspar age spectra are dominated by Neoproterozoic apparent ages and constrain basement exhumation from mid-crustal depths (~10 km) to within a few kilometers from the surface during the Neoproterozoic. Samples were also collected across the north-striking, steeply west-dipping Montezuma fault with known Laramide movement that bounds the eastern Rocky Mountain range front. Contrasting $^{40}Ar/^{39}Ar$ K-feldspar-derived thermal histories from opposing sides of the fault require two episodes of Neoproterozoic fault movement. Overall, rocks to the west record multiple diffusion domain (MDD) thermal histories that indicate cooling interpreted to be due to 4 to 7 km of basement exhumation between 1000 and 800 Ma whereas rocks to the east were exhumed later between 750 and 600 Ma. Assuming the present-day fault geometry was established in the

Proterozoic, west-side-up throw beginning late in the Grenville orogeny (ca. 1000 Ma) accommodated east-west shortening. West-side-down extensional movement at ca. 750 Ma is inferred to be associated with the incipient rifting of the supercontinent Rodinia.

1.2 Introduction

Metamorphic and igneous basement rocks currently exposed in the southwestern U.S. were originally intruded and/or metamorphosed in the middle crust (10-20 km) during the accretion of volcanic island arc terranes onto southwest Laurentia during the Proterozoic (Condie, 1982). The present-day distribution of these Precambrian rocks is shown in Figure 1.1 along with major physiographic provinces. The erosion and tectonism that brought these rocks to the surface was a cumulative response to multiple events, including the Proterozoic assembly and breakup of the Rodinian supercontinent, the Pennsylvanian-Permian Ancestral Rocky Mountain orogeny, the late Cretaceous-Early Tertiary Laramide orogeny, and Neogene Rio Grande rifting (Mallory, 1958; Dickinson and Snyder, 1978; Reed et al., 1987; Chapin and Cather, 1994; Karlstrom et al., 1999a; Karlstrom et al., 2004). Overall the younger events are better understood relative to a Precambrian history which is obscured by several geologic factors: 1) Precambrian crystalline rock outcrops comprise only a small fraction of the rocks presently exposed at the surface; 2) The Precambrian sedimentary record in the southwestern U.S. has been almost completely removed by erosion or was never deposited; and 3) Most thermochronologic systems do not record Neoproterozoic apparent ages (Wilkes and Chapin, 1997; Karlstrom et al., 1997; Shaw et al., 2005).

The Great Unconformity (Powell, 1876) represents the crystalline basement-sedimentary contact in the southwestern U.S. and varies in age from Mesoproterozoic to Paleozoic. In Arizona, the basement had been exhumed and eroded as early as 1.30 to 1.25 Ga (e.g. Apache Group, Link et al., 1993; Stewart et al., 2001; Grand Canyon Supergroup, Timmons et al., 2005). In northern New Mexico, Mississippian clastic and

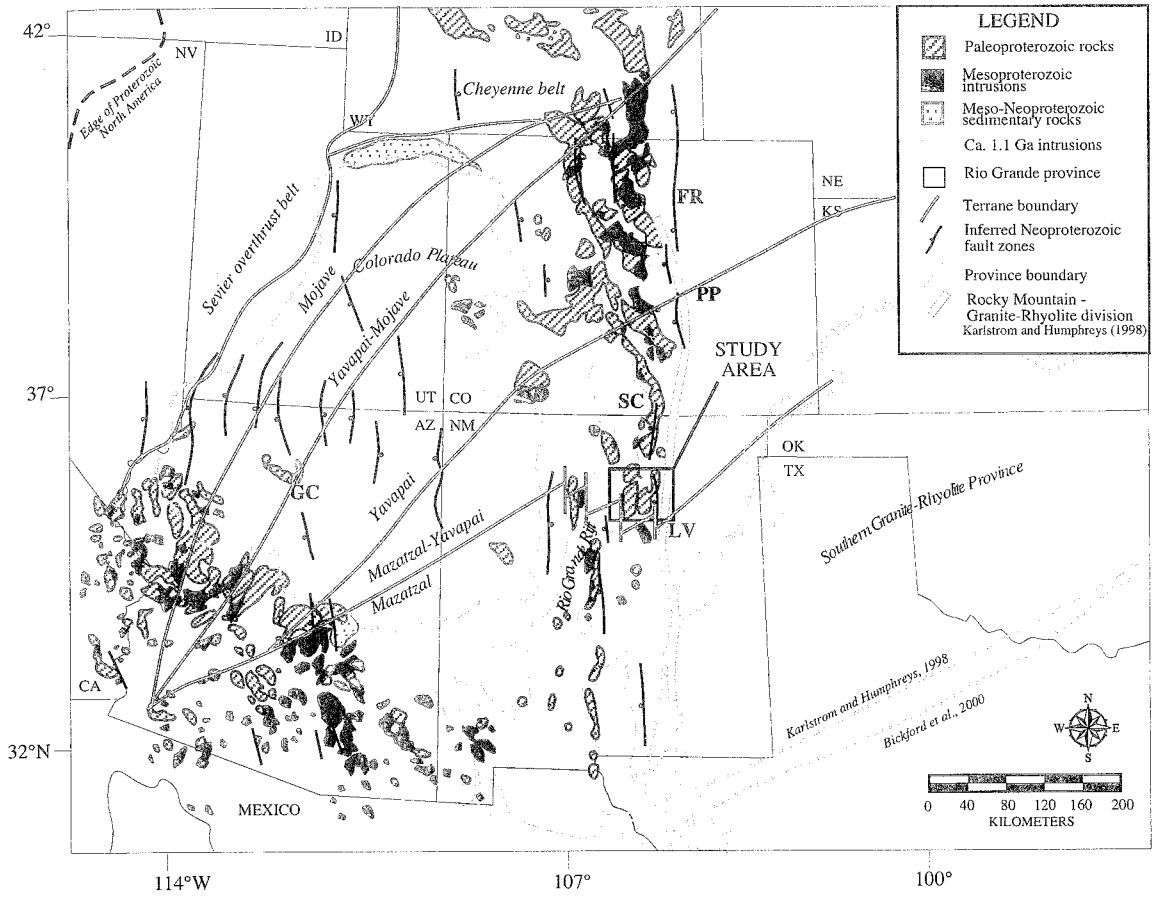

Figure 1.1: Map showing the distribution of Proterozoic rocks exposed in the southwestern U.S. North-striking Ancestral Rocky Mountain and Laramide-age faults inferred to have had a Neoproterozoic origin (Timmons et al., 2001) are marked and indicate a relative sense of displacement for ca. 800 Ma movement (ball on down-dropped side). Faults that define the present-day boundary of the Rocky Mountains and the Great Plains include the Montezuma fault (LV) and other range-bounding faults (i.e. Rampart Range fault (FR). The approximate boundary between the ca. 1.4 Ga volcanic and subvolcanic rocks of the Granite-Rhyolite Province and coeval mid-crustal intrusive rocks exposed in the Rocky Mountains is shown in gray (after Karlstrom and Humphreys, 1998). Compiled from Karlstrom and Humphreys (1998), Bickford et al. (2000), Timmons et al. (2001), and Karlstrom et al. (2004).

marine rocks overly the basement (Baltz and Myers, 1999). Thick sequences of Pennsylvanian and Cretaceous arkosic sediments throughout the Rocky Mountain region indicate Ancestral Rocky Mountain and Laramide tectonism was responsible for at least some basement denudation (Mallory, 1958; Dickinson and Snyder, 1978; Kluth and Coney, 1980), but in general, major basement erosion was pre-Mississippian. The timing of basement exhumation is therefore critical in deciphering Proterozoic fault ancestry, Neoproterozoic tectonism, and the development of the Great Unconformity in New Mexico.

Recent studies have sought to constrain the timing of Neoproterozoic tectonism in the southwestern U.S. Timmons et al. (2001; 2005) recognize syndepositional faults in the Grand Canyon Supergroup that record distinct episodes of extension at ca. 1100 and 800 Ma that generated northwest- and north-striking fault zones, respectively, inferred to have developed during the Grenville orogeny and the rifting of the Rodinian supercontinent. The authors also propose that these Precambrian faults accommodated Phanerozoic deformation and support the long-held contention that the orientation and distribution of younger fault zones and uplifts in the western U.S. have been influenced by zones of weakness established during the Proterozoic (Miller et al., 1963; Weimer, 1980; Karlstrom and Humphreys, 1998; Karlstrom et al., 1999b; Marshak et al., 2000).

$^{40}Ar/^{39}Ar$ K-feldspar thermochronology can be used to evaluate crustal thermal histories, and is an important tool in reconstructing basement exhumation when structural or sedimentological evidence is limited or missing (Heizler and Harrison, 1998; McDougall and Harrison, 1999). Existing $^{40}Ar/^{39}Ar$ K-feldspar data from Precambrian rocks in the southwestern U.S. demonstrate that basement cooling during the Proterozoic

occurred at different times across the region and reflects differential exhumation between structural blocks (Heizler, 1998; Strickland et al., 2003; Timmons, 2004; Timmons et al., 2005). This paper presents $^{40}Ar/^{39}Ar$ step heating data for hornblende, mica, and K-feldspar separates from Precambrian basement rocks exposed in the Sangre de Cristo Range of north-central New Mexico and cuttings from basement-penetrating wells to the east in the subsurface of the Las Vegas basin, in order to determine when mid-crustal rocks in this area were exhumed to relatively shallow crustal depths and cooled below 175°C. $^{40}Ar/^{39}Ar$ K-feldspar thermochronology is used to identify differential exhumation of distinct structural blocks, and constrain the timing of fault development and reactivation.

1.3 Sample locations and methods

Samples of Proterozoic granite, tonalite, pegmatite, and schist that record U-Pb and Pb-Pb dates ranging from 1.72 to ~1.40 Ga (Bauer and Pollock, 1993) were collected at eight locations along a roughly west to east transect from Santa Fe, NM to Las Vegas, NM (Fig. 1.2). This sampling traverse is perpendicular to the north-striking Picuris-Pecos and Montezuma fault zones and was designed to determine if there are variations in the thermal histories recorded by opposing sides of the faults. Drill cuttings from three petroleum exploration wells east of Las Vegas (Fig. 1.3), approximately 30 kilometers from Hermit Peak, were also obtained from the New Mexico Bureau of Geology and Mineral Resources. Cuttings provide samples of crystalline basement rocks present in the subsurface of the Las Vegas basin. Depth to basement varies significantly in the subsurface of the Las Vegas basin (Broadhead et al., 2002); sampled depths for the three

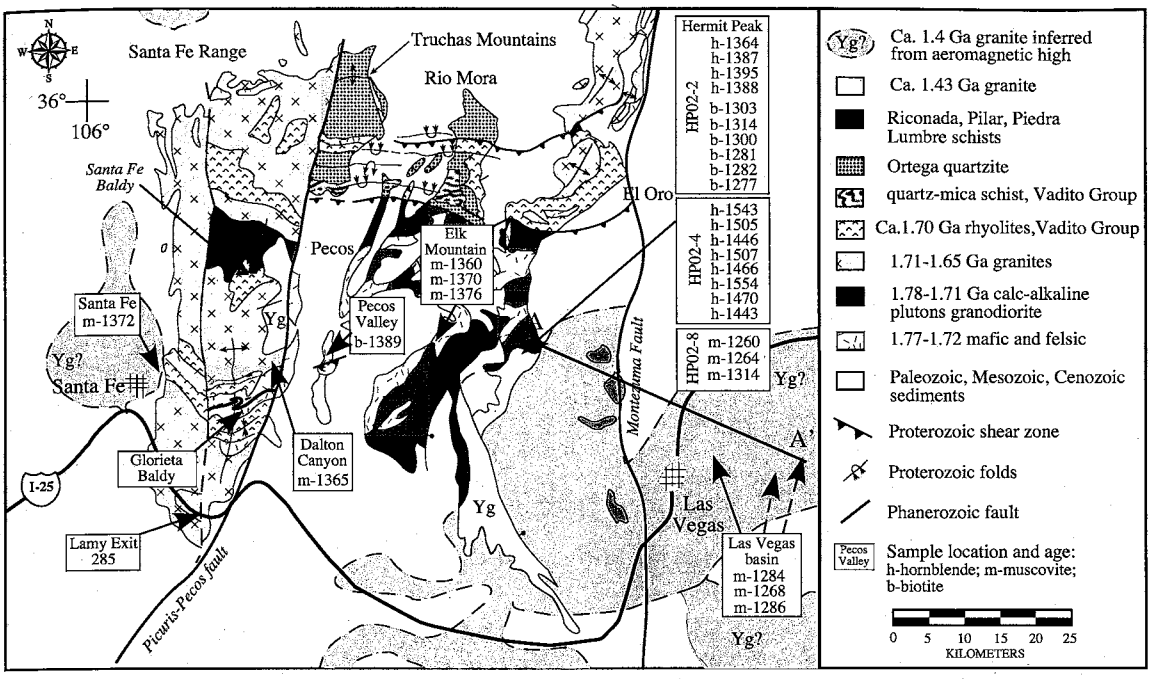

Figure 1.2: Generalized geologic map of the southern Sangre de Cristo Range, New Mexico showing the locations of sampling areas and $^{40}Ar/^{39}Ar$ dates. Sampling was conducted approximately perpendicular to the strike of the Picuris-Pecos and Montezuma fault zones to maximize potential K-feldspar thermal history variation associated with throw across these faults. A-A' delineates the cross section profile of Figure 3. Adapted from Karlstrom et al. (2004).

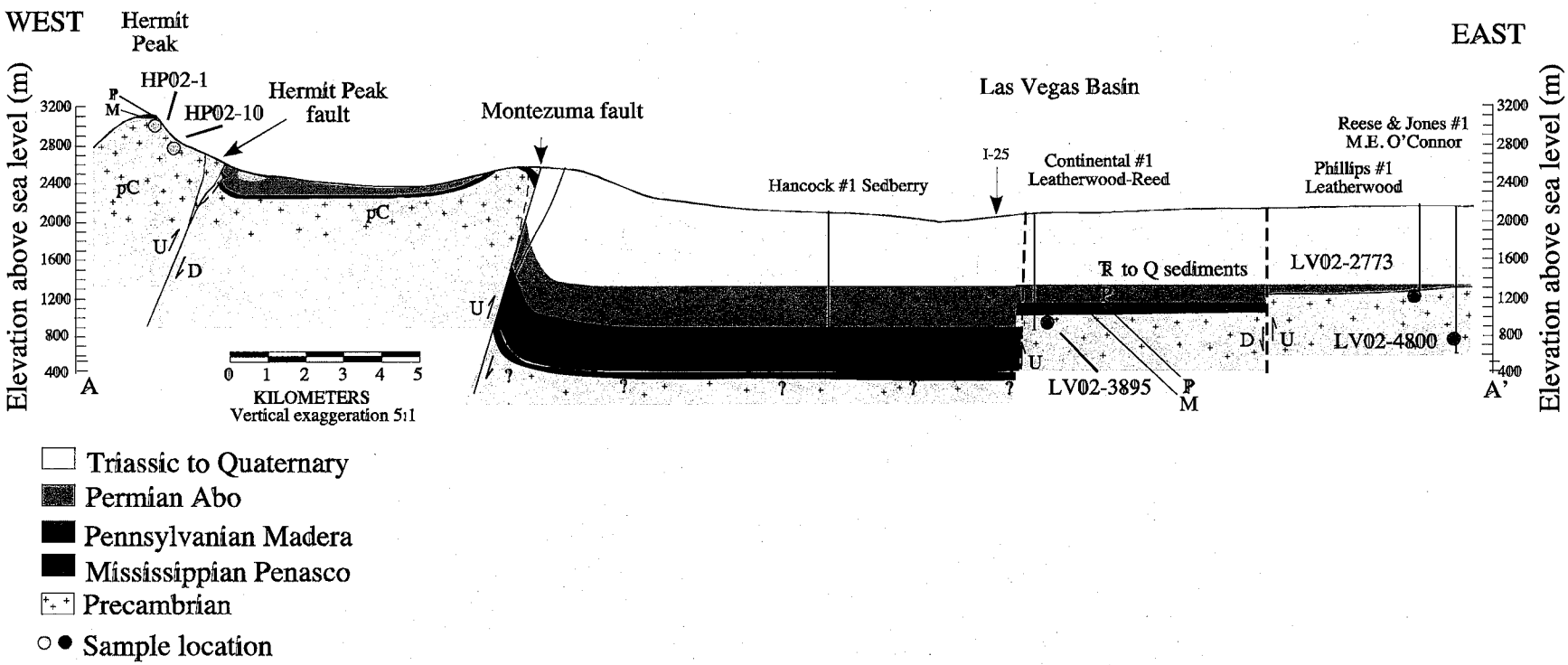

Figure 1.3: Generalized geologic cross section of the eastern Rocky Mountain range front from Hermit Peak to Reese and Jones #1 exploration well showing approximate depths to Precambrian basement, Paleozoic sediments, and undifferentiated Triassic to Quaternary sediments. Missing Mississippian and Pennsylvanian sediments in portions of the subsurface indicate Ancestral Rocky Mountain displacement on subsurface faults. Sample locations are shown in black and gray. Compiled from data from Baltz and Myers (1999) and Broadhead, R. (unpublished well log data).

wells used in this study were 925, 1300, and 1600 meters (Fig. 1.3). Mineral separates were prepared by standard magnetic and heavy liquid techniques (Heizler et al., 1999). Grain fractions ranging from 600 to 180 μm were hand picked to obtain a monomineralic separate. A detailed description of analytical techniques and parameters employed by the NMGRL is presented in DR1.

1.4 $^{40}Ar/^{39}Ar$ Results

1.4.1 $^{40}Ar/^{39}Ar$ results for hornblende, muscovite, and biotite

$^{40}Ar/^{39}Ar$ age spectra for hornblende, muscovite, and biotite from the Sangre de Cristo Range are presented in Figures 1.4, 1.5, and 1.6. Dates from this and previous studies are compiled in Tables 1.1 and 1.2 and complete step heating data are provided in DR2. Overall, very few samples yield plateau ages with 3 or more consecutive heating steps that have acceptable MSWD values (see DR1). Preferred ages are assigned to complex spectra and are calculated from the weighted mean age of selected steps that typically comprise the bulk of the spectra. Anomalously young and old apparent ages from initial and final heating steps are excluded. Although deciding which steps should be used for the preferred age is somewhat subjective, these ages allow comparison between samples distributed on a regional scale despite complexities with individual age spectra. Preferred ages are commonly accompanied by high MSWD values, however we do not expect statistical behavior in the step heating data because of likely argon gradients caused by alteration and/or complex thermal histories. In other instances, particularly with saddle-shaped spectra, the youngest step(s) are considered a maximum

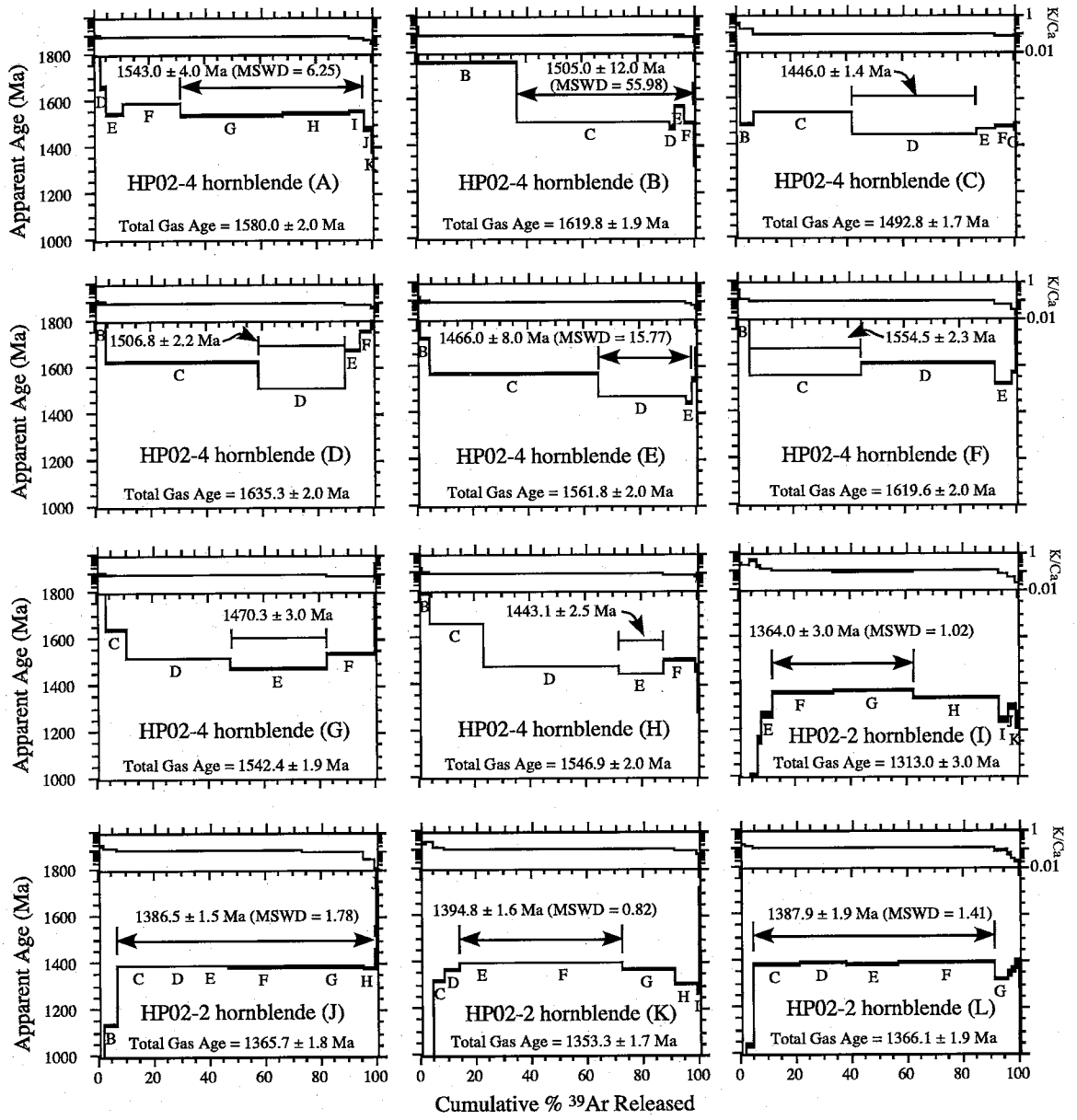

Figure 1.4: $^{40}Ar/^{39}Ar$ age spectra for multiple analyses of hornblende from amphibolite samples (HP02-2 and HP02-4) collected near the summit of Hermit Peak. Spectra are complex and assigned ages are generally the minimum apparent age.

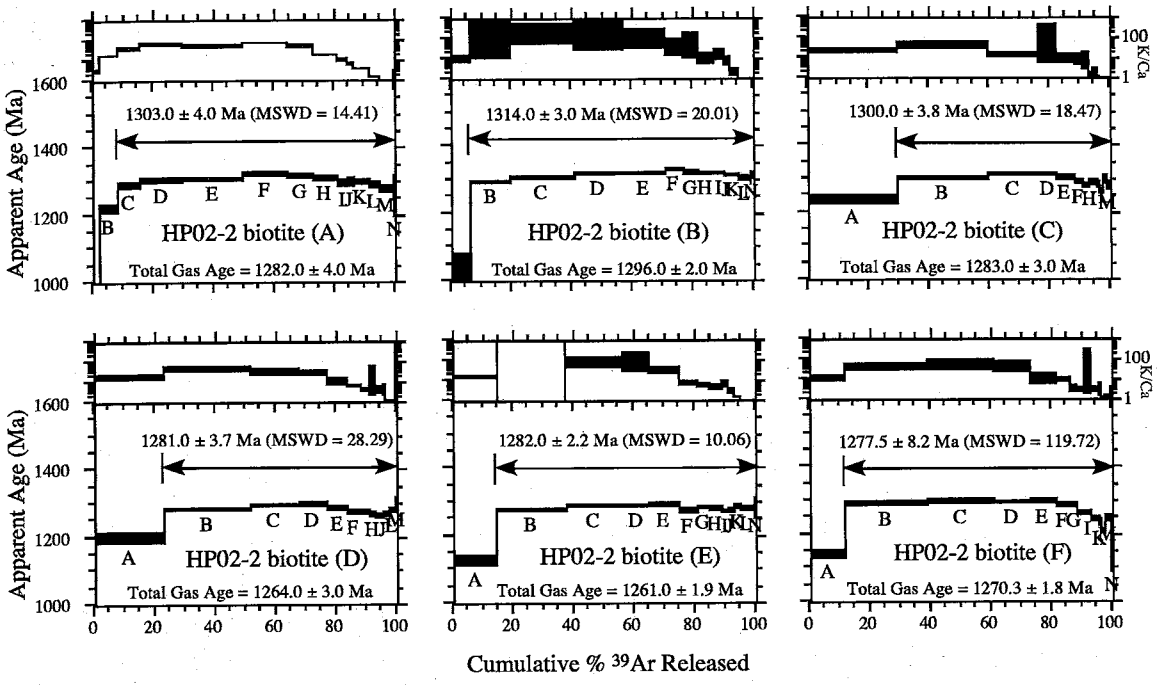

Figure 1.5: Six $^{40}Ar/^{39}Ar$ age spectra for HP02-2 biotite from a biotite-hornblende schist near Hermit Peak summit. All spectra are complex and yield preferred closure ages of 1300±25 Ma.

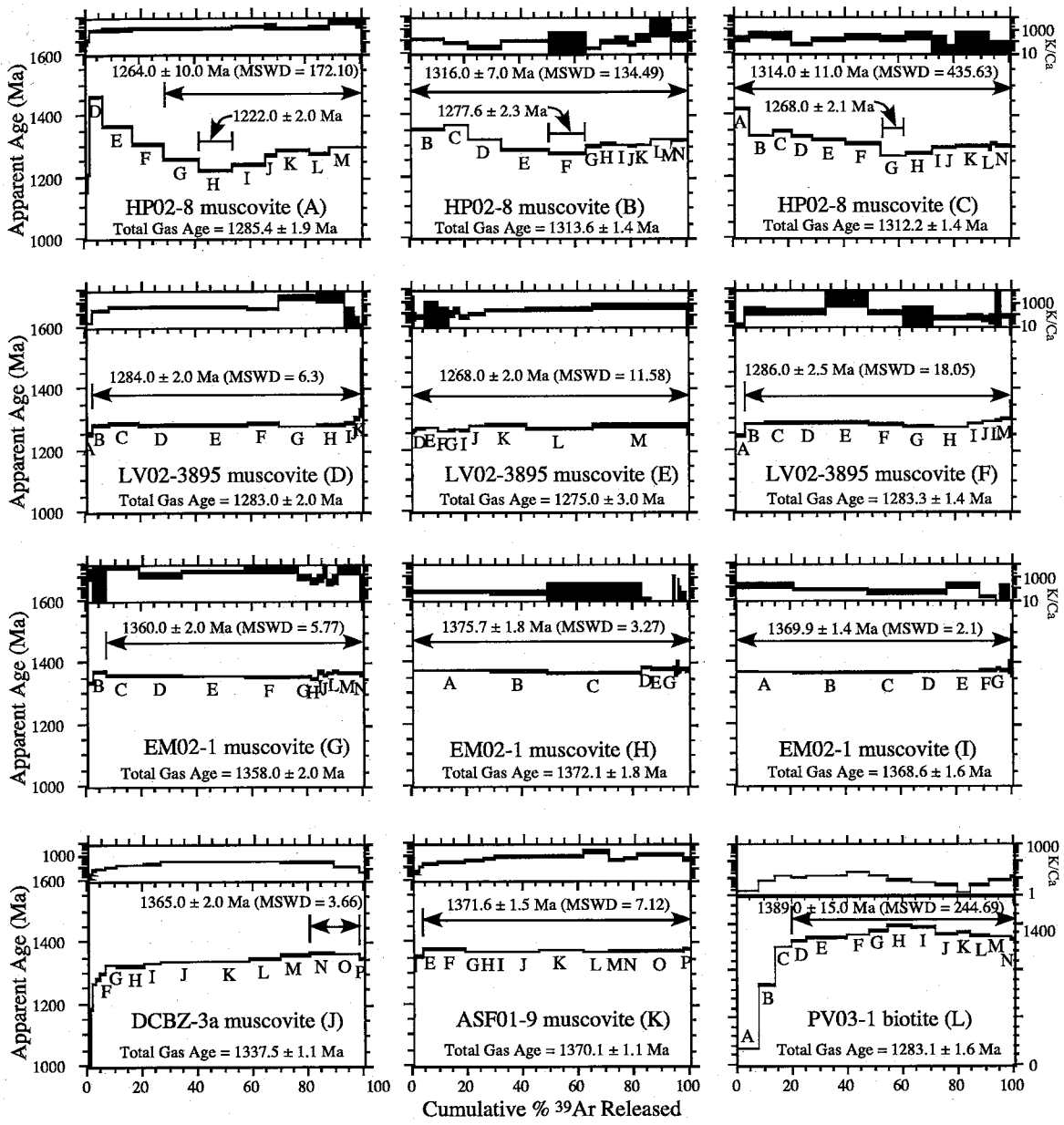

Figure 1.6: $^{40}Ar/^{39}Ar$ age spectra for muscovite and biotite from the southern Sangre de Cristo range and the subsurface of the Las Vegas basin. Multiple analyses were conducted on several samples to explore possible grain-to-grain age variations. Muscovites generally decrease in age across the range along a west to east trend.

Table 1.1: Age and location of samples dated in this study.

Sample	Rock type	Location	UTM		Mineral	Fig	Prefered age (Ma)	TGA (Ma)
HP02-4	amphibolite	Hermit Peak	461880	3955315	hbl	4A	1543.0±4.0††	1580.0±2.0
		Hermit Peak			hbl	4B	1505.0±12.0††	1619.8±1.9
		Hermit Peak			hbl	4C	1446.0±1.4†††	1492.8±1.7
		Hermit Peak			hbl	4D	1506.8±2.2†††	1635.3±2.0
		Hermit Peak			hbl	4E	1466.0±8.0†††	1561.8±2.0
		Hermit Peak			hbl	4F	1554.5±2.3†††	1619.6±2.0
		Hermit Peak			hbl	4G	1470.3±3.0†††	1542.4±1.9
		Hermit Peak			hbl	4H	1443.1±2.5†††	1546.9±2.0
HP02-2	bi-hbl schist	Hermit Peak	461848	3955357	hbl	4I	1364.0±3.0†††	1313.0±3.0
		Hermit Peak			hbl	4J	1386.5±1.5†	1365.7±1.8
		Hermit Peak			hbl	4K	1394.8±1.6†††	1353.3±1.7
		Hermit Peak			hbl	4L	1387.9±1.9†	1366.1±1.9
		Hermit Peak			bi	5A	1303.0±4.0††	1282.0±4.0
		Hermit Peak			bi	5B	1314.0±3.0††	1296.0±2.0
		Hermit Peak			bi	5C	1300.0±3.8††	1283.0±3.0
		Hermit Peak			bi	5D	1281.0±3.7††	1264.0±3.0
		Hermit Peak			bi	5E	1282.0±2.2††	1261.0±1.9
		Hermit Peak			bi	5F	1277.5±8.2††	1270.3±1.8
HP02-8	granite	Hermit Peak	462063	3955088	ms	6A	1264.0±10.0††	1285.4±1.9
		Hermit Peak			ms	6B	1316.0±7.0††	1313.6±1.4
		Hermit Peak			ms	6C	1314.0±11.0††	1312.2±1.4
LV02-3895	granite	Las Vegas Basin	489275	3939144	ms	6D	1284.0±2.0††	1283.0±2.0
		Las Vegas Basin			ms	6E	1268.0±2.0††	1275.0±3.0
		Las Vegas Basin			ms	6F	1286.0±3.0††	1283.3±1.4
EM02-1	pegmatite	Elk Mountain	451917	3959382	ms	6G	1360.0±2.0††	1358.0±2.0
		Elk Mountain			ms	6H	1375.7±1.8††	1372.1±1.8
		Elk Mountain			ms	6I	1369.9±1.4††	1368.6±1.6
DCBZ01-3a	granite	Dalton Canyon	432194	3950939	ms	6J	1365.0±2.0†††	1337.5±1.1
ASF01-9	granite breccia	Santa Fe-Hyde Park	419630	3953775	ms	6K	1371.6±1.5††	1370.1±1.1
PV03-1	tonalite	Pecos River Valley	439277	3952397	bi	6L	1389.0±15.0††	1283.1±1.6
ASF01-9	granite breccia	Santa Fe-Hyde Park	419630	3953775	Kspar	7a	n/a	889.5±0.8
LAMY02-1	granite	I-25 Exit 285	420568	3934479	Kspar	7d	n/a	984.9±1.7
TP02-4	gneiss	Glorieta Baldy	427639	3945204	Kspar	7g	n/a	1169.0±2.0
MG01-1a	granite	Dalton Canyon	430946	3949904	Kspar	7j	n/a	863.3±0.8
PVBR01-3	granodiotite	PecosValley	439277	3952397	Kspar	8a	n/a	983.6±0.5
EM02-1	pegmatite	Elk Mountain	451917	3959382	Kspar	8d	n/a	956.5±1.6
HP02-01	granite	Hermit Peak	462613	3955371	Kspar	8j	n/a	987.1±1.7
HP02-10	granite	Hermit Peak	462446	3952222	Kspar	8g	n/a	973.1±1.5
LV02-2773	granite	Las Vegas Basin	491500	3936000	Kspar	9a	n/a	812.8±3.0
LV02-3895	granite	Las Vegas Basin	489275	3939144	Kspar	9d	n/a	948.1±1.5
LV02-4800	granite	Las Vegas Basin	497200	3938000	Kspar	9g	n/a	851.0±1.4

Notes:
hbl = hornblende
bi = biotite
ms = muscovite
Ksp = K-feldspar
Fig = Corresponding figure number for age spectrum in manuscript
Preferred age = Time of bulk closure to argon diffusion
TGA = Total gas age
† = plateau age; †† = age calculated from selected steps; ††† = age calculated from one or two steps
All errors are 1σ and do not include error in decay contants or fluence monitor age

Table 1.2: Compilation of $^{40}Ar/^{39}Ar$ dates for samples from the southern Sangre de Cristo Range.

Sample	Mineral	Location	Reported Age (Ma)[3]	TGA (Ma)	Ref
WB15B	hornblende	Pecos	1388.8±5.0	1360.4±3.0	1
WB23	hornblende	Pecos	1401.0±5.0	1340.0±1.8	1
RP87	muscovite	Pecos Valley	1270.2±6.0	1252.8±1.8	1
RP-34	muscovite	Pecos Valley	1367.2±1.9	1362.4±1.9	1
SFP	muscovite	Maclure Reservior	1362.3±2.0	1366.1±1.9	2
SF21	muscovite	Maclure Reservior	1386.8±4.0	1376.5±1.9	2
SF22	muscovite	Santa Fe Mtns	1336.1±3.0	1334.4±1.8	2
SF23	muscovite	Maclure Reservior	1352.1±1.4	1337.0±1.8	2
K01-SF	muscovite	Santa Fe Baldy	1266.2±6.0	1264.8±1.1	2
SF3	muscovite	Maclure Reservior	1332.1±4.0	1319.4±1.8	2
SF3	biotite	Maclure Reservior	1224.6±1.8	1086.0±1.6	2
K01-SF	biotite	Santa Fe Baldy	1207.4±3.0	1198.6±1.0	2
RP36	biotite	Pecos Valley	1442.6±5.0	1309.8±2.0	1
RP28B	biotite	Pecos Valley	1360.4±2.0	1337.2±1.8	1
81SF7	biotite	Santa Fe	1151.4±1.5	1151.5±1.6	2
SF12	biotite	Santa Fe	1118.1±4.0	1111.0±1.5	2
WB-6	K-feldspar	Pecos Valley	-	947.2±1.8	1
RP-70	K-feldspar	Pecos Valley	-	1066.1±1.9	1
RP-34	K-feldspar	Pecos Valley	-	880.1±1.6	1
RP-87	K-feldspar	Pecos Valley	-	933.3±1.8	1

Notes

[1] Melis (2001)

[2] Erslev et al. (2004)

[3] Ages calculated for ^{40}K total decay constant= 5.476e-10/a; Fish Canyon sanidine = 28.27 Ma.

All errors are 1σ and do not include error in decay constant or fluence monitor age

TGA = Total gas age

age for argon closure as excess argon typically associated with this behavior would cause the apparent age to be too old.

Hornblende dates for hornblende±biotite schists from Hermit Peak are useful in determining the higher temperature history of the rocks in the area (T_c~500 to 550°C). Sample HP02-4 is an amphibolite body within the Hermit Peak granite and eight replicate analyses of individual aliquots of 1 to 4 crystals yielded complex, non-reproducible age spectra (Fig. 1.4, A-H). Initial heating steps generally yield apparent ages older than 1.8 Ga, suggesting the presence of excess argon, as rocks in northern New Mexico are younger than 1.8 Ga (Karlstrom et al., 2004). Following the initial old ages, the spectra record an overall decrease in age with highly variable minima. As a means to describe the apparent ages of these hornblende, each is assigned an age that typically reflects the youngest step that may record a maximum age for hornblende closure between ~1440 and 1555 Ma (Figs. 1.4A-H). Total gas ages range from 1490 to 1635 Ma. In contrast to the chaotic age spectra, the K/Ca spectra for all eight analyses are quite uniform and record consistent values of ~0.1 indicating that the sample is probably homogeneous, and thus age variability is not obviously associated with, for instance, alteration. There is only a slight decrease in K/Ca at the final high temperature steps that is probably due to degassing of Ca-bearing inclusions such as plagioclase, epidote, apatite, and/or titanite. Because the highly variable ages do not correlate to variable K/Ca (which is often the case e.g. Marcoline et al., 1999; Shaw et al., 2005) we suggest the primary cause for age variability is due to a non-uniform ^{40}Ar distribution related to a complex thermal history (see Discussion).

Four replicate analyses of one to four crystals of HP02-2 hornblende, located ~10 m from HP02-4, yielded consistent and reproducible age spectra (Figs. 1.4 I-L). All spectra show initial steps with young apparent ages (<1000 Ma) and high K/Ca values that suggest minor argon loss and/or inclusion of a non- retentive high K phase. Two spectra (HP02-2b and d) record well-defined plateau segments (MSWD ~1) with analytically identical plateau ages of ~1388 Ma. Samples HP02-2a and c are slightly more complex with somewhat hump-shaped patterns with assigned ages of 1364 and 1395 Ma, respectively. The preferred age for this hornblende is 1387±2 Ma based on the high quality spectra from HP02-2b and d (Figs. 1.4 J, L).

Six replicate analyses of one to four crystals of biotite from HP02-2 yielded complex age spectra (Figs. 1.5 A-F). Age spectra are characterized by low apparent ages during the initial heating steps attributed to minor argon loss or ^{39}Ar recoil implantation into non-K-bearing phases (i.e. chlorite). Overall the spectra are hump-shaped with intermediate steps being older than the low and high temperature steps. K/Ca spectra are also hump-shaped, and likely reflect chlorite alteration and Ca-bearing inclusions. Total gas ages for replicate splits are variable and range from 1261 to 1296 Ma. If the hump-shaped spectra are solely due to ^{39}Ar recoil redistribution, the total gas ages for complex biotites have been shown to be meaningful (e.g. Heizler et al., 1988; Lo and Onstott, 1989). If the age gradients are related to argon loss the older part of the spectra might provide the best closure age. Biotite plateau dates for this sample were determined from all but the first heating step and range from about 1315 to 1280 Ma. An additional difficulty in determining a definitive age for this sample is the poor ability of the step-heating method to resolve non-uniform argon distributions in micas that have experience

slow cooling and/or complex thermal histories. For instance, Hodges et al. (1994) demonstrated that fairly flat spectra could have significant internal age variability related to slow cooling. Due to spectra complexities and different possible age assignments it is only possible to estimate that the biotite record cooling through about 350-300°C at about 1300±25 Ma.

Three single muscovite crystals from a coarse K-feldspar-muscovite segregation in the Hermit Peak granite (HP02-8) were analyzed separately and also give complex results (Figs. 1.6 A-C). The spectra are distinctly saddle-shaped with initial apparent ages of ~1375 to 1425 Ma that progressively drop to a minimum age between ~1222 and 1278 Ma. The spectra then climb before defining a fairly flat segment at ~1300 Ma for the highest temperature steps. K/Ca values are somewhat variable but typical of muscovite and range between ~10 and 1000. Age assignment for this sample is difficult because individual heating steps do not define a common age. The age spectra structure is not interpreted to be caused by the presence of excess argon because the oldest apparent ages do not exceed geologically realistic dates. The disparity between apparent ages for each heating step may reflect an internal age gradient that is poorly resolved with the age spectrum method. Three ages are reported for each analysis: the total gas age, the age of the youngest intermediate heating step (a minimum age), and the age calculated from selected heating steps. These ages range from 1315 to ~1220 Ma and highlight the difficulty in assigning a single, unambiguous age to these complex age spectra. Most likely the complex age spectra indicate intracrystalline age variations that principally result from slow cooling (cf. Hodges et al., 1994). At best it can be argued that the total

gas ages can record the time of bulk closure of the sample (~350°C) at ~1300 Ma. This is similar to the interpretation of biotite results from Hermit Peak.

LV02-3895 single crystal muscovites from the subsurface of the Las Vegas basin were analyzed in three separate experiments (Figs. 1.6 D-F). Age spectra are relatively well behaved and most heating steps yield similar apparent ages between 1270 and 1290 Ma. K/Ca values are fairly uniform and are typically 100. Total gas ages for these replicates overlap within 2σ error and range from 1275 to 1283 Ma. The plateau ages are similar and range from 1268 to 1286 Ma and indicate bulk closure to argon loss at about 1275±10 Ma.

Three muscovite localities west of Hermit Peak were investigated. Three single crystals of EM02-1 from the Elk Mountain pegmatite district were analyzed and yielded total gas ages between 1358 and 1372 Ma (Figs. 1.6 G-I). The spectra are fairly flat (MSWD's 2.1-5.8) and have plateau ages between 1360 and 1376 Ma indicating cooling below ~350°C at this time. Two additional muscovite separates from the Dalton Canyon and Santa Fe areas were also analyzed (Figs. 1.6 J-K). Multiple grains from sample DCBZ-3a produced an age spectrum with a well-defined age gradient. Following an initial steep gradient, the bulk of the spectrum climbs gradually from 1340 to 1370 Ma. K/Ca values are high and typically about 100 to 300. The total gas age for this sample is 1338 Ma and the assigned closure age for this sample is 1365 Ma determined from the two oldest steps in the age spectrum. The age gradient may partially record argon loss associated with protracted cooling. A single grain muscovite sample ASF01-9 produced a fairly flat age spectrum with 95% of the total ^{39}Ar released defining a plateau age of 1372 Ma. The total gas age is 1370 Ma and average K/Ca value is ~900.

Biotite from a moderately K-metasomatized tonalite in the Pecos River valley (PV03-1) yields a disturbed hump-shaped age spectrum characterized by low apparent ages during the initial heating steps that climb to an age maximum before dropping to younger ages during the final heating steps (Fig. 1.6 L). Chlorite alteration results in overall low K/Ca values that vary irregularly between 1 and about 10. The low K_2O (~4%) is also a consequence of chlorite alteration. Age spectrum complexities likely reflect argon loss and/or ^{39}Ar recoil in chloritized biotite (cf. Lo and Onstott, 1989). The oldest part of the spectrum yields a weighted mean age of 1389±15 Ma that may record cooling below ~300°C at this time.

1.4.2 $^{40}Ar/^{39}Ar$ K-feldspar thermochronology

Much of the following discussion regarding the thermal evolution of the basement in northern New Mexico hinges on $^{40}Ar/^{39}Ar$ K-feldspar thermal histories generated from incremental heating analyses. DR3 provides a detailed example of the methods used to extract the thermal history from the K-feldspar data (see also; Sanders and Heizler, 2005). The K-feldspar results are interpreted within the framework of the multiple diffusion domain (MDD) model (Lovera et al., 1989, 1997, 2002). A thermal history can be retrieved from the $^{40}Ar/^{39}Ar$ age spectrum data where laboratory heating temperature, heating duration, and cumulative % ^{39}Ar released for each step are known. Thermal models for this study were generated from $^{40}Ar/^{39}Ar$ age spectrum data using algorithms created by O. Lovera (DR3) and follow the methods outlined by Quidelleur et al. (1997). Two possible thermal histories are constructed for each sample, one from an

unconstrained model that allows reheating events, and one from a monotonic model that only allows cooling from an initially high temperature.

1.4.3 $^{40}Ar/^{39}Ar$ K-feldspar results and MDD thermal models

K-feldspar separates from basement rocks between Santa Fe and the Las Vegas basin yield complex $^{40}Ar/^{39}Ar$ age spectra and variable MDD thermal history models (Figs. 1.7-1.9). Eight K-feldspar age spectra and thermal models from samples from the Sangre de Cristo Range, west of Las Vegas, and the four analyses of Melis (2001) from the same area are all similar (Figs. 1.7, 1.8) but are distinct from three samples from the Las Vegas basin (Fig. 1.9). In general, initial heating steps for Sangre de Cristo samples yield steep age gradients beginning between 300 and 600 Ma that climb to between 1000 and 1100 Ma at 100% ^{39}Ar released. Thermal history models are characterized by accelerated cooling between ~1000 and 800 Ma from above 300°C to 175°C or less. Although samples from the Sangre de Cristo Range have remarkably similar thermal histories interpreted as a common thermal signature for the basement, Figure 1.10 demonstrates there is some variability between individual models. These variations are probably related to error in the models due to spectra complexity, argon kinetics, etc. and complexity in geology on the order of tens of square kilometers. However, compared to the Las Vegas basin sample models located to the east of the Montezuma fault zone, the Sangre de Cristo models have remarkable overlap.

Modeled monotonic thermal histories for samples ASF01-9, LAMY02-1, PVBR01-3, HP02-1, and HP02-10 (Figs. 1.7c, f; Figs. 1.8c, i, l) show that rocks were 300-350°C or hotter at 1200 Ma. Most samples began to retain argon at about 1000 Ma

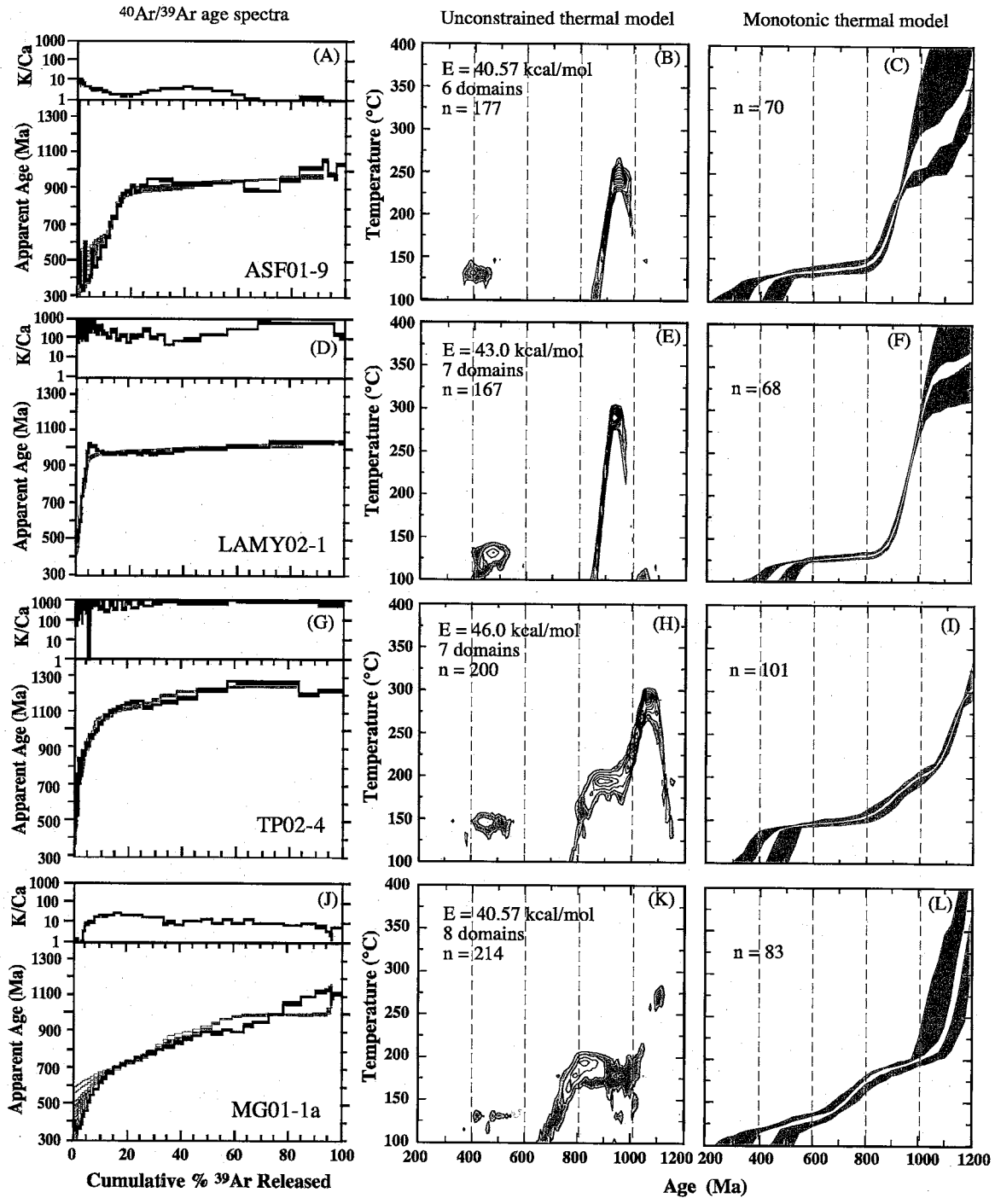

Figure 1.7: Measured (black) and modeled (gray) $^{40}Ar/^{39}Ar$ age spectra, and unconstrained and monotonic MDD thermal models generated for K-feldspar from Santa Fe (ASF01-9), I-25 Lamy exit (LAMY02-1), Glorieta Baldy (TP02-4), and Dalton Canyon (MG01-1a).

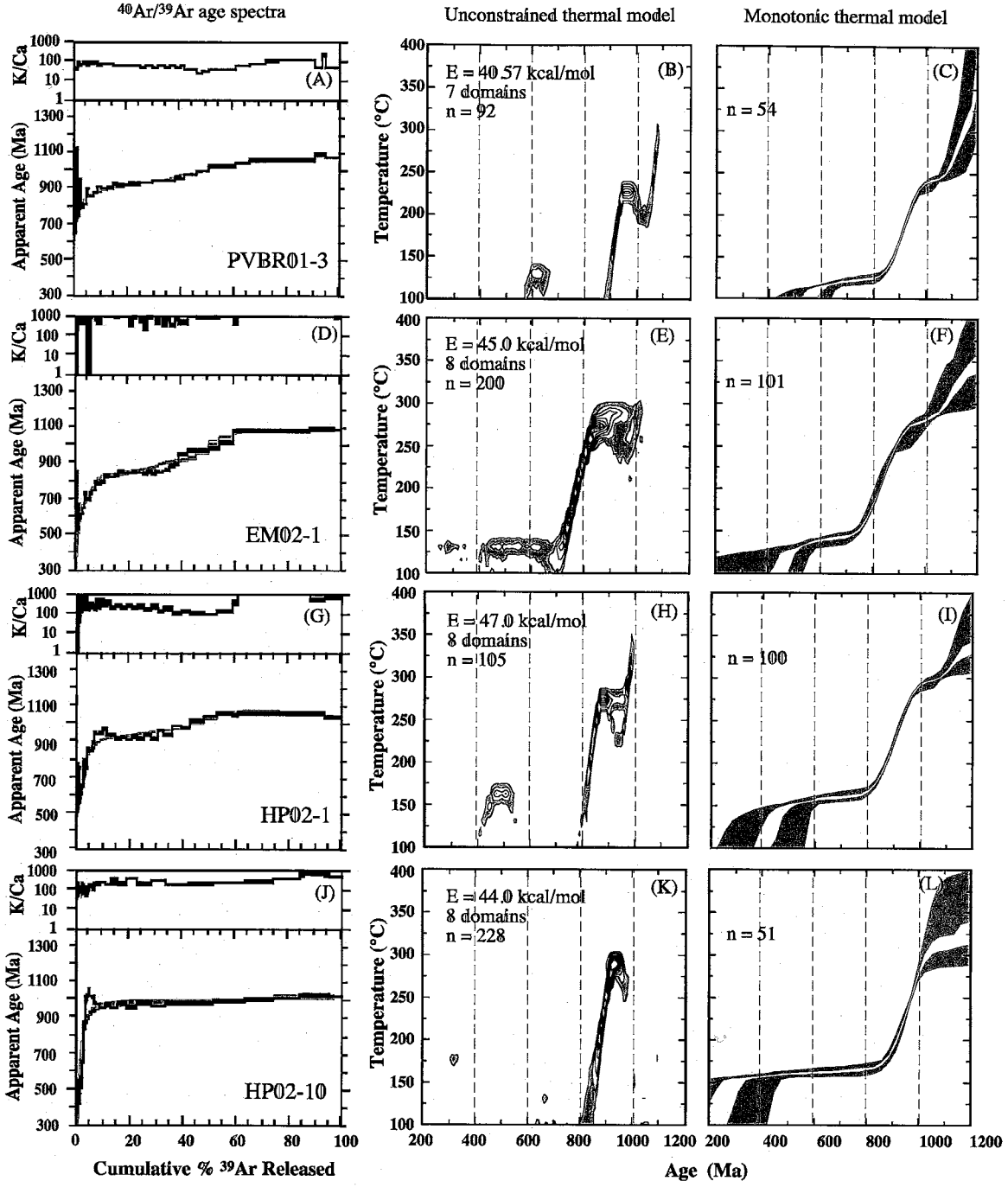

Figure 1.8: Measured (black) and modeled (gray) $^{40}Ar/^{39}Ar$ age spectra, and unconstrained and monotonic MDD thermal models generated for K-feldspar from the Pecos River valley (PVBR01-3), Elk Mountain (EM02-1), Hermit Peak summit (HP02-1), and Hermit Peak base (HP02-10).

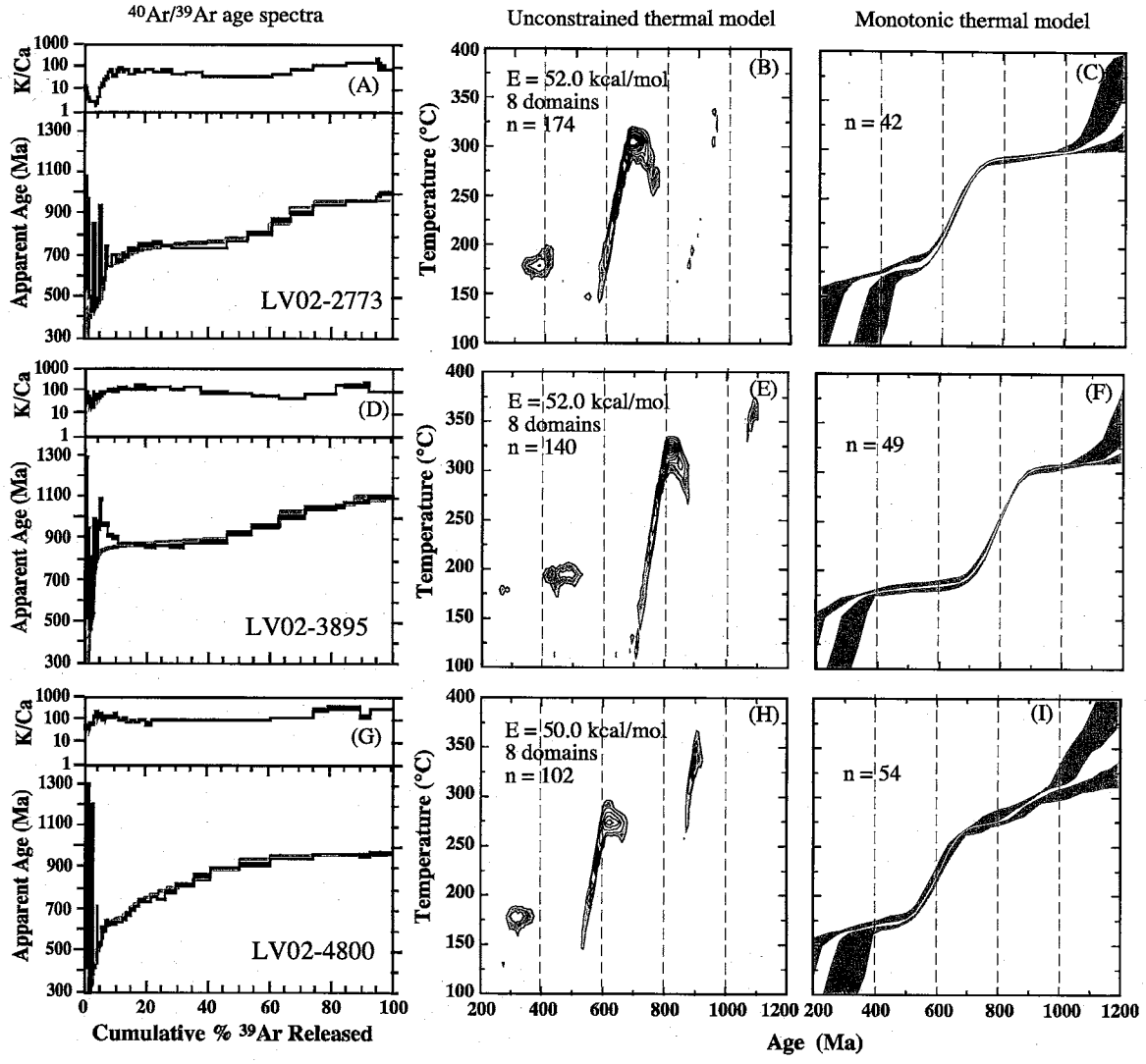

Figure 1.9: Measured (black) and modeled (gray) $^{40}Ar/^{39}Ar$ age spectra, and unconstrained and monotonic MDD thermal models generated for basement K-feldspar recovered from petroleum exploration well cuttings in the Las Vegas basin: Phillips Leatherwood #1 (LV02-2773); Continental Leatherwood-Reed #1 (LV02-3895); Reese & Jones #1 O'Connor (LV02-4800).

and thermal histories show temperatures of ~200 to 300°C at this time. Samples cooled between 1000 and 800 Ma and reached ~150°C by 800 Ma. TP02-4 (Fig. 1.7i) passed through 300°C earlier at ~1200 Ma. The anomalous age of this sample relative to other K-feldspars may be due to excess argon present in the large diffusion domains (cf. Foster et al., 1990), or it could indicate that this sample actually cooled earlier than the majority of the K-feldspars.

MG01-1a (Fig. 1.7k) is also anomalous with respect to most modeled thermal histories and shows cooling from >350 to 200°C between 1200 and 1000 Ma followed by slow cooling to ~150°C by 800 Ma. Thermal models for this sample, however, are based on a model age spectrum (Fig. 1.7k; gray spectrum) that does not closely mimic the age pattern derived from the measured age spectrum (Fig. 1.7k; black spectrum). The poor fit between measured and modeled spectra yields a thermal history that is probably suspect and therefore is not considered further.

Samples collected from the base and summit of Hermit Peak (HP02-10 and HP02-1, respectively; Figs. 1.8j, g) are separated by ~700 meters, and span one of the biggest vertical exposures of basement rock in northern New Mexico. The high elevation rocks, that represent higher crustal levels, should have cooled earlier than low elevation rocks, and record older apparent ages if argon kinetic parameters are equal. The thermal histories are nearly identical and indicate that the overall results are not sensitive to relatively small (~1 km) vertical separations.

Most K-feldspar age spectra record minimum apparent ages between ~300 and 600 Ma during initial heating steps. These parts of the age spectra contain important information for the low temperature part of the thermal history, but the thermal histories

have high uncertainty because this section of the spectra only comprise a very small amount of the total argon released and are somewhat contaminated with excess argon. This part of the age spectra is typically characterized by a steep age gradient nearly asymptotic to the age axis, further enhancing error in modeling the timing of final argon closure or resolving low temperature thermal events. To account for the steep initial gradient observed in the lower temperature portion of most age spectra, monotonic cooling models require the samples to reside in the 150 to 125°C temperature range for hundreds of millions of years following the main cooling event. Alternatively, the unconstrained models (Figs. 1.7b, e, h, k; 8b, e, h, k), while recording the same major cooling event between 1000 and 800 Ma, allow the samples to cool below 100°C with later Phanerozoic reheating, causing minimal argon loss from low retentivity diffusion domains. The timing of possible reheating events is somewhat variable between models and generally falls between ~600 to 350 Ma. Six of eight unconstrained thermal models from this study and two of three of Melis (2001) have similar temperature history profiles and suggest possible reheating to about 150 to 175°C around 500 Ma.

K-feldspars from the subsurface of the Las Vegas basin record significantly different thermal histories compared to those from the Sangre de Cristo Range and indicate that cooling through ~300°C initiated later than 1000 Ma (Figs. 1.9c, f, i). All three samples exhibit excess argon for several of the initial heating steps, but climb from minimum apparent ages of about 400 Ma to ages of 1000-1100 Ma (Figs. 1.9a, d, g). Similar monotonic cooling histories modeled for LV02-2773 and LV02-4800 suggest these rocks were at about 275°C until ca. 700 to 800 Ma, after which they show accelerated cooling to ~175°C by 500 Ma. Sample LV02-3895, located several

kilometers west of the other basin samples and on a different structural block (Fig. 1.9f, Fig. 1.3), displays a different thermal history interpreted as earlier cooling between 900 and 700 Ma. The unconstrained thermal models for these three samples also show significant cooling at these same times indicated by the monotonic models, and in addition show that the initial steep age gradient can be modeled with subsequent reheating between 300 and 500 Ma (Figs. 1.9b, e, h). As mentioned, LV02-3895 is from a discrete structural block and therefore may record a distinct thermal history. Alternatively, because this K-feldspar age spectrum has a pronounced intermediate age maxima it may be yielding an inaccurate thermal history thus MDD modeling may be inappropriate (cf. Lovera et al., 2002). Discrepancies in the timing of exhumation among the three Las Vegas basin model thermal histories cannot be explained by differences in K-feldspar argon retentivities and activation energies. It appears that sample LV02-3895 effectively records a unique cooling history distinct from the other basin K-feldspars or that the intermediate age hump is identifying a sample that should be treated cautiously due to potential ^{39}Ar recoil, contaminant K-bearing phases, recrystallization, etc. (cf. Lovera et al., 2002).

1.5 Discussion

1.5.1 Post- 1.4 Ga cooling in the southern Sangre de Cristo Range

Combining the new $^{40}Ar/^{39}Ar$ data from this study with published results (Karlstrom et al., 1997; Melis, 2001; Erslev et al., 2004; Shaw et al., 2005) provides an extensive data set to evaluate the thermal history of the basement in the southern Sangre de Cristo Range following ca. 1.4 Ga tectonism. The assigned ages recorded by

hornblende, muscovite, and biotite are interpreted as the times at which these minerals cooled below their nominal argon closure temperature (500-550°C hornblende, 350-400°C muscovite, and 300-350°C biotite; McDougall and Harrison (1999)). In general the thermochronology supports long mid-crustal residence of Paleoproterozoic rocks at temperatures around 300 to 350°C following ca. 1.4 Ga reheating to or above 500°C. This residence endured until regional basement exhumation initiated at ca. 1000 Ma as recorded by the K-feldspar data represented here.

Hornblendes analyzed in this and previous studies (Figs. 1.4a-l; Table 1.1) yield apparent ages indicating temperatures >500°C in the Sangre de Cristo basement following ca. 1.4 Ga plutonism and metamorphism (e.g. Melis, 2001). In the Hermit Peak area, the Hermit Peak granite has no U-Pb zircon dates, but has been interpreted as a 1.4 Ga pluton (Karlstrom et al., 2004). Recall that the two different hornblende samples (HP02-2 and HP02-4) located within 10 meters of one another yield dramatically different age spectra (Figs. 1.4 A-I) that are interpreted to result from closure temperature variations. HP02-4 is interpreted to be more retentive than HP02-2 and thus was not completely reset during 1.4 Ga heating. If the Hermit Peak granite were 1.4 Ga, amphibolites would have reached nearly magmatic temperatures at the margins of the intrusion and would have consequently been heated above any reasonable closure for hornblende thereby resulting in ages less than 1.4 Ga. It therefore appears the Hermit Peak crystalline rocks are older than 1.4 Ga, and experienced a thermal and deformation history similar to the other Paleoproterozoic rocks in the region.

Muscovite dates for rocks from Santa Fe to the Las Vegas basin subsurface display a trend of older apparent ages in the western part of the Sangre de Cristo Range

with younger ages eastward (Fig. 1.2). Overall, ages from Santa Fe to Elk Mountain are between about 1365 and 1375 Ma whereas the Hermit Peak muscovite sample is about 1300±25 Ma and the Las Vegas basin sample is ~1275±10 Ma. This regional trend may reflect differential cooling following the ca. 1.4 Ga thermal perturbation as basement rocks to the west cooled through about ~350 to 400°C around 1375 Ma, approximately 50 to 100 m.y. before the rocks to the east. To account for this, either 1) the rocks in the west are structurally higher in the crust and cooled sooner during regional exhumation, or; 2) rocks in the west were differentially exhumed by means of faulting or block rotation while rocks to the east remained deeper and hotter.

Biotite dates from across the region display much more age variation than the muscovite data, and do not define a similar spatial trend. Compiled biotite ages vary by as much as 300 m.y. between samples less than 10 km apart (i.e. SF-12 and RP-36; Fig. 1.2; Table 1.2). Additionally, samples from the summit of Santa Fe Baldy (elev. 3847 m; Fig. 1.2) that might be expected to preserve some of the oldest apparent ages yield the youngest. Although biotite is more commonly affected by excess argon than muscovite, a 300 m.y. discrepancy is not a consequence of excess argon as we would expect many biotites to record geologically unacceptable ages older than ~1.4 Ga which they do not (cf. Shaw et al., 2005). Instead, biotite has a wide range of closure temperatures (300-400°C; McDougall and Harrison, 1999) and the fairly random distribution of ages likely indicates that the exposed basement resided in a temperature window that caused some biotites to lose more argon than others. This is supported by the K-feldspar data that indicate >300°C temperatures between 1.2 and 1.0 Ga.

1.5.2 Neoproterozoic exhumation, fault reactivation, and the development of the Great Unconformity

The present-day elevation of the Precambrian-Mississippian unconformity varies across the southern Sangre de Cristo Range. Samples east of the Picuris-Pecos fault zone were collected within a few hundred vertical meters of the Precambrian-Paleozoic contact. To the west, this relationship is not constrained because no Paleozoic sediments are preserved. K-feldspar samples collected at Glorieta Baldy (TP02-4), Elk Mountain (EM02-1) and Hermit Peak (HP02-1) are all located above ~3000 m elevation whereas samples from the Pecos River valley (PVBR01-3a), Macho Canyon (MG01-1a), and Interstate 25 (LAMY02-1) are lower at ~2200 m. The present vertical separation is caused by post-Mississippian displacement on structures related to Ancestral Rocky Mountain, Laramide, and Rio Grande rift tectonism such as the Picuris-Pecos and Montezuma fault zones. Because the Precambrian-Paleozoic unconformity is interpreted to have little relief at the time of formation, and is laterally extensive across the region (Baltz and Myers, 1999), it serves as an excellent marker to examine the net basement displacement from these relatively young tectonic events. Contrasting earlier Precambrian ancestry of these structures requires techniques such as $^{40}Ar/^{39}Ar$ K-feldspar thermochronology to document movement prior to the Paleozoic.

MDD models generated for K-feldspar from the Sangre de Cristo Range display an overall common cooling signature from ca. 1000 to 800 Ma interpreted to record exhumation of the basement through ~300 to 175°C. There is minor spread between thermal models due to either the accuracy of the model kinetic parameters and/or poorly behaved age spectra. At first order, however, K-feldspar thermal histories in the Sangre

de Cristo Range basement indicate that the region behaved as a unified structural block as it underwent an estimated 4-7 km of net basement exhumation from 1.4 to 0.5 Ga (geothermal gradient 20°C/km to 30°C/km)(Fig. 1.10).

To the east of the Sangre de Cristo Range, thermal histories for K-feldspar from the subsurface of the Las Vegas basin indicate that cooling from 300 to 150°C occurred later, between 750 and 600 Ma (Fig. 1.10). Two samples (LV02-2773, LV02-4800) suggest that the basement in this area remained relatively hot and deep (300-350°C) while the rocks in the Sangre de Cristo Range were being exhumed. Cooling of these samples began between 750 and 700 Ma and samples cooled to 175°C by ~600 Ma. As previously mentioned, LV02-3895 has a slightly different thermal history relative to the other two subsurface samples and may be inaccurate due to its non-ideal age spectrum or it may represent a real geologic difference. Well log data and sedimentary relationships in the subsurface of the Las Vegas basin show this sample is separated from the other two by a fault that was active during Ancestral Rocky Mountain time (Fig. 1.3; Broadhead, unpub. data). Further east, the remnant Ancestral Rocky Mountain Sierra Grande uplift is identified in the subsurface. Although sample LV02-3895 could be recording an important thermal history discontinuity across a discrete fault, the first order variation observed between the Sangre de Cristo block relative to the Las Vegas basin samples is the most significant.

The Sangre de Cristo Range is presently separated from the Las Vegas basin by the north-striking Montezuma fault (Fig. 1.2; Baltz and Myers, 1999; Magnani et al., 2005). The fault is mapped as a west dipping reverse fault with dip varying along strike ranging between 40° and 70°(Baltz and Myers, 1999). Seismic reflection data across

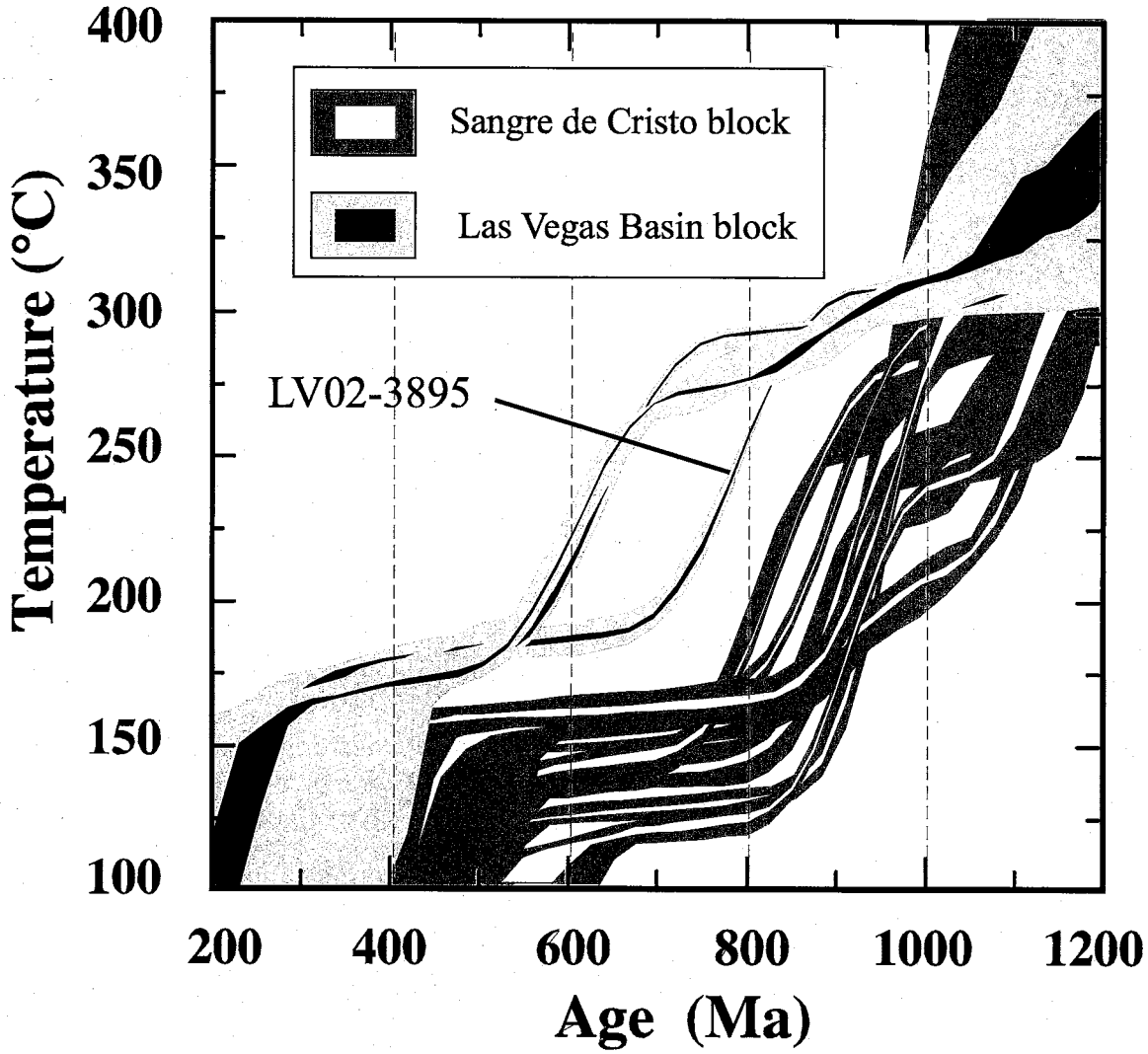

Figure 1.10: Measured (black) and modeled (gray) $^{40}Ar/^{39}Ar$ age spectra, and unconstrained and monotonic MDD thermal models generated for basement K-feldspar recovered from petroleum exploration well cuttings in the Las Vegas basin: Phillips Leatherwood #1 (LV02-2773); Continental Leatherwood-Reed #1 (LV02-3895); Reese & Jones #1 O'Connor (LV02-4800).

north-striking faults along the Sangre de Cristo range front, including the Sapello fault north of the Montezuma fault, corroborate this and show a west-dipping listric geometry extending to approximately 12 km below the Sangre de Cristo Range (Magnani et al., 2005). Mississippian sediments at the summit of Hermit Peak correlate with those at the basal sedimentary contact of the Las Vegas basin (Baltz and Myers, 1999) and indicate ~1100 m of throw on the Montezuma fault since the Mississippian. Because these blocks record different Neoproterozoic thermal histories that cannot be explained by Phanerozoic faulting, it appears the Montezuma fault initiated at least as early as 1000 Ma and has subsequently been reactivated by later tectonic events (e.g. Ancestral Rocky Mountain orogeny, Laramide orogeny). In this scenario, at ca. 1000 Ma the Sangre de Cristo block began significant differential exhumation relative to the Las Vegas block that was accommodated by the Montezuma fault with 4 to 7 km of west-side-up throw. Around 750 Ma, the fault was reactivated as a west-side-down extensional structure such that the Las Vegas block was exhumed and cooled. We envision high elevation in the Las Vegas block at this time in which cooling was facilitated largely by erosion.

The modeled temperature decrease of the Sangre de Cristo basement between 1000 and 800 Ma is interpreted to record exhumation that brought the mid-crustal basement rocks from 10-12 km depth to ~3-5 km. The final depth of the basement rocks following the major denudation pulse is difficult to estimate. Monotonic cooling models show that the Sangre de Cristo basement could have remained at ~125-150°C for hundreds of millions of years, whereas unconstrained models indicate the basement could have continued to cool after 800 Ma and then been reheated subsequently. Assuming a geothermal gradient of 25°C/km, monotonic thermal models suggest the Sangre de Cristo

basement was ~125°C or cooler by 800 Ma which would correlate to crustal depths of about of 4 to 5 km or less. Models for the Las Vegas basin basement suggest these rocks were overall a little hotter following major Neoproterozoic exhumation and resided at 5 to 7 km depth or less by 600 Ma. Unconstrained models permit samples to cool below 100°C after major exhumation, and could reflect much shallower final depths between 4 kilometers and the surface. Cambrian plutons in the southern Rocky Mountains intrude Precambrian basement requiring that Precambrian rocks were at least several kilometers deep during this time (McMillan and McLemore, 2004) which is supported by the K-feldspar thermal histories. Alternatively, if samples came near the surface by ~800 Ma, they would require subsequent burial and reheating to ~150°C so that the age spectra would record ages between ~500 and 800 Ma.

The Great Unconformity is described as either an exhumed late Precambrian surface, or as a compound surface with early Paleozoic modification (Baltz and Myers, 1999). Baltz and Myers (1999) reasoned that the development of this surface required extensive erosion of Precambrian crystalline rock, but the expected volume of sediment is absent from the Paleozoic sedimentary record. They therefore concluded that this surface likely formed in the late Precambrian and was slightly modified by periods of erosion prior to Mississippian sedimentation. The youngest $^{40}Ar/^{39}Ar$ K-feldspar apparent ages recorded by four samples range between 340 and 400 Ma (ASF01-9, LV02-4800, HP02-10, MG01-1a). An additional four samples record apparent ages between 400 and 500 Ma (LAMY02-1, LV02-2773, LV02-3895, TP02-4), whereas EM02-1 and HP02-1 show that their youngest apparent ages are between 500 and 600 Ma. These ages reflect argon loss from the least retentive diffusion domains and indicate that these samples were hotter

than ~175°C since the late Neoproterozoic. If the basement rocks were at the surface by the late Neoproterozoic as suggested by Baltz and Myers (1999), the youngest apparent ages recorded by the basement rocks should be Neoproterozoic, not Paleozoic. Given that there are no thick sequences of Paleozoic sedimentary rocks that could cause burial-related argon loss, ca. 1000 Ma late-Grenville tectonism and ca. 750 Ma rifting are favorable times for major basement exhumation and denudation but did not bring the presently exposed basement to the surface. We can constrain the pre-Mississippian surface modification proposed by Baltz and Myers (1999) to between the Cambrian and Mississippian based on Cambrian plutons and Paleozoic $^{40}Ar/^{39}Ar$ K-feldspar apparent ages. Three to four kilometers of basement removal during the early Paleozoic would represent the final significant surface modification prior to Mississippian sedimentation.

The youngest apparent ages are difficult to reconcile as being related to significant Paleozoic burial or basement removal. However, these ~300 Ma ages likely record fluid circulation at or near the unconformity. An event of this nature that either caused minor argon loss or incipient K-feldspar growth (cf. Lee and Parsons, 2003) is supported by Geissman and Harlan (2002) who recognize a late-Paleozoic chemical remagnetization event in the crystalline basement rock underlying Paleozoic sediments in New Mexico and Colorado. They attribute this event to extensive fluid flow along the Precambrian-Paleozoic contact. Fluid temperatures are estimated to be ~200°C or less (Geissman and Harlan, 2002), thus potentially hot enough to cause argon loss from low retentivity diffusion domains in K-feldspar. Apatite fission track ages from the Santa Fe range fall between 44 and 74 Ma indicating cooling below 120°C at this time (Kelly and Chapin, 1995), and there are no existing zircon fission track ages for this area. While

these ages are significant in constraining the young exhumation history of the southern Sangre de Cristo range, the data do not help to reconcile the Paleozoic history.

1.5.3 Timing of fault initiation along the eastern Rocky Mountain range front

Timmons et al. (2001) propose a northwest-southeast maximum principal stress direction for the southwestern U.S. during late-Grenville collision (ca. 1.1 Ga). Our data support four to seven kilometers of west-side-up throw on the Montezuma fault at ca. 1000 Ma that requires east-west shortening of a similar magnitude. The northerly strike of the fault is not consistent with a reverse fault generated in the stress orientation of Timmons et al. (2001). It is, however, difficult to know the true stress orientation at a given point on the Grenville front and stresses are also unlikely to have been homogenous. If the Montezuma fault initiated late in the Grenville orogeny, it could represent an area of principally east-west shortening. Alternatively, the Montezuma fault may have formed prior to 1.1 Ga, and accommodated oblique-slip during the Grenville orogeny consistent with northwest-southeast shortening (cf. Timmons et al., 2001).

1.5.4 Establishment of the Rocky Mountain/Granite-Rhyolite provincial boundary

Structural offset between ca. 1.3 to 1.4 Ga volcanic and subvolcanic rocks in the subsurface of eastern New Mexico, and mid-crustal granitic/metamorphic rocks of similar age in the Rocky Mountains requires an estimated 10 km of west-side-up throw (Karlstrom and Humphreys, 1998; Karlstrom et al., 2004). The preserved Mississippian/basement unconformity indicates only minor regional basement erosion since this time, and therefore the exposure contrast between the Rocky Mountains and the

Granite-Rhyolite province was evidently developed during the early Paleozoic and/or Precambrian. Despite the fact that the Montezuma fault accommodated significant Precambrian basement erosion, the subsurface basement data from the Las Vegas basin indicate that it does not represent the primary boundary between 1.4 Ga mid-crustal rocks and the Granite-Rhyolite province. Because the argon thermochronology data from coarse-grained K-feldspar-muscovite bearing subsurface rocks are similar to Rocky Mountain basement data, the provincial boundary must be east of our sub-surface samples. A system of buried faults east of Las Vegas is likely responsible for the offset.

1.6 Summary and Conclusions

Combined $^{40}Ar/^{39}Ar$ dates for hornblende, muscovite, and biotite and K-feldspar MDD thermal histories from the southern Sangre de Cristo Range and the Las Vegas basin subsurface yield a rich record of the timing of basement cooling and exhumation following ca. 1.4 Ga metamorphism in northern New Mexico. These data are used to reconstruct a model exhumation history for the Proterozoic basement in the region (Fig. 1.11). Detailed $^{40}Ar/^{39}Ar$ thermochronology is successful in deciphering complex tectonic histories in areas that cannot be constrained by sedimentological or structural information. In the southern Sangre de Cristo Range, New Mexico, this method is used to recognize the punctuated intracratonic effects of supercontinent assembly and break-up including fault reactivation and the timing basement denudation related to the development of the Great Unconformity.

- Hornblende dates in the Sangre de Cristo Range indicate Paleoproterozoic rocks were reheated to >500°C during ca. 1.4 Ga metamorphism and in general, cooled below ~500°C by ~1380 Ma. Muscovite and biotite yield a range of ages and indicate

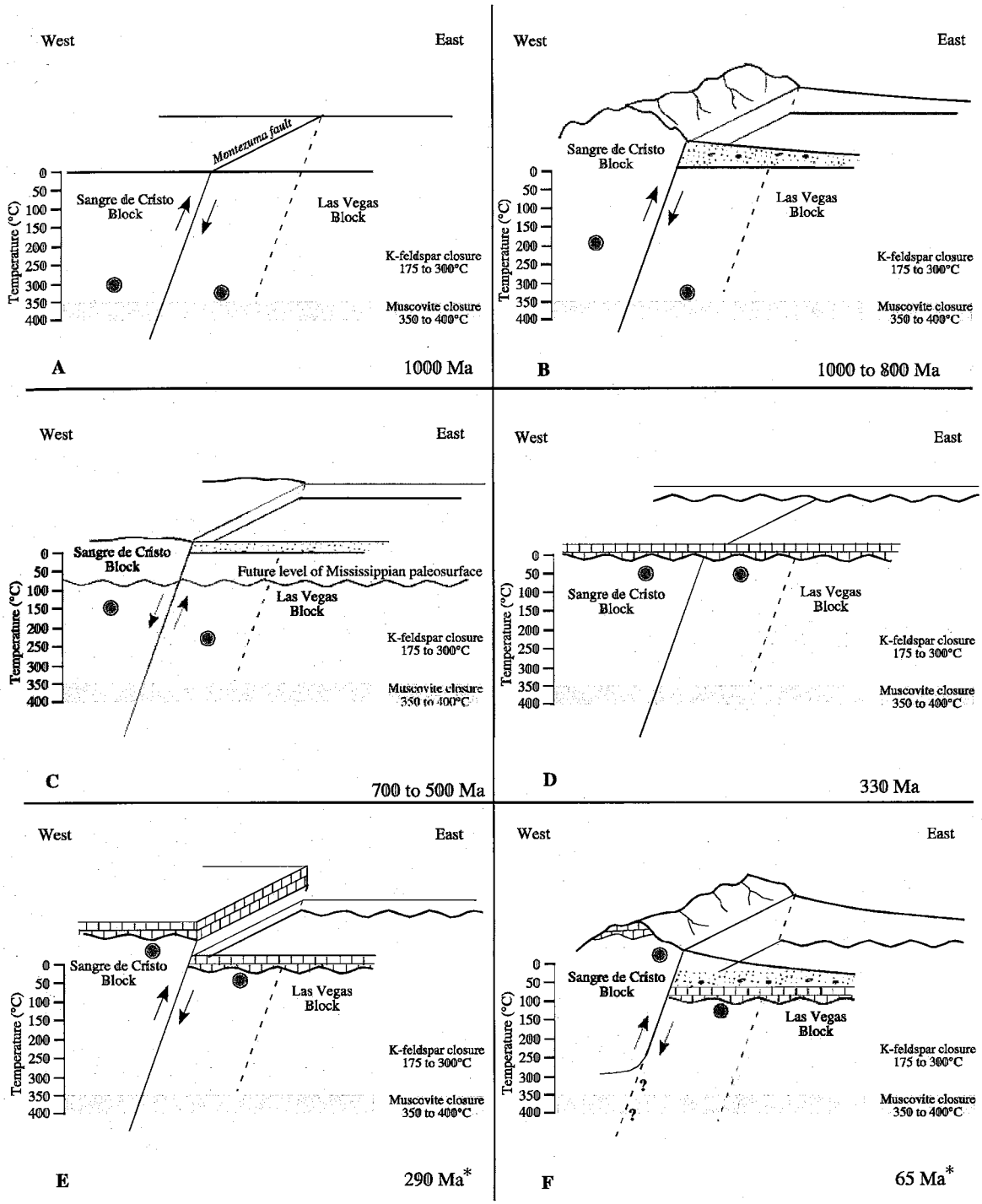

*after Baltz and Myers (1999)

Figure 1.11: Conceptual model for the tectonic evolution of the southern Sangre de Cristo Range constructed from $^{40}Ar/^{39}Ar$ hornblende and mica ages and K-feldspar thermal histories for Proterozoic basement rocks in the region. In general, Sangre de Cristo basement was exhumed ca. 1000 Ma relative to the Las Vegas basement that was not exhumed until ca. 750 Ma. The Montezuma fault accommodated displacement at these times indicating a protracted history of fault reactivation from the Precambrian to the Phanerozoic.

basement rocks in the Sangre de Cristo Range and the Las Vegas basin resided at ~300 to 400°C between 1.4 and 1.1 Ga.

- K-feldspar MDD thermal histories for the Sangre de Cristo Range record basement cooling from ~300 to 150°C between ca. 1000 and 800 Ma interpreted as 4 to 7 km of basement exhumation in the late-Grenville (Figs. 1.11 A and B). Las Vegas basin K-feldspar thermal histories indicate they remained deeper during Sangre de Cristo basement exhumation. Differential displacement between the Sangre de Cristo and Las Vegas basin basement was accommodated by the Montezuma fault during the late-Grenville.

- Thermal histories for Las Vegas basin K-feldspars indicate cooling between ~750 and 600 Ma at which time samples are interpreted to have been exhumed relative to the Sangre de Cristo basement (Fig. 1.11 C). At this time, the Montezuma fault was reactivated during the incipient rifting of Rodinia. Final exhumation of the Precambrian basement likely occurred in the Late Cambrian. Both the Sangre De Cristo and Las Vegas blocks were at a similar structural level prior to Mississippian sedimentation (Fig. 1.11D).

- The Montezuma fault was reactivated during Ancestral Rocky Mountain tectonism (Fig. 1.11 E) and again during the Laramide orogeny (Fig. 1.11F).

CHAPTER 2: $^{40}AR/^{39}AR$ K-FELDSPAR THERMOCHRONOLOGY OF MICROTEXTURALLY COMPLEX FELDSPAR, SANGRE DE CRISTO RANGE, NEW MEXICO: IMPLICATIONS FOR UNRAVELING PROTEROZOIC THERMAL AND METASOMATIC HISTORIES

2.1 Abstract

$^{40}Ar/^{39}Ar$ K-feldspar thermochronology studies identify several previously unrecognized episodes of localized K-metasomatism of Precambrian basement rocks in the southern Sangre de Cristo Range, north-central New Mexico. K-feldspar textures are complex and it is only through combining mineralogic and thermochronology studies that the metasomatic events can be documented. Primary igneous plagioclase grains are partially replaced by secondary K-feldspar. The secondary grains, analyzed by the $^{40}Ar/^{39}Ar$ method, revealed multiple age populations suggestive of episodic metasomatic events between the Neoproterozoic and Devonian. In addition to replacement of primary plagioclase by metasomatic K-feldspar, detailed BSE, SEM, and CL-SEM imaging indicate that pegmatitic perthitic microcline was also replaced by secondary patch perthite. Microsampling and single-grain $^{40}Ar/^{39}Ar$ step heating of both primary and secondary grains reveal that discrete age populations are preserved in megacrystic microcline at the sub-millimeter scale. Primary film perthites yield $^{40}Ar/^{39}Ar$ total gas ages of 1100-950 Ma similar to basement K-feldspars elsewhere in the southern Sangre de Cristo Range that record regional cooling related to post-1400 Ma exhumation. In

contrast, patch perthites record mineral growth ages of 800, 700, 600, and 400 Ma, only the first of which was recognized in previous studies. These ages are interpreted to record the timing of multiple metasomatic fluid flow events in the basement rocks.

Beyond the local significance of identifying previously unrecognized metasomatic events, the documentation of distinct age populations within microtexturally complex K-feldspar shows that single microcline crystals have the potential to record both thermal history and hydrologic/metasomatic histories. Investigation of the geochemistry and genetic origin of metasomatic fluids via fluid inclusion work suggests that non-magmatic, evolved crustal fluids circulated within areas of high permeability such as faulted, fractured, and brecciated zones of basement rock. The association of metasomatism with brittle faults and breccias in the Pecos area hints at a coeval relationship between deformation and fluid migration. Coupled with the regional geologic history, episodic K-metasomatism in the Pecos area is interpreted as evidence for widespread Neoproterozoic intraplate deformation in the southwestern U.S. associated with the insipient break up of Laurentia. Overall these results indicate that Neoproterozoic fluid flux events involved infiltration and alteration by alkaline (<300°C) fluids during regional exhumation and denudation. Paleozoic secondary K-feldspar indicates a substantially younger episode of fluid infiltration during Devonian time.

2.2 Introduction

Proterozoic basement rocks in northern New Mexico consist of crystalline and metamorphosed supracrustal rocks and a variety of granitoids that were exhumed from 10-15 km depths after 1.4 Ga (Grambling et al., 1989). The history of tectonic processes responsible for this denudation remains poorly resolved, but is hypothetically related to punctuated Mesoproterozoic, Neoproterozoic, and Ancestral Rocky Mountain events (Marshak et al., 2000). The Precambrian-Mississippian unconformity in northern New Mexico indicates that the 10-15 km deep crystalline basement (Grambling et al., 1989) had been exhumed to the surface without major tilting by Mississippian-Pennsylvanian time.

Thermochronology techniques can be used to determine cooling ages and thermal histories of minerals to infer the geological evolution of the crystalline basement. In the southern Sangre de Cristo Range in north-central New Mexico, methods such as $^{40}Ar/^{39}Ar$ dating and apatite fission track (AFT) thermochronology have deciphered a rich tectonic history of regional cooling, basement uplift, erosion, and fault reactivation since the Proterozoic (Kelley and Chapin, 1995; Karlstrom et al., 1997; Melis, 2001; Erslev et al., 2004; Shaw et al., 2005; Sanders et al., 2006). Results to date indicate that mica $^{40}Ar/^{39}Ar$ ages are mainly 1.4 Ga (Karlstrom et al., 1997; Melis, 2001; Sanders et al., 2006) and AFT ages are mainly post-70 Ma (Kelley and Chapin, 1995). Additional thermochronometers are needed to constrain the timing of geologic events within the one billion year duration of the development of the Great Unconformity.

The goal of this paper is to evaluate the regional basement thermal history using K-feldspar multiple diffusion domain (MDD) modeling (cf. Lovera et al., 1989). This

paper builds on Sanders et al. (2006; Chapter 1) in expanding the geographic area and in examining microtexturally complex K-feldspars that have the potential to reveal metasomatic and cooling events during denudation. The Pecos River valley (Figure 1.2) was identified as having both microclines that yield dominantly Mesoproterozoic $^{40}Ar/^{39}Ar$ apparent ages, and secondary, metasomatic K-feldspars with a range of total gas ages, some of which were Neoproterozoic and distinctly younger than primary microcline (Melis, 2001; Erslev et al., 2004; Sanders et al., 2006). Further sampling showed that some pegmatitic microcline also gave $^{40}Ar/^{39}Ar$ total gas ages similar to those of the younger, secondary K-feldspars. Although Mesoproterozoic (>1.0 Ga) apparent ages appear common and typical for basement K-feldspars throughout the southern Sangre de Cristo Range (Sanders et al., 2006), Neoproterozoic apparent ages are, to date, restricted to the Pecos River valley. Unlike young apparent ages in the Las Vegas basin that were explained by differential offset (Sanders et al., 2006), Pecos age discontinuities cannot be reconciled by faulting because they occur at an outcrop and even a hand sample scale. To understand these results in the context of the regional tectonic history, and to resolve age variations in terms of the MDD model, a comprehensive investigation of the timing of K-metasomatism, the nature and origin of metasomatic fluids, and thermal impacts fluids had on the $^{40}Ar^*$ in primary microcline was conducted.

Beyond a local tectonic significance, this study has implications for the use of the MDD method for unraveling metasomatic as well as cooling events. Secondary K-feldspar in the Pecos area is not dissimilar to documented K-feldspar growth of diverse ages in sedimentary, volcaniclastic, and granitoid rocks throughout North America

(Mensing and Faure, 1983; Roddy et al., 1988; Duffin, 1989; Dunbar et al., 1994; Rougvie and Sorensen, 2002; Liu et al., 2003). In the western U.S., secondary K-feldspar grew within fault zones and beneath long-lived playa basins in Arizona, California, Colorado, and New Mexico (Roddy et al., 1988; Warnock and van de Kamp, 1999; Beratan, 1999; Ennis et al., 2000). Drill core from the subsurface of the mid-continent indicates intense K-feldspar alteration profiles at the Precambrian-Paleozoic unconformity that grade downward several meters to apparently unaltered protolith (eg. Mensing and Faure, 1983). In all of these occurrences, K-feldspars exhibit a range of replacement microtextures indicative of dissolution of the primary host mineralogy and reprecipitation of K-feldspar during fluid-rock interaction. Although fluid compositions and thermal conditions under which this reaction proceeds are broadly constrained (Kastner and Siever, 1979), the presence of secondary K-feldspar necessitates a driving mechanism ultimately linked with regional tectonic perturbation, whether it be localized fluid flow along a fault or widespread basinal fluid migration. Thus, this chapter provides a case study of the use of combined textural studies of K-feldspar replacement and microtextural variation with $^{40}Ar/^{39}Ar$ thermochronology and MDD interpretation to examine metasomatic events.

2.3 Geologic setting and tectonic history of the southern Sangre de Cristo Range

Proterozoic basement rocks exposed in the Pecos River valley consist of amphibolite, tonalite, granodiorite, and granite lithologies that record the crustal accretion and subsequent metamorphism and plutonism in northern New Mexico (Figure 2.1). The oldest rocks in the area comprise the Jones metavolcanic suite (1.72 Ga; Pb-Pb galena; U-

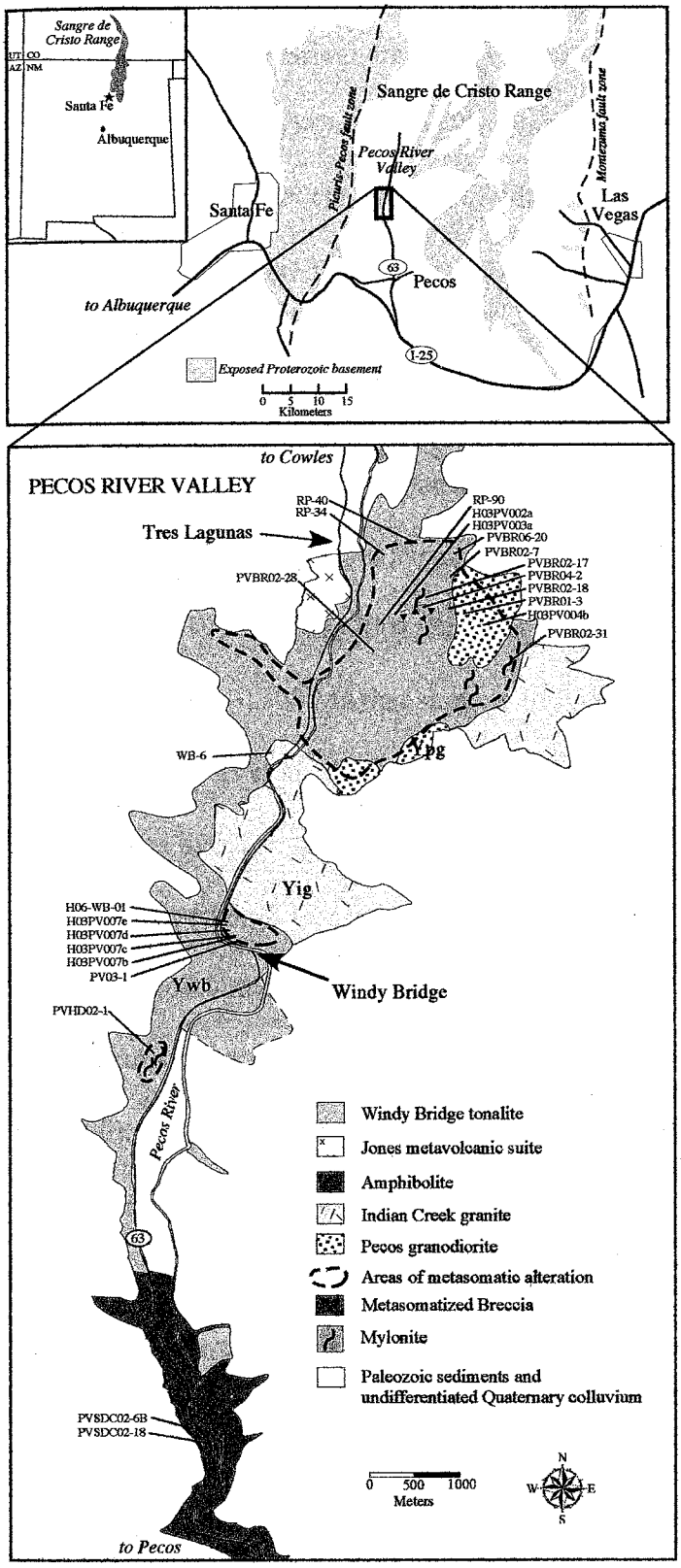

Figure 2.1: Map shows the location of the Sangre de Cristo Range and exposed Precambrian basement in northern New Mexico (upper), and the Precambrian geology of the Pecos river valley (lower). Sample locations are marked and dashed outlines indicate areas of observed K-metasomatism of the basement rock. Modified after Bauer et al. (1995), Melis (2001), and Erslev et al. (2004).

Pb zircon; Stacey et al., 1976; Bowring, 1987 *in* Robertson and Condie, 1989). Other units include the Windy Bridge tonalite (1.71 Ga zircon; Bowring and Condie, 1982), Indian Creek granite (1.65 Ga zircon; Bowring, 1984 *in* Robertson and Condie, 1989), Macho creek granite (1.48 Ga zircon; Bowring, 1984 *in* Robertson and Condie, 1989), and Pecos granodiorite (U-Pb unknown, 1.34 Ga biotite; Melis, 2001). $^{40}Ar/^{39}Ar$ dates for hornblende and micas constrain the ambient basement temperature during the Mesoproterozoic as a function of their nominal argon closure temperatures (McDougall and Harrison, 1999). Hornblende dates are ~1400 Ma and mark basement cooling below 550 to 500°C following ca. 1400 Ma regional metamorphism (Grambling et al., 1989; Karlstrom et al., 1997; Melis, 2001; Shaw et al., 2005). Micas yield a range of ages between ~1350 and ~1200 Ma that support cooling of the basement below ~350 to 300°C by 1200 Ma (Sanders et al., 2006). Several additional mica dates obtained subsequent to those published by Sanders et al. (2006) are in agreement with earlier results and are presented in Appendix 2.1.

The oldest apparent ages recorded by K-feldspars are ~1200 Ma indicating basement temperatures of ~300°C and an inferred depth of ~10 km at that time (Sanders et al., 2006). K-feldspar MDD thermochronology (Lovera et al., 1989) indicates that basement rocks in the Sangre de Cristo Range cooled and were exhumed to within several kilometers of the surface between 1000 and 800 Ma during late-Grenville contraction (Sanders et al., 2006). Crystalline rocks to the east of the range-bounding Montezuma fault (Figure 1.2) cooled below 200°C later (between 750 and 600 Ma) as a result of extension related to the break up of Laurentia (Timmons et al., 2001; Sanders et al., 2006). These data are interpreted to indicate at least two periods of differential

movement in the Proterozoic and indicate that Phanerozoic throw (Ancestral Rocky mountain, Laramide; Baltz and Myers, 1999) is the result of reactivation of Proterozoic structures (Sanders et al., 2006).

Throughout the southern Sangre de Cristo Range, basement rocks are unconformably overlain by Mississippian carbonate and marine facies rocks marking the progradation of the Paleozoic ocean into the cratonic interior. Older sedimentary rocks are absent, although to the southeast, from the Tucumcari basin to western Texas, the Mesoproterozoic sediments of the Debaca group constitute, although primarily in the subsurface, the most proximal Precambrian sedimentary sequence (Amarante et al., 2000). Baltz and Myers (1999) proposed that the Mississippian unconformity resulted from a final Paleozoic modification of the Neoproterozoic erosional surface.

2.4 Analytical techniques

2.4.1 Microprobe imaging and quantitative analysis

Electron microprobe imaging was conducted at the New Mexico Institute of Mining and Technology on a three spectrometer Cameca SX-100, and at the University of New Mexico on a JEOL 5800LV scanning electron microprobe. Backscattered electron (BSE) images of polished thin sections, polished grain mounts, and unpolished grains, as well as scanning electron (SEM) images of unpolished grains were collected on the Cameca. Quantitative X-ray chemical data analyses for mineral phases were collected on the Cameca microprobe with an accelerating voltage of 15kV and a 20nA beam with a 10 μm diameter. Quantitative data were calibrated relative to standards for the respective mineral, and weight percent values were calculated based on the

appropriate number of oxygen atoms for the given mineral composition. The JEOL microprobe was used for SEM and cathodoluminesence SEM (CL-SEM) imaging of polished thin sections and polished grain mounts. The CL detector uses a parabolic mirror light collecting element connected to a high-sensitivity photomultiplier. Three color filters (red, green, blue) were used to differentiate wavelength emissions within the ultraviolet to infrared spectrum.

2.4.2 $^{40}Ar/^{39}Ar$ Geochronology

2.4.2.1 Sample preparation

Samples of K-altered and unaltered Proterozoic granodiorite, tonalite, and coarse pegmatitic segregations were collected from the Pecos River valley (Figure 2.1). Mineral separates were prepared by Frantz magnetic separation, rinsed and dried, and grain fractions ranging from 600 to 180 microns were hand picked to obtain a monomineralic separate for imaging and analysis. K-feldspar samples for single-grain analyses were mounted on double-sided carbon tape on an aluminum disk and etched over a tray of 40 mL 48-51% HF acid at 2 cm height for 20 seconds after techniques of Waldron et al. (1994). Samples were gently rinsed with deionized water, dried, and lightly coated with carbon for BSE and SEM imaging. Following imaging, grains of interest were removed, weighed, and placed in 24-hole aluminum disks with Fish Canyon sanidine in a known geometry. Bulk separates were weighed and wrapped in copper foil before being loaded into machined aluminum disks which were stacked vertically for irradiation.

2.4.2.2 Mass spectrometer parameters

Argon isotopes were analyzed with a MAP 215-50 mass spectrometer equipped with either a Blazers 217 or a Johnston electron multiplier operating in static mode with a Nier source. The multipliers are typically operated to yield a gain of about 7000-10,000 above the Faraday. Resolution at 5% peak-height at mass 40 was typically 450-600.Analyses were conducted between 1998 and 2007 and mass spectrometer sensitivity values for furnace and laser extraction lines, discrimination, interfering reaction correction factors, irradiation time, and extraction line and total system blanks are presented Table A2.3. Detailed description of analytical methods can be found in the New Mexico Bureau of Geology and Mineral Resources open file report OF-AR-1 at http://geoinfo.nmt.edu/publications/openfile/argon/home.html.

2.4.2.3 Furnace step heating

Samples were step heated in a double vacuum molybdenum resistance furnace. K-feldspar separates wrapped in Cu-foil were heated with high resolution (~45 steps) heating schedules, and isothermal steps were conducted to help evaluate excess argon contamination (e.g. Harrison et al., 1993). Some NM-201 single-grain K-feldspars were heated using non-isothermal, abbreviated (17 steps) heating schedules due to small sample size (<100 μg). Gas released reacted with a SAES GP-50 getter operating at ~450°C during heating followed by a second stage of clean up using 2 SAES GP-50 getters (one at 20°C, one at ~450°C) and a tungsten filament operated at ~2000°C. Typically, K-feldspar steps were gettered for 2 minutes. The furnace thermocouple was

calibrated by melting Cu-foil and true sample temperature was between 35 to 100°C lower than thermocouple temperature. Heating schedules were adjusted by this amount, and corrected sample temperatures are reported. Furnace blank and mass spectrometer background values were determined by running a 15 minute, 650 to 800°C hot blank prior to each analysis.

2.4.2.4 Irradiations, flux monitoring, and age calculations

Samples were irradiated in machined aluminum disks at the McMaster University reactor, Ontario, the USGS Triga reactor, Denver, or the Texas A&M reactor, College Station. Fluence gradients were measured using Fish Canyon sanidine placed in holes of known geometry in the aluminum disks. Typically, 4 single crystals from each position were analyzed to determine the J-value. Mean values for each location were fit with a sine curve and J-values for unknowns were extrapolated based on their geometric relation. J-factor errors are estimated at 0.1 to 0.2% (1σ). Correction factors for interfering reactions were measured using CaF_2 and K-glass included with the samples during irradiation. Four to five grains of each are typically fused to obtain a weighted mean value for each factor. Total gas ages and errors are calculated by quadratically summing isotopic measurements for all steps.

2.4.2.5 Monitor age and decay constants

The assigned age of Fish Canyon sanidine is 28.27 Ma and the total ^{40}K decay constant is 5.476e-10/a (Kwon et al., 2002). At present there is no accepted value for the age of FC sanidine (Renne et al., 1998; Lanphere et al., 2001). However there has been

considerable recent work towards determining and evaluating the monitor age and ^{40}K decay constants (Min et al., 2000; Kwon, et al., 2002; Kuiper, 2008). These recent papers have recognized that $^{40}Ar/^{39}Ar$ ages based on an age of 28.02 Ma for FC sanidine and decay constants recommended by Steiger and Jäger (1977) yield younger results compared to U/Pb ages for samples that should not be discordant. In the near future it is expected that new decay constants for ^{40}K will be recommended based upon the U/Pb system and therefore ages reported here use the values of Kwon et al. (2002) in anticipation of this change. We recognize that the values used here will likely not be the final accepted values, but feel that they best reflect our present knowledge.

2.4.3 U-Pb Epidote Geochronology

U-Pb analyses of secondary epidote were conducted to constrain the timing of mineral growth and vein formation. Mineral separation, inductively coupled plasma mass spectrometry (ICP-MS), isotope dissolution, and thermal ionization mass spectrometry (TIMS) were conducted at the University of Wyoming, Laramie, WY. Epidote separates were first analyzed by ICP-MS to determine if a given sample had sufficient uranium and radiogenic lead for isotope dissolution analysis and age determination. Granodiorite and sheared granodiorite samples PVBR02-7, PVBR02-17, PVBR02-27, and PVBR02-30 were submitted in 2003 for preliminary analyses of which PVBR02-17 proved to be the only potential candidate for age analysis. Samples PVBR02-17, PVBR02-31, PVBR04-2, PVBR04-3, PVHD02-1, and H03PV004c were tested with ICP-MS in 2006 and samples PVBR02-31, PVBR04-3, and H03PV004c and additional material of PVBR02-17 were chosen for dissolution.

Epidote mineral separates were sieved and separated by standard hand picking techniques and classified by color, texture, and clarity. Three representative grains of each distinctive group were mounted on glass slides with double sided tape and loaded into a sealed canister under a LSX-200 laser ablation system with a Nd-YAG laser and argon plasma flow. Two single line ablations were performed to detect ^{238}U and ^{206}Pb, ^{207}Pb, and ^{208}Pb using an ELAN 6000 ICP-MS.

At least three aliquots of epidote from each sample with sufficient uranium and radiogenic lead (generally twice the U than Pb) were separated in a petrie dish in alcohol for dissolution and TIMS analysis. Average grain dimensions were estimated using a 100 mesh measuring screen and dry sample weight was approximated using the total surface area of multiple grains multiplied by the average thickness and density (3.0 mg/mm^3). Estimated Pb load was calculated by multiplying the sample weight by the estimated Pb concentration (3 ppm). Sufficient epidote was collected so that the estimated Pb load was between 2 and 3 ng.

Epidote dissolution and chemistry were adapted from methods developed by Krogh (1973) and Parrish et al. (1987). Samples were dissolved in HF and HNO_3 in microbombs with HBr-HCl ion exchange chemistry. A mixed $^{208}Pb/^{235}U$ tracer was added to aliquots of dissolved sample. Later analyses employed mixed $^{205}Pb/^{233}U/^{235}U$ tracer (ET535). Lead and uranium samples were loaded onto single rhenium filaments with silica gel and graphite, respectively. Isotopic compositions were measured in multi-collector, static mode on a VG Sector 54 mass spectrometer. Mass discrimination factors $0.06 \pm 0.04\%$ to $0.086 \pm 0.06\%$/amu for lead and $0 \pm 0.1\%$/amu for uranium were determined by replicate analyses of NIST SRM 981 and U-500, respectively. Samples

spiked with the ET tracer used an internal uranium fractionation measurement. Procedural blanks averaged 10 pg lead except for one batch with 100 pg. Uranium blanks were consistently 0.6 pg. Corrected ratios, uncertainties, and isochron dates were calculated using PBDAT (Ludwig, 1988), PbMacDAT (Isachsen, 2003) and ISOPLOT programs (Ludwig, 1991). The data reduction programs use the decay constants recommended by the I.U.G.S. Subcommission on Geochronology (Steiger and Jäger, 1977): 0.155125 x 10^{-9}/yr for ^{238}U, 0.98485 x 10^{-9}/yr for ^{235}U and present-day $^{238}U/^{235}U$ = 137.88.

2.4.4 Fluid inclusion gas analysis

Fluid inclusion gas compositions for secondary, patch perthite and coexisting epidote (PVBR04-2) were analyzed to evaluate the gas chemistry of metasomatic fluids. Separates were crushed in a vacuum anvil extraction system at the New Mexico Institute of Mining and Technology. Gas released during each crush was analyzed and this process was repeated until gas release from fluid inclusions was exhausted. Two measurements each on ~10 mg epidote and K-feldspar were collected for Pecos samples. Gas was measured on dual Pfeiffer Prisma Quadstar quadrapole mass spectrometers (accelerating voltage 1300V for organic; 1500V for inorganic) with a 2mA emission current in dynamic mode. Samples were prepared in a 0.7% NaOH solution for 24 hours and dried at 100°C. Analyses were corrected relative to CO_2 to normalize values between dual detectors to overcome gas fractionation issues. Unknowns were calibrated relative to Hansonburg fluorite to partially overcome fractionation of CO_2 and CO.

2.5 K-metasomatism in the Pecos River valley

K-metasomatism has variably affected most Proterozoic rocks in the Pecos River valley indiscriminate of lithology and manifests as a variety of occurrences and replacement microtextures. Miller et al. (1963) documented hydrothermal alteration in the southern Sangre de Cristo mountains and initially noted partial replacement of felsites by pink microcline in the Ortega quartzite (Figure 1.2). The following sections describe the K-feldspar veins and replacement of primary plagioclase by K-feldspar in the Pecos area, as well as the geochemistry of replacement mineralogy, temperature, chemistry, and origin of alteration fluids. Figure 2.1 shows the approximate geographic location of metasomatic alteration (cross-hatch) as well as locations for samples referred to below and in Table 2.1.

2.5.1 Occurrence and associated mineralization

Red to pink secondary K-feldspar ± epidote veins up to a millimeter wide cut basement rocks in the Pecos area and commonly have centimeter-scale hematite vein selvages (Figure 2.2a,b). Replacement style changes gradationally to a disseminated *in situ* replacement of primary sodic plagioclase by K-feldspar±epidote away from veins (Figure 2.3), and in areas, basement rocks are overprinted severely and resemble pink-red granite rather than the typically black and white appearance of locally unaltered tonalite and granodiorite (Fig 2.4). In some instances veins are irregular and/or sub-parallel (eg. Figure 2.3), however in the Tres Lagunas area, weathering along planar fractures with secondary K-feldspar±epidote allows blocks of granodiorite to preferentially break and expose metasomatized fracture surfaces. Fracture orientations (n=32) are shown on a

TABLE 2.1: AGES, LOCATIONS, AND DESCRIPTIONS OF SAMPLES DATED IN THIS STUDY

Sample	UTM		TGA (Ma)	Fig.	Sample Description
presumed microcline (multiple-grain)					
H03PV007d	437946	3950330	1020.1±2.4	2.21A	coarse-grained K-feldspar-albite-biotite segregation
PVBR01-3	439277	3952397	995.6±0.9	2.21B	microcline in tonalite
H03PV007e	437946	3950330	983.7±2.2	2.21C	medium-grained K-feldspar-quartz vein
WB-6	438920	3951153	955.0±2.3	2.21D	Indian Creek granite
H03PV002a	438719	3952293	894.8±2.6	2.21E	K-feldspar-quartz vein
RP-34	439600	3953100	886.3±2.1	2.21F	pegmatite
H03PV003a	438940	3952310	870.9±2.3	2.21G	K-feldspar-quartz vein
PVBR02-28	438694	3952002	853.9±3.0	2.21H	coarse-grained K-feldspar-muscovite pegmatite
PVIG02-1	440625	3960659	849.7±2.4	2.21I	coarse-grained K-feldspar-muscovite pegmatite
secondary K-feldspar (multiple-grain)					
PVSDC02-18	437889	3946025	1037.3±1.6	2.22A	fracture controlled K-feldspar veinlets
RP-40B	439300	3952350	959.6±1.5	2.22B	metasomatized tonalite
PVBR02-18	439247	3952273	876.4±1.5	2.22C	fine-grained replacement K-feldspar after aplite
H03PV004b	439277	3952397	863.1±1.1	2.22D	fractured and metasomatized tonalite
PVBR02-17	439247	3952273	838.9±1.5	2.22E	highly metasomatized tonalite mylonite
PVBR02-17B	439247	3952273	814.0±1.7	2.22F	highly metasomatized tonalite mylonite
H03PV007c	437946	3950330	828.7±1.2	2.22G	minor K-feldspar replacement of plagioclase in tonalite
PVBR02-31	439079	3951592	804.4±1.4	2.22H	highly metasomatized tonalite mylonite
RP-90A	438920	3952460	736.6±1.3	2.22I	highly metasomatized tonalite mylonite
PVSDC02-6B	437834	3946025	726.2±1.3	2.22J	K-feldspar replacement of plagioclase in amphibolite
PVBR02-7	439159	3952594	697.7±1.5	2.22K	coarse-grained metasomatic epidote and K-feldspar vein
PVHD02-1	437299	3949547	594.2±1.2	2.22L	highly metasomatized sheared tonalite
PV03-01	437946	3950330	404.9±0.5	2.22M	K-feldspar replacement of plagioclase in tonalite
H03PV007b	437946	3950330	369.4±0.8	2.22N	K-feldspar replacement of plagioclase in tonalite
H06-WB-01	437946	3950330	658.1±1.2	2.22O	K-feldspar replacement of plagioclase in tonalite
film[1] and patch[2] pethite K-feldspar (single-grain)					
PVBR02-28-07[1]	438694	3952002	968.1±1.2	2.23A	coarse-grained K-feldspar-muscovite pegmatite
PVBR02-28-05[1]	438694	3952002	951.22±0.93	2.23B	
PVBR02-28-15[2]	438694	3952002	802.59±0.57	2.23C	
PVBR02-28-13[2]	438694	3952002	759.51±0.69	2.23D	
PVBR06-20-22[1]	439600	3953100	1026.94±0.78	2.23E	coarse-grained microcline with K-feldspar veinlets
PVBR06-20-40[1]	439600	3953100	1063.72±0.72	2.23F	
PVBR06-20-33[1]	439600	3953100	1054.22±0.74	2.23G	
PVBR06-20-12[2]	439600	3953100	833.45±0.61	2.23H	
PVBR06-20-44[2]	439600	3953100	1109.38±0.76	2.23I	
PVBR04-2-03[2]	439277	3952250	597.9±1.1	2.23J	coarse-grained K-feldspar pegmatite
PVBR04-2-04[2]	439277	3952250	656.3±1.4	2.23K	
PVBR04-2-05[2]	439277	3952250	599.5±1.7	2.23L	
PVBR04-2-06[1]	439277	3952250	763.4±1.2	2.23M	
PVBR04-2-07[1]	439277	3952250	811.4±2.0	2.23N	
PVBR04-2-08[1]	439277	3952250	792.8±2.4	2.23O	

Notes: TGA = Total Gas Age; Fig. = corresponding figure number for age spectrum in Chapter 2; All errors reported at 1σ and do not include error in decay constants or fluence monitor age.

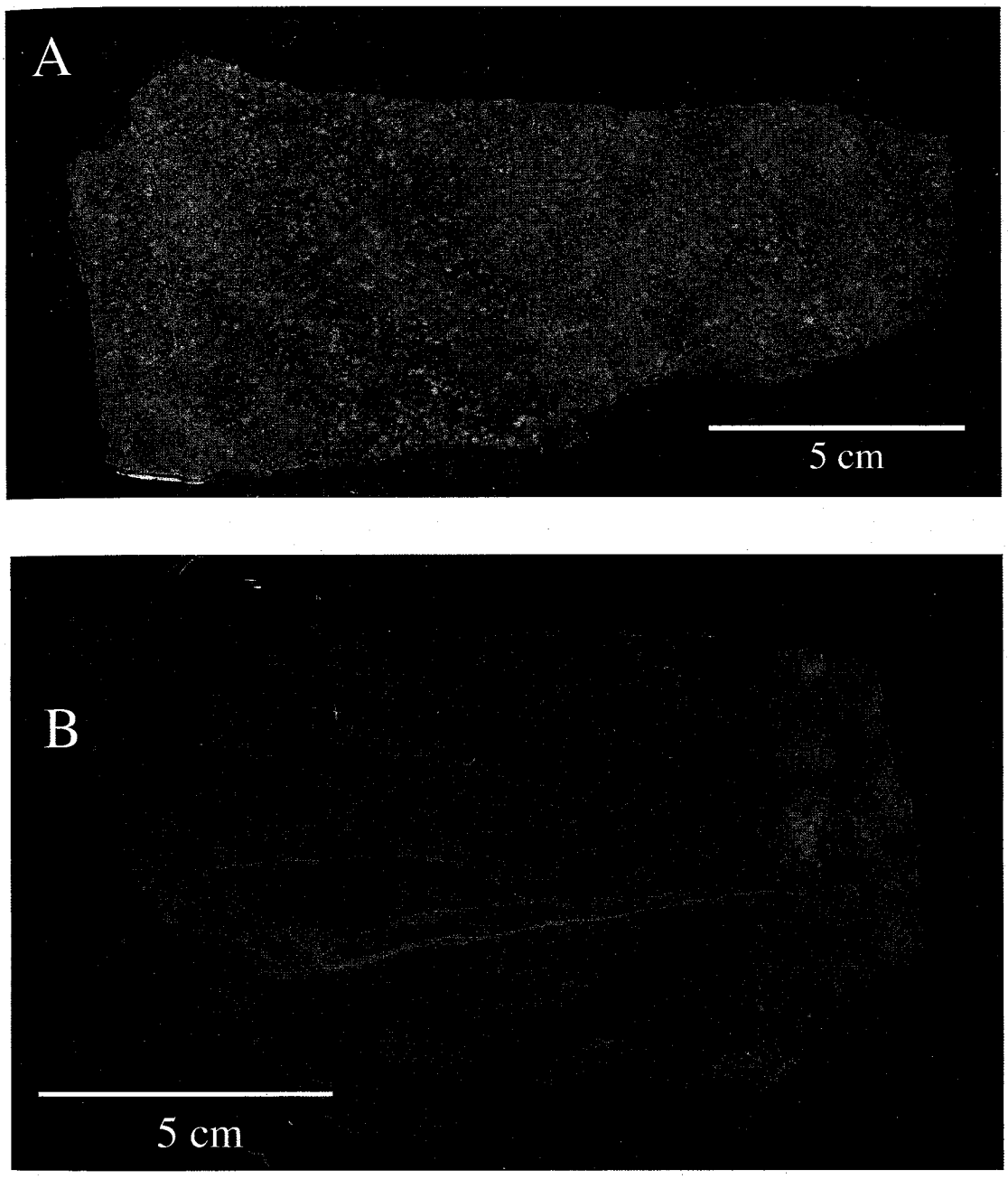

Figure 2.2: Scanned images of slabbed amphibolites with cross-cutting K-feldspar+epidote veins. A medium-grain plagioclase-amphibole segregation (A; PVSDC02-18) from a generally fine-grained amphibolite (B; PVSDC02-6B) shows multiple vein selvages of secondary K-feldspar around sub-parallel epidote veins. The fine-grained amphibolite (B) has a coarse plagioclase segregation on the right. Both the coarse plagioclase segregation and the finer-grainer amphibolite are cut by multiple epiodote veinlets. The plagioclase is replaced by secondary K-feldspar and hematite (red) in both the segregation and the matrix of the sample.

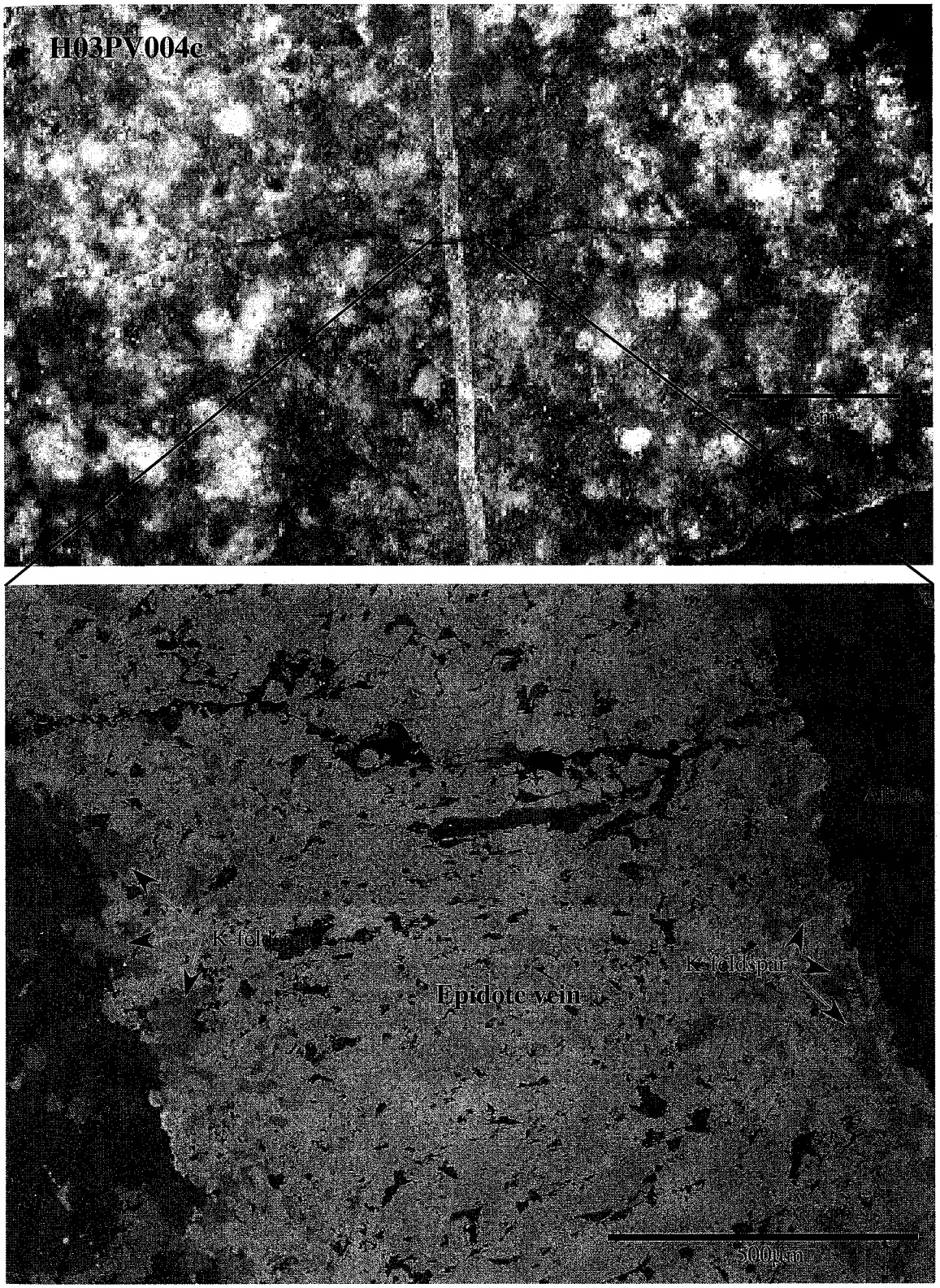

Figure 2.3: Scanned epidote vein cross-cutting the Pecos granodiorite (H03PV004c) and corresponding BSE image. The K-feldspar-hematite vein selvage is apparent in the hand sample, and in BSE the secondary K-feldspar is concentrated along, and incorporated into the epidote at the contact between the vein and, in this case, the albite host. Secondary feldspar occurs in a more disseminated style distal from the vein selvage.

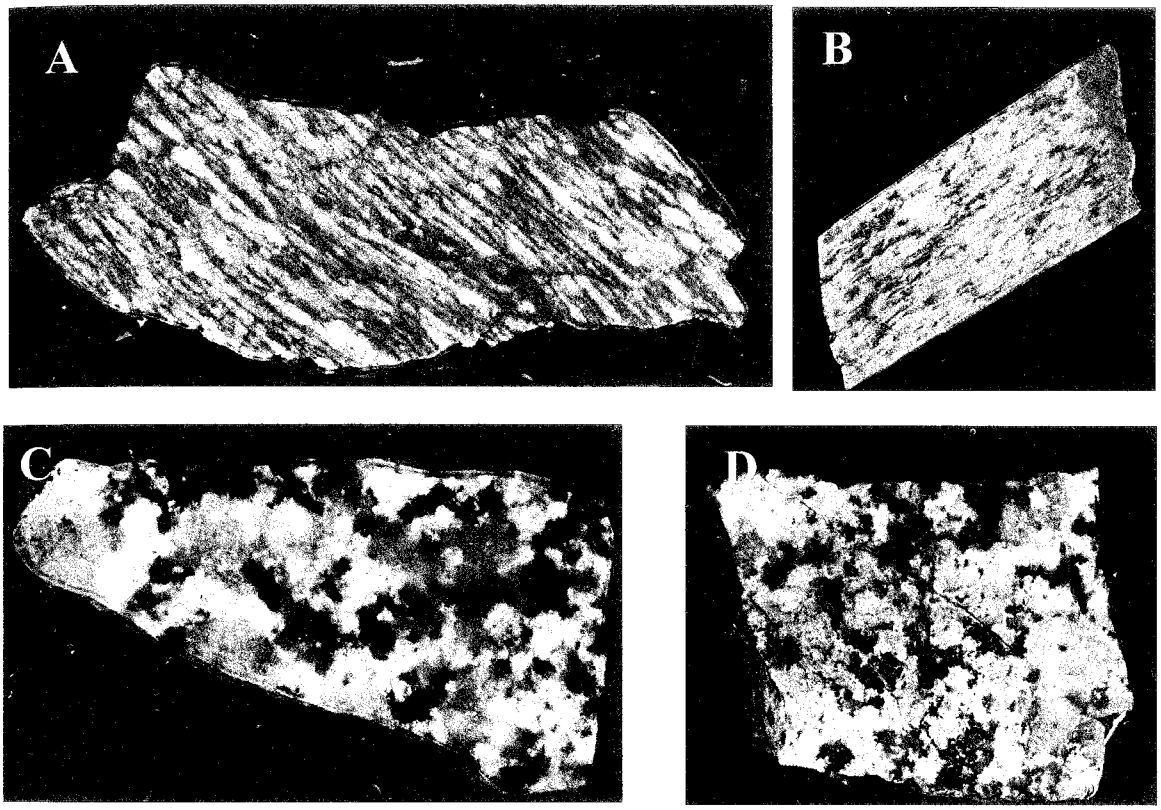

Figure 2.4: Scanned slabs of sheared granodiorite (A) and tonalite (C) and metasomatized counterparts (B,D). The overall pink coloration in altered samples is the result of secondary K-feldspar + hematite replacement of the primary mineralogy. Biotite is chloritized and granular epidote is visible in upper right part of image B. The largest sample (A) measures 14 cm long; all samples shown at same scale.

stereonet plot in Figure 2.5, and although the data are variable, several trends emerge. These include a set of north-north-west striking metasomatized fractures/veins with a near-vertical east to west dip, a north-west vertical set, a west-north-west set variably dipping to the east, and a final north-east striking set with a moderate east dip. These data are presented along with average measurements (n=unknown) for joint set trends recognized by Miller et al. (1963) in the southern portion of the Precambrian exposure of the Sangre de Cristo range. There is remarkable overlap between the Miller et al. (1963) regional trends and three trends recognized in the metasomatized fractures near Tres Lagunas (Figure 2.5) with the exception of a west-north-west, variably east dipping fracture set not mentioned by Miller et al. (1963).

Within the same Tres Lagunas area the intensity of metasomatic replacement, in terms of abundant secondary K-feldspar, epidote, and chloritization of primary biotite, increases with proximity to brecciated zones. Melis (2001) first recognized these breccias and proposed a syntectonic link between the brittle deformation and metasomatic fluid infiltration. Subsequent fieldwork has identified several sub-parallel north-north-east trending zones of brecciated basement rock with significant metasomatic overprinting (Figure 2.6; Figure 2.1). Breccias in sheared granodiorite display clast rotation and are cohesive presumably due to silica (±K-feldspar) cementation.

Tonalite at the Windy Bridge road-cut (Figure 2.1) hosts five styles of primary and secondary K-feldspar occurrences (Figure 2.7). There is a ~10 cm wide medium-grained, pink K-feldspar-quartz vein cutting the tonalite (H03PV007e; Figure 2.7a), as well as a thicker (30 cm), coarse-grained albite-microcline-biotite pegmatitic vein (H03PV007d; Figure 2.7b). A 2 mm red K-feldspar veinlet (H06-WB-01) also cuts the

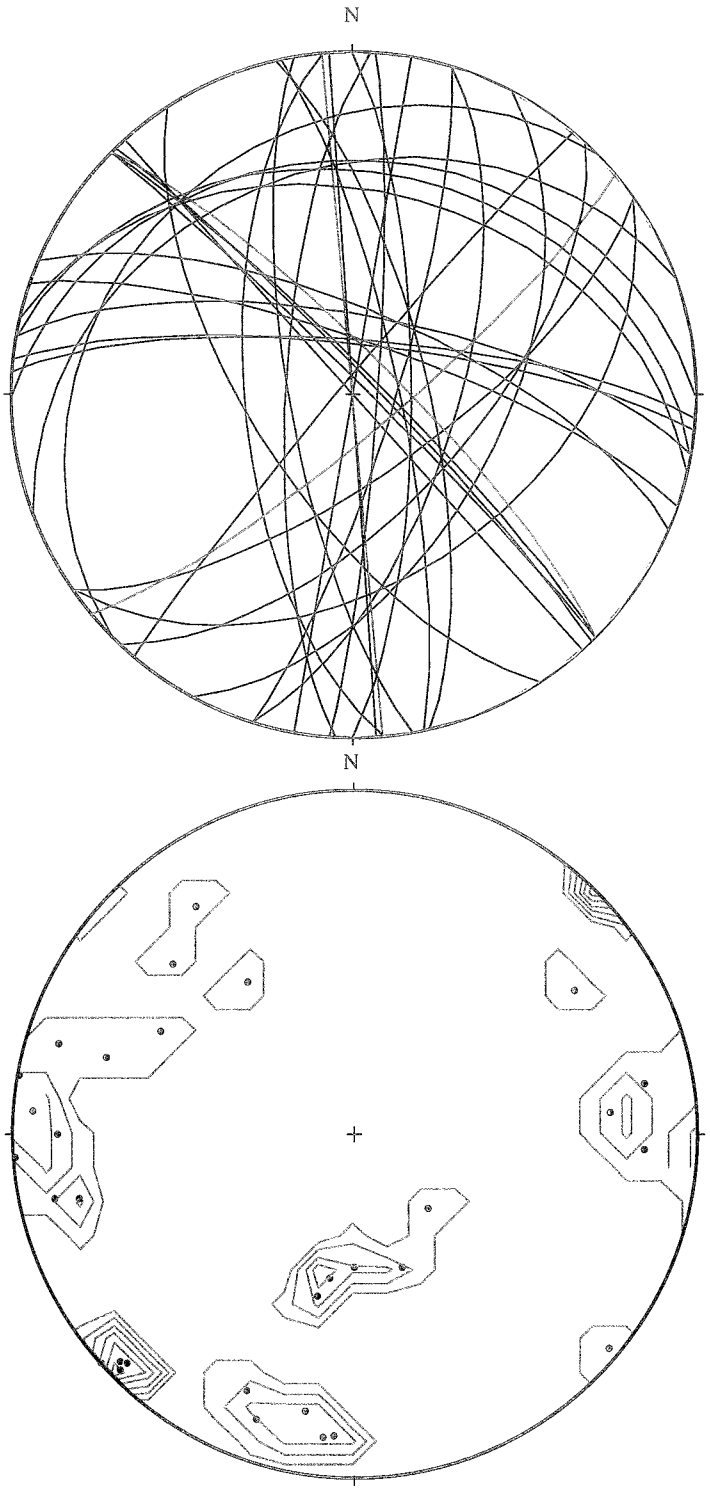

Figure 2.5: Equal area stereonet plots of metasomatized fracture surfaces in granodiorite in the Tres Lagunas area showing great circles (top) and contoured poles to planes (bottom). Great circles (black) are shown relative to measurements for the average joint orientations in the southern portion of the Sangre de Cristo range (red) as measured by Miller et al. (1963). Overall, there is good correlation between the Miller et al. (1963) data and the limited measurements from metasomatized fractures/joints that reveal approximately N-S, NW-SE, and NE-SW fracture trends. A set of ~E-W striking variably north dipping fractures is potentially unique to the Tres Lagunas area.

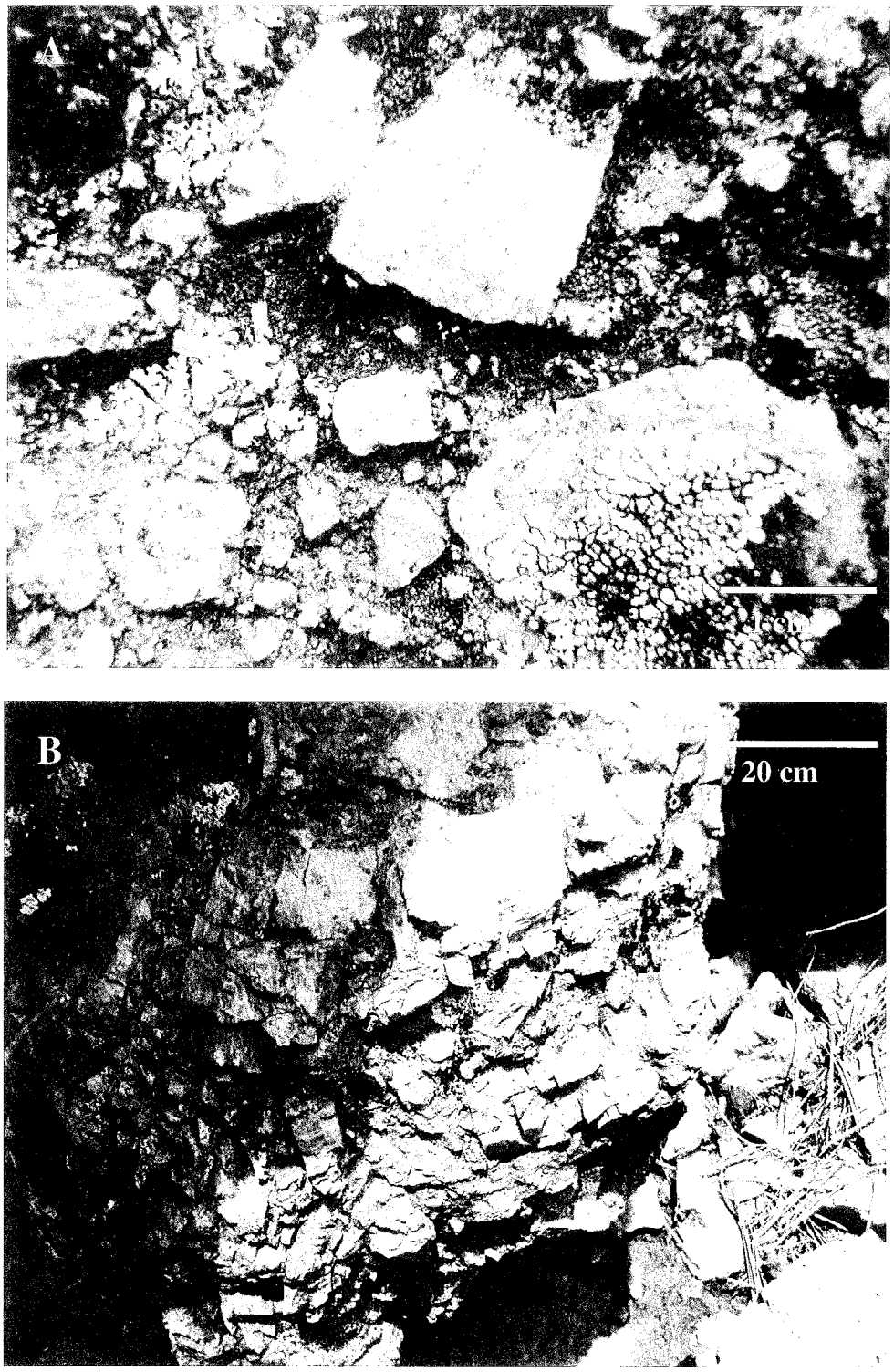

Figure 2.6: Photographs of two breccia occurrences in the Tres Lagunas area show rotated clasts in a finer-grained matrix. The degree of metasomatism is greater in the top example, and more subtle in the bottom breccia.

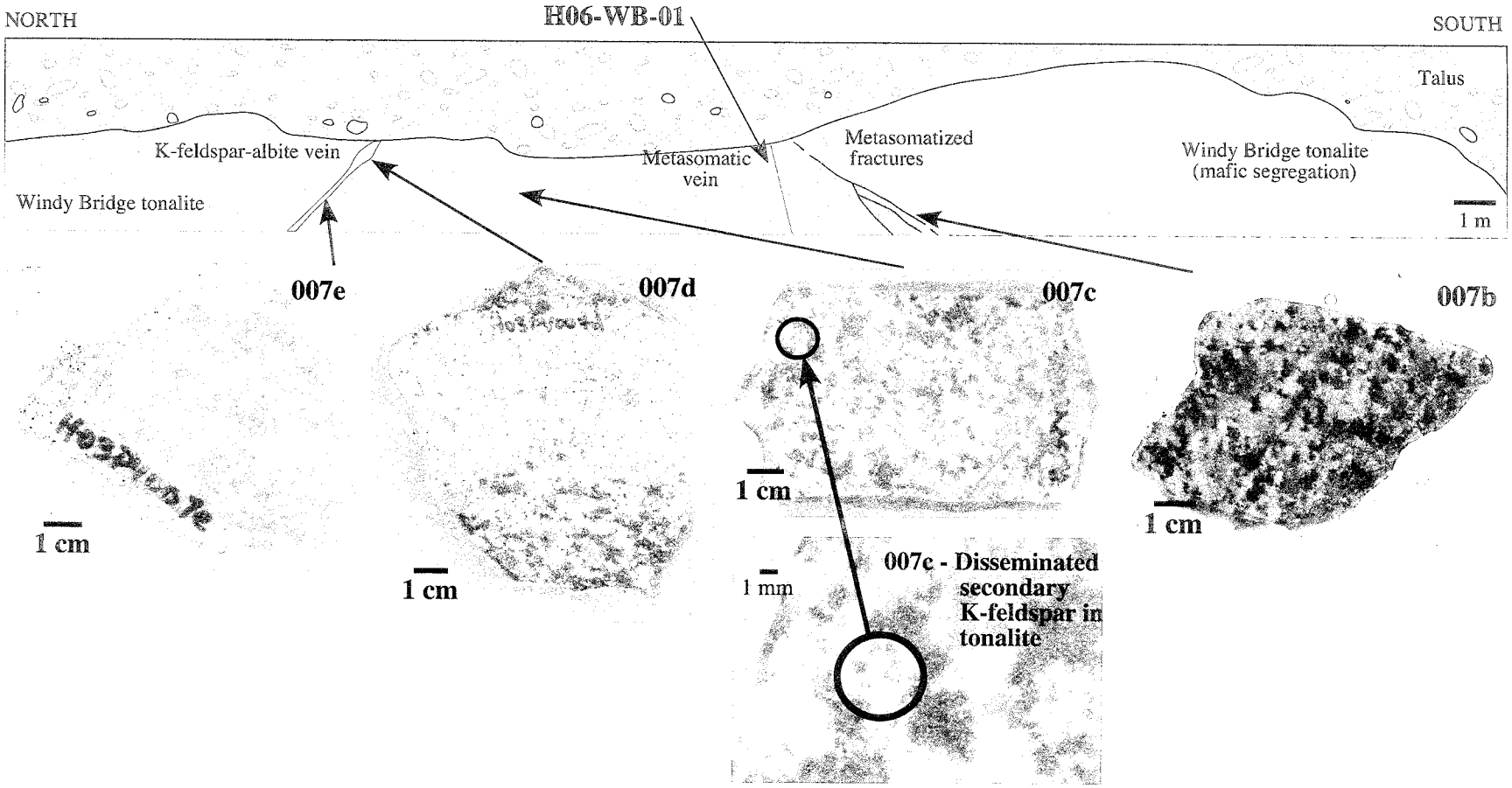

Figure 2.7: Cross-section of the east-side of the road-cut just north of the Windy Bridge picnic area. There are five different occurrences of K-feldspar within the host tonalite including coarse- and medium-grained K-feldspar±plagioclase segregations (007d, 007e), disseminated replacement of plagioclase (007c), preferential replacement of plagioclase along fractures (007b), and secondary K-feldspar veins (H06-WB-01; not shown).

same outcrop, and occasionally disseminated replacement of turbid plagioclase grains is observed (H03PV007c; Figure 2.7c). Samples PV03-1 and H03PV007b are a deep red K-feldspar replacement of plagioclase grains localized along fractures in the tonalite although no prominent vein is observed (Figure 2.7d; Figure 2.8). Metasomatism does not appear to be spatially associated with the Precambrian-Paleozoic unconformity in the Pecos area as there is no relationship between degree of alteration and proximity to the paleosurface. Metasomatized basement rocks at Windy Bridge, for example, are ~300 meters below the unconformity.

2.5.2 Replacement textures and mineral geochemistry

2.5.2.1 K-feldspar

Salmon-pink colored K-feldspar is observed replacing white, turbid primary plagioclase in amphibolite, tonalite, and granodiorite. In particular, the cores of plagioclase grains are preferentially replaced by K-feldspar-epidote-sericite (Figure 2.9). Scanning electron microscopy (SEM) images of altered plagioclase show that intragranular replacement by K-feldspar is patchy (Figure 2.10a) but shows an overall linearity and geometry within most grains suggestive of an internal crystallographic control on the distribution of replacement K-feldspar (Figures 2.10b). Figure 2.10c shows a backscatter electron (BSE) image of nearly complete replacement of plagioclase by K-feldspar and sericite. Samples PV03-01 and H03PV007b were collected from a fracture set and have a replacement adularia texture not seen in other samples (Figure 2.10d). The adularia habit is revealed by hydrofluoric acid vapor-etching of grain fragments (cf. Waldron et al., 1994), and in map (001) view appears as a mosaic of

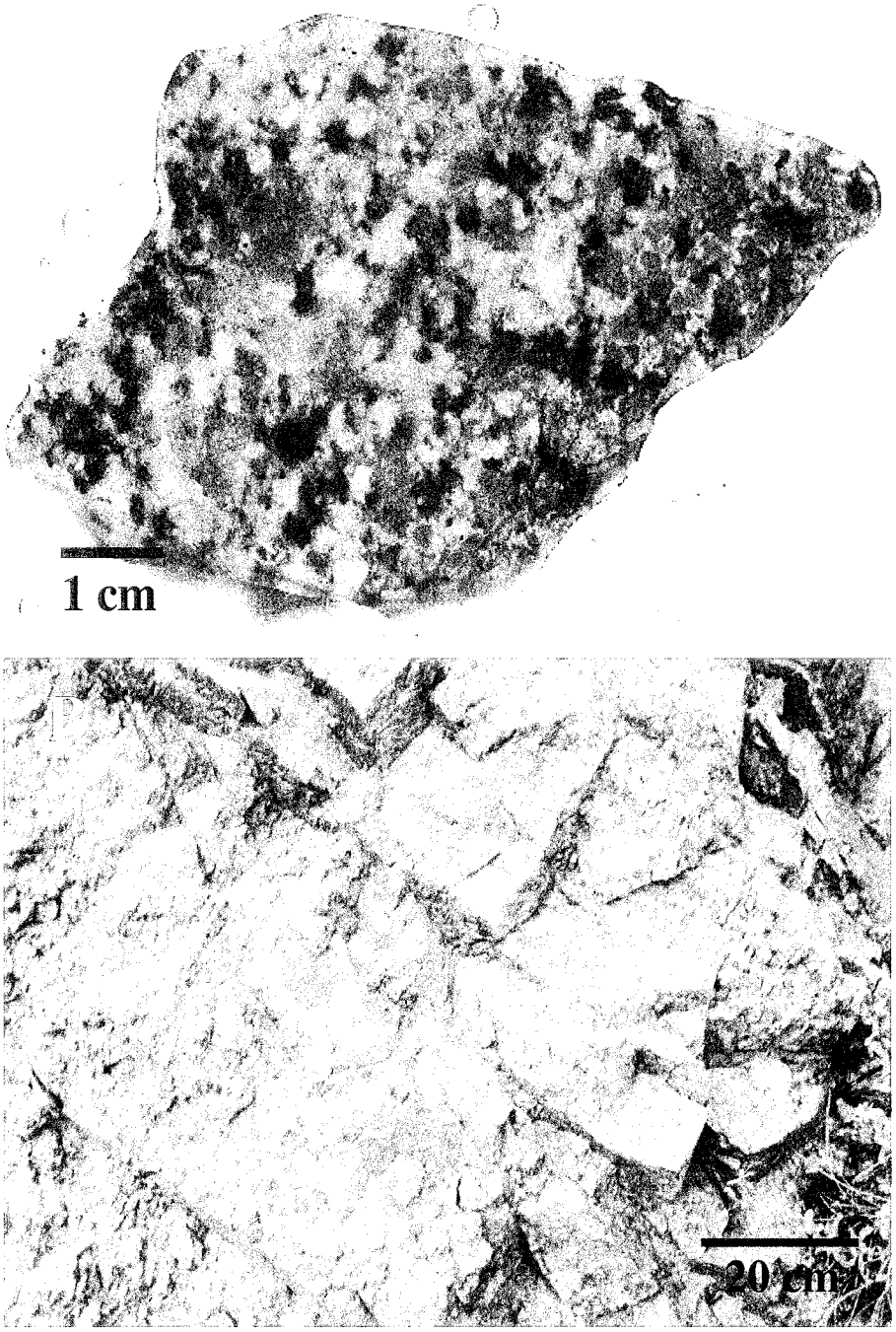

Figure 2.8: Images of a scanned metasomatized tonalite slab (A) and the outcrop it was sampled from at the Windy Bridge road-cut (B). Scanned slab (A) of tonalite sample H03PV007b shows secondary K-feldspar replacement of the cores of primary plagioclase grains. The degree of replacement decreases away from the right edge of the sample where the original fracture was (B). Unlike other secondary K-feldspar veins from Tres Lagunas, for example, this particular occurrence is not associated with an actual vein, but appears rather to have resulted from fluid infiltration along fractures in the tonalite (B).

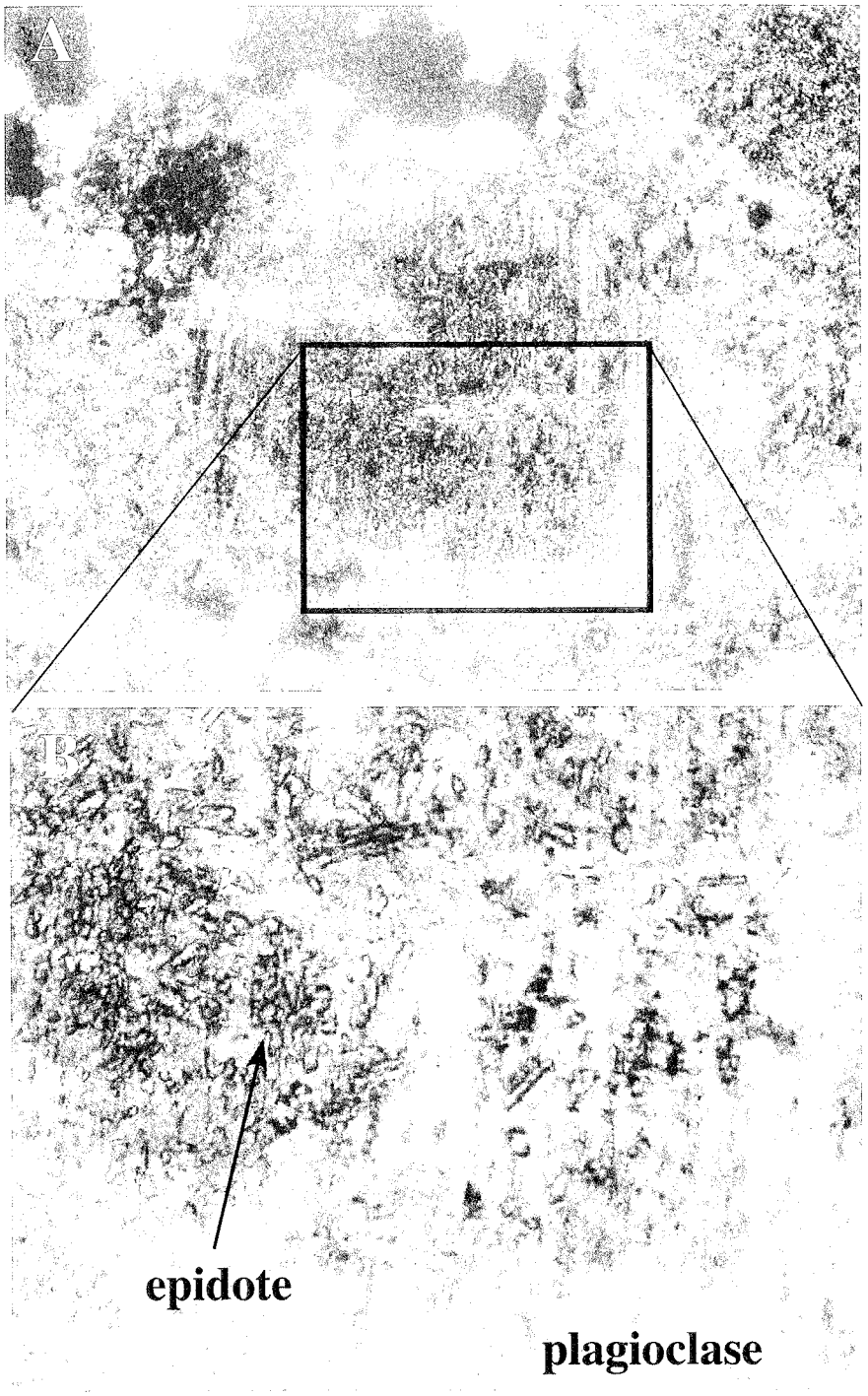

Figure 2.9: Photomicrograph of altered plagioclase in sample PV03-1. Crossed-nichols (A; 4x mag.) show remnant albite twinning at the grain margins of plagioclase with grain interior altered to secondary K-feldspar, epidote, and sericite. Abundant epidote grains are visible in uncrossed-nichols (B; 10x mag.)

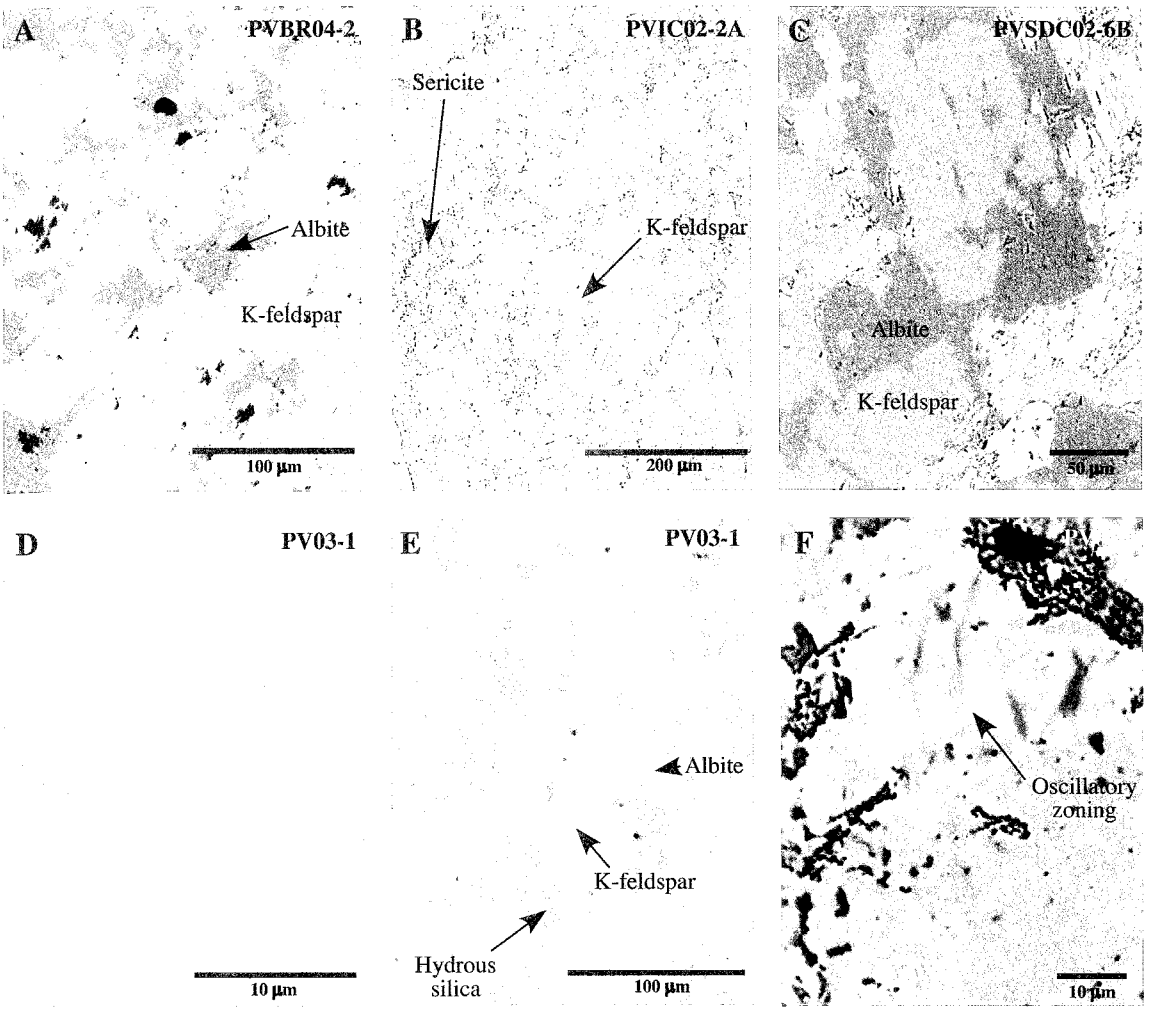

Figure 2.10: Scanning (SEM) and backscattered (BSE) electron microprobe images of secondary K-feldspar microtextures showing replacement of primary microcline and plagioclase grains. Figure A is a polished section (PVBR04-2) and shows albite (dark gray) and K-feldspar (light gray) patch perthite in place of former pegmatitic K-feldspar film perthite. Figure B is a relict plagioclase grain in the Windy Bridge tonalite (PVIC02-2A) now completely replaced by metasomatic K-feldspar (light gray) and sericite (pitted areas). Figure C is also a nearly complete replacement of a sodic plagioclase grain (dark gray; PVSDC02-6B) in an amphibolite by K-feldspar (light gray). Figures D, E, and F are images of the same sample from a metasomatized fracture in the Windy Bridge tonalite (PV03-1; H03PV007b). Figure D is a SEM image of a grain mount etched in hydrofluoric vapor that shows a mosaic of diamond-shaped adularia habit K-feldspar. This replacement occurs as layers within the host plagioclase and is a map view perspective (010) of the K-feldspar stringers seen in cross-section in Figure E. Figure E is a polished thin section that shows a plagioclase grain partially replaced by secondary K-feldspar (light gray) and hydrous silica (dark gray). Note the linearity of secondary K-feldspar suggestive of a crystallographic control by the host mineral on the propagation of replacement into the grain interior. Figure F is a higher magnification image that shows oscillatory zonation within secondary K-feldspar indicative of aqueous dissolution and reprecipitation. Zoning could be associated with incorporation of low temperature trace or rare earth elements during replacement.

diamond shaped subgrains ranging from ~30 by 20 μm to less than 3 by 2 μm (Figure 2.10d). Adularia replacement occurs along planes inter-layered with remnant primary plagioclase and the long axes of the adularia grains alternate orthogonally to each other between different layers. In cross-sectional view (010) of the replacement adularia planes in polished thin section, the planes appears as linear, parallel K-feldspar stringers a few microns thick (Figure 2.10e). At higher resolution, replacement K-feldspar shows μm-scale oscillatory chemical zonation (Figure 2.10f). Metasomatic subgrains are the product of aqueous dissolution and reprecipitation reactions at relatively low temperatures (0 to 300°C; Kastner and Siever, 1979; I. Parsons, pers. comm.). One SEM image of the adularia habit shows prismatic, euhedral epidote prism emerging from the altered plagioclase matrix (Figure 2.11), but it is unclear if the epidote formed much earlier in the geologic history of the plagioclase or is cogenetic with the adularia precipitation.

Primary microcline in the Pecos area appears unaffected by metasomatic fluids despite near complete alteration of coexisting plagioclase (Figure 2.12). Some pegmatitic microclines, however, have also undergone partial replacement by metasomatic K-feldspar and albite that have formed areas of opaque, pink patch perthite within the original clear film perthite grains (Figure 2.13). Areas of less replacement appear to have a framework of pink tubes as well as microfractures within the clear film perthite (Figure 2.13). SEM and cathodoluminescence SEM (CL-SEM) images show the boundary between phases is optically distinct and replacement patch perthite has no luminescence in contrast to primary microcline which has a characteristic blue wavelength luminescence (Mariano, 1988; Figures 2.13a). These zones of secondary K-feldspar are

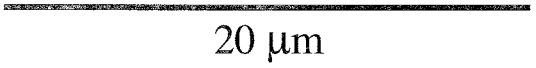

Figure 2.11: SEM image of a HF etched grain fragment from an altered plagioclase core in tonalite sample PV03-1. Euhedral epidote prisms emerge from the mosaic of diamond-shaped adularia habit replacement K-feldspar.

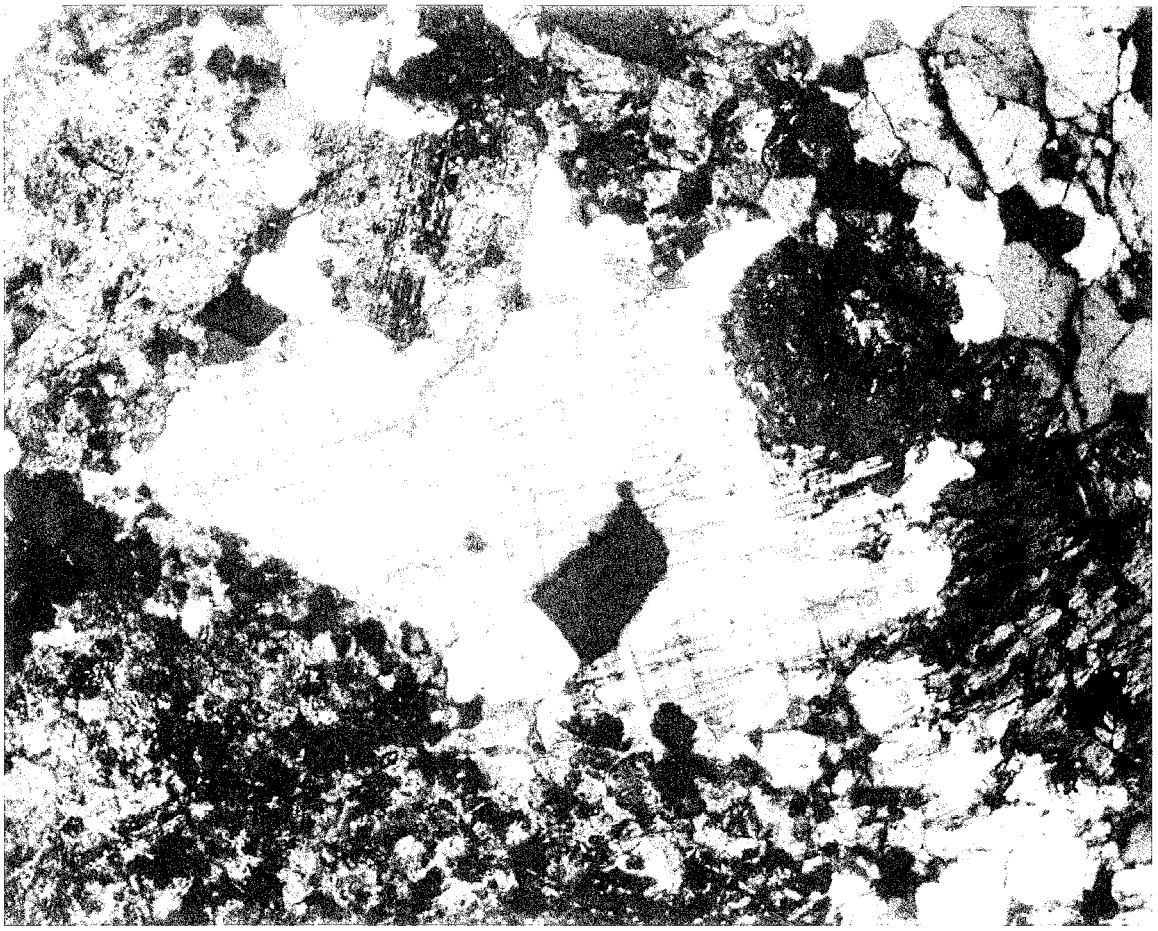

Figure 2.12: Photomicrograph (4x magnification) of microcline in granodiorite sample H03PV004c. Microcline appears relatively unaffected by alteration and tartan twinning is preserved despite near complete replacement of surrounding plagioclase by secondary K-feldspar, sericite, and epidote.

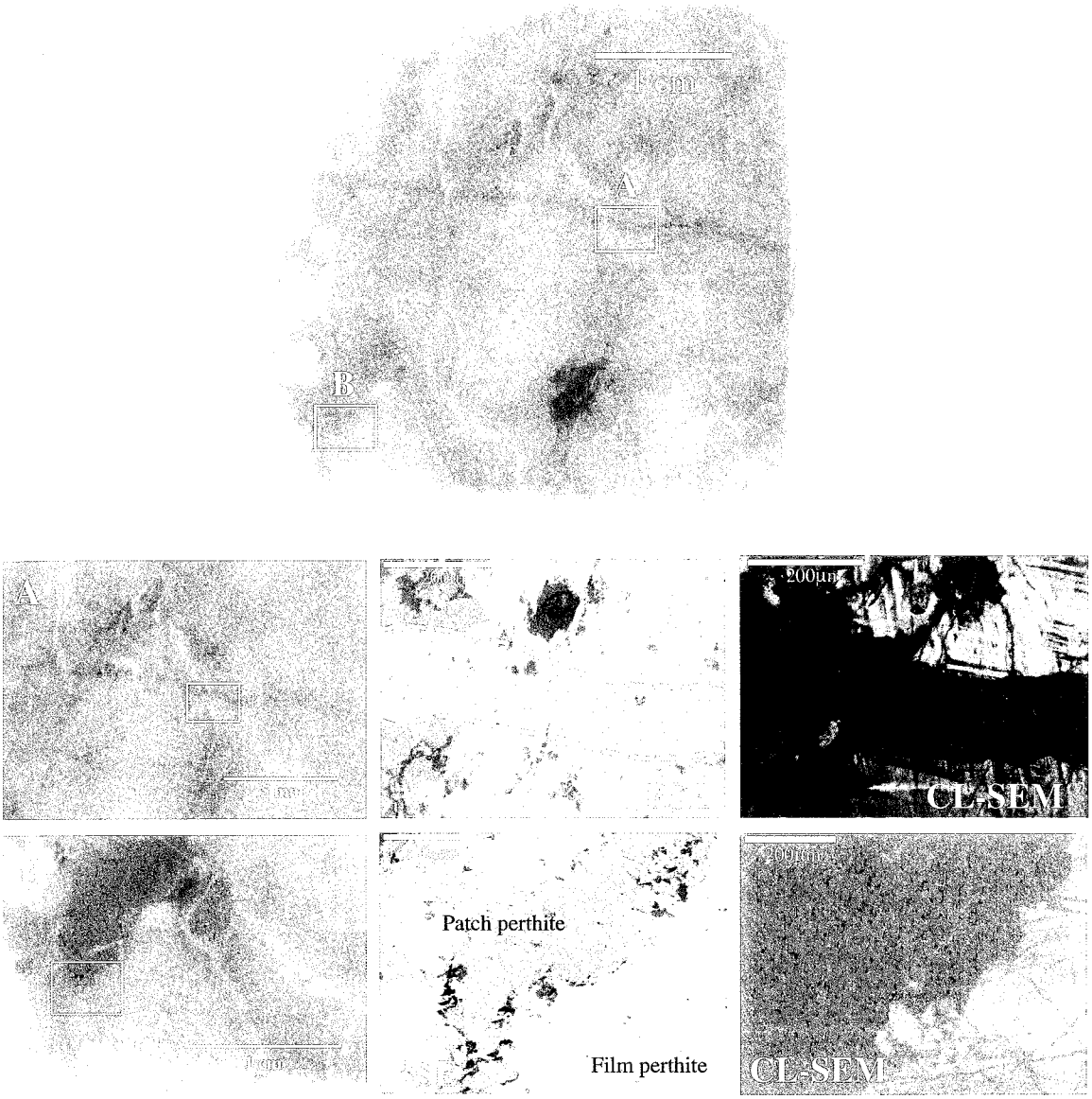

Figure 2.13: Scanned thick section of a microtexturally complex pegmatitic microcline from sample PVBR04-2B with BSE and CL-SEM images of the same areas of pink patch perthite seen optically. Figure A is a cross-cutting secondary K-feldspar veinlet that cuts both the film and patch perthite sub-grains indicating it formed later than the patch perthite. In BSE, the similar chemistry of the film perthite and the veinlet render the cross-cutting relationship essentially invisible. The veinlet stands out dramatically in CL-SEM, however, due to its non-luminescent nature. The patch perthite areas in this image are also non-luminescent. It is even apparent in the luminescent areas of the film perthite that partial replacement along microfractures and crystallographic features has occurred. Figure B shows a boundary between a primary, clear film perthite and secondary K-feldspar-albite patch perthite. Even the film perthite is cross-cut by a network of pink K-feldspar stringers that appear to mimic the cleavage habit of the microcline. The BSE image shows a scalloped, yet well-defined boundary between the patch and film perthite. In CL-SEM, patch perthite is non-luminescent as is the secondary K-feldspar in the microfractures in film perthite.

interpreted not to luminesce because metasomatic or authigenic K-feldspar is generally pure with respect to activator elements (Kastner and Siever, 1979). Alternatively, reprecipitated K-feldspars have a high degree of ordering and do not develop electron vacancies that cause cathodoluminescence in magmatic K-feldspar (Finch and Klein, 1999). Stringers of secondary K-feldspar a few microns in width are visible with CL-SEM and cut the film perthite indicating that in some instances even 'pristine' film perthite that preserves the primary igneous texture has been variably affected by metasomatic fluids (Figure 2.13b). CL-SEM images of a less-altered film perthite areas show what appears to be tartan twinning (Figures 2.14), however, because twinning is an optical property observed through polarized light, it does not explain the chemical effect as shown by the CL. The apparent twinning texture is an image of partial replacement of microcline (white) by secondary K-feldspar (black) possibly along the pericline and albite twinning planes or dissolution networks facilitated by exsolution dislocations and enhanced microporosity (cf. Waldron et al., 1994; Fitz Gerald et al., 2006). Microfractures containing metasomatic K-feldspar are visible in these areas indicating fluids infiltrated along cracks as well as exploited crystallographic features (Figure 2.13).

2.5.2.2 Epidote

Epidote is common throughout the Pecos River valley and was initially investigated in this study for its use as a U-Pb geochronometer independent of the $^{40}Ar/^{39}Ar$ method because of its apparent paragenetic association with metasomatic K-feldspar. When preliminary U-Pb data suggested that distinct textural types of epidote record discrete periods of epidote growth, effort was made to attempt to petrographically

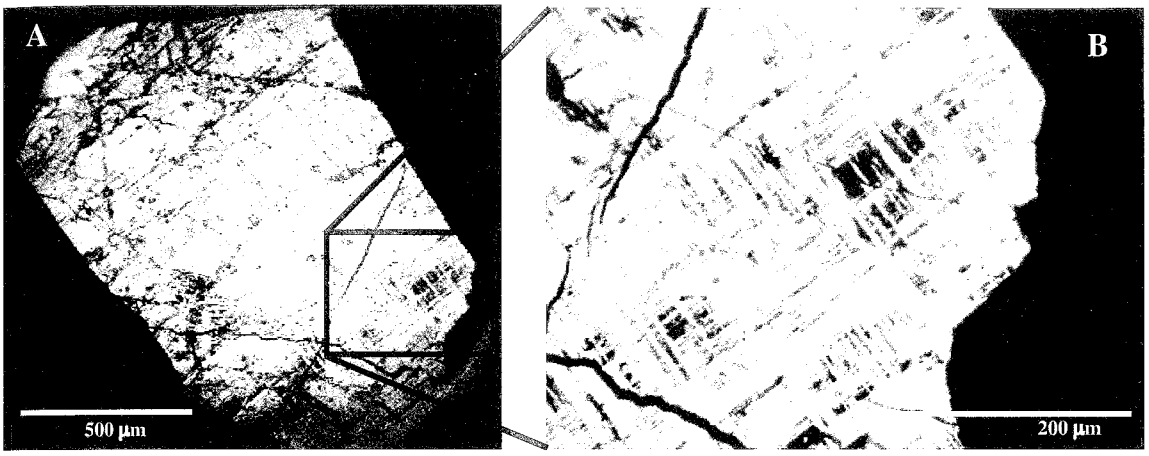

Figure 2.14: CL-SEM image of a polished grain mount of sample PVBR06-20. This grain is separated from the patch perthite region of metasomatized pegmatitic microcline. CL-SEM imaging reveals a lattice-work of luminescent and non-luminescent areas reminiscent of tartan twinning in microcline. Black areas are non-luminescent secondary K-feldspar. Fluids infiltrated along crystallographic features resulting in the partial replacement of the grain interior that mimics the twinning habit of the K-feldspar.

identify and chemically 'fingerprint' epidotes of differing ages. A useful overview of epidote chemical and structural information, phase stability, formation temperatures, and selected occurrences is compiled in Liebscher and Franz (2004), and in particular, in sections by Bird and Spieler (2004) and Grapes and Hoskin (2004).

In the Pecos River valley, epidote is associated with pink-red secondary K-feldspar veins, fills small vugs and fractures, and occurs as a replacement mineral in primary plagioclase cores (Figures 2.2b, 2.9). In many cases epidote appears paragenetically associated, if not cogenetic with metasomatic K-feldspar precipitation. For example, Figure 2.3 is a BSE image of an epidote vein cutting the Pecos granodiorite with fine-grained secondary K-feldspar along the vein periphery. In some highly metasomatized pegmatitic segregations (PVBR04-2) euhedral epidote grains up to 0.5 mm are randomly disseminated throughout the opaque, turbid patch perthite areas.

Individual grains that fill open spaces in fractures or vugs are typically prismatic and do not exceed several millimeters in diameter or length. Grains vary in color and clarity including opaque dark green, transparent apple green, and transparent olive green. A sheared, metasomatized granodiorite sample (PVBR02-17) contains veins with both crystalline epidote as well as a texturally distinct polycrystalline/granular epidote (Figure 2.15). Some euhedral crystalline epidote grains are overgrown by the granular epidote. This sample and these particular textures are discussed further in the following U-Pb epidote geochronology section. Unfortunately, the two phases were not distinct in thin section with BSE, but polished grain mount SEM quantitative data of the individual phases are discussed below. In a nearby sample (~250 m) of undeformed, metasomatized granodiorite, two generations of epidote are also observed (Figure 2.16). In this sample,

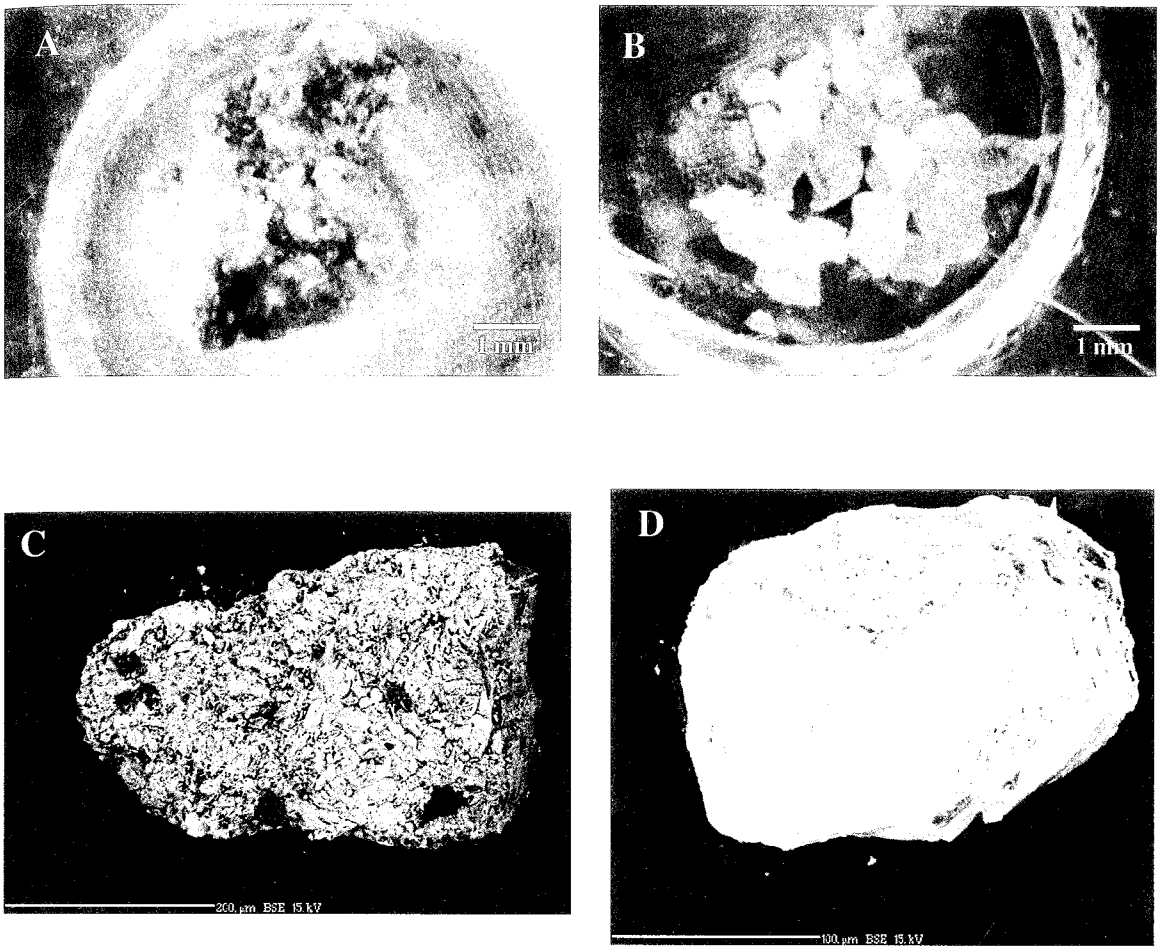

Figure 2.15: Photographs (A,B) and BSE images (C,D) of granular and crystalline varieties of epidote from sheared granodiorite sample PVBR02-17. Crystalline epidote (B) is translucent apple green with broad crystal faces in contrast to the opaque dark green composite nature of the granular epidote (A).

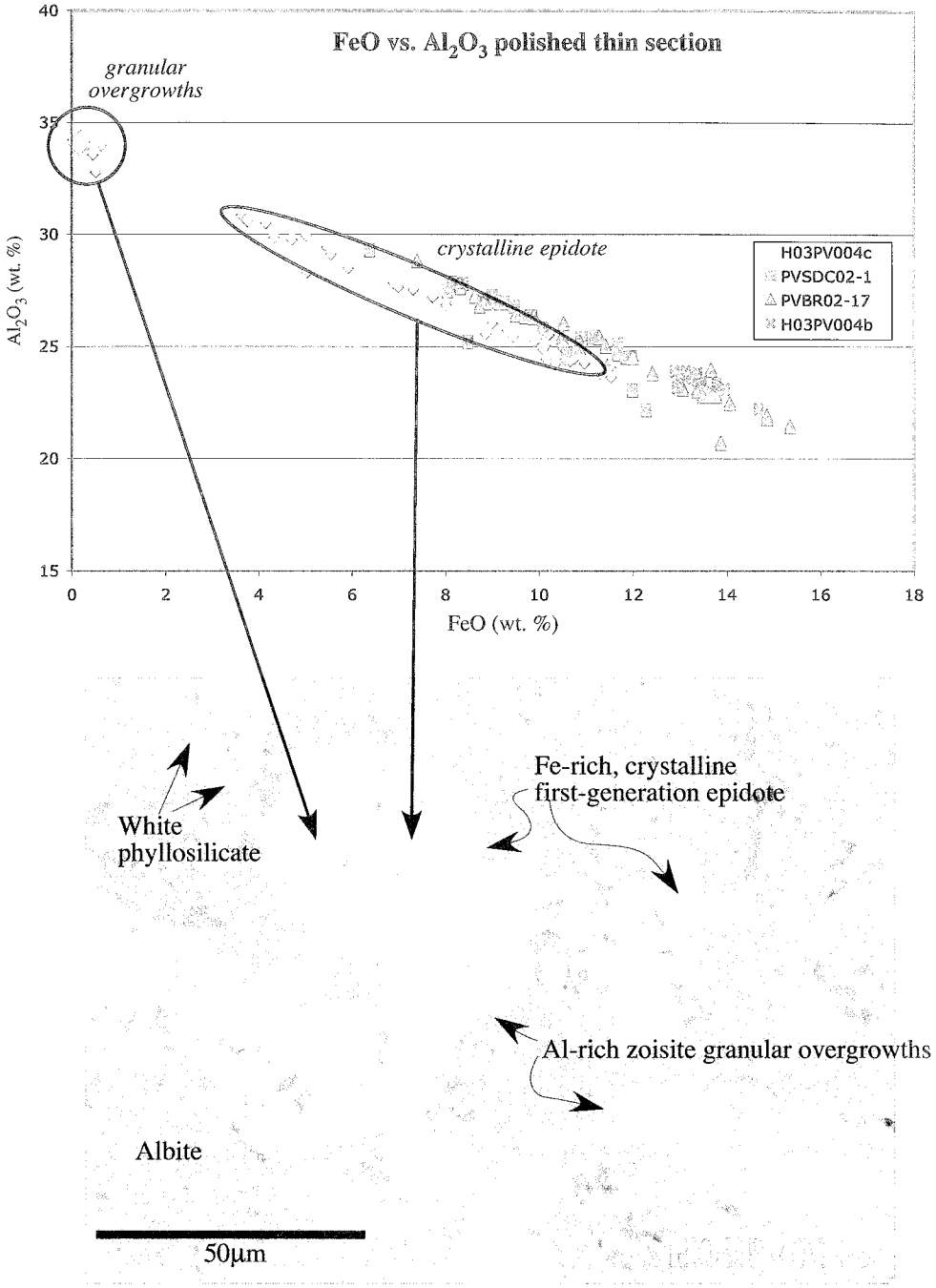

Figure 2.16: FeO vs. Al_2O_3 plot of epidote compositions for four samples from the Pecos river valley. BSE image shows crystalline, euhedral epidote cores overgrown by granular, cryptocrystalline rims in sample H03PV004c. In general, Fe-Al compositions plot along a mixing line that reflects either the solid solution of these chemical species or a progressive change in fluid composition with time. The granular overgrowths in H03PV004c are a zoisite composition suggesting that late-stage fluids were iron-poor or epidote grew during a later event from iron-poor fluids.

euhedral crystalline epidote cores are overgrown by chemically distinct (see below) anhedral rims.

Quantitative SEM data for weight percent FeO and Al_2O_3 of epidote grains in thin section and grain mount for four samples in the Pecos area are plotted in Figure 2.16 and complete data are given in Table 2.2. In general, samples overlap compositionally and plot along a solid solution mixing line for Al and Fe in the epidote structure $Ca_2Al_2FeSi_3O_{12}(OH)$. PVBR02-17 has a compositional range between 7.4 and 15.4 wt% FeO. PVSDC02-1 epidotes vary between 6.4 and 12.3 wt% FeO, and H03PV004b has a tighter range of 12.9 to 14.7 wt% FeO. H03PV004c has a bimodal compositional distribution that reflects the chemical difference between the euhedral cores and anhedral overgrowth rims seen in Figure 2.16. Crystalline cores have a compositional range between 3.6 and 11.5 wt% FeO whereas overgrowths are of a zoisite end-member composition with 0 to 0.6 wt% FeO and up to 34.8 wt% Al_2O_3. Interestingly, both H03PV004b and H03PV004c are Pecos granodiorite within ~250 m of each other, however there is no compositional overlap in epidote FeO content and no zoisite overgrowths are observed in H03PV004b. Overall, epidotes from the Pecos River valley, excluding zoisite overgrowths, differ in FeO content by as much as ~12 wt% and up to 8 wt% within single samples. Multiple quantitative analyses on single epidote grains indicate there is a range of up to 3.8 wt% FeO in some grains whereas others appear chemically homogenous (H03PV004b).

Quantitative data for the granular and crystalline textural types of epidote separated from sample PVBR02-17 (Figure 2.15) are presented in Figure 2.17, but show no difference in X_{Fe} between textural types as seen in H03PV004c. Epidote

TABLE 2.2: SCANNING ELECTRON MICROPROBE QUANTATATIVE DATA FOR PECOS EPIDOTE. WEIGHT PERCENT CALCULATED RELATIVE TO 8 OXYGENS.
X_{Fe}=Fe(mol)/(Fe(mol)+Al(mol))

H03PV004c Epidote

FeO (wt%)	FeO(mol)/100g ep	Al_2O_3 (wt%)	Al_2O_3(mol)/100g ep	Al(mol)/100g ep	$100*X^{Fe}$
0.02	0.0003	34.34	0.3368	0.6736	0.0413
0.04	0.0006	34.29	0.3363	0.6726	0.0827
0.05	0.0007	34.15	0.3349	0.6699	0.1038
0.07	0.0010	34.28	0.3362	0.6724	0.1447
0.08	0.0011	34.75	0.3408	0.6816	0.1631
0.14	0.0019	34.28	0.3362	0.6724	0.2889
0.15	0.0021	33.91	0.3326	0.6652	0.3129
0.18	0.0025	34.31	0.3365	0.6730	0.3709
0.21	0.0029	34.40	0.3374	0.6748	0.4313
0.22	0.0031	34.03	0.3338	0.6675	0.4566
0.28	0.0039	34.23	0.3357	0.6714	0.5770
0.45	0.0063	33.93	0.3328	0.6656	0.9323
0.45	0.0063	33.68	0.3303	0.6607	0.9391
0.49	0.0068	34.06	0.3341	0.6681	1.0104
0.51	0.0071	32.90	0.3227	0.6454	1.0879
0.63	0.0088	34.09	0.3343	0.6687	1.2943
3.63	0.0505	30.99	0.3039	0.6079	7.6734
3.76	0.0523	30.70	0.3011	0.6022	7.9953
4.15	0.0578	30.62	0.3003	0.6006	8.7728
4.33	0.0603	29.98	0.2940	0.5881	9.2952
4.71	0.0656	29.88	0.2931	0.5861	10.0593
5.02	0.0699	30.05	0.2947	0.5894	10.5970
5.03	0.0700	28.41	0.2786	0.5573	11.1603
5.46	0.0760	29.54	0.2897	0.5794	11.5941
5.55	0.0772	29.23	0.2867	0.5734	11.8727
5.92	0.0824	28.62	0.2807	0.5614	12.7982
6.89	0.0959	27.94	0.2740	0.5481	14.8915
6.99	0.0973	27.78	0.2725	0.5449	15.1487
7.31	0.1017	27.65	0.2712	0.5424	15.7954
7.73	0.1076	27.32	0.2679	0.5359	16.7192
8.01	0.1115	26.97	0.2645	0.5290	17.4051
9.00	0.1253	26.16	0.2566	0.5131	19.6210
8.86	0.1233	25.68	0.2519	0.5037	19.6658
9.32	0.1297	25.83	0.2533	0.5067	20.3831
9.45	0.1315	25.56	0.2507	0.5014	20.7813
9.94	0.1383	25.46	0.2497	0.4994	21.6923
9.91	0.1379	25.35	0.2486	0.4973	21.7145
10.21	0.1421	25.64	0.2515	0.5029	22.0298
10.13	0.1410	25.16	0.2468	0.4935	22.2198
10.09	0.1404	24.99	0.2451	0.4902	22.2687
10.15	0.1413	24.56	0.2409	0.4818	22.6743
10.51	0.1463	25.03	0.2455	0.4910	22.9543
10.34	0.1439	24.33	0.2386	0.4772	23.1682
10.59	0.1474	24.81	0.2433	0.4867	23.2458
10.55	0.1468	24.54	0.2407	0.4814	23.3738
10.72	0.1492	24.76	0.2428	0.4857	23.5004
10.83	0.1507	24.94	0.2446	0.4892	23.5538
10.66	0.1484	24.46	0.2399	0.4798	23.6189
10.76	0.1498	24.61	0.2414	0.4827	23.6771
10.96	0.1525	24.37	0.2390	0.4780	24.1908
11.3	0.1573	23.96	0.2350	0.4700	25.0729
11.3	0.1573	23.91	0.2345	0.4690	25.1121
11.51	0.1602	24.18	0.2372	0.4743	25.2475
11.53	0.1605	23.75	0.2329	0.4659	25.6207

PVBR02-17 Epidote

FeO (wt%)	FeO(mol)/100g ep	Al_2O_3 (wt%)	Al_2O_3(mol)/100g ep	Al(mol)/100g ep	$X^{Fe}*100$
8.63	0.1201	27.28	0.2676	0.5351	18.3314
9.71	0.1351	26.36	0.2585	0.5171	20.7208
9.89	0.1376	26.34	0.2583	0.5167	21.0367
10.52	0.1464	26.06	0.2556	0.5112	22.2653
13.87	0.1930	20.72	0.2032	0.4064	32.2017
13.36	0.1859	23.05	0.2261	0.4521	29.1410
10.87	0.1513	24.85	0.2437	0.4874	23.6855
13.60	0.1893	22.93	0.2249	0.4498	29.6187
13.66	0.1901	23.99	0.2353	0.4706	28.7755

10.87	0.1513	25.19	0.2471	0.4941	23.4408
13.06	0.1818	23.13	0.2269	0.4537	28.6034
11.45	0.1594	24.14	0.2368	0.4735	25.1801
11.28	0.1570	25.42	0.2493	0.4986	23.9458
13.77	0.1916	22.81	0.2237	0.4474	29.9883
13.49	0.1878	22.82	0.2238	0.4476	29.5497
13.65	0.1900	22.85	0.2241	0.4482	29.7682
14.85	0.2067	21.93	0.2151	0.4302	32.4536
15.35	0.2136	21.47	0.2106	0.4211	33.6554
14.06	0.1957	22.49	0.2206	0.4412	30.7276
11.41	0.1588	25.04	0.2456	0.4912	24.4321
8.73	0.1215	26.85	0.2633	0.5267	18.7453
8.85	0.1232	26.99	0.2647	0.5294	18.8743
9.51	0.1324	26.44	0.2593	0.5186	20.3318
14.85	0.2067	21.83	0.2141	0.4282	32.5539
11.99	0.1669	24.54	0.2407	0.4814	25.7428
12.41	0.1727	23.83	0.2337	0.4674	26.9809
10.49	0.1460	25.46	0.2497	0.4994	22.6211
8.31	0.1157	27.79	0.2726	0.5451	17.5034
7.39	0.1029	28.86	0.2831	0.5661	15.3751

PVSDC02-18 Epidote

FeO (wt%)	FeO(mol)/100g ep	Al_2O_3 (wt%)	Al_2O_3(mol)/100g ep	Al(mol)/100g ep	$X^{Fe*}100$
10.93	0.1521	25.41	0.2492	0.4984	23.3836
9.26	0.1289	26.99	0.2647	0.5294	19.5776
9.08	0.1264	27.05	0.2653	0.5306	19.2358
8.38	0.1166	27.84	0.2730	0.5461	17.5987
8.04	0.1119	27.52	0.2699	0.5398	17.1699
9.85	0.1371	26.40	0.2589	0.5179	20.9318
8.48	0.1180	25.25	0.2476	0.4953	19.2435
9.47	0.1318	26.83	0.2631	0.5263	20.0281
8.15	0.1134	27.89	0.2735	0.5471	17.1733
6.38	0.0888	29.35	0.2879	0.5757	13.3626
8.81	0.1226	26.99	0.2647	0.5294	18.8051
10.59	0.1474	24.74	0.2426	0.4853	23.2962
11.98	0.1667	23.10	0.2266	0.4531	26.8992
12.27	0.1708	22.22	0.2179	0.4359	28.1510
11.97	0.1666	24.57	0.2410	0.4820	25.6876
11.67	0.1624	25.16	0.2468	0.4935	24.7613
11.67	0.1624	24.69	0.2422	0.4843	25.1143
11.18	0.1556	25.49	0.2500	0.5000	23.7342
10.08	0.1403	25.85	0.2535	0.5071	21.6717
10.89	0.1516	25.42	0.2493	0.4986	23.3109
8.33	0.1159	27.65	0.2712	0.5424	17.6113
9.00	0.1253	27.30	0.2678	0.5355	18.9570
9.16	0.1275	26.98	0.2646	0.5292	19.4130
11.85	0.1649	24.55	0.2408	0.4816	25.5112
11.67	0.1624	24.80	0.2432	0.4865	25.0308

H03PV004b Epidote

FeO (wt%)	FeO(mol)/100g ep	Al_2O_3 (wt%)	Al_2O_3(mol)/100g ep	Al(mol)/100g ep	$X^{Fe*}100$
13.35	0.1858	23.67	0.2321	0.4643	28.5806
13.45	0.1872	23.36	0.2291	0.4582	29.0039
13.78	0.1918	23.39	0.2294	0.4588	29.4789
13.37	0.1861	23.87	0.2341	0.4682	28.4397
12.89	0.1794	23.95	0.2349	0.4698	27.6345
13.35	0.1858	23.57	0.2312	0.4623	28.6671
13.96	0.1943	23.15	0.2270	0.4541	29.9654
13.46	0.1873	23.45	0.2300	0.4600	28.9401
13.26	0.1846	23.67	0.2321	0.4643	28.4428
13.78	0.1918	23.19	0.2274	0.4549	29.6577
13.12	0.1826	23.94	0.2348	0.4696	27.9980
14.67	0.2042	22.26	0.2183	0.4366	31.8617
13.23	0.1841	23.72	0.2326	0.4653	28.3538
12.93	0.1800	23.22	0.2277	0.4555	28.3207
13.01	0.1811	23.79	0.2333	0.4667	27.9550

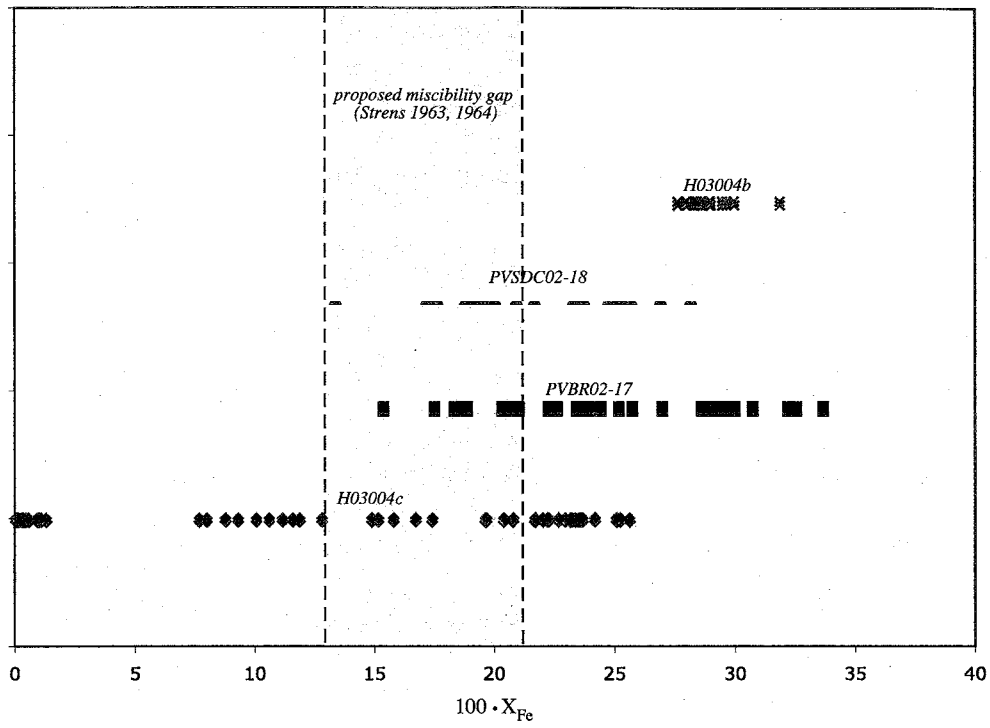

Figure 2.17: Epidote compositions for four epidote samples expressed as $Fe^{3+}/Fe^{3+} + Al$ (also referred to as X_{Fe}), and shown relative to the proposed miscibility gap of Strens (1963, 1964). Three sample compositions fall within the gap. This behavior is recognized in epidote from hydrothermal systems (Bird and Spieler, 2004).

compositional values expressed as molar fraction ($100*X_{Fe}$) are plotted in Figure 2.17 relative to the proposed compositional miscibility gap of Strens (1964). All three samples have compositional ranges that overlap the miscibility gap, however, Bird and Spieler (2004) noted that in low temperature environments, such as geothermal fields, epidote is documented to have a spread in X_{Fe} values within the miscibility gap related to low temperature disordering.

2.5.3 Metasomatic fluid chemistry and epidote growth temperature

Metasomatism of basement rocks in the Pecos River valley has resulted in an overall enrichment in potassium, typically at the expense of primary sodic plagioclase *via* replacement by K-feldspar. This reaction is represented by the following equation 2.1 in which Al, Si, and O are conserved, K^+ is introduced from an external source, and cation species are exchanged:

Eq. 2.1

$K^+ + NaAlSi_3O_8 \Leftrightarrow KAlSi_3O_8 + Na^+$ (in Senderov, 1973; Munha et al., 1980)

albite *K-feldspar*

Fluid activity and temperature conditions under which this reaction occurs are described by Giggenbach (1984) and shown in Figure 2.18 as a function of temperature versus the log of aNa^+/aK^+. With increasing temperature, a descending fluid will increase in Na^+ activity and eventually fall within the albite stability field resulting in albitization of a host rock. The reverse situation, as recorded by K-feldspar replacement of plagioclase in the Pecos area, is the result of ascending, cooling fluids with a log Na^+/K^+ activity value

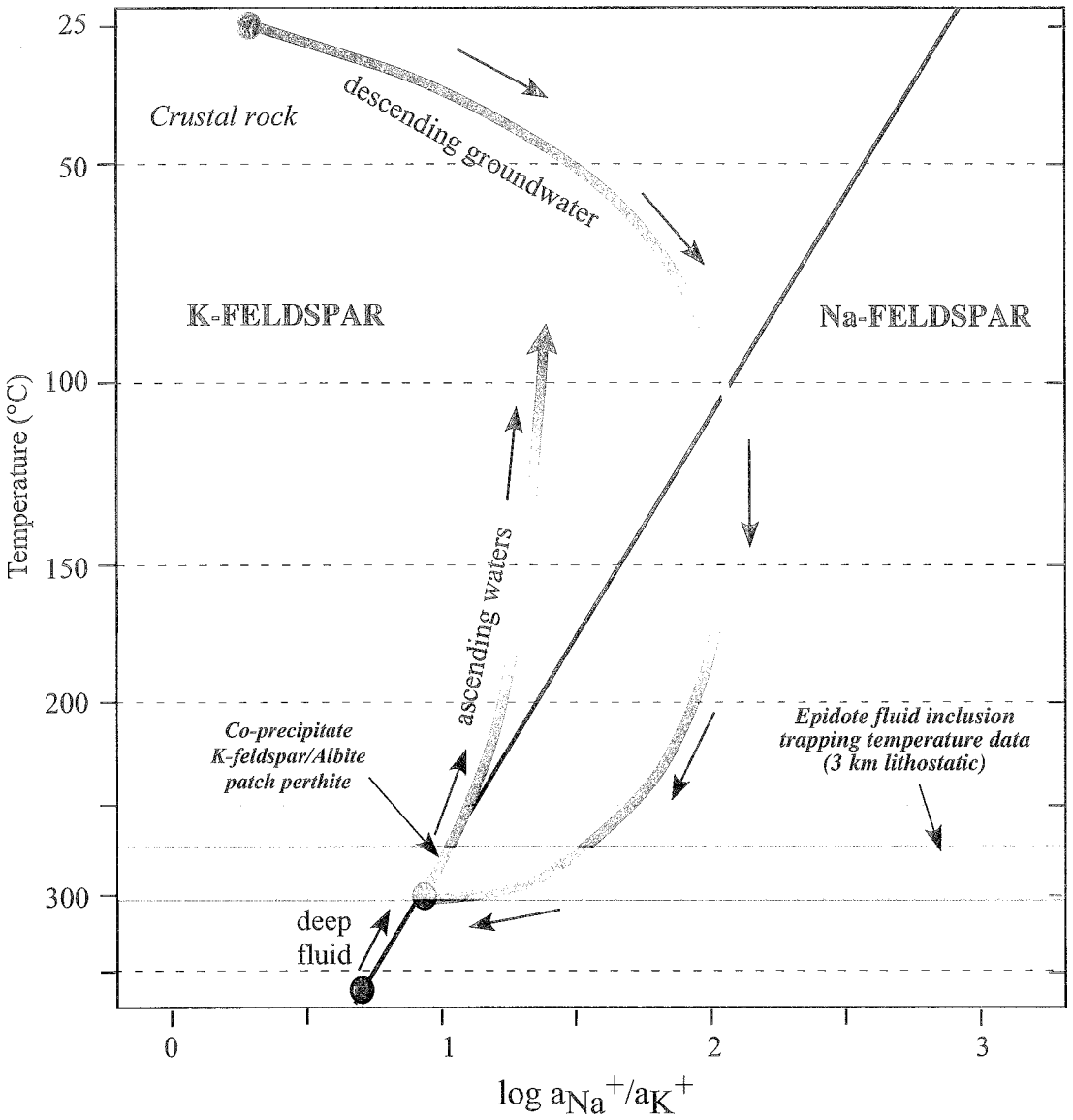

Figure 2.18: Fluid model shows the phase stability of K-feldspar and albite relative to fluid temperature, Na-K activity, and approximate Pecos alteration fluid temperatures based on epidote fluid inclusion data (modified from Giggenbach (1984). Fluid paths indicate descending, warming groundwater will precipitate albite at higher temperatures (depending on the sodium content), while ascending, cooling fluids support lower temperature K-feldspar precipitation. Partial replacement of plagioclase by K-feldspar seen in the Pecos area indicates that fluid composition and temperature fall within the K-feldspar stability field. Co-precipitation of secondary K-feldspar and albite patch perthite in microcline suggests fluid composition/temperature fall along the phase stability boundary. Based on epidote fluid inclusion data, the estimated temperature of alteration reflects a Na-K activity of <1 for metasomatic fluids. In the context of this phase stability diagram, the replacement mineralogy in the Pecos area supports a low-temperature, alkaline alteration fluid.

between 1 and 1.5 and a temperature of less than ~275°C (Figure 2.18; Giggenbach, 1984). Most altered plagioclase grains show only a partial replacement by K-feldspar at the micron-scale indicating that while this cation exchange occurred, plagioclase never achieved chemical equilibrium with the infiltrating fluid.

Although the above scenario implies addition of K^+ from an external source, chemical species can also be leached and liberated from mineral constituents of the host rock during alteration. For example, the following reaction (Eq. 2.2) describes the alteration assemblage observed in metasomatized tonalite or granodiorite and derives the K^+ from the chloritization of biotite in the presence of water.

Eq. 2.2

$$3(Na,Ca)AlSi_3O_8 + 2K(Mg,Fe)_3(AlSi_3O_{10})(OH)_2 \Rightarrow 2KAlSi_3O_8 + Ca_2(Al,Fe)Al_2O(SiO_4)\text{-}(Si_2O_7)OH \pm (Mg,Fe)_3(Si,Al)_4O_{10}(OH)_2\cdot(Mg,Fe)_3(OH)_6 + 6SiO_2 + 3Fe_2O_3 + Na^+$$

$$\textit{oligoclase} + \textit{biotite} \Rightarrow \textit{orthoclase} + \textit{epidote}\pm\textit{chlorite} + \textit{quartz} + \textit{hematite} + Na^+$$

As in the first reaction, Na^+ is still removed from the system by aqueous transport, but the process involves the dominant constituents of the host rock and accounts for the entire suite of alteration minerals. Whether metasomatism was achieved by either of these end-member scenarios is uncertain, although a combination of K^+ introduced from an external source as well as derived from the alteration of the primary mineralogy is possible.

Epidote occurs in a wide variety of geologic environments from high-pressure metamorphic terranes to low-pressure/low temperature geothermal systems (cf. Liebscher

and Franz, 2004). Consequently, the temperature of epidote formation is also widely variable. Drill holes in geothermal systems offered the first opportunity to sample alteration assemblages and measure the temperature and pressure of coexisting geothermal fluids (eg. White and Sigvaldason, 1963). One complication with this approach is the dynamic character of geothermal systems and the resulting spatial migration of isotherms with the development, maturation, and demise of a given system. This introduces some uncertainty that the present-day measured down-hole temperatures truly reflect the temperature of epidote growth. There is, however, general agreement in the literature that hydrothermal epidote may form at temperatures below 200°C (Seki, 1972; Reyes, 1990, 1998) but is common at temperatures between 220 and 260°C (Shizamu and Yajima, 1973; Elders et al., 1984; Ragnarsdottir et al., 1984; Doi et al., 1998; Reyes, 1998), or higher (Browne, 1978).

In order to determine the temperature of epidote formation fluid inclusion microthermometry measurements were made on rare, 3-4 μm, primary two-phase (vapor-liquid) epidote inclusions for samples PVBR04-2 and PVBR02-7 (Table 2.3). Epidote grains in doubly polished thin section were selected based on the presence of inclusions and cut out of the thin section to fit under the analytical chamber of the heating/cooling stage. No daughter minerals were observed, and inclusions suspected of necking were avoided. Three inclusions in different epidote grains in sample PVBR04-2 yield homogenization temperatures of 210, 285, and 305°C and ice melting temperatures of -4, -23, and -13°C, respectively. Four inclusions in a single field of view from sample PVBR02-7 homogenized between 260 and 265°C and had T_m values of -2 to -2.5°C. Salinities determined from T_m data for PVBR02-7 range between 3.39 and 4.18 weight

TABLE 2.3: FLUID INCLUSION MICROTHERMOMETRY DATA FOR PECOS EPIDOTE

Sample	Host Mineral	Type	Phases	T_m ice	T_h	Salinity	T_t (lithostatic)			T_t (hydrostatic)		
							1 km	2 km	3 km	1 km	2 km	3 km
PVBR02-7†	epidote	P	L + V	-2 to -2.5	260 to 265	3.39 to 4.18	271	286	306	263	269	275
PVBR02-7†	epidote	P	L + V	-2 to -2.5	260 to 265	3.39 to 4.18	271	286	306	263	269	275
PVBR02-7†	epidote	P	L + V	-2 to -2.5	260 to 265	3.39 to 4.18	271	286	306	263	269	275
PVBR02-7†	epidote	P	L + V	-2 to -2.5	260 to 265	3.39 to 4.18	271	286	306	263	269	275
PVBR04-2	epidote	P	L + V	-23	285	> 23.18	300	310	321	289	295	300
PVBR04-2	epidote	P	L + V	-13	305	16.89	320	330	360	310	318	324
PVBR04-2	epidote	P	L + V	-4	210	6.45	229	241	262	218	225	232

Data provided by D. Canales in 2007. P = Primary, L = Liquid, V = Vapor, $T_{m\,ice}$ = melting temperature of ice (all temperatures reported in degrees Celcius) ; T_h = homogenization temperature. T_t = trapping temperature. Salinity reported in equivalent weight percent NaCl (Bodnar, 1992; Appendix F). †Range in values for sample PVBR02-7 results from the measurements reported from a population (n=4) of fluid inclusions within a single grain. Tratpping temperatures calculated from liquid vapor curves from Roedder and Bodnar (1980).

percent, and >23.18, 16.89, and 6.49 weight percent for PVBR04-2. High salinities may indicate a suspect sample containing hydrocarbon gas species. Isochor slopes were calculated from homogenization temperatures (T_h) and salinities using Flincor fluid inclusion microthermometry software. Trapping temperatures for inclusions were determined from isochor values for both lithostatic and hydrostatic pressure equivalents of 1, 2, and 3 kilometers depth because the exact nature and depth of alteration is not exactly known (Roedder, 1984). These values, therefore, bracket the approximate temperature range of epidote formation. The four inclusions from sample PVBR02-7 yield trapping temperatures between 271 and 306°C for lithostatic pressures and 263 to 275°C for hydrostatic pressures. The three individual inclusions from sample PVBR04-2 have trapping temperatures based on lithostatic pressures that range from 300 to 321°C, 320 to 360°C, and 229 to 262°C. Temperatures based on hydrostatic pressures range from 289 to 300°C, 310 to 324°C, and 218 to 232°C. Overall, temperatures of epidote formation determined from fluid inclusion data are within the range of reported temperatures compiled in Liebscher and Franz (2004).

Fluid inclusion gas chemistry for secondary patch perthite and coexisting epidote for sample PVBR04-2 was analyzed by *in vaccuo* crushing to evaluate the source of metasomatic fluids. Analytical data are plotted on a fluid source discrimination diagram of CO_2/CH_4 versus N_2/Ar in Figure 2.19 and presented in Table 2.4 (Blamey and Norman, 2002). Patch perthite fluid inclusions with CO_2/CH_4 values between 2.0 and 2.7 and N_2/Ar values between 28.4 and 39.1. Epidote inclusions have CO_2/CH_4 values between 0.6 and 0.8 and N_2/Ar values between 49.7 and 60.2. All sample gas compositions plot within the evolved crustal fluid regime (Figure 2.19).

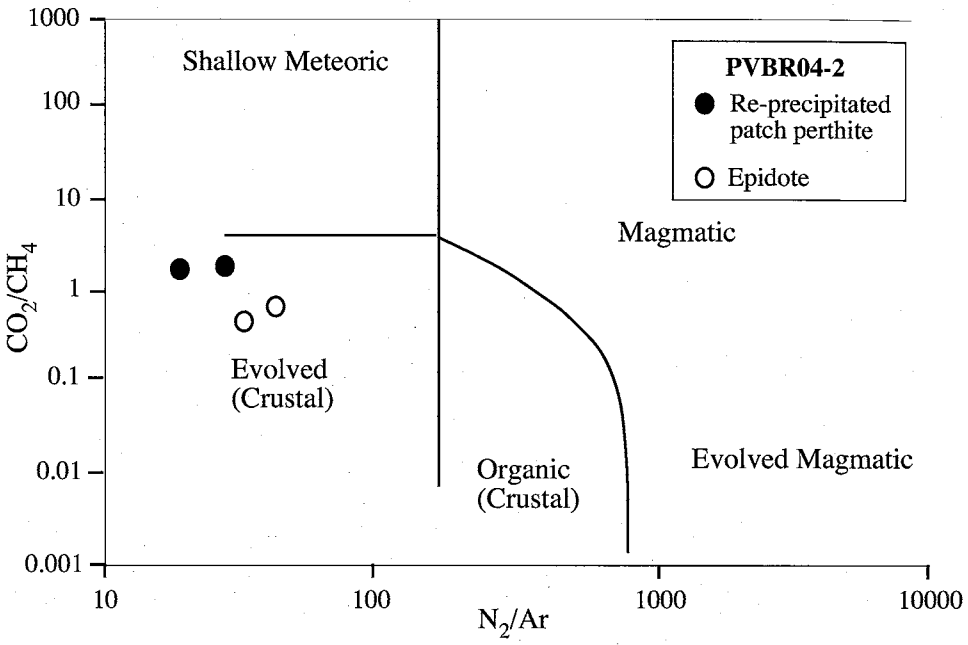

Figure 2.19: Fluid inclusion gas compositions for secondary K-feldspar and epidote shown relative to CO_2/CH_4 and N_2/Ar. Two analyses for each separate fall within the evolved crustal fluid regime (after Blamey and Norman, 2002).

TABLE 2.4: Measured and corrected fluid inclusion gas species and values.

	PVBR04-2				Hansonburg Fluorite (standard)		
	Epidote		K-feldspar				
	Crush 1	Crush 2	Crush 1	Crush 2	Crush 1	Crush 2	Crush 3
measured							
H2	6.132E-11	5.595E-10	3.453E-10	2.62E-10	9.169E-12	2.121E-11	9.911E-11
He	1.034E-12	5.377E-11	1.021E-12	7.335E-13	4.407E-12	4.476E-12	2.976E-11
CH4	1.495E-10	1.18E-09	6.619E-10	4.519E-10	2.288E-10	1.218E-10	4.755E-10
H2O	4.94E-09	0.000000637	3.257E-07	0.000000129	0.000000286	1.067E-07	0.000003295
H2O(fit)	2.47E-08	0.000001496	9.432E-07	5.036E-07	8.298E-07	3.909E-07	0.000003564
CO	0	0	0	0	0	0	0
N2	1.329E-10	2.678E-09	9.708E-09	4.816E-09	0	1.004E-10	2.133E-10
C2H4	2.121E-12	2.501E-11	4.019E-11	2.325E-11	2.967E-11	6.8E-12	8.543E-11
C2H6	1.554E-11	1.028E-10	1.029E-10	4.021E-11	2.411E-11	8.001E-12	3.877E-10
H2S	2.626E-13	2.789E-11	2.279E-11	9.213E-12	2.277E-11	8.715E-12	3.718E-10
Ar	2.206E-12	5.385E-11	2.482E-10	1.695E-10	1.139E-13	3.552E-12	3.121E-12
C3H6	1.981E-12	2.262E-11	2.257E-11	9.825E-12	2.82E-13	8.213E-13	1.087E-10
C3H8	7.115E-12	0	1.05E-11	0	0	9.936E-12	0
CO2	1.15E-10	7.36E-10	1.817E-09	8.853E-10	3.559E-09	1.528E-09	1.362E-08
C4H8	0	2.141E-11	1.817E-11	7.104E-12	9.554E-12	4.115E-12	7.986E-11
C4H10	2.868E-16	2.51E-11	1.441E-11	5.503E-12	2.335E-11	7.193E-12	1.287E-10
SO2	4.398E-12	2.748E-11	1.477E-11	2.888E-12	3.061E-11	3.615E-12	2.653E-10
Benzene	3.818E-12	3.789E-11	2.669E-11	1.176E-11	7.161E-12	3.398E-12	4.3E-11
Burst size	5.898E-09	0.000000446	2.325E-07	6.512E-08	0.000000231	8.874E-08	0.000002636
Sum	5.4372E-09	6.42551E-07	3.38754E-07	1.35695E-07	2.89949E-07	1.08532E-07	3.31091E-06
SUM(fit)	2.51972E-08	1.50155E-06	9.56254E-07	5.10295E-07	8.33749E-07	3.92732E-07	3.57991E-06
corrected							
H2	0.243360413	0.037261464	0.036109637	0.051342832	0.001099731	0.005400629	0.002768504
He	0.004103631	0.003580963	0.000106771	0.00014374	0.000528576	0.001139708	0.000831306
CH4	0.59331999	0.078585393	0.069217981	0.088556587	0.027442312	0.031013513	0.013282452
H2O	90.85565617	99.13605033	96.14634952	95.06601032	98.6380374	98.31198932	99.51942895
H2O(fit)	98.02678088	99.63029435	98.63483913	98.68797773	99.52635662	99.53351595	99.5555398
CO	0	0	0	0	0	0	0
N2	0.527439643	0.178348883	1.015211003	0.943767476	0	0.025564505	0.005958248
C2H4	0.008417603	0.001665611	0.004202856	0.004556186	0.003558625	0.00173146	0.002386372
C2H6	0.061673529	0.006846253	0.010760735	0.007879753	0.002891758	0.002037267	0.010829877
H2S	0.001042179	0.001857412	0.002383257	0.001805426	0.002731038	0.00221907	0.010385732
Ar	0.008754942	0.003586291	0.025955436	0.033216069	1.36612E-05	0.000904433	8.71809E-05
C3H6	0.007861986	0.001506442	0.002360251	0.001925356	3.38231E-05	0.000209125	0.003036388
C3H8	0.028237269	0	0.001098034	0	0	0.002529969	0
CO2	0.456399992	0.049015974	0.190012195	0.173487821	0.42686708	0.389069359	0.380456356
C4H8	0	0.001425859	0.001900122	0.001392135	0.001145908	0.001047788	0.002230782
C4H10	1.13822E-06	0.001671605	0.001506921	0.001078395	0.002800603	0.001831529	0.003595061
SO2	0.017454323	0.001830107	0.001544568	0.000565947	0.003671369	0.000920475	0.007410798
Benzene	0.01515248	0.00252339	0.002791098	0.002304548	0.000858892	0.000865221	0.001201147
corrected ratio							
H2/N2	0.461399549	0.208924571	0.035568603	0.054401993			
He/N2	0.007780286	0.020078417	0.000105171	0.000152305			
CH4/N2	1.124905944	0.440627334	0.068180882	0.093833056			
H2O/N2	37.17080512	237.8640777	33.54964977	26.78571429			
H2O(fit)/N2	185.8540256	558.6258402	97.15698393	104.5681063			
CO/N2	1E-30	1E-30	1E-30	1E-30			
C2H4/N2	0.015959368	0.009339059	0.004139885	0.004827658			
C2H6/N2	0.116930023	0.038386856	0.010599506	0.008349252			
H2S/N2	0.001975922	0.010414488	0.002347548	0.001912998			
Ar/N2	0.016598947	0.02010829	0.025566543	0.035195183			
C3H6/N2	0.014905944	0.008446602	0.002324887	0.002040075			
C3H8/N2	0.053536494	1E-30	0.001081582	1E-30			
CO2/N2	0.865312265	0.274831964	0.187165225	0.183824751			
C4H8/N2	1E-30	0.007994772	0.001871652	0.001475083			
C4H10/N2	2.15801E-06	0.009372666	0.001484343	0.00114265			
SO2/N2	0.033092551	0.010261389	0.001521426	0.000599668			
Benzene/N2	0.028728367	0.014148618	0.002749279	0.00244186			
N2/Ar	60.24478694	49.73073352	39.11361805	28.41297935			
CO2/CH4	0.769230769	0.623728814	2.745127663	1.959061739			

2.5.4 U-Pb Epidote geochronology

As in many radiometric systems, the retentivity of radiogenic lead in epidote is a function of closure empirically estimated between 670-750°C (Dahl, 1997). Because $^{40}Ar/^{39}Ar$ hornblende and mica dates indicate that the Pecos basement was cooler than ~400°C by 1350 Ma (Karlstrom et al., 1997; Sanders et al., 2006), any epidote date younger than this should represent a mineral growth age. Consequently U-Pb analysis of vein epidote has the potential to directly date the timing of hydrothermal activity (<1350 Ma). Eight picks of PVBR02-17, three picks of H03PV004c, and one pick each of PVBR04-3 and PVBR02-31 were analyzed and results are shown in Figure 2.20 and complete analytical data is presented in Table 2.5. Overall, the data are only marginally radiogenic ($^{206}Pb/^{204}Pb$ from 23 to 54) with little spread within individual samples. With the exception of PVBR02-17, individual Pb-Pb dates are largely dependent on assigned initial lead isotopic compositions and have correspondingly large uncertainties. The date from PVBR02-17 crystalline epidote is the best constrained as six of eight picks plot on a $^{207}Pb/^{204}Pb$ vs. $^{206}Pb/^{204}Pb$ chord with a mean standard weighted deviation (MSWD) of 1.82 and a calculated age of 1123±140 Ma (2σ; Figure 2.20). A single data point for a granular epidote pick gives a distinctly younger date and its model age is highly dependent on the model value for Pb_o. A two-point chord between the granular pick and upper crust Pb_o values of Zartman and Doe (1981) yields a date of 561±120 Ma. The same pick reduced with model Pb_o values for lower crust, mantle, and orogene yield dates of 923±88, 806±98, and 659±110 Ma, respectively. Assuming that Pb_o isotopic values are in the vicinity of reservoir values of Zartman and Doe (1981), the intersection of the crystalline chord and those reservoirs is closest to mantle model values with an age of

TABLE 2.5: U-Pb TIMS results for epidote separates, Pecos, New Mexico

				Corrected Ratios												
Sample	Est. wt. (mg)	U (ppm)	Pb (ppm)	$^{206}Pb/^{204}Pb$	error (%)	$^{207}Pb/^{204}Pb$	error (%)	$^{208}Pb/^{204}Pb$	error (%)	$^{238}U/^{204}Pb$	error (%)	$^{235}U/^{204}Pb$	Rho 6/4-7/4	Rho 6/4-8/4	Rho Alpha-Mu	Rho Beta-Nu
PVBR02-17	*crystalline=1123±140 Ma (MSWD=1.82) 6 pt Pb/Pb isochron; granular=806±98 Ma 1 pt w/ZD mantle value*															
granular, polyx, br-gr 5gr	0.280	10.76	6.32	44.714	0.493	17.228	0.348	37.945	0.359	148.17	0.793	1.075	0.773	0.615	0.880	0.538
crystalline, clear, lt gr 17gr	0.300	12.81	6.58	51.088	0.378	18.037	0.150	38.750	0.168	182.78	0.689	1.326	0.702	0.223	0.858	0.548
xtalline pk 3 25gr	0.310	4.31	2.08	53.522	5.370	18.255	1.230	38.454	0.438	198.54	8.720	1.440	0.983	-0.509	0.999	0.977
xtalline pk 4 15gr	0.250	10.58	7.84	49.415	0.510	17.898	0.195	62.784	0.375	152.73	0.920	1.108	0.704	0.928	0.885	0.565
xtalline pk 5 4gr	0.340	7.96	4.68	43.788	0.411	17.467	0.148	38.893	0.167	148.45	0.786	1.077	0.674	0.223	0.908	0.547
gran coating dk-gr 2 gr	1.180	3.89	2.13	52.882	0.301	18.132	0.138	39.965	0.163	176.40	0.562	1.279	0.678	0.350	0.816	0.493
gran coating, br-gr 15gr	0.617	4.35	3.28	39.039	2.200	17.144	0.438	39.338	0.569	114.31	4.590	0.829	0.700	0.400	0.074	0.073
xtalline pk 6 20gr	0.084	22.90	15.54	41.128	3.500	17.336	0.679	38.891	0.700	125.18	6.900	0.908	0.750	0.350	0.048	0.047
H03PV004c																
crystalline, cldy, gr pk 1 >50gr	1.238	6.09	11.64	24.061	0.139	16.030	0.155	36.090	0.240	34.89	0.594	0.253	0.750	0.410	0.259	0.257
crystalline, cldy, gr pk 2 >50gr	1.299	5.37	9.53	24.634	0.120	16.046	0.181	36.178	0.240	37.92	0.245	0.275	0.730	0.400	0.631	0.630
crystalline, cldy, gr pk 3 >50gr	1.110	4.79	9.81	23.516	0.126	15.964	0.182	36.101	0.240	32.31	0.261	0.234	0.770	0.420	0.612	0.610
PVBR04-3																
crystalline, clear, gr pk 1 >50gr	0.990	10.51	15.80	28.537	0.203	16.393	0.184	37.858	0.250	48.07	0.552	0.349	0.720	0.430	0.372	0.372
PVBR02-31																
crystalline, clear, gr pk 1 >50gr	0.928	6.61	4.40	26.818	0.585	16.310	0.207	42.207	0.380	112.16	2.137	0.813	0.710	0.410	0.104	0.103

Sample: polyx=polycrystalline, cldy=cloudy, br-gr=brownish green, lt gr=light green, dk-gr=dark green, gran=granular coating, gr=number of grains
Atomic ratios corrected for blank of 10 to 100 pg Pb, 0.6 pg U and mass discrimination (0.06 ± 0.04% to 0.086 ± 0.06%/amu Pb and 0±0.1%/amu U)
Errors reported in percent at 2σ
Rho = error correlation coefficients
Granular date is two point chord between Zartman and Doe (1981) model mantle value at 800 Ma (6/4=16.850, 7/4=15.390) with uncertainties estimated at 0.5%. Chord from crystalline data intersects this value, so using the model value for the initial is marginally supported by sample data.

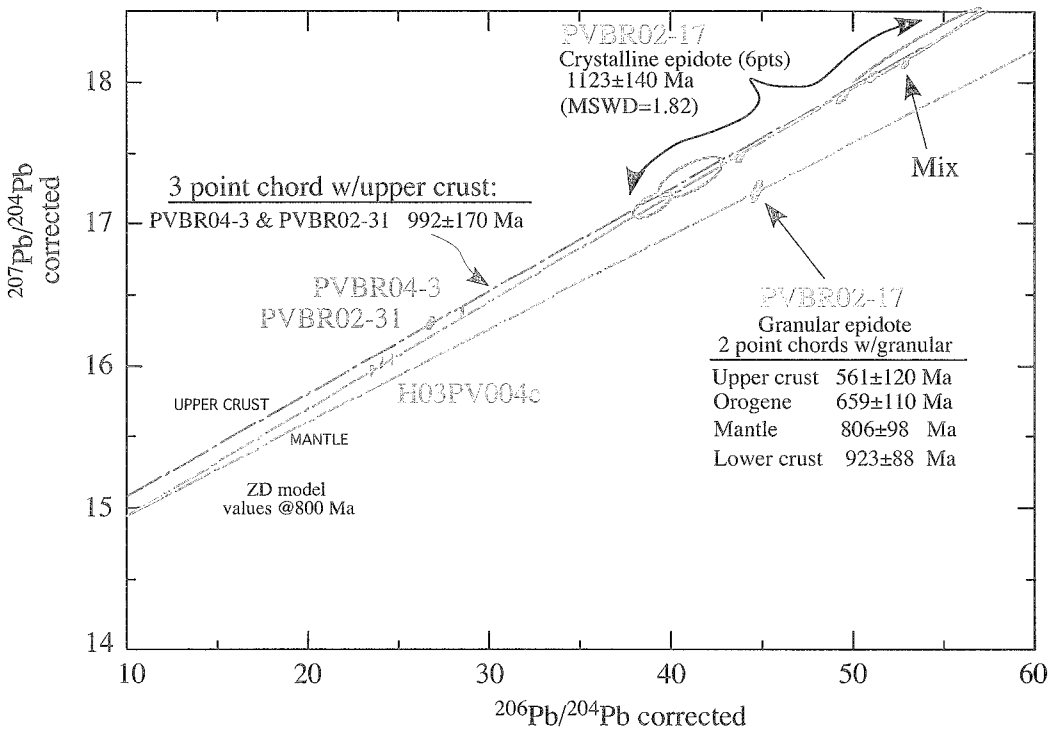

Figure 2.20: Pb-Pb isochron plot for Pecos epidote samples PVBZR02-17, PVBR04-3, PVBR02-31, and H03PV004c. Green lines are chords for crystalline and granular epidote from sample PVBR02-17. Six points for the crystalline epidote yield an age of 1123±140Ma. One granular point is heavily influenced by the model Pb values but is distinctly younger. The purple line is a three point chord with samples PVBR04-3, PVBR02-31, and the upper crust model Pb value.

806±98 Ma. The age of this pick was not reproducible in replicate analyses of granular epidote although one fraction plots between the granular and crystalline chord and is interpreted as a mixture of the two textural types.

Three data points for H03PV004c are clustered and relatively non-radiogenic resulting in high age uncertainty (Figure 2.20). However, these data plot on top of the PVBR02-17 chord and are interpreted to be of similar age. Samples PVBR02-31 and PVBR04-3 are not particularly radiogenic either, but plot distinctly above the chord from PVBR02-17. Either they are a different age than PVBR02-17 and H03PV004c, or they are the same age with different initial lead isotopic compositions. Unfortunately, with only one data point each, the choice of initial lead compositions has a large leveraging effect on the calculated age. If Pb_o values were close to those of PVBR02-17, the sample would be older than PVBR02-17 (~1200-1350 Ma), however if the initial lead isotopic composition was more radiogenic, similar to Zartman and Doe (1981) upper crust values, these samples would be younger. A three-point chord reduced with upper crust Pb_o model values yields an age of 992±170 Ma. Overall, U-Pb analyses of all Pecos epidote samples have high internal uncertainty, but indicate epidote growth occurred during the Neo- and Late Mesoproterozoic.

2.5.5 $^{40}Ar/^{39}Ar$ K-feldspar results

Both primary microcline and secondary K-feldspar separates were sampled to constrain a cooling/exhumation history as well as the timing of metasomatic alteration in the Pecos River valley. K-feldspar results and MDD models in Sanders et al. (2006) reflect significant basement cooling between 1000 and 800 Ma in the southern Sangre de

Cristo mountains and by ca. 800 suggest rocks resided at ~150°C or less. Similar results are seen in Pecos area microclines (eg. PVBR01-3), however, as discussed below, some microcline (and many secondary K-feldspars) are dominated by younger Neoproterozoic apparent ages. To record these apparent ages, the basement needs to be at hot temperatures (>400°C) at ca. 900 Ma in contrast to MDD thermal models. There is, therefore, an apparent incompatibility between these young microcline ages and the regional thermal history. Based on microtextural observations, some microclines were microsampled (0.1 to 0.4 mg), characterized, and dated as single grains to attempt to reconcile these data.

2.5.5.1 Multiple grain microcline

Multiple grains of nine suspected primary microcline from pegmatites, granodiorite, and granite from the northern part of the Pecos River valley were analyzed and are dominated by Neoproterozoic and Mesoproterozoic apparent ages (Figures 2.1). $^{40}Ar/^{39}Ar$ age spectra for multiple grain K-feldspar analyses are presented in Figure 2.21 and isotopic data for all multiple grain analyses are given in Table A2.4. Several milligrams of each sample were analyzed, and, in general, yield $^{40}Ar/^{39}Ar$ age spectra that show initial steep age gradients over the first 10% of the total ^{39}Ar released, minimal excess argon component, and K/Ca values generally between 10 and 1000 (Figures 2.21.a-i). Five analyses have spectra characterized by increasingly old apparent ages over the course of the heating experiment and apparent ages that climb to over 1000 Ma (Figures 2.21a-e). In contrast, four samples yield significantly younger flat or slightly climbing age segments with no apparent dates greater than 1000 Ma (with the exception

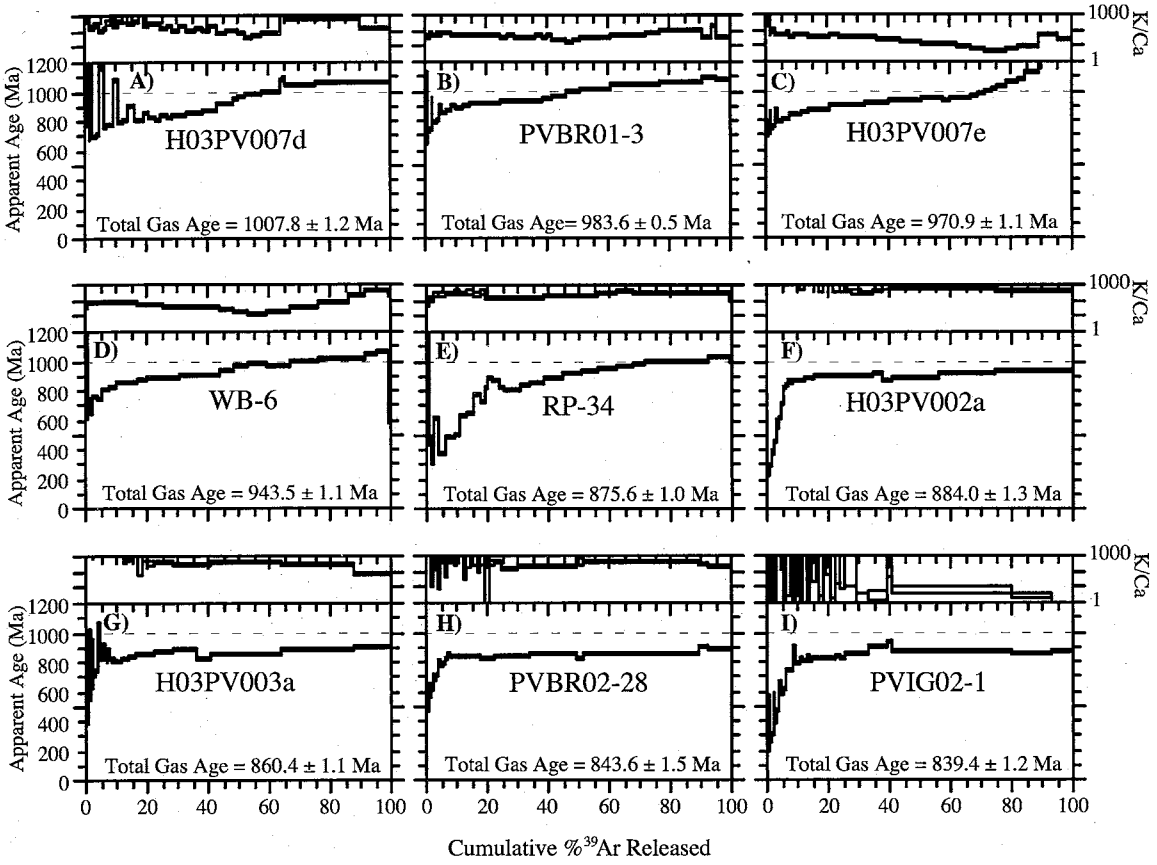

Figure 2.21: $^{40}Ar/^{39}Ar$ age spectra for presumed primary microcline from the Pecos river valley.

of initial excess argon in H03PV003a) (Figures 2.21f-i). Spectra for samples H03PV007d, PVBR01-3, and WB-6 have fairly flat segments corresponding to 10 to 40% of the total gas released before climbing to apparent ages older than 1000 Ma (Figures 2.21.a,b,d). Total gas ages are 1008, 984, and 944 Ma, respectively. Sample H03PV007e yields an age spectrum that increases gradually between 10 and 70% of the cumulative ^{39}Ar released before climbing abruptly to old apparent ages suggestive of a high retentivity diffusion domain or high temperature excess argon component (Lovera et al., 1989; Foster at al., 1990; Figure 2.21c). The total gas age is 971 Ma. The age spectrum for RP-34 climbs progressively (315 to 1038 Ma) throughout the analyses with the exception of some oscillation between 20 and 30% of the total ^{39}Ar released and has a total gas age of 876 Ma (Figure 2.21f). H03PV002a yields an age spectrum that climbs gradually and a total gas age of 884 Ma (Figure 2.21f). Samples H03PV003a, PVBR02-28, and PVIG02-1 yield age spectra with total gas ages of 860, 844, and 839 Ma, respectively (Figures 2.21g-i).

2.5.5.2 Multiple grain secondary K-feldspar

Secondary, metasomatic K-feldspar from veins and replaced plagioclase grains were sampled throughout the Pecos River valley from Dalton canyon to Tres Lagunas. $^{40}Ar/^{39}Ar$ age spectra for fifteen multiple-grain metasomatic K-feldspar analyses yield a range of total gas ages between 1025 and 365 Ma and are commonly characterized by undulatory age behavior (Figure 2.22). Analytical data are presented in Table A2.4. K/Ca values are also highly variable and range between ~1 and 1000. PVSDC02-18 and RP-40B have similar spectra shapes that have initial steep age gradients that level slightly

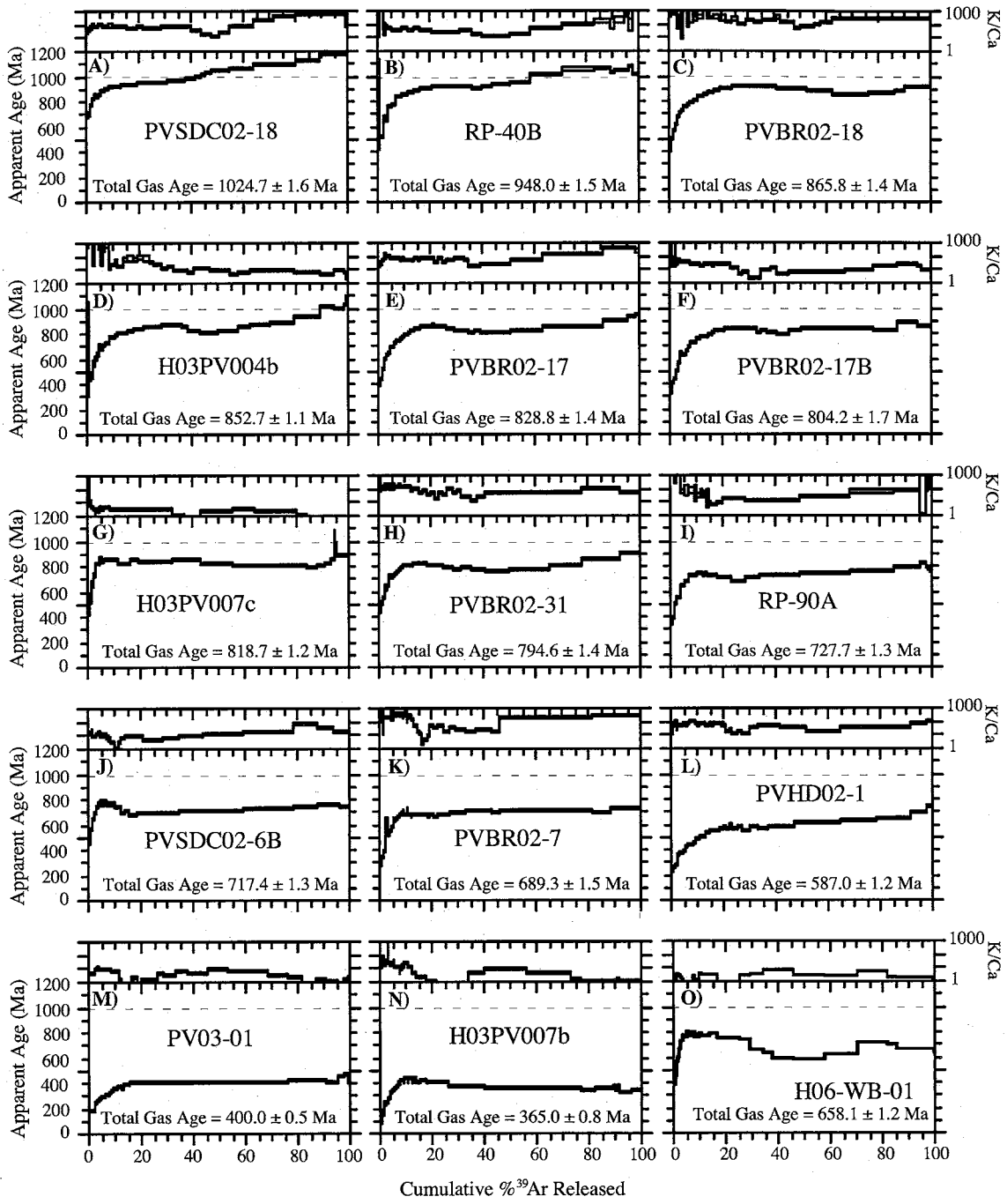

Figure 2.22: $^{40}Ar/^{39}Ar$ age spectra for secondary K-feldspar in the Pecos river valley.

between 10% and 30% and 15% and 50%, respectively, before climbing to progressively older apparent ages (Figures 2.22a, b). Total gas ages are 1025 and 948 Ma. PVBR02-18 yields a complex age spectrum characterized by a hump over the initial 75% of the cumulative ^{39}Ar released and a total gas age of 866 Ma (Figure 2.22c). Samples H03PV004b, PVBR02-17, and PVBR02-17B all yield similar undulatory spectra with intermediate humps comprising the initial ~40% of the total ^{39}Ar released and total gas ages of 853, 829, and 804 Ma, respectively (Figures 2.22d-f). The duplicate analyses of PVBR02-17 demonstrate some variability in argon release behavior and yield slightly different total gas ages. H03PV007c yields an age spectrum with a less pronounced hump although apparent ages get progressively younger between 5 and 85% of the total ^{39}Ar released (Figure 2.22g). The total gas age is 819 Ma. The age spectrum for PVBR02-31 has a hump over the initial 40% cumulative ^{39}Ar released and a total gas age of 795 Ma (Figures 2.22h). RP-90A and PVSDC02-6B yield spectra with small humps comprising <25% of the total ^{39}Ar released and total gas ages of 728 and 717 Ma, respectively (Figures 2.22i,j). PVBR02-7, PVHD02-1, and PV03-1 yield age spectra with little or no undulatory behavior and total gas ages of 689, 587, and 400 Ma, respectively (Figures 2.22k-m). H03PV007b has an age spectrum with progressively decreasing apparent ages between 10 and 100% of the total ^{39}Ar released and a total gas age of 365 Ma (Figure 2.22n). H06-WB-01 yields a complex age spectrum with old apparent ages for initial heating steps followed by younger apparent ages for higher temperature steps (Figure 2.22o). Total gas age is 658 Ma and K/Ca values are less than 10.

2.5.5.3 Single grain K-feldspar analyses

Single-grain separates were sampled from three pegmatitic microclines in the Tres Lagunas area that contained both patch and film perthite microtextures. Grains were approximately 500 μm cubes and weighed between 0.05 and 0.35 mg. Age spectra are shown in Figure 2.23 and complete analytical data are given in Table A2.5. Two analyses of film perthite and two of patch perthite from sample PVBR02-28 yield dramatically different age spectra and total gas ages. Film perthites (PVBR02-28-05, PVBR02-28-07) were analyzed with different step heating schedules but age spectra have similar total gas ages of 951 and 968 Ma, respectively, and show only slight undulatory behavior (Figures 2.23a,b). Overall, age spectra climb moderately and the oldest apparent ages for individual steps are 1023 and 1080 Ma. K/Ca values are between ~50 and 350. Patch perthite grains (PVBR02-28-13, PVBR02-28-15) yield generally flat age spectra with total gas ages of 760 and 803 Ma, respectively (Figures 2.23c,d). PVBR02-28-15 has young initial apparent ages (~500 Ma) that climb to a flat segment within the first 10% cumulative ^{39}Ar released. K/Ca values are, on average, 200 to 350. PVBR02-28-13 has a complex age spectrum that is poorly resolved by the heating schedule. K/Ca values are similar to the other patch analysis.

Three film perthite grains and two patch perthite grains were analyzed from sample PVBR06-20. All three film perthites (PVBR06-20-22, 33, 40) yield age spectra that climb from initially low apparent ages (300-600 Ma) to relatively flat segments (1000-1100 Ma) that comprise 70-80% of the total gas released. These samples have total gas ages of 1027, 1054, and 1064 Ma, respectively (Figures 2.23e-g). All three spectra exhibit a short flat section of 800 to 900 Ma apparent ages between 10 and 20%

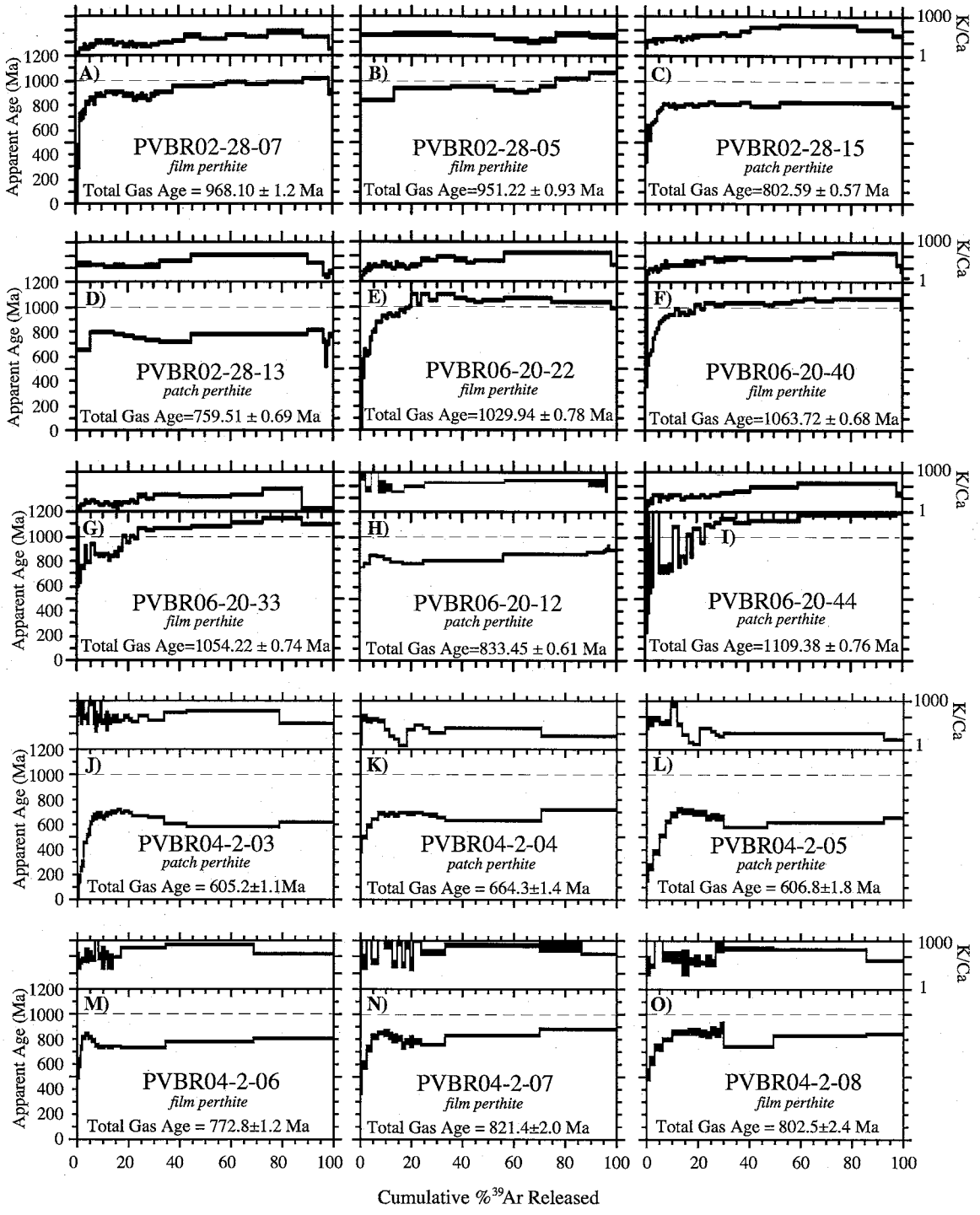

Figure 2.23: $^{40}Ar/^{39}Ar$ age spectra for single grain film and patch perthite analyses microsampled from pegmatitic microcline PVBR02-28, PVBR06-20, and PVBR04-2.

of the spectra. K/Ca values range between 1 and 1000. Patch perthite analyses yield one age spectrum (PVBR06-20-12) with slight undulatory behavior, K/Ca values generally between 100 and 1000, and a total gas age of 833 Ma (Figure 2.23h). Approximately 64% of the total gas released was during steps I and J (1150°C, 1200°C). The other spectrum (PVBR06-20-44) has isothermal heating steps with old initial apparent ages characteristic of excess argon and a total gas age of 1109 Ma (Figure 2.23i). Seventy-five percent of the cumulative gas released has apparent ages between 1100 and 1200 Ma that may also reflect excess argon. K/Ca values climb from 1 to ~350 during the heating analyses.

Three analyses each of film and patch perthite from sample PVBR04-2 yield complex age spectra characterized by undulatory behavior over the initial 10 to 40% of the total gas released (Figures 2.23j-o). Total gas ages for patch perthite grains are 598, 656, and 600 Ma, and 763, 811, and 793 Ma for film perthite. In all analyses >50% of the total gas released was during the final two or three steps. K/Ca values are generally between 10 and 1000 except for patch perthites PVBR04-2-04 and PVBR04-2-05 that have values between 1 and ~100. Overall, both film and patch perthite separates for this sample are distinctly younger than the film and patch perthites from the other two microcline samples. Film perthite from PVBR04-2 are actually similar in age to the patch perthites of PVBR02-28 and one patch perthite from PVBR06-20.

2.5.6 Evaluation of thermal effects on ^{40}Ar in primary microcline

Sanders et al. (2006) interpreted the ca. 800-900 Ma gradient of ages to result form argon loss related to long term crustal residence. As presented, but not discussed in

detail, thermal histories that allow for earlier cooling followed by a thermal spike around 800 Ma can produce the measured K-feldspar spectra as well. This reheating model implies exhumation significantly earlier than preferred by Sanders et al. (2006). In light of the two generations of K-feldspar in the Pecos area, at the suggested fluid temperatures of ca. 280°C it is possible that younger ages (~800 Ma) in microcline are not related to slow cooling, but rather an episodic event at 800 Ma. In order to quantify effects of reheating and potential episodic argon loss related to metasomatism, MDD thermal models were generated to compare measured age spectra to spectra modeled with a 800 Ma thermal pulse. Model input parameters are given in Table 2.6.

The automated multiple diffusion domain (MDD) modeling software created by O. Lovera is intended to recover thermal histories from measured $^{40}Ar/^{39}Ar$ K-feldspar age spectra until a good match between measured and modeled spectra is recovered. Similarly, manual input parameters for age and temperature are used to back out a modeled age spectrum. This second method is used in the following section to evaluate the thermal effects of metasomatic fluids on $^{40}Ar^*$ loss from primary microcline within zones of intense alteration. This is important because if fluid associated with secondary K-feldspar growth are ~280°C, they will likely cause at least partial resetting of primary K-feldspar that could yield inaccurate estimates of the regional thermal history. Fluid temperatures, as discussed above, are estimated to be about 280°C to 320°C although the following models incorporate a greater range in fluid temperature. Understanding the impact of a thermal event in this temperature range is critical in interpreting the modeled MDD thermal histories, particularly, in terms of partial resetting versus crustal residence.

TABLE 2.6: MODEL INPUT PARAMETERS FOR A COLD (75°C) CA. 900 MA BASEMENT THERMAL HISTORY, AND PARAMETERS FOR VARIED TEMPERATURE AND DURATION OF CA. 800 MA THERMAL SPIKE.

best fit 75°C@899 Ma	
Age (Ma)	Temp (°C)
1400	550
1200	420
1000	350
900	255
899	75
800.005	75
700	25
460	25
400	25
350	25
330	25
0	25

reheat of best fit 0.5 m.y.	
Age (Ma)	Temp (°C)
1400	550
1200	420
1000	350
900	255
899	75
800.005	75
800	280
799.5	280
799.495	75
700	25
460	25
400	25
350	25
330	25
0	25

reheat of best fit 0.25 m.y.	
Age (Ma)	Temp (°C)
1400	550
1200	420
1000	350
900	255
899	75
800.005	75
800	280
799.75	280
799.745	75
700	25
460	25
400	25
350	25
330	25
0	25

reheat of best fit 1 m.y.	
Age (Ma)	Temp (°C)
1400	550
1200	420
1000	350
900	255
899	75
800.005	75
800	280
799	280
798.995	75
700	25
460	25
400	25
350	25
330	25
0	25

reheat of best fit 50,000	
Age (Ma)	Temp (°C)
1400	550
1200	420
1000	350
900	255
899	75
800.005	75
800	280
799.95	280
799.945	75
700	25
460	25
400	25
350	25
330	25
0	25

50,000 years @280°C	
Age (Ma)	Temp (°C)
1400	550
1200	420
1000	350
900	255
899	75
800.005	75
800	280
799.95	280
799.945	75
700	25
460	25
400	25
350	25
330	25
0	25

50,000 years @300°C	
Age (Ma)	Temp (°C)
1400	550
1200	420
1000	350
900	255
899	75
800.005	75
800	300
799.95	300
799.945	75
700	25
460	25
400	25
350	25
330	25
0	25

50,000 years @310°C	
Age (Ma)	Temp (°C)
1400	550
1200	420
1000	350
900	255
899	75
800.005	75
800	310
799.95	310
799.945	75
700	25
460	25
400	25
350	25
330	25
0	25

50,000 years @320°C	
Age (Ma)	Temp (°C)
1400	550
1200	420
1000	350
900	255
899	75
800.005	75
800	320
799.95	320
799.945	75
700	25
460	25
400	25
350	25
330	25
0	25

The first model presented is a monotonic cooling fit to the measured spectrum for sample PVBR01-3 (Figure 2.24a). This sample is a pristine microcline within an area of intense metasomatism. Published results have interpreted this sample as either having cooled in the late-Grenville (1000 Ma) followed by hundreds of millions of years of crustal residence at ~125°C or having cooled below 125°C by 900 Ma followed by a later reheating event (Sanders et al., 2006). The model presented here has manual input values that force the second situation and allow the sample to cool to 75°C by 899 Ma. The resulting model age spectrum (green) purposely deviates from the measured data (black) over the initial 15% of the total ^{39}Ar released. The purpose of this model is to compare a situation in which ca. 800 reheating related to metasomatism is partly responsible for the form of the measured spectrum rather than prolonged residence at ~125°C. The following sections discuss the effects of a reheating event on the <125°C at 800 Ma model age spectrum (green).

The measured and modeled spectra from above are presented in Figure 2.24b and are shown with four additional model spectra representing short duration thermal spikes at 800 Ma. These models are isothermal and were kept at 280°C at 800 Ma for 0.05, 0.25, 0.5, and 1.0 Ma. These thermal perturbations influence the initial 30% of the calculated age spectra and produces the age gradient between 800 and 900 Ma. There is progressive fractional loss of ^{40}Ar * over this portion of the model age spectra as a function of the duration of the thermal event. A 280°C, 0.25 Ma duration thermal event provides a model spectrum that best fits the measured spectrum. Because both time and temperature control argon loss, models that vary the temperature of a constant duration thermal pulse were also constructed. Figure 2.24c presents the measured and modeled

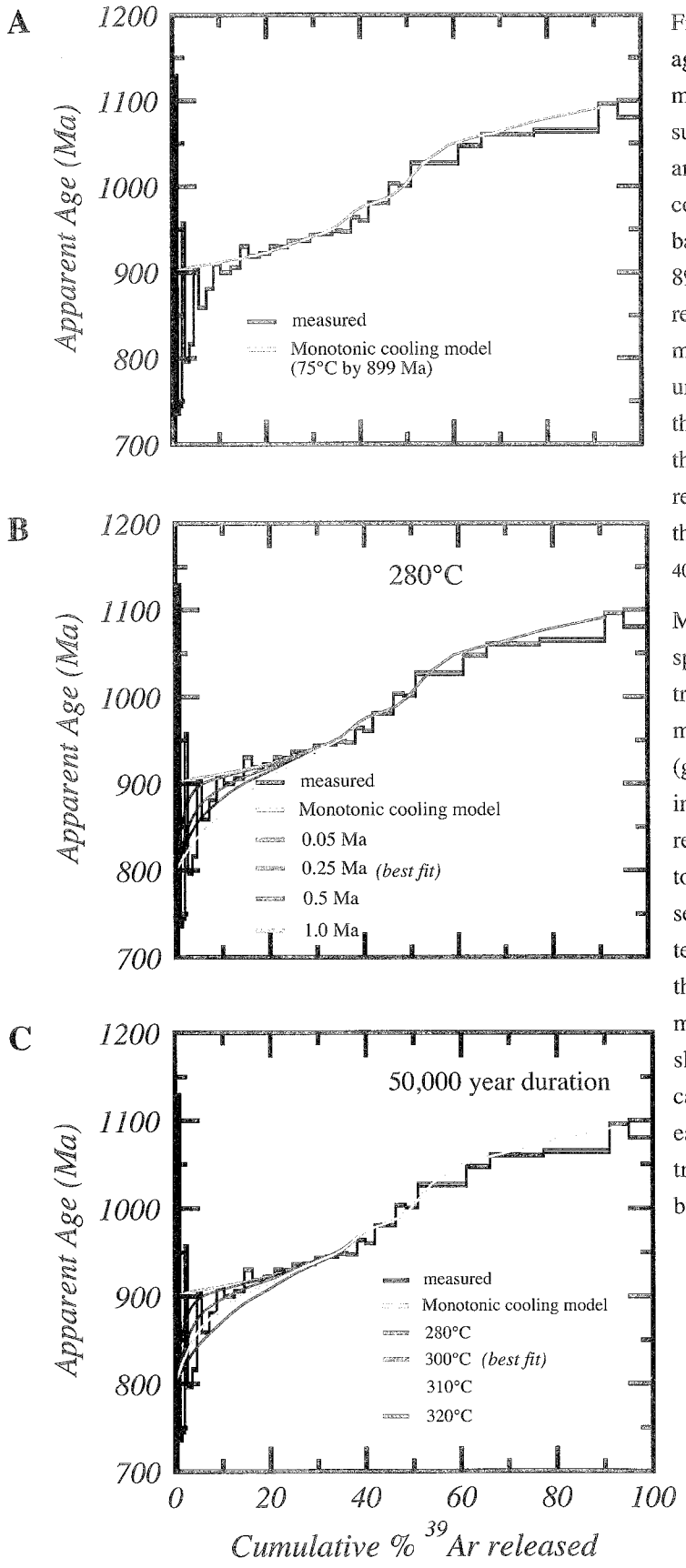

Figure 2.24: Measured and modeled age spectra for sample PVBR01-3 microcline. Figure A plots the measured spectrum (black) in contrast to an age spectrum for a monotonic cooling fit to the data that allows the basement to have cooled to 75°C by 899 Ma (green). Subsequently, this results in a mismatch between the measured and modeled data. Figures B and C attempt to reconcile this mismatch with the assumption that the model spectrum (green) represents the true geologic history, and the measured data are the result of $^{40}Ar^{*}$ loss during alteration at ~800 Ma. Figure B shows the two age spectra, as well as, model age spectra that reflect reheating of the monotonic cooling age spectrum (green) to 280°C at 800 Ma for varying durations. Durations of the reheating event range from 0.05 Ma to 1.0 Ma, and the best fit is represented by a 0.25 Ma event at this temeprature. Figure C demonstrates that similar effects can result from a much shorter heating duration with slightly higher temperatures. In this case, 0.05 Ma at 300°C produces essentially the same model age spectra as a heating event 20°C cooler, but five times longer.

data of Figure 2.24a and four models with the same duration of 50 Ka but variable temperatures of 280, 300, 310, and 320 °C. Similarly to Figure 2.24b, only the initial 30% of the model age spectra undergo progressive argon loss as a function of increasing temperature. The 310°C pulse provides the best-fit model. These models show metasomatism can affect microcline that cooled prior to 800 Ma, and thus the temperature conditions of the migrating fluids need to be considered when evaluating the basement exhumation history. Also, these models show that moderately high temperature fluids will not substantially degas "primary" K-feldspar thereby indicating that the primary K-feldspars can record the true cooling (exhumation) history of the region.

2.6 Discussion

Neoproterozoic total gas ages recorded by secondary K-feldspar and some pegmatitic microcline in the Pecos River valley are too young to fit with multiple diffusion domain (MDD) cooling histories for other microcline in the area as well as throughout the southern Sangre de Cristo Range (Sanders et al., 2006). A potential resolution to this incompatibility requires secondary K-feldspar to grow below its argon closure temperature (<350°C), where $^{40}Ar/^{39}Ar$ dating will record a mineral growth age rather than a cooling age. While this is an acceptable hypothesis for K-feldspar veins and replacement of plagioclase, it does not explain ~800 Ma ages for some pegmatitic microclines that are expected to be primary and therefore older. The following discusses how investigating a variety of K-feldspar occurrences and replacement microtextures has validated this hypothesis that multiple age populations of secondary K-feldspar represent

the timing of mineral growth during punctuated periods of metasomatism. Young microcline ages are furthermore shown to result from patch perthite replacement of the primary film perthite microtexture. These results are significant in that they benefit our understanding of the $^{40}Ar/^{39}Ar$ system and K-feldspar thermochronology by incorporating a mineralogic perspective, and contribute to understanding the overall chronology of the tectonic evolution of the southwestern U.S.

2.6.1 Implications for K-feldspar thermochronology

Several secondary K-feldspar samples in the Pecos River valley (PVSDC02-18, RP-40B) yield $^{40}Ar/^{39}Ar$ age spectra similar to basement microcline from other areas of the Sangre de Cristo Range. They are interpreted as having formed during the Mesoproterozoic and experienced a similar cooling history as the basement rocks in the region. Younger dates for secondary K-feldspar are interpreted as mineral growth ages rather than cooling ages. This is based principally on the fact that these samples have MDD deduced argon kinetic parameters that require ca. 350°C Neoproterozoic temperatures not compatible with most primary K-feldspar data. Similarly, microsampling of coexisting subgrains of film and patch perthite shows they have similar laboratory derived argon retentivities that will not allow young samples to be explained by overall low closure temperatures. Consequently, the young ages of the patch perthites within the pegmatitic megacrysts are also interpreted as a mineral growth age related to the K-metasomatism in the area.

Parsons et al. (1988) documented a spread in $^{40}Ar/^{39}Ar$ total gas ages for cryptoperthitic alkali feldspars from the Klokken syenite intrusion in Greenland that are

also variably replaced by patch perthite. Rather than argue that patch perthite grew at a much younger time relative to the pristine primary cryptoperthite, his interpretation is quite different and suggests that patch perthite is 'leaky' in nature and attributes young ages to $^{40}Ar^*$ loss over geologic time. His arguments are explored in more detail in Chapter 3, and challenges the fundamental MDD assumption that requires $^{40}Ar^*$ loss in nature to operate by the same mechanisms and pathways as ^{39}Ar in the laboratory. The discussion here continues with the assertion that laboratory derived kinetic parameters are accurate to the first order, and that the Pecos secondary K-feldspar ages are best explained by crystal growth ages. The range of secondary K-feldspar total gas ages from the Pecos area could be explained in the context of the Parsons et al. (1988) model as a single event followed by indiscriminate, with respect to laboratory parameters, degrees of $^{40}Ar^*$ loss, but this would neglect the internal reproducibility of age spectra between duplicate analyses of the same sample (PVBR02-17 and 17B), age similarities between secondary K-feldspars from different geographic locations (eg. PVSDC02-6B and RP-90A), and experimentally derived argon retentivities. Instead it appears that metasomatic effects seen in the Pecos area are the result of a complex history of multiple fluid events over time.

2.6.1.1. Hump-shaped age spectra

Determination of the exact timing of metasomatism is somewhat complicated by undulatory behavior of age spectra for secondary K-feldspars (eg. Figure 2.22). In some cases, intermediate age maxima are up to ~100 Ma older than apparent ages for higher temperature heating steps (eg. PVSDC02-6B, Figure 2.22j). Lovera et al. (2002) describe

hump-shaped age spectra in the context of K-feldspar recrystallization and repartitioning of $^{40}Ar^*$. The intermediate age maximum is explained by release of old argon, formerly sited in a retentive domain, from a less retentive location (recrystallization at 150°C; Lovera et al., 2002). Consequently the initial portion of the age spectra that corresponds to the degassing of low retentivity domains has old apparent ages. In this model, diffusion domains essentially undergo a restructuring and repartition $^{40}Ar^*$ into a new architecture of diffusion domains during mineral recrystallization (Lovera et al., 2002). While this model explains the shape of the age spectra, it is not process oriented and does not expand on, in particular, the mechanism for retaining $^{40}Ar^*$ during mineral modification. In the Pecos area, for example, patch perthite (recrystallized from film perthite) yield much younger total gas ages than the film perthite and suggest $^{40}Ar^*$ was lost during recystallization, not retained or redistributed.

Hump-shaped age spectra are also documented for feldspar partially to completely replaced by secondary K-feldspar (Girard and Onstott, 1991; Warnock and van de Kamp, 1999; Liu et al., 2003). Warnock and van de Kamp (1999) discuss a different potential cause for this behavior in secondary and hydrothermally altered K-feldspar. They recognize that precipitated adularia rims on detrital K-feldspar cores in the Fountain Formation, Colorado, yield hump-shaped spectra when impure mixtures are analyzed, and infer that multiple populations of K-feldspar with different activation energies produce the undulatory behavior. Even in the pure detrital K-feldspar separate, a small intermediate age maximum is observed that is interpreted again as a mixture of the detrital component and secondary adularia that infiltrated microcracks and was not avoided during sampling (Warnock and van de Kamp, 1999). This explanation appears

most relevant for causing the hump-shape behavior in Pecos samples because multiple populations of K-feldspar are also recognized in the Pecos area, and there exists a high potential to sample a mixture of primary and secondary components, particularly in multiple grain analyses. The presence of sericite, particularly in replaced plagioclase grains, may also exacerbate the intermediate age maxima. An extreme example of this is seen in the age spectrum for a near complete replacement of plagioclase by K-feldspar and abundant sericite in sample PVIC02-3 (Fig 2.25). The dramatic hump-shaped behavior is interpreted as the result of degassing of older sericite (degassed by ca. 800°C; Parry et al., 1997) that grew earlier in the geologic history of the basement.

2.6.1.2. Fluid temperature implications for primary K-feldspar

Microsampling, characterization, and $^{40}Ar/^{39}Ar$ analyses of respective textural types indicate distinct $^{40}Ar/^{39}Ar$ ages are preserved by film and patch perthite (Figure 2.26). Film perthite samples yield generally older apparent ages than patch perthite counterparts and have age spectra compatible with the regional basement thermal history (except PVBR04-2 which is discussed below). Patch perthite, on the other hand, yield consistently younger, Neoproterozoic apparent ages that, with one exception (PVBR06-20-44), document the timing of fluid interaction. As discussed earlier, the preservation of discrete age populations at the sub-grain scale can be explained by secondary K-feldspar growth below the argon closure temperature. The question then arises if metasomatic fluids were hot enough to cause ^{40}Ar * loss from the host microcline, and what implications, either locally or regionally, do these fluid pulses have for interpreting basement K-feldspar age spectra and MDD models?

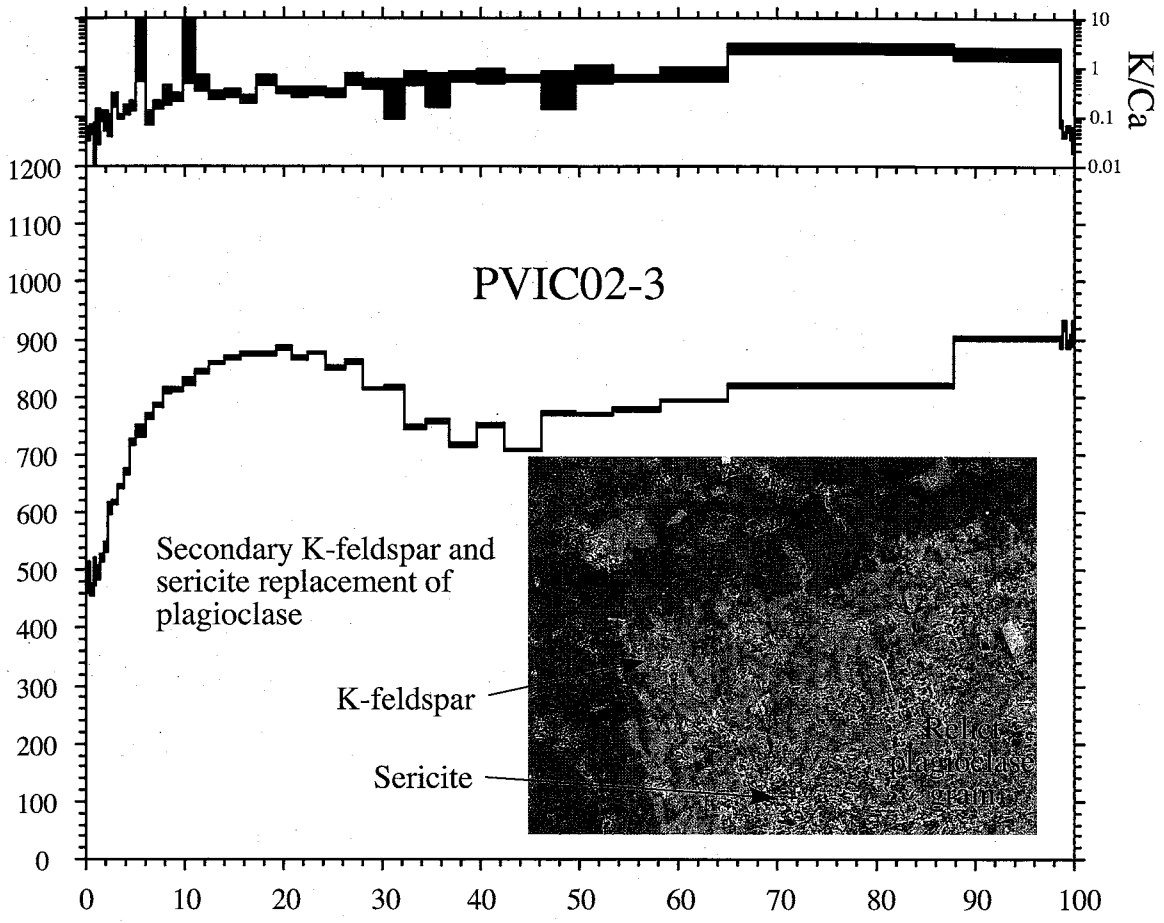

Figure 2.25: Age spectrum and photomicrograph of altered plagioclase in tonalite sample PVIC02-3. ^{40}Ar contribution from sericite in the plagioclase core may be causing, at least in part, the hump-shaped behavior of the age spectrum.

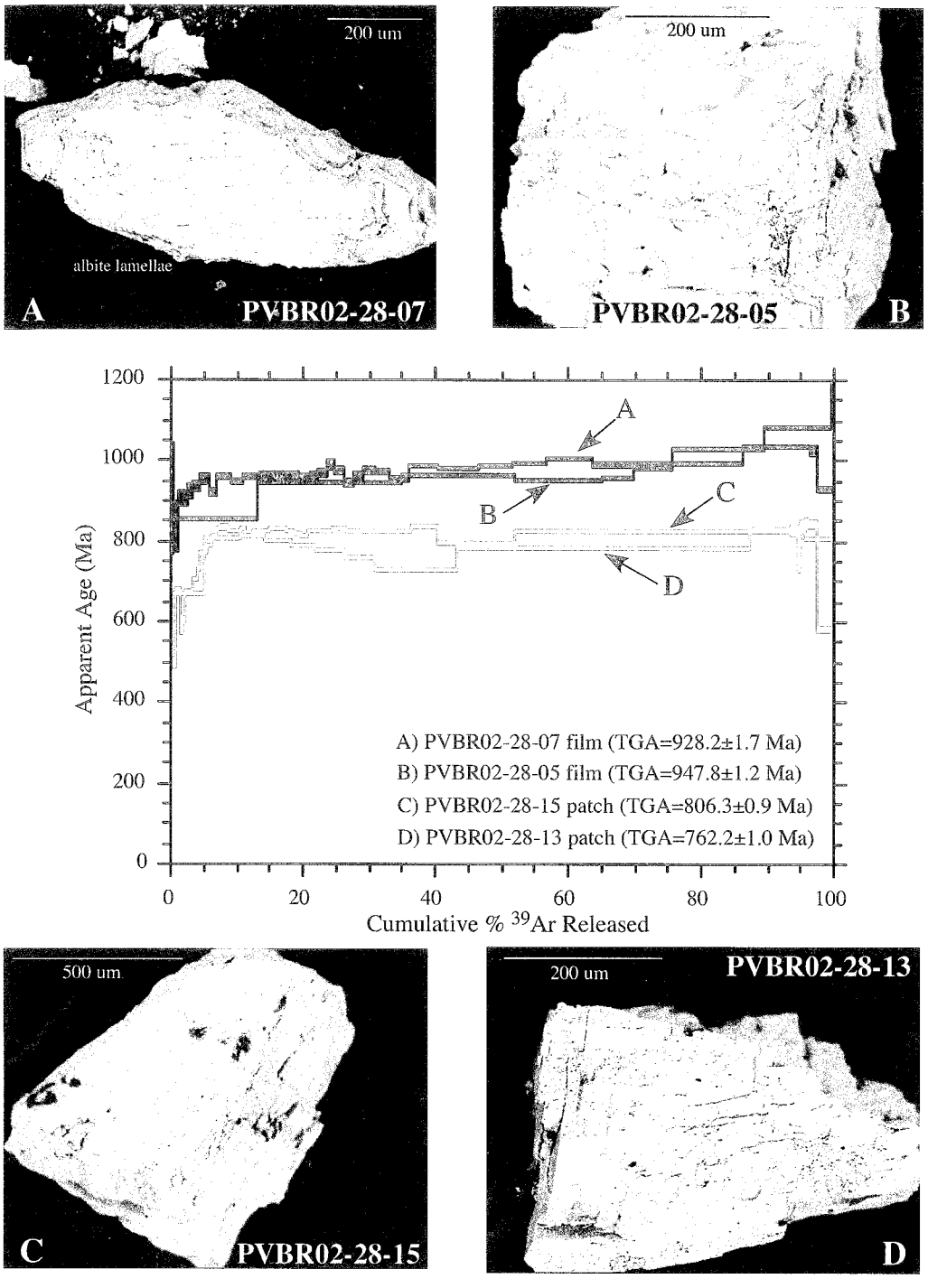

Figure 2.26: $^{40}Ar/^{39}Ar$ age spectra for film and patch perthite from pegmatitic microcline sample PVBR02-28. Two film perthite sub-grains (A,B) yield similar age spectra that climb to apparent ages >1000 Ma at high temperature heating steps. Patch perthite sub-grains (C,D), however, have no apparent ages greater than ~850 Ma and yield relatively flat age segments with ca. 800 Ma total gas ages. Multiple-grain separate analysis of PVBR02-28 yields a similar young total gas age suggesting the pink patch perthite was inadvertently sampled.

Fluid temperatures, based on the presence of epidote and fluid inclusion microthermometry, are estimated at ~280°C. This relies cautiously on the fact that epidote is cogenetic with metasomatic K-feldspar, and, while this is unmistakable in some situations, it is more dubious in others. Using this temperature, model age spectra are constructed to investigate the effects of variable fluid temperatures and hydrothermal durations on a primary microcline that was cold (75°C) by 899 Ma (Section 2.5.6). Recall that a measured age spectrum fits the modeled radiogenic argon loss from the microcline during a 280°C fluid event that lasted ~250,000 years (Figure 2.24). Alternatively, and for contrast, a 50,000 year pulse of ~310°C fluid has virtually the same effect. While the geologic ramifications of these models are quite different and discussed in the following section, the implications are that a primary microcline can withstand fairly long duration thermal spikes without causing significant $^{40}Ar^*$ loss. Sanders et al. (2006) presented unconstrained MDD thermal models for basement microcline in the Sangre de Cristo Range, but overall these models overlap with the monotonic cooling models and, consequently, a regional Neoproterozoic slow cooling history was preferred over a reheating event. If the fluid events documented in the Pecos area were widespread and are underappreciated in the geologic record of northern New Mexico, this interpretation needs revision. Although presently there is no preconception that metasomatism is widespread outside the Pecos valley, most basement K-feldspar age spectra can be modeled with a small percentage of argon loss related to a Neoproterozoic reheating event (e.g. PVBR01-3; Figure 2.24; Sanders et al., 2006). With respect to the conclusions of Sanders et al. (2006), this situation would allow the Sangre de Cristo basement to cool to below 125°C by 899 Ma instead of 150°C as predicted by the

monotonic cooling model. In terms of crustal position, this would place the basement several kilometers closer to the surface by the Early Neoproterozoic than is predicted by the monotonic models. The greater, regional variations in K-feldspar age spectra and thermal histories between the Sangre de Cristo Range and the Las Vegas basin (Sanders et al., 2006) cannot be reconciled by Neoproterozoic thermal perturbation at the temperatures and durations discussed for the Pecos area.

2.6.2 Geologic evolution of the Pecos valley and regional implications

The Paleo- to Mesoproterozoic magmatic and metamorphic history of the basement lithologies in the southern Sangre de Cristo Range is described by numerous authors (Miller et al., 1963; Robertson and Moench, 1979; Bowring and Condie, 1982; Grambling et al., 1989; Robertson and Condie, 1989; Melis, 2001; Sanders et al., 2006). The post-magmatic/post-metamorphic history of these rocks is the particular focus of this study primarily because in areas such as the Pecos valley, potassium metasomatism has left a chemical overprint with the potential to reveal geologic and tectonic information about the time period represented by the Great Unconformity. The age of alteration minerals, geochemistry and temperature of metasomatic fluids, and phase stability are all threads of information that characterize the origin and timing of fluid-basement interaction in the Pecos area. This information is used to discriminate a tectonic affinity for this style of alteration, and, in a greater scope, show how deformation and metasomatism in the southern Sangre de Cristo Range tie in with tectonic events regionally.

2.6.2.1. Timing of metasomatism

Ages of both epidote and secondary K-feldspar dates in the Pecos area indicate there have been persistent periods of K-metasomatism in the Pecos area since the Mesoproterozoic. The best-constrained Pb-Pb isochron age for crystalline epidote from the Pecos River valley is from sample PVBR02-17 and is 1123±140 Ma (Figure 2.20). Other epidote analyses are poorly constrained but overall are in agreement with this general age range for epidote growth. Two secondary K-feldspar samples (PVSDC02-18, RP-40B) yield age spectra consistent with mineral growth prior to ca. 1100 Ma. K-feldspar from one sample (PVSDC02-18) occurs as vein selvages surrounding an epidote vein. The ages of these K-feldspar samples are consistent with reported Mesoproterozoic epidote dates and are interpreted as an early episode of K-feldspar growth above the $^{40}Ar^*$ closure temperature.

A second event is broadly constrained at ca. 800 Ma. One analysis of a granular cryptocrystalline epidote from PVBR02-17 hints at a second, ca. 800-900 Ma period of epidote growth although these data were not reproducible. Similarly, the oldest $^{40}Ar/^{39}Ar$ apparent age recorded by secondary K-feldspar from this sample is ~980 Ma, but only 895 Ma in a duplicate analysis (PVR02-17B). Despite the large error of the epidote results, there appears to be poor agreement between Neoproterozoic K-feldspar apparent ages and the Mesoproterozoic U-Pb epidote data unless these phases are not, in fact, cogenetic, but grew at different times. To reconcile both epidote and K-feldspar dates, secondary K-feldspar in this particular sample appears to have formed later than the crystalline epidote, perhaps at the same time as the suspected ca. 800-900 Ma granular epidote growth.

Subsequent 700, 600, and 400 Ma events are suggested by younger K-feldspars. Although total gas ages for multiple grain analyses of secondary K-feldspar range between 1025 and 365 Ma (n=15), there is a broad similarity in age among some samples suggesting a potential episodic nature to K-metasomatism. The oldest secondary K-feldspars (PVSDC02-18, RP-40B) have age spectra that resemble those of primary microcline throughout the southern Sangre de Cristo Range (Figure 2.27; Sanders et al., 2006) and are interpreted to have formed during the Mesoproterozoic and cooled along with the rest of the basement during the Neoproterozoic. The timing of this K-feldspar formation may be the most compatible with local U-Pb epidote dates. Six samples yield slight undulatory age spectra with total gas ages between 795 and 866 Ma that are broadly lumped into a ca. 800 Ma event (PVBR02-18, H03PV004b, PVBR02-17, PVBR02-17B, H03PV007c, PVBR02-31). A potential ca. 700 Ma event is represented by three samples (RP-90A, PVSDC02-6B, PVBR02-7). PVHD02-1 and H06-WB-01 (587 and 658 Ma, respectively) have ages similar to patch perthite from sample PVBR04-2, although the spectra are more complex than other secondary K-feldspars. There is a final Paleozoic event (365-400 Ma; H03PV007b, PV03-1) recorded by adularia habit replacement K-feldspar. Single grain total gas ages for replacement patch perthite are variable but also support metasomatism between 760 and 830 Ma (PVBR02-28-15, PVBR02-28-13, PVBR06-20-12). Three patch perthite analyses from sample PVBR04-2 yield total gas ages that suggest replacement between 598 and 656 Ma and overlap temporally with samples PVHD02-1 and H06-WB-01. This sample is a bit unusual, however, in that coexisting film perthite have total gas ages between 763 and 811 Ma unlike film perthite from other pegmatitic microcline that record significantly older

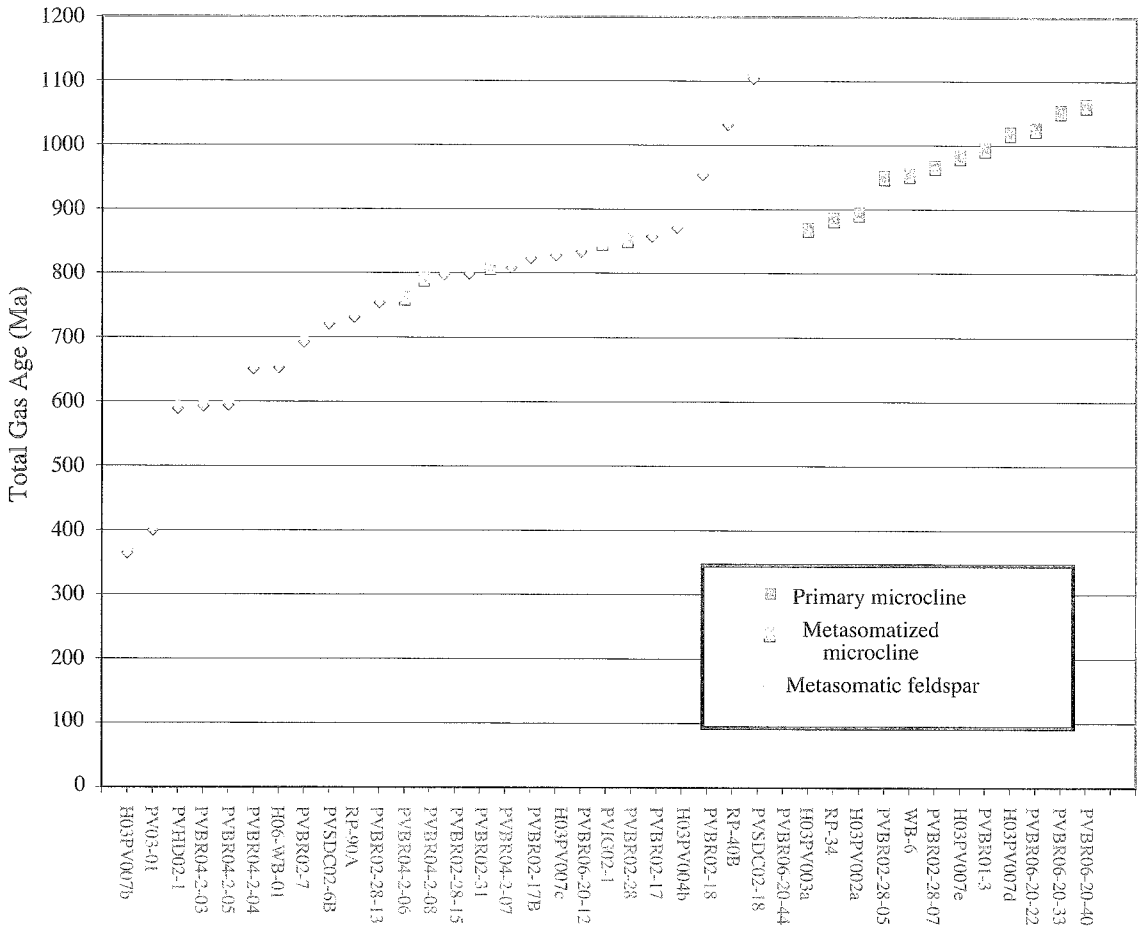

Figure 2.27: Diagram showing the age distribution of presumed primary and secondary K-feldspar total gas ages. Microcline samples suspected of partial replacement by secondary K-feldspar are represented by blue squares.

apparent ages (eg. PVBR02-28-07). It is difficult to explain why these film perthites are young without assuming that the film perthites were either thermally reset at this location, or replaced by patch perthite at ca. 800 Ma and again at ca. 600 Ma in which case the film perthite sample was contaminated by 800 Ma patch perthite. CL-SEM images of this sample show that even presumably pristine microcline can contain significant replacement K-feldspar (Figures 2.13, 2.14). Overall, the range in total gas ages for all secondary K-feldspar in the Pecos valley is attributed to episodic fluid flow in fractures and breccias in basement rocks, as well as along mineral grain and sub-grain boundaries. The metasomatic overprints of each event are recorded due to the long-lived susceptibility of the basement mineralogy to intermittent alteration.

2.6.2.2. Metasomatism, deformation, and tectonism

There is an obvious association between metasomatic fluid flow and brittle structures in the Pecos River valley, particularly in the Tres Lagunas area. Most apparent are metasomatized fractures in the Pecos granodiorite, but intermittent zones of brecciated, intensely metasomatized basement collectively suggest that alteration was contemporaneous with, or post-dated deformation. Metasomatized fracture orientations are similar to average regional joint trends described by Miller et al. (1963) for the southern Sangre de Cristo Range, and include an additional east-west, variably north dipping fracture set that may or may not be unique to this particular area (Figure 2.5). While these similarities in fracture/joint orientations are interesting, they are not diagnostic in terms of the timing of deformation relative to metasomatism. Alteration fluids may have exploited this regional fabric of pre-existing brittle structures, or

alternatively metasomatism was coeval with local and regional deformation. Regardless, ca. 700-900 Ma total gas ages for secondary K-feldspar in and surrounding these fractures and brecciated areas, and lack of deformation in overlying Paleozoic rocks constrain the timing of deformation to the Neoproterozoic (or earlier).

Despite its prevalence in the Pecos River valley, K-metasomatism is not currently recognized in the breccias of the Picuris-Pecos fault several kilometers to the west (eg. Deer Creek canyon, Macho Canyon). Neoproterozoic brittle deformation in the Pecos area, and more regionally, on the Montezuma fault, however, indicates considerable tectonism during certain intervals of this time period (Melis, 2001; Sanders et al., 2006). This offers an opportunistic time for some of the documented strike-slip displacement on the Picuris-Pecos fault to occur (Miller et al., 1963; Bauer and Ralser, 1995; Erslev et al., 2004). To date, any connection between lateral displacement on the Picuris-Pecos fault and K-metasomatism in the Pecos valley remains tentative.

K-feldspar replacement of plagioclase is a significant mineralogic indicator of the chemical nature of alteration fluids and can discriminate the tectonic setting during metasomatism. Numerous studies of metasomatism have been conducted on rocks of diverse age and tectonic setting. In virtually every occurrence (rocks of any age), this style of replacement is linked to circulation of low temperature (<300°C) alkaline fluids in fault zones and intracratonic sedimentary basins (Gonterman, 1973; Kastner and Siever, 1979; Mensing and Faure, 1983; Giggenbach, 1984; Hearn and Sutter, 1985; Chapin and Lindley, 1986; Roddy et al., 1988; Duffin, 1989; Lidiak and Ceci, 1991; Dunbar et al., 1994; Leisling et al., 1995; Beratan, 1999; Davidson, 1999; Ennis et al., 1999; Warnock and van de Kamp, 1999; Rougvie and Sorensen, 2002; Liu et al., 2003).

In some of these other case studies, as for the Pecos, metasomatism lasted for tens to hundreds of millions of years (Warnock and van de Kamp, 1999; Liu et al., 2003), with multiple events taking advantage of persistent weak zones in the crust (Roddy et al., 1988; Warnock and van de Kamp, 1999).

Metasomatic fluid temperatures in the Pecos area are estimated within the general range (~280°C) based on epidote fluid inclusion trapping temperatures. Epidote chemical compositions vary in iron and aluminum content both between coexisting grains and within single grains (Figure 2.16). It is uncertain if this chemical variation represents a change in fluid chemistry with time, however, zoisite rims on some epidote grains indicate iron-poor fluids were present during either late-stage mineralization or a later hydrothermal pulse. There is a potential, therefore, that during metasomatism fluid compositions evolved to an iron-poor chemistry, possibly as the consequence of hematite and continued epidote precipitation. Fluid inclusion gas analyses for epidote and coexisting patch perthite indicate a fluid gas chemistry characteristic of an evolved crustal source (Blamey and Norman, 2002). Collectively, phase stability and alteration geochemistry in the Pecos area support a fluid regime developed in the cratonic interior not dissimilar to other K-metasomatic occurrences in North America.

The geology and association of alteration fluids with brittle deformation structures (breccias) supports a tectonic setting in which deformation and faulting increased basement permeability allowing presumably contemporaneous circulation of metasomatic fluids. This model is favored over a scenario similar to the North American mid-continent where fluid flow along the basement-sedimentary interface facilitated the development of a widespread alteration profile on the bedrock (cf. Gonterman, 1973).

This is primarily because no alteration profile is observed at the Mississippian-Precambrian unconformity in the Pecos area and the effects of metasomatism are prevalent throughout the basement with no spatial association to the paleosurface. This does not preclude development of a similar alteration profile in the Pecos area, in fact, removal of a saprolite may represent a final modification to the paleosurface prior to Mississippian sedimentation. Percolation and infiltration of basinal brines in the Devonian, in particular, could account for the similar replacement habit and ages of Pecos valley adularia and samples throughout the mid-continent (Liu et al., 2003). During Neoproterozoic metasomatism, however, basement rocks are interpreted to have been ~150°C (Sanders et al., 2006), that, assuming a geothermal gradient of 25°C/km, places the basement at around 6 km depth at this time. Therefore, fluid flow in the shallow crust along brittle features such as faults or areas of enhanced weakness and permeability is the most appropriate mechanism for K-metasomatism in the Pecos valley (Roddy et al., 1988). The geochemistry of alteration fluids is characteristic of low temperature (~280°C) evolved crustal brines also compatible with circulation along fault and fracture zones in an intracratonic setting.

The sedimentary rocks of the Neoproterozoic Chuar group in the Grand Canyon are interpreted as basin deposits related to the break-up of the Rodinian supercontinent (Dehler et al., 2001; Timmons et al., 2001). Although the distribution of sedimentation in such basins during the Neoproterozoic is unclear (Link et al., 1993; Fletcher, 2005), this tectonic environment would provide an ideal situation for both the evolution of basinal brines and fluid circulation along basin-bounding and inter-basin faults. The episodic nature of metasomatism during the Neoproterozoic suggests that the mechanism(s)

driving alteration and deformation persisted over hundreds of millions of years and is compatible with the time frame of long-lived lithospheric modification.

The timing of episodic metasomatism in the Pecos area temporally overlaps periods of tectonism documented both locally on the Montezuma fault, as well as regionally in the Grand Canyon. Based on K-feldspar MDD thermal models, Sanders et al. (2006) interpret two periods of movement on the Montezuma fault between 1000 and 800 Ma and between 750 and 600 Ma related to the assembly and break-up of the Rodinian supercontinent. Documented ca. 800 Ma extension in the Grand Canyon is also attributed to rifting of the supercontinent at this time (Timmons et al., 2001; 2005). Collectively, these limited but critical pieces of information portray a tectonically dynamic Neoproterozoic geologic history in the southwestern U.S. Perhaps not surprising then, is that although only roughly constrained, the timing of ca. 800 Ma metasomatism in the Pecos River valley is coeval with Montezuma faulting and the inferred exhumation of the Sangre de Cristo Range (Figure 2.28; Sanders et al., 2006). Ca. 700 Ma and younger Neoproterozoic metasomatic events also overlap the timing of reactivated throw on the fault. Although there is documented Ancestral Rocky and Laramide faulting, currently there is no recognized secondary K-feldspar of those ages in the Sangre de Cristo mountains. There is the potential this is being overlooked, fluid characteristics were different at these times, or the crustal depth that such replacement may have occurred at is not exposed.

Although there is no clear link between K-metasomatism in the Pecos area and faulting on the Montezuma fault or in the Grand Canyon, the ages of metasomatic overprints and deformation are suggestive that the recurrence of these ca. 800 Ma and

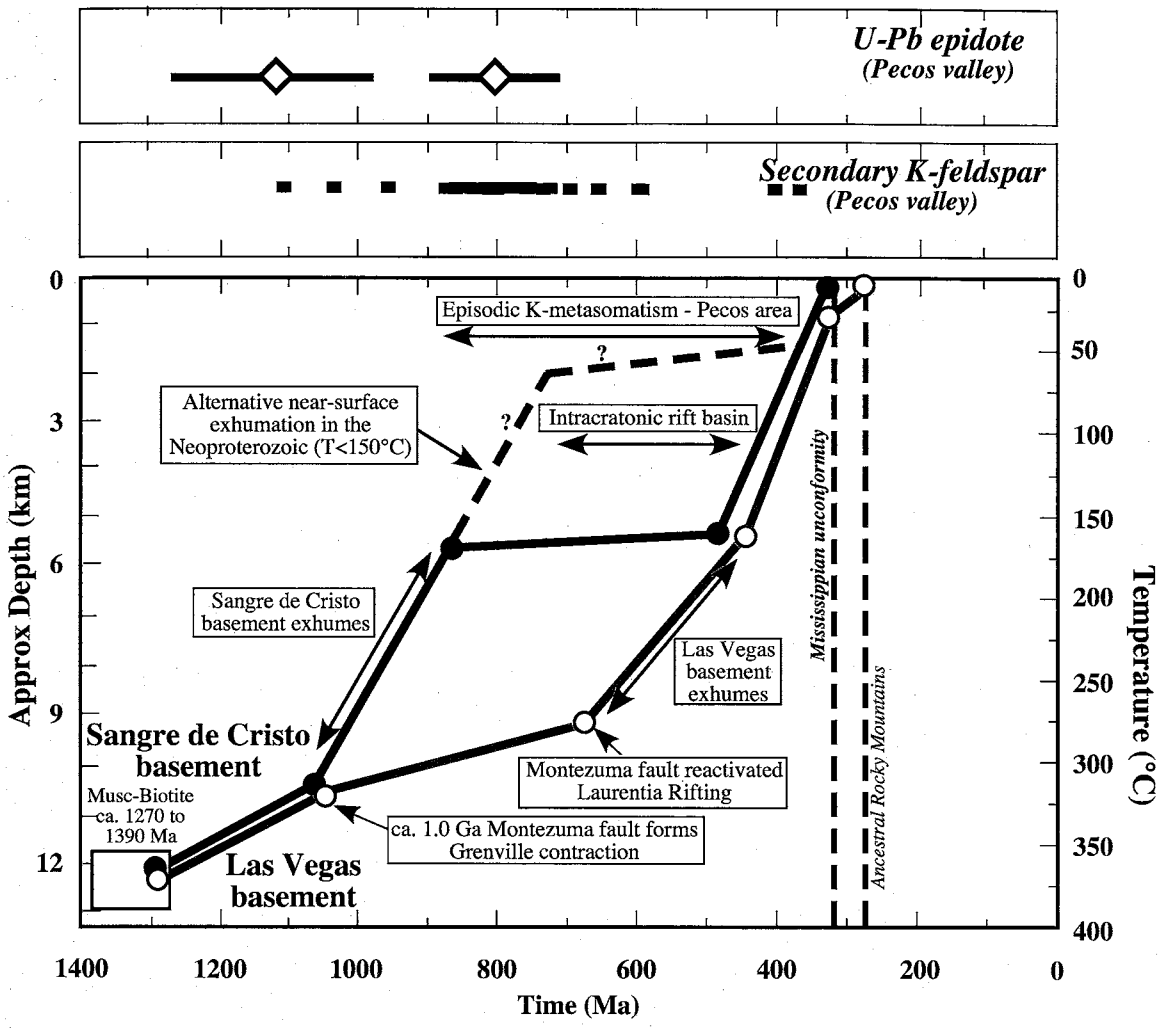

Figure 2.28: Geological exhumation history of basement rocks in the Sangre de Cristo Range and the Las Vegas basin shown with the timing of episodic epidote and secondary K-feldspar growth in the Pecos river valley. Dotted line indicates feldspar that grew before regional basement cooling and the growth ages is unknown. Epidote data include uncertainties. Divergence in cooling paths between the Sangre de Cristo and Las Vegas basement ca. 1000 Ma marks the onset of differential exhumation accommodated by the Montezuma fault zone. By ca. 850 Ma the basement rocks of the Pecos area were exhumed to a relatively shallow crustal level (T<150°C) where they were infiltrated by alkaline brines. Renewed movement on the Montezuma fault at ~750 Ma during the incipient rifting of Laurentia uplifted the Las Vegas basement relative to Sangre de Cristo rocks. Additional pulses of metasomatic fluids in the Pecos area overlap with this period of extension and rift basin development. A final documented period of metasomatism in the Devonian altered the basement prior to the final modification of the Precambrian erosional surface and Mississippian sedimentation. Geothermal gradient ~30°C/km. Adapted from Erslev et al. (2004) and Sanders et al. (2006).

700 Ma ages in the geologic record is providing a significant piece of information about the tectonic evolution of the southwestern U.S. Figure 2.29 shows the distribution of $^{40}Ar/^{39}Ar$ weighted mean ages for 47 primary and secondary K-feldspar (Table 2.7) from the Pecos valley and throughout the Sangre de Cristo Range. In some cases, age spectra had two flat segments. Because the shape of a K-feldspar age spectra is a consequence of its thermal history these flat segments are geologically significant and two weighted mean ages were calculated. It is apparent that secondary K-feldspars yield overall younger apparent ages than primary K-feldspars which is not surprising as secondary K-feldspar is a replacement phenomenon and primary K-feldspars record basement cooling ages. Of significance, however, is the number of Neoproterozoic apparent ages recorded by primary K-feldspars, and the overlap of young weighted mean ages with secondary K-feldspar ages. While secondary K-feldspars are generally dominated by Neoproterozoic ages, Figure 2.29 demonstrates that these ages are also represented in the age spectra for primary K-feldspars. This plot is not especially helpful in distinguishing the relative importance of basement cooling (through 200-300°C) in the Neoproterozoic versus reheating to 200-300°C by metasomatic fluids. However, both would be expected at 5-10 km depths as rocks were unroofed by a combination of intracratonic faulting, and reheating to 200-300°C would be active at still shallower depths of ~several kilometers in zones of weakness and extension driven fluid flux (similar to the Rio Grande Rift). Overall, the common preservation of 700-950 Ma K-feldspar ages in both primary and secondary K-feldspar in the southwestern U.S. is interpreted here as evidence for continental-scale, but likely partitioned, lithospheric extension processes (similar to Basin and Range or Rio Grande Rift) during the Neoproterozoic.

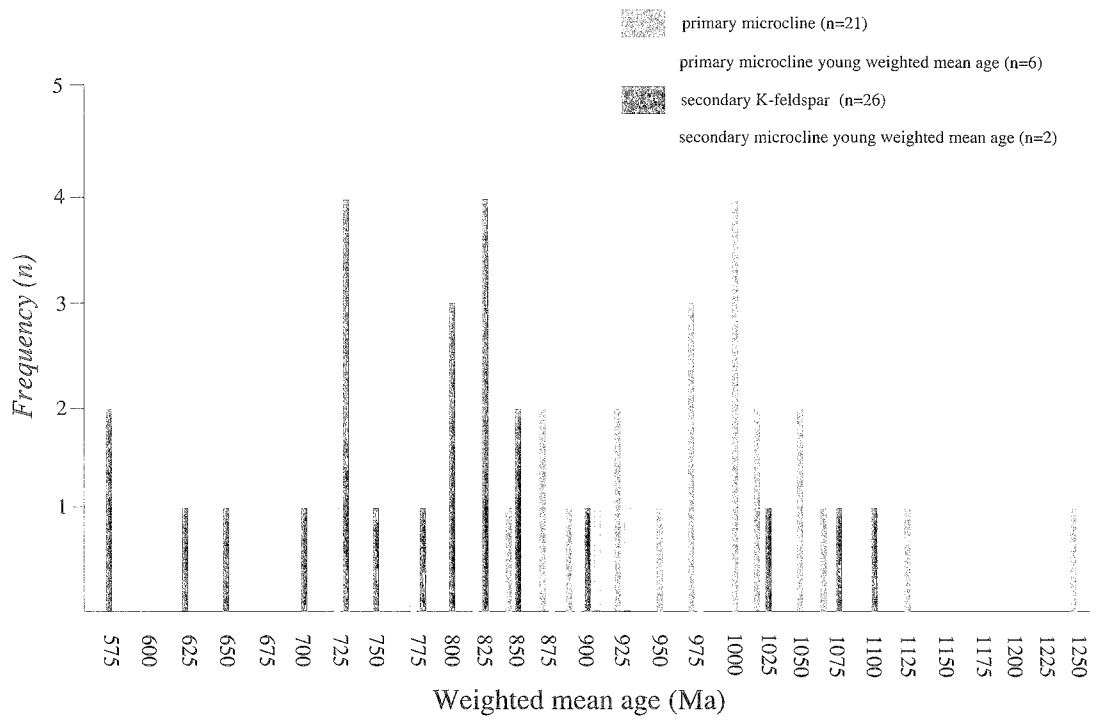

Figure 2.29: Histogram of weighted mean ages for primary (blue) and secondary (red) K-feldspar from the Pecos River valley and southern Sangre de Cristo Range. Plateau ages were assigned to the flat section(s) of the age spectra. Some spectra have two flat sections and thus two ages were calculated for a single sample. The younger of these two forced plateau ages is represented by hollow histogram bars. Overall, secondary K-feldspars are younger than ages recorded by primary microcline, and there is a greater spread in ages recorded by secondary K-feldspar than primary microcline. Ages for primary microcline (blue, hollow) overlap with secondary K-feldspar ages (red) suggesting contemporaneous metasomatism and regional tectonism in the Neoproterozoic.

Table 2.7: Compilation of ages for primary and secondary K-feldspar from the Pecos River valley and the southern Sangre de Cristo Range. The ages were calculated from the flat section(s) of the age spectra.

Sample	Steps	Forced plateau age (Ma)	%^{39}Ar
Presumed primary microcline			
ASF01-9	Y-ZK	955±12	59.5
LAMY02-1	ZA-ZT	980±10	89.8
TP02-4	ZP-ZT	1250±30	54.1
PVBR01-3	T-ZC	979±7	21.9
	ZL-ZQ	1127±15	34.0
EM02-1	W-ZG	827±3	16.6
	ZQ-ZT	1064±6	40.4
HP02-1	ZC-ZI	905±7	16.0
	ZP-ZS	1042±6	40.6
HP02-10	ZD-ZT	1001±12	92.0
LV02-2773	ZB-ZJ	730±8	32.2
	ZQ-ZT	985±8	5.3
LV02-3895	ZE-ZL	883±6	35.0
	ZQ-ZS	1085±14	10.7
LV02-4800	ZP-ZT	982±9	39.9
H03PV007d	R-Y	830±30	13.8
	ZR-ZT	1065±11	34.5
H03PV007e	ZA-ZI	948±5	27.3
WB-6	K-P	791±11	27.2
	S-W	882±15	38.5
H03PV002a	ZJ-ZT	911±9	79.8
RP-34	Z-ZC	1000±20	32.5
H03PV003a	ZN-ZT	880±20	75.4
PVBR02-28-07	AG-AM	932±10	49.6
PVBR02-28-05	B-G	870±40	70.1
PVBR06-20-22	AH-AN	1006±9	60.1
PVBR06-20-40	AC-AO	1002±9	76.4
PVBR06-20-33	AB-AK	1048±17	76.3
Secondary K-feldspar			
PVBR02-28	*V-ZT*	*861±8*	*92.8*
PVIG02-1	*ZC-ZT*	*835±16*	*86.2*
PVSDC02-18	*V-ZE*	*942±7*	*22.6*
	ZN-ZP	*1076±20*	*25.3*
RP-40B	*N-U*	*915±5*	*24.9*
	Y-ZC	*1048±11*	*25.3*
PVBR02-18	*X-ZR*	*903±7*	*82.8*
H03PV004b	*W-ZN*	*847±11*	*52.6*
PVBR02-17	*X-ZO*	*838±11*	*78.5*
PVBR02-17B	*Y-ZT*	*862±9*	*81.0*
H03PV007c	*W-ZO*	*828±9*	*87.3*
PVBR02-31	*X-ZR*	*805±13*	*86.6*
RP-90A	*K-Y*	*725±13*	*85.1*
PVSDC02-6B	*ZH-ZT*	*738±15*	*87.7*
PVBR02-7	*R-ZT*	*708±6*	*92.0*
PVHD02-1	*V-ZM*	*592±11*	*61.2*
PV03-1	*Q-ZN*	*388±2*	*80.8*
H03PV007b	*ZD-ZT*	*372±9*	*82.5*
PVBR02-28-15	*Q-AP*	*775±5*	*92.8*
PVBR02-28-13	*C-K*	*734±18*	*88.4*
PVBR06-20-12	*D-M*	*800±20*	*92.5*
PVBR06-20-44	*AJ-AO*	*1103±19*	*70.5*
PVBR04-2-03	*S-AK*	*653±7*	*20.4*
PVBR04-2-04	*G-S*	*640±20*	*92.5*
PVBR04-2-05	*G-S*	*589±18*	*90.0*
PVBR04-2-06	*K-S*	*730±20*	*92.7*
PVBR04-2-07	*N-T*	*800±40*	*81.9*
PVBR04-2-08	*H-S*	*770±20*	*89.2*

2.7 Conclusions

Characterization of replacement textures and $^{40}Ar/^{39}Ar$ analyses of secondary K-feldspar in the Pecos area provide unique insights into the tectonic history of northern New Mexico, as well as, $^{40}Ar/^{39}Ar$ K-feldspar systematics and the MDD model. Microsampling sub-grain textures such as patch perthite from a film perthite microcline is an important contribution to K-feldspar thermochronology because it has the potential to discern both regional cooling histories and subsequent fluid events. These pieces of information have to be resolved in the context of mineral growth relative to $^{40}Ar^*$ closure temperature, argon retentivities, fluid temperature, and duration of alteration. Age spectra that exhibit undulatory behavior also complicate understanding the timing of secondary K-feldspar growth. This behavior is common in age spectra from replacement K-feldspars (eg. Warnock and van de Kamp, 1999), and likely stems from a mixture of multiple generations of K-feldspar and possibly sericite. Despite these complications and caveats, microsampling and microtexture characterization is a necessary, and potentially powerful, direction for K-feldspar thermchronology, particularly in areas with complex tectonic and fluid histories.

In the Pecos River valley, Precambrian basement lithologies are overprinted by multiple K-metasomatic events that record a complex tectonic history of brittle deformation and hydrothermal alteration since the Neoproterozoic. While primary microclines yield $^{40}Ar/^{39}Ar$ age spectra consistent with inferred basement cooling during the Early Neoproterozoic (Sanders et al., 2006), secondary K-feldspars record a range of mineral growth ages that support punctuated fluid alteration in the Mesoproterozoic, at ca. 800 Ma, ca. 700 Ma, ca. 600 Ma, and ca. 400 Ma. The association of metasomatism

with fractures and breccias suggests alteration was coeval with deformation and is linked to local and regional tectonism. Secondary K-feldspar dates therefore constrain the timing of brittle deformation in the Pecos valley to the Neoproterozoic or earlier, and leave open the possibility of contemporaneous Proterozoic slip on the nearby Picuris-Pecos fault. Ca. 800 and 700 Ma secondary K-feldspar growth in the Pecos area also overlaps the inferred timing of movement on the Montezuma fault, and, in a more regional context, extensional faulting in the Grand Canyon (Timmons et al., 2005; Sanders et al., 2006). Replacement microtextures and metasomatic fluid characteristics are indicative of low temperature (<300°C), saline brines typically found in extensional basins and along faults (Chapin and Lindley, 1986; Roddy et al., 1988). Collectively, metasomatism and deformation in the Pecos, and ca. 800 Ma regional faulting, extension, and possible basin development related to the rifting of the Rodinian supercontinent support a tectonically active Neoproterozoic. The ca. 800 Ma signature seen in K-feldspar cooling ages, as secondary mineral growth, and deformation hints at a regional connection between tectonic and hydrologic processes. The recurrence of this age in the K-feldspar record is likely not coincidental, but is rather indicating that intraplate tectonism, basin development, and crustal fluid flow was prevalent in the southwestern U.S. during the Neoproterozoic.

CHAPTER 3: EVALUATION OF MICROTEXTURES AND ^{40}AR and ^{39}AR BEHAVIOR IN ALKALI FELDSPARS FROM THE KLOKKEN INTRUSION, GREENLAND: IMPLICATIONS OF SINGLE GRAIN ANALYSES AND HEAT-TREATMENT EXPERIMENTS FOR K-FELDSPAR THERMOCHRONOLOGY

3.1 Abstract

^{40}Ar/^{39}Ar analyses of multiple and single grain fragments of alkali feldspar from the Precambrian Klokken intrusion, Greenland, were conducted to evaluate the age distribution and diffusive behavior of ^{39}Ar and ^{40}Ar* in microtexturally diverse samples. Sub-milligram, single grain cryptoperthite analyses yield ages similar to the age of the intrusion whereas patch perthite sub-grains record variable ages with age spectra steps as young as ~400 Ma. Previous work proposes that young ages result from low argon retention (closure temperature ~125°C) and long-term crustal residence at about this temperature. This is not supported by laboratory derived closure temperatures, therefore a sequence of experiments involving isothermal heat treatment for up to 24 h at 650, 700, 900, 1000, and 1100°C prior to irradiation, were conducted to explore accuracy of measured kinetic parameters. Good correspondence between measured and model age spectra from multiple diffusion domain analysis of these experimental changes indicates that the laboratory derived kinetic data predict geological closure temperatures for Klokken samples that are accurate to a first order and are not anomalous relative to 100's of published K-feldspar samples. In light of the new geochronology results and establishment of robust closure temperatures, the geological history of the Klokken

intrusion is re-evaluated relative to published histories to include an Early Paleozoic low-temperature fluid modification event. Fluids that were localized within porous laminated syenite layers effectively reset the K-Ar clock of patch perthites. This event is likely connected to regional burial associated with the Caledonian orogeny. The nature of this apparent microtextural modification and its coupling to argon transport is poorly understood, but it is potentially related to the susceptibility of microporous features (i.e. nanotunnels, micropores) common to patch perthites that interact with fluids. This work indicates that further study that capitalizes on the collaborative expertise of mineralogists and argon thermochronologists has excellent potential to reveal linkages between argon transport and microtexture development.

3.2 Introduction

Early investigations into the use of plutonic alkali feldspar as a geochronometer for the K-Ar dating method demonstrated that the mineral consistently yielded younger ages than coexisting biotite, and therefore could not be used to retrieve meaningful geologic information (Dalrymple and Lanphere, 1969). Subsequent to the development of the $^{40}Ar/^{39}Ar$ technique, this behavior in K-feldspar was explained in terms of diffusive loss of $^{40}Ar^*$ as a function of argon closure in slowly cooled intrusions (Harrison and McDougall, 1982; Heizler et al., 1988). Lovera et al. (1989) refined this interpretation with recognition that the Arrhenius behavior derived from laboratory degassing of ^{39}Ar potentially contained a wealth of information about the diffusion characteristics of K-feldspar. They concluded that K-feldspar Arrhenius and age spectrum data could be explained in the context of a distribution of discrete diffusion domains, and could yield a unique thermal history for slowly cooled samples. This multiple diffusion domain (MDD) model provided the foundation for $^{40}Ar/^{39}Ar$ K-feldspar thermochronology and instigated numerous geological applications and coincident experimental evaluations of the method (see McDougall and Harrison, 1999 for an overview). Especially during the developmental phase of the MDD model, there was criticism that laboratory derived kinetic parameters could not be extracted from step-heating data and that the diffusion domains predicted by argon degassing required an observable mineralogical link. This occurred despite the fact that MDD derived thermal histories pertaining to a wide variety of geologic problems gave sensible results with other independent structural or thermometric data. In a significant way, criticisms by workers such as Parsons et al. (1988; 1999), Villa (1994, 1997); Turner and Wang (1992), Foland (1994) and Lee

(1995) drove MDD practitioners to explore issues related to diffusivity changes caused by the step-heating process, and to attempt to identify possible diffusion boundaries. Notably, companion papers by Lovera et al. (1993) and Fitz Gerald and Harrison (1993) conducted detailed experiments on MH-10 orthoclase to evaluate assumptions of the MDD method and to mineralogically identify diffusion domains. In their opinion they successfully concluded that the MDD method was robust with respect to providing laboratory derived diffusion parameters that were accurate for the natural transport of radiogenic argon and that at least some diffusion domain boundaries could be identified that matched the size and proportion predicted by MDD methods. Further work by Lovera et al. (1997 and 2002) continued to develop the method, addressed some reasons for complexity and also cautioned that not all samples yielded accurate thermal histories. It was therefore up to the researcher to be diligent in applying the method to data that did not provide good correlations between laboratory transport of ^{39}Ar and the natural transport of $^{40}Ar^*$. These efforts were somewhat unsuccessful in convincing all workers of the viability of the method, and especially Parsons et al. (1999) took exception to the use of the MDD method and claimed that none of the underlying assumptions of the model were fulfilled on the basis of mineralogical considerations.

An attempt to partially overcome the stalemate between the "Harrison camp" and the "Parsons camp" was undertaken during a visit by Ian Parsons to the Australian National University (ANU) in 2006 where Parsons was to conduct TEM investigations of K-feldspar with John Fitz Gerald and where Mark Harrison was acting director. The ANU argon laboratory choose to apply modern MDD laboratory and modeling approaches to the Klokken (a Precambrian intrusion in Greenland) alkali feldspars that

were used extensively by Parsons to challenge the MDD method. From this work it was shown by McLaren et al. (2007) that indeed the findings of Parsons et al. (1988) seemed to be correct in that application of the MDD method did not lead to sensible thermal history results. Unfortunately the work of McLaren et al. (2007) did little to advance any understanding of why the MDD approached failed to yield sensible thermal histories. It also failed to instill concern amongst MDD practitioners that the method was flawed in general.

Now, nearly exactly 20 years after Heizler et al. (1988) and Parsons et al. (1988) simultaneously argued that K-feldspar could and could not yield sensible thermal history data from laboratory derived diffusion coefficients and age spectra, a collaborative effort by them has led to this chapter that once again attempts to understand the Klokken intrusion alkali feldspars. This chapter explores the mineralogical and argon isotope systematics of Parsons et al.'s (1988) foundational alkali feldspar samples by combining expertise in mineralogy and argon systematics along with detailed microsampling methods to extract a logical linkage between feldspar age, laboratory derived closure temperature, microtexture, and geological history.

A brief introduction of the Klokken alkali feldspar mineralogy and argon systematics is warranted prior to delving into this experimental effort. Parsons et al. (1988) recognized that the different $^{40}Ar/^{39}Ar$ age spectra shapes and total gas ages correlated with microtexturally distinct feldspar. Specifically, pristine, glassy cryptoperthitic feldspar yields total gas ages consistent with the reported U-Pb zircon age of the intrusion; whereas turbid, micropore-rich, deuterically coarsened patch perthite

samples yield variably younger ages. On the basis that deuteric alteration occurred relatively soon after emplacement ($<10^5$ a), the authors concluded that patch perthite samples are young due varying degrees of $^{40}Ar^*$ loss from their inherently *leaky* crystal structure. It was further suggested that $^{40}Ar^*$ does not degas in the laboratory by the same pathways and mechanisms as it does in nature. This insinuation, if accurate, clearly nullifies the MDD method for Klokken samples and could have far reaching implications in general for the application of the $^{40}Ar/^{39}Ar$ K-feldspar thermochronology technique.

The failure of the Parson's et al. (1988) study and the subsequent MDD study by McLaren et al. (2007) to resolve differences in Klokken apparent ages is that Arrhenius plots for supposed *leaky* samples yield argon closure temperatures too high to allow radiogenic argon to escape within the constraints that the region remained below about 150°C since the Precambrian. Deuterically altered Klokken patch perthite therefore present a situation where the natural retentivity of $^{40}Ar^*$ appears substantially lower than that of nucleogenic ^{39}Ar, contrary to assumptions of the MDD model. Even if it is asserted that the Klokken region experienced a much hotter temperature history, the close spatial association of the samples coupled with their similar closure temperatures yields inconsistency that calls into question the validity of the MDD method.

Cleary there is a correct explanation for the conflicting results and, because the Klokken intrusion hosts a diverse suite of microtexturally distinct feldspar, there is the potential to investigate the apparent decoupling of ^{39}Ar and $^{40}Ar^*$ from both a mineralogical and argon perspective. The experiments in this study are designed to compare and contrast the behavior of these isotopes in Klokken samples to provide better insight into mechanisms controlling the so-called *leakiness* of patch perthite, and to

evaluate the overall suggestion that this behavior might be inherent in all K-feldspars used for thermochronology studies. $^{40}Ar/^{39}Ar$ age spectrum experiments that sample at the single crystal fragment level provide insight unachievable by previous bulk analyses and prove to be very enlightening with respect to the geochronology of the system. Also, argon experiments that focus on the relationship between transport of $^{40}Ar^*$ and ^{39}Ar in the context of observable chemical and microtextural changes are key towards developing logical conclusions about the MDD method and the Klokken thermal history. Finally, collaborative, open-minded exchange between mineralogy and argon systematics can bring about advancement in both disciplines and potentially reconcile presently opposing views.

3.3 Geology of the Klokken gabbro-syenite complex

The Klokken intrusion is one of ten Proterozoic alkalic intrusions that comprise the Gardar igneous province in south Greenland. The ages of these intrusions group into two populations indicating discrete magmatic events at ca. 1300 and ca. 1160 Ma potentially associated with a Proterozoic rift system (Upton, 1974; Upton and Emeleus, 1987). Rock types associated with the intrusions are typically syenite, gabbro, and alkalic granite that intrude basement granitic-gneiss. The Klokken stock was a shallow intrusion (≤3 km) and present lateral exposure is approximately 2.5 by 4.5 km (Parsons, 1979). A U-Pb zircon age of 1166.3±1.2 Ma (2σ) indicates that the Klokken intruded during the younger of the two Proterozoic magmatic pulses (Harper, 1988). The petrology and mineralogy of the of the intrusion has been investigated in detail by

Parsons (1979), Parsons and Butterfield (1981), Brown et al. (1983), Parsons and Becker (1987), Brown and Parsons (1988), and Parsons et al. (1988).

The intrusion is composed primarily of interlayered dark, granular syenites and white to cream-colored, laminated syenites that constitute the 650 m thick exposure (Parsons, 1979). Individual layers can be tens of meters thick and stretch laterally up to a kilometer (Parsons, 1979). Lamination in laminated syenite layers is due to the horizontal alignment of the feldspar phenocrysts (parallel to 010) that are generally elongate and can exceed 2 cm in length. Feldspar phenocrysts in the granular syenite are smaller and generally no larger than several millimeters. Laminated syenites provided conduits for fluids interpreted to be of a late-stage, deuteric origin that modified the feldspar microtextures while the granular syenites were impermeable and remained unaffected (Brown and Parsons, 1984). These microtextural modifications, and their impact on the $^{40}Ar/^{39}Ar$ system are discussed in detail below. Following emplacement, the Klokken intrusion is interpreted to have cooled to <300°C within 100,000 years, and has remained unaffected by any subsequent thermal perturbation, metamorphism, or significant deformation (Parsons et al., 1988; Burgess et al., 1992).

3.4 Prior investigations linking feldspar microtextures to argon diffusion

Application of K-feldspar thermochronology and MDD modeling to geologic problems is, in part, based on the ability to recover kinetic parameters (activation energy and D) specific to a given feldspar from step-heating data. There is generally minimal focus on sample characterization in terms of microtextures because the parameters of interest are deduced from argon degassing behavior and not from structural or textural

information. The overall conformity of activation energies extrapolated from many analyses suggests that while K-feldspar are microtexturally complex, any differential effect that textural, structural, or chemical differences have on $^{40}Ar^*$ and ^{39}Ar degassing behavior amongst samples are second order (Lovera et al., 1997). The studies discussed below represent the few that have investigated feldspar microtextures in relation to argon degassing behavior. They also investigate potential modifications to the natural degassing behavior that might be coupled to feldspar structural changes related to heating during argon extraction.

Benson Mines orthoclase was studied by Foland (1974) who concluded that the effective diffusion length-scale of this gem quality material is the physical grain size. The sample was revisited by Xu and Foland (1991) and Foland (1994) who pre-heated 127 μm diameter grain fragments at 700°C for 3 weeks prior to irradiation. When compared to unheated results, the step heating analysis of the treated sample yielded an age spectrum that was younger than the predicted spectrum modeled for argon loss at this temperature and duration. The initial diffusivities for the heated sample plotted higher on the Arrhenius diagram than the untreated sample suggesting a decrease in sample retentivity during low temperature steps as a result of the heat-treatment. The authors conclude that cracking and spallation during heating, or argon trapping at high temperature steps account for these changes and discrepancies between predicted and observed degassing behavior. Heizler et al. (1999) found a similar behavior using sanidine from the Oligocene Fish Canyon tuff. They concluded that problems with cracking and spallation were important when the physical crystal size dominated the diffusion length-scale, but also argued that this was unimportant for MDD work on

microtexturally complex K-feldspars that apparently have diffusion dimensions much smaller than commonly used grain sizes for argon analysis.

Parsons et al. (1988) analyzed bulk separates (37 to 49 mg) of microtexturally distinct alkali feldspar from the Klokken intrusion, Greenland, and found different total gas ages for different feldspar varieties that had evidently experienced the same thermal history. While cryptoperthitic feldspar yield total gas ages compatible with the reported U-Pb zircon age, the apparently deuterically altered coarse patch perthites yielded apparent ages 100's of Ma younger. This observation prompted the authors to refute the ability of $^{40}Ar/^{39}Ar$ K-feldspar thermochronology to retrieve an accurate geologic history on the basis that feldspars leak $^{40}Ar^*$, and $^{40}Ar^*$ does not behave the same in a natural environment as it does in the laboratory. Also, because cryptoperthites are retentive of argon and are composed of a myriad of perthitic and twin interfaces, they proposed that these coherent boundaries are not pathways by which argon can easily degas. The saddle-shape behavior of some Klokken age spectra is interpreted by Parsons et al. (1988) to reflect displacive changes in the feldspar structure and shearing of the silicate framework at high temperature steps. They recognize that this effect is rapid and occurs on the time-scale of a step-heating analysis unlike reported rates for cation homogenization or Al-Si disordering. Alternatively, they state that this saddle-shape can be explained by non-diffusive argon loss below 1000°C during step heating.

Burgess et al. (1992) re-evaluated the microtextures of Klokken alkali feldspars using a laser probe to determine total gas ages for particular spots within a given, microtexturally complex grain. Results corroborate Parsons et al. (1988) findings that pristine cryptoperthites record an $^{40}Ar/^{39}Ar$ age compatible with the intrusive age whereas

turbid, patch perthite are younger. Using the observed size distribution of patch perthite sub-grains (<200 nm to 1 μm) and calculated argon loss from patch perthite, Burgess et al. (1992) suggested that the young age of the patch perthites was compatible with the fine scale diffusion dimension and a geologic history that held the Klokken syenite at about 120°C since crystallization.

Microstructural changes in heat-treated orthoclase sample MH-10 were investigated by Fitz Gerald and Harrison (1993). Aliquots with a grain size of ~200 μm were heated at 750, 950 and1100°C for 71 minutes prior to irradiation. Samples were observed optically and with TEM but only minor changes to microstructures were noted. Microcracking was observed in minor deuterically coarsened areas and narrow exsolution lamellae were potentially homogenized, but the cross-hatched and tweed texture remained. The authors conclude that the heating time at this temperature was too short to cause significant microtextural modification, and that consequently, step-heating experiments that are routinely performed on a similar time-scale do not impose significant changes that would compromise laboratory derived kinetic parameters.

In a companion paper, Lovera et al. (1993) addressed changes in kinetic properties of the same heat-treated MH-10 K-feldspars. In short, they reported that heating to 750°C decreased the initial D/r^2 by a factor of 3 relative to unheated data, and increased the activation energy from 48 to 54 kcal/mol. Similar results were found for the 950 and 1100°C heat-treated samples, except that the very initial D/r^2 values were less than those given by unheated samples. These heat-treatment experiments, along with crushing and special irradiation experiments led Lovera et al. (1993) to conclude that

there is very minor consequences of heating towards the ability to link ^{39}Ar behavior in the laboratory to the natural transport of $^{40}Ar^*$.

A very significant advancement in reconciling multiple diffusion domains with microtextural features come from the work of Fitz Gerald et al. (2006). Their study on sub-solvus microcline from the Shap granite, United Kingdom, identified pull-apart defects and nanotunnels at the TEM scale in optically pristine samples. Nanotunnels are fluid coarsened defects that originally form due to strain between the albite and K-feldspar interface. Heat-treatment of these samples (600 and 1000°C; 148 to 5748 hours) showed that the albite lamellae chemically homogenized but the nanotunnels persisted as did the twin and tweed textures. Fitzgerald et al. (2006) concluded, that, while cation diffusion occurs rapidly within the time frame and temperature range of a typical argon step heating experiments, microtextures associated with the Si, Al-O framework can persist to high temperatures. This work provided strong evidence that multiple diffusion domain behavior for K-feldspar could be directly linked to the ubiquitous occurrence of nanotunnels and because the nanotunnels were stable during step heating could provide both natural and laboratory pathways for argon transport.

3.5 Analytical techniques

3.5.1 Microprobe imaging and qualitative analysis

Electron microprobe imaging was conducted at the New Mexico Institute of Mining and Technology on a three-spectrometer Cameca SX-100 microprobe. Backscattered electron (BSE) and scanning electron (SEM) images of polished grain mounts and unpolished grains were collected. Qualitative X-ray chemical lines cans

were conducted on selected polished grains using either a 10 μm or a 1 μm diameter 20 nA beam with an accelerating voltage of 15kV. In preparation for SEM imaging, unpolished grain mounts were mounted on double-sided carbon tape on an aluminum disk and etched over a tray of 40 mL 48-51% HF acid at 2 cm height for 20 seconds after techniques of Waldron et al. (1994). Samples were gently rinsed with deionized water and dried prior to a light carbon coating.

3.5.2 $^{40}Ar/^{39}Ar$ Geochronology

3.5.2.1 Sample preparation

Four samples of the Klokken syenite were investigated that include two cryptoperthite-bearing granular units (140182, 140115) and two patch perthite-bearing laminated units (43738, 140025). Samples were crushed in a mortar and pestle and sieved to obtain monomineralic grain fractions typically between 32 and 80 mesh, magnetically separated, and treated with heavy liquids to concentrate the alkali feldspar. The low-density fraction (<2.58g/cm^3) was rinsed and hand picked under a binocular microscope to obtain grain fragments (also referred to simply as grains) void of biotite, hornblende, or inclusions. Biotite and hornblende were separated from the magnetic fraction. Following imaging, grains of interest were removed, weighed, and placed in 24-hole aluminum disks with Fish Canyon sanidine in a known geometry. Bulk separates were weighed and wrapped in copper foil before being loaded into machined aluminum disks which were stacked vertically for irradiation.

3.5.2.2 Mass spectrometer parameters

Argon isotopes were analyzed with a MAP 215-50 mass spectrometer equipped with a Blazers 217 electron multiplier operating in static mode with a Nier source. The multipliers are typically operated to yield a gain of about 10,000 above the Faraday and resolution at 5% peak-height at mass 40 was about 450. Analyses were conducted between May and November 2007 and mass spectrometer sensitivity, discrimination, interfering reaction correction factors, irradiation time, and extraction line and total system blanks are presented Appendix Table A2.3. Detailed description of analytical methods can be found in the New Mexico Bureau of Geology and Mineral Resources open file report OF-AR-1 at http://geoinfo.nmt.edu/publications/openfile/argon/home.html.

3.5.2.3 Furnace step heating

Samples were step heated in a double vacuum molybdenum resistance furnace. K-feldspar separates wrapped in Cu-foil were heated with high resolution (~45 steps) heating schedules, and isothermal steps were conducted to help evaluate excess argon contamination (e.g. Harrison et al., 1993). Single-grain K-feldspar were heated using either non-isothermal, abbreviated (11-16 steps) heating schedules, or long (up to 41 steps), isothermal schedules depending on the mass of the grains. Shorter (8 steps) heating schedules were used for hornblende and biotite analyses. Gas released reacted with a SAES GP-50 getter operating at ~450°C during heating followed by a second stage of clean up using 2 SAES GP-50 getters (one at 20°C, one at ~450°C) and a tungsten filament operated at ~2000°C. Typically, K-feldspar steps were gettered for 2

minutes. The furnace thermocouple was calibrated by melting Cu-foil and true sample temperature was between 35 and 100°C lower than thermocouple temperature. Heating schedules were adjusted by this amount, and corrected sample temperatures are reported. Furnace blank and mass spectrometer background values were determined by running a 15 minute, 650 to 800°C hot blank prior to each analysis.

3.5.2.4 Irradiations, flux monitoring, and age calculations

Samples were irradiated in machined aluminum disks at the USGS Triga reactor in Denver, CO. Fluence gradients were measured using Fish Canyon sanidine placed in holes of known geometry in the aluminum disks. Typically, 4 single crystals from each position were analyzed to determine the J-value. Mean values for each location were fit with a plane function or were interpolated from adjacent locations to derive J-values for unknowns with an estimated precision of 0.1 to 0.2% (1σ). Correction factors for interfering reactions were measured using CaF_2 and K-glass included with the samples during irradiation. Four to five grains of each are typically fused to obtain a weighted mean value for each factor. Total gas ages and errors are calculated by quadratically summing isotopic measurements for all steps. The assigned age of Fish Canyon sanidine is 28.27 Ma and the total ^{40}K decay constant is 5.476e-10/a (Kwon et al., 2002). At present there is no accepted value for the age of FC sanidine (Renne et al., 1998; Lanphere et al., 2001), however there as been considerable recent work towards determining and evaluating the monitor age and ^{40}K decay constants (Min et al., 2000; Kwon et al., 2002, Kuipper et al., 2008).

3.5.3. Heat-treatment methods

Alkali feldspar aliquots from cryptoperthite sample 140182 and predominantly patch perthite samples 43738 and 140025 were preheated under vacuum prior to irradiation in the same furnace used for age spectrum experiments. The low-density mineral separate fractions of Klokken samples were weighed, wrapped in Cu-packets, and weighed again as a means of sample identification in the case identifying markings are obscured by the heating process. The samples heated to 1100°C were wrapped in graphite foil. Packets were loaded into a cylindrical Mo-crucible liner 1.4 cm in diameter, stacked tightly to a height of ~8 mm attempting to minimize any vertical temperature gradient. A small piece of copper foil capped the samples to hold them in place and then the liner was inserted into the crucible, pumped down and readied for sample degassing. The furnace thermocouple was calibrated by copper foil melting tests, and observed in real-time by video to correct for the insulating effect of the crucible and liner relative to the position of the thermocouple. Heating schedules were adjusted accordingly based on the calculated temperature offset from the melting point of Cu (1084.5°C). Reproducibility of two Cu foil calibration tests was within 3°C with a calculated offset of -50°C. Degassing experiments used manual operation of the temperature control to ensure no overshoot of the target temperature and also to minimize the time necessary to achieve the temperature set point. Samples were heated at 650°C for 14 h, 700°C for 24 h and at 900°C, 1000°C, and 1100°C all for 4 h. After heating, samples were removed from foil packets and grains were selected for BSE imaging and $^{40}Ar/^{39}Ar$ analysis.

3.6 Results

3.6.1 Description of feldspar samples

Four hand samples of syenite from the Klokken intrusion, Greenland, were acquired from I. Parsons at the University of Edinburgh, U.K., and belong to the same suite of samples analyzed in Parsons et al. (1988). Samples 140182 and 140115 are granular syenites that contain pristine cryptoperthitic alkali feldspar, and samples 43738 and 140025 are laminated syenites with a variable mixture of cryptoperthite and turbid patch perthite. All sample numbers correspond to the Grønlands Geologiske Undersøgelse (GGU) archive collection that these rocks belong to. The feldspar compositions and microtextures have been well documented and imaged petrographically, by electron microprobe, and with transmission electron microscopy (Brown et al., 1983; Brown and Parsons, 1984; Brown and Parsons, 1988; Parsons et al., 1988; Burgess et al., 1992; Lee et al., 2007).

3.6.1.1 Cryptoperthites

Samples 140182 and 140115 are medium to fine-grained, gray-black granular syenites that contain pristine, glass-clear, cryptoperthitic feldspar (Figure 3.1). Feldspar grains are slightly yellow and resemble sanidine in appearance. BSE images of polished grains are generally featureless with the exception of minor patch perthite in occasional grain fragments (Figure 3.2). BSE images of HF-etched, unpolished grains show the distinctive diamond-mesh pattern characteristic of braid cryptoperthite (Figure 3.3). At the TEM scale, the braid cryptoperthite consists of a mosaic of diamond-shaped lozenges of twinned albite ~60 to 200 nm in length that are separated by zigzag bands of low

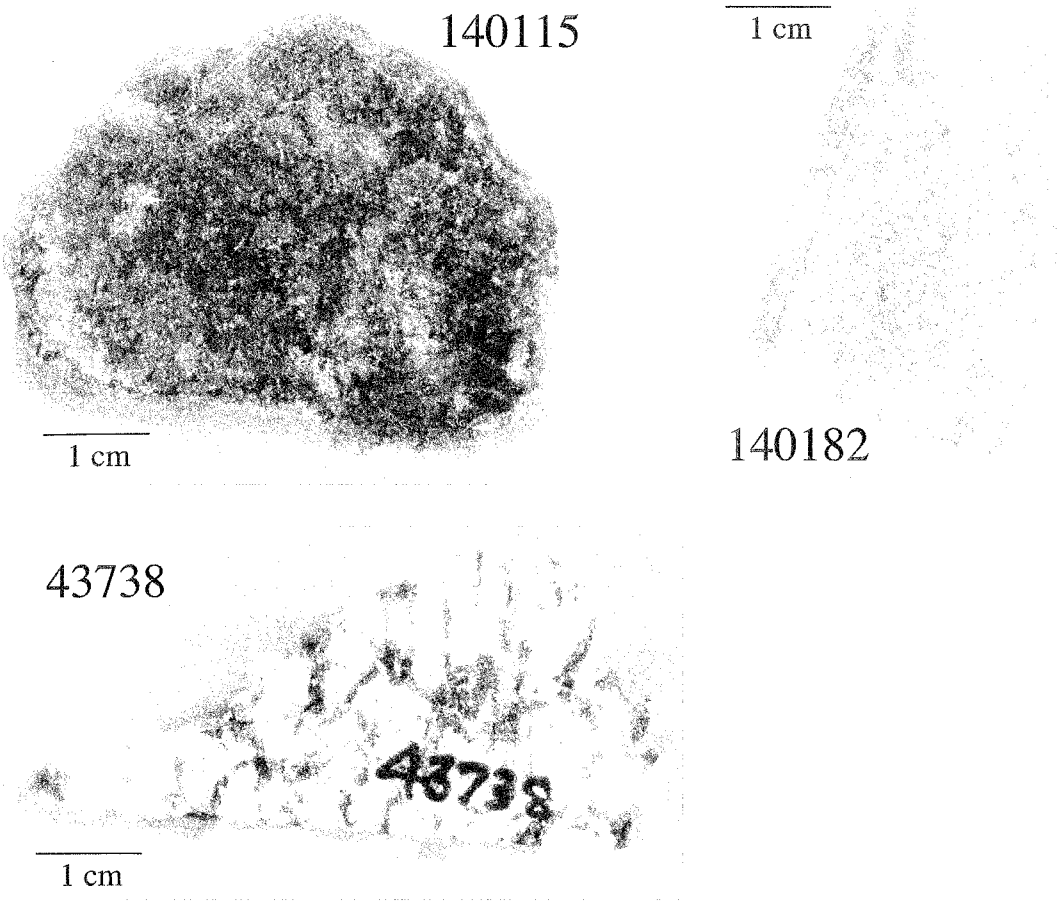

Figure 3.1: Scanned slabs of Klokken granular syenite samples 140182 and 140115, and layered syenite samples 43738 and 140025.

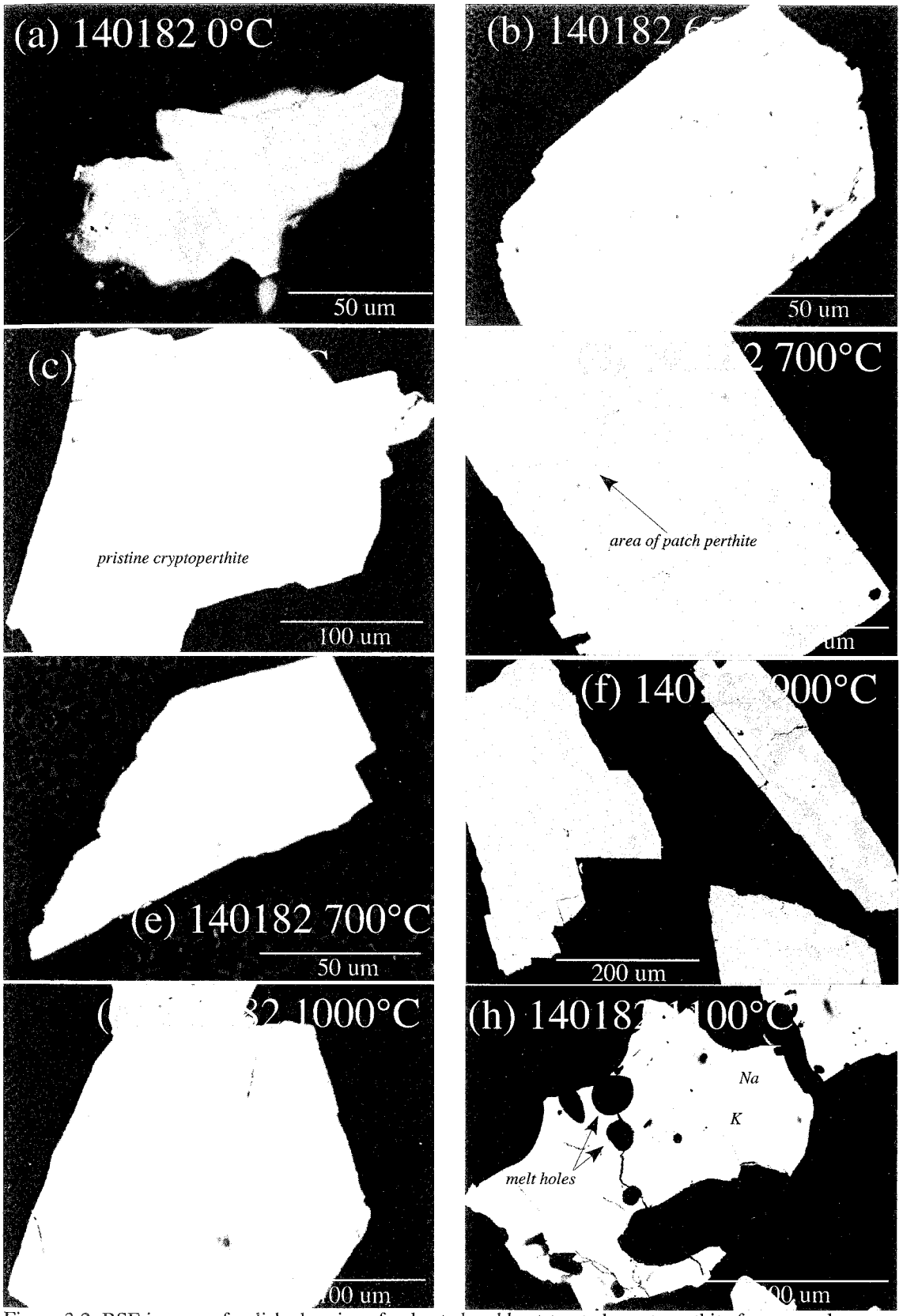

Figure 3.2: BSE images of polished grains of unheated and heat-treated cryptoperthite from sample 140182. Little change is seen in pristine samples with heating to 1000°C. At 1100°C melt holes and sample fusing occurs, but patch perthite areas are still not completely homogenized.

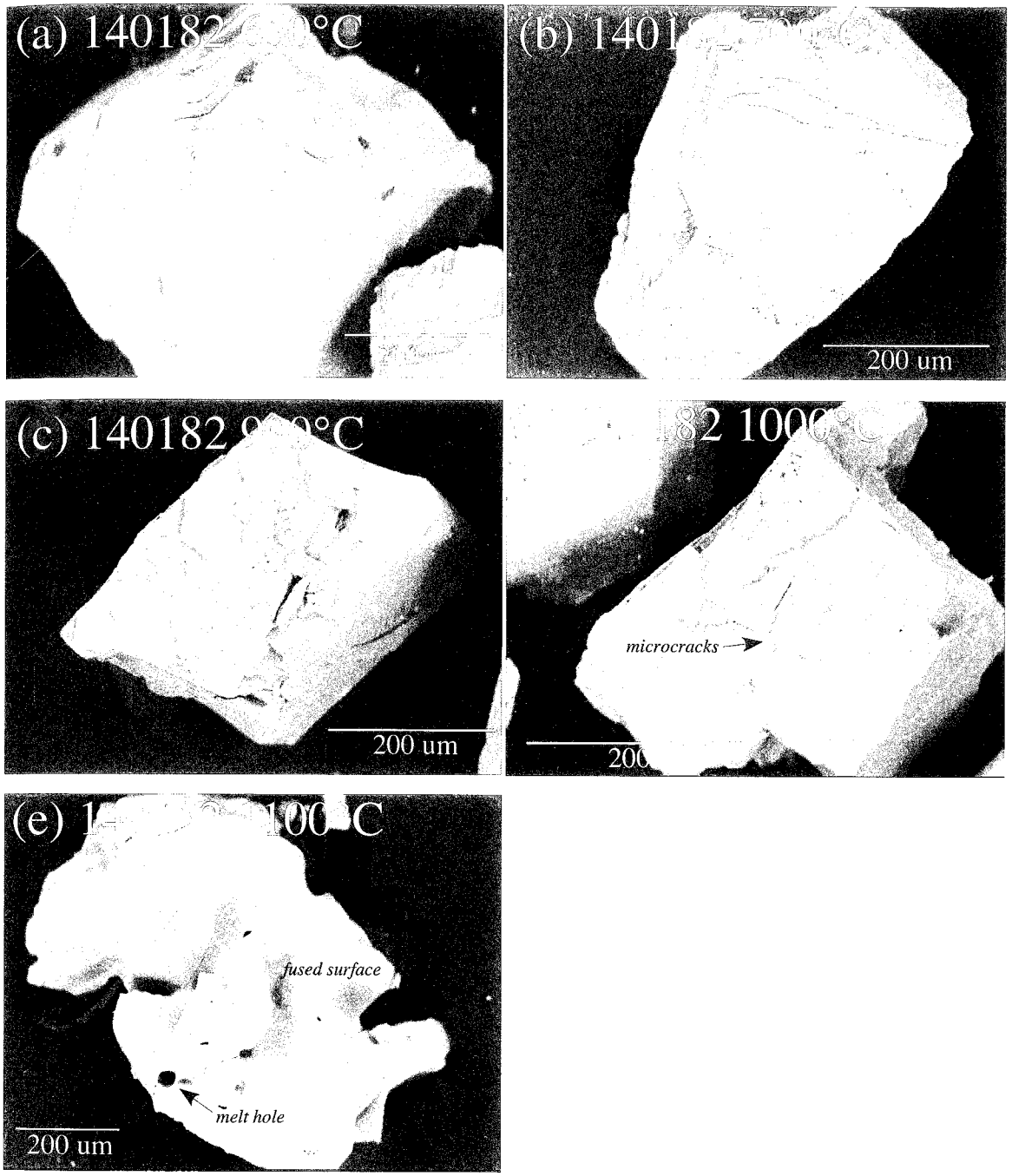

Figure 3.3. BSE images of heat-treated, etched cryptoperthite grains from sample 140182. Little change is observed in samples heated to 1000°C with the exception of minor cracking (d). 1100°C heating caused significant melting and fused surfaces.

microcline (Figure 3.4; Parsons et al., 1988). The braid habit forms in feldspar with compositions between $Ab_{80}Or_{20}$ and $Ab_{30}Or_{70}$ as intergrowths orient to minimize the elastic strain energies at the lamellar interfaces (Willaime and Brown, 1974; Parsons and Brown, 1984). Ultimately, elastic strain energy results from the different unit cell dimensions of adjacent K-feldspar and albite intergrowths in exsolved feldspar (Parsons and Brown, 1984). Because strain energies develop during the crystallization and cooling of alkali feldspar, preservation of cryptoperthitic microtextures indicates the crystalline structure has not been affected by deformation or hydrothermal alteration subsequent to the initial emplacement and cooling (Parsons et al., 1988). Bulk compositions for feldspars from samples 140182 and 140115 are $Ab_{55.3}An_{2.8}Or_{41.9}$ and $Ab_{56.5}An_{2.0}Or_{41.5}$, respectively, as reported in Parsons et al. (1988).

3.6.1.2 Patch perthites

Samples 43738 and 140025 are microtexturally more complex than the cryptoperthite samples, and contain variable mixtures of crypto- and patch perthite subgrains. Both samples are variably white and opaque due to areas of considerable turbidity caused by micropores resulting from the alteration of the cryptoperthite to albite and microcline sub-grains. This modification is believed to have occurred within $\sim 10^5$ years after emplacement as a result of deuteric fluid circulation in the laminated syenite layers of the intrusive body while granular syenites remained unaffected (Parsons et al., 1988). The replacement of cryptoperthite by patch perthite sub-grains occurs in the presence of fluid by a process known as an *un-zipping reaction* (cf. Brown and Parsons, 1984). As fluids infiltrate sub-grain boundaries and grain interiors, dissolution-

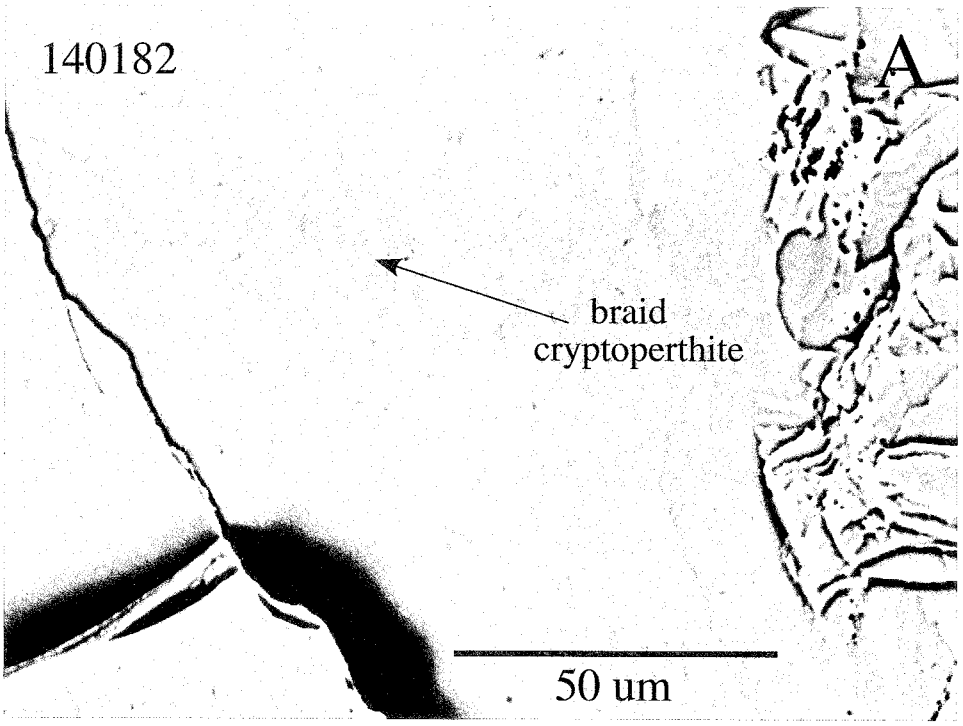

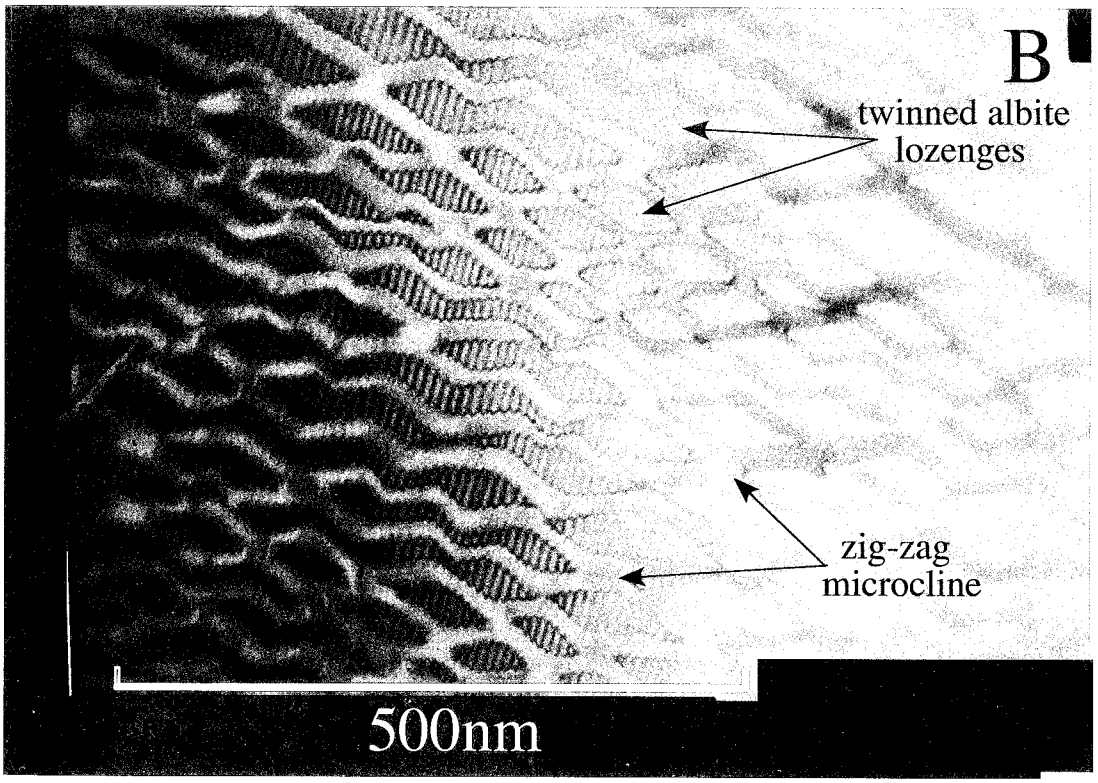

Figure 3.4: BSE and TEM images of Klokken braid cryptoperthite. The upper image (A) shows the subtle braid pattern relief on an etched grain fragment of sample 140182. TEM image (B) shows the sub-micron architecture of the braid perthite is composed of twinned albite lozenges separated by zig-zag bands of microcline.

reprecipitation reactions are driven by the release of elastic strain energy at lamellar interfaces. This results in the reorganization of the feldspar structure to the lower-energy patch perthite state and an overall coarsening of the microtextures. The temperature of deuteric fluids are estimated to have been <450°C (Brown and Parsons, 1984).

Individual patches of albite and microcline are irregular and range in diameter from <200 nm up to ~100 μm in turbid Klokken feldspars (Brown and Parsons, 1984; Burgess et al., 1992). BSE images of HF vapor etched, unpolished grain mounts of samples 43738 and 140025 show areas of pitted patch perthite and remnant zones of the primary cryptoperthite microtextures (Figure 3.5). Figure 3.5a shows patch perthite and albite with twinning in sample 43738. Similar patch perthite with remnant primary braid cryptoperthite is seen in 140025 (Figure 3.5b). The bulk composition for sample 140025 is $Ab_{66.9}\,An_{1.0}\,Or_{32.1}$ (Parsons et al., 1988). The composition of 43738 has not been determined, but is estimated by Parsons et al. (1988) to be between $Ab_{66.9}\,An_{1.0}\,Or_{32.1}$ and $Ab_{56.4}An_{0.5}Or_{43.1}$.

3.6.1.3 Heat-treated feldspar

Following heat treatment, grains were selected from the different temperature runs from samples 140182, 43738, and 140025 and were either mounted on carbon tape and HF vapor etched, or set in epoxy and polished for BSE imaging in order to visually evaluate any physical and chemical changes that occurred during heating. Representative grains from each experiment are shown in Figures 3.2, 3.3, 3.6, 3.7, 3.8, and 3.9.

Etched grains from the 650 to 1000°C aliquots for pristine cryptoperthite sample 140182 show little noticeable effects from heating with the possible exception of rare

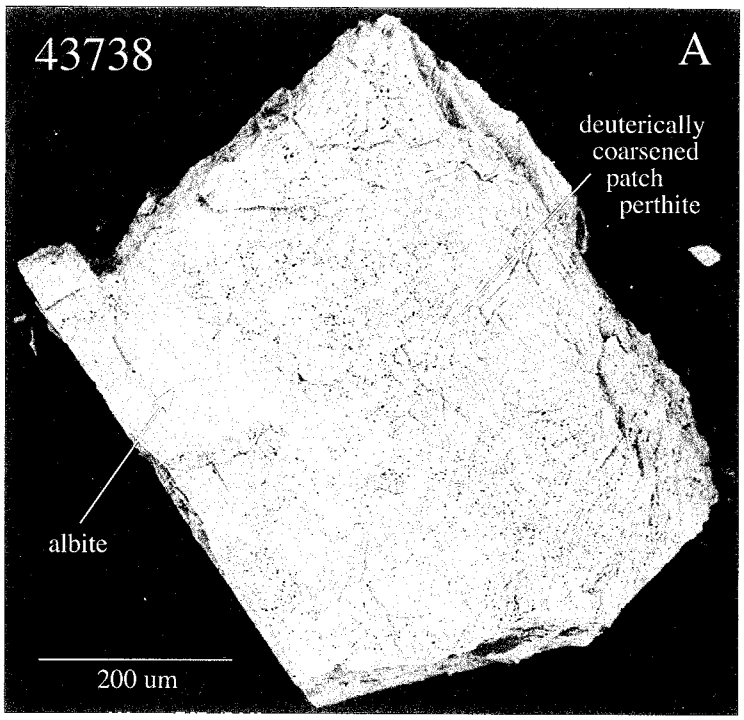

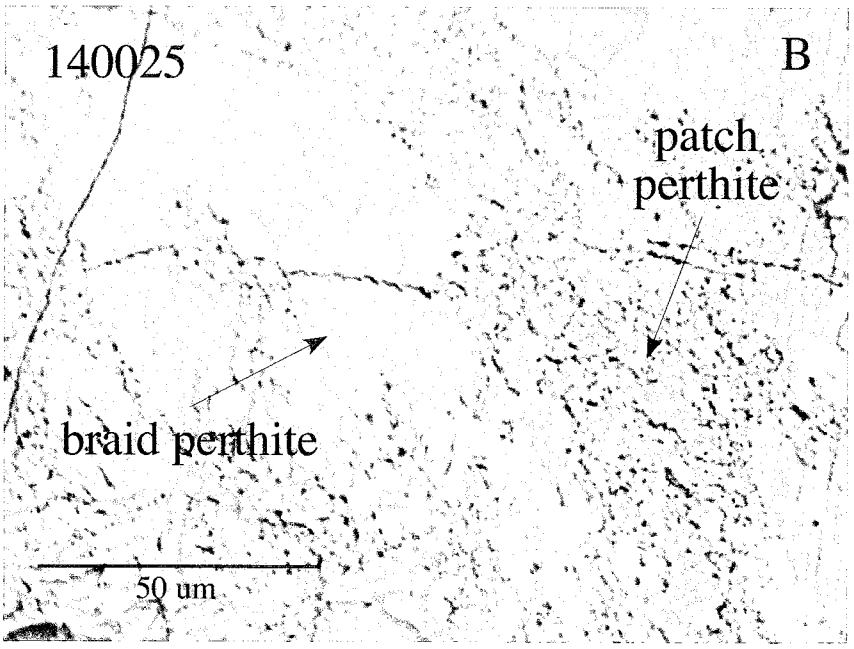

Figure 3.5: BSE images of etched grains of samples 43738 (A) and 140025 (B). Sample 43738 shows subtle albite twins on pristine albite and areas of microporous patch perthite. Sample 140025 has areas of remnant, pristine braid perthite with porous patch perthite.

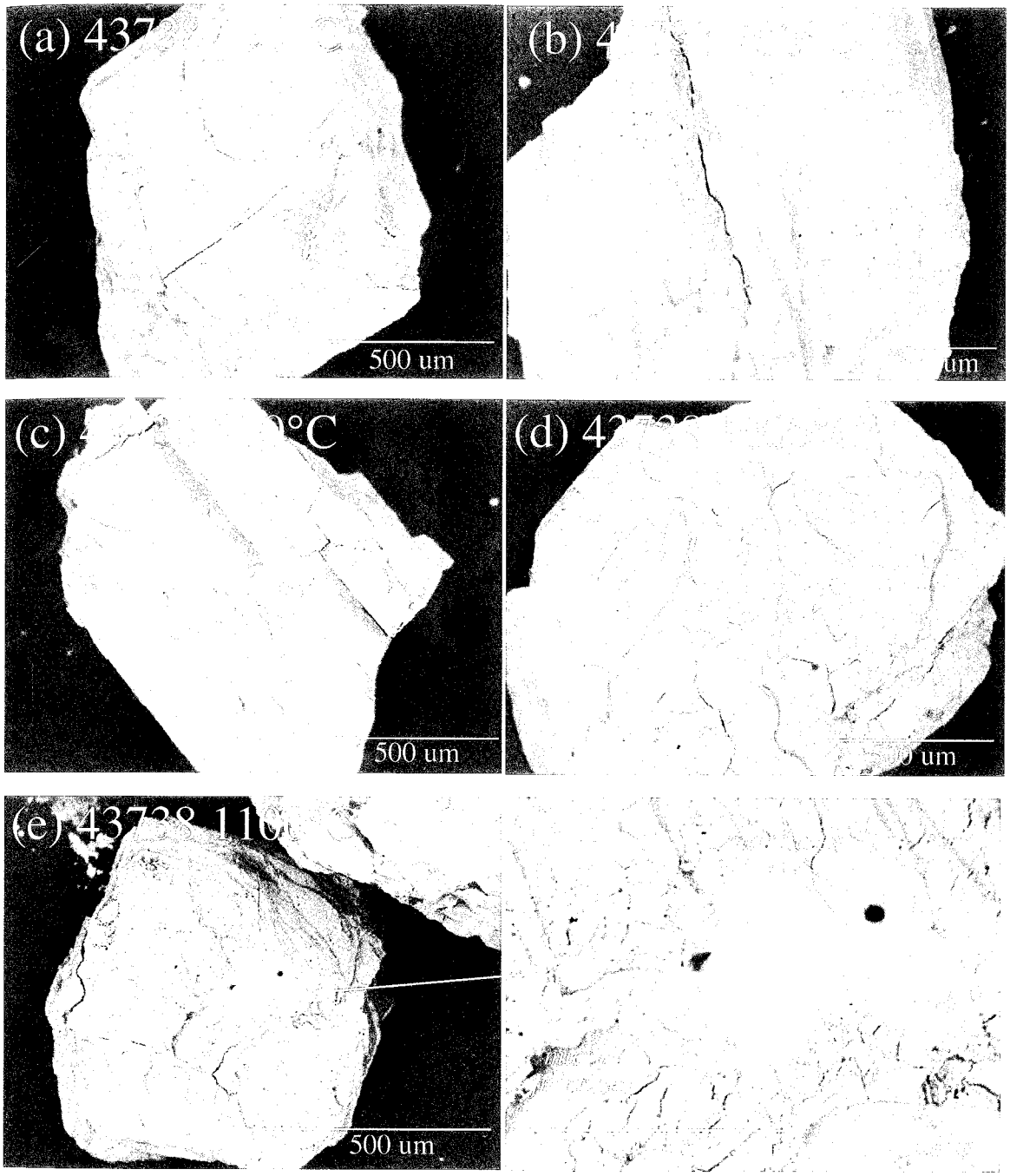

Figure 3.6: BSE images of heat-treated, etched patch perthite grains from sample 43738. The patch perthite texture is relatively unaffected by heating to 650°C or 700°C as shown by the visible chemical contrast (mean z; a,b). This contrast becomes progressively more faint at 900°C and 1000°C (c,d) and has disappeared by 1100°C (e). Microfractures in patch perthite, melt holes, and glass extruded from melt holes also form by 1100°C, but albite twinning remains unaffected.

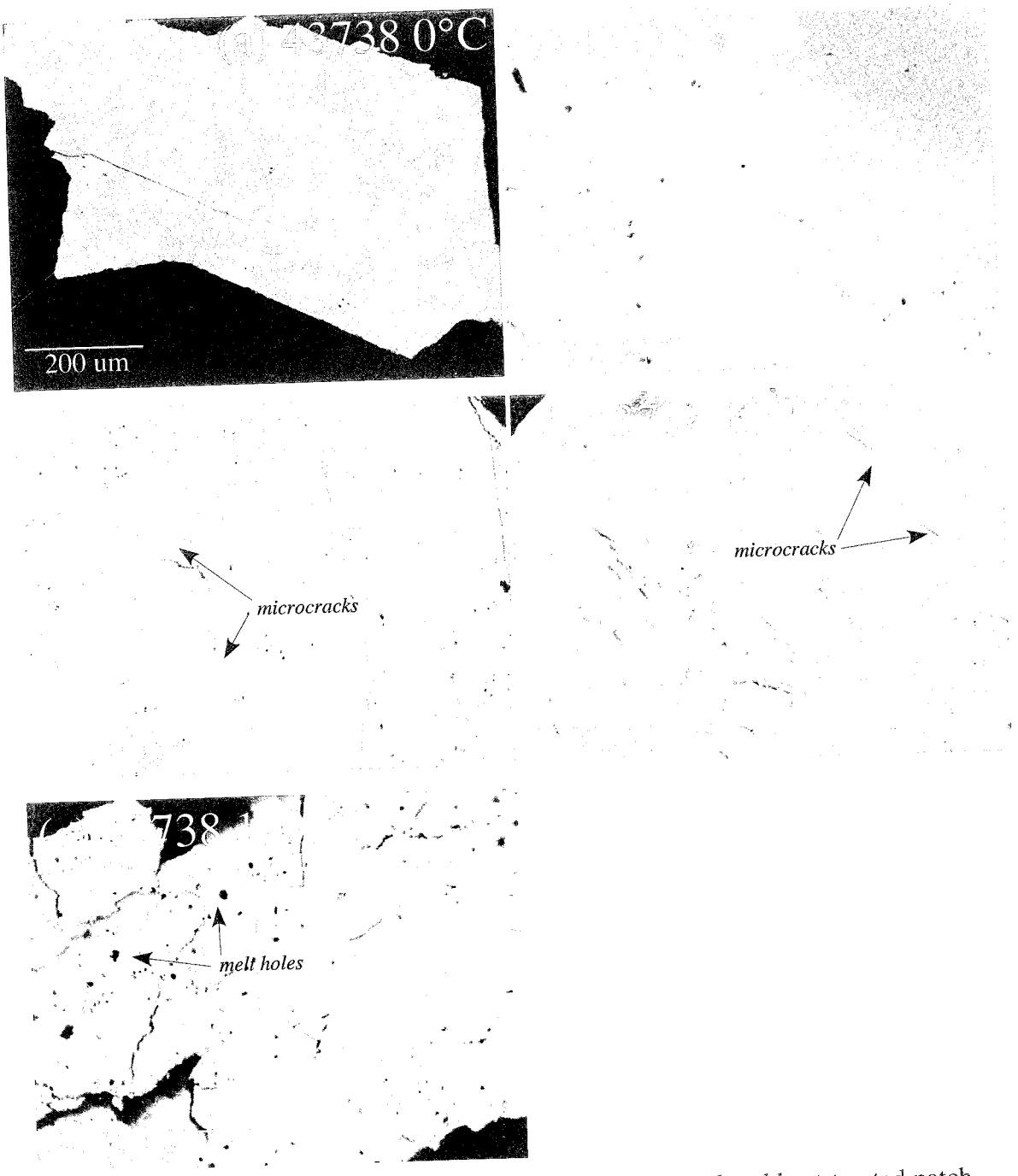

Figure 3.7: BSE images of polished grain mounts of unheated and heat-treated patch perthite from sample 43738. The patch perthite texture becomes less distinct with increased heating temperature as the K and Na phases chemically homogenize. Microcracks are observed in the sample heated to 900°C (c). Abundant melt holes form by 1100°C, although the sample failed to completely homogenize at this temperature (e).

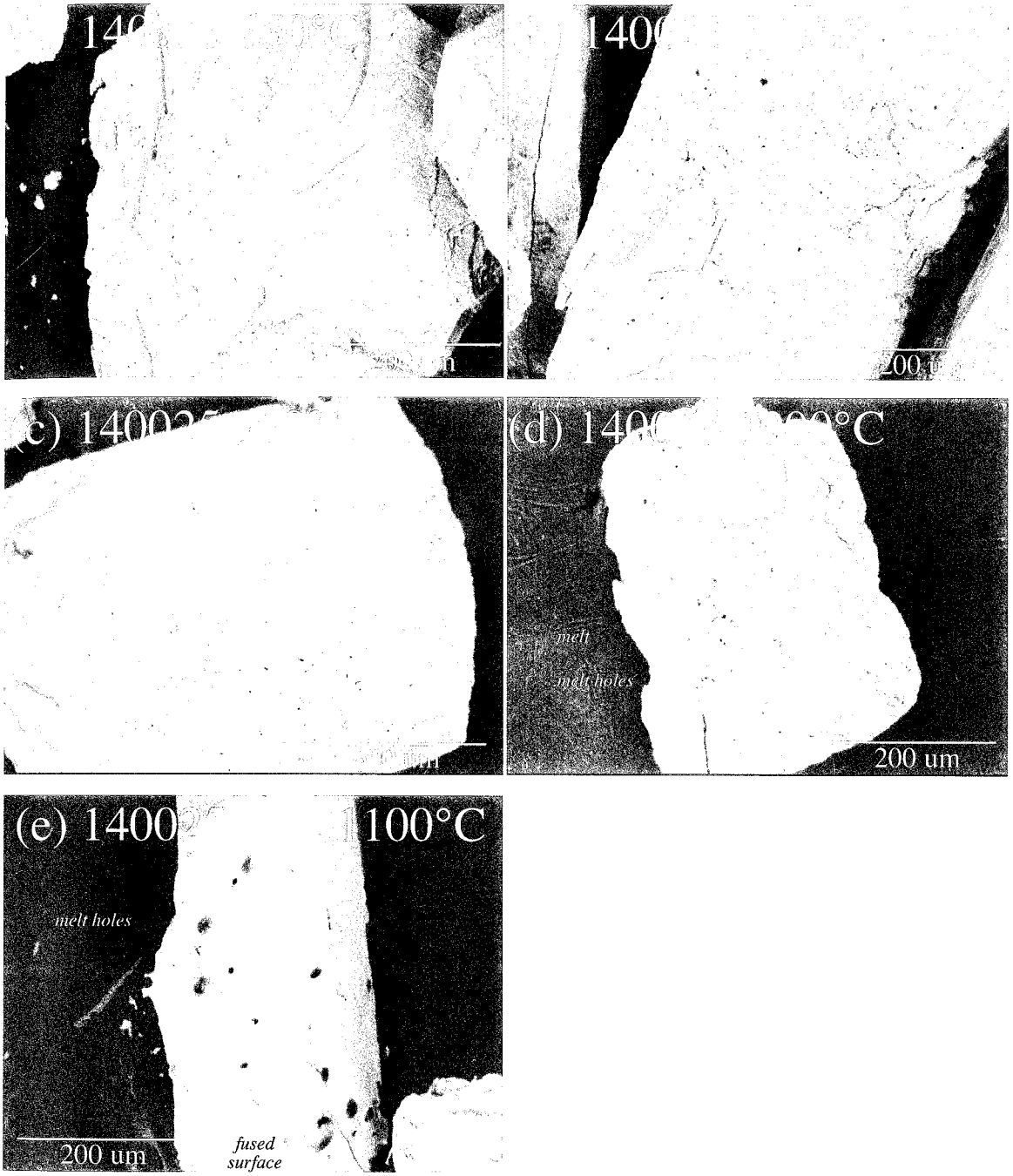

Figure 3.8. BSE images of heat-treated, etched patch perthite grains from sample 140025. The patch perthite texture progressively disappears with increased heating (a,b,c) and is no longer visible in a sample heated to 1000°C (d). Glass melt and melt holes form by 1000°C (d). The sample heated to 1100°C has large melt-gas holes that form crater-like features on the surface of an otherwise generally featureless, fused surface (e).

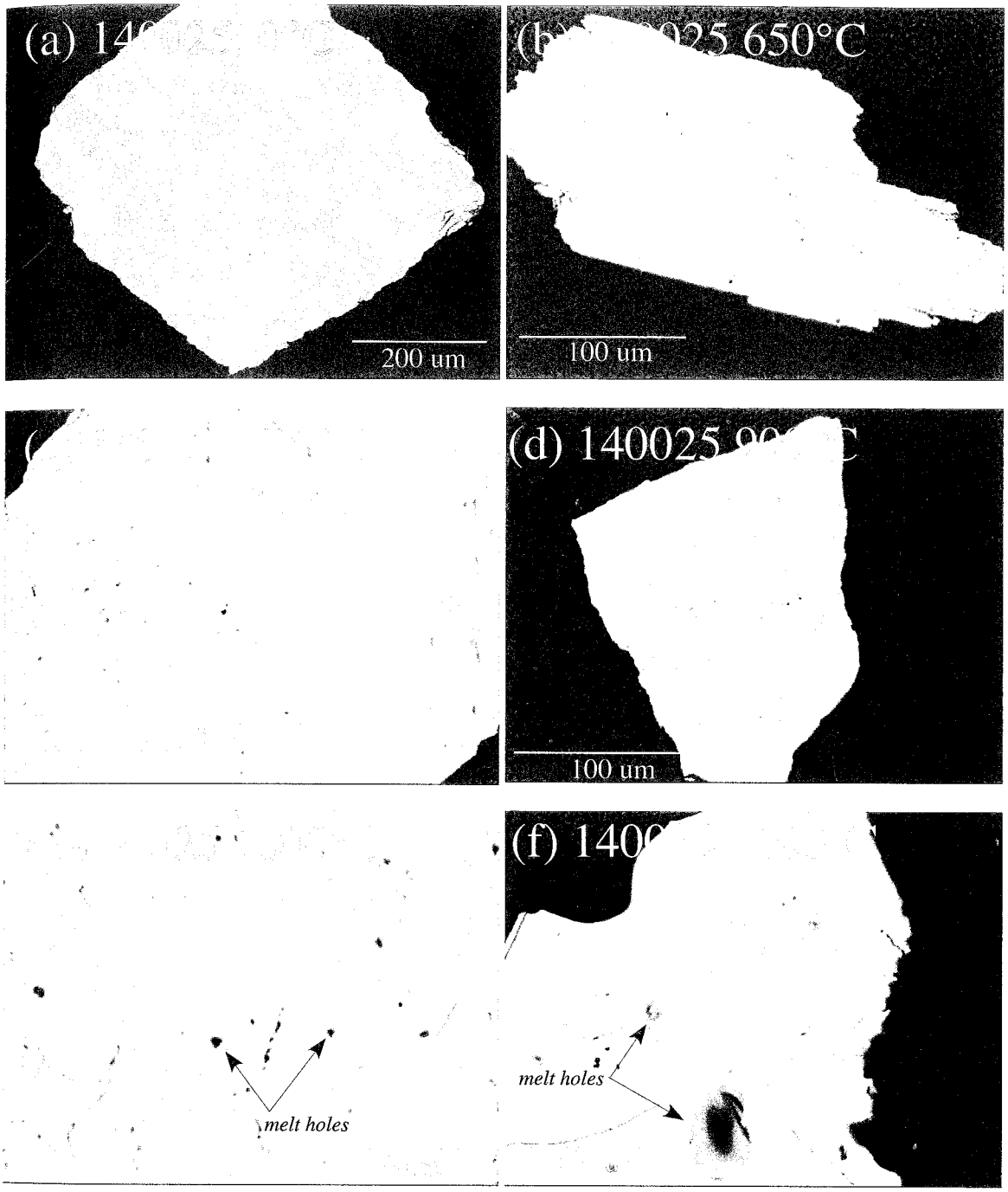

Figure 3.9: BSE images of polished grain mounts of unheated and heat-treated patch perthite from sample 140025. The sample has homogenized significantly by 1000°C (e), but still does not achieve complete homogenization even at 1100°C (f). Melt holes are visible in the grains heated to 1000°C and 1100°C (e,f).

microfractures in the 1000°C sample (Figure 3.3a-d). The 1100°C heating sample is remarkably different and grains are melted and fused together with open pits that resemble microfumeroles or melt holes that have bubbled and extruded a glassy, transparent melt (Figure 3.3e). The surface appears reflective and glassy due to melting. Polished grain mounts of this sample are generally featureless with the exception of minor patch perthite areas. Rounded, hollow melt holes, glass in some melt holes, and microfractures are seen in the 1100°C heat-treated sample.

Etched grain mounts of patch perthite sample 43738 show that the patch perthite microtexture persists through the 650, 700, and 900°C heating experiments, although the visual contrast in chemical compositions (mean z) in BSE images decreases progressively with higher temperature heat-treatment. The 1000°C heat-treated sample preserves little evidence of any chemical heterogeneity and is significantly cracked along cleavage planes, and grain boundaries, particularly in the patch perthite areas (Figures 3.7d, 3.10). The sample shows only the initial signs of incongruent melting at 1100°C indicated by small glassy flows extruded from melt holes (Figure 3.6e, f). Polished grains show a similar progressive homogenization of the initial chemical contrast with increasing heat-treatment temperature (Figures 3.7). There is significant cracking by 900°C, again primarily focused along cleavage planes but more frequently within areas of patch perthite (Figure 3.7c). The 1100°C treated sample has numerous small melt holes but still shows the sample is not completely homogenized (Figure 3.7e).

Etched grains of mixed cryptoperthite and patch perthite sample 140025 also show a gradual homogenization of albite and K-feldspar between 650°C and 900°C, and any chemical variation is gone by 1000°C (Figure 3.8). Some microfractures are seen in

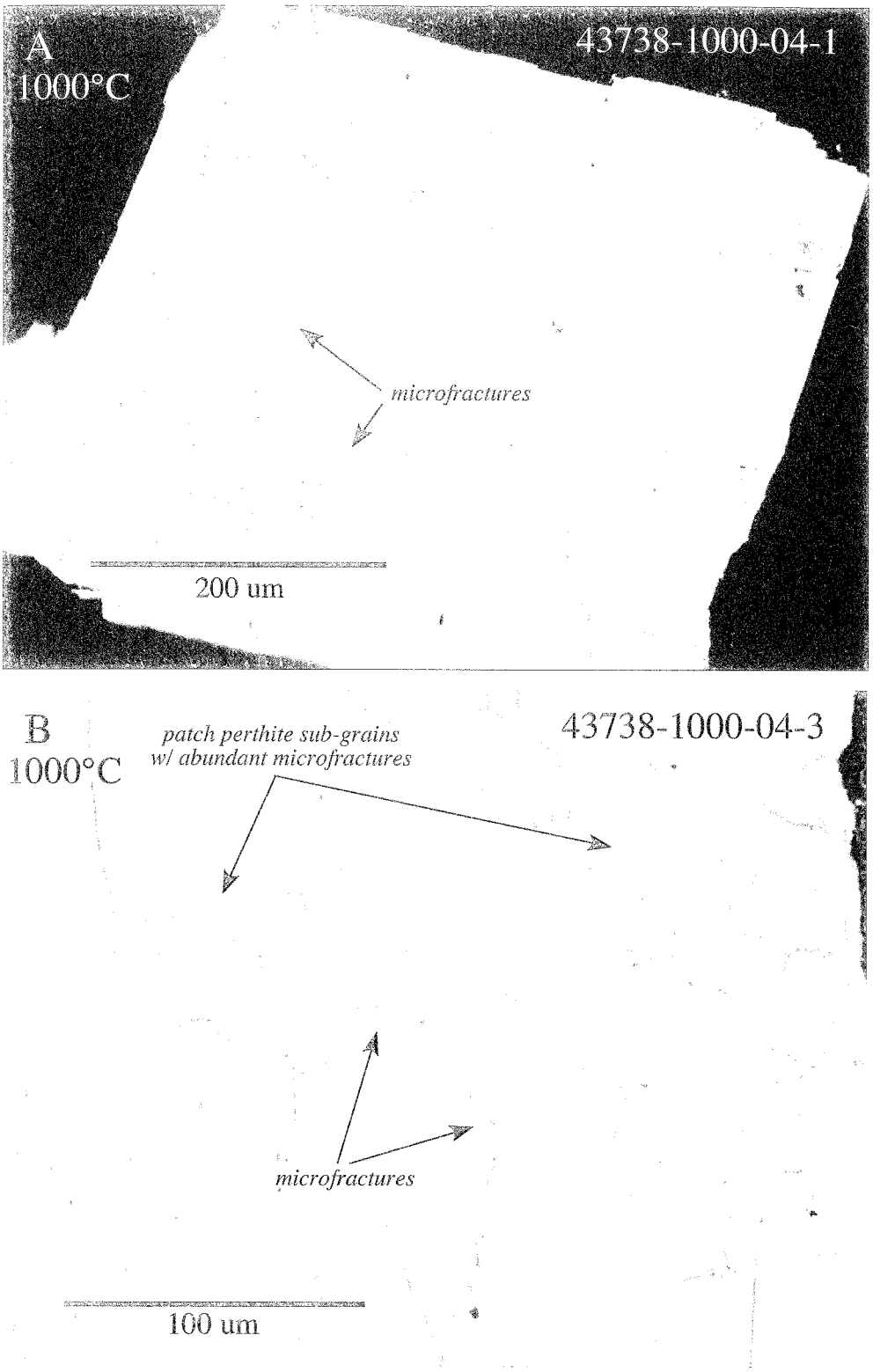

Figure 3.10: BSE images of polished, 1000°C heat-treated patch perthite grains from sample 43738 show microfractures along cleavage planes (A) as a result of heating. Microfractures are abundant in deuterically coarsened areas within sub-grains and along sub-grain boundaries (B).

the 900°C sample, and melt extrusions and melt holes are observed in the 1000°C sample. Etched grains of the 1100°C treated sample have round melt holes overlain by extruded melt (Figure 3.8e). Grains appear fused and generally textureless. Polished grains also show homogenization of the albite and K-feldspar with heating (Figures 3.9). There is still considerable heterogeneity, however, up to 1000°C. Melt holes have also formed by this temperature, and the sample is significantly melted by 1100°C although some chemical heterogeneity still persists.

3.6.2 Electron microprobe qualitative analytical results

SEM qualitative line scans were conducted across sodic and potassic phase boundaries of unheated and heat-treated Klokken samples 140182, 43738, and 140025 (Figure 3.11). K and Na were measured to evaluate inter-grain cation homogenization during the various pre-irradiation heating temperatures. Line scan data were acquired in both beam-scanning and stage-scanning mode. Beam-scanning mode uses a moving 10 μm diameter electron beam to analyze points across the sample, and counts per second were recorded every 0.11 μm. Stage-scanning mode employs a 1 μm stationary beam with a mobile stage and has higher precision than beam-scanning with counts per second recorded every 0.02 μm. On average, transects are 20 um long.

Line-scans are plotted in Figure 3.12 and show a distinct chemical transition across phase boundaries. Sample 140182 is dominated by pristine cryptoperthite, however, areas of patch perthite are observed and targeted for line scan profiling. For instance, the 700°C heat-treated data show high Na and low K content in the albite and the inverse in the microcline (Figure 3.12a). Due to a poor sample polish and inconsistent

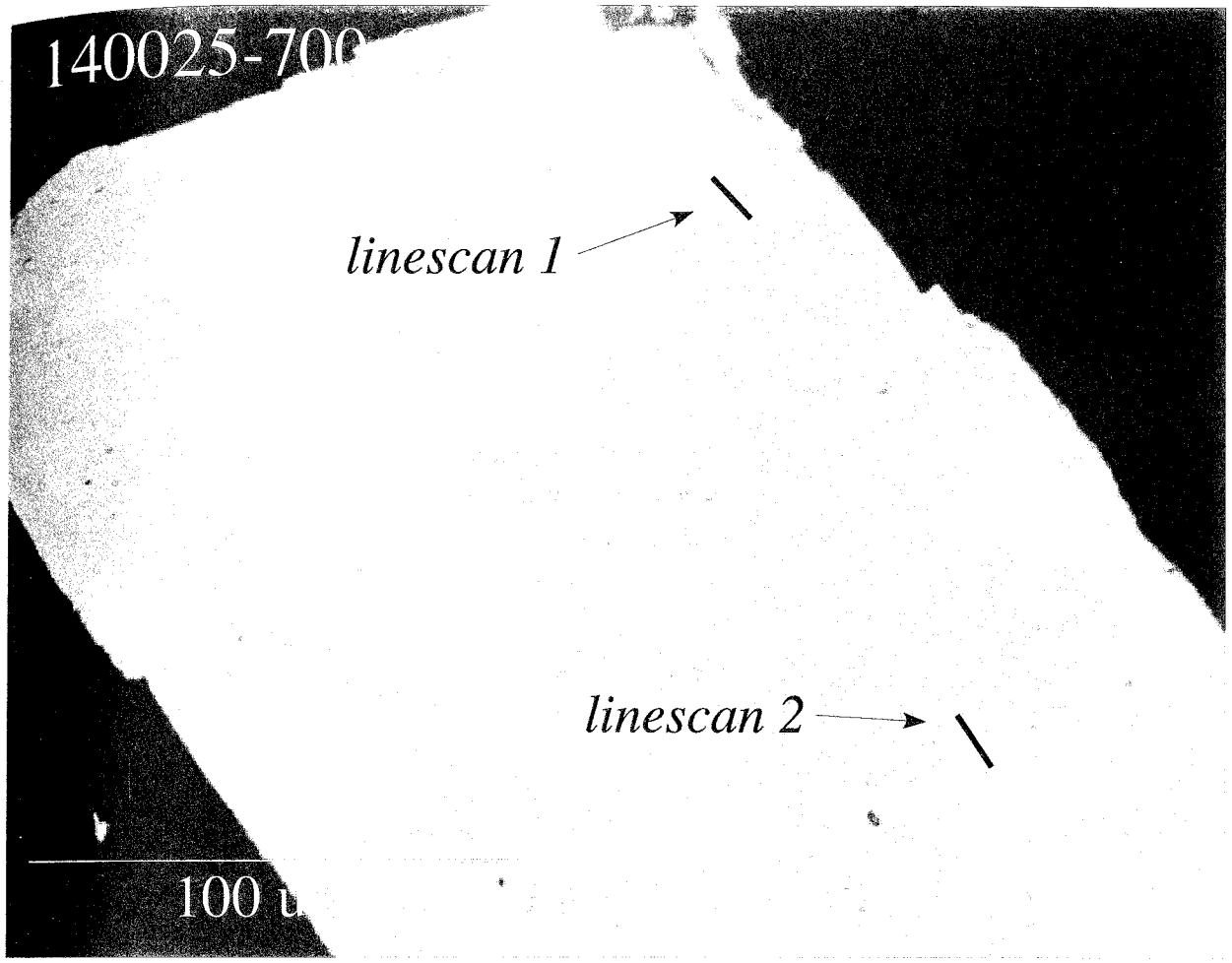

Figure 3.11: BSE image of a polished heat-treated patch perthite grain showing line scan positions across phase boundaries.

data there is no reliable line scan data for unheated sample 140182, but they are not expected to provide results significantly different from the low-temperature (650, 700°C) heated samples (Figure 3.12a).

In all three samples there is a systematic correlation between alkali concentration (expressed as counts per second) and the temperature of the heat-treatment. The line scan for the 700°C heat-treatment of cryptoperthite sample 140182 indicates a higher K-content in the potassic phase than the 900°C sample which in turn has a higher content than the 1000 or 1100°C samples (Figure 3.12a). The result of this effect is a general flattening of the chemical gradients across grain boundaries, that progresses until chemical homogenization is achieved in the 1100°C heated grains.

Patch perthite sample 43738 behaves differently than the previous sample in that K and Na never completely homogenizes even after 4 hours of heating at 1100°C (Figure 3.12b). Line scans document a progressive decrease in the K content of the microcline with increased heat-treatment temperature, but chemical components never plot as a horizontal line across phase boundaries indicative of cation equilibrium. Curiously, while the microcline shows a progressive decrease in K and a complimentary increase in Na with hotter heat-treatments, the relative abundance of these species in the albite remains relatively unchanged. There is a little variability between Na values in the albite, but it is only minor compared to the compositional changes observed in the other two feldspar samples (Figure 3.12a, c). It appears the temperature necessary for this sample to completely homogenize is higher than 1100°C.

Line scan data for mixed cryptoperthite and patch perthite sample 140025 are an ideal example of the progressive homogenization of the albite and K-feldspar with

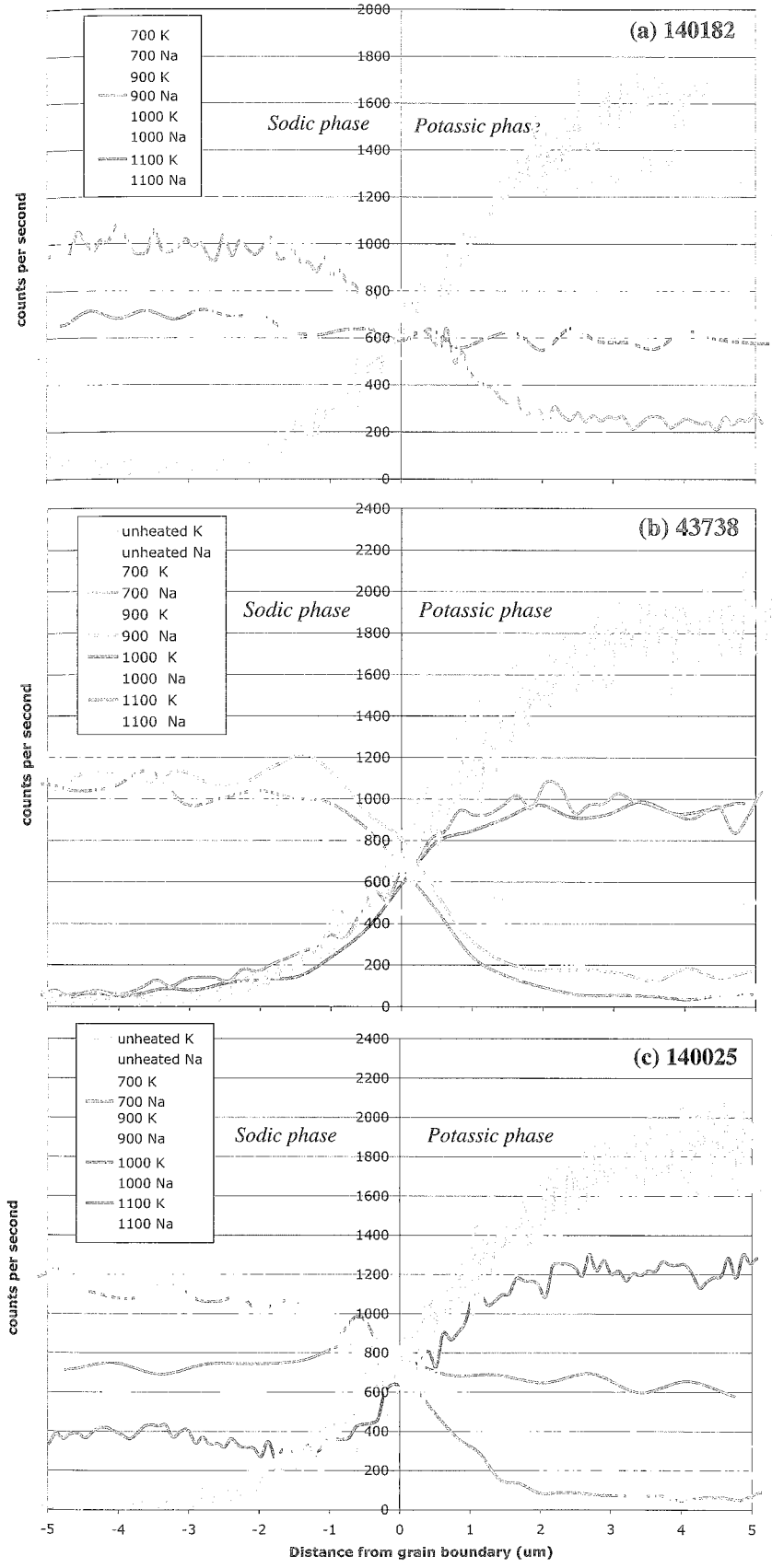

Figure 3.12: Qualitative SEM line scans for unheated and heat-treated Klokken samples. Line scans show a progressive flattening with increasing heat-treatment temperature. Horizontal lines indicate chemical homogenization resulting from high temperature heat-treatment.

increasing temperature (Figure 3.12c). The K and Na components steadily decrease or increase in the respective phases until achieving a generally flat line for the 1100°C heat-treated sample indicating complete chemical homogenization.

3.6.3 $^{40}Ar/^{39}Ar$ results for hornblende and biotite analyses

Biotite and hornblende analyses for sample 140025 and a hornblende analysis for sample 43738 yield age spectra with dates of 1174.4±3.4, 1159.9±8.1, and 1146.0±8.1 Ma, respectively, calculated from a flat segment comprising >90% of the total gas released Figure 3.13. Complete isotopic data are given in Appendix Table A3.1. Total gas ages are 1160.5±1.6, 1164.6±1.8, and 1155.0±1.6 Ma. K/Ca values for the biotite analysis range between ~10 and 100, and between 0.1 and 1 for hornblende samples. The biotite date is older than the reported U-Pb date. Because the spectrum is flat, this does not appear to be an excess argon phenomenon. It is conceivable there is poor correlation between the ^{40}K and U series isotope decay constants or inaccuracy in the monitor age, but overall the age of the biotite is close to the reported intrusion age (1166.3±1.2 Ma). Hornblende dates are consistent with the reported U-Pb zircon age for the Klokken intrusion and indicate post-emplacement cooling to <500°C by 1146 Ma.

3.6.4 $^{40}Ar/^{39}Ar$ results for multiple feldspar grain analyses

$^{40}Ar/^{39}Ar$ age spectra for multiple grain analyses of Klokken samples 140182, 140115, 43738, and 140025 are presented in Figure 3.14 and complete isotopic data are given in Appendix Tables A3.2, 3.3, 3.4, and 3.5. Cryptoperthite samples 140115 and 140182 yield flat, well-behaved age spectra with total gas ages of 1140.1±4.2 and

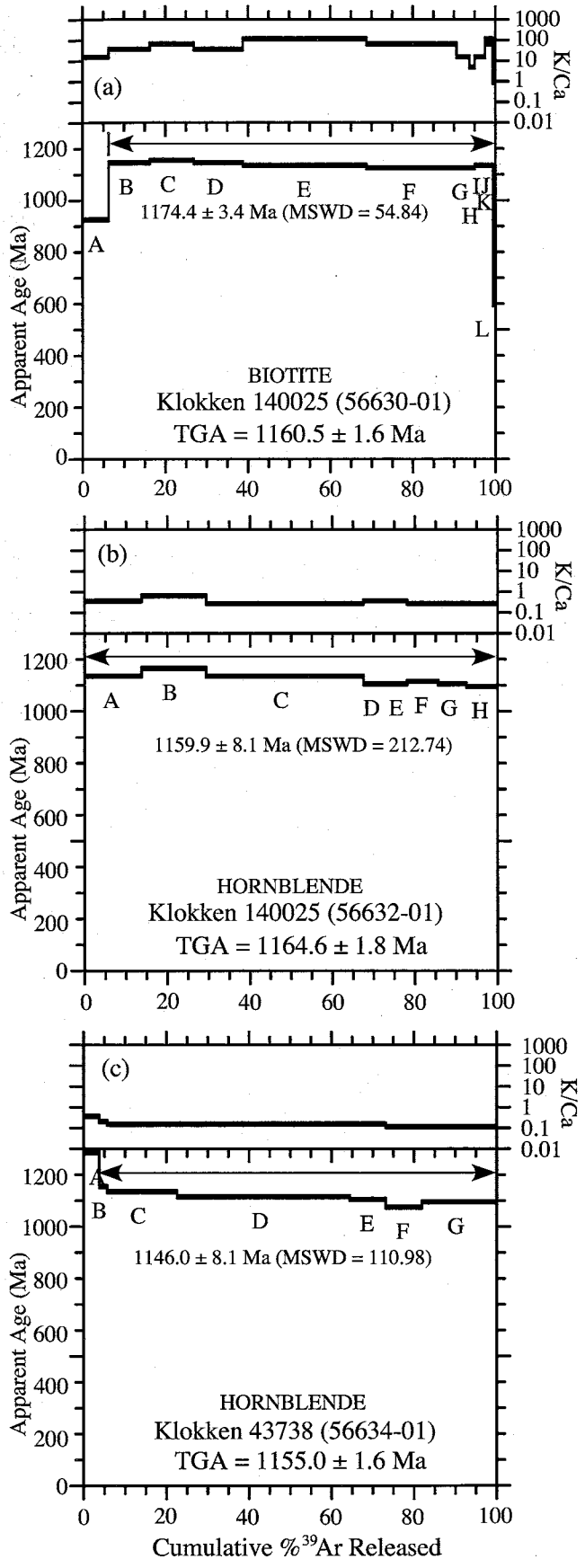

Figure 3.13: $^{40}Ar/^{39}Ar$ age spectra for hornblende and biotite separates from Klokken syenite samples.

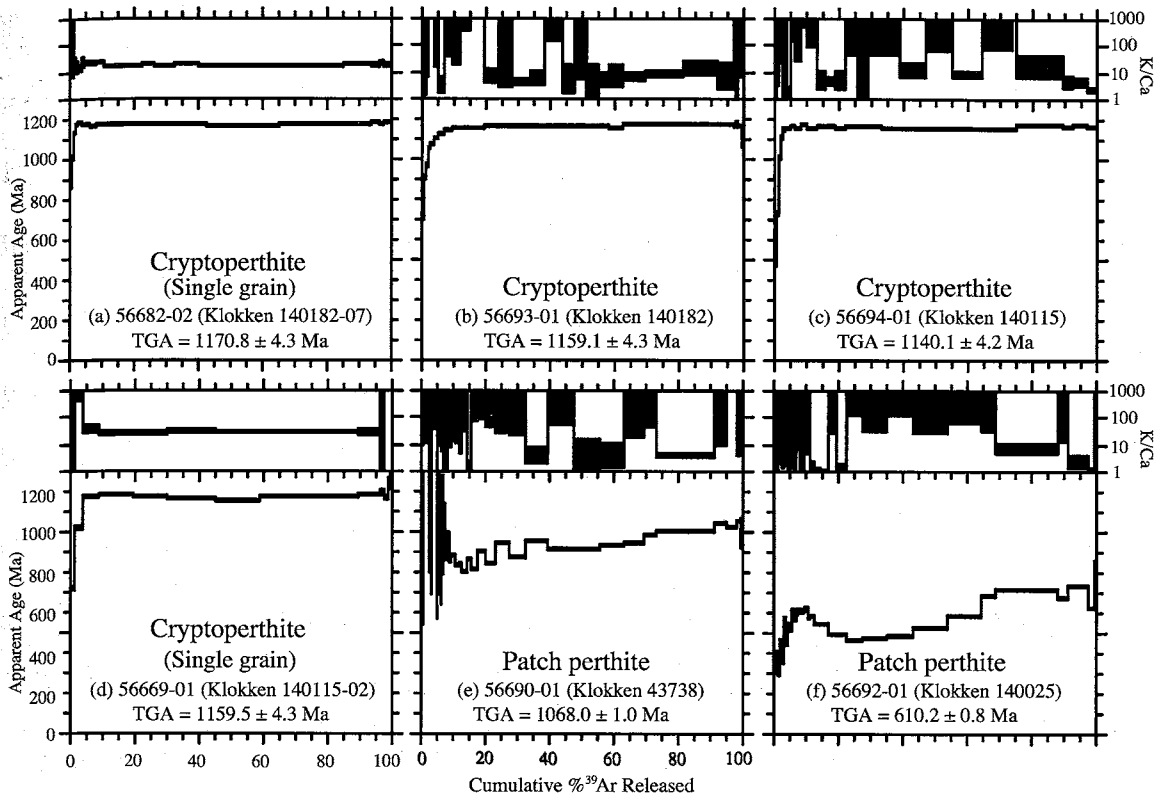

Figure: 3.14: $^{49}Ar/^{39}Ar$ age spectra for four multiple grain and two single grain analyses for Klokken cryptoperthite and patch perthite.

1159.1±4.3 Ma, respectively. Age spectra have initially young apparent ages that climb abruptly to the flat segment over the first 3 to 10% of the gas released (Figures 3.14a,b). K/Ca values for these samples, and other multiple grain analyses, have large uncertainties because the ^{37}Ar (half-life = 35.1 days) that is used as a proxy for Ca had decayed to near background levels during the long interval between irradiation and analysis. Patch perthite sample 43738 yields a more complex age spectrum characterized by geologically unacceptable old apparent ages (>1166 Ma) for the initial steps of the triplicate isothermal replicate heating steps (Figure 3.14e). This behavior is indicative of the presence of excess argon and is observed over the initial 10% of the gas released. Following the degassing of the excess argon component, the age spectrum climbs gradually from ~800 to ~1100 Ma. The total gas age is 1068.0±1.0 Ma. Sample 140025 yields a hump-shaped spectrum with a total gas age of 610.2±0.8 Ma (Figure 3.14f). The hump portion dominates the first 25% of the total gas released and the spectrum then rises gradually to ca. 770 Ma. Figure 3.15 shows the variation in age spectra between all four Klokken samples. Overall, spectra are similar in shape to spectra in Parsons et al. (1988), with the exception of 140182 that has a flatter age spectrum in this study and a total gas age within error of the reported crystallization age for the Klokken syenite. Total gas ages differ from Parsons et al. (1988) reported data, but the general age distribution of old cryptoperthite and younger patch perthite is consistent.

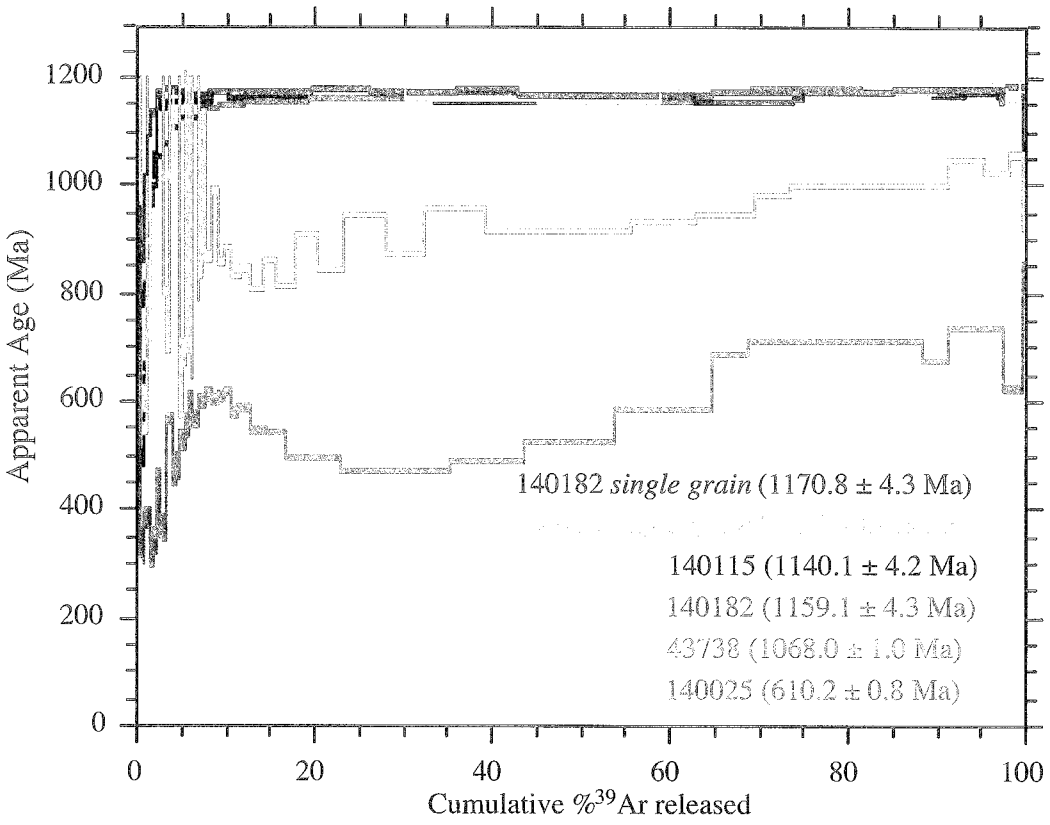

Figure 3.15: $^{40}Ar/^{39}Ar$ age spectra for four multiple grain and two single grain analyses of Klokken feldspar. Patch perthite samples 43738 and 140025 yield complex age spectra in contrast to the relatively well-behaved cryptoperthitic samples. Multiple and single grain cryptoperthite have similar age spectra and total gas ages.

3.6.5 $^{40}Ar/^{39}Ar$ results for single feldspar grain analyses

Age spectra for single grain (fragment) analyses of the four Klokken samples are presented in Figures 3.14, 3.16, and 3.17 and complete isotopic data are given in Appendix Table A3.X. One analysis each of the cryptoperthite samples (140182, 140115) was conducted and yield well-behaved flat age spectra with total gas ages of 1170.8±4.3 and 1159.5±4.3 Ma, respectively, that are within error of the U-Pb zircon date (Figure 3.14a, d). The shapes of the spectra are similar to the respective multiple grain analyses although total gas ages for single grain analyses are older. Both single grain analyses have younger initial apparent ages that climb abruptly to the flat segment over the first 5% of the total gas released. Corresponding images of selected single grains are shown in Figure 3.18.

Twelve single grains of patch perthite sample 43738 were analyzed and yield a range of total gas ages from 970.2 Ma to 1238.0 Ma (Figure 3.16). These particular minimum and maximum values are from analyses with large uncertainties related to minute crystal sizes (0.01 mg). Ages for bigger grains with smaller uncertainties range between 996.2 to 1141.1 Ma. Overall, age spectra are complex and characterized by old initial apparent ages related to the presence of excess argon over the initial 5 to 25% of the total gas released that is followed by gradually rising ages over the remainder of the analyses. K/Ca values are consistently about 10 for most analyses. Figure 3.19 shows all age spectra (excluding 43738-01 and 43738-02) on the same plot and demonstrates the spread between the flat segments of the various age spectra.

Nine single grains of sample 140025 were analyzed and age spectra are shown in Figure 3.17. Complete isotopic data are given in Appendix Table A3.6. Samples exhibit

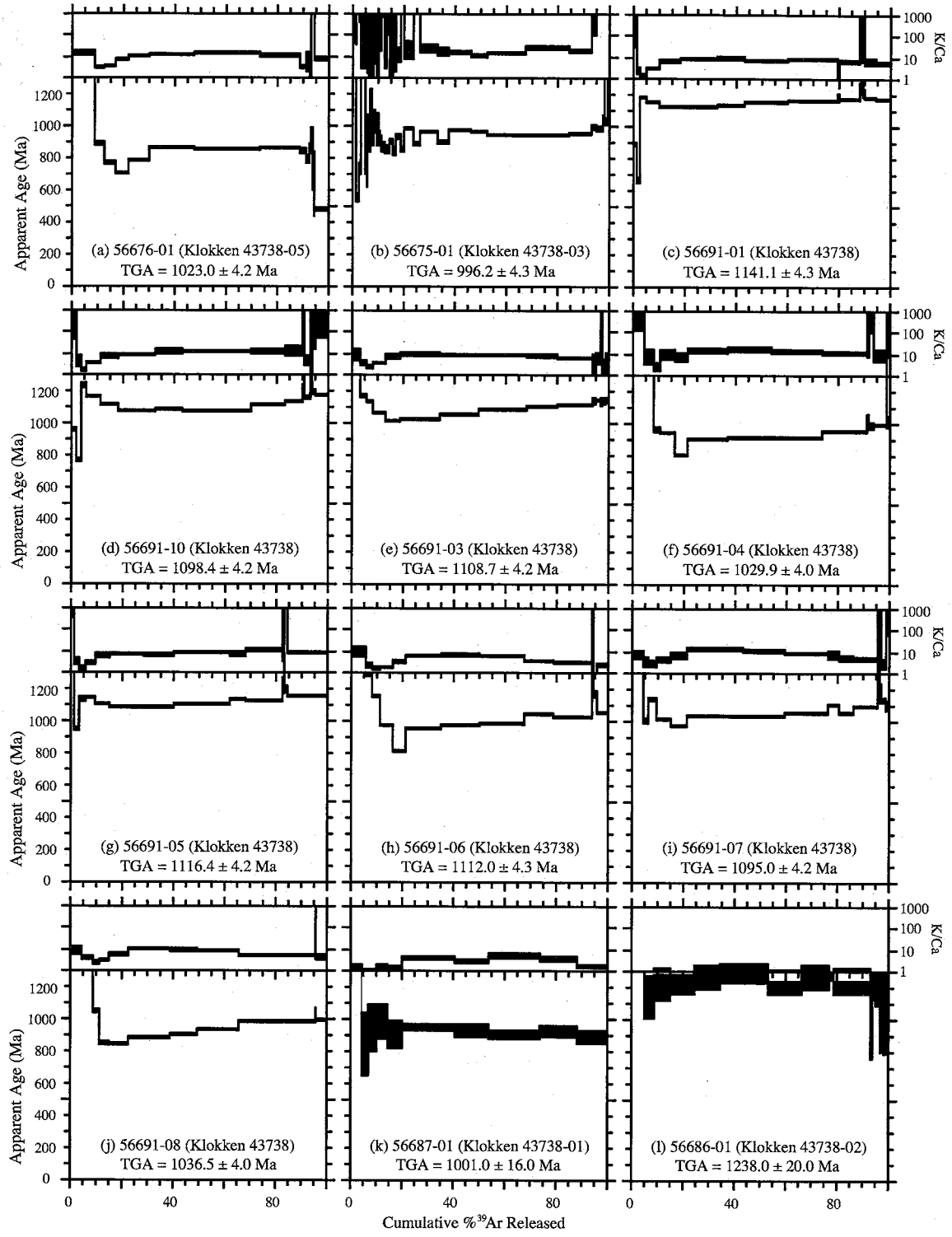

Figure 3.16: $^{40}Ar/^{39}Ar$ age spectra for single grain analyses of patch perthite from sample 43738.

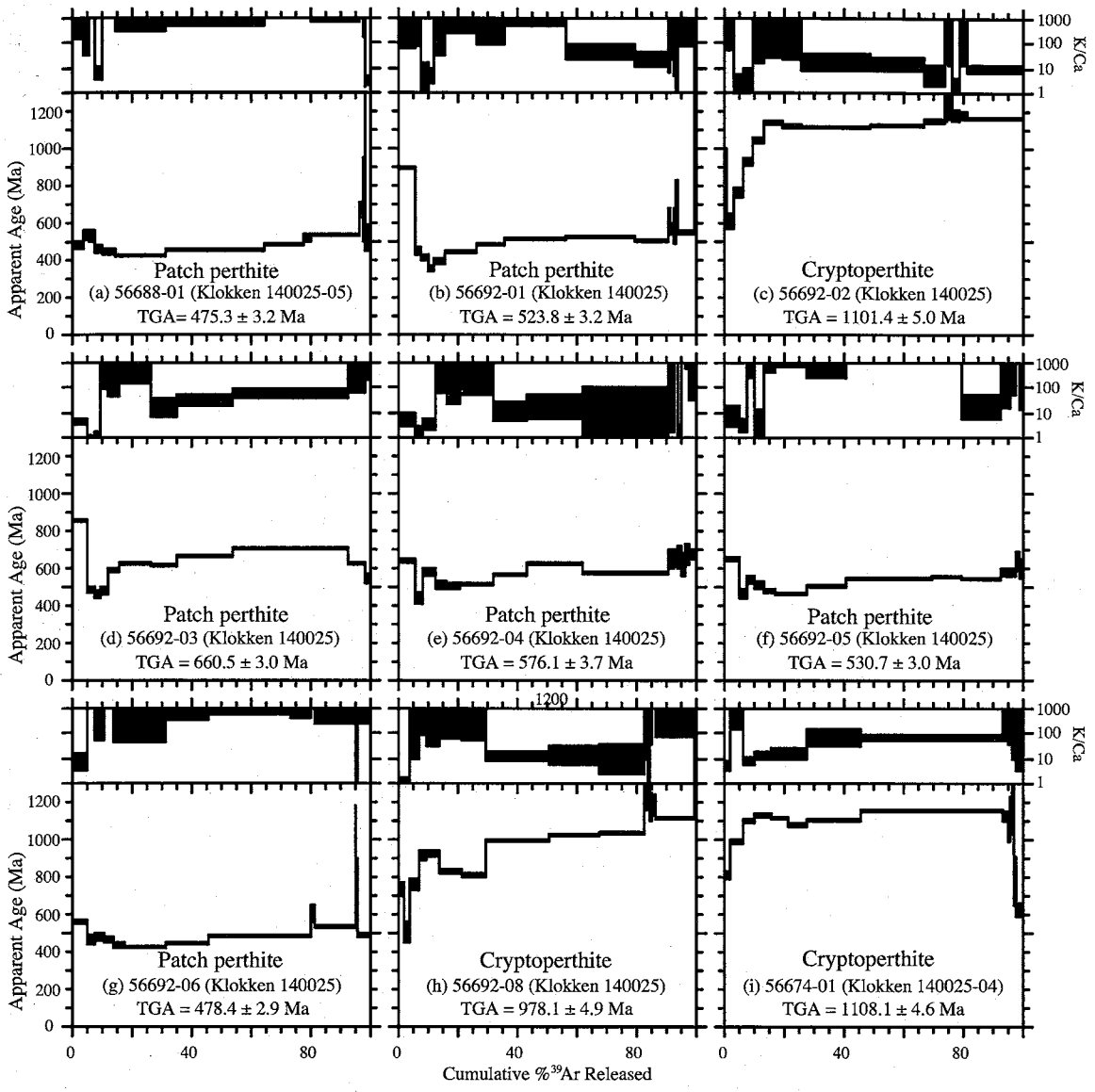

Figure 3.17: $^{40}Ar/^{39}Ar$ age spectra for single grain analyses of cryptoperthite and patch perthite from sample 140025.

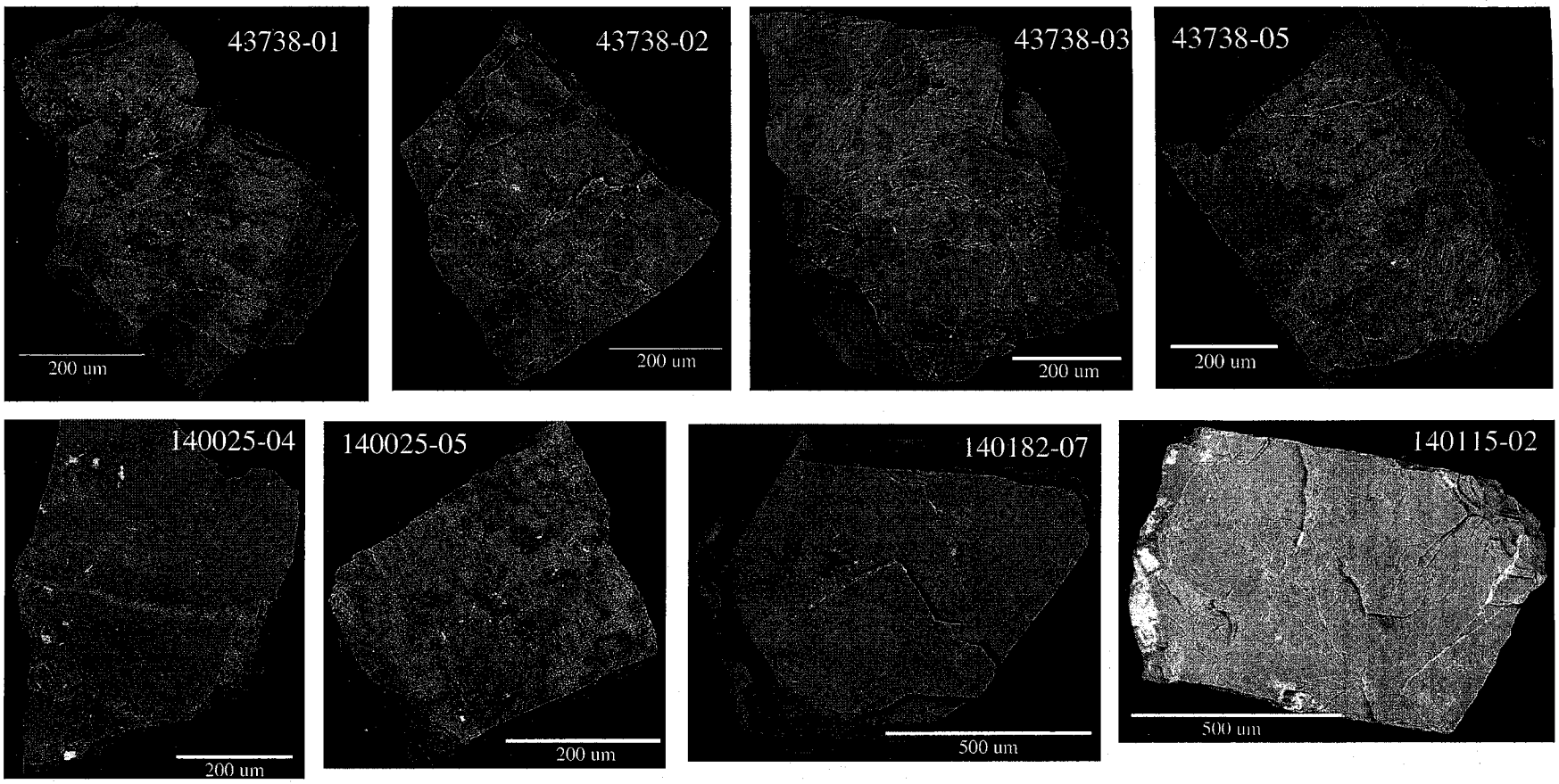

Figure 3.18: BSE images of HF-etched single grains of Klokken feldspar. Grains are actual samples analyzed in single grain experiments.

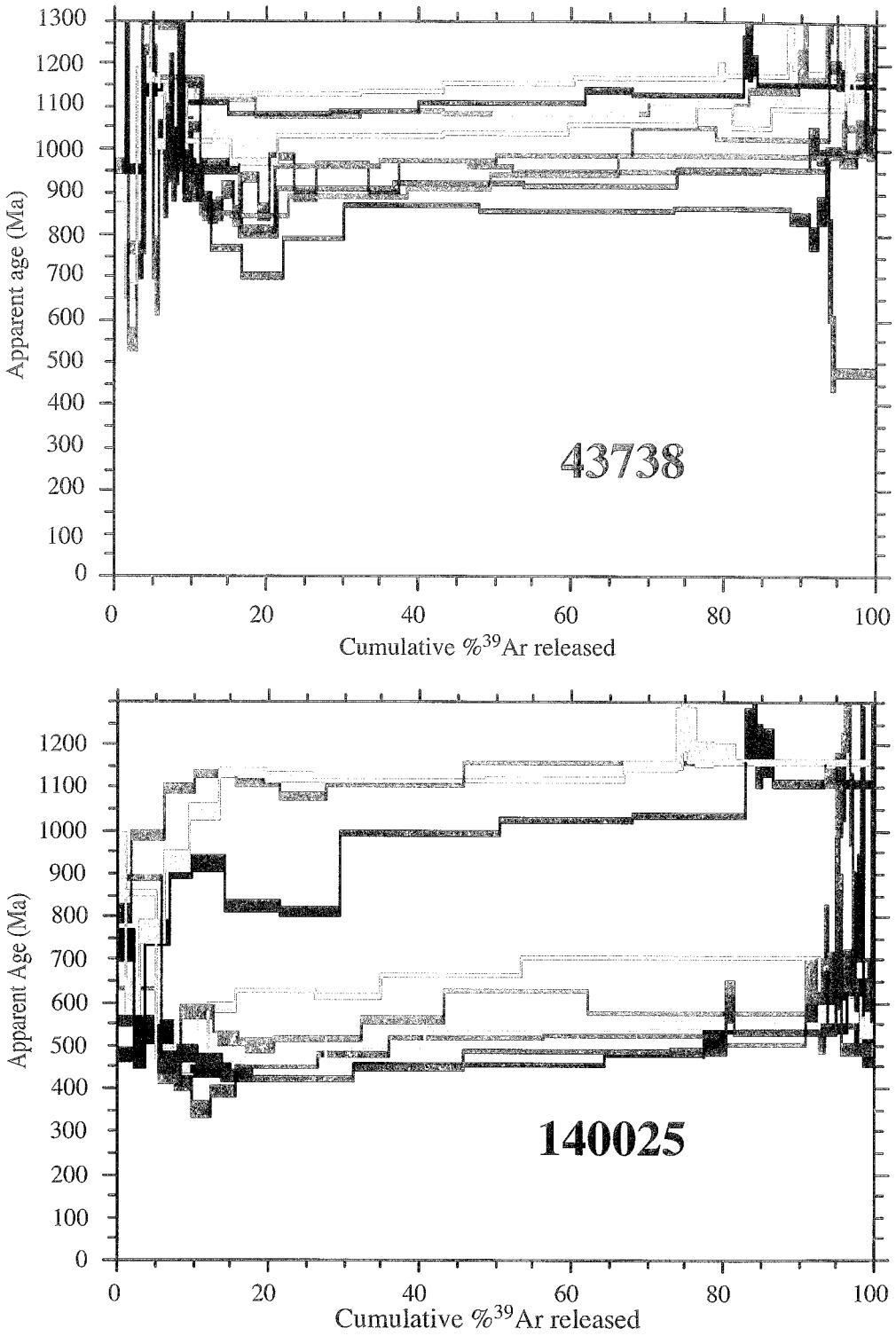

Figure 3.19: Compiled $^{40}Ar/^{39}Ar$ age spectra for single grain analyses from Klokken samples 43738 and 140025. While data for sample 43738 are spread out, age spectra for sample 140025 are distinctly bimodal.

complex age spectra with minor excess argon, but also have flat segments. Age spectra and total gas ages for this sample indicate a distinct bimodal age distribution represented by a 475 to 660 Ma population (n=6) and a 978 to 1108 Ma group (n=3) (Figures 3.17, 3.9). K/Ca values are variable between 1 and ~1000 and appear overall to be lower in the older sample population (Figures 3.17c,h,i) than the younger samples, although some young samples have low K/Ca values as well (Figure 3.17e).

3.6.6 $^{40}Ar/^{39}Ar$ results for heat-treated feldspar

3.6.6.1 Age spectra

$^{40}Ar/^{39}Ar$ age spectra for multiple grain analyses of heat-treated feldspar are presented in Figure 3.20 and complete isotopic data are given in Appendix Tables A3.2-3.5. Overall, the three heat-treated samples (140182, 43738, and 140025) reflect progressive $^{40}Ar^*$ loss as a function of heating temperature. This is seen in the shape of the age spectra for the various heating temperatures and is quantified by the total gas ages (Figure 3.20; Table 3.1). Cryptoperthite 140182 has the least complex unheated age spectrum of all three samples characterized by a relatively flat segment for ~95% of the total gas released (black; Figure 3.20). The 650°C and 700°C heated samples yield similar age spectra with progressively older apparent ages that define their broadly curving, convex downwards shape (green and red). Apparent ages for the high-temperature heating steps approach, but do not record apparent ages as old as the unheated data. The 900 and 1000°C age spectra are similar in appearance to each other and generally yield stair-stepped shapes (blue and yellow). The maximum apparent ages recorded are 1116 and 934 Ma, respectively. The 1100°C heat-treated sample yields an

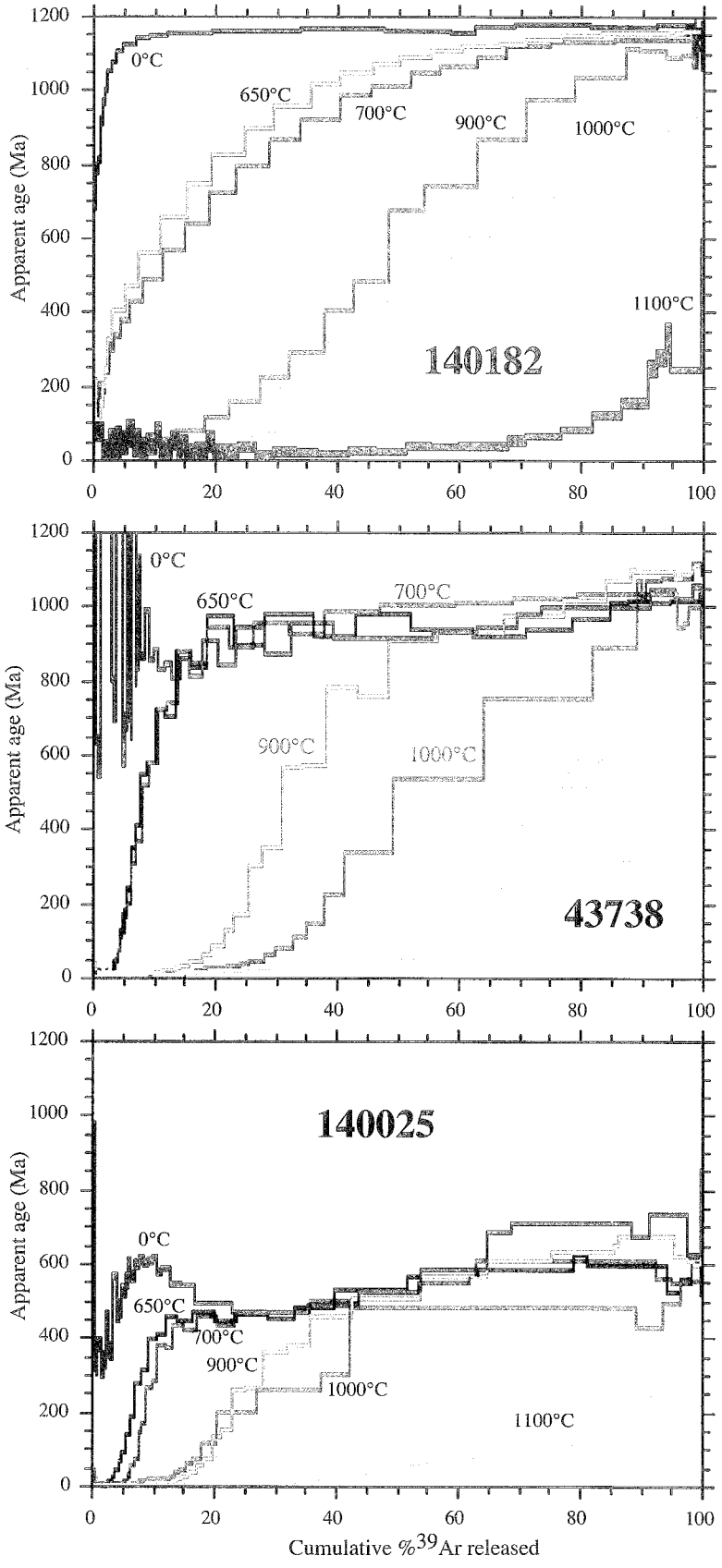

Figure 3.20: Measured age spectra for Klokken heating experiments. Colors correspond to the heating temperature, and age spectra show progressive $^{40}Ar^*$ loss due to the heating prior to irradiation.

TABLE 3.1: LIST OF MULTIPLE GRAIN AND SINGLE GRAIN FELDSPAR SAMPLES ANALYZED FROM THE KLOKKEN INTRUSION, TOTAL GAS AGES, AND ANALYTICAL PARAMETERS.

Sample	Run ID	Total Gas Age	Irradiation	Run Date	Discrimination	Furnace Sensitivity	Temp offset (°C)	Irrad time (hours)
Multiple grain analyses								
140115	56694	1140.1±4.2	NM-201	11/14/07	1.005±0.001	8.5859E-17	70	45
140182	56693	1159.1±4.3	NM-201	11/15/07	1.005±0.001	8.5859E-17	70	60
140182-650	57030	978.8±1.2	NM-206	11/17/07	1.005±0.001	8.5859E-17	70	60
140182-700	57034	930.5±1.2	NM-206	11/16/07	1.005±0.001	8.5859E-17	70	60
140182-900	57037	614.8±0.9	NM-206	11/18/07	1.005±0.001	8.5859E-17	70	60
140182-1000	57040	462.3±0.8	NM-206	11/24/07	1.005±0.001	8.5859E-17	70	60
140182-1100	57043	71.6±2.3	NM-206	12/2/07	1.005±0.001	8.5859E-17	70	60
43738	56690	1068.0±1.0	NM-201	12/5/07	1.005±0.001	8.5859E-17	70	60
43738-650	57032	884.7±1.1	NM-206	11/20/07	1.005±0.001	8.5859E-17	70	60
43738-700	57033	918.7±1.1	NM-206	11/23/07	1.005±0.001	8.5859E-17	70	60
43738-900	57036	706.5±0.9	NM-206	11/25/07	1.005±0.001	8.5859E-17	70	60
43738-1000	57039	497.8±0.7	NM-206	11/27/07	1.005±0.001	8.5859E-17	70	60
43738-1100	57042	177.9±0.3	NM-206	11/30/07	1.005±0.001	8.5859E-17	70	60
140025	56692	610.2±0.8	NM-201	12/3/07	1.005±0.001	8.5859E-17	70	45
140025-650	57031	481.9±0.7	NM-206	11/19/07	1.005±0.001	8.5859E-17	70	60
140025-700	57035	483.6±0.7	NM-206	11/22/07	1.005±0.001	8.5859E-17	70	60
140025-900	57038	433.4±0.5	NM-206	11/26/07	1.005±0.001	8.5859E-17	70	60
140025-1000	57041	364.2±0.5	NM-206	11/29/07	1.005±0.001	8.5859E-17	70	60
140025-1100	57044	186.8.1±0.3	NM-206	12/1/07	1.005±0.001	8.5859E-17	70	60
Single grain analyses								
140115-02	56669-01	1159.5±4.3	NM-201	5/17/07	1.00141±0.0007	1.2818E-16	100	45
140182-07	56682	1170.8±4.3	NM-201	5/18/07	1.00141±0.0007	1.2818E-16	100	45
43738-01	56687	1001.0±16.0	NM-201	7/19/07	1.0017±0.0007	1.3625E-16	30	45
43738-02	56686	1238.0±20.0	NM-201	7/20/07	1.0017±0.0007	1.3625E-16	30	45
43738-03	56675-01	996.2±4.3	NM-201	5/17/07	1.00141±0.0007	1.2818E-16	100	45
43738-05	56676-01	1023.0±4.2	NM-201	5/11/07	1.0028±0.00056	1.2812E-16	100	45
43738	56691-01	1141.1±4.3	NM-201	8/6/07	1.00298±0.0017	1.0246E-16	30	45
43738	56691-10	1098.4±4.2	NM-201	8/7/07	1.00298±0.0017	1.0246E-16	30	45
43738	56691-03	1108.7±4.2	NM-201	8/7/07	1.00298±0.0017	1.0246E-16	30	45
43738	56691-04	1029.9±4.0	NM-201	8/7/07	1.00298±0.0017	1.0246E-16	30	45
43738	56691-05	1116.4±4.2	NM-201	8/8/07	1.00298±0.0017	1.0246E-16	30	45
43738	56691-06	1112.0±4.3	NM-201	8/9/07	1.00327±0.0007	1.0533E-16	30	45
43738	56691-07	1095.0±4.2	NM-201	8/9/07	1.00327±0.0007	1.0533E-16	30	45
43738	56691-08	1036.5±4.0	NM-201	8/11/07	1.00325±0.0071	1.1140E-16	30	45
140025-04	56674-01	1108.1±4.6	NM-201	5/11/07	1.0028±0.00056	1.2812E-16	100	45
140025-05	56688-01	475.3±3.2	NM-201	5/16/07	1.00141±0.0007	1.2818E-16	100	45
140025	56692-01	523.8±3.2	NM-201	8/3/07	1.0017±0.0007	9.5721E-17	30	45
140025	56692-02	1101.4±5.0	NM-201	8/3/07	1.0017±0.0007	9.5721E-17	30	45
140025	56692-03	660.5±3.0	NM-201	8/4/07	1.0017±0.0007	9.5721E-17	30	45
140025	56692-04	576.1±3.7	NM-201	8/4/07	1.0017±0.0007	9.5721E-17	30	45
140025	56692-05	530.7±3.0	NM-201	8/4/07	1.0017±0.0007	9.5721E-17	30	45
140025	56692-06	478.4±2.9	NM-201	8/4/07	1.0017±0.0007	9.5721E-17	30	45
140025	56692-08	978.1±4.9	NM-201	8/4/07	1.0017±0.0007	9.5721E-17	30	45

age spectrum dominated by young apparent ages with high uncertainties that reflect the near zero age due to preheating (brown). Apparent ages climb to as old as 653 Ma over the last 50% of the total gas released.

The age spectrum for patch perthite sample 43738 (unheated) is characterized by unacceptably old apparent ages (>1166 Ma) during initial heating steps indicative of excess argon (brown; Figure 3.20b). Most of this component was apparently degassed during the heat treatment, but may still persist in the 650 and 700°C heat-treated age spectra causing the observed age oscillation of isothermal replicate heating steps between 10% and 55% of the spectrum (black and red). In general, the 650 and 700°C heat-treated age spectra have similar concave-up shapes over the initial 40% of the total gas released that climb steeply from 0 to ca. 850 Ma over the initial 15% of the total gas released. The 700°C age spectrum then climbs gradually to ~1078 Ma, but the 650°C spectrum has a slight drop in apparent age between 55% and 80% of the gas released before climbing to ~1033 Ma. Consequently, the total gas age for the 650°C heat-treated sample (884.7±1.1 Ma) is younger than the 700°C sample (918.7±1.1 Ma). The 900°C, 1000°C, and 1100°C spectra all have similar convex-up shapes. The initial 15% of the age spectrum for the 900°C heated sample is characterized by steps with apparent ages <40 Ma (green). The spectrum then rises abruptly to ca. 950 Ma where it climbs more moderately to ~1100 Ma. The age spectrum for the 1000°C heated sample is also dominated by near zero ages over the initial ~25% of the total gas released before it climbs to ~1067 Ma (blue). The 1100°C age spectrum has young apparent ages over the initial 50% of the gas released (<44 Ma; yellow). The spectrum then climbs to a

maximum age of 518 Ma before dropping to ~402 Ma over the last 15% of the total gas released.

The measured age spectrum for unheated feldspar from sample 140025 has a hump over the initial 20% of the total gas released then climbs gradually from ~467 Ma to ~734 Ma (brown; Figure 3.20c). All heat-treated samples have age spectra with a concave-up shape. The 650 and 700°C spectra have similar shapes and climb abruptly from 0 to ca. 450 Ma over the initial 15% of the total gas released then climb gradually to approximately 600 Ma. The 900°C, 1000°C, and 1100°C spectra all yield young apparent ages during initial heating steps then climb to 627, 548, and 263 Ma, respectively.

3.6.6.2 Arrhenius diagrams and log r/r_o plots

Arrhenius and log (r/r_o) plots of measured ^{39}Ar data from step heating analyses of untreated and heat-treated feldspar from Klokken samples 140182, 43738, and 140025 are presented in Figure 3.21. Data are plotted as the inverse of the furnace temperature against the diffusion coefficient for a given heating step to construct the Arrhenius diagram. Heating schedules with isothermal replicate steps are critical to identifying a shift in D/r^2 values at a single temperature interpreted as gas evolution from a mixture of different size diffusion domains (cf. Lovera et al., 1989). In practice an Arrhenius law, or reference line (r_o), is calculated from the slope(s) of a segment plotted between the diffusion coefficient of the last isothermal step at one temperature and the diffusion coefficient calculated for the first step of the next, higher temperature range. The slope of the Arrhenius law is proportional to the activation energy (E) of a sample. Although

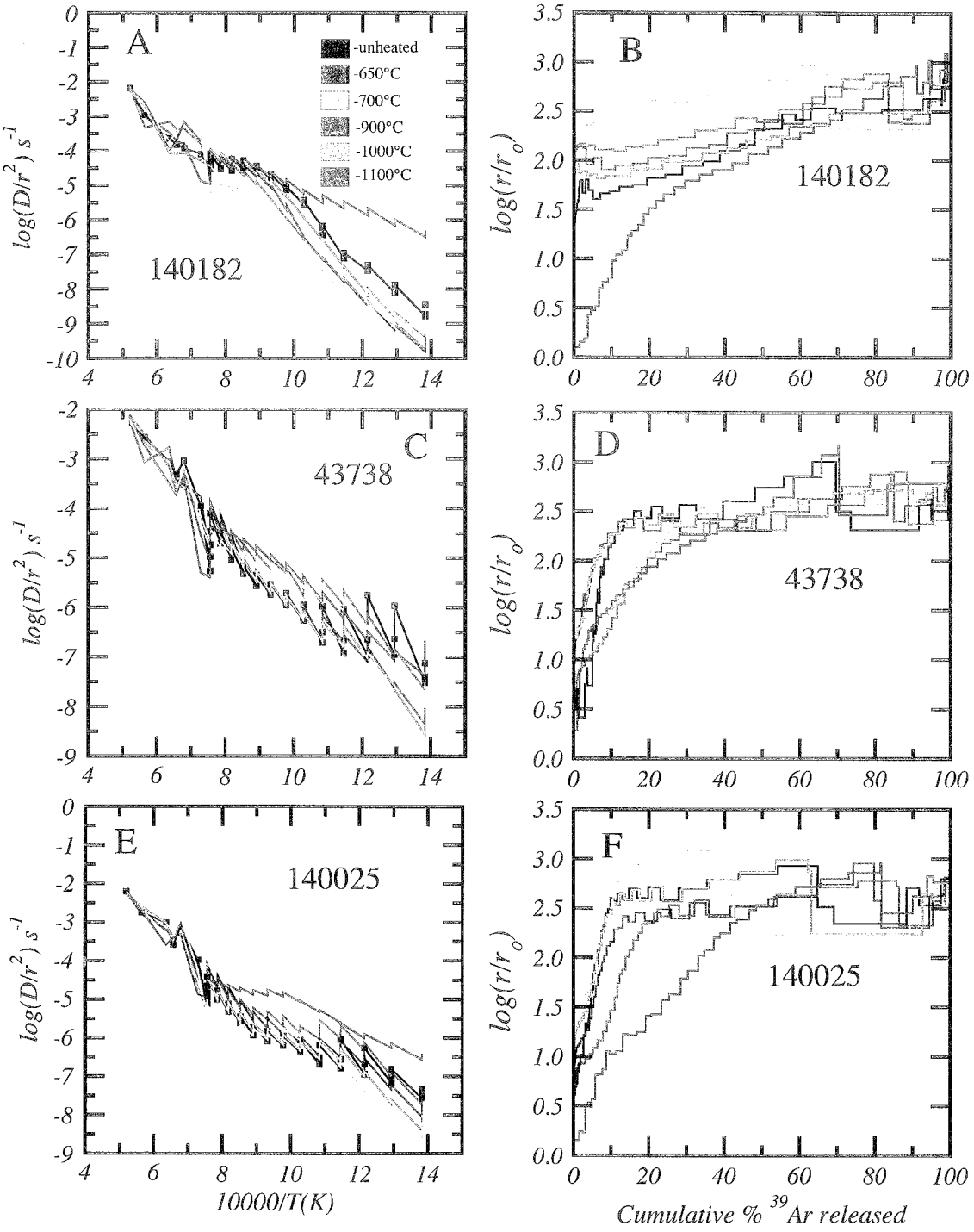

Figure 3.21: Arrhenius and logr/r_o plots for multiple grain analyses of untreated and heat-treated samples.

this method is highly sensitive to furnace calibration, the small percentage of total gas released during low temperature heating steps, and small sample weights, it is a method to establish the kinetic parameters of a given sample. For complete details and methods for both Arrhenius and log (r/r_o) calculations see DR3 of Sanders et al. (2006).

Arrhenius plots for untreated and heat-treated Klokken samples 140182, 43738, and 140025 are presented in Figure 3.21. Overall, heat-treated samples show a decrease in initial D/r^2 relative to unheated samples with the exception of the 1100°C heat-treated samples that, in samples 140182 and 140025, have significantly higher D/r^2 values (Figures 3.21a, e). However, there is internal variability between samples, which precludes a consistent observation between a progressive increase in argon retentivity and heat-treatment temperature. Data for sample 140025 hint at such a trend and initial D/r^2 values for the 650, 700, and 1000°C heat-treated analyses are progressively lower (Figure 3.21e). The maximum decrease in initial D/r^2 seen in sample 140182 is from –8.44 for untreated data to about -9.80 for both the 650°C heat-treated analyses. Sample 43738 decreases from -7.12 for the unheated sample to a minimum value of -8.57 for the 700°C heat-treated sample. Sample 140025 decreases from -7.33 for the unheated analysis to a minimum of -8.65 for the 1000°C heat-treated sample.

Plotting all data to a constant reference Arrhenius law allows the log r/r_o plots to directly reflect variations in apparent diffusion length as well as overall argon retentivity. This assumes that all splits of individual samples have equal activation energies. The log (r/r_o) plots for unheated and heat-treated Klokken samples are shown in Figure 3.21. Overall, plots are similar in shape for a given sample. Cryptoperthite sample 140182 shows a gradual shift to higher r/r_o values for the 650 to 1000°C heat-treated samples

relative to the unheated sample, and indicates an increase in bulk argon retentivity. The 1100°C heat-treated sample plots much lower than the other samples showing that it is significantly less retentive of ^{39}Ar. Log r/r_o plots for heat-treated patch perthite samples 43738 have initially higher values than the untreated data and demonstrate that heat treatment resulted in a more retentive sample. By about 5% ^{39}Ar loss, the 650 and 700°C samples are nearly identical to the untreated sample, but the 900, 1000, and 1100°C plots indicate a less retentive behavior between about 0 and 30% of gas release. Log r/r_o plots for heat-treated sample 140025 show that the initially lower D/r^2 values compared to the unheated sample only comprise about 2-4% of the total ^{39}Ar released and that, except for the 700°C sample, heat treated samples are slightly less retentive compared to the unheated sample. Like sample 43738, the 700°C heat-treatment sample is very similar in shape and position to the data for the unheated sample, but the 650°C shows higher D/r^2 values. The 900°C heat-treated sample is very similar to the other patch perthite sample in that they both show lower retentivities over the first few 10's of percent of the spectrum followed overall correspondence to the unheated sample. The 1100°C sample plot is very similar to that of the 140182 1100°C analysis, and demonstrates a significant reduction in retentivity compared to unheated material.

3.6.6.3 Activation energies

Activation energies are calculated for each sample from the ^{39}Ar released during step heating analyses, and are used in subsequent calculation of domain distributions and model age spectra. Activation energy is the most difficult parameter to measure accurately when doing MDD analysis. This is because the smallest diffusion domain

commonly only holds a small fraction of the total gas and degassing of larger diffusion domains cause a reduction in the slope defined by the early released gas. These Klokken samples are particularly difficult because of poor linearity as well as complex zigzag patterns like that shown by the Arrhenius plot of unheated 43738 (Figure 3.21). Using line segments that connect the final step of a set of isothermal steps with the first step of the next higher isothermal group is a means of recovering E (Sanders et al., 2006; DR3). This method generally provides line segments with steeper slopes as compared to using multiple low temperature points. Due to the general saw-tooth pattern of K-feldspar Arrhenius plots, a slope is calculated for each of the segments described above and, based on the consistency of the slope values, an E for the sample is assigned. Activation energy values for given line segments are plotted versus cumulative percent ^{39}Ar (Figure 3.22). The ^{39}Ar values correspond to, in the case of triplicate isothermal steps, the amount of the total gas released from the second and third isothermal step at a given temperature and the first heating step of the next higher temperature isothermal set. This plot allows for a better visualization of the change and/or constancy of E throughout the analysis and shows that cryptoperthite sample 140182 has the most consistent E of ~50 kcal/mol during the step-heating analyses (blue; Figure 3.22). Activation energies for the other two samples are more variable in any given analysis, but generally fall within a similar ~50±10 kcal/mol range over the initial 10-20 percent of the total gas released. Most activation energies deviate from this range as the step heating analyses proceed to higher temperature steps, and reflect the steeper slopes of Arrhenius segments recovered during this portion of the experiment. Activation energies for all 1100°C heat-treated feldspar generally range between ~20 and 35 kcal/mol and are very constant over ~70% of the

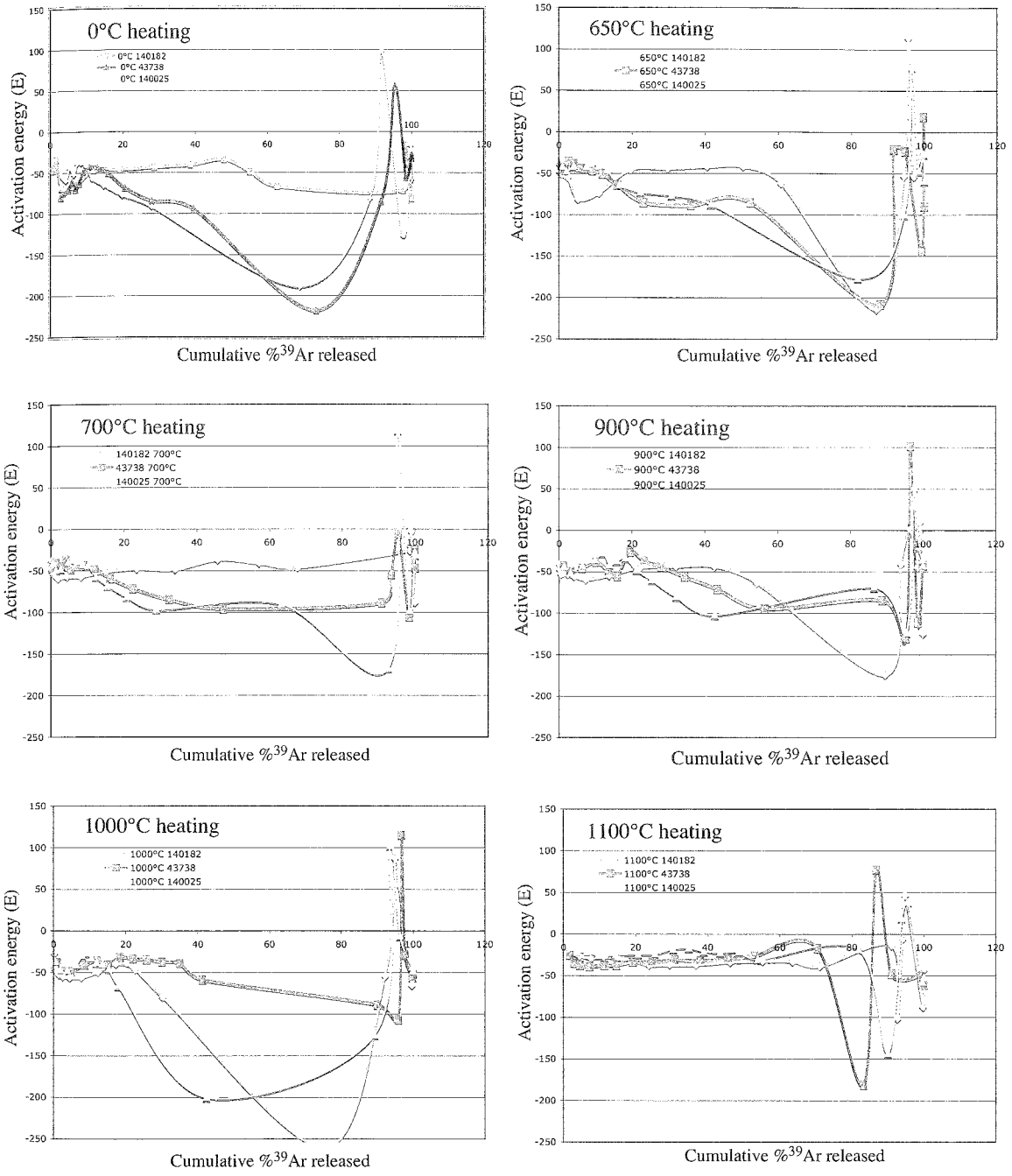

Figure 3.22: Plots of activation energies versus cumulative percent ^{39}Ar released for all unheated and heat-treated Klokken samples. Activation energies were calculated from the segment slopes on respective Arrhenius diagrams.

total gas released. The complex oscillation of all plots towards the end of the experiment results from non-diffusive argon loss related to melting of the sample during the final, high temperature steps.

For modeling purposes all samples were assigned an E of 50 kcal/mol. This is somewhat arbitrary and falls within the range of 46±6 kcal/mol that Lovera et al. (1997) reported for an average value based on over 100 K-feldspars. Although E is important in determining the bulk argon retentivity, its choice is made less important by compensation with the initial diffusion coefficient (y-intercept on the Arrhenius plot). As E increases, D also increases thus the net retentivity for different choices of E are not vastly different such that accuracy of final models is not highly dependent on accuracy of E and D_o/r_o^2.

3.7 Multiple diffusion domain (MDD) modeling

3.7.1 MDD modeling of untreated Klokken feldspar

Recall that the ultimate goal of this experimental effort on Klokken alkali feldspar is to explain old cryptoperthites with younger patch perthites. It is not possible to explain age discrepancy by simple slow cooling of two variably retentive samples because laboratory derived closure temperatures are similar. However, if the cryptoperthites are yielding overall accurate ^{39}Ar diffusion parameters they can be used to construct a thermal history of the region using the MDD method. The steep initial age gradient over the first 5 to 20% of the cryptoperthite spectra can be modeled by either long term crustal residence at about 150°C between 1150 and 400 Ma or by a discrete thermal event between 400 and 550 Ma. This later situation is modeled to show the magnitude of time and temperature required by potential hydrothermal and/or burial events to produce the

measured cryptoperthite with the ultimate goal of determining if the patch perthite young ages can be explained by microtextural modification related to a localized fluid flow event that severely affected the patch perthites but only caused minor argon loss in cryptoperthite samples.

Model age spectra were created for samples 140182 and 140015 that assumed the samples had cooled rapidly after emplacement to 100°C by 1135 Ma and remained thermally unaffected since (green; Figure 3.23). These models fit the old part of the measured spectra well and then are subjected to thermal spikes associated with a hypothetical 20 ka hydrothermal event at ca 530 or 430 Ma with fluid temperatures of 250°C to create the steep initial age gradient (red, blue; Figure 3.23). Fluid temperature and event duration were chosen arbitrarily but reflect a minor thermal perturbation that does not necessitate a magmatic driving force, but rather circulation of meteoric or evolved crustal fluids. The ca. 530 Ma timing of the modeled event was based on the approximate age of young single grains for sample 140025. The ca. 430 Ma modeled event was based on the approximate timing of the Caledonian orogeny in east Greenland that represents a distal, although regional, tectonic event (e.g. Andresen and Hartz, 2001).

Both reheating models provide excellent fits to the measured cryptoperthite age spectra and indicate that minor $^{40}Ar^*$ loss in these samples can be resolved by a short-lived, moderate to low temperature thermal event in the Paleozoic. The models are not unique, as both time and temperature could be varied significantly to provide acceptable model fits, but they do demonstrate that the temperature magnitude is compatible with the measured spectra, and provide a range of possibilities for considering fluid histories that might have more severely degassed patch perthites without overly degassing the

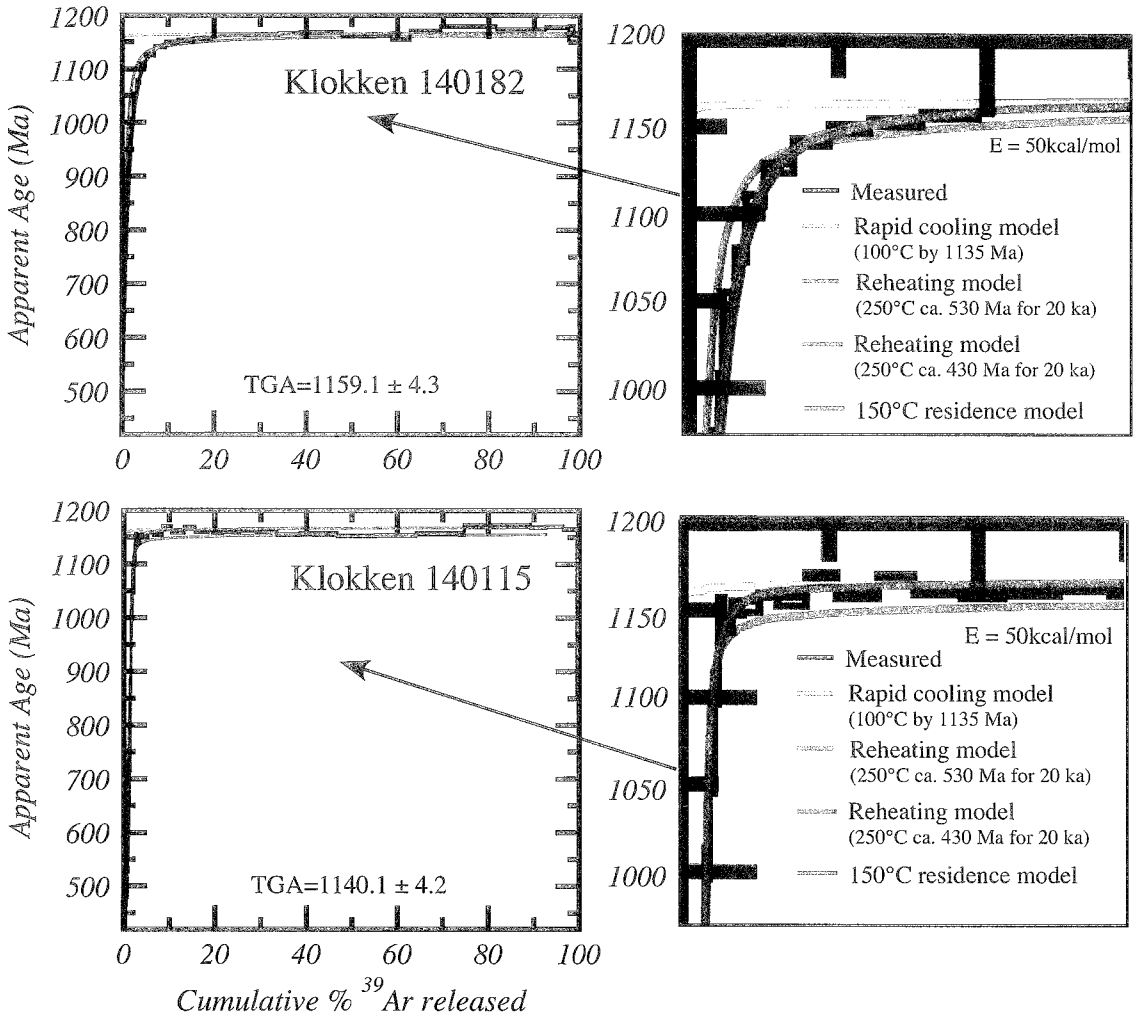

Figure 3.23: Measured and modeled $^{40}Ar/^{39}Ar$ age spectra for cryptoperthite samples 140182 and 140115. Measured data (black) were fit with a rapid cooling model that forced the Klokken intrusion to be 100°C by 1135 Ma (green). The rapid cooling history model was then modeled with 530 and 430 Ma thermal spikes to 250°C for 20 ka (blue, red). A long-term isothermal (150°C) crustal residence model is shown in purple. Close-ups show good agreement between measured data and modeled argon loss related to the thermal spikes.

cryptoperthites. They also leave open the possibility of a potentially unrecognized and undocumented fluid event in East Greenland during the Paleozoic.

3.7.2 MDD modeling of heat-treated Klokken feldspar

The advancement of this feldspar heating experiment over that conducted by Lovera et al. (1993) is that here both the Arrhenius data and the age spectrum data are used to understand potential changes to diffusion characteristics caused by the step-heating process. ^{39}Ar can only record the kinetic properties of the sample after the heating has been completed, whereas the transport of $^{40}Ar^*$ is a function of the entire isothermal heat treatment. Three end member situations can be envisioned for the behavior of $^{40}Ar^*$ and ^{39}Ar in the context of model results. If heating prior to irradiation causes no change in the geologically correct diffusion characteristics there should be a perfect correlation between the retentivity predicted by ^{39}Ar, the amount of $^{40}Ar^*$ lost and the known laboratory induced thermal history. In contrast, if the sample is changed immediately upon the beginning of heat-treatment and does not progress thereafter, the loss of $^{40}Ar^*$ will still be predicted by the degassing of ^{39}Ar following irradiation. In this case, a model spectrum based on the known laboratory induced thermal history will fit the measured spectrum, but will have no geological relevance. A third situation is where the sample undergoes progressive change during heat-treatment (e.g. chemical homogenization of K-feldspar and albite; slow melting) that also progressively changes the retentivity of $^{40}Ar^*$. Here, the loss of $^{40}Ar^*$ will reflect the average retentivity of the sample whereas ^{39}Ar will only measure the state of the sample when it was removed from the heat-treatment. If the sample becomes progressively more retentive during heat-treatment, model spectra will

under predict the total $^{40}Ar^*$ loss and the opposite is true if the sample becomes progressively less retentive.

Lovera et al. (1993) suggested that minor increase in argon retentivity observed in heat-treated samples would have little affect on the MDD model because domains are degassed of argon prior to their change. Based on this, samples should lose more $^{40}Ar^*$ than predicted by ^{39}Ar. In order to test this, the Arrhenius data from the Klokken heat-treated samples are modeled in two fashions and then used to construct model age spectra based on the laboratory induced thermal history. In one instance (measured models) a model age spectrum is generated using the domain distribution modeled from the actual fractional loss of ^{39}Ar from the individual heat-treated samples. In addition, a model spectrum (unheated models) for each heat-treated sample is calculated using the kinetic parameters given by the unheated sample. In the case where heating prior to irradiation causes a progressive increase in retentivity, the measured models should show an older model spectrum whereas the models for unheated samples should provide a younger model spectrum with the actual measured spectrum falling somewhere in between. Stated simply, if model spectra deviate from measured spectra they would imply that $^{40}Ar^*$ and ^{39}Ar are decoupled and potentially violate the primary assumption of the MDD model.

Prior to imposing the laboratory induced isothermal history on the samples, a measure of the geological thermal history must be established (the initial concentration distribution of $^{40}Ar^*$ needs to be determined). To do this, standard MDD modeling is performed to fit the unheated age spectra by inputting thermal histories until a reasonable match between measured and model spectra are obtained. These thermal histories do not require geological accuracy. In the case of the cryptoperthite sample 140182 a good

match to the unheated spectrum shown previously in Figure 3.23. For the more complex patch perthite samples it is less straightforward to obtain a single geological thermal history that will apply to all heat-treated samples. For example, unheated sample 140025 has a hump-shaped age spectrum that does not allow a good model spectrum to be obtained from any thermal history. In this case, the 650°C heat-treated spectrum which does not show this hump spectrum and is only minorly outgassed prior to irradiation can be used to determine the initial $^{40}Ar^*$ concentration. A model fit for this spectrum was overlain on the disturbed spectrum for the unheated sample and matched the intermediate sections fairly well (Figure 3.24). This thermal history was subsequently used for the other heat-treated samples of Klokken 140025. The 700°C heat-treated sample 43738 is also modeled with a different thermal history to allow a better fit between measured and modeled data. Recall the age distribution for single grain analyses of this sample exhibits a substantial spread in total gas ages and thus a single thermal history cannot be used for all samples to represent the starting concentration.

Measured and modeled data are shown in Figures 3.25, 3.26, and 3.27. Overall, measured models and unheated models coupled with the known isothermal degassing history provided good modeled spectra compared to those measured for the 650°C and 700°C runs. For example, the 700°C heat-treated sample 140025 demonstrates an excellent fit between models and measured data (Figure 3.26b). The 650°C run of 140182 demonstrates more spread between models (Figure 3.25a). In this case, the measured kinetic model over-predicts the $^{40}Ar^*$ retention in the sample relative to the measured spectrum. This behavior is a reflection of the increased retentivity seen in the measured Arrhenius data compare to the unheated sample (Figures 3.21). The unheated

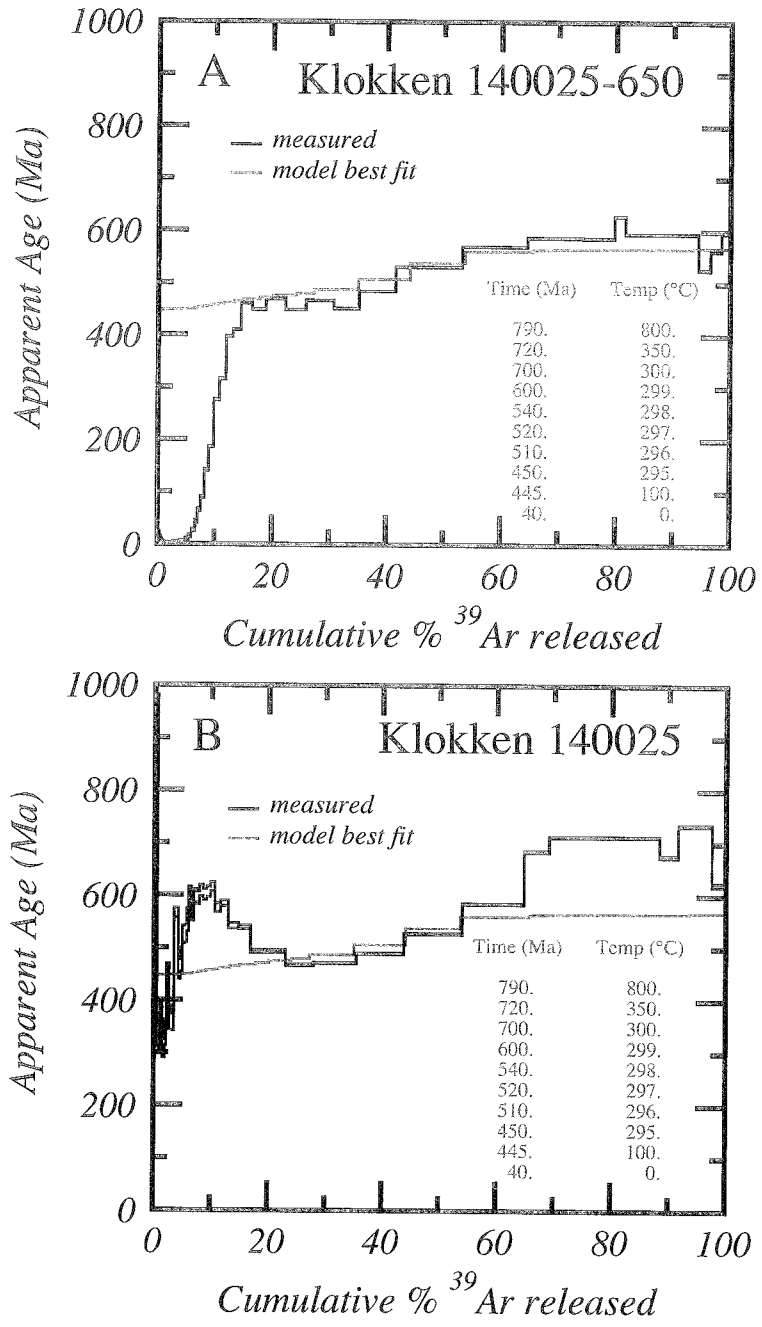

Figure 3.24: Measured (black) and modeled (red) spectra for heated and untreated Klokken sample 140025 (black). Model input parameters are shown in red.

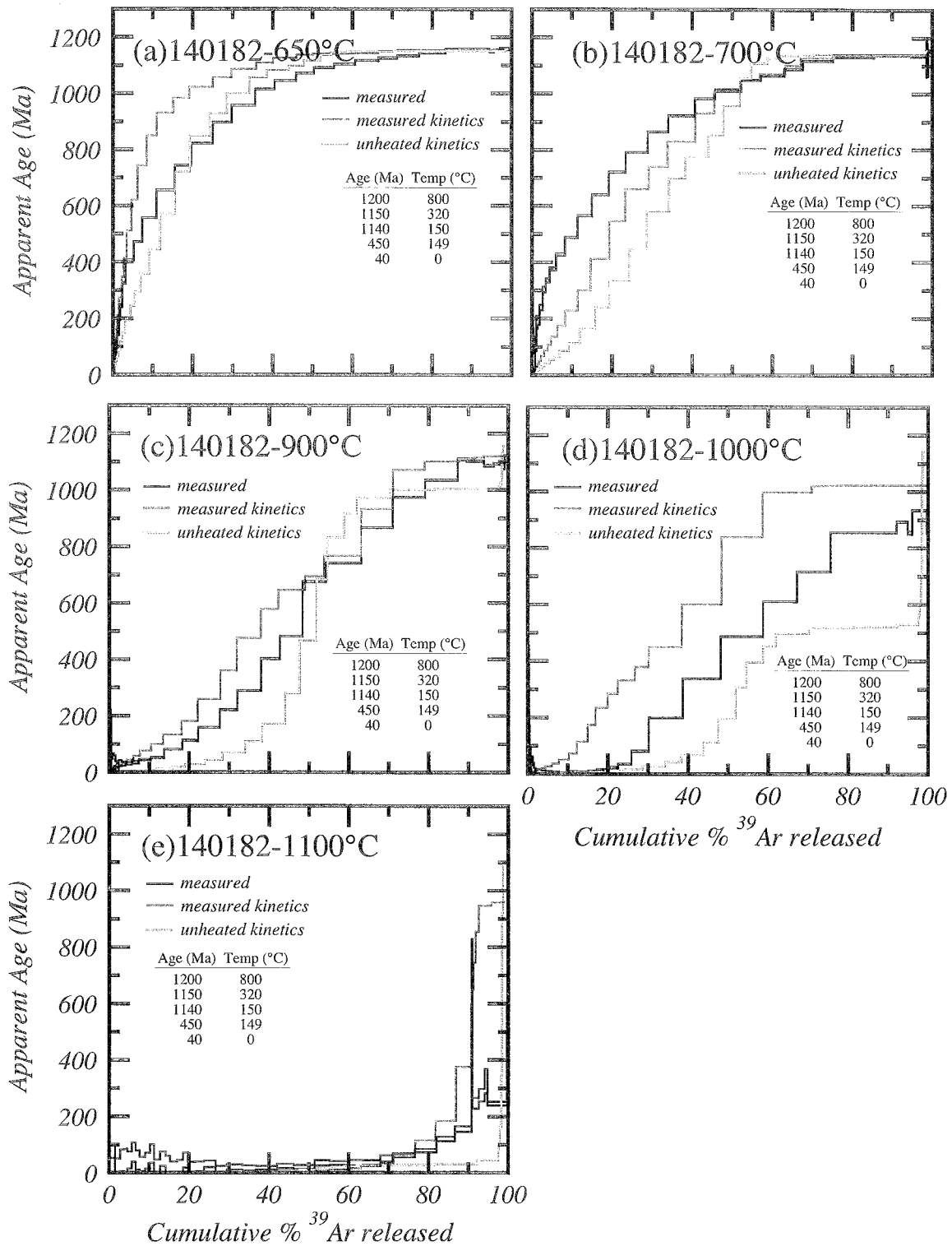

Figure 3.25: Measured and modeled age spectra for sample 140182 heat-treated feldspar. Models impose the laboratory heating temperature and duration on the presumed geologic history of the Klokken intrusion that allows the sample to cool rapidly following emplacement. Measured kinetic models use the kinetic parameters calculated from heat-treated samples. Unheated kinetic models use the kinetics from unheated samples.

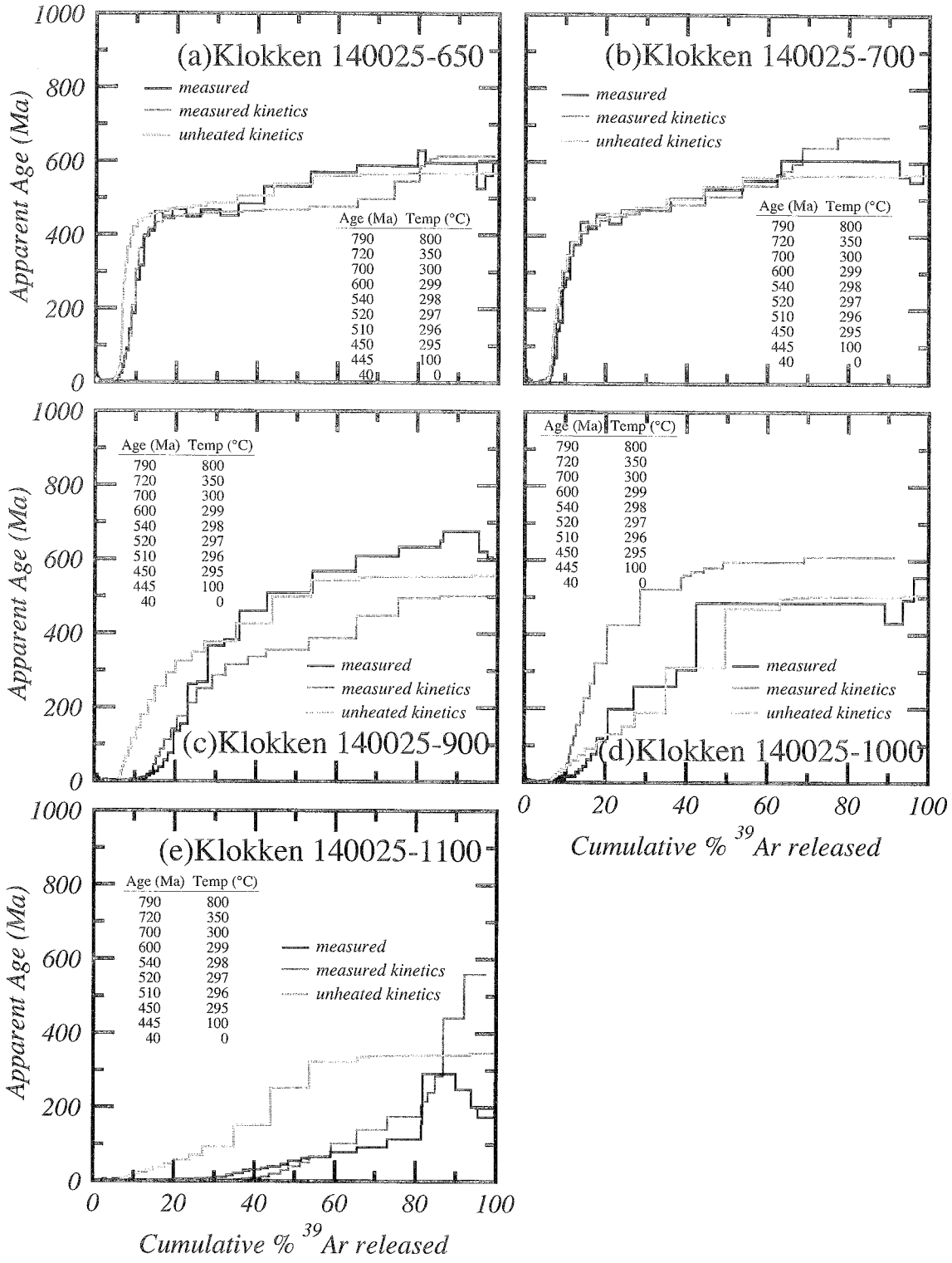

Figure 3.26: Measured and modeled $^{40}Ar/^{39}Ar$ age spectra for heat-treated Klokken sample 140025. Measured kinetic models (red) calculated from the diffusion kinetics for the heated sample, and unheated kinetic models from the kinetics of the unheated sample. Model input cooling histories are also given.

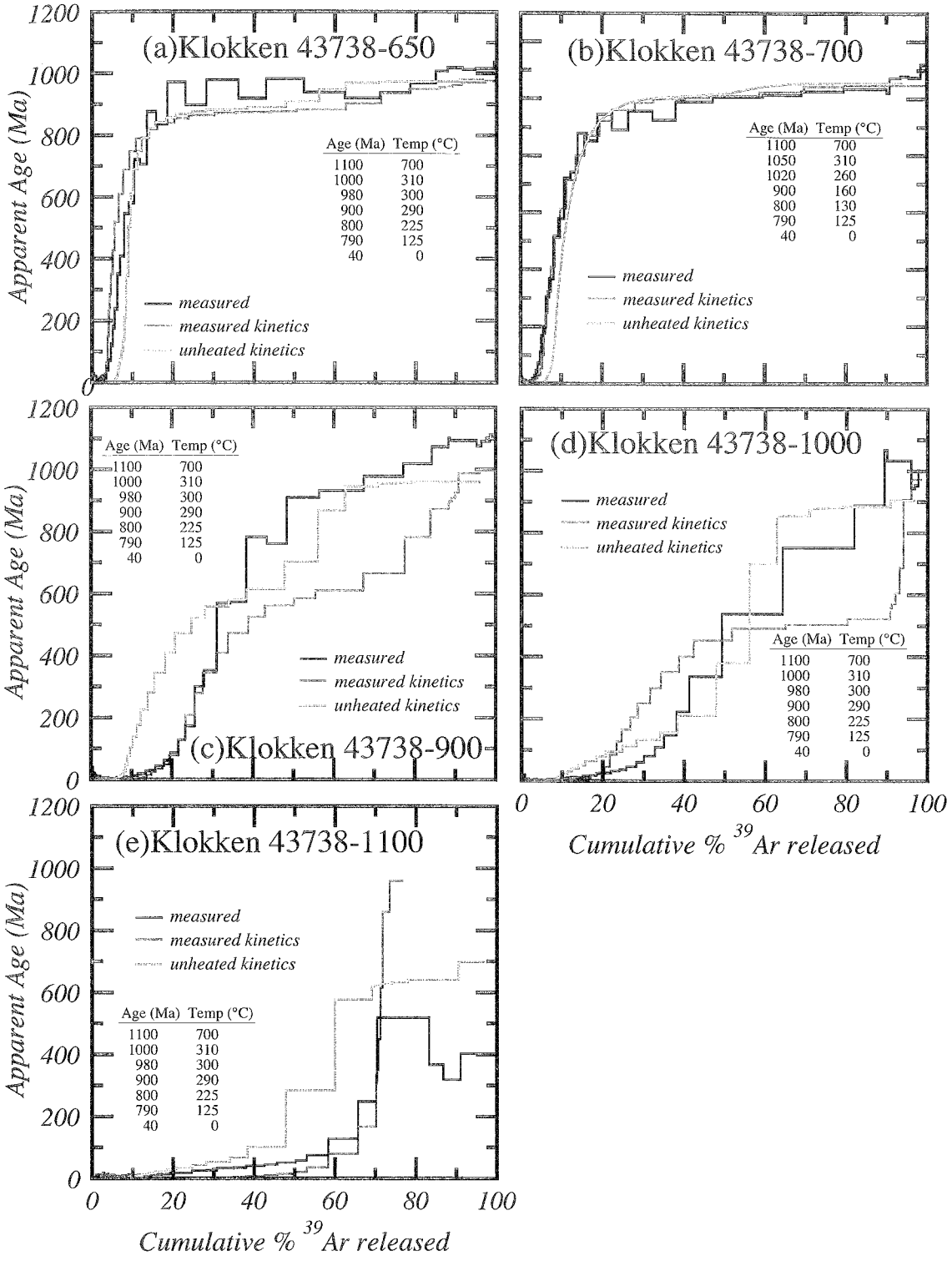

Figure 3.27: Measured and modeled $^{40}Ar/^{39}Ar$ age spectra for heat-treated Klokken sample 43738. Measured kinetic models (red) calculated from the diffusion kinetics for the heated sample, and unheated kinetic models from unheated samples. Model input cooling histories are also given.

kinetic model is a better fit, although there is still some discrepancy. Models for the 700°C heat-treated sample 140182 also do not fit the measured data perfectly (Figure 3.25b). The 900°C heat-treated samples for Klokken 43738 and 140025 demonstrate that there is no consistent rule for change in retentivity caused by heating relative to unheated material. Here the age model age spectra for 140025 appears less retentive after heating, whereas 43738 appears more retentive following heating (Figure 3.26c). This might be best explained by variation between sample splits as there is no prior reason that the unheated samples need to have identical kinetic parameters to the heated splits, especially considering the small sample size and likelihood of heterogeneous populations of patch and cryptoperthite within single grain fragments. Despite some inconsistencies, the overall good correlation between measured and model age spectra for 650 and 700°C heat-treated material suggests both ^{39}Ar and $^{40}Ar^*$ behave similarly in the laboratory environment and remain essentially unaffected by the heat-treatment. At higher temperatures of heat treatment there does appear to be a significant breakdown in this correlation such that degree of $^{40}Ar^*$ loss during isothermal heating at 900°C and 1000°C is not well predicted by the behavior of ^{39}Ar. This is seen in the deviation of model spectra from one another and the measured spectrum (Figures 3.25c, 3.2 6c,d, 3.27d). Perhaps the change in retentivity is progressive with increasing temperature but lack of a consistent trend for all samples makes this difficult to accurately evaluate.

Complexities encountered in these data sets are not unanticipated, especially considering these samples are much less homogeneous in both composition and argon behavior compared to samples previously used for experimental studies like this. Sample heterogeneity, while avoided as best as possible by careful hand picking is inherent to

Klokken feldspar. There are a number of other factors that introduce possible error and include accuracy of assigned activation energies, modeled domain distributions and even the true heat-treatment temperatures. Despite this, the lower temperature (650-700°C) heat-treatment does not appear to significantly affect the diffusion kinetics recovered from step heating experiments. This is less true of the higher temperature heat-treatment, as model age spectra calculated from the measured diffusion kinetics of ^{39}Ar, in general, over predict the retentivity of $^{40}Ar^*$ for measured samples suggesting that the feldspar has become more retentive because of heat treatment. This apparent decoupling of isotopes in high temperature heat-treated samples likely has little effect on the ability to retrieve geologically accurate diffusion coefficients and activation energies from step heating analyses because samples are not isothermally degassed prior to conducting MDD analyses and activation energies are determined from low temperature (~400 to 600°C) steps.

3.8 Discussion

3.8.1 Heating experiments, diffusion behavior, and microtextural modification

Parsons et al. (1988), McLaren et al. (2007) and now this study have documented that the laboratory derived diffusion parameters for crypto and patch perthite yield similar argon retention estimates. This similarity cannot be reconciled with the interpretation for the Klokken thermal history proposed by Parsons et al. (1988) and requires that either the laboratory derived closure temperatures are not geologically relevant or that the thermal/fluid history at Klokken is more complex than previously published. If the laboratory degassing of ^{39}Ar is not analogous to the natural transport of $^{40}Ar^*$, the change

between laboratory and natural behavior either occurs immediately upon the initial heating of the sample during the first step of argon extraction or that the Klokken patch-perthite samples have become more retentive of argon after the time that they were once leaky of $^{40}Ar^*$.

The first explanation is perhaps viable considering that K-feldspars are not completely stable during argon extraction (Lovera et al., 1993; Fitz Gerald et al., 1993; 2006). However, isothermal heat-treatment experiments conducted here demonstrate a good correlation between measured and predicted age spectra for samples heated to 700°C or less. If this is not geologically relevant then something must change during heating to increase argon retentivity in the patch perthites and decrease it in the cryptoperthites. The magnitude of this increase or decrease can be put into perspective by comparing predictions made by Parsons et al. (1988) and Burgess et al. (1992) about the natural transport boundaries and length scales that are based on microtextural observations with the measured Arrhenius parameters. Parsons et al. (1988) argued that the physical grain-size of the cryptoperthites approximated the diffusion length because cryptoperthite are fully coherent and do not act as diffusion boundaries. Also, Burgess et al. (1992) identified subgrain mosaics within the patch microclines and estimated a diffusion length of about 1 μm that provided a low closure temperature (~125°C) that would explain the young age of the patch perthites. These length estimates are represented on the Arrhenius plot by assuming that the E and D_o values of K-feldspar determined by Foland (1974) are representative of all alkali feldspar. Analyzed cryptoperthite fragments have half-widths of about 200 μm (eg. Figure 3.3) that when coupled with Foland's kinetic parameters yield the Arrhenius law shown in Figure 3.28.

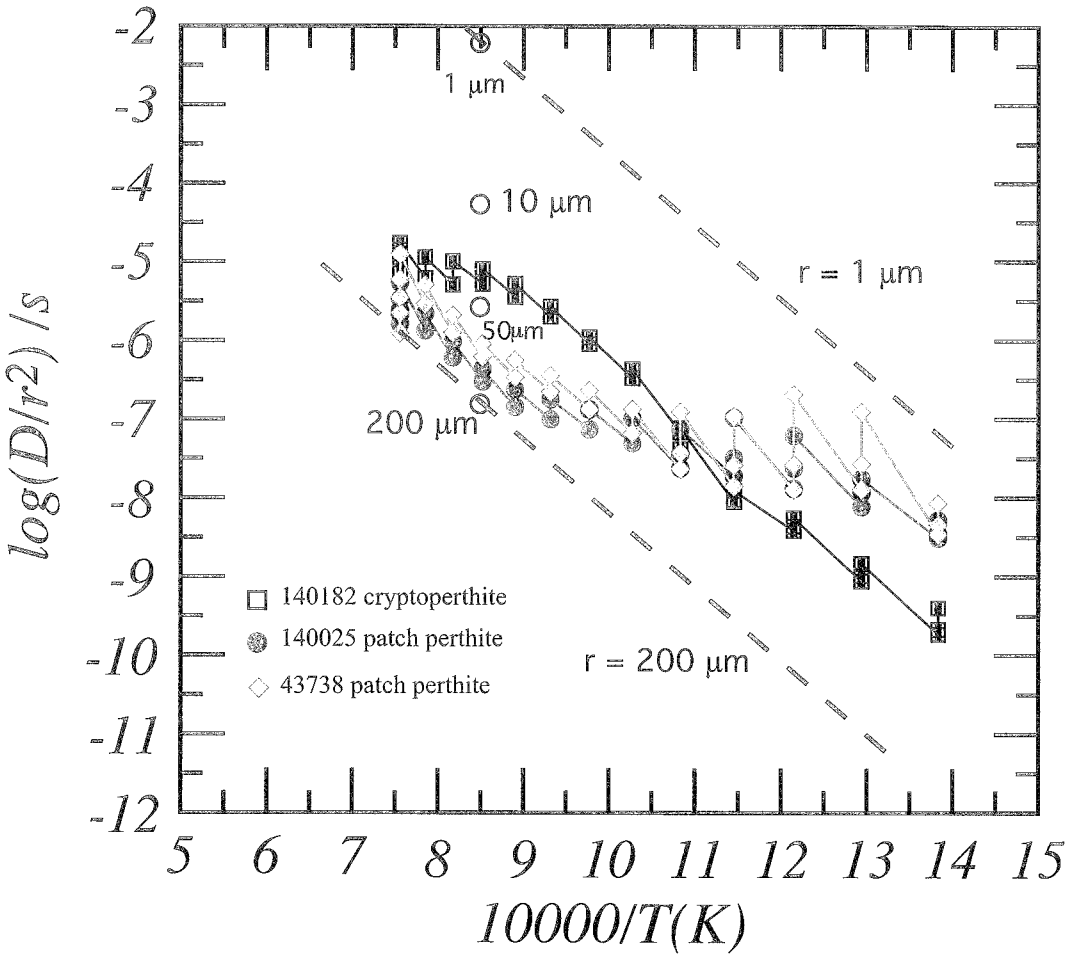

Figure3.28:Arrhenius diagram for unheated Klokken alkali feldspars assuming spherical diffusion geometry. For reference, dashed lines represent Arrhenius laws for 1 and 200 μm diffusion radius using E and D_o from Foland (1974). Labeled open circles represent position on the Arrhenius plot for diffusion radii ranging from 1 to 200 μm again using E and D_O of Foland (1974). Measured Arrhenius data show poor agreement to the diffusion radius predicted by Parsons et al. (1988) for cryptoperthite who suggested that physical grain size represents diffusion length. Also, Burgess et al. (1992) suggested a 1 μm diffusion length for patch perthite that again shows poor agreement with measured Arrhenius parameters.

The Arrhenius law for the patch-perthites plots much higher on the Arrhenius diagram than cryptoperthites because of the much smaller (1 μm) assumed diffusion dimension (Figure 3.28). The measured Arrhenius data for the unheated Klokken samples do not agree with the length scales suggested by Parsons et al. (1988) or by Burgess et al. (1992). In the case of the cryptoperthites, the laboratory heating would have to cause significant reduction of argon retention whereas for the patch perthites the laboratory heating would have to substantially increase the retentivity. For instance, in order to explain the measured D/r^2 values at 900°C, the suggested 1 μm diffusion dimension for patch perthites would have to increase to about 200 μm to explain the measured Arrhenius data. This change may result as the albite and K-feldspar patches undergo chemical homogenization as observed in the heated sample images, however there appears to be only very little chemical change until at least 900°C (e.g. Figure 3.12). In contrast, the 200 μm crystals of cryptoperthite would have to undergo a size reduction during heating to ~30 μm fragments (Figure 3.28). This could result from cracking during heating, however no obvious signs of excessive microfracturing are observed in images of heat-treated cryptoperthites (Figures 3.2. 3.3. 3.5, 3.6, 3.7, 3.8). In summary, the measured Arrhenius data for cryptoperthite sample 140182 shows a decrease in argon retentivity as a result of heating, whereas patch perthite samples 43738 and 140025 show an initial drop in retentivity but an overall increase in apparent diffusion length of the sample after pre-heating above 700°C. Differences in the kinetic behavior of these samples after heat-treatment are likely due to the microtextural differences between the cryptoperthite and patch perthite. Specifically, the mechanisms and pathways controlling argon diffusivity are responding differently to heating because of the inherent structural

differences between the strain-controlled cryptoperthite and deuterically-coarsened patch perthite. Partial annealing of the feldspar structure and reduction of diffusion pathways, either in size or in number, might explain the increase in argon retentivity in the cryptoperthite, but does not account for enhanced diffusivities in patch perthite samples. Patch perthite samples have numerous micropores that developed between sub-grains during deuteric alteration and also as enlarged nanotunnels features in patch microcline. These features may play a role in this behavior, particularly if heat-treatment improves the interconnectivity of these features with argon diffusion pathways. Samples heated to 1100°C are, for the most part, partially to mostly melted and therefore information from these samples is not particularly useful or applicable, except that the common practice of holding a sample at 1100°C during argon extraction for MDD analysis should be considered more quantitatively in the context of a sample's bulk composition and incongruent melting temperature.

Based on these experiments it seems excessively *ad hoc* to require laboratory-induced changes to the microtextures that would return D/r^2 values common to almost all K-feldspars used for MDD analysis. It could be argued that all alkali feldspars are compromised by heating resulting in the commonality of D/r^2 values. If this is true, there would be no explanation of why most MDD derived thermal histories are accurate relative to other thermochronometric methods or why they yield geologically acceptable results when constrained by multiple and independent methods. Under the suggestion here that the laboratory derived closure temperatures for Klokken samples are accurate to first order, the thermal history for the Klokken intrusion needs to be reevaluated.

3.8.2 Implications of $^{40}Ar/^{39}Ar$ dates for Klokken samples: A revised thermal history

$^{40}Ar/^{39}Ar$ age spectra and assigned ages for mafic separates from Klokken samples are consistent with the reported intrusion age of 1166.3±1.2 Ma. Incremental step heating analyses of braid cryptoperthite samples 140182 and 140115 yield flat spectra and ages also compatible with emplacement and cooling at this time. Single-grain analyses of remnant braid cryptoperthite in deuterically altered sample 140025 give ages compatible with the intrusion age. Patch perthite sub-grains, on the other hand, yield dominantly Paleozoic total gas ages indicating discrete age populations are preserved in the partially replaced sample. This is significant in that, despite pervasive replacement of the primary cryptoperthite, careful microsampling and sample characterization can be used to recover meaningful geologic information. This also demonstrates that complexities in multigrain age spectra reported in prior studies (Parsons et al., 1988; McLaren et al., 2007) can be explained by mixing of microtexturally and temporally distinct populations.

All Klokken samples have experienced the same regional thermal history since emplacement because the are very close spatially to each other (<1 km). Young samples cannot be explained simply by thermally induced argon loss, because temperatures nearing 400°C for short durations are required to degas the patch perthites that in turn would also substantially degas the cryptoperthite samples as well. Rather than a regional thermal event *per se*, infiltration of a moderately high temperature (<300°C) fluid in the porous laminated syenite layers may explain these ages and closure temperature estimates. This fluid exploited the microporous patch-perthite and was coincident with microstructural modification and the resulting argon loss hundreds of millions of years after magmatism. The minor argon loss observed in cryptoperthite samples can be

after magmatism. The minor argon loss observed in cryptoperthite samples can be explained by this short-duration, low-temperature fluid pulse in the Paleozoic and possibly records heating associated with burial and regional tectonism related to the onset of the Caledonian orogeny. The nature of the microtextural modification remains speculative and requires additional high-resolution microbeam analysis. Modification is potentially driven by the same thermodynamic principles that describe the unzipping reaction of cryptoperthite in the presence of fluids. A great difficulty is determining which microtextures and subgrains correlate to any potential modification event, and at what scale this mechanism is operating. The inherently complex patch-perthite sub-grain microtextures have been described in detail in a number of studies and attributed exclusively to post-magmatic deuteric alteration within 10^5 years after emplacement. Resolving potential points of contention between a strictly mineralogical perspective and a geochronologic one is the only way to alleviate the stalemate between K-feldspar thermochronology practitioners and their critics. These results present a solid case that, in the context of MDD theory, require a rethinking of the fluid-rock history of the laminated syenite units within the Klokken stock. While the specifics of the mechanism(s) responsible for argon loss during fluid-rock interaction are vague, the same critics of K-feldspar thermochronology have argued that microtextural modification of feldspar persists to low temperatures and is specifically important with respect to $^{40}Ar^*$ transport (*i.e.* Parsons et al., 1999). The ages and closure temperature estimates here seem to support a low temperature modification and it will be key to directly image a potential microtextural candidate to explain young patch perthite ages. Recent progress in feldspar micro-imaging has identified discrete nanotunnels associated with dislocations in

feldspar exsolution lamellae that are believed to be controlling features for argon transport (Fitz Gerald et al., 2006). Nanotunnels are also shown to persist during high temperature isothermal heating experiments demonstrating these features persist despite chemical homogenization. Nanotunnels are also thought to become enlarged during fluid-rock interaction resulting in faceted micropores at the edge of albite exsolution lamellae. This suggests a feature that may control argon degassing behavior in feldspar has an inherent susceptibility to fluid infiltration and structural modification. This rationale provides a potential explanation for young Klokken patch perthite subgrains that invokes coupled argon transport and fluid modification.

Further work remains regarding the specific problems at Klokken as well as the need to recognize and then understand how low temperature modifications to microtextures are related to $^{40}Ar^*$ loss. Microtextures common to patch perthites may inherit a predetermined susceptibility to fluid alteration based on their original magmatic and deuteric history. Determining the timing of microtextural modification by microsampling and single grain K-feldspar analyses will be an important aspect in understanding modification history. On the basis that the MDD model accurately represents the geologic history of feldspar, mineralogists and petrologists can benefit from temporal information. By the same token, MDD practitioners will benefit by recognizing microtextural changes that can be properly understood within temperature and fluid histories.

3.9 Conclusion

$^{40}Ar/^{39}Ar$ step heating of sub-milligram feldspar grain fragments from the Klokken intrusion demonstrates that discrete ages correlated with microtexture can be resolved, even within a single, deuterically altered grain. This information shows that early $^{40}Ar/^{39}Ar$ work misinterpreted age spectra for at least one mixed cryptoperthite and patch perthite sample (140025) due to bulk sampling of altered and unaltered phases, and, in part explains the complexity of the early data. Microsample analyses of patch perthite from sample 140025 also show this microtexture records apparent ages much younger than the intrusion age (400-660 Ma). Isothermal heating experiments and evaluation of the ^{39}Ar and $^{40}Ar^*$ diffusive behavior in Klokken patch perthite and cryptoperthite indicate these feldspars, despite different ages and microtextures, can be characterized by similar kinetics and yield diffusion behavior typical of K-feldspar from numerous other studies. This leads to a re-evaluation of the geologic history at Klokken in which Early Paleozoic ages result from fluid infiltration that perhaps is related regionally to the Caledonian orogeny. The microporous nature of patch perthite in Klokken laminated syenites evidently endows this microtexture with a particular susceptibility to fluid modification unlike cryptoperthite in granular syenite that are generally unaffected. Microtextural modification may be a ubiquitous occurrence in other patch perthites and emphasizes the necessity of collaborative efforts between mineralogists and argon thermochronologists.

4.1 References Cited

Amarante, J.F.A., Kelly, S.A., and Miller, K.C., 2002, Characterization of the Proterozoic basement in Mescalero #1, Guadalupe County, New Mexico: American Association of Petroleum Geologists Rocky Mountains session meeting, AAPG Bulletin 84, p. 1235.

Amarante, J.F.A., Kelley, S.A., Heizler, M.T., Barnes, M.A., Miller, K.C., Anthony, E., 2005, Characterization and age of the Mesoproterozoic Debaca sequence in the Tucumcari basin, New Mexico *in* Karlstrom, K. E., and Keller, G. R., eds., The Rocky Mountain Region-An Evolving Lithosphere: Tectonics, Geochemistry, and Geophysics: American Geophysical Union Monograph 154; in press.

Andresen, A. and Hartz, E., 2001, Caledonian magmatism in East Greenland; an update: Geological Society of America Abstracts with Programs, v. 33, no. 1, p. 31.

Baltz, E.H. and Myers, D.A., 1999, Stratigraphic framework of upper Paleozoic rocks, southeastern Sangre de Cristo Mountains, New Mexico, with a section on speculations and implications for regional interpretation of Ancestral Rocky Mountains paleotectonics: New Mexico Bureau of Mines and Mineral Resources Memoir 48, 272 p.

Bauer, P. W., and Pollock, T.R., 1993, Compilation of Precambrian isotopic ages in New Mexico: New Mexico Bureau of Mines and Mineral Resources, Open-file Report 389, 130 p.

Bauer, P.W. and Ralser, S., 1995, The Picuris-Pecos fault – repeatedly reactivated from Proterozoic to Neogene, in Bauer, P.W., Kues, B.S., Dunbar, N.W., Karlstrom, K.E., and Harrison, B., eds., Geology of the Santa Fe region, New Mexico, Guidebook 46, New Mexico Geological Society, p. 111-115.

Bauer, P.W., Daniel, C.F., Lucas, S.G., Barker, J.M., and Kottlowski, F.E., 1995, Second-day road log, from Santa Fe to Pecos, Rowe, Bernal, Romeroville, and Mineral Hill, *in* Bauer, P.W., Kues, B.S., Dunbar, N.W., Karlstrom, K.E., and Harrison, B., eds., Geology of the Santa Fe region, New Mexico: New Mexico Geological Society Forty-sixth field conference guidebook, p. 29-55.

Beratan, K.K., 1999, Miocene potassium metasomatism, Whipple Mountains, southeastern California: A datable tracer of extension –related fluid transport: Geology, v. 27, no. 3, p. 259-262.

Bickford, J.M., Soegaard, K., Nielsen, K.C., McLelland, J.M., 2000, Geology and geochronology of Grenville-age rocks in the Van Horn and Franklin Mountains area, west Texas; implications for the tectonic evolution of Laurentia during the Grenville: Geological Society of America Bulletin, v. 112, no.7, p. 1134-1148.

Bird, D. and Speiler, A.R., 2004, Epidote in geothermal systems: Reviews in Mineralogy and Geochemistry, v. 56, p. 235-300.

Blamey, N.J.F. and Norman, D.I., 2002, New Interpretations of Geothermal Fluid Inclusion Volatiles: Ar/He and N^2/Ar ratios – A better indicator of Magmatic Volatiles and Equilibrium Gas Geothermometry: Proceedings of the 27th Annual Geothermal Reservoir Engineering, Stanford University, San Francisco, CA.

Bodnar, R.J., 1992, Revised Equation and Table for Freezing-Point Depressions of H2O-salt fluid inclusions: PACROFI IV Abstract Volume.

Bowring, S.A., 1984, *in* Robertson, J.M., and Condie, K.C., 1989, Geology and geochemistry of early Proterozoic volcanic and subvolcanic rocks of the Pecos greenstone belt, Sangre de Cristo Mountains, New Mexico, *in* Grambling, J.A., and Tewksbury, B.J., eds., Proterozoic Geology of the southern Rocky Mountains, Volume 235: Geological Society of America Special Paper, p. 119-146.

Bowring, S.A., and Condie, K.C., 1982, U-Pb zircon ages from northern and central New Mexico: Geological Society of America Abstracts with Programs, v. 14, p. 304.

Broadhead, R.F., Frisch, K.E., Jones, G., 2002, Geologic structure and petroleum source rocks of the Tucumcari Basin, east-central New Mexico: New Mexico Bureau of Mines and Mineral Resources Open File Report 460, 27 p.

Broadhead, R.F., unpublished data, New Mexico Bureau of Geology and Mineral Resources, 801 Leroy Place, Socorro, New Mexico, 87801.

Brown, W.L., and Parsons, I., 1984, The nature of potassium feldspar, exsolution microtextures and development of dislocations as a function of composition in perthitic alkali feldspars: Contributions to Mineralogy and Petrology, v. 86, p. 335-341.

Brown, W.L., and Parsons, I., 1988, Zoned ternary feldspars in the Klokken intrusion: exsolution microtextures and mechanisms: Contributions to Mineralogy and Petrology, v. 98, no. 4, p. 444-454.

Brown, W.L., Becker, S.M., and Parsons, I., 1983, Cryptoperthites and cooling rate in a layered syenite pluton: A chemical and TEM study: Contributions to Mineralogy and Petrology, v. 82, p. 13-25.

Browne, P.R.L., 1978, Hydrothermal alteration in active geothermal systems: Annual Reviews in Earth and Planetary Science, v. 6, p. 229-250.

Burgess, R., Kelley, S.P., Parsons, I., Walker, F.D.L., and Worden, R.H., 1992, $^{40}Ar/^{39}Ar$

analysis of perthite microtextures and fluid inclusions in alkali feldspars from the Klokken syenite, South Greenland: Earth and Planetary Science Letters, v. 109, p. 147-167.

Cather, S.M., Timmons, J.M., Karlstrom, K.E., 2005, Regional inferences for the 1.4Ga-Holocene lateral slip history of the Picuris-Pecos and related faults, northern New Mexico: New Mexico Geological Society guidebook 56, p. 29-34.

Chapin, C.E., and Cather, S.M., 1994, Tectonic setting of the axial basins of the northern and central Rio Grande rift; in Keller, G.R., and Cather S.M., Basins of the Rio Grande Rift: Structure stratigraphy and tectonic setting: GSA Special Paper 291, p. 5-25.

Chapin, C.E., and Lindley, J.I., 1986, Potassium metasomatism of igneous and sedimentary rocks in detachment terranes and other sedimentary basins: Economic implications: Arizona Geological Society Digest, v. 16, p. 118-126.

Condie, K.C., 1982, Plate-tectonics model for Proterozoic continental accretion in the southwestern United States: Geology, v. 10, no. 1, p. 37-42.

Cosca, M.A. and O'Nions R.K., 1994, A re-examination of the influences of composition on argon retentivity in metamorphic calcic amphiboles: Chemical Geology, v. 112, no. 1-2, p. 39-56.

Dahl, P.S., 1997, A crystal-chemical basis for Pb retention and fission-track annealing systematics in U-bearing minerals, with implications for geochronology. Earth and Planetary Science Letters v.150. p. 277-290.

Dalrymple, G.B. and Lanphere, M.A., 1969, Potassium-argon dating: Freeman, San Francisco.

Davidson, G.J., 1999, Feldspar metasomatism along a Proterozoic rift-basin margin-"Smoke" around a base-metal "fire" (HYC deposit, Australia) or a product of background diagenesis: Geological Society of America Bulletin, v. 111, no. 5, p. 663-673.

Dehler, C.M., Elrick, M., Karlstrom, K.E., Smith, G.A., Crossey, L.J., and Timmons, J.M., 2001, Neoproterozoic Chuar Group (~800-742 Ma), Grand Canyon: a record of cyclic marine deposition during global cooling and supercontinent rifting: Sedimentary Geology, v. 141-142, p. 465-499.

Dickinson, W. R. and Snyder, W. S., 1978, Plate tectonics of the Laramide orogeny, *in* Mattews, V., III, 1978, Laramide folding associated with basement block faulting in the western United States: Geologic Society of America Memior 151, p. 355-366.

Doi, N., Kato, O., Ikeuchi, K., Komatsu, R., Miyazaki, S., Akaku, K., and Uchida, T., 1998, Genesis of the plutonic-hydrothermal system around Quaternary granite in the Kakkonda geothermal system, Japan: Geothermics, v. 27, p. 663-690.

Duffin, M.E., 1989, Nature and origin of authigenic K-feldspar in Precambrian basement rocks of the North American midcontinent: Geology, v. 17, p. 765-768.

Dunbar, N.W., Chapin, C.E., Ennis, D.J., Campbell, A.R., 1994, Trace element and mineralogical alteration associated with moderate and advanced degrees of K-metasoamtism in a rift basin at Socorro, New Mexico: New Mexico Geological Society Guidebook, 45th Field Conference, Mogollon Slope, West-Central New Mexico and East-Central Arizona, p. 225-231.

Elders, W.A., Bird, D.K., Williams, A.E., and Schiffman, P., 1984, Hydrothermal flow regime and magmatic heat source of the Cerro Prieto geothermal system, Baja, California, Mexico: Geothermics, v. 13, p. 27-47.

Ennis, D.J., Dunbar, N.W., Campbell, A.R., Chapin, C.E., 2000, The effects of K-metasomatism on the mineralogy and geochemistry of silicic ignimbrites near Socorro, New Mexico; Chemical Geology, v. 167, p. 285-312.

Erslev, E.A., Fankhauser, S.D., Heizler, M.T., Sanders, R.E., Cather, S.M., 2004, Strike-slip tectonics and thermochronology of northern New Mexico: A field guide to critical exposures in the southern Sangre de Cristo Mountains *in* Nelson, E.P., and Erslev, E.A., eds., Field trips in the southern Rocky Mountains, U.S.A: Geological Society of America Field Guide 5, p. 15-40.

Finch, A.A., and Klein, J., 1999, The causes and petrological significance of cathodoluminescence emissions from alkali feldspars: Contributions to Mineralogy and Petrology, V. 135, p. 234-243.

Fitz Gerald, J.D., Parsons, I., and Cayzer, N., 2006, Nanotunnels and pull-aparts: Defects of exsolution lamellae in alkali feldspars: American Mineralogist, v. 91, p. 772-783.

Fitz Gerald, J.D. and Harrison, T.M., 1993, Argon diffusion domains in K-feldspar I: microstructures in MH-10: Contributions to Mineralogy and Petrology, v. 113, p. 367-380.

Foland, K.A., 1974, ^{40}Ar diffusion in homogenous orthoclase and an interpretation of Ar diffusion in K-feldspar: Geochimica et Cosmochimica Acta, v. 38, p. 151-166.

Foland, K.A., Hubacher, F.A., and Arehart, G.B., 1992, $^{40}Ar/^{39}Ar$ dating of fine-grained samples: An encapsulated-vial procedure to overcome the problem of ^{39}Ar recoil loss: Chemical Geology (Isotope Geoscience Section), v. 102, p. 269-276.

Foland, K.A., 1994, Argon diffusion in feldspars *in* Feldspars and their reactions (ed. I. Parsons, p. 415-447. Kluwer, Dordrecht.

Foster, D.A., Harrison, T.M., Copeland, P. and Heizler, M.T., 1990, Effects of excess argon within large diffusion domains on K-feldspar age: Geochimica et Cosmochimica Acta, v. 54, p. 1699-1708.

Geissman, J.W. and Harlan, S.S., 2002, Late Paleozoic remagnetization of Precambrian crystalline rocks along the Precambrian/Carboniferous nonconformity, Rocky Mountains: a relationship among deformation, remagnetization, and fluid migration: Earth and Planetary Science Letters, v. 203, p. 905-924.

Giggenbach, W. F., 1984, Mass transfer in hydrothermal alteration systems-a conceptual approach: Geochimica et Cosmochimica Acta, v. 48, p. 2693-2711.

Girard, J.P., and Onstott, T.C., 1991, Application of $^{40}Ar/^{39}Ar$ laser-probe and step-heating techniques to the dating of diagenetic K-feldspar overgrowths: Geochimica et Cosmochimica Acta, v. 55, no. 12, p. 3777-3793.

Gonterman, J.R., 1973, Petrographic study of the Precambrian basement rocks of Ohio [M.S. thesis]: Columbus, Ohio State University, 139 p.

Grambling, J.A., Williams, M.L., Smith, R.F., and Mawer, C.K., 1989, The role of crustal extension in the metamorphism of Proterozoic rocks in New Mexico *in* Grambling J.A., and Tewksbury, B.J., eds., Proterozoic geology of the southern Rocky Mountains: Geological Society of America Special Paper 235, p. 87-110.

Grapes, R.M., and Hoskin, P.W.O., 2004, Epidote group minerals in low-medium pressure metamorphic terranes: Reviews in Mineralogy and Geochemistry, v. 56, p. 301-345.

Harper, C.L., 1988, On the Nature of Time in Cosmological Perspective: Ph.D. Thesis, University of Oxford

Harrison, T.M., Heizler, M.T., Lovera, O.M., 1993, *In vacuo* crushing experiments and K-feldspar thermochronometry. Earth. Planet. Science Letters, 117, 169-180.

Harrison, T.M., Heizler, M.T., Lovera O.M. and Wenji, C., 1994, A chlorine disinfectant for excess argon. Earth Planet. Sci. Lett., 123, 95-104.

Hearn, P.P. Jr., and Sutter, J.F., 1985, Authigenic potassium feldspar in Cambrian carbonates: Evidence of Alleghanian brine migration: Science, v. 228, p. 1529-1531.

Heizler, M.T., Lux, D.R., Decker, E.R., 1988, The age and cooling history of the Chain of Ponds and Big Island Pond plutons and the Spider Lake Granite, west-central Maine and Quebec: American Journal of Science, v. 288, no. 9, p. 925-952.

Heizler, M.T., 1998, Filling the thermochronological void in parts of the Southwestern U.S.: Geological Association of Canada/Mineralogical Association of Canada Annual meeting Program with Abstracts, p. 76.

Heizler, M.T. and Harrison, T.M., 1998, The thermal history of the New York basement determined from $^{40}Ar/^{39}Ar$ K-feldspar studies: Journal of Geophysical Research, v. 103, p. 29,795-29,814.

Heizler, M.T., Perry, F.V., Crowe, B.M., Peters, L., and Appelt, R., 1999, The age of Lathrop Wells volcanic center; an $^{40}Ar/^{39}Ar$ dating investigation: Journal of Geophysical Research Solid Earth and Planets, v. 104, no. 1., p. 767-804.

Hodges, K.V., Hames, W.E., Bowring, S.A., 1994, $^{40}Ar/^{39}Ar$ age gradients in micas from high-temperature low-pressure metamorphic terrain; evidence for very slow cooling and implications for the interpretation of age spectra: Geology, v. 22, no. 1, p. 55-58.

Isachsen, C., 2003, Macintosh code for PbDAT data reduction program for Excel: Earthtime website: Pb_MacDat_5.

Karlstrom, K.E., Dallmeyer, R.D., Grambling, J.A., 1997, $^{40}Ar/^{39}Ar$ evidence for 1.4 Ga regional metamorphism in New Mexico: Implications for thermal evolution of lithosphere in the southwestern USA; Journal of Geology, v.105, p. 205-223.

Karlstrom, K.E. and Humphreys, E.D., 1998, Persistent influence of Proterozoic accretionary boundaries in the tectonic evolution of southwestern North America: Interaction of cratonic grain and mantle modification events: Rocky Mountain Geology, v. 33, no. 2, p. 161-179.

Karlstrom, K.E., Harlan, S., Williams, M.L., McLelland, J., Geissman, J.W., Ahall, Karl-Inge, 1999a, Refining Rodinia: Geologic evidence for the Australia-Western U.S. connection in the Proterozoic; GSA Today, v. 9, no. 10, p. 1-6.

Karlstrom, K.E., Cather, S.M., Kelley, S.A., Heizler, M.T., Pazzaglia, F.J., Roy, M., 1999b, Sandia Mountains and Rio Grande Rift: Ancestry of structures and history of deformation: New Mexico Geological Society Guidebook, 50th field conference, Albuquerque Geology, p. 155-165.

Karlstrom, K. E., Amato, J. M., Williams, M. L., Heizler, M.T., Shaw, C. A., Read, A. S., and Bauer, P., 2004, Proterozoic tectonic evolution of the New Mexico region: A synthesis, *in* Mach, G. H. and Giles, K. A. eds., The geology of New Mexico, A geologic history: New Mexico Geological Society, Special Publication 11, p. 1-34.

Kastner M., and Siever, R., 1979, Low temperature feldspars in sedimentary rocks: American Journal of Science, v. 279, p. 435-479.

Kelly, S.A. and Chapin, C.E., 1995, Apatite fission-track thermochronology of southern Rocky Mountain-Rio Grande rift-western High Plains provinces: New Mexico Geological Society Guidebook, 46th field conference, Geology of the Santa Fe Region, p. 87-96.

Kluth, C.F. and Coney, P.J., 1980, Plate tectonics of the Ancestral Rocky Mountains: Geology, v. 9, p. 10-15.

Kwon, J., Min, K., Bickel, P., and Renne, P. R., 2002, Statistical methods for jointly estimating decay constants of ^{40}K and age of dating standard: Mathematical Geology, v. 34, no. 2, p. 45-474

Lanphere, M.A., and Baadsgaard, H., 2001, Precise K-Ar, $^{40}Ar/^{39}Ar$, Rb-Sr, and U/Pb mineral ages from the 27.5 Ma Fish Canyon tuff reference standard. Chem. Geol. 175, 653-671.

Lee, M.R. and Parsons, I., 2003, Microtextures of authigenic Or-rich feldspar in the Upper Jurassic Humber Group, UK North Sea: Sedimentology, v. 50, no. 3, p. 597-608.

Lee, M.R., Parsons, I., Edwards, P.R., and Martin, R.W., 2007, Identification of cathodoluminescence activators in zoned alkali feldspars by hyperspectral imaging and electron-probe microanalysis: American Mineralogist, v. 92, p. 243-253.

Leising, J.F., Tyler, S.W., and Miller, W.W., 1995, Convection of saline brines in enclosed lacustrine basins: A mechanism for potassium metasomatism: Geological Society of America Bulletin, v. 107, no. 10, p. 1157-1163.

Lidiak, E.G., and Ceci V.M., 1991, Authigenic K-feldsapr in the Precambrian basement of Ohio and its effect on tectonic discrimination of the granitic rocks: Canadian Journal of Earth Science, v. 28, p. 1624-1634.

Liebscher, A. and Franz, G (eds.), 2004, Epidotes: Reviews in Mineralogy and Geochemistry, v. 56, Mineralogical Society of America/Geochemical Society, Washington D.C., 628 p.

Link, P.K.(Ed.), Christie-Blick, N., Devlin, W.J., Elston, D.P., Horodyski, R.J., Levy. M., Miller, J.M.G, Pearson, R.C., Prave, A., Stewart, J.H., Winston, D., Wright, L.A., Wrucke, C.T., 1993, Middle and Late Proterozoic stratified rocks of the western U.S. Cordillera, Colorado Plateau, and Basin and Range province *in* Reed Jr., J.C., Bickford, M.E., Houston, R.S., Link, P.K., Rankin, D.W., Sims, P.K., Van Schmus, W.R.(Eds.), Precambrian: Conterminous U.S. DNAG C-2, p. 463-596.

Liu, J., Hay, R.L., Deino, A., Kyser, T.K., 2003, Age and origin of authigenic K-feldspar in uppermost Precambrian rocks in the North American midcontinent: Geological Society of America Bulletin, v. 115, no. 4, p. 422-433.

Lo, C. and Onstott, T.C., 1989, ^{39}Ar recoil artifacts in chloritized biotite: Geochimica et Cosmochimica Acta, v. 53, no. 10, p. 259-274.

Lochman-Balk, C., 1971, The Cambrian of the craton of the United States, *in* Holland, C.H., ed., Cambrian of the New World, lower Paleozoic rocks of the World, v. 1: New York, Wiley Interscience, p. 79-167.

Lovera, O.M., Richter, F.M., Harrison, T.M., 1989, ^{40}Ar/^{39}Ar thermochronology for slowly cooled samples having a distribution of domain sizes: Journal of Geophysical Research, v. 94, p. 17,917-17,935.

Lovera, O.M., Harrison, T.M., Richter, F.M., 1991, Diffusion domains determined by 39Ar released during step heating, Journal of Geophysical Research, v. 96, p. 2057-2069.

Lovera, O.M, Heizler, M.T., and Harrison, T.M., 1993, Argon diffusion domains in K-feldspar II: kinetic properties of MH-10: Contributions to Mineralogy and Petrology, v. 113, p. 381-393.

Lovera, O.M., Grove, M., Harrison, T.M., 1997, Systematic analysis of K-feldspar ^{40}Ar/^{39}Ar step heating results; I, Significance of activation energy determination: Geochimica et Cosmochimica Acta, v. 61, no. 15, p. 3171-3192.

Lovera, O.M., Grove, M., Harrison, T.M., 2002, Systematic analysis of K-feldspar ^{40}Ar/^{39}Ar step heating results II: Relevance of laboratory argon diffusion properties to nature; Geochimica et Cosmochimica Acta, v. 66, no. 7, p. 1237-1255.

Ludwig, K.R., 1988, PBDAT for MS-DOS, a computer program for IBM-PC compatibles for processing raw Pb-U-Th isotope data, version 1.24: U.S. Geological Survey, Open-File Report 88-542.

Magnani, M.B., Levander, A., Erslev, E.A., Bolay-Koenig, N., Karlstrom, K.E., 2005, Listric thrust faulting in the Laramide front of north-central New Mexico guided by Precambrian basement structures *in* Karlstrom, K. E., and Keller, G. R., eds., The Rocky Mountain Region-An Evolving Lithosphere: Tectonics, Geochemistry, and Geophysics: American Geophysical Union Monograph 154; in press.

Mallory, W. W., 1958, Pennsylvanian coarse arkosic redbeds and associated mountains in Colorado: RMAG symposium on Pennsylvanian Rocks of the Colorado and adjacent areas, p. 17-20.

Marcoline, J. R., Heizler, M. T., Goodwin, L. B., Ralser, S., Clark, J., 1999, Thermal, structural, and petrological evidence for 1400-Ma metamorphism and deformation in central New Mexico: Rocky Mountain Geology, v. 34, no.1, p. 93-119.

Mariano, A.N., 1988, Some further applications of cathodoluminescence *in* Marshall, D, (ed.) Cathodoluminescense of geological materials: Unwin Hyman, Boston, USA, p. 94-123.

Marshak, S., Karlstrom, K.E., Timmons, J.M., 2000, Inversion of Proterozoic extensional faults: An explanation for the pattern of Laramide and Ancestral Rockies intracratonic deformation, United States: Geology, v. 28, p. 735-738.

McClaren, S., Dunlap, W.J., and Powell, R., 2007, Understanding K-feldspar , $^{40}Ar/^{39}Ar$ data: reconciling models, methods and microtextures: Journal of the Geological Society, London, v. 164, p. 941-944.

McDougall, I. and Harrison, T.M., 1999, Geochronology and thermochronology by the $^{40}Ar/^{39}Ar$ method: Oxford University Press, New York, 269 p.

McMillian, N.J. and McLemore, V. T., 2004, Cambrian-Ordivician magmatism and extension in New Mexico and Colorado *in* Cather, S.M., McIntosh, W.C., and Kelly, S.A. eds.: Tectonics, geochronology, and volcanism in the Southern Rocky Mountains and Rio Grande Rift: New Mexico Bureau of Geology and Mineral Resources, 801 Leroy Pl., Socorro, NM, 87801, p. 1-12.

Melis, E.A., 2001, $^{40}Ar/^{39}Ar$ K-feldspar thermochronologic constraints on the brittle tectonic and uplift history of the southern Sangre de Cristo Mountains, Northern New Mexico since 1100 Ma: [M.S. Thesis], New Mexico Institute of Mining and Technology, Socorro, New Mexico, 87801.

Mensing, T.M. and Faure, G., 1983, Identification and age of neoformed Paleozoic feldspar (adularia) in a Precambrian basement core from Scioto County, Ohio, USA: Contributions to Mineralogy and Petrology, v. 82, p. 327-333.

Miller, J.P., Montgomery, A., Sutherland, P.K., 1963, Geology of Part of the Sangre de Cristo Mountains; New Mexico State Bureau of Mines and Mineral Resources Memoir 11, 106 p.

Min, K., Mundil, R., Renne, P. R., and Ludwig, K. R., 2000, A test for systematic errors in $^{40}Ar/^{39}Ar$ geochronology through comparison with U/Pb analysis of a 1.1 Ga rhyolite: Geochimica et Cosmochimica Acta, v. 64, p. 73-98.

Munha, J., Fyfe, W.S., and Kerrich, R., 1980, Adularia: The characteristic mineral of felsic spillites: Contributions to Mineralogy and Petrology, v. 75, p. 15-19.

Myrow, P.M., Taylor, J.F., Miller, J.F, Ethington, R.L., Ripperdan, R.L., Allen, J., 2003,

Fallen arches: Dispelling myths concerning Cambrian and Ordovician paleogeography of the Rocky Mountain region; GSA Bulletin, v.115, no. 6, p. 695-713.

O'Nions, R.K., Smith, D.G.W., Baadsgaard, H., Morton, R.D., 1969, Influence of chemical composition on argon retentivity in metamorphic calcic amphiboles from south Norway: Earth and Planetary Science Letters, v. 5, no. 5, p. 339-345.

Onstott, T. C., and Peacock, M.W., 1987, Argon Retentivity of hornblendes: a field experiment in a slowly cooled metamorphic terrane: Geochimica et Cosmochimica Acta, v. 51, p. 281-293.

Parry, W.T., Wilson, P.N., Jasumback, M.D., and Heizler, M.T., 1997, Clay mineralogy an $d^{40}Ar/^{39}Ar$ dating of phyllic and argillic alteration at Bingham, Utah: Geological Society of America Abstracts with Programs 26, no. 6, s.282.

Parsons, I., 1978, Feldspars and fluids in cooling plutons: Mineralogical Magazine, v. 42, p. 1-17.

Parsons I., 1979, The Klokken gabbro-syenite complex, South Greenland: cryptic variation and origin of inversely graded layering: Journal of Petrology, v. 20, p. 653-694.

Parsons, I. and Butterfield, A.W., 1981, Sedimentary features of the Nunarssuit and Klokken syenites, S. Greenland: Journal of the Geological Society of London, v. 138, p. 289-306.

Parsons, I. and Brown, W.L., 1984, Feldspars and the thermal history of igneous rocks *in* Brown, W.L., ed., Feldspars and feldspathoids: structure, properties, and occurrences: NATO ASI Series C: Reidel Publishing Company: Dordrecht, p. 317-371.

Parsons, I. and Becker, S.M., 1987, Layering, compaction and post-magmatic processes in the Klokken intrusion *in* Parsons, I., ed., Origins of Igneous Layering: D. Reidel Publishing Company: Dordrecht, p. 29-92.

Parsons, I., Rex, D.C., Guise, P., and Halliday, A.N., 1988, Argon-loss by alkali feldspars: Geochimica et Cosmochimica Acta, v. 52, p. 1097-1112.

Parsons, I., 2005, Written and personal communication, Department of Geology and Geophysics, The University of Edinburgh, UK.

Powell, J.W., 1876, Exploration of the Colorado River of the West: Washington D.C., Smithsonian Institution, 291 p.

Press, W. H., Teukolsky, S.A., Vetterling, W.T., Flannery, B.P., 1992, Numerical recipes in FORTRAN: the art of scientific computing, Cambridge University Press, 2nd ed., 963 p.

Quidelleur, X., Grove, M., Lovera, O.M., Harrison, T.M., Yin, A., 1997, Thermal evolution and slip history of the Renbu Zedong Thrust, southeastern Tibet: Journal of Geophysical Research, v. 102, n. B2, p. 2659-2679.

Ragnarsdottir, K.V., Walther, J.V., and Arnorsson, S., 1984, Description and interpretation of the composition of fluid and alteration mineralogy in the geothermal system, at Svartsengi, Iceland: Geochimica et Cosmochimica Acta, v. 48, p. 1535-1553.

Reed, J.C. Jr., Bickford, M.E., Premo, W.R., Aleinikoff, J.N., Pallister, J.S., 1987, Evolution of the Early Proterozoic Colorado province: Constraints from U-Pb geochronology: Geology, v. 15, p. 861-865.

Renne, P. R., Swisher, C. C., Deino, A. L., Karner, D. B., Owens, T. L., and DePaolo, D.J., 1998, Intercalibration of standards, absolute ages and uncertainties in $^{40}Ar/^{39}Ar$ dating: Chemical Geology, v. 145, no. 1-2, p. 117-152.

Reyes, A.G., 1990, Petrology of Philippine geothermal systems and the application of alteration mineralogy to their assessment: Journal of Volcanology and Geothermal Research, v. 43, p. 279-309.

Reyes, A.G., 1998, Petrology and mineral alteration in hydrothermal systems: From diagenesis to volcanic catastrophes: The United Nations University, Geothermal Training Programme, Reykjavik, Iceland.

Roedder, E., 1984, Fluid Inclusions *in* Reviews in Mineralogy, v. 12: Washington D.C., Mineralogical Society of America, p. 263.

Robertson, J.M., and Condie, K.C., 1989, Geology and geochemistry of early Proterozoic volcanic and subvolcanic rocks of the Pecos greenstone belt, Sangre de Cristo Mountains, New Mexico, *in* Grambling, J.A., and Tewksbury, B.J., eds., Proterozoic Geology of the southern Rocky Mountains, Volume 235: Geological Society of America Special Paper, p. 119-146.

Robertson and Moench, 1979, The Pecos greenstone belt; a Proterozoic volcano-sedimentary sequence in the southern Sangre de Cristo mountains, New Mexico: New Mexico Geological Society 30th conference guidebook, Guidebook of Santa Fe Country, p. 165-173.

Roddy, M.S., Reynolds, S.J., Smith, B.M., Ruiz, J., 1988, K-metasomatism and detachment-related mineralization, Harcuvar Mountains, Arizona: Geological Society of America Bulletin, v. 100, p. 1627-1639.

Rougvie, J.R., and Sorenson, S.S., 2002, Cathodoluminescence record of K-metasomatism in ash-flow tuffs: Grain-scale mechanisms and large-scale geochemical implications: Geology, v. 30, no. 4, p. 307-310.

Sanders, R.E. and Heizler, M.T., 2005, Extraction of MDD thermal histories from $^{40}Ar/^{39}Ar$ K-feldspar step heating data: NMBGMR Open File Report OF-AR 26.

Sanders, R.E., Heizler, M.T., Goodwin, L.B., 2006, $^{40}Ar/^{39}Ar$ thermochronology constraints on the timing of Proterozoic basment exhumation and fault ancestry, southern Sangre de Cristo Range, New Mexico: Geological Society of America Bulletin, v. 118, no. 11/12, p. 1489-1506.

Seki, Y., 1972, Lower-grade stability limit of epidote in light of natural occurrences: Journal of the Geological Society of Japan, v. 78, p. 405-413.

Senderov, E.E., 1973, The relation between Na/K ratios in thermal waters to feldspar-analcime equilibria: Geochemistry International, no. 12, p. 1831-1837.

Shaw, C. A., Heizler, M.T., and Karlstrom, K. E, 2005, Mid-Crustal temperatures during ca. 1.4 Ga metamorphism in the southwestern United States: A regional synthesis of $^{40}Ar/^{39}Ar$ data *in* Karlstrom, K. E., and Keller, G. R., eds., The Rocky Mountain Region-An Evolving Lithosphere: Tectonics, Geochemistry, and Geophysics: American Geophysical Union Monograph 154; in press.

Shimazu, M., and Yajima, J., 1973, Epidote and wairakite in drill cores at the Hachimantai geothermal area, northeastern Japan: Journal of the Japanese Association of Mineralogy, Petrology, and Economic Geology, v. 68, p. 363-371.

Stacey, J.S., Doe, B.R., Silver, L.T., and Zartman, R.E., 1976, Plumbotectonics IIA, Precambrian masiive sulfide deposits: United States Geological Society Open-File Report 76-476.

Steiger, R. H., and Jäger, E., 1977, Subcommission on geochronology: Convention on the use of decay constants in geo- and cosmochronology: Earth and Planetary Science Letters, v. 36, p. 359-362.

Stewart, J.H., Gehrels, G.E., Barth, A.P., Link, P.K., Christie-Blick, N., and Wruke, C.T., 2001, Detrital zircon provenance of Mesoproterozoic to Cambrian arenites in the western United States and northwestern Mexico: Geological Society of America Bulletin, v. 113, no. 10, p. 1343-1356.

Strickland, D., Heizler, M. T., Selverstone, J., and Karlstrom, K. E., 2003, Proterozoic evolution of the Zuni Mountains, western New Mexico: Relationship to the Jemez

Lineament and implications for a complex cooling history: New Mexico Geological Society Guidebook, 54th Field Conference, Geology of the Zuni Plateau, p. 109-117.

Taylor, J.R., 1982, An introduction to error analysis: The study of uncertainties in physical measurements: Univ. Sci. Books, Mill Valley, CA, 270 p.

Timmons, J.M., Karlstrom, K.E., Dehler, C.M., Geissman, J.W., Heizler, M.T., 2001, Proterozoic multistage (ca. 1.1 and 0.8 Ga) extension recorded in the Grand Canyon Supergroup and establishment of northwest- and north-trending tectonic grains in the southwestern United States: Geological Society of America Bulletin, v. 113, no. 2, p. 163-180.

Timmons, J. M., 2004, Mesoproterozoic tectonic evolution of southwestern North America: protracted intracratonic deformation, sedimentation, and differential exhumation in Grand Canyon and the Rocky Mountain region [Dissertation thesis]: University of New Mexico, Albuquerque, New Mexico, 87131.

Timmons, J. M., Karlstrom, K. E., Heizler, M. T., Bowring, S. A., Gehrels, G. E., and Crossey, L. J., 2005, Tectonic inferences from the ca. 1254 -1100 Ma Unkar Group and Nankoweap Formation, Grand Canyon: Intracratonic deformation and basin formation during protracted Grenville orogenesis: Geological Society of America Bulletin, in press.

Turner, G. and Wang, S., 1992, Excess argon, crustal fluids and apparent isochrons from crushing K-feldspar: Earth and Planetary Science Letters, 1, 155-157.

Upton, B.G.J., 1974, The alkaline province of south-west Greenland *in* Sorensen, H., ed., The alkaline rocks: London: Wiley, p. 221-238.

Upton, B.G.J. and Emeleus, C.H., 1987, Mid-Proterozoic alkaline magmatism in Southern Greenland: The Gardar province *in* Fitton, J.G., and Upton, B.G.J., eds., Alkaline Igneous Rocks: Geological Society of London Special Publication 30, p. 449-471.

Villa, I. M., 1994, Multipath Ar transport in K-feldspar deduced from isothermal heating experiments: Earth and Planetary Science Letters, 122, p. 393-401.

Villa, I. M., 1997, Direct determination of ^{39}Ar recoil distance: Geochimica et Cosmochimica Acta, 61, p. 689-691.

Waldron, K.A., Lee, M.R., and Parsons, I., 1994, The microstructures of perthitic alkali feldspars revealed by hydrofluoric acid etching: Contributions to Mineralogy and Petrology, v. 116, p. 360-364.

Warnock, A.C. and van de Kamp, P.C., 1999, Hump-shaped ^{40}Ar/^{39}Ar age spectra in K-

feldspar and evidence for Cretaceous authigenesis in the Fountain Formation near Eldorado Springs, Colorado; Earth and Planetary Science Letters, v. 174, p. 99-111.

Weimer, R.J., 1980, Recurrent movement on basement faults, a tectonic style for Colorado and adjacent Areas: RMAG symposium, p. 23-35.

White, D.E., and Sigvaldason, G.E., 1963, Epidote in hot-spring systems, and depth of formation of propylitic epidote in epithermal ore deposits: United States Geoloigcal Survey Professional Paper 450-E:80-84.

Wilks, M. and Chapin, C.E., 1997, The New Mexico Geochronology Database: Digital Data Series, Database DDS DBI, New Mexico Bureau of Geology and Mineral Resources.

Willaime, C. and Brown, W.L., 1974, A coherent elastic model for the determination of the orientation of exsolution boundaries: application to the feldspars: Acta Crystallography, v. A30, p. 316-331.

Xu, Y-p and Foland, K.A., 1991, Diffusion of Ar isotopes in irradiated minerals during $^{40}Ar/^{39}Ar$ incremental heating: Eos Trans Am Geophys Union, Spring Meeting Suppl 72 (17): 291.

Zartman, R.E. and Doe, B.R., 1981, Plumbotectonics-the model. Tectonophysics, v. 75, p. 135-162.

Data repository 1: $^{40}Ar/^{39}Ar$ analytical techniques

Mass spectrometer parameters

Argon isotopes were analyzed with a MAP 215-50 mass spectrometer equipped with a Johnston electron multiplier operating in static mode with a Nier source. The multiplier is operated at ~2.2 kV and yields a gain of about 7000 above the Faraday. Analyses were conducted in three intervals between 2001 and 2003 during which time mass spectrometer sensitivity ranged from 1.68e-16 to 1.73e-16 mol/pA (NM-145), 2.47e-16 to 2.50e-16 mol/pA (NM-158), and 2.70e-16 mol/pA (NM-164) for furnace analyses and 9.05e-17 to 9.37e-17 mol/pA (NM-145), 1.35e-16 to 1.36e-16 mol/pA (NM-158), and 1.55e-16 mol/pA (NM-164) for laser analyses. One AMU discrimination values were 1.00535±0.00031, 1.00484±0.00092 and 1.0052±0.00121 in favor of light isotopes for NM-145, NM-157, and NM-164, respectively. Resolution at 5% peak-height at mass 40 was typically 600. Detailed description of analytical methods can be found in the New Mexico Bureau of Geology and Mineral Resources open file report OF-AR-1 at http://geoinfo.nmt.edu/publications/openfile/argon/home.html.

Furnace step-heating

Samples were step heated in a double vacuum molybdenum resistance furnace. K-feldspar separates wrapped in Cu-foil were heated with high resolution (~45 steps) heating schedules, and isothermal steps were conducted to help evaluate excess argon contamination (e.g. Harrison et al., 1993). The gas released reacted with a SAES GP-50 getter operating at ~450°C during heating followed by a second stage of clean up using 2 SAES GP-50 getters (one at 20°C, one at ~450°C) and a tungsten filament operated at

~2000°C. Typically K-feldspar steps were gettered for 2 minutes. The furnace thermocouple was calibrated by melting Cu-foil and true furnace temperature was 35 or 45°C lower than thermocouple temperature. Heating schedules were adjusted by this amount, and corrected sample temperatures are reported in data tables.

Furnace blank and background values were determined by running a 15 minute, 800°C hot blank prior to each analysis. In December 2001 blank and background values were 770, 15, 0.9, 8, and $3.3x10^{-18}$ moles and 590, 7, 0.7, 6, and $2.8x10^{-18}$ moles in October 2002 for masses 40, 39, 38, 37, and 36, respectively.

Laser step-heating

Hornblende, muscovite, and biotite were heated using a defocused Synrad 50 Watt CO_2 laser. Extracted gas was gettered using 2 GP-50 getters operating at 20°C and ~450°C, a tungsten filament at 2000°C, and a cold finger at -140°C.

Blanks and backgrounds were run throughout the step heating experiments. Samples were analyzed in three batches at which times blank and background values were 250, 3.5, 0.4, 1.5, $1.0x10^{-18}$ moles in December 2001, 592, 0.3, 0.7, $2.2x10^{-18}$ moles in May 2003, and 500, 4.8, 0.7, 4.8, and $0.90x10^{-18}$ moles in June 2003 for masses 40, 39, 38, 37, and 36, respectively.

Irradiations, flux monitoring, and age calculations

Samples were irradiated in machined Al disks in the 5C position at the McMaster University reactor, Ontario, for 52.800 MW hours (irradiation NM-145), 41.717 MW hours (irradiation NM-158), and 99.95 MW hours (irradiation NM-164). Fluence

gradients were measured using Fish Canyon sanidine placed in holes of known geometry in the Al disks. Typically, 4 single crystals from each position were analyzed to determine the J-value. Mean values for each location were fit with a sine curve and J-values for unknowns were extrapolated based on their geometric relation. J-factor errors are estimated at 0.1 to 0.2% (1σ). Correction factors for interfering reactions were measured using CaF_2 and K-glass included with the samples during irradiation. Four to five grains of each are typically fused to obtain a weighted mean value for each factor and are: NM-145 $(^{39}Ar/^{37}Ar)_{Ca} = 0.0007\pm0.00002$; $(^{36}Ar/^{37}Ar)_{Ca} = 0.00027\pm0.000005$; $(^{40}Ar/^{39}Ar)_{K} = 0.031\pm0.001$; NM-158 $(^{39}Ar/^{37}Ar)_{Ca} = 0.00075\pm0.00003$; $(^{36}Ar/^{37}Ar)_{Ca} = 0.000292\pm0.000006$; $(^{40}Ar/^{39}Ar)_{K} = 0.0296\pm0.0005$, and NM-164 $(^{39}Ar/^{37}Ar)_{Ca} = 0.0007\pm0.00005$; $(^{36}Ar/^{37}Ar)_{Ca} = 0.00027\pm0.00001$; $(^{40}Ar/^{39}Ar)_{K} = 0.02559\pm0.0005$.

Age assignments were handled several ways depending on the complexity of the age spectrum. Ideally, a plateau age is assigned where greater than 50% of the total ^{39}Ar released yields 3 consecutive heating steps with an MSWD of ~1. However, most spectra for this study are complex and weighted means of chosen steps rarely yield MSWD values that fall within the 95% confidence window for n-1 degrees of freedom. Despite this, we still report the weighted mean ages (Taylor, 1982) as plateau ages and increase the weighted mean error by multiplying by the square root of the MSWD. As mentioned in the text, we generally do not attempt to compare data within the cited precision as there are many geological reasons why individual samples will have variable ages and why individual spectra will have internal discordance. Total gas ages and errors are calculated by quadradically summing of all steps and are at times used as our best approximation of the argon closure age.

Monitor age and decay constants

The assigned age of Fish Canyon sanidine is 28.27 Ma and the total ^{40}K decay constant is 5.476e-10/a (Kwon et al., 2002). At present there is no accepted value for the age of FC sanidine (Renne et al., 1998; Lanphere et al., 2001), however there as been considerable recent work towards determining and evaluating the monitor age and ^{40}K decay constants (Min et al., 2000, Kwon, et al., 2002). These recent papers have recognized that $^{40}Ar/^{39}Ar$ ages based on an age of 28.02 Ma for FC sanidine and decay constants recommended by Steiger and Jäger (1977) yield younger results compared to U/Pb ages for samples that should not be discordant. In the near future it is expected that new decay constants for ^{40}K will be recommended based upon the U/Pb system and therefore ages reported here use the values of Kwon et al. (2002) in anticipation of this change. We recognize that these values used here will likely not be the final accepted values, but feel that they best reflect our present knowledge.

Sample preparation

Samples of Proterozoic granite, tonalite, pegmatite, and schist were collected at eight locations along a roughly west to east transect from Santa Fe, NM to Las Vegas, NM. This sampling traverse is perpendicular to the north-striking Picuris-Pecos and Montezuma fault zones and was designed to determine if there are variations in the thermal histories recorded by opposing sides of the faults. Drill cuttings from three basement penetrating petroleum exploration wells east of Las Vegas, NM, approximately 30 kilometers from Hermit Peak, were also obtained from the New Mexico Bureau of

Geology and Mineral Resources. Cuttings provide samples of crystalline basement rocks present in the subsurface of the Las Vegas basin. Depth to basement varies and these three samples are from 925, 1300 and 1600 m. Mineral separates were prepared by standard magnetic and heavy liquid techniques. Grain fractions ranging 600 to 180 microns were hand picked to obtain a monomineralic separate. Separates were weighed and wrapped in copper foil before being loaded into machined aluminum disks which in turn were stacked vertically for irradiation.

DR2. $^{40}Ar/^{39}Ar$ analytical data for samples from the Sangre de Cristo Range and Las Vegas basin, New Mexico.

	ID	Power/Temp (W/°C)	$^{40}Ar/^{39}Ar$	$^{37}Ar/^{39}Ar$	$^{36}Ar/^{39}Ar$ (x 10^{-3})	$^{39}Ar_K$ (x 10^{-15} mol)	K/Ca	$^{40}Ar^*$ (%)	^{39}Ar (%)	Age (Ma)	±1σ (Ma)
	HP02-4 A, E4:157, 1 to 4 xls hornblende, J=0.0188187, D=1.0052±0.00172, NM-157, Lab#=53558-01										
#	A	1.5	278.3	3.325	499.5	0.797	0.15	47.1	0.5	2272	22
#	B	3.0	318.0	5.589	224.9	1.07	0.091	79.2	1.3	3197.4	11.9
#	C	4.0	106.7	4.819	29.62	1.48	0.11	92.2	2.3	1916.2	6.9
#	D	4.5	80.17	5.674	7.142	2.47	0.090	97.9	4.0	1660.6	5.3
#	E	5.0	70.91	5.746	2.908	9.27	0.089	99.4	10.4	1545.9	3.0
#	F	5.5	73.58	5.709	2.552	30.4	0.089	99.6	31.3	1586.5	2.3
	G	6.0	70.20	5.728	2.396	53.1	0.089	99.6	67.9	1537.7	2.3
	H	7.5	70.64	5.742	2.338	34.1	0.089	99.7	91.4	1544.5	2.8
	I	8.5	71.44	7.444	3.501	8.15	0.069	99.4	97.0	1554.5	4.3
#	J	10	66.30	9.437	5.066	3.58	0.054	98.9	99.5	1473.8	7.3
#	K	12	60.46	14.07	7.357	0.798	0.036	98.3	100.0	1380	10
	Total gas age ± 1σ			n=11		145.2				1579.6	2.4
	WMA ± 1σ	steps G-I		n=3	MSWD=6.25	95.4	0.087		65.7	1542.6	4.3
	HP02-4 B, E4:157, 1 to 4 xls hornblende, J=0.0188187, D=1.00484±0.00092, NM-157, Lab#=53558-10										
#	A	1.5	351.2	2.082	409.9	0.602	0.25	65.6	0.9	3059	18
#	B	3.0	87.46	5.713	6.687	24.1	0.089	98.3	36.7	1761.2	1.9
	C	4.0	67.77	5.766	2.557	36.6	0.088	99.6	91.0	1500.6	1.8
	D	4.5	68.21	6.007	10.08	1.44	0.085	96.3	93.2	1473.7	7.0
	E	5.0	72.67	6.474	4.604	2.28	0.079	98.8	96.6	1566.0	5.2
	F	5.5	67.79	7.144	3.966	1.89	0.071	99.1	99.4	1497.1	5.1
#	G	6.0	65.43	7.252	27.85	0.157	0.070	88.3	99.6	1348	38
#	H	7.5	67.19	12.28	13.10	0.268	0.042	95.7	100.0	1456	24
	Total gas age ± 1σ			n=8		67.4				1619.8	1.9
	WMA ± 1σ	steps C-F		n=4	MSWD=55.98	42.3	0.087		62.7	1505	12
	HP02-4 C, E4:157, 1 to 4 xls hornblende, J=0.0188187, D=1.00484±0.00092, NM-157, Lab#=53558-12										
#	A	1.5	182.5	1.540	316.9	1.60	0.33	48.8	1.9	1798	13
#	B	2.5	73.73	2.954	24.29	3.93	0.17	90.6	6.5	1488.1	4.5
#	C	3.4	70.60	5.679	3.239	30.1	0.090	99.3	41.9	1539.9	1.7
	D	4.5	64.23	5.657	2.492	37.8	0.090	99.6	86.4	1446.0	1.4
#	E	5.0	65.88	6.016	3.542	5.54	0.085	99.1	92.9	1467.6	3.3
#	F	5.5	66.74	7.098	3.586	5.67	0.072	99.3	99.6	1482.7	3.3
#	G	6.0	69.73	7.329	15.77	0.372	0.070	94.2	100.0	1474	17
	Total gas age ± 1σ			n=7		84.9				1492.8	1.7
	WMA ± 1σ	steps D-D		n=1	MSWD=0.00	37.8	0.090		44.5	0.0	0.0
	HP02-4 D, E4:157, 1 to 4 xls hornblende, J=0.0188187, D=1.00484±0.00092, NM-157, Lab#=53558-14										
#	A	1.5	363.5	3.841	445.8	0.553	0.13	63.8	1.0	3073	14
#	B	2.5	121.9	5.188	36.31	1.61	0.098	91.5	3.8	2069.8	5.9
#	C	3.5	76.18	5.964	2.814	31.0	0.086	99.5	58.1	1623.2	2.1
	D	4.5	68.13	5.900	2.424	17.9	0.086	99.6	89.4	**1506.8**	**2.2**
#	E	5.0	80.30	7.124	5.389	3.08	0.072	98.7	94.8	1672.3	3.8
#	F	5.5	85.68	7.781	4.538	2.49	0.066	99.2	99.2	1749.8	3.9
#	G	6.0	92.38	10.21	-4.1574	0.162	0.050	102.2	99.5	1873	29
#	H	7.5	109.5	12.10	-0.5330	0.300	0.042	101.0	100.0	2066	19
	Total gas age ± 1σ			n=8		57.0				1635.3	2.0
	Step D										

	ID	Power/Temp (W/°C)	$^{40}Ar/^{39}Ar$	$^{37}Ar/^{39}Ar$	$^{36}Ar/^{39}Ar$ (x 10^{-3})	$^{39}Ar_K$ (x 10^{-15} mol)	K/Ca	$^{40}Ar^*$ (%)	^{39}Ar (%)	Age (Ma)	±1σ (Ma)
	HP02-4 E, E4:157, 1 to 4 xls hornblende, J=0.0188187, D=1.00484±0.00092, NM-157, Lab#=53558-16										
#	A	1.5	329.6	3.267	342.5	0.650	0.16	69.4	0.9	3050	14
#	B	2.5	86.96	5.420	14.97	2.37	0.094	95.4	4.2	1721.3	5.9
#	C	3.5	72.21	5.767	2.120	43.5	0.088	99.8	65.3	1568.6	2.2
	D	4.5	65.59	5.819	2.305	22.3	0.088	99.7	96.5	1468.4	2.0
	E	5.0	63.93	7.294	3.238	1.23	0.070	99.4	98.2	1441.2	6.6
#	F	5.5	69.64	9.908	1.740	1.10	0.051	100.4	99.8	1540.2	6.2
#	G	6.0	76.90	13.22	4.460	0.157	0.039	99.7	100.0	1640	35
	Total gas age ± 1σ			n=7		71.3				1561.8	2.0
	WMA ± 1σ	steps D-E		n=2	MSWD=15.77	23.5	0.087		33.0	1466.2	7.5
	HP02-4 F, E4:157, 1 to 4 xls hornblende, J=0.0188187, D=1.00484±0.00092, NM-157, Lab#=53558-29										
#	A	1.5	354.2	1.742	341.5	0.869	0.29	71.5	1.1	3202	12
#	B	2.5	107.5	4.417	22.48	2.49	0.12	94.1	4.1	1950.2	5.1
	C	3.5	71.44	5.823	2.774	33.4	0.088	99.5	44.4	**1554.5**	**2.0**
#	D	4.5	74.94	5.692	2.107	39.3	0.090	99.8	92.0	1608.0	2.3
#	E	5.0	69.23	8.239	4.432	4.98	0.062	99.1	98.0	1518.9	3.7
#	F	5.5	71.48	16.94	4.852	1.43	0.030	99.9	99.8	1567.4	6.6
#	G	6.0	84.97	29.80	3.444	0.137	0.017	101.6	99.9	1786	32
#	H	7.5	109.0	29.20	-5.2474	0.068	0.017	103.6	100.0	2106	51
	Total gas age ± 1σ			n=8		82.6				1619.6	2.0
	Step C										
	HP02-4 G, E4:157, 1 to 4 xls hornblende, J=0.0188187, D=1.00484±0.00092, NM-157, Lab#=53558-37										
#	A	1.5	387.8	4.504	387.8	0.578	0.11	70.5	0.7	3321	17
#	B	2.5	101.9	5.183	35.99	1.75	0.098	90.0	2.8	1835.0	5.8
#	C	3.0	77.95	5.935	4.276	6.34	0.086	99.0	10.3	1641.9	3.6
#	D	3.5	68.74	5.926	2.598	31.4	0.086	99.6	47.5	1515.3	1.8
	E	4.0	65.74	5.853	2.416	29.7	0.087	99.6	82.6	**1470.3**	**2.9**
#	F	5.0	70.30	7.065	3.206	14.2	0.072	99.5	99.4	1538.2	2.7
#	G	6.0	69.32	6.208	-14.1360	0.325	0.082	106.7	99.8	1597.2	17.4
#	H	7.5	71.11	4.005	-41.1861	0.084	0.13	117.6	99.9	1729	55
#	I	8.5	88.47	2.704	-14.0368	0.056	0.19	104.9	100.0	1847	83
	Total gas age ± 1σ			n=9		84.3				1542.4	1.9
	Step E										
	HP02-4 H, E4:157, 1 to 4 xls hornblende, J=0.0188187, D=1.00484±0.00092, NM-157, Lab#=53558-39										
#	A	1.5	417.9	3.596	413.5	0.544	0.14	70.8	0.8	3442	15
#	B	2.5	95.86	5.057	25.47	1.76	0.10	92.6	3.3	1797.1	5.4
#	C	3.0	78.76	5.734	2.891	13.5	0.089	99.5	22.9	1658.6	2.4
#	D	3.5	66.18	5.804	2.500	33.6	0.088	99.6	71.8	1476.6	2.4
	E	4.0	64.06	5.889	2.670	11.1	0.087	99.5	88.0	**1443.1**	**2.5**
#	F	5.0	68.22	6.827	3.874	7.62	0.075	99.1	99.1	1503.5	2.4
#	G	6.0	66.35	9.118	6.199	0.356	0.056	98.3	99.6	1469	13
#	H	7.5	67.85	8.218	20.63	0.172	0.062	92.0	99.8	1424	24
#	I	8.5	72.75	7.157	58.17	0.109	0.071	77.1	100.0	1321	41
	Total gas age ± 1σ			n=9		68.7				1546.9	2.0
	Step E									**1443.1**	**2.5**

	ID	Power/Temp (W/°C)	$^{40}Ar/^{39}Ar$	$^{37}Ar/^{39}Ar$	$^{36}Ar/^{39}Ar$ (x 10^{-3})	$^{39}Ar_K$ (x 10^{-15} mol)	K/Ca	$^{40}Ar^*$ (%)	^{39}Ar (%)	Age (Ma)	±1σ (Ma)
	HP02-2 I, C11:157, 1 to 4 xls hornblende, J=0.0192598, D=1.0052±0.00172, NM-157, Lab#=53555-01										
#	A	1.5	149.6	1.989	477.4	0.220	0.26	5.8	1.3	283	97
#	B	3.0	73.36	2.322	140.5	0.409	0.22	43.6	3.6	878	34
#	C	4.0	45.37	1.267	26.81	0.411	0.40	82.7	6.0	994	17
#	D	4.5	50.97	2.540	18.67	0.332	0.20	89.6	7.9	1153	16
#	E	5.0	54.42	3.731	10.19	0.610	0.14	95.0	11.5	1264	12
	F	5.5	58.18	5.016	4.335	3.80	0.10	98.5	33.5	1360.8	4.7
	G	6.0	58.23	5.068	3.294	5.01	0.10	99.0	62.5	1366.9	3.8
#	H	7.5	56.37	4.903	2.794	5.24	0.10	99.2	92.8	1337.8	3.8
#	I	8.5	51.79	6.592	6.486	0.585	0.077	97.3	96.2	1242	11
#	J	10	53.06	11.44	2.524	0.506	0.045	100.3	99.1	1296	12
#	K	12	53.24	22.55	18.11	0.158	0.023	93.3	100.0	1240	34
	Total gas age ± 1σ			n=11		17.3				1312.7	3.1
	WMA ± 1σ		steps F-G	n=2	MSWD=1.02	8.8	0.10		51.0	1364.5	3.1
	HP02-2 J, C11:157, 1 to 4 xls hornblende, J=0.0192598, D=1.00484±0.00092, NM-157, Lab#=53555-14										
#	A	1.5	125.3	2.385	344.7	2.20	0.21	18.8	2.0	685	23
#	B	2.5	53.53	3.423	31.30	4.95	0.15	83.2	6.4	1132.8	4.2
	C	3.0	59.55	4.595	3.489	18.9	0.11	98.9	23.3	1387.0	1.9
	D	3.2	59.44	4.733	2.625	12.9	0.11	99.3	34.8	1389.7	2.0
	E	3.5	59.24	4.627	2.194	12.7	0.11	99.5	46.2	1388.1	2.1
	F	4.0	59.02	4.686	2.069	30.0	0.11	99.6	73.0	1385.4	1.9
	G	5.0	59.05	5.407	2.795	24.9	0.094	99.3	95.3	1383.7	3.1
	H	5.5	58.82	13.05	6.034	4.45	0.039	98.7	99.3	1379.3	3.4
#	I	7.5	64.19	45.38	23.60	0.480	0.011	94.8	99.7	1448	16
#	J	10	243.7	49.19	515.7	0.259	0.010	39.1	99.9	1944	38
#	K	12	518.0	78.24	1565.8	0.090	0.007	11.9	100.0	1484	112
	Total gas age ± 1σ			n=11		111.9				1365.7	1.8
	WMA ± 1σ		steps C-H	n=6	MSWD=1.78	103.9	0.10		92.9	1386.5	1.5
	HP02-2 K, C11:157, 1 to 4 xls hornblende, J=0.0192598, D=1.00484±0.00092, NM-157, Lab#=53555-16										
#	A	1.5	144.2	2.091	421.1	2.00	0.24	13.8	1.8	593	21
#	B	2.5	50.16	1.893	63.58	3.10	0.27	62.8	4.5	866.6	7.1
#	C	3.0	57.12	3.540	8.821	4.39	0.14	95.9	8.3	1317.5	3.4
#	D	3.2	58.02	4.242	1.845	6.35	0.12	99.6	13.9	1368.9	3.3
	E	3.5	59.56	4.669	1.629	20.4	0.11	99.8	31.7	1396.3	2.0
	F	4.0	59.54	4.610	2.020	46.3	0.11	99.6	72.2	1393.9	1.6
#	G	5.0	58.20	4.978	2.757	21.2	0.10	99.3	90.8	1368.8	2.2
#	H	5.5	54.62	5.930	3.963	9.12	0.086	98.7	98.8	1303.9	2.2
#	I	7.5	52.29	9.216	3.577	0.944	0.055	99.4	99.6	1272.0	8.0
#	J	10	97.40	19.13	140.1	0.403	0.027	59.0	99.9	1374	22
#	K	12	296.9	92.03	800.5	0.064	0.006	22.8	100.0	1593	122
	Total gas age ± 1σ			n=11		114.3				1353.3	1.7
	WMA ± 1σ		steps E-F	n=2	MSWD=0.82	66.7	0.11		58.3	1394.8	1.6

	ID	Power/Temp (W/°C)	$^{40}Ar/^{39}Ar$	$^{37}Ar/^{39}Ar$	$^{36}Ar/^{39}Ar$ (x 10^{-3})	$^{39}Ar_K$ (x 10^{-15} mol)	K/Ca	$^{40}Ar^*$ (%)	^{39}Ar (%)	Age (Ma)	±1σ (Ma)
	HP02-2 L, C11:157, 1 to 4 xls hornblende, J=0.0192598, D=1.00484±0.00092, NM-157, Lab#=53555-30										
#	A	1.5	62.97	2.809	131.7	0.637	0.18	38.5	1.6	701	24
#	B	2.5	47.29	3.579	26.99	0.986	0.14	83.7	4.0	1036.4	9.7
	C	3.0	59.46	4.537	3.637	6.92	0.11	98.8	21.2	1384.6	2.9
	D	3.2	59.21	4.617	1.602	6.58	0.11	99.8	37.5	1390.6	2.9
	E	3.5	58.88	4.699	1.840	7.63	0.11	99.7	56.4	1384.2	3.3
	F	4.0	59.42	4.789	2.504	14.1	0.11	99.4	91.3	1389.9	2.2
#	G	5.0	55.96	6.454	5.679	1.83	0.079	97.9	95.8	1319.3	6.0
#	H	5.5	57.76	9.751	8.354	0.457	0.052	97.1	96.9	1343	15
#	I	7.5	59.23	17.46	13.48	0.643	0.029	95.6	98.5	1358	11
#	J	10	97.87	25.51	142.6	0.564	0.020	59.0	99.9	1383	20
#	K	12	317.9	99.77	1083.5	0.025	0.005	1.8	100.0	203	497
	Total gas age ± 1σ			n=11		40.3				1366.1	1.9
	WMA ± 1σ	steps C-F		n=4	MSWD=1.41	35.2	0.11		87.3	1387.9	1.9
	HP02-2 A, E7:157, 1 to 4 xls biotite, J=0.0193994, D=1.0052±0.00172, NM-157, Lab#=53560-01										
#	A	1.0	582.2	0.1682	1915.2	2.49	3.0	2.8	2.6	501	122
#	B	1.4	74.53	0.0299	86.69	5.44	17.1	65.6	8.2	1218.0	6.6
	C	1.7	60.91	0.0124	27.58	7.11	41.1	86.6	15.5	1286.5	3.9
	D	2.0	56.94	0.0086	11.21	13.7	59.6	94.2	29.6	1301.8	3.1
	E	2.4	55.28	0.0099	4.654	19.6	51.3	97.5	49.8	1306.5	2.3
	F	2.7	55.51	0.0075	2.946	13.9	68.0	98.4	64.1	1319.2	2.6
	G	3.0	54.86	0.0097	1.607	8.63	52.7	99.1	73.0	1314.8	2.8
	H	3.5	55.01	0.0287	3.042	7.65	17.8	98.4	80.9	1310.1	3.1
	I	3.8	54.70	0.0514	5.150	3.23	9.9	97.2	84.3	1294.0	4.8
	J	4.2	54.83	0.0847	4.904	2.15	6.0	97.4	86.5	1297.5	4.8
	K	5.0	54.04	0.1376	2.543	4.96	3.7	98.6	91.6	1296.1	3.0
	L	6.0	54.20	0.3291	4.554	3.51	1.6	97.6	95.2	1288.9	4.1
	M	8.0	53.53	1.198	5.475	4.45	0.43	97.2	99.8	1274.2	4.0
	N	10	54.88	0.2650	13.68	0.185	1.9	92.7	100.0	1253	30
	Total gas age ± 1σ			n=14		96.9				1282.1	4.0
	WMA ± 1σ	steps C-N		n=12	MSWD=14.41	89.0	41.8		91.8	1303.0	3.8
	HP02-2 B, E7:157, 1-4 xls biotite, J=0.0193994, D=1.00484±0.00092, NM-157, Lab#=53560-10										
#	A	1	298.0	0.0484	874.8	24.8	10.5	13.2	6.2	1038	22
	B	1.4	60.61	0.0047	25.10	55.2	107.9	87.8	20.0	1294.1	2.0
	C	1.7	55.46	0.0028	5.259	85.1	179.7	97.2	41.3	1306.6	1.7
	D	2.0	55.39	0.0030	2.663	63.7	171.8	98.6	57.2	1318.5	1.7
	E	2.4	55.14	0.0053	2.066	54.2	96.2	98.9	70.7	1317.3	1.8
	F	2.7	55.88	0.0144	2.247	24.3	35.5	98.8	76.8	1329.1	1.8
	G	3.0	55.53	0.0116	2.675	19.1	43.9	98.6	81.6	1321.0	1.8
	H	3.5	55.30	0.0482	2.499	21.7	10.6	98.7	87.0	1318.0	2.6
	I	3.8	55.30	0.0330	2.512	13.9	15.5	98.7	90.4	1317.9	2.1
	J	4.2	55.09	0.0716	3.025	8.05	7.1	98.4	92.5	1311.7	2.6
	K	5.0	55.32	0.2525	3.901	9.80	2.0	98.0	94.9	1311.5	2.8
	L	6.0	54.85	0.5949	3.946	15.8	0.86	98.0	98.8	1303.9	2.6
	M	8.0	55.02	0.9436	4.636	1.02	0.54	97.6	99.1	1304.1	9.0
	N	10	55.38	0.6542	3.873	3.63	0.78	98.0	100.0	1313.6	4.2
	Total gas age ± 1σ			n=14		400.4				1296.0	2.3
	WMA ± 1σ	steps B-N		n=13	MSWD=20.01	375.5	105.6		93.8	1314.4	2.9

	ID	Power/Temp (W/°C)	$^{40}Ar/^{39}Ar$	$^{37}Ar/^{39}Ar$	$^{36}Ar/^{39}Ar$ (x 10^{-3})	$^{39}Ar_K$ (x 10^{-15} mol)	K/Ca	$^{40}Ar^*$ (%)	^{39}Ar (%)	Age (Ma)	±1σ (Ma)
	HP02-2 C, E7:157, 1-4 xls biotite, J=0.0193994, D=1.00484±0.00092, NM-157, Lab#=53560-34										
#	A	1.0	105.6	0.0251	188.2	53.3	20.3	47.3	29.4	1237.6	6.1
	B	1.4	54.44	0.0124	3.199	55.1	41.1	98.3	59.8	1299.4	1.9
	C	1.7	54.65	0.0348	1.607	29.6	14.7	99.1	76.1	1311.3	1.7
	D	2.0	54.91	0.0102	2.099	11.4	50.0	98.9	82.4	1313.2	2.4
	E	2.4	54.29	0.0544	1.821	10.2	9.4	99.0	88.0	1304.0	2.6
	F	2.7	53.99	0.0597	3.162	5.55	8.6	98.3	91.1	1291.9	3.2
	G	3.0	53.31	0.0701	3.604	3.25	7.3	98.0	92.9	1277.7	3.7
	H	3.5	53.51	0.3676	2.857	2.84	1.4	98.5	94.4	1285.7	4.8
	I	3.8	53.89	0.2722	3.740	1.91	1.9	98.0	95.5	1287.5	4.8
	J	4.2	53.61	0.5515	3.814	2.04	0.93	98.0	96.6	1282.9	4.9
	K	5.0	52.38	1.087	3.579	2.01	0.47	98.1	97.7	1263.4	5.6
	L	6.0	53.72	0.8449	1.543	1.86	0.60	99.3	98.7	1297.1	4.8
	M	8.0	53.48	1.302	4.899	2.28	0.39	97.5	100.0	1276.4	6.2
	Total gas age ± 1σ			n=13		181.3				1282.7	2.5
	WMA ± 1σ	steps B-M		n=12	MSWD=18.47	127.9	26.9		70.6	1300.2	3.8
	HP02-2 D, E7:157, 1-4 xls biotite, J=0.0193994, D=1.00484±0.00092, NM-157, Lab#=53560-36										
#	A	1.0	123.3	0.0267	255.5	81.8	19.1	38.7	23.2	1196.5	7.6
	B	1.4	54.39	0.0114	6.364	100.8	44.9	96.5	51.8	1282.3	2.0
	C	1.7	53.84	0.0170	2.192	54.9	30.0	98.8	67.4	1294.1	2.0
	D	2.0	53.94	0.0192	1.957	34.5	26.6	98.9	77.2	1297.2	1.7
	E	2.4	53.42	0.0513	2.518	23.6	10.0	98.6	83.9	1285.3	2.0
	F	2.7	52.62	0.0849	2.261	14.6	6.0	98.7	88.1	1272.5	1.9
	G	3.0	52.76	0.1239	2.756	9.99	4.1	98.5	90.9	1272.4	2.4
	H	3.5	52.42	0.0440	2.797	8.40	11.6	98.4	93.3	1266.1	3.1
	I	3.8	52.31	0.1309	3.751	7.31	3.9	97.9	95.4	1259.3	2.7
	J	4.2	52.45	0.1288	3.082	3.33	4.0	98.3	96.3	1265.4	3.6
	K	5.0	52.56	0.5652	3.110	4.19	0.90	98.3	97.5	1268.0	3.3
	L	6.0	53.16	0.5080	3.319	7.36	1.0	98.2	99.6	1277.5	2.3
	M	8.0	55.25	-0.0074	5.501	1.43	-	97.1	100.0	1301.6	5.4
	Total gas age ± 1σ			n=13		352.1				1264.4	2.6
	WMA ± 1σ	steps B-M		n=12	MSWD=28.29	270.3	28.1		76.8	1280.8	3.7
	HP02-2 E, E7:157, 1-4 xls biotite, J=0.0193994, D=1.00484±0.00092, NM-157, Lab#=53560-38										
#	A	1.0	111.7	0.0310	229.2	57.4	16.4	39.3	14.2	1124.9	7.0
	B	1.4	54.41	-0.0040	7.414	95.1	-	96.0	37.8	1277.1	1.7
	C	1.7	53.64	0.0064	2.611	75.8	79.8	98.6	56.5	1288.5	1.9
	D	2.0	53.47	0.0064	1.697	33.5	79.8	99.1	64.8	1290.3	1.8
	E	2.4	53.56	0.0165	1.859	41.2	31.0	99.0	75.0	1291.0	1.9
	F	2.7	52.74	0.0731	2.406	24.3	7.0	98.7	81.0	1273.9	2.7
	G	3.0	53.20	0.0918	2.579	16.2	5.6	98.6	85.1	1281.2	2.3
	H	3.5	52.88	0.1207	1.805	16.4	4.2	99.0	89.1	1279.5	2.3
	I	3.8	52.50	0.0829	2.372	7.11	6.2	98.7	90.9	1269.8	2.7
	J	4.2	52.63	0.1689	2.431	8.24	3.0	98.7	92.9	1272.1	2.3
	K	5.0	53.57	0.3573	2.845	8.37	1.4	98.5	95.0	1286.7	2.6
	L	6.0	52.90	0.8103	2.580	19.2	0.63	98.7	99.7	1277.3	2.6
	M	8.0	51.50	1.098	-2.5780	0.427	0.46	101.7	99.8	1280	15
	N	10	54.07	0.8178	4.789	0.614	0.62	97.5	100.0	1286	11
	Total gas age ± 1σ			n=14		403.9				1261.0	1.9
	WMA ± 1σ	steps B-N		n=13	MSWD=10.06	346.5	41.5		85.8	1282.0	2.2

	ID	Power/Temp (W/°C)	$^{40}Ar/^{39}Ar$	$^{37}Ar/^{39}Ar$	$^{36}Ar/^{39}Ar$ ($\times 10^{-3}$)	$^{39}Ar_K$ ($\times 10^{-15}$ mol)	K/Ca	$^{40}Ar^*$ (%)	^{39}Ar (%)	Age (Ma)	±1σ (Ma)
	HP02-2 F, E7:157, 1-4 xls biotite, J=0.0193994, D=1.00484±0.00092, NM-157, Lab#=53560-40										
#	A	1.0	99.99	0.0493	187.2	29.8	10.4	44.7	11.6	1139.3	5.7
	B	1.4	56.55	0.0121	11.88	70.2	42.2	93.8	38.9	1291.5	1.8
	C	1.7	54.68	0.0094	4.607	57.4	54.4	97.5	61.2	1296.3	2.0
	D	2.0	54.31	0.0136	3.497	29.8	37.6	98.1	72.8	1295.7	1.8
	E	2.4	54.18	0.0538	2.789	22.0	9.5	98.5	81.4	1297.1	2.7
	F	2.7	53.61	0.0574	3.284	12.5	8.9	98.2	86.2	1284.6	2.4
	G	3.0	53.89	0.1612	4.011	5.38	3.2	97.8	88.3	1286.0	2.9
	H	3.5	52.53	0.1668	4.343	7.45	3.1	97.6	91.2	1260.2	3.9
	I	3.8	52.37	0.0244	3.821	4.30	20.9	97.8	92.9	1259.8	3.1
	J	4.2	51.62	0.1917	4.886	7.36	2.7	97.2	95.8	1241.1	2.8
	K	5.0	50.97	0.1996	4.326	2.25	2.6	97.5	96.7	1232.4	5.1
	L	6.0	49.79	0.5525	5.238	2.86	0.92	97.0	97.8	1206.8	3.8
	M	8.0	51.70	0.4084	4.301	4.90	1.2	97.6	99.7	1246.2	3.1
	N	10	44.97	0.3331	7.408	0.848	1.5	95.2	100.0	1103.6	8.9
	Total gas age ± 1σ			n=14		257.0				1270.3	1.8
	WMA ± 1σ	steps B-N		n=13	MSWD=119.72	227.2	33.8		88.4	1277.5	8.2
	HP02-8 A, E5:157, single xl muscovite, J=0.0190109, D=1.0052±0.00172, NM-157, Lab#=53559-01										
#	A	1.0	38.96	0.0245	17.82	1.99	20.8	86.5	0.4	903.3	6.0
#	B	1.4	47.74	0.0058	4.045	2.98	88.0	97.5	1.0	1157.0	3.7
#	C	1.7	49.64	0.0033	0.8343	4.66	152.9	99.5	1.9	1208.7	3.0
#	D	2.0	64.68	0.0006	0.1433	21.4	879.7	99.9	6.2	1463.2	2.4
#	E	2.4	58.52	0.0004	0.1017	52.5	1176	99.9	16.7	1364.7	2.1
#	F	2.7	55.06	0.0004	0.1180	58.3	1183	99.9	28.4	1306.9	2.2
	G	3.0	52.16	0.0003	0.0704	64.0	1466	100.0	41.2	1257.1	1.9
	H	3.5	50.17	0.0004	0.1145	60.2	1323	99.9	53.2	1221.9	1.8
	I	3.8	51.29	0.0003	0.1146	57.3	1589	99.9	64.7	1241.8	2.0
	J	4.2	52.84	0.0003	0.0476	22.8	2026	100.0	69.3	1269.2	2.6
	K	5.0	53.86	0.0004	0.0731	58.0	1162	100.0	80.9	1286.5	2.1
	L	6.0	53.17	0.0004	0.1299	38.6	1412	99.9	88.6	1274.5	2.1
	M	8.0	54.45	0.0001	0.0693	47.6	7096	100.0	98.1	1296.6	2.2
	N	10	54.52	0.0000	0.2088	9.31	14619	99.9	100.0	1297.1	2.5
	Total gas age ± 1σ			n=14		499.6				1285.4	1.9
	WMA ± 1σ	steps G-N		n=8	MSWD=172.10	357.8	######		71.6	1264.3	9.8

ID	Power/Temp (W/°C)	$^{40}Ar/^{39}Ar$	$^{37}Ar/^{39}Ar$	$^{36}Ar/^{39}Ar$ (x 10^{-3})	$^{39}Ar_K$ (x 10^{-15} mol)	K/Ca	$^{40}Ar^*$ (%)	^{39}Ar (%)	Age (Ma)	±1σ (Ma)
HP02-8 B, E5:157, single xl muscovite, J=0.0190109, D=1.00484±0.00092, NM-157, Lab#=53559-10										
B	1.4	57.95	0.0034	0.0598	143.4	147.9	100.0	12.2	1355.6	1.9
C	1.7	58.76	0.0068	0.1264	104.9	75.2	99.9	21.1	1368.5	2.5
D	2.0	55.89	0.0141	0.1185	139.1	36.1	99.9	32.9	1320.8	1.9
E	2.4	53.91	0.0043	0.0871	201.2	119.2	100.0	50.0	1287.4	2.2
F	2.7	53.35	-0.0018	0.1262	162.2	-	99.9	63.8	1277.6	2.2
G	3.0	54.80	0.0180	0.2757	61.1	28.3	99.9	69.0	1301.6	2.2
H	3.5	54.88	0.0051	0.0861	65.5	100.2	100.0	74.5	1304.0	2.2
I	3.8	54.90	0.0037	0.1464	50.1	136.5	99.9	78.8	1304.0	1.8
J	4.2	54.77	0.0078	0.2762	34.4	65.3	99.9	81.7	1301.2	1.9
K	5.0	54.84	0.0029	-0.0361	58.6	177.4	100.0	86.7	1303.9	1.9
L	6.0	55.83	0.0002	0.0466	87.3	2227	100.0	94.1	1320.3	1.8
M	8.0	55.87	-0.0210	1.514	6.41	-	99.2	94.7	1313.5	3.0
N	10	55.78	0.0022	0.2431	62.9	227.4	99.9	100.0	1318.5	1.5
Total gas age ± 1σ			n=13		1177.1				1313.6	1.4
WMA ± 1σ	steps B-N		n=13	MSWD=134.49	1177.1	282.4		100.0	1314.0	6.4
HP02-8 C, E5:157, single xl muscovite, J=0.0190109, D=1.00484±0.00092, NM-157, Lab#=53559-14										
A	1.0	62.22	0.0034	1.037	62.5	148.4	99.5	5.4	1420.1	1.7
B	1.4	56.57	0.0019	0.0943	102.3	274.4	100.0	14.2	1332.5	2.0
C	1.7	57.55	0.0019	0.1476	81.6	273.7	99.9	21.2	1348.4	2.1
D	2.0	56.30	0.0082	0.0402	85.7	62.5	100.0	28.6	1328.1	2.1
E	2.4	55.68	0.0033	0.0876	137.1	156.3	100.0	40.5	1317.5	2.6
F	2.7	54.97	0.0025	0.0816	143.4	206.8	100.0	52.8	1305.6	1.7
G	3.0	52.77	0.0031	0.0510	109.1	162.7	100.0	62.2	1268.0	1.9
H	3.5	53.31	0.0021	0.0005	111.5	245.2	100.0	71.8	1277.5	1.8
I	3.8	54.35	-0.0023	0.0563	61.9	-	100.0	77.2	1295.1	3.3
J	4.2	54.35	-0.0097	0.0955	40.0	-	99.9	80.6	1294.9	1.5
K	5.0	54.64	-0.0012	0.0109	132.3	-	100.0	92.0	1300.2	2.4
L	6.0	54.05	-0.0630	0.1273	12.6	-	99.9	93.1	1289.4	2.5
M	8.0	54.95	-0.0076	0.2663	20.8	-	99.9	94.9	1304.2	1.9
N	10	54.59	-0.0038	-0.0592	58.9	-	100.0	100.0	1299.7	1.4
Total gas age ± 1σ			n=14		1159.6				1312.2	1.4
WMA ± 1σ	steps A-N		n=14	MSWD=435.63	1159.6	139.0		100.0	1314	11
LV02-3895 D, Q2:157, single xl muscovite, J=0.0186725, D=1.0052±0.00172, NM-157, Lab#=53565-01										
# A	1.0	57.45	0.0191	15.01	2.77	26.7	92.3	2.5	1256.1	4.3
B	1.4	55.16	0.0023	2.345	6.49	220.0	98.7	8.3	1280.7	3.0
C	1.7	55.03	0.0012	0.2713	12.3	409.4	99.9	19.2	1288.8	2.2
D	2.0	54.59	0.0010	0.3387	19.4	492.6	99.8	36.5	1281.2	2.7
E	2.4	54.53	0.0011	0.0734	24.7	446.2	100.0	58.6	1281.5	2.3
F	2.7	54.87	0.0017	0.3295	12.6	305.3	99.8	69.8	1285.9	2.2
G	3.0	54.47	0.0002	0.2847	15.8	2171	99.8	83.9	1279.3	2.4
H	3.5	54.57	0.0002	0.1430	10.9	2327	99.9	93.6	1281.9	2.2
I	3.8	55.05	-0.0009	0.0968	4.14	-	99.9	97.3	1290.2	3.6
J	4.2	55.17	-0.0031	-1.6419	2.06	-	100.9	99.2	1300.8	5.6
K	5.0	55.75	-0.0103	-3.5731	0.796	-	101.9	99.9	1320	10
N	10	57.69	-0.0799	-33.1316	0.130	-	117.0	100.0	1488	41
Total gas age ± 1σ			n=12		112.0				1283.0	2.0
WMA ± 1σ	steps B-N		n=11	MSWD=6.30	109.3	828.6		97.5	1284.2	2.4

	ID	Power/Temp (W/°C)	$^{40}Ar/^{39}Ar$	$^{37}Ar/^{39}Ar$	$^{36}Ar/^{39}Ar$ (x 10^{-3})	$^{39}Ar_K$ (x 10^{-15} mol)	K/Ca	$^{40}Ar^*$ (%)	^{39}Ar (%)	Age (Ma)	±1σ (Ma)
	LV02-3895 E, Q2:157, single xl muscovite, J=0.0186725, D=1.00484±0.00092, NM-157, Lab#=53565-12										
#	A	1.0	63.74	-0.0619	63.40	3.59	-	70.6	0.1	1113.2	5.3
	B	1.4	54.90	-0.0014	5.733	16.3	-	96.9	0.7	1259.3	2.1
	C	1.7	53.79	0.0066	0.9161	35.5	77.4	99.5	1.9	1264.6	1.8
	D	2.0	54.32	0.0075	1.187	97.7	67.7	99.4	5.3	1272.4	2.9
	E	2.4	54.28	-0.0008	0.8927	122.0	-	99.5	9.6	1273.0	1.7
	F	2.7	53.55	-0.0015	0.7785	113.6	-	99.6	13.5	1261.3	1.8
	G	3.0	53.60	0.0044	0.1205	54.9	116.7	99.9	15.4	1265.4	1.4
	H	3.5	53.69	0.0022	0.1356	65.9	232.3	99.9	17.7	1266.9	2.2
	I	3.8	53.43	0.0083	0.3409	98.3	61.5	99.8	21.1	1261.4	3.0
	J	4.2	54.48	0.0045	0.2654	162.9	113.5	99.9	26.8	1279.6	1.9
	K	5.0	54.73	0.0022	0.1362	428.3	228.5	99.9	41.7	1284.6	2.6
	L	6.0	53.84	0.0019	0.0855	687.6	263.0	100.0	65.6	1269.7	3.9
	M	8.0	54.38	0.0012	0.0556	986.5	422.3	100.0	99.9	1278.9	6.1
	N	10	52.99	-0.3217	-0.0581	1.81	-	100.0	100.0	1255.2	6.3
	Total gas age ± 1σ			n=14		2874.9				1274.8	2.6
	WMA ± 1σ	steps B-N		n=13	MSWD=11.58	2871.3	286.4		99.9	1268.2	2.3
	LV02-3895 F, Q2:157, single xl muscovite, J=0.0186725, D=1.00484±0.00092, NM-157, Lab#=53565-16										
#	A	1.0	55.95	0.0321	12.37	39.0	15.9	93.5	3.9	1243.7	3.1
	B	1.4	54.83	0.0025	0.5565	71.8	204.8	99.7	11.1	1284.1	1.6
	C	1.7	55.06	0.0032	0.2948	101.9	160.0	99.8	21.3	1289.3	1.6
	D	2.0	55.06	0.0034	0.2477	115.5	151.5	99.9	32.9	1289.6	1.8
	E	2.4	55.08	0.0003	0.1649	153.4	1829	99.9	48.2	1290.3	2.4
	F	2.7	54.54	0.0043	0.1577	129.4	119.0	99.9	61.2	1281.1	1.7
	G	3.0	54.23	-0.0016	0.1766	102.0	-	99.9	71.4	1275.8	2.3
	H	3.5	54.04	0.0100	0.0513	132.0	50.8	100.0	84.7	1273.3	1.4
	I	3.8	54.79	0.0084	0.0494	49.5	60.6	100.0	89.6	1286.0	1.8
	J	4.2	55.05	0.0126	0.0284	29.0	40.3	100.0	92.5	1290.4	2.0
	K	5.0	55.03	0.0122	-0.0443	16.4	41.8	100.0	94.2	1290.4	2.1
	L	6.0	55.18	-0.0006	-0.0232	21.5	-	100.0	96.3	1292.9	2.3
	M	8.0	55.68	0.0083	-0.1275	35.8	61.7	100.1	99.9	1301.8	2.0
#	N	10	56.87	-0.0733	-5.3066	1.04	-	102.7	100.0	1346.5	9.8
	Total gas age ± 1σ			n=14		998.2				1283.3	1.4
	WMA ± 1σ	steps B-M		n=12	MSWD=18.05	958.2	375.7		96.0	1285.9	2.5
	EM02-1 G, Q1:157, single xl muscovite, J=0.0187679, D=1.0052±0.00172, NM-157, Lab#=53564-01										
#	A	1.0	62.70	0.0003	17.88	7.67	1506	91.6	2.5	1334.8	3.5
#	B	1.4	60.02	-0.0003	0.9172	13.7	-	99.5	7.1	1372.9	2.6
	C	1.7	59.14	0.0001	0.3967	35.0	8546	99.8	18.7	1361.1	2.7
	D	2.0	58.89	0.0004	0.0443	46.9	1272	100.0	34.3	1358.7	2.2
	E	2.4	58.79	0.0002	0.1464	67.4	2283	99.9	56.7	1356.6	1.9
	F	2.7	58.56	0.0001	0.1329	59.7	3464	99.9	76.6	1352.9	2.2
	G	3.0	58.71	0.0006	0.2180	13.4	865.2	99.9	81.0	1355.0	2.8
	H	3.5	58.46	0.0012	0.2939	8.55	439.3	99.9	83.9	1350.5	3.2
	I	3.8	59.48	0.0007	-0.0385	4.56	684.2	100.0	85.4	1368.6	4.0
	J	4.2	58.91	0.0002	-0.4671	5.22	3008	100.2	87.1	1361.6	3.0
	K	5.0	59.27	0.0016	0.0917	5.10	312.7	100.0	88.8	1364.7	3.0
	L	6.0	59.74	0.0007	-0.2220	5.67	698.2	100.1	90.7	1373.8	3.2
	M	8.0	59.47	0.0001	0.0816	25.6	5052	100.0	99.2	1368.0	2.4
	N	10	59.47	-0.0006	1.067	2.41	-	99.5	100.0	1363.3	4.7
	Total gas age ± 1σ			n=14		300.9				1358.4	2.0
	WMA ± 1σ	steps C-N		n=12	MSWD=5.77	279.6	3178		92.9	1360.0	2.1

	ID	Power/Temp (W/°C)	$^{40}Ar/^{39}Ar$	$^{37}Ar/^{39}Ar$	$^{36}Ar/^{39}Ar$ (x 10^{-3})	$^{39}Ar_K$ (x 10^{-15} mol)	K/Ca	$^{40}Ar^*$ (%)	^{39}Ar (%)	Age (Ma)	±1σ (Ma)
	EM02-1 H, Q1:157, single xl muscovite, J=0.0187679, D=1.00484±0.00092, NM-157, Lab#=53564-14										
	A	1.0	61.48	0.0090	5.509	63.1	56.7	97.4	28.4	1374.6	2.3
	B	1.4	59.82	0.0110	0.2948	46.3	46.5	99.9	49.2	1372.6	1.8
	C	1.7	59.36	-0.0022	0.0991	75.2	-	100.0	83.0	1366.1	2.9
	D	2.0	60.44	0.0508	-0.1205	7.13	10.0	100.1	86.2	1384.7	2.9
	E	2.4	60.23	0.1006	0.3178	8.86	5.1	99.9	90.2	1379.4	2.8
	F	2.7	60.29	0.0850	0.2776	5.30	6.0	99.9	92.6	1380.4	2.9
	G	3.0	60.16	0.0740	0.9242	3.45	6.9	99.6	94.1	1375.3	3.2
	H	3.5	60.32	0.0052	0.0321	2.52	98.5	100.0	95.3	1382.0	4.4
	I	3.8	59.85	-0.3961	2.389	1.01	-	98.8	95.7	1362.2	7.3
	J	4.2	60.57	-0.2160	-2.3810	0.748	-	101.1	96.1	1396.9	8.4
	K	5.0	59.93	0.0111	1.914	1.14	46.1	99.1	96.6	1366.7	6.6
	L	6.0	60.25	0.0197	1.825	1.68	25.9	99.1	97.3	1372.2	6.0
	M	8.0	60.29	0.0235	0.9328	4.39	21.7	99.5	99.3	1377.2	3.1
	N	10	60.72	0.1674	2.603	1.56	3.0	98.8	100.0	1376.4	5.4
	Total gas age ± 1σ			n=14		222.4				1372	2
	WMA ± 1σ		steps A-N	n=14	MSWD=3.27	222.4	30.0		100.0	1376	2
	EM02-1 I, Q1:157, single xl muscovite, J=0.0187679, D=1.00484±0.00092, NM-157, Lab#=53564-16										
	A	1.0	64.60	0.0030	17.21	86.4	170.0	92.1	21.0	1369.1	2.3
	B	1.4	59.54	0.0064	0.5765	110.8	80.1	99.7	48.0	1366.7	1.9
	C	1.7	59.49	0.0094	0.4920	65.7	54.3	99.8	64.0	1366.4	1.9
	D	2.0	59.65	0.0109	0.2901	51.4	46.7	99.9	76.5	1369.9	1.9
	E	2.4	59.59	0.0031	0.2440	48.1	166.0	99.9	88.2	1369.1	1.8
	F	2.7	59.83	0.0259	0.5211	25.9	19.7	99.7	94.5	1371.8	2.3
	G	3.0	60.25	0.1168	0.5685	5.74	4.4	99.7	95.9	1378.5	3.3
	H	3.5	59.81	0.0115	-0.0042	12.5	44.2	100.0	98.9	1373.9	2.2
	I	3.8	60.25	-0.0613	1.743	1.10	-	99.1	99.2	1372.5	7.3
	J	4.2	60.12	-0.2271	-0.1790	0.568	-	100.1	99.3	1379	12
	K	5.0	60.65	-0.7171	-1.5807	0.663	-	100.7	99.5	1393	10
	L	6.0	59.75	-0.3774	-1.3318	0.971	-	100.6	99.7	1378.5	8.2
	M	8.0	60.14	-0.2325	3.849	0.574	-	98.1	99.9	1360	12
#	N	10	60.51	-0.4035	4.584	0.536	-	97.7	100.0	1363	12
	Total gas age ± 1σ			n=14		410.9				1368.6	1.6
	WMA ± 1σ		steps A-M	n=13	MSWD=2.10	410.3	94.1		99.9	1369.9	1.4
	DCBZ-3a J, G3:145, muscovite, J=0.0097154, D=1.00535±0.00031, NM-145, Lab#=52784-01										
#	A	1.0	78.04	0.0296	38.29	0.534	17.3	85.5	0.8	912.2	2.4
#	B	1.4	97.96	0.0142	13.20	0.588	35.9	96.0	1.7	1185.1	2.3
#	C	1.7	104.2	0.0068	3.719	0.753	75.5	98.9	2.9	1267.4	2.5
#	D	2.0	105.7	0.0052	2.410	0.960	97.7	99.3	4.4	1283.4	1.9
#	E	2.3	107.4	0.0048	1.676	1.28	106.0	99.5	6.4	1300.8	1.6
#	F	2.7	110.5	0.0037	1.631	2.45	137.8	99.6	10.2	1326.9	1.5
#	G	3.0	110.0	0.0030	1.253	2.97	168.7	99.7	14.8	1324.0	1.3
#	H	3.3	110.0	0.0026	1.195	3.34	198.5	99.7	20.0	1324.2	1.6
#	I	3.6	110.9	0.0022	0.7990	3.96	232.5	99.8	26.2	1332.7	1.2
#	J	4.0	111.4	0.0015	0.6152	11.8	330.0	99.8	44.4	1337.7	1.5
#	K	4.5	111.5	0.0015	0.6673	8.78	332.5	99.8	58.1	1338.7	1.8
#	L	5.0	112.5	0.0015	0.6419	7.40	337.1	99.8	69.6	1346.9	1.8
#	M	5.5	114.0	0.0015	0.6068	6.74	329.8	99.8	80.0	1359.3	1.3
	N	6.0	114.9	0.0015	0.7865	5.91	333.6	99.8	89.2	1366.9	1.2
	O	8.0	114.7	0.0039	1.802	5.77	131.6	99.5	98.2	1363.0	1.6
#	P	9.0	115.7	0.0118	11.12	1.16	43.1	97.2	100.0	1348.1	2.4
	Total gas age ± 1σ			n=16		64.4				1337.5	1.1
	WMA ± 1σ		steps N-O	n=2	MSWD=3.66	11.7	233.8		18.2	1365.4	2.1

	ID	Power/Temp (W/°C)	$^{40}Ar/^{39}Ar$	$^{37}Ar/^{39}Ar$	$^{36}Ar/^{39}Ar$ (x 10^{-3})	$^{39}Ar_K$ (x 10^{-15} mol)	K/Ca	$^{40}Ar^*$ (%)	^{39}Ar (%)	Age (Ma)	±1σ (Ma)
	ASF01-9 K, H5:145, muscovite, J=0.0097408, D=1.00535±0.00031, NM-145, Lab#=52788-01										
#	A	1.0	103.7	0.0654	43.21	0.204	7.8	87.7	0.6	1157.9	4.2
#	B	1.4	109.6	0.0156	5.598	0.210	32.8	98.5	1.2	1311.9	4.1
#	C	1.7	113.9	0.0082	4.108	0.316	62.3	98.9	2.2	1352.9	4.4
#	D	2.0	113.9	0.0038	4.097	0.492	134.5	98.9	3.6	1352.2	2.1
	E	2.3	116.8	0.0023	3.630	1.79	225.7	99.1	9.0	1377.9	1.4
	F	2.7	116.5	0.0015	1.768	3.43	330.0	99.6	19.2	1380.0	2.0
	G	3.0	115.4	0.0010	2.537	2.19	493.0	99.4	25.7	1369.4	1.6
	H	3.3	114.9	0.0008	1.190	1.39	650.5	99.7	29.9	1368.4	1.8
	I	3.6	115.1	0.0006	1.805	1.68	808.8	99.5	34.9	1368.2	1.4
	J	4.0	114.9	0.0006	1.133	3.63	893.8	99.7	45.7	1368.1	1.1
	K	4.5	115.4	0.0005	0.8374	5.45	974.6	99.8	62.0	1373.1	1.0
	L	5.0	114.7	0.0003	0.9670	3.05	1960	99.8	71.1	1367.5	1.4
	M	5.5	115.2	0.0010	1.182	1.80	516.1	99.7	76.5	1371.1	1.6
	N	6.0	115.6	0.0008	1.329	1.48	677.4	99.7	80.9	1373.5	1.5
	O	8.0	115.2	0.0004	0.7571	5.62	1250	99.8	97.6	1372.2	1.5
	P	9.0	116.3	0.0010	1.639	0.791	508.0	99.6	100.0	1379.0	2.7
	Total gas age ± 1σ			n=16		33.5				1370.1	1.1
	WMA ± 1σ	steps E-P		n=12	MSWD=7.12	32.3	890.9		96.4	1371.6	1.5
	PV03-01 L, L5:164, 0.21 mg biotite, J=0.015, D=1.0052±0.00121, NM-164, Lab#=54026-01										
#	A	1.0	7.055	0.2876	2.059	5.81	1.8	91.7	7.4	168.5	1.3
#	B	1.4	40.49	0.0688	3.346	4.99	7.4	97.6	13.7	849.5	2.3
#	C	1.7	66.46	0.0368	2.116	4.73	13.9	99.1	19.8	1254.1	2.9
	D	2.0	70.69	0.0442	0.9630	4.26	11.5	99.6	25.2	1316.0	3.5
	E	2.4	73.30	0.0385	1.282	11.2	13.3	99.5	39.4	1349.3	2.4
	F	2.7	75.31	0.0216	0.9546	6.62	23.6	99.6	47.8	1376.5	2.9
	G	3.0	78.82	0.0376	0.7211	5.36	13.6	99.7	54.6	1422.1	3.2
	H	3.5	83.05	0.0634	0.8293	6.38	8.0	99.7	62.8	1474.2	3.5
	I	3.8	81.52	0.0857	0.6219	6.89	6.0	99.8	71.5	1456.3	2.5
	J	4.2	75.66	0.1291	0.4897	6.26	4.0	99.8	79.5	1383.0	3.4
	K	5.0	77.23	0.3545	0.3179	3.63	1.4	99.9	84.1	1404.1	4.4
	L	6.0	74.23	0.1284	0.4510	5.24	4.0	99.8	90.8	1364.6	3.0
	M	8.0	73.65	0.0630	0.0157	6.27	8.1	100.0	98.8	1358.7	3.4
	N	10	71.65	0.0411	-0.1255	0.972	12.4	100.1	100.0	1333.1	5.0
	Total gas age ± 1σ			n=14		78.6		K2O=9.58 %		1283.1	1.6
	WMA ± 1σ	steps D-N		n=11	MSWD=244.69	63.0	10.0		80.2	1389	15

ID	Power/Temp (W/°C)	$^{40}Ar/^{39}Ar$	$^{37}Ar/^{39}Ar$	$^{36}Ar/^{39}Ar$ (x 10^{-3})	$^{39}Ar_K$ (x 10^{-15} mol)	K/Ca	$^{40}Ar^*$ (%)	^{39}Ar (%)	Age (Ma)	±1σ (Ma)
PVBR-3, H:2:144, 2.95 mg K-feldspar, J=0.0094167, D=1.00535±0.00031, NM-144, Lab#=52786-01										
BA	450	58.16	-0.0063	9.657	0.378	-	95.1	0.0	765.6	5.9
C	450	50.17	0.0078	8.670	0.870	65.5	94.9	0.1	676.5	3.2
D	500	151.8	0.0089	7.905	1.243	57.3	98.5	0.3	1604.6	3.5
E	500	46.59	0.0098	4.557	2.111	51.9	97.1	0.5	648.1	1.9
F	500	47.11	0.0106	3.568	2.127	48.3	97.8	0.7	657.8	1.9
G	550	91.50	0.0129	3.208	3.437	39.6	99.0	1.0	1126.1	1.2
H	550	53.14	0.0109	1.892	4.67	46.7	98.9	1.5	734.5	1.5
I	550	53.86	0.0066	1.639	4.65	77.5	99.1	2.0	743.3	1.5
J	600	73.47	0.0079	1.856	6.11	64.6	99.3	2.6	954.4	1.4
K	600	58.15	0.0071	0.9753	9.04	71.7	99.5	3.6	793.98	0.91
L	600	59.97	0.0064	0.8733	9.13	79.5	99.6	4.5	814.4	1.3
M	650	67.95	0.0079	0.6680	10.39	64.8	99.7	5.6	900.89	0.93
N	650	63.74	0.0066	0.5042	15.28	77.3	99.8	7.2	856.6	1.0
O	650	65.77	0.0064	0.3838	14.95	79.2	99.8	8.7	878.72	0.85
P	700	68.50	0.0082	0.5831	15.26	62.0	99.7	10.3	906.90	0.84
Q	700	67.54	0.0075	0.3213	20.70	68.4	99.9	12.4	897.6	1.2
R	700	68.06	0.0070	0.2606	19.79	72.5	99.9	14.5	903.3	1.1
S	750	70.43	0.0088	0.3064	16.98	58.1	99.9	16.2	927.8	1.2
T	750	69.29	0.0083	0.2156	23.30	61.2	99.9	18.6	916.2	1.0
U	750	69.64	0.0083	0.2495	21.46	61.5	99.9	20.8	919.8	1.2
V	800	70.40	0.0097	0.2587	15.62	52.8	99.9	22.4	927.7	1.2
W	800	70.36	0.0090	0.2381	20.65	56.6	99.9	24.6	927.26	0.91
X	850	71.00	0.0105	0.2146	21.99	48.6	99.9	26.8	934.0	1.0
Y	850	71.06	0.0095	0.2975	24.18	54.0	99.9	29.3	934.3	1.1
Z	900	71.71	0.0113	0.3019	21.13	45.3	99.9	31.5	941.07	0.97
ZA	900	71.84	0.0099	0.3516	24.52	51.3	99.9	34.0	942.23	0.81
ZB	950	72.21	0.0104	0.4192	19.38	49.1	99.8	36.0	945.8	1.3
ZC	950	72.15	0.0089	0.5468	19.91	57.2	99.8	38.1	944.76	0.96
ZD	1000	73.81	0.0109	0.6639	16.98	46.9	99.7	39.8	961.4	1.1
ZE	1000	73.43	0.0097	0.5369	18.93	52.6	99.8	41.8	957.92	0.98
ZF	1050	75.55	0.0153	0.9329	19.52	33.4	99.6	43.8	978.2	1.2
ZG	1050	75.53	0.0147	0.8686	22.84	34.7	99.7	46.2	978.2	1.1
ZH	1100	77.92	0.0215	1.287	20.77	23.8	99.5	48.3	1000.85	0.99
ZI	1100	77.61	0.0178	1.120	25.31	28.7	99.6	50.9	998.22	0.83
ZJ	1100	80.18	0.0129	0.8400	97.9	39.5	99.7	61.0	1024.5	1.8
ZK	1100	82.29	0.0084	0.8865	48.3	61.1	99.7	66.0	1044.9	1.3
ZL	1100	83.72	0.0079	1.160	60.6	64.8	99.6	72.3	1057.9	1.5
ZM	1200	83.57	0.0052	0.7320	47.8	98.7	99.7	77.2	1057.7	1.2
ZN	1300	84.10	0.0047	0.9083	134.3	108.8	99.7	91.0	1062.3	2.1
ZO	1400	87.43	0.0112	1.075	26.03	45.8	99.6	93.7	1093.6	1.1
ZP	1660	87.36	0.0025	0.8614	12.81	204.7	99.7	95.1	1093.5	1.2
ZQ	1660	85.78	0.0123	1.111	48.0	41.5	99.6	100.0	1077.8	1.2
Total gas age ± 1σ			n=42		969.3		K2O=13.40 %		993.20	0.46

ID	Power/Temp (W/°C)	$^{40}Ar/^{39}Ar$	$^{37}Ar/^{39}Ar$	$^{36}Ar/^{39}Ar$ (x 10^{-3})	$^{39}Ar_K$ (x 10^{-15} mol)	K/Ca	$^{40}Ar^*$ (%)	^{39}Ar (%)	Age (Ma)	±1σ (Ma)
ASF01-9, H:4:145, 2.98 mg K-feldspar, J=0.0096403, D=1.00535±0.00031, NM-145, Lab#=52787-01										
A	450	311.7	0.0703	547.8	1.225	7.3	48.1	0.9	1632.0	8.4
B	450	73.35	0.0523	164.9	0.649	9.8	33.5	1.3	388.6	10.7
C	450	55.46	0.0524	104.7	0.439	9.7	44.2	1.6	387.2	9.4
D	500	56.79	0.0559	75.35	0.329	9.1	60.8	1.8	524.4	10.3
E	500	31.51	0.0666	31.70	0.804	7.7	70.3	2.4	353.0	4.0
F	500	29.55	0.0789	27.72	0.754	6.5	72.3	2.9	341.5	4.3
G	550	59.59	0.1118	68.19	1.204	4.6	66.2	3.8	588.1	4.6
H	550	29.03	0.1218	14.15	1.458	4.2	85.6	4.8	391.9	2.6
I	550	30.28	0.1376	13.13	1.250	3.7	87.2	5.6	413.8	2.8
J	600	56.32	0.1715	65.91	1.464	3.0	65.4	6.7	554.9	4.0
K	600	35.00	0.1641	15.75	1.713	3.1	86.7	7.8	468.4	2.2
L	600	35.60	0.1583	7.055	1.389	3.2	94.2	8.8	511.1	2.4
M	650	51.57	0.1931	45.84	1.646	2.6	73.8	10.0	570.2	3.0
N	650	40.08	0.2055	6.046	1.819	2.5	95.6	11.2	573.7	2.2
O	650	44.03	0.2127	3.750	1.506	2.4	97.5	12.3	632.3	2.3
P	700	55.92	0.3079	24.90	1.480	1.7	86.9	13.3	701.3	2.9
Q	700	54.40	0.3147	8.778	2.232	1.6	95.3	14.9	739.8	2.1
R	700	59.53	0.3004	5.788	1.729	1.7	97.2	16.1	809.1	2.2
S	750	65.61	0.3811	18.80	1.385	1.3	91.6	17.0	834.3	3.2
T	750	64.67	0.3202	3.505	1.840	1.6	98.4	18.3	873.7	2.7
U	750	66.07	0.2780	4.171	1.644	1.8	98.2	19.4	886.7	2.8
V	800	68.81	0.3291	16.48	1.367	1.6	93.0	20.4	877.0	3.2
W	800	68.89	0.2918	4.504	2.119	1.7	98.1	21.9	916.0	2.2
X	850	68.99	0.3125	15.59	2.688	1.6	93.4	23.7	881.8	2.1
Y	850	69.32	0.2195	6.297	4.102	2.3	97.3	26.6	914.8	1.5
Z	900	73.13	0.1857	7.155	6.72	2.7	97.1	31.3	952.4	1.4
ZA	900	71.81	0.1375	3.663	6.68	3.7	98.5	35.9	949.2	1.2
ZB	950	69.80	0.1376	4.558	4.97	3.7	98.1	39.4	925.3	1.6
ZC	950	70.01	0.1251	5.100	5.30	4.1	97.9	43.0	925.8	1.6
ZD	1000	70.27	0.1335	5.761	5.03	3.8	97.6	46.5	926.5	1.2
ZE	1000	70.58	0.1362	6.819	5.45	3.7	97.2	50.3	926.5	1.6
ZF	1050	71.40	0.1679	8.377	5.41	3.0	96.6	54.1	930.3	1.4
ZG	1050	72.28	0.1920	10.67	5.50	2.7	95.7	57.9	932.5	1.6
ZH	1100	75.48	0.3036	18.31	6.18	1.7	92.9	62.2	942.5	1.7
ZI	1100	73.51	0.4160	27.94	8.09	1.2	88.8	67.8	891.4	1.5
ZJ	1100	73.59	0.5342	28.46	11.47	0.96	88.6	75.8	890.7	1.3
ZK	1100	77.29	0.5478	22.65	10.73	0.93	91.4	83.3	948.5	1.4
ZL	1100	81.70	0.4049	16.21	12.33	1.3	94.2	91.8	1013.2	1.2
ZM	1200	86.71	0.7832	16.98	3.092	0.65	94.3	94.0	1061.5	2.4
ZN	1300	85.17	1.589	38.48	2.980	0.32	86.8	96.1	983.2	2.4
ZO	1400	81.04	0.9190	30.37	1.069	0.56	89.0	96.8	964.3	3.8
ZP	1660	84.26	0.7342	16.40	4.59	0.69	94.3	100.0	1038.8	1.6
Total gas age ± 1σ			n=42		143.8		K2O=1.92 %		896.11	0.86

ID	Power/Temp (W/°C)	$^{40}Ar/^{39}Ar$	$^{37}Ar/^{39}Ar$	$^{36}Ar/^{39}Ar$ (x 10^{-3})	$^{39}Ar_K$ (x 10^{-15} mol)	K/Ca	$^{40}Ar^*$ (%)	^{39}Ar (%)	Age (Ma)	±1σ (Ma)
TP02-4, A:1:157 , 2.36 mg K-feldspar, J=0.0186268, D=1.0052±0.00172, NM-157, Lab#=53525-01										
A	430	404.4	0.0047	32.22	4.11	108.0	97.6	0.2	3876.8	5.5
B	430	33.38	0.0021	5.475	1.94	239.6	95.1	0.3	848.1	4.5
C	430	37.97	0.0021	3.258	1.63	244.7	97.5	0.4	956.8	4.4
D	430	20.54	0.0031	3.229	1.56	165.4	95.3	0.5	567.1	4.5
E	480	27.43	0.0018	2.161	2.30	286.0	97.7	0.6	738.5	3.4
F	480	19.98	0.0001	0.9064	2.52	4887	98.7	0.7	570.2	2.8
G	480	15.71	0.0018	0.0360	2.34	286.2	99.9	0.9	467.8	2.9
H	480	17.89	0.0032	4.801	2.55	159.2	92.1	1.0	487.8	3.5
I	530	27.54	0.0011	0.8174	3.05	457.5	99.1	1.2	750.1	2.7
J	530	18.13	0.0043	-0.0796	3.68	118.4	100.1	1.3	531.2	2.1
K	530	19.11	0.0027	0.2127	3.46	187.7	99.7	1.5	553.8	2.1
L	530	20.83	0.0015	0.1313	3.99	331.9	99.8	1.7	597.0	2.3
M	580	31.57	0.0011	0.7721	6.10	480.0	99.3	2.1	839.0	2.3
N	580	25.15	0.0009	0.0493	6.9	599.0	99.9	2.4	700.6	2.0
O	580	27.35	0.0010	-0.0499	6.40	515.1	100.1	2.7	751.5	2.0
P	580	27.95	0.0002	0.6191	5.71	3294	99.3	3.0	760.6	2.3
Q	630	33.33	0.0013	0.2902	7.1	378.9	99.7	3.4	879.5	2.0
R	630	32.28	0.0007	0.0325	8.9	688.8	100.0	3.9	858.9	1.7
S	630	33.60	0.0003	0.1353	8.0	1588	99.9	4.3	886.1	2.1
T	680	35.91	0.0019	0.6296	9.8	265.8	99.5	4.8	930.8	2.0
U	680	35.01	-0.0002	0.0976	10.8	-	99.9	5.4	915.6	2.0
V	680	35.69	0.0008	0.0307	8.5	672.9	100.0	5.8	929.9	2.1
W	730	38.00	0.0009	0.4051	10.8	555.2	99.7	6.4	974.4	1.8
X	730	37.16	0.0009	0.1016	12.5	598.9	99.9	7.0	959.3	1.8
Y	730	38.04	0.0006	0.3002	11.7	833.4	99.8	7.7	975.8	1.9
Z	780	38.93	0.0010	0.1803	12.2	520.9	99.9	8.3	994.1	1.8
ZA	780	39.53	0.0009	0.2081	15.5	588.7	99.8	9.1	1005.9	2.0
ZB	830	41.15	0.0016	0.1622	19.8	327.8	99.9	10.1	1037.5	1.8
ZC	830	41.91	0.0001	0.2145	22.5	7615	99.8	11.3	1051.8	1.9
ZD	880	43.35	0.0020	0.2776	26.3	261.0	99.8	12.7	1078.8	1.9
ZE	880	44.46	0.0008	0.1257	28.7	627.6	99.9	14.2	1100.4	1.9
ZF	930	45.39	0.0015	0.3340	28.6	342.7	99.8	15.7	1116.6	2.1
ZG	930	45.85	0.0003	0.2803	32.5	1661	99.8	17.4	1125.4	2.3
ZH	980	46.83	0.0016	0.4900	34.1	326.4	99.7	19.2	1142.1	1.9
ZI	980	46.88	0.0007	0.2732	37.7	703.5	99.8	21.2	1144.2	1.7
ZJ	1030	47.59	0.0014	0.5516	47.2	364.5	99.7	23.6	1155.5	2.0
ZK	1030	47.95	0.0006	0.3113	43.8	855.6	99.8	25.9	1163.3	2.0
ZL	1100	46.03	0.0012	0.6700	63.5	429.9	99.6	29.2	1126.4	2.2
ZM	1100	46.80	0.0007	0.5228	61.9	703.1	99.7	32.5	1141.4	2.2
ZN	1100	47.76	0.0007	0.6161	106.4	755.0	99.6	38.1	1158.3	2.0
ZO	1100	48.77	0.0008	0.6938	149.0	642.9	99.6	45.9	1176.0	2.5
ZP	1100	51.65	0.0006	0.6313	215.4	785.3	99.6	57.1	1227.1	3.1
ZQ	1180	54.37	0.0005	0.6656	55.7	1022	99.6	60.0	1273.5	2.2
ZR	1280	53.99	0.0007	0.7014	449.7	750.5	99.6	83.6	1266.9	4.3
ZS	1380	50.23	0.0007	0.6953	144.4	759.8	99.6	91.1	1202.0	2.3
ZT	1670	51.23	0.0008	0.7010	169.5	616.8	99.6	100.0	1219.3	2.6
Total gas age ± 1σ			n=46		1910.9		K2O=16.70 %		1188.0	2.0

ID	Power/Temp (W/°C)	$^{40}Ar/^{39}Ar$	$^{37}Ar/^{39}Ar$	$^{36}Ar/^{39}Ar$ (x 10^{-3})	$^{39}Ar_K$ (x 10^{-15} mol)	K/Ca	$^{40}Ar^*$ (%)	^{39}Ar (%)	Age (Ma)	±1σ (Ma)
LV02-4800, A:4:157, 2.76 mg K-feldspar, J=0.0184739, D=1.0052±0.00172, NM-157, Lab#=53527-01										
A	430	417.5	0.0111	35.46	3.90	46.2	97.5	0.2	3912.0	5.5
B	430	36.75	0.0066	2.655	1.55	77.8	97.9	0.3	929.8	6.2
C	430	32.44	0.0066	3.223	1.33	77.6	97.1	0.4	836.5	7.0
D	430	26.84	0.0062	3.257	1.49	82.5	96.4	0.4	712.8	6.3
E	480	29.50	0.0073	1.422	2.35	70.0	98.6	0.6	784.6	4.1
F	480	16.51	0.0116	0.3067	2.64	43.9	99.5	0.7	482.9	3.6
G	480	15.11	0.0107	1.526	2.69	47.8	97.0	0.9	436.9	3.7
H	480	13.59	0.0103	0.5228	3.05	49.7	98.9	1.0	404.0	3.0
I	530	56.85	0.0126	0.9709	6.54	40.4	99.5	1.4	1305.9	2.7
J	530	10.99	0.0121	-0.1876	5.16	42.0	100.5	1.7	338.2	2.0
K	530	11.03	0.0092	-0.0479	4.91	55.7	100.1	1.9	338.2	2.1
L	530	10.00	0.0083	0.1190	5.37	61.7	99.7	2.2	307.8	2.0
M	580	50.46	0.0082	0.8546	11.6	62.6	99.5	2.8	1197.9	2.5
N	580	12.82	0.0074	0.3280	7.9	68.5	99.2	3.3	384.8	1.6
O	580	14.07	0.0042	0.1531	7.5	120.8	99.7	3.7	419.9	1.7
P	580	14.24	0.0029	0.1260	7.6	176.7	99.7	4.1	424.6	1.6
Q	630	26.31	0.0043	0.7479	9.2	119.1	99.2	4.6	717.5	1.8
R	630	17.22	0.0043	0.0903	9.1	118.6	99.8	5.1	503.0	1.5
S	630	18.31	0.0033	0.1317	8.2	156.3	99.8	5.5	530.3	1.7
T	680	21.56	0.0055	0.5448	10.7	92.9	99.3	6.1	607.5	1.7
U	680	20.91	0.0040	0.0416	12.1	128.4	99.9	6.7	595.4	1.4
V	680	21.57	0.0039	0.0123	10.7	131.8	100.0	7.3	611.7	1.5
W	730	22.89	0.0046	0.1096	12.7	111.6	99.9	8.0	642.4	1.5
X	730	22.20	0.0044	-0.0563	14.6	116.9	100.1	8.8	627.2	1.5
Y	730	22.12	0.0040	-0.0309	13.3	127.9	100.0	9.5	625.1	1.3
Z	780	22.25	0.0032	0.0668	14.2	157.7	99.9	10.3	627.6	1.5
ZA	780	22.06	0.0045	0.0183	17.0	114.1	100.0	11.2	623.3	1.3
ZB	830	22.70	0.0061	0.1750	20.7	83.3	99.8	12.3	637.5	1.3
ZC	830	23.20	0.0049	0.0618	21.9	104.0	99.9	13.5	650.1	1.6
ZD	880	24.23	0.0074	0.3307	24.6	68.6	99.6	14.8	672.4	1.4
ZE	880	25.24	0.0055	0.2781	26.1	93.6	99.7	16.2	696.2	1.6
ZF	930	25.90	0.0070	0.4630	29.0	72.9	99.5	17.8	710.3	1.3
ZG	930	27.06	0.0055	0.3459	32.0	93.1	99.6	19.5	737.3	1.5
ZH	980	26.82	0.0074	0.3724	36.8	69.4	99.6	21.5	731.8	1.3
ZI	980	28.02	0.0055	0.3951	41.4	92.2	99.6	23.7	758.5	1.4
ZJ	1030	27.56	0.0059	0.5747	51.2	85.8	99.4	26.5	747.0	1.4
ZK	1030	29.17	0.0054	0.5149	56.4	94.4	99.5	29.5	783.2	1.5
ZL	1100	30.85	0.0055	0.5971	110.3	93.6	99.4	35.4	819.1	1.6
ZM	1100	32.62	0.0056	0.4407	104.9	91.1	99.6	41.1	857.9	1.8
ZN	1100	34.57	0.0061	0.4526	169.8	84.0	99.6	50.2	898.5	2.1
ZO	1100	35.60	0.0057	0.4567	182.2	88.9	99.6	60.1	919.5	2.2
ZP	1100	36.76	0.0044	0.3423	259.3	116.8	99.7	74.0	943.7	1.8
ZQ	1180	37.76	0.0020	0.1442	93.3	255.4	99.9	79.1	964.9	1.8
ZR	1280	37.75	0.0017	0.1721	197.8	308.8	99.9	89.7	964.5	1.7
ZS	1380	37.47	0.0041	0.1782	54.9	125.4	99.9	92.7	958.9	1.8
ZT	1670	38.06	0.0019	0.2852	135.8	269.5	99.8	100.0	970.1	1.7
Total gas age ± 1σ			n=46		1855.7		K2O=13.98 %		877.2	1.5

ID	Power/Temp (W/°C)	$^{40}Ar/^{39}Ar$	$^{37}Ar/^{39}Ar$	$^{36}Ar/^{39}Ar$ (x 10^{-3})	$^{39}Ar_K$ (x 10^{-15} mol)	K/Ca	$^{40}Ar^*$ (%)	^{39}Ar (%)	Age (Ma)	±1σ (Ma)
LV02-3895, A:5:157, 2.15 mg K-feldspar, J=0.0187113, D=1.0052±0.00172, NM-157, Lab#=53528-01										
A	430	1019.7	0.0177	83.58	2.37	28.8	97.6	0.2	5435.4	5.9
B	430	70.76	0.0055	13.10	0.84	92.0	94.5	0.2	1481.7	7.4
C	430	51.94	-0.0089	7.331	0.680	-	95.8	0.3	1201.3	7.9
D	430	39.14	0.0087	8.148	0.77	58.9	93.8	0.3	954.7	7.6
E	480	58.75	0.0129	6.705	1.23	39.6	96.6	0.4	1321.2	5.2
F	480	30.31	0.0062	4.110	1.55	82.8	96.0	0.5	793.0	4.4
G	480	23.44	0.0089	2.890	1.50	57.2	96.4	0.6	642.9	4.4
H	480	27.06	0.0087	5.500	1.77	58.6	94.0	0.7	710.3	3.9
I	530	56.75	0.0120	6.593	2.98	42.5	96.6	0.9	1288.3	3.3
J	530	22.03	0.0136	3.540	2.91	37.4	95.2	1.1	604.1	2.8
K	530	18.79	0.0125	3.598	2.77	40.9	94.3	1.3	522.4	2.3
L	530	21.46	0.0117	3.053	3.14	43.5	95.8	1.6	593.6	2.2
M	580	37.85	0.0193	5.189	3.70	26.5	95.9	1.8	946.2	3.1
N	580	15.80	0.0190	1.648	4.18	26.9	96.9	2.1	459.4	1.9
O	580	16.75	0.0200	1.375	3.84	25.5	97.6	2.4	486.4	1.7
P	580	17.09	0.0202	1.474	3.72	25.3	97.5	2.6	494.5	2.2
Q	630	30.78	0.0174	3.342	3.19	29.4	96.8	2.8	808.4	2.9
R	630	18.44	0.0101	1.362	3.38	50.6	97.8	3.1	530.2	1.8
S	630	20.78	0.0082	1.439	2.95	62.5	98.0	3.3	588.7	2.4
T	680	39.77	0.0132	3.320	4.46	38.7	97.5	3.6	995.9	3.0
U	680	27.64	0.0115	1.372	4.22	44.4	98.5	3.9	751.3	2.3
V	680	29.87	0.0091	1.047	3.66	56.3	99.0	4.1	803.4	2.9
W	730	38.36	0.0107	1.558	4.67	47.7	98.8	4.5	978.2	2.8
X	730	36.41	0.0092	0.7784	5.67	55.5	99.4	4.8	943.5	2.4
Y	730	38.13	0.0076	0.5742	5.91	66.9	99.6	5.3	979.4	2.3
Z	780	44.14	0.0066	1.416	8.5	77.2	99.1	5.8	1091.1	2.1
ZA	780	37.47	0.0063	0.3395	10.6	81.3	99.7	6.6	967.5	1.9
ZB	830	37.62	0.0058	0.5854	16.6	88.0	99.5	7.7	969.1	1.9
ZC	830	34.94	0.0049	0.1361	21.1	105.0	99.9	9.2	917.1	1.5
ZD	880	34.54	0.0049	0.3822	27.8	103.3	99.7	11.1	907.4	1.7
ZE	880	33.14	0.0041	0.2036	34.0	123.7	99.8	13.4	879.2	1.5
ZF	930	33.11	0.0045	0.4644	40.1	113.4	99.6	16.2	876.8	1.5
ZG	930	32.73	0.0037	0.2868	48.0	138.9	99.7	19.5	870.0	1.5
ZH	980	32.45	0.0040	0.3172	52.6	127.0	99.7	23.1	863.8	1.5
ZI	980	32.49	0.0036	0.2659	62.9	141.0	99.8	27.5	865.0	1.7
ZJ	1030	32.37	0.0043	0.3894	68.2	119.2	99.6	32.2	861.8	1.5
ZK	1030	33.00	0.0038	0.2558	81.5	133.5	99.8	37.8	875.8	1.7
ZL	1100	33.42	0.0066	0.3705	119.6	76.9	99.7	46.1	884.1	1.5
ZM	1100	35.59	0.0074	0.3241	116.3	68.7	99.7	54.1	929.4	1.7
ZN	1100	37.08	0.0094	0.3307	132.8	54.2	99.7	63.3	959.8	1.7
ZO	1100	39.52	0.0108	0.4600	124.1	47.1	99.7	71.8	1007.6	1.8
ZP	1100	41.74	0.0069	0.4278	141.8	74.0	99.7	81.6	1051.0	2.1
ZQ	1180	42.19	0.0028	0.4118	37.0	180.1	99.7	84.2	1059.7	2.0
ZR	1280	43.04	0.0032	0.2544	100.5	158.3	99.8	91.1	1076.8	2.1
ZS	1380	43.40	0.0028	0.4346	18.0	180.4	99.7	92.4	1082.7	2.2
ZT	1670	44.30	0.0057	0.4221	110.6	90.2	99.7	100.0	1099.6	1.9
Total gas age ± 1σ			n=46		1448.6		K2O=13.83 %		988.0	1.6

ID	Power/Temp (W/°C)	$^{40}Ar/^{39}Ar$	$^{37}Ar/^{39}Ar$	$^{36}Ar/^{39}Ar$ (x 10^{-3})	$^{39}Ar_K$ (x 10^{-15} mol)	K/Ca	$^{40}Ar^*$ (%)	^{39}Ar (%)	Age (Ma)	±1σ (Ma)
EM02-1, A:8:157, 1.97 mg K-feldspar, J=0.0195129, D=1.0052±0.00172, NM-157, Lab#=53530-01										
A	430	490.4	0.0027	44.66	2.85	188.8	97.3	0.2	4260.7	6.0
B	430	32.83	0.0021	11.54	1.50	240.0	89.6	0.3	827.7	6.1
C	430	27.27	0.0006	7.321	1.34	785.8	92.1	0.4	727.4	5.7
D	430	23.83	-0.0012	4.822	1.59	-	94.0	0.5	661.6	4.9
E	480	30.81	0.0005	1.895	2.51	1017	98.2	0.7	846.5	3.6
F	480	19.20	0.0004	2.169	3.37	1421	96.7	0.9	563.7	2.5
G	480	18.73	-0.0003	1.975	3.60	-	96.9	1.2	552.8	2.5
H	480	18.03	0.0006	2.036	4.55	839.6	96.7	1.5	533.8	2.3
I	530	22.73	0.0008	0.9003	5.86	623.5	98.8	1.9	662.9	1.9
J	530	20.02	0.0005	0.4559	7.9	1055	99.3	2.5	597.9	1.7
K	530	20.57	0.0009	0.3976	8.3	581.4	99.4	3.0	612.4	1.6
L	530	21.81	0.0002	0.2704	10.0	2299	99.6	3.7	644.6	1.4
M	580	25.31	0.0007	0.3232	10.4	695.0	99.6	4.5	729.9	1.5
N	580	23.98	0.0000	0.2523	14.0	-	99.7	5.4	698.5	1.3
O	580	25.10	0.0004	0.0146	14.0	1149	100.0	6.4	727.2	1.4
P	580	25.93	0.0001	0.1882	16.1	9431	99.8	7.5	745.5	1.6
Q	630	28.15	0.0002	0.2109	15.0	2642	99.8	8.6	797.4	1.5
R	630	27.54	0.0000	0.1038	19.4	10607	99.9	9.9	784.0	1.8
S	630	28.01	0.0000	0.2421	19.2	10328	99.7	11.3	794.0	1.6
T	680	29.56	0.0003	0.1190	23.1	1723	99.9	12.9	830.0	1.6
U	680	29.22	0.0002	0.0832	26.8	2953	99.9	14.8	822.6	1.5
V	680	29.54	0.0003	0.0464	24.1	1488	100.0	16.5	830.2	1.8
W	730	30.48	0.0002	0.0017	24.3	2132	100.0	18.2	851.6	1.7
X	730	30.16	0.0002	0.1216	26.5	2061	99.9	20.0	843.7	1.6
Y	730	30.09	0.0000	0.0788	21.8	1322	99.9	21.5	842.3	1.6
Z	780	30.45	0.0006	0.1222	19.3	865.2	99.9	22.9	850.0	1.6
ZA	780	30.17	0.0001	0.0673	20.6	7057	99.9	24.3	844.3	2.0
ZB	830	30.12	0.0006	0.0959	21.6	836.4	99.9	25.8	843.0	1.4
ZC	830	29.96	0.0000	0.0421	21.2	24412	100.0	27.3	839.7	1.5
ZD	880	30.29	0.0004	0.0853	20.6	1220	99.9	28.8	846.8	1.8
ZE	880	30.05	0.0004	0.2008	21.1	1234	99.8	30.2	840.7	1.7
ZF	930	30.35	0.0010	0.0862	19.6	534.5	99.9	31.6	848.1	1.8
ZG	930	30.36	0.0004	0.4798	20.1	1294	99.5	33.0	845.7	2.0
ZH	980	30.78	0.0008	0.1457	19.6	605.1	99.9	34.4	857.3	1.8
ZI	980	30.84	0.0006	0.3072	21.3	879.8	99.7	35.9	857.7	1.8
ZJ	1030	32.16	0.0016	0.5088	22.3	310.2	99.5	37.4	885.4	1.7
ZK	1030	32.61	0.0007	0.3933	26.1	698.0	99.6	39.3	896.1	1.5
ZL	1100	35.15	0.0012	0.4759	46.4	421.2	99.6	42.5	950.2	1.5
ZM	1100	36.00	0.0005	0.5474	49.8	1092	99.6	46.0	967.5	1.9
ZN	1100	36.06	0.0007	0.4352	61.7	761.5	99.6	50.3	969.5	1.8
ZO	1100	36.85	0.0006	0.5096	54.4	854.6	99.6	54.1	985.5	1.9
ZP	1100	38.42	0.0005	0.7523	78.5	1069	99.4	59.6	1016.4	1.7
ZQ	1180	41.40	0.0008	0.6445	19.2	637.0	99.5	60.9	1076.9	2.3
ZR	1280	41.83	0.0003	0.5927	389.3	1814	99.6	88.2	1085.6	2.6
ZS	1380	42.07	0.0003	0.6795	139.1	1721	99.5	97.9	1089.9	1.9
ZT	1670	42.13	0.0005	1.313	30.2	977.0	99.1	100.0	1087.4	1.9
Total gas age ± 1σ			n=46		1429.8		K2O=14.29 %		980.6	1.6

ID	Power/Temp (W/°C)	$^{40}Ar/^{39}Ar$	$^{37}Ar/^{39}Ar$	$^{36}Ar/^{39}Ar$ (x 10^{-3})	$^{39}Ar_K$ (x 10^{-15} mol)	K/Ca	$^{40}Ar^*$ (%)	^{39}Ar (%)	Age (Ma)	±1σ (Ma)
LV02-2773, A:7:157, 2.02 mg K-feldspar, J=0.0193112, D=1.0052±0.00172, NM-157, Lab#=53529-01										
A	430	548.1	0.0401	37.42	3.80	12.7	98.0	0.3	4439.5	6.5
B	430	30.76	0.0382	2.138	1.20	13.3	98.0	0.4	836.8	6.6
C	430	25.07	0.0435	2.551	1.04	11.7	97.0	0.5	702.3	6.7
D	430	23.33	0.0498	1.716	1.18	10.2	97.8	0.6	666.2	5.6
E	480	42.52	0.0534	2.774	1.95	9.5	98.1	0.7	1078.3	4.2
F	480	20.08	0.0767	1.126	2.29	6.6	98.4	0.9	589.3	3.4
G	480	20.77	0.1004	2.325	2.22	5.1	96.7	1.1	597.9	3.8
H	480	18.68	0.1087	1.631	2.57	4.7	97.5	1.3	549.5	3.3
I	530	37.10	0.1055	1.858	5.00	4.8	98.5	1.6	974.8	2.8
J	530	17.33	0.1511	1.051	4.50	3.4	98.3	2.0	518.5	2.0
K	530	16.42	0.1671	0.9393	4.62	3.1	98.4	2.3	495.1	2.1
L	530	13.92	0.1821	0.4009	5.03	2.8	99.3	2.7	431.1	1.7
M	580	31.49	0.1750	1.889	8.7	2.9	98.3	3.4	855.0	2.1
N	580	14.37	0.2689	0.6612	6.9	1.9	98.8	3.9	441.5	1.7
O	580	14.76	0.2383	0.5168	6.21	2.1	99.1	4.4	453.6	1.6
P	580	15.87	0.1224	0.3367	6.40	4.2	99.4	4.9	484.8	1.9
Q	630	35.27	0.0428	1.263	11.8	11.9	99.0	5.8	940.1	2.1
R	630	18.90	0.0321	0.4060	7.8	15.9	99.4	6.4	564.3	1.7
S	630	19.67	0.0205	0.2525	7.1	24.9	99.6	7.0	585.3	1.9
T	680	26.27	0.0161	0.6688	10.7	31.6	99.3	7.8	744.1	1.8
U	680	22.17	0.0097	0.2050	10.7	52.8	99.7	8.6	648.5	1.6
V	680	22.08	0.0080	0.2309	9.5	63.6	99.7	9.3	646.2	1.7
W	730	24.40	0.0127	0.3045	12.0	40.2	99.6	10.3	702.1	1.4
X	730	22.89	0.0082	0.1269	13.0	62.3	99.8	11.3	666.9	1.3
Y	730	23.24	0.0067	0.1297	12.0	76.3	99.8	12.2	675.3	1.5
Z	780	24.67	0.0087	0.1680	13.5	58.6	99.8	13.2	709.6	1.3
ZA	780	24.09	0.0072	0.1378	15.5	70.7	99.8	14.4	696.0	2.1
ZB	830	25.34	0.0112	0.1486	20.6	45.6	99.8	16.0	725.6	1.7
ZC	830	25.41	0.0081	0.0953	22.4	63.4	99.9	17.7	727.7	1.4
ZD	880	26.37	0.0097	0.2526	28.4	52.8	99.7	19.9	749.2	1.5
ZE	880	26.33	0.0078	0.2306	30.2	65.2	99.7	22.2	748.4	1.3
ZF	930	27.01	0.0097	0.3390	38.8	52.4	99.6	25.2	763.4	1.4
ZG	930	26.15	0.0086	0.3034	41.8	59.1	99.7	28.5	743.6	1.6
ZH	980	25.69	0.0111	0.4275	58.9	45.8	99.5	33.0	732.1	1.3
ZI	980	25.71	0.0099	0.3989	72.2	51.4	99.5	38.6	732.7	1.5
ZJ	1030	25.77	0.0145	0.4743	104.0	35.3	99.5	46.6	733.7	1.4
ZK	1030	27.29	0.0133	0.4081	85.9	38.4	99.6	53.2	769.6	1.4
ZL	1100	28.95	0.0154	0.4055	102.9	33.2	99.6	61.1	807.7	1.4
ZM	1100	31.80	0.0112	0.2819	72.4	45.5	99.7	66.7	871.9	1.7
ZN	1100	33.45	0.0075	0.2630	96.6	68.0	99.8	74.2	907.7	1.7
ZO	1100	35.13	0.0048	0.2069	137.3	106.0	99.8	84.7	943.8	1.7
ZP	1100	36.24	0.0035	0.3143	129.1	147.0	99.7	94.7	966.4	1.8
ZQ	1180	37.25	0.0025	0.2334	10.8	205.6	99.8	95.5	987.6	2.0
ZR	1280	37.46	0.0048	0.2390	10.1	105.3	99.8	96.3	992.0	2.0
ZS	1380	37.98	0.0058	0.0723	16.6	88.2	99.9	97.6	1003.5	1.9
ZT	1670	38.15	0.0071	0.5690	31.5	71.9	99.6	100.0	1004.0	1.6
Total gas age ± 1σ			n=46		1297.6		K2O=12.78 %		852.1	1.4

ID	Power/Temp (W/°C)	$^{40}Ar/^{39}Ar$	$^{37}Ar/^{39}Ar$	$^{36}Ar/^{39}Ar$ (x 10^{-3})	$^{39}Ar_K$ (x 10^{-15} mol)	K/Ca	$^{40}Ar^*$ (%)	^{39}Ar (%)	Age (Ma)	±1σ (Ma)
HP02-1, B:8:157, 1.71 mg K-feldspar, J=0.0193992, D=1.0052±0.00172, NM-157, Lab#=53545-01										
A	430	637.5	-0.0027	66.03	1.54	-	96.9	0.1	4682.4	8.9
B	430	47.01	-0.0068	9.436	0.655	-	94.1	0.2	1130.5	9.1
C	430	36.28	-0.0046	11.82	0.546	-	90.4	0.2	898.4	9.7
D	430	27.02	-0.0121	12.24	0.560	-	86.6	0.3	682.8	9.4
E	480	35.15	-0.0029	8.216	0.74	-	93.1	0.4	896.8	6.7
F	480	23.77	-0.0022	4.834	1.19	-	94.0	0.5	656.8	4.5
G	480	18.71	0.0010	3.294	1.26	510.1	94.8	0.6	539.2	4.7
H	480	20.88	-0.0012	2.602	1.21	-	96.3	0.7	600.7	4.8
I	530	28.03	0.0019	2.415	1.52	271.2	97.5	0.8	775.8	3.7
J	530	18.96	-0.0034	2.058	1.93	-	96.8	1.0	555.2	3.5
K	530	18.37	0.0008	1.273	2.23	609.1	97.9	1.2	545.9	2.7
L	530	19.05	0.0021	1.468	2.92	247.5	97.7	1.5	562.3	2.3
M	580	26.52	0.0091	1.143	3.19	56.0	98.7	1.8	749.3	2.6
N	580	20.68	0.0023	0.9702	3.73	217.7	98.6	2.1	607.9	2.1
O	580	21.37	0.0006	0.7075	4.15	850.9	99.0	2.5	627.4	1.9
P	580	22.36	0.0009	0.2792	4.99	538.5	99.6	2.9	655.1	1.8
Q	630	28.16	0.0026	0.7073	5.29	196.1	99.3	3.4	790.5	2.3
R	630	25.04	0.0016	0.4322	5.75	327.0	99.5	3.9	719.1	1.9
S	630	26.34	0.0012	0.4619	6.18	408.9	99.5	4.5	749.8	1.9
T	680	31.44	0.0024	0.4010	8.5	217.0	99.6	5.3	866.2	2.2
U	680	30.76	0.0020	0.4944	10.1	254.5	99.5	6.2	850.6	1.7
V	680	32.69	0.0023	0.2066	8.4	226.3	99.8	6.9	894.9	1.9
W	730	35.54	0.0031	0.3562	10.9	165.9	99.7	7.9	954.8	1.7
X	730	35.03	0.0016	0.2050	13.6	310.4	99.8	9.2	945.0	2.0
Y	730	35.21	0.0013	0.2843	13.4	383.8	99.8	10.4	948.3	1.9
Z	780	36.11	0.0016	0.1001	12.3	312.9	99.9	11.5	968.3	1.8
ZA	780	34.54	0.0014	0.1888	18.3	372.4	99.8	13.2	934.7	1.8
ZB	830	34.78	0.0027	0.2126	18.1	187.6	99.8	14.8	939.7	1.7
ZC	830	33.65	0.0021	0.3589	24.2	241.5	99.7	17.0	914.6	1.7
ZD	880	33.88	0.0024	0.1789	20.2	210.1	99.8	18.8	920.6	1.7
ZE	880	33.40	0.0022	0.1793	26.8	231.2	99.8	21.3	910.4	1.8
ZF	930	34.09	0.0027	0.2869	22.9	187.1	99.8	23.3	924.4	1.6
ZG	930	33.53	0.0025	0.1479	24.6	201.6	99.9	25.6	913.3	1.7
ZH	980	34.65	0.0033	0.2499	27.5	152.9	99.8	28.1	936.7	1.7
ZI	980	33.70	0.0024	0.2434	30.0	208.4	99.8	30.8	916.5	1.8
ZJ	1030	35.97	0.0038	0.3726	25.9	134.3	99.7	33.1	963.7	1.7
ZK	1030	34.70	0.0028	0.4085	34.8	183.7	99.7	36.3	936.7	1.6
ZL	1100	37.10	0.0050	0.5012	40.3	102.9	99.6	39.9	986.3	1.7
ZM	1100	36.63	0.0045	0.4610	30.9	114.3	99.6	42.7	976.9	1.8
ZN	1100	38.31	0.0050	0.3935	58.3	101.8	99.7	48.0	1011.9	1.8
ZO	1100	39.80	0.0055	0.4951	56.1	92.1	99.6	53.1	1041.2	1.9
ZP	1100	40.83	0.0040	0.5158	67.8	128.2	99.6	59.3	1061.8	2.2
ZQ	1180	40.23	0.0014	0.3270	19.8	353.3	99.8	61.1	1050.8	2.0
ZR	1280	40.82	0.0004	0.2800	299.2	1308	99.8	88.2	1062.9	3.1
ZS	1380	40.75	0.0011	0.3862	60.8	481.2	99.7	93.7	1060.8	2.0
ZT	1670	39.43	0.0007	0.4590	68.9	707.3	99.7	100.0	1034.1	2.0
Total gas age ± 1σ			n=46		1101.9		K2O=12.76 %		1010.9	1.7

ID	Power/Temp (W/°C)	$^{40}Ar/^{39}Ar$	$^{37}Ar/^{39}Ar$	$^{36}Ar/^{39}Ar$ (x 10^{-3})	$^{39}Ar_K$ (x 10^{-15} mol)	K/Ca	$^{40}Ar^*$ (%)	^{39}Ar (%)	Age (Ma)	±1σ (Ma)
HP02-10, E:1:157, 2.38 mg K-feldspar, J=0.0187144, D=1.0052±0.00172, NM-157, Lab#=53556-01										
A	430	531.1	0.0114	46.62	2.39	44.6	97.4	0.2	4325.1	6.5
B	430	30.04	0.0038	6.706	0.98	136.0	93.4	0.2	770.0	6.8
C	430	23.10	0.0062	7.986	0.620	81.9	89.8	0.3	598.2	8.0
D	430	18.09	0.0033	3.312	0.82	152.9	94.6	0.3	506.6	6.3
E	480	18.94	0.0105	1.157	0.88	48.8	98.2	0.4	544.6	5.8
F	480	12.91	0.0085	2.268	1.10	60.0	94.8	0.5	375.7	4.4
G	480	12.20	0.0032	2.378	1.34	161.4	94.2	0.6	355.0	4.1
H	480	12.60	0.0039	1.961	1.27	130.5	95.4	0.7	369.7	4.2
I	530	18.89	0.0077	1.931	1.86	66.4	97.0	0.8	537.4	3.3
J	530	14.40	0.0083	2.989	2.03	61.6	93.9	1.0	411.0	3.4
K	530	13.56	0.0098	0.6281	2.42	52.0	98.6	1.1	407.1	2.7
L	530	14.10	0.0057	0.9663	2.80	90.2	98.0	1.3	419.0	2.2
M	580	19.38	0.0044	0.5978	3.03	116.7	99.1	1.6	559.9	2.2
N	580	15.60	0.0048	0.3262	3.36	105.7	99.4	1.8	464.4	1.9
O	580	17.13	0.0054	0.6478	3.64	93.8	98.9	2.1	501.9	1.7
P	580	19.19	0.0061	0.6711	3.76	83.4	99.0	2.3	554.5	1.9
Q	630	22.52	0.0032	-0.0087	3.24	160.1	100.0	2.6	641.4	2.1
R	630	23.29	0.0061	0.5881	2.98	83.3	99.3	2.8	655.7	2.2
S	630	25.43	0.0054	0.7565	2.80	94.5	99.1	3.0	704.9	2.5
T	680	32.97	0.0056	0.7297	3.77	90.8	99.3	3.3	872.3	2.4
U	680	32.01	0.0055	0.7312	3.51	93.5	99.3	3.5	851.9	2.3
V	680	34.50	0.0055	0.7759	3.64	92.4	99.3	3.8	904.2	2.4
W	730	39.75	0.0064	0.5775	3.64	80.1	99.6	4.0	1011.6	2.4
X	730	39.11	0.0048	0.3840	4.93	106.6	99.7	4.4	1000.2	2.4
Y	730	40.23	0.0041	0.2576	5.80	124.2	99.8	4.8	1022.8	2.4
Z	780	41.95	0.0049	0.3515	6.39	103.6	99.8	5.3	1055.5	2.2
ZA	780	40.16	0.0032	0.2885	10.5	158.8	99.8	6.0	1021.3	1.9
ZB	830	39.74	0.0045	0.3816	12.1	113.4	99.7	6.9	1012.5	1.9
ZC	830	38.13	0.0027	0.1295	14.6	188.8	99.9	8.0	982.1	1.9
ZD	880	37.90	0.0027	0.2894	16.8	187.0	99.8	9.2	976.5	2.0
ZE	880	36.82	0.0024	0.1268	23.6	214.8	99.9	10.9	955.8	1.9
ZF	930	37.56	0.0030	0.3734	31.7	170.2	99.7	13.2	969.2	1.9
ZG	930	36.83	0.0020	0.1127	34.2	259.2	99.9	15.7	956.0	1.6
ZH	980	38.06	0.0027	0.3002	47.1	188.6	99.8	19.1	979.7	1.7
ZI	980	37.16	0.0015	0.2412	50.6	347.8	99.8	22.8	962.1	1.9
ZJ	1030	38.01	0.0025	0.3543	76.6	206.3	99.7	28.3	978.4	1.8
ZK	1030	37.26	0.0017	0.2293	74.7	295.7	99.8	33.7	964.0	1.9
ZL	1100	38.23	0.0028	0.2707	119.3	181.8	99.8	42.4	983.3	1.8
ZM	1100	38.10	0.0026	0.1935	124.9	193.6	99.9	51.4	981.2	1.9
ZN	1100	38.55	0.0023	0.1756	166.0	221.6	99.9	63.4	990.3	2.1
ZO	1100	39.37	0.0020	0.1824	152.2	255.0	99.9	74.4	1006.4	1.7
ZP	1100	39.44	0.0015	0.2265	133.5	346.6	99.8	84.1	1007.5	1.6
ZQ	1180	40.29	0.0010	0.2572	20.3	534.2	99.8	85.6	1024.0	1.6
ZR	1280	40.26	0.0006	0.2113	113.8	864.5	99.8	93.8	1023.6	2.1
ZS	1380	40.26	0.0008	0.3587	24.8	601.2	99.7	95.6	1022.8	1.7
ZT	1670	40.07	0.0011	0.3994	60.4	446.5	99.7	100.0	1018.9	1.8
Total gas age ± 1σ			n=46		1380.8		K2O=11.91 %		996.9	1.6

ID	Power/Temp (W/°C)	$^{40}Ar/^{39}Ar$	$^{37}Ar/^{39}Ar$	$^{36}Ar/^{39}Ar$ (x 10^{-3})	$^{39}Ar_K$ (x 10^{-15} mol)	K/Ca	$^{40}Ar^*$ (%)	^{39}Ar (%)	Age (Ma)	±1σ (Ma)
LAMY02-1, A:11:157, 2.04 mg K-feldspar, J=0.0192267, D=1.0052±0.00172, NM-157, Lab#=53532-02										
A	430	59.88	0.0056	15.01	3.57	90.7	92.6	0.3	1324.6	3.7
B	430	18.85	-0.0038	2.763	1.66	-	95.7	0.4	542.8	3.4
C	430	16.75	-0.0003	2.966	1.49	-	94.8	0.5	485.6	3.9
D	430	16.76	0.0009	2.788	1.48	575.4	95.1	0.7	487.3	3.1
E	480	17.32	0.0010	1.873	1.92	486.4	96.8	0.8	509.4	3.5
F	480	17.26	0.0026	1.184	2.53	193.4	98.0	1.0	513.3	2.0
G	480	18.23	0.0025	0.7187	2.11	208.1	98.8	1.2	542.5	3.3
H	480	18.72	0.0013	2.233	2.41	406.9	96.5	1.4	543.6	2.7
I	530	20.66	0.0023	1.642	3.18	222.5	97.6	1.7	597.9	1.9
J	530	20.43	0.0023	0.6471	4.21	219.0	99.1	2.0	599.5	1.9
K	530	21.79	0.0032	0.6265	3.21	159.9	99.2	2.3	633.6	2.1
L	530	23.09	0.0010	0.6049	3.87	528.6	99.2	2.6	665.8	2.0
M	580	26.18	0.0020	1.189	3.93	254.5	98.7	2.9	735.5	2.1
N	580	27.13	0.0016	0.6077	4.65	312.0	99.3	3.3	761.8	1.9
O	580	29.92	0.0008	0.5609	4.22	626.8	99.4	3.6	825.3	2.4
P	580	32.73	0.0046	0.4802	4.66	111.8	99.6	4.0	887.7	2.1
Q	630	35.74	0.0032	0.7181	4.04	158.9	99.4	4.3	950.1	2.7
R	630	37.12	0.0012	0.6184	5.25	442.4	99.5	4.8	979.3	2.2
S	630	38.33	0.0015	0.3232	5.30	345.3	99.8	5.2	1005.7	2.8
T	680	39.46	0.0014	0.4881	5.32	364.6	99.6	5.6	1027.5	2.3
U	680	39.01	0.0010	0.3421	7.4	504.9	99.7	6.2	1019.4	2.2
V	680	38.82	0.0007	0.2290	7.1	682.2	99.8	6.8	1016.1	2.6
W	730	38.71	0.0018	0.3650	9.2	277.2	99.7	7.6	1013.2	2.2
X	730	37.92	0.0021	0.3908	10.5	245.9	99.7	8.4	997.1	2.1
Y	730	37.42	0.0016	0.4446	11.5	320.1	99.6	9.4	986.4	2.0
Z	780	37.11	0.0030	0.3868	10.5	167.7	99.7	10.2	980.4	2.0
ZA	780	36.77	0.0033	0.2381	15.2	153.1	99.8	11.4	974.3	2.1
ZB	830	36.49	0.0054	0.1485	19.3	94.2	99.9	13.0	969.1	1.7
ZC	830	36.58	0.0023	0.2763	23.6	217.3	99.8	14.9	970.1	2.2
ZD	880	36.80	0.0062	0.1823	20.8	82.0	99.9	16.6	975.4	1.9
ZE	880	36.75	0.0041	0.2219	28.1	125.7	99.8	18.9	974.1	1.7
ZF	930	37.18	0.0085	0.3603	21.4	60.2	99.7	20.7	982.1	1.8
ZG	930	36.97	0.0047	0.1691	28.7	109.4	99.9	23.0	979.0	2.3
ZH	980	36.76	0.0041	0.3342	26.9	123.1	99.7	25.2	973.6	1.7
ZI	980	36.99	0.0021	0.2655	29.2	243.4	99.8	27.6	978.8	1.8
ZJ	1030	36.61	0.0051	0.4780	34.1	99.1	99.6	30.4	969.7	1.7
ZK	1030	37.34	0.0036	0.4097	31.4	140.9	99.7	32.9	985.0	2.1
ZL	1100	36.89	0.0113	0.6211	44.3	45.0	99.5	36.5	974.4	1.5
ZM	1100	37.68	0.0074	0.4953	47.7	69.3	99.6	40.4	991.5	1.7
ZN	1100	37.99	0.0063	0.3885	70.4	80.4	99.7	46.2	998.4	2.2
ZO	1100	38.26	0.0039	0.4765	127.9	132.3	99.6	56.6	1003.4	1.9
ZP	1100	38.67	0.0019	0.4799	133.0	265.4	99.6	67.4	1011.7	2.2
ZQ	1180	38.46	0.0008	0.2615	57.9	622.8	99.8	72.1	1008.7	1.9
ZR	1280	39.79	0.0009	0.2485	295.6	565.2	99.8	96.2	1035.5	2.8
ZS	1380	40.21	0.0032	0.5150	26.0	158.1	99.6	98.3	1042.2	1.8
ZT	1670	40.31	0.0041	1.194	20.3	123.7	99.1	100.0	1040.2	2.3
Total gas age ± 1σ			n=46		1227.0		K2O=12.02 %		995.0	1.7

ID	Power/Temp (W/°C)	$^{40}Ar/^{39}Ar$	$^{37}Ar/^{39}Ar$	$^{36}Ar/^{39}Ar$ (x 10^{-3})	$^{39}Ar_K$ (x 10^{-15} mol)	K/Ca	$^{40}Ar^*$ (%)	^{39}Ar (%)	Age (Ma)	±1σ (Ma)
MG01-1a, J:1:145, 3.25 mg K-feldspar(?), J=0.0095489, D=1.00535±0.00031, NM-145, Lab#=52790-01										
A	450	79.79	2.143	186.8	1.515	0.24	31.0	0.8	387.5	8.3
B	450	27.95	0.7130	17.64	0.887	0.72	81.5	1.3	359.4	4.3
C	450	25.92	0.4026	11.90	0.782	1.3	86.5	1.7	354.2	4.2
D	500	25.23	0.7817	9.002	0.463	0.65	89.7	2.0	357.1	8.3
E	500	25.04	1.039	7.270	1.451	0.49	91.7	2.8	362.0	2.3
F	500	26.95	0.4165	6.449	1.312	1.2	93.0	3.5	391.7	2.7
G	550	28.98	0.1446	4.301	1.579	3.5	95.6	4.3	428.5	2.1
H	550	31.07	0.0636	3.806	2.278	8.0	96.4	5.5	458.9	1.8
I	550	34.32	0.0427	2.658	2.027	11.9	97.7	6.6	506.9	2.1
J	600	37.67	0.0496	3.191	2.033	10.3	97.5	7.7	548.6	2.0
K	600	39.71	0.0309	1.920	3.195	16.5	98.6	9.5	579.5	1.6
L	600	42.84	0.0238	1.444	2.937	21.4	99.0	11.0	620.6	1.8
M	650	44.64	0.0262	0.9979	2.920	19.5	99.3	12.6	644.5	2.2
N	650	47.05	0.0218	0.7057	4.67	23.4	99.6	15.1	674.8	1.3
O	650	49.09	0.0188	0.6965	4.411	27.1	99.6	17.5	699.2	1.3
P	700	50.70	0.0233	1.051	3.981	21.9	99.4	19.7	717.0	1.2
Q	700	52.27	0.0211	1.008	5.88	24.2	99.4	22.8	735.6	1.1
R	700	53.94	0.0212	0.8825	5.06	24.1	99.5	25.6	755.4	1.2
S	750	55.24	0.0264	0.9916	4.215	19.3	99.5	27.8	769.9	1.5
T	750	56.52	0.0266	0.7326	6.05	19.2	99.6	31.1	785.3	1.1
U	750	58.02	0.0288	1.346	4.64	17.7	99.3	33.6	800.3	1.3
V	800	59.53	0.0654	1.698	3.093	7.8	99.2	35.3	816.1	1.8
W	800	59.75	0.0508	1.978	4.396	10.0	99.0	37.6	817.6	1.4
X	850	61.62	0.0668	1.318	5.92	7.6	99.4	40.8	840.5	1.2
Y	850	63.61	0.0472	1.170	6.21	10.8	99.5	44.2	862.7	1.4
Z	900	65.19	0.0472	1.320	6.95	10.8	99.4	47.9	879.3	1.2
ZA	900	66.75	0.0343	0.9894	7.09	14.9	99.6	51.8	897.0	1.2
ZB	950	66.48	0.0593	1.170	6.78	8.6	99.5	55.4	893.7	1.2
ZC	950	67.96	0.0373	1.034	7.04	13.7	99.6	59.2	909.8	1.1
ZD	1000	67.02	0.0522	1.625	7.75	9.8	99.3	63.4	898.0	1.4
ZE	1000	70.63	0.0395	1.220	7.20	12.9	99.5	67.3	937.3	1.1
ZF	1050	72.81	0.0599	2.383	10.26	8.5	99.0	72.8	956.37	0.90
ZG	1050	77.02	0.0582	1.992	10.27	8.8	99.2	78.4	1000.6	1.2
ZH	1100	82.99	0.0710	3.220	12.43	7.2	98.9	85.1	1056.3	1.6
ZI	1100	87.14	0.0621	1.937	10.03	8.2	99.3	90.5	1100.0	1.2
ZJ	1100	90.06	0.0813	3.379	7.10	6.3	98.9	94.3	1123.6	1.6
ZK	1100	93.82	0.1447	12.34	2.180	3.5	96.1	95.5	1134.2	3.4
ZL	1100	99.91	0.2024	30.47	1.012	2.5	91.0	96.0	1141.1	4.2
ZN	1300	84.82	0.3499	7.490	0.537	1.5	97.4	96.3	1062.2	6.0
ZO	1400	87.55	0.0860	5.506	1.146	5.9	98.1	96.9	1093.9	3.2
ZP	1660	89.99	0.0932	7.135	5.69	5.5	97.7	100.0	1112.5	1.4
Total gas age ± 1σ			n=41		185.3		K2O=2.29 %		871.65	0.80

Isotopic ratios corrected for blank, radioactive decay, and mass discrimination, not corrected for interferring reactions.
Ages calculated relative to FC-2 Fish Canyon Tuff sanidine interlaboratory standard at 28.27 Ma.
Errors quoted for individual analyses include analytical error only, without interferring reaction or J uncertainties.
Total gas age calculated by recombining isotopic measurements of all steps.
Total gas age error calculated by recombining errors of isotopic measurements of all steps.
WMA (weighted mean age) is inverse-variance-weighted mean of selected steps.
WMA age error is inverse-variance-weighted mean error (Taylor, 1982) times root MSWD where MSWD>1.
WMA and total gas ages incorporate uncertainties in interferring reaction corrections and J factors.
Isotopic abundances after Steiger and Jager (1977). Decay constant for ^{40}K is 5.476e-10/a after Kwon et al. (2002).
# symbol preceding sample ID denotes analyses excluded from WMA age calculations.
Discrimination = 1.00535±0.00031, 1.00484±0.00092, and 1.0052±0.00121 for NM-145, NM-157, and NM-164, respectively.
Correction factors:

$(^{39}Ar/^{37}Ar)_{Ca}$ = 0.0007±0.00003(NM-145); 0.00075±0.00003(NM-158); 0.0007±0.00005(NM-164)

$(^{36}Ar/^{37}Ar)_{Ca}$ = 0.00027±0.000005(NM-145); 0.000292±0.000006(NM-158); 0.00027±0.00001(NM-164)

$(^{38}Ar/^{39}Ar)_{K}$ = 0.01077

$(^{40}Ar/^{39}Ar)_{K}$ = 0.031± 0.001(NM-145); 0.0296±0.0005(NM-158); 0.02559±0.001487(NM-164)

Data repository 3: Open-File Report - Methods for obtaining thermal histories from $^{40}Ar/^{39}Ar$ K-feldspar step heating data

DR3.1 Introduction

This overview of $^{40}Ar/^{39}Ar$ K-feldspar thermochronology summarizes the theory and methodology of the Multiple Diffusion Domain (MDD) model with specific examples to illustrate the procedures used at the New Mexico Geochronology Research Laboratory (NMGRL). Geochronology relies on the accumulation of a radiogenic daughter isotope that is produced by the radioactive decay of a parent isotope. The parent to daughter ratio is combined with known decay constant(s) to calculate a date for a sample. The calculated date may be a meaningful geological age (i.e. time of an eruption, growth of a mineral, etc.) provided the sample is a closed system with no gain or loss of the parent or daughter isotopes. Thermochronology is based on the same basic principles of geochronology, but rather than a date being related to a specific event, thermochronological data records the time when a sample passes through a certain temperature (Dodson, 1973). This temperature is defined as the closure temperature and reflects the temperature when the sample effectively ceases to loose a daughter product by diffusion. There are many themochronometers amongst the variety of radioactive decay schemes and closure temperatures are highly variable (McDougall and Harrison, 1999). For the K-Ar system, hornblende appears to have the highest closure temperature of about 500°C (Harrison, 1981) followed by micas that range between about 300 and 400°C (Robins, 1974; Harrison et al., 1985; Hames and Bowring, 1994; Grove and Harrison, 1996). Homogeneous orthoclase was determined to have a closure temperature of about 300°C (Foland, 1974). Foland (1974) also suggested that microcline would have a lower closure temperature due to fine-scale mircotextures. Significant work throughout the past two decades has utilized and explored the argon systematics of K-feldspar (see

McDougall and Harrison, 1999 for a review). There are probably many factors that contribute to argon loss in this microstructurally complex mineral and the overall utility of $^{40}Ar/^{39}Ar$ dating is still debated (e.g. Parsons et al., 1999; Lovera et al., 1997; 2002).

For $^{40}Ar/^{39}Ar$ K-feldspar thermochronology at the NMGRL, we adopt the MDD model of Lovera et al. (1989) to extract thermal histories from step-heating data. This method views K-feldspars as having a number of different size diffusion domains each of which has a different closure temperature typically between ~300 and 175°C. Diffusion domains are discrete areas of varying length and are assumed to be separated by boundaries that are maintained at zero argon concentration. Given sufficient time and temperatures near or in excess of the closure temperature of a particular domain, radiogenic argon will diffuse to the domain boundary and escape from the K-feldspar. Because argon loss in K-feldspars occurs in the temperature range equivalent to those found at mid- to shallow crustal levels, K-feldspar $^{40}Ar/^{39}Ar$ thermochronology is an useful method for understanding the thermal history of an important crustal region. In addition, the K-feldspar system is sensitive to moderate thermal perturbations and therefore can be used to determine the timing of episodic argon loss events related to, for instance, magmatism, geothermal activity or burial.

DR3.2 K-feldspar $^{40}Ar/^{39}Ar$ data and plots

DR3.2.1 Age spectrum diagrams

The thermal history recorded by a K-feldspar can be determined by combining the age spectrum data and the laboratory degassing behavior of ^{39}Ar. The age spectrum is a measurement of the natural radiogenic ^{40}Ar ($^{40}Ar^*$) concentration distribution within the sample, whereas the degassing of the reactor-produced ^{39}Ar during step-heating is a measure of the K-feldspar closure temperatures. Below we demonstrate the steps used to recover thermal histories from $^{40}Ar/^{39}Ar$ K-feldspar step heating data. The first step is to create the age spectrum by high-resolution (~45 steps) step heating (Fig. 1a). Heating

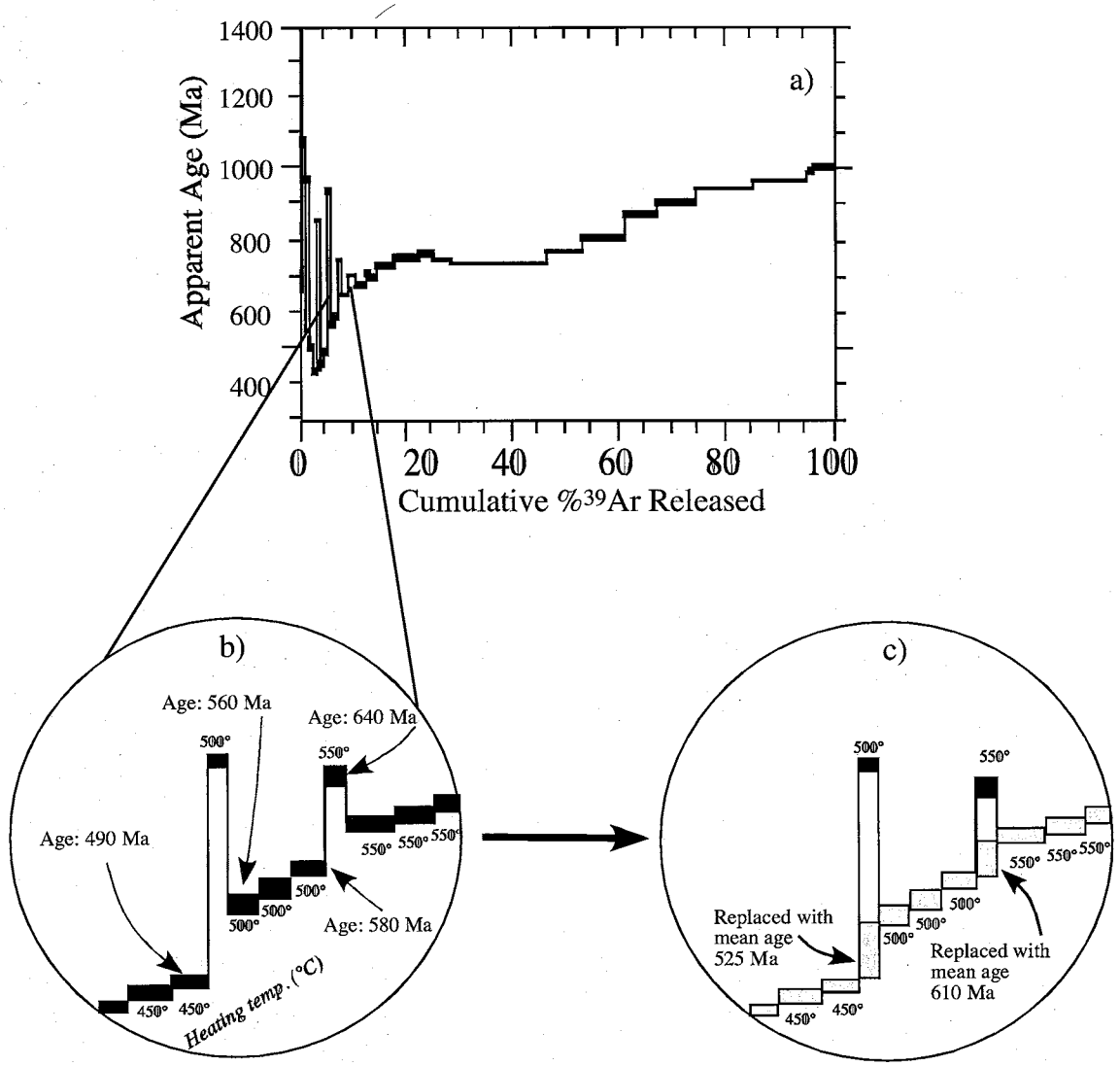

Fig. 1. Age spectrum diagram and excess argon corrections. 1a. Common age spectrum for many K-feldspars with initially old ages indicating excess ^{40}Ar contamination followed by an overall increasing age gradient revealing the non-uniform $^{40}Ar^*$ concentration profile developed by argon loss associated with slow-cooling and/or reheating events. 1b. Isothermal replicate heating steps demonstrate a characteristic behavior with the first step yielding an anomalously old age caused by degassing of fluid inclusions that host excess ^{40}Ar. 1c. Method of correcting anomalous ages involves substituting old ages with the mean age of the preceding and following steps. The error bar is expanded to fill the age space between the preceding and following steps.

schedules typically begin at 400°C and include three to four isothermal steps for many of the lower temperature settings (Fig. 1b). The isothermal steps serve two primary purposes. The first is to resolve excess ^{40}Ar that is common in most K-feldspars. The excess ^{40}Ar appears to be cited in thermally distinct reservoirs as the first isothermal step commonly records an anomalously old apparent age relative to the next isothermal steps at a given temperature (Figs 1a, b). When the next higher isothermal temperature group is carried out the 1st step is once again anomalously old and is followed by younger apparent ages (Fig. 1b). This behavior is thought to be caused by decrepitation of fluid inclusions that contain excess ^{40}Ar (Harrison et al., 1993, 1994). After initial decrepitation caused by the first of the isothermal replicate steps, the age typically decreases and then rises more uniformally as the true distribution of $^{40}Ar^*$ is less disturbed by the fluid-inclusion hosted excess argon. Moving to the next highest temperature of isothermal replicates causes decrepitation of new fluid inclusions that again causes the apparent age to increase significantly (Fig. 1a, b).

Because MDD theory does not allow for excess argon contamination, the anomalously old steps need correction prior to modeling the age spectrum. Harrison et al. (1993) developed a method to correct for fluid inclusion hosted excess argon though the recognition that the old apparent ages were correlated to Cl that is monitored by measuring $^{38}Ar_{Cl}$. Using the Harrison et al. (1993) approach for many of the Precambrian samples analyzed at the NMGRL, yields Cl-corrected ages that are negative indicating that the Cl cannot all be correlated to excess argon and thus the method of Harrison et al. (1993) is generally not employed. Rather, it is assumed that when the apparent age reaches a minimum for a given set of isothermal heating steps the measured age accurately records the true $^{40}Ar^*$ distribution. To correct the anomalously old apparent ages that are given by the 1st isothermal step they are decreased to the mean value of the previous and following steps (Fig. 1b, c). This procedure results in a corrected age spectrum that only records an overall increasing spectrum and is the spectrum used for

thermal history modeling.

DR3.2.2 Arrhenius diagrams

The second purpose of the isothermal steps is to evaluate whether the calculated diffusion coefficients for the initial heating steps on the Arrhenius diagram are approximately the same. An Arrhenius diagram is a plot of inverse temperature (1/T) and frequency-factor length scale parameter (D/r^2) for each heating step (Fig. 2a). The frequency-factor length scale ratio is determined from the fraction of ^{39}Ar released and the duration of each heating step assuming a plane-sheet geometry (eqs. 1 and 2).

$$f=1-(8/\pi^2)\exp(-\pi^2 Dt/4r^2) \quad \text{for } 0.45\leq f\leq 1 \quad \text{eq. 1}$$

$$f=(2/((\pi^{1/2}))(Dt/r^2)^{1/2} \quad \text{for } 0\leq f\leq 0.60 \quad \text{eq. 2}$$

where D = diffusion coefficient; f = fraction ^{39}Ar released; r = diffusion half width; t = time at temperature.

The slope of the Arrhenius data is a function of the activation energy (E) of a sample, however with multiple diffusion domains contributing gas to each temperature step the true slope can be difficult to determine. Lovera et al. (1989) demonstrated that the initial heating steps could yield diffusion coefficients with a slope that accurately records the true E if the gas released is dominated by only one of the diffusion domains. Subequal diffusion coefficients for isothermal replicate heating steps indicates gas release that is dominated by a single domain (Fig. 2b – data segment 1), whereas significant decreases of the diffusion coefficient during replicate temperature steps indicates gas evolution from a mixture of different domain sizes (Fig. 2b – data segment 2). Because up to 4 replicate isothermal steps are typically used for these samples the overall slope of the initial segment of the Arrhenius plot is generally underestimated by linear regression of

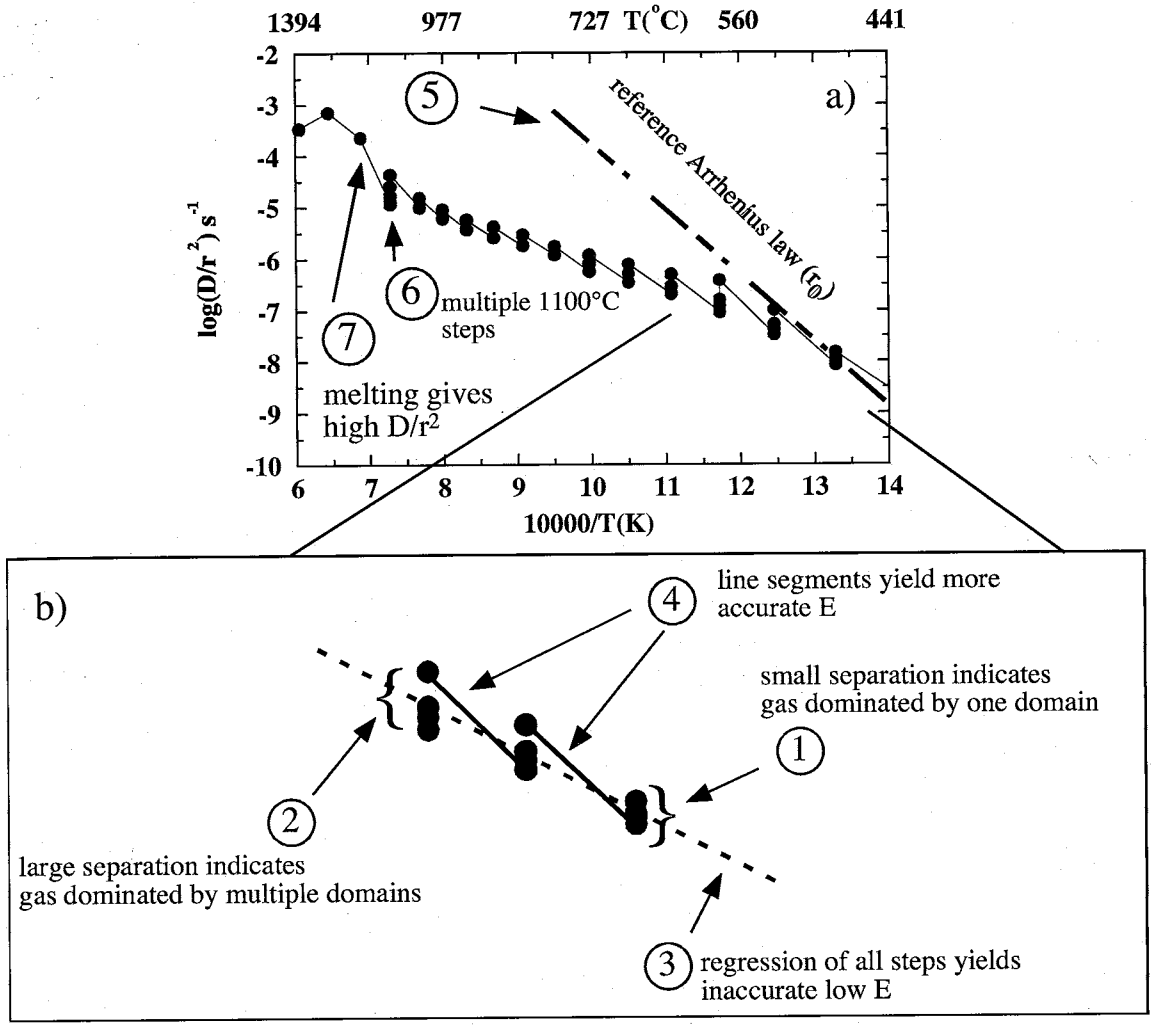

Fig. 2 Arrhenius diagram. 1a. Typical K-feldspar Arrhenius diagram for samples containing multiple diffusion domains. 1b. Expansion of initial part of the Arrhenius diagram to demonstrate characteristic data and choice of best E. 1, when isothermal steps yield similar $\log(D/r_2)$ values it is inferred that gas released is dominated by a single domain, whereas 2, shows significant decrease of $\log(D/r_2)$ values for isothermal steps that indicate a transition to degassing of larger diffusion domains. 3, regression of all initial data would provide an E that is underestimated due to ^{39}Ar derived from multiple domains. 4, line segments connecting last step of isothermal group with 1st step of next highest temperature isothermal group can be used to better determine the slope (E) of r_o. 5, by convention the reference Arrhenius law is projected through initial heating steps such that the initial steps on $\log(r/r_o)$ are zero. 6, several steps at 1100°C are carried out to degas the sample prior to the onset of melting. 7, once the temperature is raised above 1100°C high apparent $\log(D/r^2)$ values are calculated due to enhanced argon loss via melting compared to diffusive argon loss. Data collected above 1100°C are not used for modeling since the argon loss from the sample is not occurring by the same mechanism that occurred in nature.

all of the diffusion coefficients (Fig. 2b – data segment 3). Therefore, we calculate the slope of line segments between the last isothermal step of a temperature group and the 1st isothermal step of the next highest temperature group (Fig 2b – data segment 4). The individual line segments that yield similar values are averaged to estimate the E for each sample. Typically, the first 3 to 5 line segments yield similar slopes that are averaged to estimate the E of the sample. For an Arrhenius diagram with Y-axis of $\log(D/r^2)$ and X-axis of 10000/T the E is given in kcal/mol via equation 3.

$$E = m*2.303*19.87 \qquad \text{eq. 3}$$

where m is slope, 2.303 is a log versus natural log conversion and 19.87 is the gas constant.

Once the E is determined, a reference Arrhenius law (r_o) with this E is projected through the initial heating steps (Fig. 2a – data segment 5). Another characteristic of the Arrhenius plot is the several isothermal heating steps conducted at 1100°C (Fig. 2a – data segment 6). Typically a K-feldspar is heated at 1100°C for several steps that total about 8 hours to facilitate substantial degassing prior to incongruent melting. Stepping above 1100°C, where the sample begins to degas via melting, is readily recognized on the Arrhenius plot by a calculated diffusion coefficient that is anomalously high relative to the projection of the lower temperature diffusion coefficients (Fig. 2a – data segment 7).

DR3.2.3 Log(r/r_o) diagrams

Recall, as small diffusion domains are exhausted of argon during initial heating steps, the slope of the Arrhenius data decrease as larger domains begin to contribute more ^{39}Ar. This, coupled with the fact that each diffusion coefficient datum on the Arrhenius plot is graphically displayed with a symbol of equal size makes it is difficult to visualize

the domain distribution of the sample. Also, the Arrhenius plot varies with heating schedule, thus making it a somewhat ineffective in representing the diffusion domain distribution. Therefore, Lovera et al. (1991) devised the $\log(r/r_o)$ plot as an alternative method of portraying the Arrhenius data (Fig. 3). This is a plot of the log of the deviation of the measured data from r_o versus cumulative $\%^{39}Ar$ released. Dividing the deviation by 2 yields the parameter $\log(r/r_o)$ that represents the change in domain size (r) necessary to depart from r_o. For a single domain sample there would be no variation between r_o and the measured data and thus the $\log(r/r_0)$ plot would be a horizontal line with value equal to zero. $\text{Log}(r/r_o)$ values increase as the measured frequency factors fall below r_o on the Arrhenius diagram. A $\log(r/r_o)$ value of 1 indicates a relative increase in diffusion domain size of 10 whereas a value of 2 means a domain size that is 100 times larger than r_o. For the example given in Fig. 3, the $\log(r/r_o)$ values climb almost immediately from zero indicating that there is very little gas in the smallest diffusion domain and the overall flat part near a value of 2 indicates that the largest diffusion domain is about 100 times larger than the reference value. The nondiffusive loss of ^{39}Ar that stems from sample melting is quite apparent on the $\log(r/r_o)$ plot as noted by a sudden drop of the $\log(r/r_o)$ value near 75% cumulative $\%^{39}Ar$ released.

DR3.3 Modeling kinetic parameters and thermal histories

Once the activation energy and the maximum value on the $\log(r/r_o)$ plot are determined, the domain distribution (i.e. volume fraction, number of domains, relative sizes) can be obtained by modeling the fraction of ^{39}Ar released relative to the heating schedule (Lovera et al., 1989; 1991). Lovera developed a set of automated routines for modeling both the ^{39}Ar fraction released and age spectrum data. We generally use these programs in a semi-automated manner by inputting our determined E and restricting the number of diffusion domains. The programs are modified from routines given in Press et al. (1992) and use a variational method to calculate a nonlinear-square fit approximation

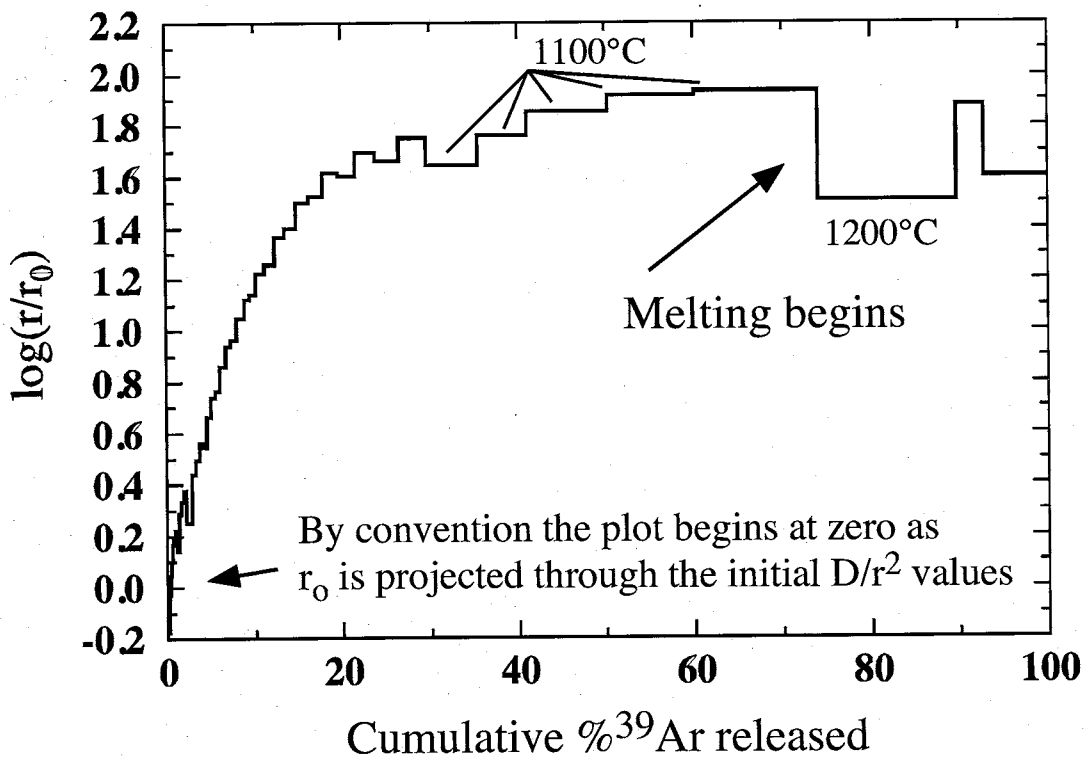

Fig. 3. Log(r/r_o) diagram. This plot is intended to provide a method to show how much ^{39}Ar is contained in an individual point on the Arrhenius plot. The log(r/r_o) value represents the relative domain size compared to r_o that has caused deviation from the reference Arrhenius law. A value of 1 indicates that r is 10 times larger than r_0 whereas a value of 2 indicates that r is 100 times larger than r_o.

of the $\log(r/r_o)$ and age spectrum diagrams. For the case of the age spectrum modeling, the thermal histories are approximated with the Chebyshev polynomials with the best-fit Chebyshev coefficients being found with the Levenberg-Marquard methods. After the kinetic parameters are determined, the measured age spectrum is forward modeled by inputting thermal histories that yield calculated spectra that match the measured ages. There are two types of thermal histories calculated by the Lovera programs. For monotonic thermal histories, the sample is only allowed to cool from an initially high temperature, whereas for the unconstrained thermal histories the sample is allowed to undergo reheating (Figs. 4, 5a, b). Individual thermal histories are accepted when they yield a model spectrum that meets the fitting criteria relative to the measured spectrum (Quidelleur et al., 1997), The individual models are contoured and displayed in two separate fashions. For the monotonic thermal histories, 90% confidence intervals are calculated for the mean as well as the overall distribution and are shown as black and grey bans, respectively (Fig. 4). For the unconstrained models, bins of time-temperature space are assigned and then the number of thermal histories that pass through an individual bin is calculated. The contour shading represents various percentages of the number of time-temperature paths that pass through individual bins relative to the total number of solutions. The background region represents a density of acceptable solutions that is less then 2% of the total number of solutions.

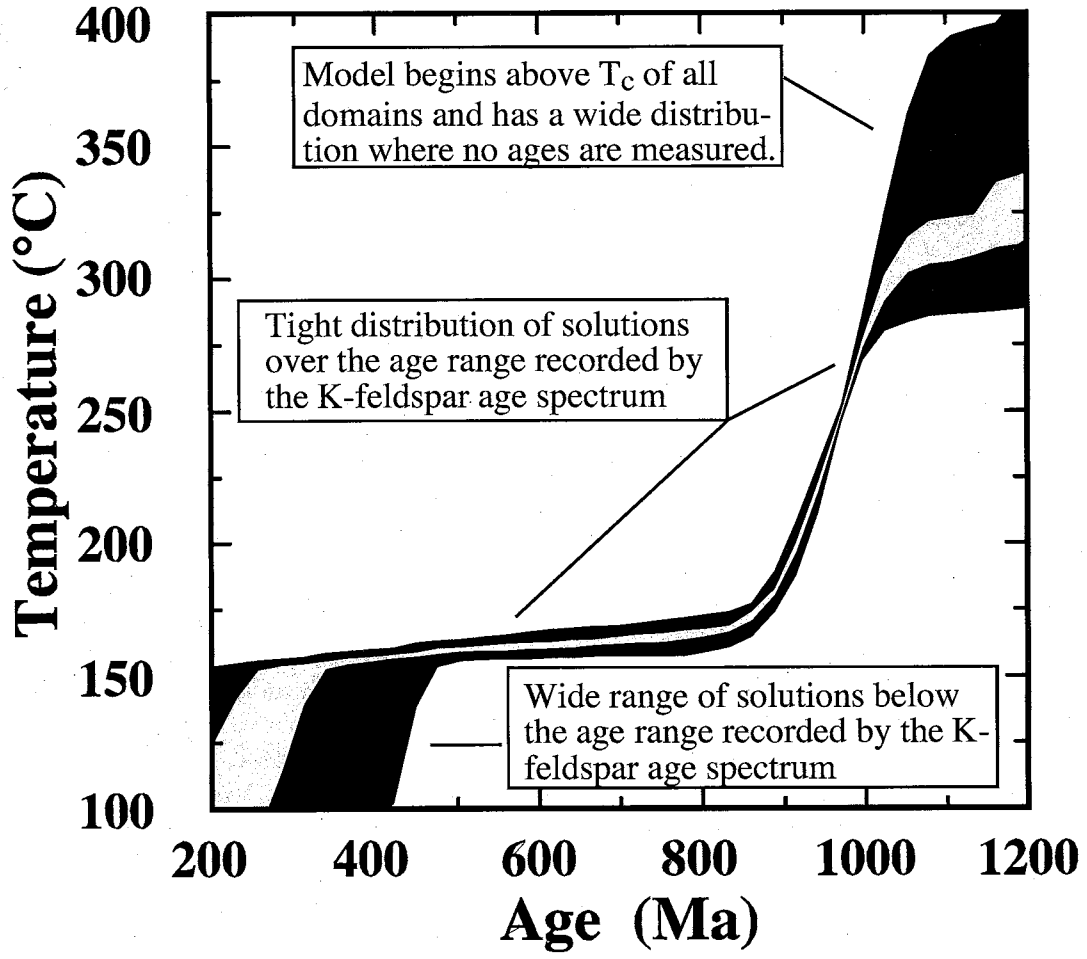

Fig. 4. Thermal histories from monotonic models. Diagram represents contoured results of thermal histories that yield calculated age spectra that match a measured age spectrum. This model only allows the sample to cool from an initially high temperature. The grey band is the 90% confidence interval of the mean, whereas the black band is the 90% confidence of the entire distribution. Large uncertainties in time-temperature space occur where there is either poor agreement between the model and measured data, or more commonly in the age regions that are younger or older than the measured data.

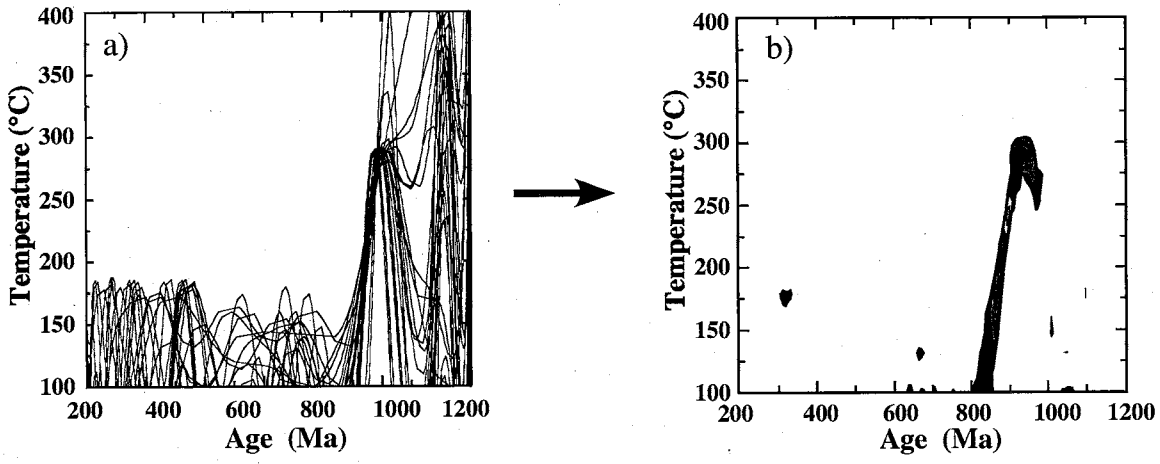

Fig. 5. Thermal histories from unconstrained models. Unconstrained thermal histories incorporate models allowed to accommodate possible reheating events. 5a, Essentially all acceptable models require the sample to be near 275°C at about 950 Ma followed by cooling soon after. Later thermal perturbations cause minor argon loss. 5b, Contoured data of all individual solutions constructed by determining the percentage of solutions that fall within discrete time-temperature bins. Warm colors reflect the highest density of solutions.

APPENDIX 2.1: $^{40}Ar/^{39}Ar$ RESULTS FOR MUSCOVITE AND BIOTITE FROM THE PECOS RIVER VALLEY, NEW MEXICO.

$^{40}Ar/^{39}Ar$ results for muscovite and biotite are presented in Table A2.1 and age spectra are shown in Figure A2.1. Complete isotopic results are given in Table A2.2. Age assignments were handled several ways depending on the complexity of the age spectrum. Ideally, a plateau age is assigned where greater than 50% of the total ^{39}Ar released yields 3 consecutive heating steps with an MSWD of ~1. However, most spectra for this study are complex and weighted means of chosen steps rarely yield MSWD values that fall within the 95% confidence window for n-1 degrees of freedom (Mahon, 1996). Despite this, we still report the weighted mean ages (Taylor, 1982) as plateau ages and increase the weighted mean error by multiplying by the square root of the MSWD. As mentioned in the text, we generally do not attempt to compare data within the cited precision as there are many geological reasons why individual samples will have variable ages and why individual spectra will have internal discordance. Total gas ages and errors are calculated by quadradically summing all steps and are at times used as our best approximation of the argon closure age.

Overall, muscovite analyses yield well-behaved age spectra with most assigned plateau ages calculated from >90% of the total ^{39}Ar released. K/Ca values range between 100 and 1000. Three replicate analyses of PVBR02-28 muscovite have segments that comprise >95% of the total ^{39}Ar released with calculated dates of 1343, 1325, and 1342 Ma (MSWD=22.64, 75.73, and 35.68, respectively)(Figures A2.1a,b,c). The best estimate for the cooling age of this pegmatite (<350-400°C) is ~1340 Ma. Two analyses

TABLE A2.1: AGES, LOCATIONS, AND DESCRIPTIONS OF MUSCOVITE AND BIOTITE DATED IN THE PECOS RIVER VALLEY.

Sample	Mineral	UTM		Total Gas Age (Ma)	Plateau Age (Ma)	MSWD	Fig.	Sample Description
PVBR02-28	M	438694	3952002	1341.7±1.7	1343.0±3.3	22.64	A2.1A	muscovite from coarse K-feldspar pegmatite in tonalite
	M			1323.6±1.6	1324.6±4.8	75.73	A2.1B	
	M			1341.9±1.6	1341.8±3.9	35.68	A2.1C	
PVBR02-28	B	438694	3952002	1305.8±4.2	---		A2.1D	biotite from coarse K-feldspar pegmatatite in tonalite
	B			1287.9±3.0	---		A2.1E	
H03PV002a	M	438920	3952460	1361.8±1.5	1369.3±3.0	14.68	A2.1F	muscovite from coarse K-feldspar-quartz segregation
	M			1335.4±1.5	1359.2±2.5	7.33	A2.1G	
H03PV007e	B	437946	3950330	1261.9±1.8	1258.5±5.1	16.58	A2.1H	biotite from large pink vein cutting tonalite
	B			1246.1±2.0	1246.9±4.8	9.92	A2.1I	
	B			1254.1±1.6	---		A2.1J	
	B			1321.2±2.2	---		A2.1K	
	B			1257.4±2.0	---		A2.1L	
	B			1266.0±1.7	1281.7±10.6	145.25	A2.1M	
PV03-1	B	437946	3950330	1360.8±1.5	---		A2.1N	biotite in moderately metasomatized tonalite
H03PV007b	B	437946	3950330	1215.3±1.8	---		A2.1O	biotite from tonalite near metasomatized fracture

Notes: Fig.-corresponding figure number for age spectrum in appendix; All errors reported at 1σ and do not include error in decay constants or fluence monitor age. M=muscovite; B=biotite.
Plateau age is the inverse variance weighted mean of selected steps; MSWD = mean standard weighted deviate; Fig. = Figure number corresponding to respective age spectra in Figure A2.1.

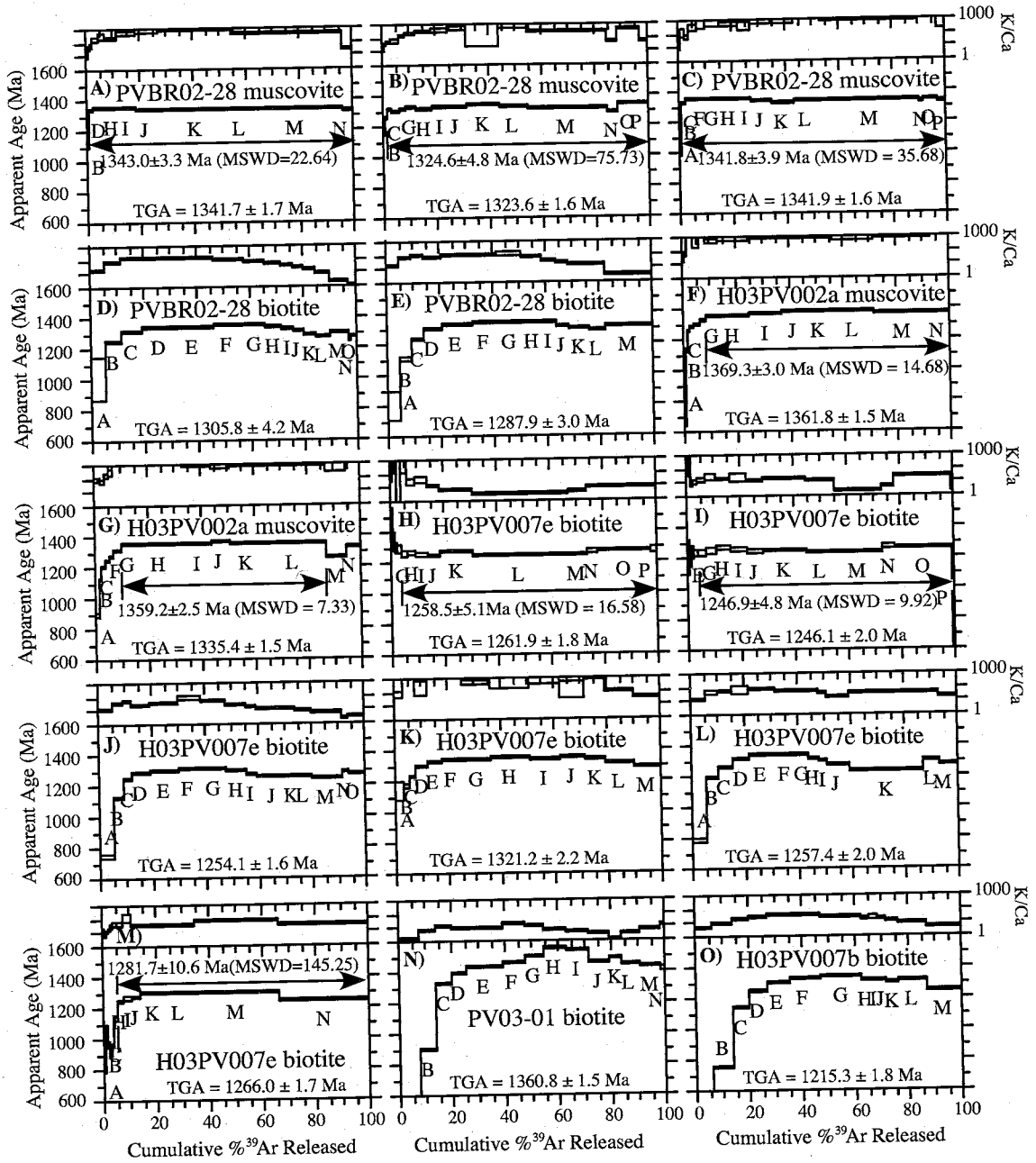

Figure A2.1: $^{40}Ar/^{39}Ar$ age spectra for muscovite and biotite from the Pecos river valley, New Mexico.

of muscovite from H03PV002a yield spectra assigned ages of 1369 and 1359 Ma calculated from 91% and 76% of the total ^{39}Ar released with MSWD values of 14.68 and 7.33 (Figures A2.1f,g). The mean age of 1364 Ma is an appropriate cooling age for the sample based on the reproducibility of the duplicate analyses. Age variability between samples of up to 45 m.y. can be attributed to differences in emplacement age of the pegmatites during ca. 1.4 Ga metamosphism. Alternatively, this can result from differences in muscovite closure temperature between samples and simply reflect regional cooling below 350-400°C around 1365 to 1340 Ma.

Biotite separates give more complex age spectra commonly characterized by hump-shape behavior interpreted as the result of ^{39}Ar recoil into chloritic zones during irradiation (cf. Lo and Onstott, 1989). K/Ca values typically vary between 10 and 100 but get as high as 1000. Two biotite separates from sample PVBR02-28 have slightly hump-shaped spectra and total gas ages of 1306 and 1288 Ma (Figures A2.1d,e). The oldest individual steps in these analyses are 1365 and 1343 Ma and represent the maximum cooling age of the samples. Old apparent ages are similar to the calculated ages for coexisting muscovite and corroborate cooling of this sample below ~350°C at ca. 1340 Ma.

Six analyses of biotite from sample H03PV007e yield complex age spectra (Figures A2.1h-m). Ages calculated for three analyses with ~95% of the total ^{39}Ar released and are 1259, 1247, and 1282 Ma (MSWD=16.58, 9.92, and 145.25). The remaining samples are characterized by hump-shaped behavior and have total gas ages of 1254, 1321, and 1257 Ma. Samples PV03-1 and H03PV007b are from the same outcrop

as H03PV007e and also have hump-shaped age spectra (Figures A2.1o,p). Total gas ages are 1361 and 1215 Ma, respectively.

Collectively, biotite exhibit more complexity in age spectra and more age variability than muscovite, typically due to the hump-shaped nature of many analyses. At the outcrop scale biotite ages vary by more than 100 Ma (Figures A2.1o,p). Differences in closure temperature between samples, coupled with slow cooling and consequently a slow transition through the argon closure temperature window for biotite (350-300°C), would allow individual grains with variable argon retentivities to yield different ages. This would be compatible with protracted, isothermal crustal residence at this temperature range in the Mesoproterozoic (Hodges, et al., 1994; Shaw et al., 2005). Even in this scenario, however, a 100 Ma age difference in biotite from the same outcrop is extreme. Minor alteration of biotite, possibly related to metasomatic fluids, is a likely culprit to explain the spread in biotite ages, and does not preclude long-term crustal residence. Overall, muscovite ages best represent the timing of basement cooling below 400-350°C at ca. 1340-1365 Ma.

TABLE A2.2: $^{40}Ar/^{39}Ar$ ANALYTICAL DATA FOR MUSCOVITE AND BIOTITE IN THE PECOS RIVER VALLEY, NEW MEXICO.

	ID	Power (Watts)	$^{40}Ar/^{39}Ar$	$^{37}Ar/^{39}Ar$	$^{36}Ar/^{39}Ar$ (x 10^{-3})	$^{39}Ar_K$ (x 10^{-15} mol)	K/Ca	$^{40}Ar^*$ (%)	^{39}Ar (%)	Age (Ma)	±1σ (Ma)
	PVBR02-28, Muscovite, J=0.0189971±0.10%, D=1.007±0.001, NM-171, Lab#=54335-01										
X	A	1	63.33	0.2760	113.7	0.57	1.8	47.0	0.2	817.0	13.0
X	B	1	54.08	0.0474	33.20	0.438	10.8	81.9	0.4	1114.0	11.0
X	C	2	52.65	0.0198	13.13	1.10	25.8	92.6	0.8	1196.9	5.5
	D	2	58.44	0.0111	5.360	1.24	46.0	97.3	1.3	1337.1	4.5
	E	2	57.90	0.0086	2.260	2.47	59.3	98.9	2.3	1343.3	3.1
	F	3	58.20	0.0026	1.720	5.1	200.1	99.1	4.3	1350.9	2.4
	G	3	58.04	0.0016	0.7630	7.2	314.9	99.6	7.1	1353.0	2.4
	H	4	58.01	0.0024	0.5390	12.2	216.2	99.7	11.8	1353.5	1.8
	I	4	57.84	0.0009	0.3760	16.4	586.4	99.8	18.3	1351.6	2.2
	J	4	57.29	0.0007	0.2900	22.5	774.2	99.9	27.0	1342.9	2.8
	K	5	57.25	0.0006	0.0790	71.5	893.5	100.0	54.9	1343.2	2.3
	L	6	57.30	0.0012	0.4280	17.6	437.6	99.8	61.8	1342.3	1.7
	M	8	57.23	0.0012	0.1300	88.6	424.5	99.9	96.4	1342.7	2.3
	N	10	56.35	0.0173	0.9870	9.3	29.5	99.5	100.0	1323.6	1.6
	Total gas age ± 1σ			n=14		256.2	202.4			1341.7	1.7
	Plateau ± 1σ steps D-N			n=11	MSWD=22.64	254.1	561.4	±294.0	99.2	1343.0	3.3
	PVBR02-28, Muscovite, J=0.0189971±0.10%, D=1.007±0.001, NM-171, Lab#=54335-02										
X	A	1	52.17	0.1288	63.10	0.77	4.0	64.3	0.3	899.7	8.0
X	B	1	50.74	0.0360	14.86	2.26	14.2	91.4	1.0	1152.7	3.2
X	C	2	54.00	0.0147	6.630	2.30	34.8	96.4	1.8	1254.9	3.8
	D	2	55.93	0.0091	1.910	4.4	56.1	99.0	3.3	1311.9	2.7
	E	2	55.63	0.0078	1.456	7.3	65.8	99.2	5.9	1309.2	1.8
	F	3	56.14	0.0033	0.9020	8.3	153.7	99.5	8.7	1320.6	2.4
	G	3	56.29	0.0024	0.6760	10.2	213.5	99.7	12.2	1324.2	1.8
	H	4	56.11	0.0018	0.4140	19.1	283.4	99.8	18.8	1322.4	1.5
	I	4	56.47	0.0015	0.2650	17.6	337.9	99.9	24.9	1329.2	2.2
	J	4	56.65	0.0010	0.1400	20.5	526.0	99.9	31.9	1333.0	1.8
	K	5	57.02	0.0004	0.1250	34.1	1214.8	99.9	43.7	1339.1	1.8
	L	6	56.50	0.0008	0.2100	32.4	671.3	99.9	54.8	1330.0	2.2
	M	8	55.92	0.0018	0.1680	87.1	288.3	99.9	84.8	1320.4	2.7
	N	10	54.00	0.0073	0.5600	11.8	69.7	99.7	88.8	1286.0	1.8
	O	15	57.58	0.0011	0.1380	23.9	484.5	99.9	97.1	1348.3	1.6
	P	20	56.98	0.0097	0.5100	8.6	52.4	99.7	100.0	1336.6	2.2
	Total gas age ± 1σ			n=16		290.7	178.2			1323.6	1.6
	Plateau ± 1σ steps D-P			n=13	MSWD=75.73	285.378	446.826±328.96		98.2	1324.63	4.782

	ID	Power (Watts)	$^{40}Ar/^{39}Ar$	$^{37}Ar/^{39}Ar$	$^{36}Ar/^{39}Ar$ (x 10^{-3})	$^{39}Ar_K$ (x 10^{-15} mol)	K/Ca	$^{40}Ar^*$ (%)	^{39}Ar (%)	Age (Ma)	±1σ (Ma)
	PVBR02-28, Muscovite, J=0.0189971±0.10%, D=1.007±0.001, NM-171, Lab#=54335-03										
X	A	1	55.15	0.0433	34.70	0.88	11.8	81.4	0.5	1125.9	6.8
	B	1	55.41	0.0062	8.730	1.03	82.3	95.3	1.0	1268.6	4.5
	C	2	57.42	0.0033	3.840	2.85	157.0	98.0	2.5	1327.4	2.7
	D	2	58.29	0.0072	1.380	2.98	70.9	99.3	4.0	1354.1	3.0
	E	2	58.08	0.0014	0.6340	5.0	375.2	99.7	6.6	1354.3	2.3
	F	3	58.00	0.0009	0.7680	6.8	560.7	99.6	10.2	1352.2	3.0
	G	3	57.99	0.0009	0.0790	9.3	600.2	100.0	15.0	1355.4	2.3
	H	4	57.68	0.0009	0.2980	13.7	554.6	99.9	22.1	1349.2	2.4
	I	4	57.71	0.0010	0.2890	9.4	500.2	99.9	27.0	1349.7	2.1
	J	4	56.78	0.0004	0.0960	14.6	1275.5	100.0	34.7	1335.3	2.7
	K	5	56.60	0.0006	0.1250	15.4	797.2	99.9	42.7	1332.1	2.2
	L	6	56.85	0.0002	0.2260	20.4	2125.9	99.9	53.3	1335.7	2.3
	M	8	57.39	0.0003	0.1020	69.9	1569.9	100.0	89.7	1345.3	2.0
	N	10	56.92	0.0007	1.200	3.55	784.9	99.4	91.6	1332.2	2.7
	O	15	57.64	-0.0004	0.3220	10.8	-	99.8	97.2	1348.5	2.0
	P	20	56.37	0.0008	0.2880	5.4	622.2	99.9	100.0	1327.5	2.6
	Total gas age ± 1σ			n=16		192.0	597.1			1341.9	1.6
	Plateau ± 1σ	steps B-P		n=15	MSWD=35.68	191.136	1123.088±562.4		99.5	1341.80	3.892
	PVBR02-28, Biotite, J=0.018992±0.10%, D=1.007±0.001, NM-171, Lab#=54337-22										
	A	1	707.8	0.0226	2264.4	11.1	22.5	5.5	5.4	1005.0	68.0
	B	1	78.31	0.0069	91.16	12.5	73.6	65.6	11.4	1243.0	3.8
	C	2	68.60	0.0035	45.00	17.0	147.9	80.6	19.6	1310.6	3.1
	D	2	61.90	0.0032	17.03	24.9	158.4	91.9	31.6	1336.9	2.2
	E	2	59.04	0.0039	4.991	29.8	132.5	97.5	46.0	1348.6	2.0
	F	3	58.57	0.0043	2.603	24.2	120.0	98.7	57.6	1352.5	2.3
	G	3	58.51	0.0054	2.986	15.6	93.8	98.5	65.1	1349.6	2.4
	H	4	58.20	0.0095	4.558	13.7	53.6	97.7	71.7	1336.7	1.8
	I	4	57.86	0.0112	5.470	9.4	45.6	97.2	76.3	1326.5	2.7
	J	4	57.28	0.0147	6.085	8.0	34.8	96.9	80.1	1313.8	2.3
	K	5	56.02	0.0208	6.200	9.1	24.6	96.7	84.5	1291.7	2.5
	L	6	54.90	0.0434	5.039	11.3	11.8	97.3	89.9	1278.5	2.5
	M	8	55.79	0.2131	4.675	14.2	2.4	97.6	96.7	1295.8	2.1
	N	10	52.86	0.3495	3.660	2.40	1.5	98.0	97.9	1250.8	3.6
	O	15	54.35	0.4042	3.920	4.16	1.3	97.9	99.9	1275.5	3.3
	P	10	57.07	0.3080	-4.9000	0.219	1.7	102.6	100.0	1365.0	18.0
	Total gas age ± 1σ			n=16		207.5	14.3			1305.8	4.2
	PVBR02-28, Biotite, J=0.018992±0.10%, D=1.007±0.001, NM-171, Lab#=54337-01										
	A	1	469.3	0.0249	1490.2	5.0	20.5	6.2	4.7	799.0	45.0
	B	1	72.81	0.0075	98.32	4.6	68.2	60.1	8.9	1104.1	4.9
	C	2	71.38	0.0045	69.21	5.1	114.4	71.3	13.6	1235.1	3.9
	D	2	65.76	0.0054	37.18	7.9	94.0	83.3	20.9	1301.7	3.2
	E	2	62.56	0.0048	20.04	12.0	106.5	90.5	32.0	1333.1	2.4
	F	3	60.08	0.0040	9.520	10.5	126.9	95.3	41.8	1343.6	2.0
	G	3	58.77	0.0041	5.520	9.4	124.4	97.2	50.5	1341.4	2.5
	H	4	58.10	0.0064	3.650	8.7	79.6	98.1	58.5	1339.5	2.0
	I	4	58.09	0.0123	3.930	5.7	41.4	98.0	63.8	1338.1	2.3
	J	4	57.00	0.0187	4.610	4.9	27.3	97.6	68.3	1316.3	2.6
	K	5	56.63	0.0269	5.220	8.1	19.0	97.3	75.8	1307.1	2.3
	L	6	55.44	0.0261	5.780	7.3	19.6	96.9	82.5	1284.0	2.5
	M	8	56.87	0.1109	5.234	18.9	4.6	97.3	100.0	1311.3	1.9
	Total gas age ± 1σ			n=13		108.1	17.9			1287.9	3.0

ID		Power (Watts)	$^{40}Ar/^{39}Ar$	$^{37}Ar/^{39}Ar$	$^{36}Ar/^{39}Ar$ (x 10^{-3})	$^{39}Ar_K$ (x 10^{-15} mol)	K/Ca	$^{40}Ar^*$ (%)	^{39}Ar (%)	Age (Ma)	±1σ (Ma)
H03PV002a, Muscovite, J=0.0189856±0.10%, D=1.007±0.001, NM-171, Lab#=54336-02											
Xi	A	1	37.00	0.0142	48.85	1.08	35.9	61.0	0.6	650.5	7.3
Xi	B	1	49.57	0.0081	14.35	1.87	62.9	91.4	1.6	1133.4	4.0
Xi	C	2	53.41	0.0004	2.660	1.81	1378.9	98.5	2.5	1264.4	3.2
Xi	D	2	54.34	0.0012	2.050	2.34	411.5	98.9	3.8	1283.6	2.4
Xi	E	2	55.65	0.0009	1.327	5.0	560.7	99.3	6.4	1309.7	1.8
Xi	F	3	56.95	-0.0002	0.9800	4.5	-	99.5	8.8	1333.1	2.1
	G	3	58.25	0.0009	0.2840	7.9	548.6	99.9	13.0	1358.2	1.9
	H	4	58.44	0.0007	0.1930	22.3	686.7	99.9	24.9	1361.7	2.0
	I	4	58.84	0.0004	0.1740	22.4	1175.6	99.9	36.8	1368.4	2.1
	J	4	59.41	0.0004	0.2160	17.5	1311.6	99.9	46.2	1377.6	2.7
	K	5	59.50	0.0005	0.1580	19.4	1020.4	99.9	56.5	1379.3	2.2
	L	6	59.46	0.0005	0.2160	28.7	1020.4	99.9	71.8	1378.4	2.2
	M	8	59.18	0.0007	0.1350	40.5	752.5	99.9	93.4	1374.2	2.3
	N	10	58.70	0.0002	0.0890	12.5	3001.2	100.0	100.0	1366.6	1.8
	Total gas age ± 1σ			n=14		187.8	727.5			1361.8	1.5
	Plateau ± 1σ	steps G-N		n=8	MSWD=14.68	171.3	1086.4	±775.4	91.2	1369.3	3.0
H03PV002a, Muscovite, J=0.0189856±0.10%, D=1.007±0.001, NM-171, Lab#=54336-01											
X	A	1	43.78	0.0057	35.85	2.46	90.3	75.8	1.2	891.7	4.7
X	B	1	46.15	0.0045	4.640	2.31	112.9	97.0	2.4	1123.1	3.1
X	C	2	50.16	0.0080	1.650	2.28	63.5	99.0	3.5	1212.6	2.8
X	D	2	52.15	0.0029	1.680	2.94	174.7	99.1	5.0	1247.5	3.0
X	E	2	53.37	0.0015	1.060	4.28	349.5	99.4	7.2	1271.9	3.3
X	F	3	56.11	0.0006	0.6220	6.4	927.6	99.7	10.4	1320.8	2.1
	G	3	58.08	0.0004	0.3790	10.4	1244.4	99.8	15.6	1354.8	2.1
	H	4	58.42	0.0003	0.0540	34.8	1882.7	100.0	33.0	1362.1	2.0
	I	4	58.39	0.0004	0.1850	21.5	1178.3	99.9	43.8	1361.0	2.7
	J	4	58.75	0.0006	0.2590	14.5	836.4	99.9	51.1	1366.5	1.9
	K	5	58.29	0.0004	0.2940	23.6	1342.6	99.9	63.0	1358.7	1.8
	L	6	57.77	0.0006	0.1140	47.0	809.8	99.9	86.6	1351.1	2.1
X	M	8	52.79	0.0005	0.4190	15.4	1133.8	99.8	94.3	1265.3	2.5
X	N	10	56.59	0.0006	0.4860	11.4	809.8	99.8	100.0	1329.5	2.6
	Total gas age ± 1σ			n=14		199.3	699.1			1335.4	1.5
	Plateau ± 1σ	steps G-L		n=6	MSWD=7.33	151.842	1223.092±392.8		76.2	1359.20	2.462
H03PV007e, Biotite, J=0.0192076±0.10%, D=1.007±0.001, NM-171, Lab#=54332-25											
X	A	1	63.10	-0.2800	-69.0000	0.021	-	132.2	0.2	1750.0	120.0
X	B	1	55.00	-0.1280	-28.1000	0.043	-	115.1	0.5	1453.0	56.0
X	C	2	54.60	-0.0230	-18.5000	0.063	-	110.0	0.9	1401.0	39.0
X	D	2	54.70	-0.0610	-5.1000	0.084	-	102.8	1.5	1337.0	30.0
X	E	2	52.69	0.0110	-5.3000	0.149	46.4	103.0	2.6	1304.0	18.0
X	F	3	53.13	-0.0180	-2.0000	0.213	-	101.1	4.1	1294.0	13.0
	G	3	51.12	-0.0051	-2.5000	0.290	-	101.5	6.2	1262.0	11.0
	H	4	52.00	0.0149	0.1500	0.464	34.2	99.9	9.6	1263.4	6.6
	I	4	51.60	0.0122	-0.3000	0.56	41.8	100.2	13.7	1258.9	6.8
	J	4	51.45	0.0362	2.050	0.68	14.1	98.8	18.5	1243.9	4.9
	K	5	52.89	0.0797	1.630	1.68	6.4	99.1	30.7	1271.6	2.8
	L	6	51.44	0.1510	2.020	5.0	3.4	98.9	67.0	1244.2	2.1
	M	8	51.31	0.0970	1.800	0.97	5.3	99.0	74.0	1242.8	4.3
	N	10	52.52	0.0500	1.910	0.51	10.2	98.9	77.7	1263.5	5.2
	O	15	53.40	0.0597	1.780	2.76	8.5	99.0	97.7	1279.6	2.9
	P	25	54.50	0.0622	5.600	0.319	8.2	97.0	100.0	1279.0	10.0
	Total gas age ± 1σ			n=16		13.8	5.8			1261.9	1.8
	Plateau ± 1σ	steps G-P		n=10	MSWD=16.58	13.238	8.729±13.009		95.9	1258.53	5.059

	ID	Power (Watts)	$^{40}Ar/^{39}Ar$	$^{37}Ar/^{39}Ar$	$^{36}Ar/^{39}Ar$ (x 10^{-3})	$^{39}Ar_K$ (x 10^{-15} mol)	K/Ca	$^{40}Ar^*$ (%)	^{39}Ar (%)	Age (Ma)	±1σ (Ma)
	H03PV007e, Biotite, J=0.0192076±0.10%, D=1.007±0.001, NM-171, Lab#=54332-26										
X	A	1	45.30	0.1330	7.000	0.024	3.8	95.2	0.3	1101.0	73.0
X	B	1	52.10	0.0430	11.70	0.029	11.9	93.3	0.6	1204.0	55.0
X	C	2	50.70	0.0060	6.200	0.053	85.0	96.4	1.2	1209.0	34.0
X	D	2	51.87	0.0580	4.500	0.084	8.8	97.4	2.2	1238.0	22.0
X	E	2	51.47	0.0473	4.200	0.173	10.8	97.6	4.2	1233.0	11.0
	F	3	51.29	0.0344	3.800	0.232	14.8	97.8	6.9	1232.0	12.0
	G	3	51.79	0.0158	2.770	0.321	32.3	98.4	10.6	1246.1	9.2
	H	4	52.48	0.0250	2.070	0.48	20.4	98.8	16.2	1262.0	6.0
	I	4	51.56	0.0197	1.180	0.52	25.9	99.3	22.2	1250.3	6.3
	J	4	51.22	0.0314	2.310	0.57	16.2	98.7	28.8	1238.5	5.8
	K	5	51.55	0.0244	1.760	1.38	20.9	99.0	44.7	1247.2	3.8
	L	6	50.82	0.0307	2.360	0.94	16.6	98.6	55.6	1231.0	3.9
	M	8	50.92	0.1981	2.430	1.50	2.6	98.6	73.0	1232.8	3.2
	N	10	52.34	0.1019	1.930	0.426	5.0	98.9	77.9	1260.4	6.5
	O	15	52.51	0.0186	1.240	1.86	27.4	99.3	99.5	1266.8	3.2
X	P	25	52.30	0.1360	27.10	0.046	3.8	84.7	100.0	1123.0	41.0
	Total gas age ± 1σ			n=16		8.6	8.6			1246.1	2.0
	Plateau ± 1σ	steps F-O		n=10	MSWD=9.92	8.223	17.962±9.375		95.3	1246.91	4.752
	H03PV007e, Biotite, J=0.0192076±0.10%, D=1.007±0.001, NM-171, Lab#=54332-02										
	A	1	75.05	0.0365	164.5	4.5	14.0	35.2	5.2	749.3	7.5
	B	1	48.00	0.0147	11.18	3.74	34.8	93.1	9.4	1131.3	3.0
	C	2	52.97	0.0100	5.870	2.74	50.9	96.7	12.5	1250.7	3.1
	D	2	54.14	0.0182	2.720	6.1	28.0	98.5	19.5	1287.6	2.1
	E	2	54.67	0.0139	0.8710	9.2	36.8	99.5	29.9	1306.2	2.4
	F	3	55.23	0.0055	0.6940	7.8	92.8	99.6	38.7	1316.6	2.2
	G	3	55.53	0.0092	0.7460	7.8	55.6	99.6	47.6	1321.5	2.2
	H	4	54.64	0.0147	0.9290	6.7	34.8	99.5	55.1	1305.3	2.0
	I	4	52.70	0.0244	1.470	3.54	20.9	99.2	59.1	1268.9	2.9
	J	4	52.58	0.0374	1.248	10.8	13.7	99.3	71.4	1268.0	2.0
	K	5	52.22	0.0358	1.320	2.15	14.3	99.3	73.8	1261.2	2.9
	L	6	52.30	0.0417	0.9900	5.1	12.2	99.5	79.6	1264.5	2.4
	M	8	53.18	0.0776	7.324	10.7	6.6	95.9	91.8	1247.0	2.2
	N	10	53.68	0.1839	1.760	1.79	2.8	99.1	93.8	1284.7	2.8
	O	15	53.09	0.1217	0.9700	5.3	4.2	99.5	99.9	1278.5	2.9
	P	20	54.78	0.8010	-2.5000	0.124	0.64	101.5	100.0	1327.0	21.0
	Total gas age ± 1σ			n=16		88.1	13.3			1254.1	1.6
	H03PV007e, Biotite, J=0.0192076±0.10%, D=1.007±0.001, NM-171, Lab#=54332-03										
	A	1	399.0	0.0056	1197.6	3.79	91.1	11.3	3.4	1139.0	33.0
	B	1	57.00	0.0011	33.64	2.06	463.8	82.6	5.3	1175.3	4.9
	C	2	56.00	0.0007	19.85	3.11	773.0	89.5	8.1	1231.1	3.0
	D	2	57.63	0.0012	12.35	4.7	425.2	93.7	12.3	1298.7	2.5
	E	2	57.45	0.0004	5.980	6.2	1186.5	96.9	17.9	1327.7	2.3
	F	3	57.30	0.0002	3.550	8.2	3401.4	98.2	25.2	1337.4	2.2
	G	3	57.08	0.0009	1.804	12.0	593.3	99.1	36.0	1342.3	2.5
	H	4	57.44	0.0009	1.161	16.3	579.8	99.4	50.6	1351.6	1.8
	I	4	57.18	0.0006	0.8280	13.1	822.9	99.6	62.4	1348.9	2.2
	J	4	57.49	0.0018	0.9970	10.6	278.8	99.5	71.9	1353.2	1.8
	K	5	56.68	0.0015	0.8190	8.4	347.1	99.6	79.4	1340.5	2.6
	L	6	55.28	0.0044	1.724	11.8	115.7	99.1	90.0	1312.2	2.4
	M	8	53.90	0.0134	1.819	11.1	38.1	99.0	100.0	1288.0	1.9
	Total gas age ± 1σ			n=13		111.4	189.2			1321.2	2.2

ID	Power (Watts)	$^{40}Ar/^{39}Ar$	$^{37}Ar/^{39}Ar$	$^{36}Ar/^{39}Ar$ (x 10^{-3})	$^{39}Ar_K$ (x 10^{-15} mol)	K/Ca	$^{40}Ar^*$ (%)	^{39}Ar (%)	Age (Ma)	±1σ (Ma)
H03PV007e, Biotite, J=0.0192076±0.10%, D=1.007±0.001, NM-171, Lab#=54332-04										
A	1	90.66	0.0284	212.2	9.4	18.0	30.8	5.5	784.4	8.2
B	1	51.87	0.0093	11.87	8.2	54.9	93.2	10.2	1199.1	2.3
C	2	53.67	0.0076	5.050	8.8	67.4	97.2	15.3	1267.4	2.1
D	2	55.74	0.0063	1.912	10.8	81.0	99.0	21.6	1319.1	2.0
E	2	56.49	0.0064	0.7300	17.1	79.5	99.6	31.6	1337.7	2.3
F	3	56.82	0.0085	0.7800	12.7	60.0	99.6	39.0	1343.0	2.3
G	3	56.99	0.0080	0.9290	8.1	63.9	99.5	43.7	1345.2	2.1
H	4	55.32	0.0101	1.039	7.6	50.6	99.5	48.1	1316.4	2.1
I	4	54.84	0.0120	1.840	5.1	42.6	99.0	51.0	1304.2	2.5
J	4	53.09	0.0219	1.761	13.9	23.3	99.0	59.1	1274.3	2.4
K	5	68.29	0.0117	61.37	48.5	43.8	73.4	87.3	1231.5	3.4
L	6	54.76	0.0125	1.652	10.3	40.9	99.1	93.3	1303.6	2.0
M	8	53.22	0.0252	1.959	11.6	20.2	98.9	100.0	1275.6	1.7
Total gas age ± 1σ			n=13		171.9	40.1			1257.4	2.0
H03PV007e, Biotite, J=0.0192076±0.10%, D=1.007±0.001, NM-171, Lab#=54332-05										
X A	1	406.0	0.0331	1264.6	0.44	15.4	8.0	0.7	881.0	47.0
X B	1	66.91	0.0362	97.80	0.194	14.1	56.8	1.0	1000.0	21.0
X C	2	54.10	0.0540	44.70	0.245	9.4	75.6	1.4	1058.0	15.0
X D	2	47.64	0.0384	37.70	0.371	13.3	76.6	2.0	969.4	8.6
X E	2	42.54	0.0253	31.10	0.55	20.2	78.4	2.9	903.3	8.1
X F	3	44.01	0.0164	26.18	0.76	31.1	82.4	4.1	965.0	5.5
X G	3	50.14	0.0120	17.96	0.78	42.5	89.4	5.3	1133.8	6.2
H	4	53.50	0.0106	8.300	1.62	48.1	95.4	7.9	1247.4	3.7
I	4	54.18	0.0031	6.740	1.61	165.7	96.3	10.5	1267.5	3.8
J	4	54.12	0.0121	4.390	2.21	42.3	97.6	14.1	1278.7	3.3
K	5	54.44	0.0106	1.660	5.4	48.0	99.1	22.7	1298.1	2.2
L	6	54.67	0.0112	0.8010	7.5	45.7	99.6	34.8	1306.4	1.8
M	8	54.49	0.0066	0.5310	19.5	77.1	99.7	65.9	1304.8	2.2
N	15	51.32	0.0115	1.003	21.3	44.5	99.4	100.0	1247.0	1.7
Total gas age ± 1σ			n=14		62.5	49.2			1266.0	1.7
Plateau ± 1σ	steps H-N		n=7	MSWD=145.25	59.179	58.996±44.944		94.7	1281.71	10.601
PV03-01, Biotite, 0.21 mg, J=0.0162972±0.09%, D=1.00484±0.00092, NM-164, Lab#=54026-01										
A	1	7.053	0.2932	2.060	2.47	1.7	91.8	7.4	182.5	1.4
B	1	40.48	0.0702	3.350	2.12	7.3	97.6	13.7	907.0	2.3
C	2	66.44	0.0375	2.120	2.01	13.6	99.1	19.8	1330.6	2.9
D	2	70.66	0.0451	0.9600	1.81	11.3	99.6	25.2	1395.0	3.6
E	2	73.28	0.0392	1.283	4.7	13.0	99.5	39.4	1429.6	2.4
F	3	75.28	0.0220	0.9600	2.81	23.1	99.6	47.8	1457.9	2.9
G	3	78.79	0.0383	0.7200	2.28	13.3	99.7	54.6	1505.3	3.2
H	4	83.02	0.0647	0.8300	2.71	7.9	99.7	62.8	1559.3	3.5
I	4	81.49	0.0873	0.6200	2.93	5.8	99.8	71.5	1540.7	2.4
J	4	75.63	0.1316	0.4900	2.66	3.9	99.8	79.5	1464.6	3.4
K	5	77.20	0.3614	0.3200	1.54	1.4	99.9	84.1	1486.6	4.5
L	6	74.20	0.1309	0.4500	2.23	3.9	99.8	90.8	1445.6	3.0
M	8	73.62	0.0642	0.0200	2.66	7.9	100.0	98.8	1439.4	3.4
N	10	71.63	0.0419	-0.1300	0.413	12.2	100.1	100.0	1412.8	5.2
Total gas age ± 1σ			n=14		33.4	5.4	K2O=3.75%		1360.8	1.5

ID	Power (Watts)	$^{40}Ar/^{39}Ar$	$^{37}Ar/^{39}Ar$	$^{36}Ar/^{39}Ar$ ($\times 10^{-3}$)	$^{39}Ar_K$ ($\times 10^{-15}$ mol)	K/Ca	$^{40}Ar^*$ (%)	^{39}Ar (%)	Age (Ma)	±1σ (Ma)
H03PV007b, Biotite, J=0.019035±0.10%, D=1.0063±0.001, NM-171, Lab#=54334-01										
A	1	111.9	0.0831	333.7	6.7	6.1	11.9	5.9	413.0	15.0
B	1	32.76	0.0413	20.21	8.6	12.4	81.8	13.5	751.8	2.5
C	2	48.32	0.0239	9.910	6.9	21.4	93.9	19.7	1136.7	2.9
D	2	53.06	0.0179	5.210	7.7	28.6	97.1	26.5	1247.6	2.5
E	2	55.63	0.0132	1.980	9.9	38.7	99.0	35.3	1308.5	2.1
F	3	56.98	0.0137	1.358	13.1	37.3	99.3	46.9	1334.4	2.0
G	3	57.26	0.0170	1.787	17.3	30.0	99.1	62.3	1336.9	1.7
H	4	56.21	0.0209	3.400	3.15	24.4	98.2	65.1	1311.2	3.7
I	4	56.48	0.0235	2.980	3.40	21.7	98.5	68.1	1318.0	2.5
J	4	56.26	0.0270	3.470	3.54	18.9	98.2	71.2	1311.8	2.7
K	5	55.84	0.0340	3.510	5.6	15.0	98.2	76.3	1304.5	2.0
L	6	56.67	0.0423	3.452	11.9	12.1	98.2	86.8	1318.8	2.2
M	8	53.04	0.0944	3.813	14.8	5.4	97.9	100.0	1254.7	1.8
Total gas age ± 1σ			n=13		112.5	13.8			1215.3	1.8

Notes:
Isotopic ratios corrected for blank, radioactive decay, and mass discrimination, not corrected for interfering reactions.
Errors quoted for individual analyses include analytical error only, without interfering reaction or J uncertainties.
Total gas age calculated by summing isotopic measurements of all steps.
Total gas age error calculated by quadratically combining errors of isotopic measurements of all steps.
Plateau age is inverse-variance-weighted mean of selected steps.
Plateau age error is inverse-variance-weighted mean error (Taylor, 1982) times root MSWD where MSWD>1.
Plateau error is weighted error of Taylor (1982).
Decay constants and isotopic abundances after Steiger and Jäger (1977).
symbol preceding sample ID denotes analyses excluded from plateau age calculations.
Ages calculated relative to FC-2 Fish Canyon Tuff sanidine interlaboratory standard at 28.27 Ma
Decay Constant (LambdaK (total)) = 5.476e-10/a
Correction factors:
NM-171: $(^{39}Ar/^{37}Ar)_{Ca}$ = 0.00074 ± 2e-05, $(^{36}Ar/^{37}Ar)_{Ca}$ = 0.000284 ± 6e-06, $(^{38}Ar/^{39}Ar)_K$ = 0.0122, $(^{40}Ar/^{39}Ar)_K$ = 0.0295 ± 0.000
NM-164: $(^{39}Ar/^{37}Ar)_{Ca}$ = 0.0007 ± 5e-05, $(^{36}Ar/^{37}Ar)_{Ca}$ = 0.00027 ± 1e-05, $(^{38}Ar/^{39}Ar)_K$ = 0.0177, $(^{40}Ar/^{39}Ar)_K$ = 0.02559 ± 0.0014

TABLE A2.3: IRRADIATION DATA, CORRECTION FACTORS, AND ANALYTICAL PARAMETERS FOR FURNACE AND LASER EXTRACTION LINES AND MASS SPECTROMETER.

Irradiation ID	Irradiation time (hrs)	Sensitivity (mol/pA)		Discrimination[1]	Correction factors			
		Furnace	CO_2 Laser		$(^{39}Ar/^{37}Ar)_{Ca}$	$(^{36}Ar/^{37}Ar)_{Ca}$	$(^{38}Ar/^{39}Ar)_{K}$	$(^{40}Ar/^{39}Ar)_{K}$
NM-84	50.000	9.9021E-17	5.35E-17	1.00258±0.00114	0.000650±0.000050	0.000260±0.000020	0.01190	0.02615±0.00006
NM-102	15.250	1.1706e-16 to 1.5736e-16	6.3059e-17 to 8.477e-17	1.00461±0.00118	0.000770±0.000200	0.000280±0.000005	0.01190	0.02620±0.00010
NM-145	52.820	1.6800e-16 to 1.7300e-16	9.0500e-17 to 9.3700e-17	1.00535±0.00031	0.000700±0.000020	0.000270±0.000005	0.01077	0.03100±0.001000
NM-157	57.120	2.3594e-16 to 2.8582e-16	1.2859e-16 to 1.6403e-16	1.00520±0.00172	0.000700±0.000020	0.000270±0.000005	0.01077	0.03160±0.00020
NM-158	41.717	2.4700e-16 to 2.5000e-16	1.3500e-16 to 1.3600e-16	1.00520±0.00172	0.000750±0.000030	0.000292±0.000006	0.01077	0.02960±0.000500
NM-164	99.950	2.60E-16	1.49E-16	1.00484±0.00092	0.000700±0.000050	0.000270±0.000010	0.01077	0.02559±0.000500
NM-171	77.150	2.6371e-16 to 2.8628e-16	1.5135e-16 to 1.6430e-16	1.00700±0.00100	0.000700±0.000020	0.000284±0.000005	0.01220	0.02950±0.00020
NM194	15.000	9.21E-17	5.28E-17	1.00200±0.00100	0.000676±0.000005	0.000276±0.000002	0.01320	0.01000±0.002000
NM-201	45.000	1.2812e-16 to 1.3248e-16	7.3500e-17 to 7.3600e-17	1.00200±0.00100	0.000700±0.000050	0.000280±0.000020	0.01300	0.01000±0.002000
NM-206	60.000	8.84E-17	4.52E-17	1.00363±0.00071	0.000700±0.000050	0.000280±0.000020	0.01300	0.01000±0.002000

	System blank									
	Furnace					CO_2 Laser				
	^{40}Ar	^{39}Ar	^{38}Ar	^{37}Ar	^{36}Ar	^{40}Ar	^{39}Ar	^{38}Ar	^{37}Ar	^{36}Ar
NM-84	1.3653E-15	<0.1e-17	<0.1e-17	<0.1e-17	8.9118E-19	---	---	---	---	---
NM-102	3.9650E-17	3.3947E-18	8.1942E-19	3.5118E-19	2.2241E-18	---	---	---	---	---
NM-145	3.0059E-16	3.0312E-18	<0.1e-17	5.0520E-18	<0.1e-17	---	---	---	---	---
NM-157	8.2448E-16	2.9622E-18	9.8740E-19	1.4811E-18	3.2091E-18	---	---	---	---	---
NM-158	4.8644E-16	4.0749E-18	<0.1e-17	1.2734E-18	<0.1e-17	---	---	---	---	---
NM-164	1.3869E-15	3.6429E-18	7.8063E-19	4.6838E-18	4.9440E-18	1.6831E-16	1.9414E-18	1.4934E-19	1.7921E-18	2.9868E-19
NM-171	2.1106E-15	2.8152E-18	<0.1e-17	8.4456E-19	5.3489E-18	3.8974E-16	6.8535E-18	6.0920E-19	2.7414E-18	1.6753E-18
NM194						---	---	---	---	---
NM-201	2.5624E-14	1.2812E-17	5.1248E-18	1.1531E-17	1.9218E-17	---	---	---	---	---
NM-206	1.7677E-15	1.5025E-18	2.6516E-17	8.8385E-18	6.1870E-18	---	---	---	---	---

[1] 1 AMU in favor of light isotopes.

TABLE A2.4: $^{40}Ar/^{39}Ar$ analytical data for multiple-grain K-feldspar separates.

ID	Temp (°C)	$^{40}Ar/^{39}Ar$	$^{37}Ar/^{39}Ar$	$^{36}Ar/^{39}Ar$ (x 10^{-3})	$^{39}Ar_K$ (x 10^{-15} mol)	K/Ca	$^{40}Ar^*$ (%)	^{39}Ar (%)	Age (Ma)	±1σ (Ma)	Time (min)
PVIG02-1, K-feldspar, 2.30 mg, J=0.0195263±0.10%, D=1.00644±0.00091, NM-157, Lab#=53531-01											
AA	450	329.7	-1.9000	170.2	0.90	-	84.7	0.1	3403.0	10.0	13.2
B	450	42.38	14.10	84.10	0.776	0.036	44.0	0.1	571.0	12.0	23.2
C	450	28.09	-0.4000	57.10	0.689	-	39.7	0.1	360.0	15.0	31.7
D	450	20.43	4.900	37.30	0.92	0.10	47.8	0.2	320.0	16.0	48.3
E	500	52.39	10.00	18.57	1.23	0.051	91.1	0.3	1207.8	7.9	13.0
F	500	9.306	0.0600	7.630	2.17	8.5	75.7	0.4	234.7	4.7	23.2
G	500	8.489	1.090	8.790	2.30	0.47	70.3	0.5	200.8	4.0	31.5
H	500	8.394	0.5400	6.870	3.13	0.94	76.3	0.7	214.4	3.8	48.2
I	550	20.16	1.710	5.540	2.07	0.30	92.6	0.8	567.2	4.0	12.8
J	550	8.766	-0.4800	2.370	3.97	-	91.6	1.1	264.9	2.2	23.0
K	550	9.403	1.310	2.170	4.98	0.39	94.3	1.4	290.9	1.9	31.3
L	550	10.30	2.330	2.820	5.49	0.22	93.7	1.7	314.9	1.6	48.0
M	600	20.36	2.370	4.410	4.43	0.22	94.5	2.0	582.6	2.5	12.6
N	600	12.78	0.2900	1.283	6.73	1.8	97.2	2.4	395.9	1.6	22.8
O	600	14.56	1.930	1.285	7.14	0.26	98.5	2.8	450.4	2.1	31.1
P	600	16.09	-0.2900	1.665	7.96	-	96.8	3.3	484.0	1.5	47.8
Q	650	23.04	-0.2900	1.920	6.31	-	97.4	3.6	663.0	2.0	13.2
R	650	19.41	0.5500	0.8200	10.1	0.93	99.0	4.3	581.0	2.4	23.3
S	650	20.95	-0.2600	0.8240	9.7	-	98.7	4.8	618.5	1.9	31.6
T	700	24.82	0.0300	0.9290	9.5	17.0	98.9	5.4	714.3	1.5	13.1
U	700	26.16	0.7700	0.7670	13.7	0.66	99.4	6.2	749.2	1.4	23.2
V	700	26.28	0.8100	0.8690	10.9	0.63	99.3	6.9	751.5	1.9	31.4
W	750	33.25	0.0000	1.570	14.2	-	98.6	7.8	902.8	1.2	13.3
X	750	28.39	0.1200	0.4120	13.3	4.3	99.6	8.6	802.1	1.3	23.5
Y	750	28.49	0.3700	0.8680	10.9	1.4	99.2	9.2	801.9	1.5	31.8
Z	800	29.95	0.1000	0.6360	10.3	5.1	99.4	9.9	836.2	1.5	13.3
ZA	800	29.15	-0.0700	0.5720	12.8	-	99.4	10.7	818.1	1.5	23.3
ZB	850	30.13	-0.0200	0.7220	14.3	-	99.3	11.6	839.3	1.7	13.5
ZC	850	29.22	0.2700	0.7540	13.7	1.9	99.3	12.4	819.3	1.8	23.6
ZD	900	29.52	0.4300	0.7840	15.2	1.2	99.3	13.4	826.2	1.6	13.4
ZE	900	29.42	0.3700	0.7920	15.8	1.4	99.3	14.4	823.8	1.4	23.5
ZF	950	29.73	0.7000	0.8200	16.5	0.73	99.4	15.4	831.4	1.4	13.6
ZG	950	29.75	-0.7200	0.5640	17.5	-	99.2	16.5	830.2	1.5	23.7
ZH	1000	29.88	0.2400	1.053	16.4	2.1	99.0	17.5	832.1	1.1	13.5
ZI	1000	29.91	0.6700	0.8960	19.5	0.76	99.3	18.8	834.7	1.3	23.5
ZJ	1050	30.34	0.3800	0.8460	22.3	1.3	99.3	20.2	844.2	1.6	13.6
ZK	1050	30.10	0.3220	1.014	27.1	1.6	99.1	22.0	837.5	1.1	23.6
ZL	1120	31.13	0.2080	0.9870	52.4	2.5	99.1	25.4	860.5	1.4	13.4
ZM	1120	31.47	0.2720	1.267	54.6	1.9	98.9	29.0	866.3	1.3	23.5
ZN	1120	23.25	126.0	-26.7000	0.071	0.004	177.0	29.0	1155.0	77.0	118.5
ZP	1120	34.02	0.2210	2.878	83.6	2.3	97.6	34.7	911.8	1.5	239.1
ZQ	1200	34.89	0.1700	1.261	20.8	3.0	99.0	36.1	940.5	1.5	8.0
ZR	1300	32.00	0.0710	0.9408	543.1	7.2	99.2	76.6	879.7	1.8	8.7
ZS	1400	31.39	0.1830	1.219	183.2	2.8	98.9	91.8	864.6	1.7	8.7
ZT	1690	31.99	1.850	2.014	94.4	0.28	98.6	100.0	876.6	1.7	8.2
Total gas age ± 1σ			n=45		1386.9	1.6		K2O=11.86%	840.3	1.2	

ID	Temp (°C)	$^{40}Ar/^{39}Ar$	$^{37}Ar/^{39}Ar$	$^{36}Ar/^{39}Ar$ (x 10^{-3})	$^{39}Ar_K$ (x 10^{-15} mol)	K/Ca	$^{40}Ar^*$ (%)	^{39}Ar (%)	Age (Ma)	±1σ (Ma)	Time (min)
PVBR01-3, K-feldspar, 2.95 mg, J=0.0094468±0.01%, D=1.00535±0.00031, NM-144, Lab#=52786-01											
A	450	1090.7	0.0260	150.4	2.103	19.6	95.9	1.0	4359.6	5.2	10.9
B	450	79.10	0.0118	20.80	1.236	43.2	92.2	1.5	957.0	11.0	21.5
BA	450	57.66	0.0112	18.20	0.380	45.6	90.7	1.7	733.0	5.8	18.7
C	450	49.99	0.0154	12.40	0.870	33.1	92.7	2.1	662.9	3.2	29.7
D	500	151.4	0.0143	10.52	1.242	35.8	98.0	2.7	1599.6	3.5	10.9
E	500	46.51	0.0130	6.100	2.107	39.2	96.1	3.6	643.4	1.9	21.4
F	500	47.03	0.0137	5.100	2.123	37.2	96.8	4.5	653.3	1.9	29.3
G	550	91.41	0.0149	4.160	3.428	34.3	98.7	6.0	1125.3	1.2	12.7
H	550	53.10	0.0124	2.590	4.66	41.2	98.6	7.9	733.6	1.5	22.7
I	550	53.82	0.0076	2.340	4.64	67.3	98.7	9.8	742.4	1.5	30.6
J	600	73.43	0.0087	2.393	6.09	58.7	99.0	12.2	954.7	1.4	12.2
K	600	58.13	0.0077	1.338	9.01	66.5	99.3	15.5	794.60	0.92	22.4
L	600	59.94	0.0070	1.233	9.11	73.3	99.4	18.7	815.1	1.3	30.7
M	650	67.93	0.0084	0.9840	10.35	60.9	99.6	22.1	901.95	0.93	12.1
N	650	63.72	0.0070	0.7190	15.23	73.4	99.7	26.8	857.9	1.0	22.2
O	650	65.76	0.0068	0.6030	14.90	75.0	99.7	30.9	880.10	0.85	30.6
P	700	68.49	0.0086	0.7980	15.21	59.4	99.7	34.8	908.36	0.84	11.9
Q	700	67.53	0.0077	0.4800	20.63	65.8	99.8	39.7	899.3	1.2	21.8
R	700	68.05	0.0073	0.4270	19.72	69.5	99.8	43.9	904.9	1.1	30.0
S	750	70.41	0.0091	0.5000	16.92	55.8	99.8	47.1	929.4	1.2	11.2
T	750	69.28	0.0086	0.3570	23.22	59.2	99.9	51.3	918.0	1.0	21.3
U	750	69.63	0.0086	0.4030	21.39	59.4	99.8	54.7	921.5	1.2	29.7
V	800	70.38	0.0100	0.4690	15.57	50.8	99.8	57.0	929.2	1.2	11.0
W	800	70.34	0.0093	0.3970	20.58	54.8	99.8	59.9	928.97	0.91	20.9
X	850	70.99	0.0108	0.3640	21.92	47.2	99.9	62.6	935.8	1.1	12.5
Y	850	71.05	0.0097	0.4330	24.10	52.4	99.8	65.5	936.1	1.1	22.6
Z	900	71.70	0.0116	0.4570	21.06	44.0	99.8	67.7	942.83	0.97	12.3
ZA	900	71.83	0.0102	0.4850	24.44	49.9	99.8	70.2	944.07	0.81	22.4
ZB	950	72.20	0.0107	0.5890	19.32	47.5	99.8	72.0	947.6	1.3	12.2
ZC	950	72.13	0.0092	0.7120	19.84	55.2	99.7	73.7	946.49	0.96	22.2
ZD	1000	73.80	0.0113	0.8570	16.93	45.4	99.7	75.1	963.1	1.1	12.0
ZE	1000	73.42	0.0100	0.7100	18.86	50.8	99.7	76.6	959.64	0.98	22.0
ZF	1050	75.54	0.0157	1.101	19.45	32.5	99.6	78.0	980.0	1.2	11.7
ZG	1050	75.52	0.0151	1.012	22.76	33.9	99.6	79.6	980.1	1.1	21.8
ZH	1100	77.91	0.0219	1.445	20.70	23.3	99.5	80.9	1002.72	0.99	11.5
ZI	1100	77.60	0.0182	1.250	25.22	28.1	99.5	82.5	1000.19	0.83	21.4
ZJ	1100	80.18	0.0131	0.8730	97.6	38.9	99.7	87.7	1026.9	1.8	152.5
ZK	1100	82.28	0.0085	0.9540	48.1	59.8	99.7	89.8	1047.2	1.3	131.1
ZL	1100	83.71	0.0080	1.214	60.4	63.5	99.6	92.2	1060.3	1.5	238.7
ZM	1200	83.57	0.0053	0.8010	47.6	95.9	99.7	93.9	1060.1	1.2	7.7
ZN	1300	84.10	0.0048	0.9330	133.8	106.9	99.7	97.9	1064.8	2.1	7.3
ZO	1400	87.41	0.0114	1.201	25.94	44.6	99.6	98.5	1095.7	1.1	6.4
ZP	1660	87.34	0.0029	1.118	12.77	178.3	99.6	98.9	1095.2	1.2	22.1
ZQ	1660	85.77	0.0125	1.179	47.8	40.7	99.6	100.0	1080.2	1.2	41.5
Total gas age ± 1σ			n=44		969.4	52.6		K2O=13.36%	1003.70	0.45	

ID	Temp (°C)	$^{40}Ar/^{39}Ar$	$^{37}Ar/^{39}Ar$	$^{36}Ar/^{39}Ar$ (x 10^{-3})	$^{39}Ar_K$ (x 10^{-15} mol)	K/Ca	$^{40}Ar^*$ (%)	^{39}Ar (%)	Age (Ma)	±1σ (Ma)	Time (min)
WB-6, 3.48 mg, J=0.0081246±0.09%, D=1.00258±0.00114, NM-84, Lab#=8847-01											
A	500	419.5	0.0140	77.08	3.56	36.6	94.6	1.4	2630.8	3.6	13.4
B	500	52.41	0.0079	6.860	2.78	64.5	96.1	2.5	626.4	1.5	21.3
C	550	62.99	0.0074	3.230	3.76	68.8	98.5	3.9	745.0	1.5	14.0
D	550	53.27	0.0072	2.623	5.27	70.8	98.6	5.8	648.4	1.3	21.8
E	600	64.47	0.0072	1.738	10.01	71.2	99.2	9.4	764.0	1.7	14.8
F	600	62.97	0.0057	1.207	9.74	89.0	99.4	12.7	750.7	1.1	21.8
G	650	69.50	0.0067	1.085	16.05	75.7	99.5	17.9	814.27	0.92	14.9
H	650	70.40	0.0061	1.013	15.26	84.1	99.6	22.5	823.0	1.4	21.9
I	700	74.49	0.0067	0.7250	23.22	75.7	99.7	29.0	862.0	1.6	14.8
J	700	74.87	0.0059	0.6470	19.07	86.3	99.8	33.9	865.8	1.5	21.8
K	750	76.17	0.0072	0.4840	21.71	70.5	99.8	39.0	878.1	1.5	12.8
L	800	77.47	0.0090	0.5770	32.7	56.8	99.8	46.1	889.8	1.7	12.7
M	850	78.41	0.0113	0.4510	36.3	45.2	99.8	53.0	898.6	1.7	12.7
N	900	79.74	0.0121	0.5100	32.7	42.1	99.8	58.6	910.5	1.6	12.8
O	950	80.15	0.0118	0.4850	28.4	43.3	99.8	63.0	914.3	1.9	11.2
P	1000	80.28	0.0114	0.7730	25.6	44.7	99.7	66.7	914.7	1.8	10.9
Q	1050	82.81	0.0167	1.349	30.2	30.6	99.5	70.7	935.8	1.6	13.1
R	1100	87.37	0.0253	2.218	30.5	20.2	99.3	74.4	973.6	1.5	12.3
S	1100	89.18	0.0300	3.209	40.3	17.0	98.9	78.9	986.9	1.6	28.0
T	1100	88.38	0.0210	2.834	50.4	24.3	99.1	83.9	980.9	1.6	57.9
U	1100	90.27	0.0122	3.043	58.9	41.8	99.0	89.1	996.7	2.1	117.9
V	1100	92.82	0.0060	3.885	62.9	85.1	98.8	93.9	1016.3	1.9	237.9
W	1100	93.92	0.0023	6.742	38.1	221.1	97.9	96.6	1018.5	1.4	421.9
X	1200	96.75	0.0013	1.540	24.47	389.5	99.5	98.2	1055.2	1.4	12.6
Y	1250	98.22	0.0012	1.911	22.66	419.9	99.4	99.6	1066.5	1.6	8.6
Z	1300	47.69	0.0023	1.980	6.88	225.8	98.8	100.0	591.5	1.1	8.5
Total gas age ± 1σ			n=26		651.4	44.8			943.6	1.1	

ID	Temp (°C)	$^{40}Ar/^{39}Ar$	$^{37}Ar/^{39}Ar$	$^{36}Ar/^{39}Ar$ (x 10^{-3})	$^{39}Ar_K$ (x 10^{-15} mol)	K/Ca	$^{40}Ar^*$ (%)	^{39}Ar (%)	Age (Ma)	±1σ (Ma)	Time (min)
RP-34, K-feldspar, 2.00 mg, J=0.0154396±0.10%, D=1.00361±0.00157, NM-102, Lab#=50033-01											
A	450	85.06	0.0035	45.44	5.45	146.6	84.2	2.7	1359.8	3.4	29.4
B	450	21.47	0.0061	11.94	2.018	83.6	83.5	3.7	445.9	2.6	37.2
C	500	21.26	0.0030	2.620	4.36	170.1	96.4	5.8	501.3	1.3	17.3
D	500	12.71	0.0030	1.710	4.96	168.9	96.0	8.0	314.6	1.0	27.4
E	550	26.91	0.0018	1.333	15.71	280.3	98.5	14.7	626.1	1.3	16.0
F	550	15.01	0.0017	0.2890	15.61	294.9	99.4	20.7	378.05	0.69	27.5
G	600	20.42	0.0018	0.3290	22.75	286.6	99.5	28.4	497.88	0.88	17.8
H	600	20.95	0.0013	0.4870	14.16	386.5	99.3	32.7	508.24	0.99	27.9
I	650	27.18	0.0016	0.6580	22.22	318.9	99.3	38.7	635.5	1.1	17.7
J	650	27.84	0.0013	0.2630	16.72	389.5	99.7	42.8	650.8	1.2	27.7
K	700	34.78	0.0018	0.8330	17.63	281.9	99.3	46.7	779.9	1.6	18.0
L	700	32.35	0.0010	0.6900	12.04	505.2	99.4	49.2	735.5	1.3	28.3
M	750	37.55	0.0029	1.006	6.49	177.2	99.2	50.5	829.3	1.7	8.1
N	800	41.64	0.0029	1.544	12.57	177.8	98.9	52.9	898.3	1.5	8.5
O	850	40.39	0.0028	1.684	14.57	185.5	98.8	55.5	875.8	1.5	8.5
P	900	37.50	0.0032	1.163	16.23	159.4	99.1	58.2	827.6	1.5	8.5
Q	950	37.10	0.0032	1.444	18.75	162.0	98.9	61.1	818.8	1.2	8.6
R	1000	37.13	0.0033	1.055	20.63	155.1	99.2	64.0	821.5	1.4	8.3
S	1050	38.26	0.0032	0.6380	26.67	159.9	99.5	67.5	843.9	1.7	8.2
T	1100	39.34	0.0031	0.8970	35.81	166.2	99.3	71.6	861.7	2.1	8.5
U	1100	41.51	0.0025	0.9430	53.0	204.4	99.3	76.8	899.2	1.5	28.5
V	1100	42.82	0.0026	1.045	48.3	200.1	99.3	80.9	921.1	1.8	58.4
W	1100	43.73	0.0024	1.479	43.4	217.0	99.0	84.0	934.4	2.2	118.5
X	1100	45.21	0.0018	2.202	47.6	278.8	98.6	87.1	955.6	1.6	238.3
Y	1100	46.68	0.0013	4.108	40.9	395.5	97.4	89.4	970.8	2.1	478.2
Z	1230	47.22	0.0017	0.9340	34.74	296.6	99.4	91.2	995.0	2.2	8.0
ZA	1280	47.73	0.0014	0.9260	163.5	357.3	99.4	98.0	1003.3	1.6	8.9
ZB	1330	49.92	0.0016	0.9630	53.3	325.0	99.4	99.7	1038.4	1.7	8.8
ZC	1430	48.09	0.0043	2.195	8.11	119.5	98.7	100.0	1003.1	2.0	8.7
Total gas age ± 1σ			n=29		798.1	246.3		K2O=9.93%	876.6	1.4	

ID	Temp (°C)	$^{40}Ar/^{39}Ar$	$^{37}Ar/^{39}Ar$	$^{36}Ar/^{39}Ar$ (x 10^{-3})	$^{39}Ar_K$ (x 10^{-15} mol)	K/Ca	$^{40}Ar^*$ (%)	^{39}Ar (%)	Age (Ma)	±1σ (Ma)	Time (min)
PVBR02-28, K-feldspar, 1.80 mg, J=0.0187266±0.10%, D=1.0052±0.00172, NM-157, Lab#=53543-01											
A	450	157.0	0.0161	78.30	1.64	31.7	85.3	0.1	2290.8	7.3	13.1
B	450	23.24	0.0164	18.89	0.99	31.1	76.0	0.1	521.0	8.0	23.3
C	450	19.32	0.0195	14.43	1.03	26.2	77.9	0.2	452.7	8.1	31.6
D	450	17.06	0.0147	11.50	0.96	34.7	80.1	0.3	415.1	7.9	48.1
E	500	16.90	0.0104	6.880	1.48	49.1	88.0	0.3	447.6	5.4	13.1
F	500	16.10	0.0093	4.810	2.05	54.9	91.2	0.5	442.6	4.1	23.1
G	500	16.67	0.0110	4.740	1.99	46.4	91.6	0.6	458.5	3.6	31.6
H	500	17.52	0.0055	4.220	2.51	92.8	92.9	0.7	484.9	3.3	48.2
I	550	23.41	0.0056	4.560	3.12	91.1	94.2	0.9	630.9	2.7	12.9
J	550	19.20	0.0059	1.780	3.19	86.9	97.3	1.1	546.9	2.5	23.0
K	550	20.76	0.0032	2.270	3.36	157.5	96.8	1.3	582.3	2.4	31.4
L	550	21.96	0.0053	2.810	3.98	97.2	96.2	1.5	608.1	2.2	48.1
M	600	26.09	0.0046	2.740	4.96	110.9	96.9	1.8	707.0	2.6	12.8
N	600	24.33	0.0035	0.8500	6.53	145.8	99.0	2.2	678.8	2.0	23.0
O	600	25.48	0.0034	1.220	6.28	152.3	98.6	2.5	703.4	2.1	31.2
P	600	26.62	0.0033	1.330	5.97	155.1	98.5	2.9	728.9	2.1	47.9
Q	650	30.16	0.0032	1.970	6.56	157.5	98.1	3.2	804.2	2.2	13.2
R	650	28.57	0.0033	0.8500	6.7	153.2	99.1	3.6	776.2	1.9	23.3
S	650	29.26	0.0026	1.210	6.20	195.5	98.8	4.0	789.2	2.1	31.7
T	700	30.69	0.0027	1.390	7.8	186.9	98.7	4.5	819.5	1.7	13.0
U	700	30.86	0.0029	0.5890	7.9	174.7	99.4	4.9	828.5	1.8	23.3
V	700	32.15	0.0016	2.010	7.4	313.0	98.2	5.4	847.2	2.0	31.6
W	750	31.88	0.0030	1.480	8.1	170.1	98.6	5.9	844.9	1.9	13.5
X	750	31.47	0.0039	0.7640	8.8	129.5	99.3	6.4	840.6	2.0	23.6
Y	750	31.57	0.0033	0.9240	7.4	154.1	99.1	6.8	841.6	2.2	31.8
Z	800	31.73	0.0031	1.119	8.0	164.1	99.0	7.3	843.8	1.8	13.4
ZA	800	31.31	0.0036	1.043	8.2	141.7	99.0	7.8	835.2	2.0	23.4
ZB	850	31.59	0.0030	1.067	10.4	171.8	99.0	8.4	841.2	1.7	13.6
ZC	850	31.54	0.0028	1.388	13.4	182.2	98.7	9.3	838.0	1.9	23.7
ZD	900	31.77	0.0028	1.551	13.9	182.9	98.6	10.1	842.0	1.7	13.5
ZE	900	31.30	0.0027	0.7910	12.0	189.0	99.3	10.9	836.6	1.7	23.6
ZF	950	31.38	0.0028	0.9460	15.2	182.2	99.1	11.8	837.4	2.0	13.7
ZG	950	31.56	0.0027	0.7800	13.7	189.0	99.3	12.7	842.3	1.8	23.7
ZH	1000	31.20	0.0029	1.317	14.7	174.7	98.8	13.6	831.2	1.9	13.7
ZI	1000	31.27	0.0025	1.198	19.2	202.5	98.9	14.9	833.4	1.9	23.6
ZJ	1050	31.38	0.0027	1.704	21.0	189.0	98.4	16.3	832.7	1.6	13.7
ZK	1050	31.49	0.0024	1.448	30.1	215.6	98.6	18.3	836.5	1.6	23.7
ZL	1120	31.60	0.0033	1.769	58.1	156.6	98.3	22.2	836.9	1.5	13.5
ZM	1120	32.10	0.0031	1.385	45.0	166.5	98.7	25.4	850.1	1.6	23.7
ZN	1120	32.12	0.0029	0.9910	53.9	174.4	99.1	29.3	853.1	1.5	58.1
ZO	1120	32.42	0.0026	0.9900	65.4	199.0	99.1	34.3	859.6	1.5	118.1
ZP	1120	32.74	0.0024	1.126	67.4	215.4	99.0	39.6	865.4	1.6	238.1
ZQ	1200	31.03	0.0021	1.597	29.0	239.5	98.5	41.9	825.7	1.8	8.2
ZR	1300	32.69	0.0011	1.346	441.5	475.9	98.8	84.4	863.0	1.9	8.6
ZS	1400	35.20	0.0024	1.616	43.3	209.9	98.6	89.4	914.0	1.7	8.7
ZT	1690	34.51	0.0026	1.703	87.7	192.7	98.5	100.0	899.1	1.8	8.3
Total gas age ± 1σ			n=46		1188.0	226.3		K2O=13.54%	841.7	1.5	

ID	Temp (°C)	$^{40}Ar/^{39}Ar$	$^{37}Ar/^{39}Ar$	$^{36}Ar/^{39}Ar$ (x 10^{-3})	$^{39}Ar_K$ (x 10^{-15} mol)	K/Ca	$^{40}Ar^*$ (%)	^{39}Ar (%)	Age (Ma)	±1σ (Ma)	Time (min)
H03PV007d, K-feldspar, 2.54 mg, J=0.0192281±0.00%, D=1.0058±0.001, NM-171, Lab#=54326-02											
A	450	870.2	0.0130	64.92	5.25	39.2	97.8	0.2	5212.5	4.9	11.9
B	450	73.47	0.0084	14.70	2.71	60.7	94.1	0.3	1543.6	4.6	22.0
C	450	52.70	0.0088	22.75	2.49	58.1	87.2	0.4	1156.3	5.1	30.3
D	450	40.09	0.0080	11.55	2.79	63.7	91.5	0.6	974.1	3.7	46.9
E	500	72.74	0.0061	4.520	4.79	83.6	98.2	0.8	1577.6	3.3	11.6
F	500	27.97	0.0070	3.010	5.66	72.6	96.8	1.0	764.7	2.1	21.7
G	500	24.74	0.0067	3.030	5.40	76.6	96.4	1.2	688.5	2.0	29.9
H	500	24.53	0.0053	3.850	6.35	96.6	95.4	1.5	677.7	2.1	46.6
I	550	84.88	0.0059	3.690	13.7	86.9	98.7	2.1	1752.4	2.8	11.3
J	550	24.67	0.0063	1.260	12.2	80.7	98.5	2.6	699.3	1.4	21.4
K	550	24.92	0.0059	1.418	12.2	85.9	98.3	3.1	704.2	1.4	29.8
L	550	25.70	0.0049	1.947	14.4	104.8	97.8	3.7	719.0	1.3	46.3
M	600	63.21	0.0058	1.707	25.7	87.5	99.2	4.8	1444.2	2.2	11.0
N	600	27.43	0.0050	0.6890	23.4	101.6	99.3	5.8	768.2	1.4	21.1
O	600	27.91	0.0034	0.7900	23.2	152.1	99.2	6.8	778.6	1.4	29.3
P	600	28.27	0.0029	0.9300	25.5	178.4	99.0	7.9	785.8	1.5	46.0
Q	650	42.30	0.0038	1.510	29.0	132.9	98.9	9.2	1077.6	1.9	10.5
R	650	28.81	0.0027	0.5230	30.8	187.4	99.5	10.5	800.7	1.4	20.6
S	650	28.99	0.0024	0.5960	28.3	210.2	99.4	11.8	804.5	1.2	29.0
T	700	34.00	0.0027	0.4820	35.6	185.7	99.6	13.3	915.1	1.4	11.5
U	700	29.26	0.0023	0.3180	35.9	217.5	99.7	14.9	812.3	1.4	21.6
V	700	29.50	0.0020	0.4880	30.5	260.3	99.5	16.3	816.6	1.2	29.9
W	750	31.53	0.0031	0.6300	34.2	163.0	99.4	17.8	860.6	1.3	11.2
X	750	29.80	0.0028	0.5090	38.9	183.2	99.5	19.6	823.2	1.4	21.3
Y	750	29.62	0.0031	0.5690	33.3	163.0	99.4	21.1	818.8	1.7	29.7
Z	800	30.60	0.0046	0.4180	33.7	110.9	99.6	22.7	841.5	1.2	12.0
ZA	800	30.03	0.0037	0.3650	38.0	139.5	99.6	24.5	829.4	1.4	22.1
ZB	850	31.00	0.0048	0.3290	45.2	106.8	99.7	26.6	850.9	1.2	11.8
ZC	850	30.39	0.0033	0.3420	47.9	155.1	99.7	28.9	837.5	1.4	21.9
ZD	900	31.71	0.0050	0.2970	48.9	102.3	99.7	31.2	866.8	1.4	12.3
ZE	900	31.30	0.0038	0.3490	49.0	135.3	99.7	33.6	857.4	1.2	22.6
ZF	950	32.42	0.0053	0.4560	46.1	96.3	99.6	35.8	881.2	1.4	12.1
ZG	950	32.40	0.0034	0.5650	48.6	150.8	99.5	38.2	880.1	1.3	22.2
ZH	1000	34.52	0.0063	0.6860	53.4	80.6	99.4	40.9	924.7	2.9	12.8
ZI	1000	34.55	0.0051	0.8100	54.3	99.3	99.3	43.6	924.6	1.1	22.6
ZJ	1050	36.09	0.0068	1.586	28.1	75.5	98.7	45.0	952.1	1.3	12.3
ZK	1050	36.60	0.0068	1.194	42.9	74.5	99.0	47.2	965.1	1.3	22.8
ZL	1100	37.92	0.0112	1.306	45.4	45.4	99.0	49.6	991.6	1.6	13.0
ZM	1100	37.92	0.0092	1.643	57.2	55.6	98.7	52.6	989.6	1.5	23.0
ZN	1100	39.38	0.0071	2.870	120.7	72.0	97.9	59.0	1011.8	1.8	57.6
ZO	1100	43.58	0.0023	4.270	12.5	226.8	97.1	59.7	1086.6	1.7	118.1
ZP	1100	43.28	0.0062	2.760	5.41	82.4	98.1	60.0	1089.5	2.6	49.9
ZQ	1200	43.13	0.0032	0.7590	10.6	162.0	99.5	60.6	1097.9	1.6	9.8
ZR	1250	40.99	0.0009	0.5270	186.6	558.8	99.6	71.0	1057.6	1.5	7.4
ZS	1350	41.74	0.0009	0.5430	290.3	555.8	99.6	88.0	1072.4	2.2	8.1
ZT	1700	42.01	0.0036	1.410	192.5	143.4	99.0	100.0	1072.7	2.2	8.0
Total gas age ± 1σ			n=46		1939.8	131.4		K2O=15.26%	1006.61	0.90	

ID	Temp (°C)	$^{40}Ar/^{39}Ar$	$^{37}Ar/^{39}Ar$	$^{36}Ar/^{39}Ar$ (x 10^{-3})	$^{39}Ar_K$ (x 10^{-15} mol)	K/Ca	$^{40}Ar^*$ (%)	^{39}Ar (%)	Age (Ma)	±1σ (Ma)	Time (min)
H03PV007e, K-feldspar, 2.08 mg, J=0.0189279±0.00%, D=1.007±0.001, NM-171, Lab#=54328-01											
A	450	135.1	0.0339	46.03	2.08	15.1	89.9	0.2	2180.2	6.9	13.4
B	450	34.14	0.0238	22.57	1.21	21.4	80.5	0.2	763.9	5.6	23.3
C	450	32.41	0.0195	19.08	1.08	26.2	82.6	0.3	748.0	5.8	31.5
D	450	28.66	0.0167	18.59	1.19	30.6	80.8	0.4	663.4	6.8	48.1
E	500	29.90	0.0210	7.510	1.80	24.3	92.6	0.5	768.7	3.1	12.3
F	500	25.35	0.0195	5.920	2.28	26.2	93.1	0.7	673.6	3.9	22.5
G	500	24.96	0.0148	5.300	2.21	34.5	93.7	0.9	668.7	3.1	30.7
H	500	26.26	0.0157	6.320	2.54	32.5	92.9	1.1	692.7	2.7	47.6
I	550	32.56	0.0196	4.230	4.25	26.0	96.2	1.4	849.2	2.6	12.1
J	550	26.81	0.0147	1.930	5.60	34.6	97.9	1.8	735.8	2.0	22.1
K	550	27.59	0.0144	2.490	5.44	35.6	97.3	2.2	749.9	1.8	30.6
L	550	27.93	0.0119	2.190	6.73	42.9	97.7	2.7	759.6	1.9	47.3
M	600	32.91	0.0147	1.475	9.8	34.7	98.7	3.4	874.3	1.5	11.8
N	600	29.10	0.0122	1.069	12.9	41.8	98.9	4.4	793.6	1.3	21.9
O	600	29.46	0.0112	0.7860	13.2	45.5	99.2	5.4	803.4	1.2	30.4
P	600	30.02	0.0095	1.188	16.1	53.9	98.8	6.6	813.3	1.8	47.0
Q	650	31.42	0.0133	0.4820	17.1	38.4	99.6	7.9	848.5	1.2	11.5
R	650	31.17	0.0115	0.3600	23.7	44.4	99.7	9.7	844.0	1.9	21.7
S	650	31.65	0.0102	0.5090	24.4	50.2	99.5	11.6	853.3	1.4	30.0
T	700	32.74	0.0130	0.3740	33.4	39.2	99.7	14.2	877.7	1.3	12.3
U	700	32.86	0.0114	0.2500	40.7	44.7	99.8	17.4	881.0	1.2	22.4
V	700	33.79	0.0106	0.2690	37.8	48.1	99.8	20.4	900.6	1.4	30.7
W	750	34.04	0.0135	0.2390	41.0	37.9	99.8	23.7	906.2	1.4	11.9
X	750	34.48	0.0130	0.2000	49.2	39.3	99.8	27.8	915.7	1.5	22.2
Y	750	35.03	0.0131	0.3670	42.9	38.9	99.7	31.4	926.0	1.3	30.5
Z	800	35.18	0.0172	0.3170	40.0	29.7	99.7	34.8	929.4	1.3	12.6
ZA	800	35.57	0.0177	0.1620	43.1	28.9	99.9	38.5	938.6	1.5	22.7
ZB	850	35.57	0.0238	0.3420	42.4	21.5	99.7	42.3	937.4	1.7	12.4
ZC	850	35.87	0.0253	0.2950	40.3	20.2	99.8	45.8	943.8	1.6	22.7
ZD	900	36.20	0.0348	0.3820	35.8	14.7	99.7	49.1	950.1	1.5	12.8
ZE	900	36.09	0.0362	0.3940	33.1	14.1	99.7	52.1	947.9	1.9	22.9
ZF	950	35.89	0.0403	0.6250	28.2	12.7	99.5	54.8	942.4	2.1	12.9
ZG	950	36.24	0.0372	0.8180	27.3	13.7	99.3	57.3	948.4	2.0	23.2
ZH	1000	36.58	0.0493	1.148	25.9	10.3	99.1	59.8	953.3	1.7	13.4
ZI	1000	36.82	0.0456	1.459	25.6	11.2	98.8	62.2	956.3	1.7	23.4
ZJ	1050	37.92	0.0654	2.200	25.7	7.8	98.3	64.7	974.3	1.6	13.2
ZK	1050	38.44	0.0691	2.498	26.8	7.4	98.1	67.4	983.0	1.6	23.4
ZL	1100	39.68	0.0963	3.108	20.5	5.3	97.7	69.4	1004.4	1.8	13.5
ZM	1100	40.67	0.1019	3.529	22.6	5.0	97.5	71.6	1021.6	1.9	23.5
ZN	1100	41.27	0.0887	2.953	33.5	5.8	97.9	75.0	1036.7	1.8	58.5
ZO	1100	42.44	0.0772	2.748	36.6	6.6	98.1	78.8	1060.8	1.2	118.4
ZP	1100	43.65	0.0545	3.608	30.9	9.4	97.6	82.0	1079.0	1.6	238.5
ZQ	1200	45.26	0.0403	0.7770	47.3	12.7	99.5	87.0	1125.2	1.4	8.6
ZR	1250	49.54	0.0080	0.5720	70.2	63.9	99.7	94.6	1204.5	2.1	8.5
ZS	1350	57.16	0.0188	1.093	13.4	27.1	99.4	96.0	1333.3	1.8	8.5
ZT	1700	56.85	0.0167	1.590	35.7	30.5	99.2	100.0	1325.7	1.8	8.3
Total gas age ± 1σ			n=46		1103.0	16.5		K2O=10.76%	969.10	0.81	

ID	Temp (°C)	$^{40}Ar/^{39}Ar$	$^{37}Ar/^{39}Ar$	$^{36}Ar/^{39}Ar$ (x 10^{-3})	$^{39}Ar_K$ (x 10^{-15} mol)	K/Ca	$^{40}Ar^*$ (%)	^{39}Ar (%)	Age (Ma)	±1σ (Ma)	Time (min)
H03PV003a, K-feldspar, 2.78 mg, J=0.0192765±0.00%, D=1.007±0.001, NM-171, Lab#=54325-01											
A	450	123.1	0.0112	77.06	2.38	45.6	81.5	0.1	1964.9	5.4	12.6
B	450	17.31	0.0067	19.40	1.09	76.1	66.8	0.1	367.0	7.0	22.7
C	450	14.55	0.0122	10.80	1.45	41.8	78.0	0.2	360.8	4.1	31.0
D	450	14.18	0.0061	12.01	1.67	83.9	74.9	0.2	339.6	5.2	47.8
E	500	25.48	0.0052	7.460	2.64	98.9	91.3	0.3	676.1	2.8	12.4
F	500	13.16	0.0055	3.650	3.22	93.6	91.8	0.4	381.4	2.3	22.6
G	500	14.04	0.0043	3.220	3.32	118.9	93.2	0.6	410.0	2.3	30.9
H	500	15.48	0.0045	3.720	3.90	114.1	92.9	0.7	446.1	1.9	47.5
I	550	40.44	0.0042	5.980	8.2	120.3	95.6	1.0	1016.6	2.0	12.1
J	550	18.70	0.0034	1.700	6.76	150.5	97.3	1.2	548.3	1.4	22.3
K	550	20.18	0.0042	1.684	6.89	122.1	97.5	1.5	586.6	1.7	30.5
L	550	21.81	0.0030	2.199	7.01	168.4	97.0	1.7	624.1	2.1	47.4
M	600	37.03	0.0033	4.820	12.2	154.6	96.2	2.2	953.6	1.8	11.9
N	600	25.06	0.0024	1.027	9.4	210.0	98.8	2.5	711.8	1.3	22.1
O	600	25.82	0.0022	1.169	8.0	229.8	98.7	2.8	728.7	1.7	30.3
P	600	26.53	0.0019	1.747	7.94	267.1	98.1	3.1	741.5	2.0	47.1
Q	650	42.04	0.0026	3.841	20.2	200.1	97.3	3.8	1061.1	2.1	11.6
R	650	30.30	0.0018	1.347	9.8	278.8	98.7	4.2	830.6	1.7	21.8
S	650	30.10	0.0016	1.870	8.7	314.9	98.2	4.5	822.5	2.0	30.3
T	700	35.17	0.0018	4.706	14.8	277.3	96.0	5.0	915.1	1.6	12.4
U	700	29.57	0.0017	0.8520	10.4	303.7	99.2	5.4	817.4	1.3	22.5
V	700	29.17	0.0018	0.8520	9.0	278.8	99.1	5.7	808.3	1.6	30.9
W	750	33.74	0.0016	3.328	14.2	316.9	97.1	6.2	893.2	1.7	12.3
X	750	29.60	0.0018	0.6930	12.8	289.9	99.3	6.7	819.1	1.8	22.8
Y	750	29.08	0.0021	0.9610	11.1	245.3	99.0	7.1	805.6	1.6	31.1
Z	800	29.81	0.0018	1.138	13.7	283.4	98.9	7.6	820.8	2.1	13.2
ZA	800	29.22	0.0016	0.5380	14.3	320.9	99.5	8.1	811.7	1.5	23.2
ZB	850	29.51	0.0016	0.7120	16.8	325.0	99.3	8.8	817.0	1.4	13.0
ZC	850	29.49	0.0015	0.5770	18.5	338.8	99.4	9.4	817.5	1.1	22.9
ZD	900	29.91	0.0023	0.8450	18.9	221.8	99.2	10.1	825.1	1.4	13.3
ZE	900	29.97	0.0020	0.5440	19.3	257.7	99.5	10.9	828.5	1.8	23.4
ZF	950	30.29	0.0023	0.7330	19.7	226.8	99.3	11.6	834.3	1.7	13.2
ZG	950	30.64	0.0020	0.7360	21.2	261.2	99.3	12.4	842.2	1.3	23.2
ZH	1000	30.88	0.0028	0.9530	20.4	184.9	99.1	13.2	846.1	1.2	13.5
ZI	1000	31.14	0.0021	0.7530	25.5	241.1	99.3	14.1	853.0	1.4	23.4
ZJ	1050	31.06	0.0023	0.6820	28.6	219.9	99.4	15.2	851.8	1.5	13.4
ZK	1050	31.41	0.0019	0.8550	37.3	263.7	99.2	16.6	858.4	1.8	23.4
ZL	1100	31.50	0.0022	1.014	48.6	235.1	99.1	18.5	859.2	1.5	13.5
ZM	1100	31.95	0.0022	0.8220	57.2	233.9	99.2	20.8	870.5	1.0	23.6
ZN	1100	32.14	0.0017	0.7310	83.4	293.6	99.3	24.0	875.1	1.5	58.6
ZO	1100	32.69	0.0020	0.7940	88.2	258.7	99.3	27.6	886.6	1.3	118.6
ZP	1100	32.85	0.0022	1.191	96.2	227.8	98.9	31.5	887.5	1.8	238.4
ZQ	1200	29.93	0.0020	0.9200	96.3	252.6	99.1	35.5	825.1	1.3	8.6
ZR	1250	31.10	0.0012	0.6374	517.1	411.1	99.4	58.3	852.9	1.9	8.5
ZS	1350	33.14	0.0014	0.6125	547.4	361.8	99.5	85.2	897.5	1.8	8.6
ZT	1700	33.67	0.0053	0.7740	276.6	96.4	99.3	100.0	908.0	1.2	8.3
Total gas age ± 1σ			n=46		2261.9	235.7		K2O=16.21%	859.48	0.92	

ID	Temp (°C)	$^{40}Ar/^{39}Ar$	$^{37}Ar/^{39}Ar$	$^{36}Ar/^{39}Ar$ (x 10^{-3})	$^{39}Ar_K$ (x 10^{-15} mol)	K/Ca	$^{40}Ar^*$ (%)	^{39}Ar (%)	Age (Ma)	±1σ (Ma)	Time (min)
H03PV002a, K-feldspar, 2.06 mg, J=0.0191087±0.00%, D=1.0063±0.001, NM-171, Lab#=54331-01											
A	450	72.37	0.0058	127.8	3.93	88.0	47.8	0.2	926.1	7.0	12.8
B	450	16.79	0.0076	33.55	2.22	67.1	40.9	0.3	224.6	5.3	22.9
C	450	12.54	0.0060	20.74	2.41	85.0	51.0	0.4	210.1	5.3	31.0
D	450	11.54	0.0064	17.62	2.72	79.7	54.8	0.5	207.6	5.3	47.8
E	500	10.76	0.0054	10.47	3.55	94.5	71.2	0.7	248.8	4.0	12.6
F	500	9.824	0.0051	7.160	4.47	100.0	78.4	0.9	250.1	2.6	22.8
G	500	10.03	0.0045	4.720	4.22	113.4	86.1	1.1	278.0	1.9	31.2
H	500	10.79	0.0069	4.730	4.44	73.9	87.0	1.3	300.6	1.7	47.9
I	550	13.29	0.0047	3.960	4.66	108.6	91.2	1.6	379.7	1.9	12.6
J	550	12.35	0.0044	2.070	5.73	116.0	95.0	1.8	368.8	1.3	22.5
K	550	13.65	0.0037	2.380	5.18	137.9	94.8	2.1	403.0	1.6	31.1
L	550	15.23	0.0038	2.590	5.52	134.3	95.0	2.3	444.7	1.8	47.4
M	600	20.74	0.0041	2.430	5.63	124.4	96.5	2.6	590.9	2.0	11.9
N	600	18.40	0.0031	1.368	6.75	164.1	97.8	2.9	538.9	1.5	22.2
O	600	19.81	0.0031	1.470	6.17	163.0	97.8	3.2	574.5	1.6	30.8
P	600	21.55	0.0041	2.230	6.38	126.0	96.9	3.5	612.7	1.7	47.6
Q	650	25.37	0.0040	1.920	5.49	127.6	97.8	3.8	707.6	2.1	12.4
R	650	25.36	0.0031	1.320	6.66	166.2	98.5	4.1	711.6	1.6	22.6
S	650	27.07	0.0036	1.640	5.97	143.7	98.2	4.4	749.5	2.0	30.8
T	700	30.49	0.0022	1.615	7.86	227.8	98.4	4.8	827.1	1.8	13.0
U	700	30.07	0.0028	0.8550	8.7	183.5	99.2	5.2	822.8	1.5	23.0
V	700	30.96	0.0021	1.369	7.89	247.7	98.7	5.6	839.0	2.0	31.4
W	750	32.27	0.0017	0.9380	9.8	309.2	99.1	6.1	870.6	1.5	12.8
X	750	31.92	0.0018	0.8060	11.6	289.9	99.3	6.7	863.9	1.4	22.8
Y	750	31.81	0.0016	0.9300	10.7	325.0	99.1	7.2	860.7	1.5	31.1
Z	800	32.20	0.0019	0.7860	10.9	268.5	99.3	7.7	869.9	2.2	13.2
ZA	800	32.30	0.0017	0.6310	13.4	305.5	99.4	8.4	873.1	1.3	23.0
ZB	850	32.54	0.0016	0.6330	15.5	320.9	99.4	9.1	878.4	1.6	12.9
ZC	850	32.53	0.0023	0.7480	17.1	219.9	99.3	10.0	877.4	1.4	23.0
ZD	900	33.04	0.0018	0.6230	19.9	283.4	99.4	11.0	889.2	1.2	13.3
ZE	900	33.26	0.0017	0.5190	21.7	309.2	99.5	12.1	894.5	1.4	23.4
ZF	950	33.38	0.0020	0.8710	21.2	260.3	99.2	13.1	894.9	1.5	13.2
ZG	950	33.59	0.0013	0.6050	24.5	398.6	99.5	14.4	901.0	1.5	23.2
ZH	1000	33.61	0.0018	0.6930	23.8	277.3	99.4	15.6	900.9	1.6	13.5
ZI	1000	33.98	0.0017	0.6560	27.5	301.9	99.4	17.0	909.0	1.5	23.5
ZJ	1050	34.17	0.0025	0.8080	28.5	207.4	99.3	18.5	912.1	1.3	13.3
ZK	1050	34.10	0.0022	0.9070	35.3	236.2	99.2	20.3	910.0	1.3	23.4
ZL	1100	34.09	0.0025	0.9940	31.4	202.5	99.1	21.9	909.3	1.5	13.5
ZM	1100	34.32	0.0026	0.8690	37.0	197.0	99.3	23.9	914.9	1.1	23.6
ZN	1100	34.16	0.0025	0.9020	42.9	208.2	99.2	26.2	911.3	1.4	41.6
ZO	1100	34.36	0.0023	1.112	68.3	224.8	99.0	29.9	914.2	1.5	117.9
ZP	1100	34.94	0.0020	1.892	59.7	256.4	98.4	33.1	921.5	1.4	238.6
ZQ	1200	32.67	0.0016	1.093	47.7	327.1	99.0	35.8	878.3	1.2	8.0
ZR	1250	33.19	0.0009	0.9230	262.6	550.4	99.2	51.0	890.4	2.2	8.5
ZS	1350	35.11	0.0009	0.8110	310.6	539.9	99.3	70.3	931.8	1.6	8.5
ZT	1700	35.24	0.0012	0.9100	433.7	427.7	99.2	100.0	933.9	2.7	8.1
Total gas age ± 1σ			n=46		1702.0	323.3		K2O=16.61%	882.5	1.1	

ID	Temp (°C)	$^{40}Ar/^{39}Ar$	$^{37}Ar/^{39}Ar$	$^{36}Ar/^{39}Ar$ (x 10^{-3})	$^{39}Ar_K$ (x 10^{-15} mol)	K/Ca	$^{40}Ar^*$ (%)	^{39}Ar (%)	Age (Ma)	±1σ (Ma)	Time (min)
PVSDC02-18, K-feldspar, 2.30 mg, J=0.0193456±0.10%, D=1.0052±0.00172, NM-157, Lab#=53537-01											
A	450	86.18	0.0553	63.07	2.94	9.2	78.4	0.2	1526.0	6.1	13.39
B	450	29.70	0.0195	17.75	1.44	26.2	82.3	0.3	706.7	6.1	23.32
C	450	27.80	0.0137	13.32	1.33	37.2	85.8	0.3	692.5	5.6	31.71
D	450	27.04	0.0098	10.17	1.49	52.1	88.9	0.4	696.5	4.3	48.36
E	500	25.34	0.0208	6.230	2.06	24.5	92.8	0.6	683.7	4.1	12.94
F	500	25.51	0.0152	4.790	2.76	33.6	94.5	0.7	698.0	2.9	23.13
G	500	25.52	0.0133	4.320	2.64	38.4	95.0	0.9	701.7	3.0	31.52
H	500	26.48	0.0106	4.520	3.01	48.1	95.0	1.1	723.2	2.8	48.25
I	550	28.33	0.0088	3.180	3.47	58.0	96.7	1.3	775.7	2.5	12.92
J	550	28.24	0.0081	2.450	4.55	62.7	97.4	1.6	778.6	2.3	23.01
K	550	28.73	0.0065	2.010	4.77	78.6	97.9	1.8	793.0	2.1	31.28
L	550	29.85	0.0056	1.250	5.63	91.1	98.8	2.2	823.4	2.2	47.93
M	600	31.51	0.0068	1.490	6.05	75.5	98.6	2.6	858.8	2.3	12.67
N	600	31.09	0.0073	1.150	8.8	70.0	98.9	3.1	851.8	1.8	22.95
O	600	31.78	0.0050	0.9770	9.4	102.0	99.1	3.7	868.1	1.8	31.29
P	600	32.61	0.0052	0.9130	11.3	98.1	99.2	4.4	886.7	1.9	47.96
Q	650	32.80	0.0062	0.4790	10.6	81.9	99.6	5.0	893.5	1.9	13.23
R	650	33.29	0.0061	0.3520	14.7	83.1	99.7	6.0	904.9	1.9	23.36
S	650	33.85	0.0048	0.3960	14.8	106.7	99.7	6.9	916.7	1.8	31.67
T	700	34.22	0.0069	0.3850	17.4	74.5	99.7	8.0	924.7	1.9	13.06
U	700	34.48	0.0074	0.1960	21.7	69.1	99.8	9.4	931.4	1.9	23.18
V	700	34.67	0.0063	0.1730	20.4	81.6	99.9	10.8	935.5	2.1	31.45
W	750	34.77	0.0078	0.2020	21.9	65.3	99.8	12.2	937.4	2.0	13.47
X	750	35.07	0.0072	0.2630	26.5	70.9	99.8	14.0	943.3	1.9	23.43
Y	750	35.40	0.0067	0.1060	24.2	76.0	99.9	15.7	951.4	1.6	31.86
Z	800	35.37	0.0087	0.1340	22.4	58.8	99.9	17.2	950.4	2.0	13.4
ZA	800	35.63	0.0077	0.2180	26.9	65.9	99.8	19.1	955.4	1.6	23.4
ZB	850	35.76	0.0081	0.2310	28.8	63.4	99.8	21.2	958.1	1.7	13.64
ZC	850	36.06	0.0062	0.2180	30.6	82.3	99.8	23.4	964.3	1.7	23.68
ZD	900	36.32	0.0068	0.2910	27.7	74.6	99.8	25.5	969.3	1.6	13.53
ZE	900	36.36	0.0054	0.2690	27.9	94.3	99.8	27.6	970.3	1.8	23.55
ZF	950	36.66	0.0067	0.2830	23.8	75.8	99.8	29.5	976.6	1.7	13.71
ZG	950	37.08	0.0063	0.4450	23.6	81.0	99.6	31.3	984.3	1.9	23.74
ZH	1000	37.80	0.0123	1.012	21.0	41.4	99.2	33.0	995.5	2.0	13.61
ZI	1000	38.44	0.0136	1.065	22.2	37.5	99.2	34.7	1008.2	1.8	23.63
ZJ	1050	39.48	0.0276	1.839	21.2	18.5	98.6	36.5	1024.7	2.0	13.77
ZK	1050	39.93	0.0210	1.708	22.0	24.2	98.7	38.3	1034.6	2.0	23.79
ZL	1120	41.23	0.0289	3.203	36.1	17.7	97.7	41.3	1052.1	2.2	13.64
ZM	1120	41.05	0.0161	2.445	39.7	31.7	98.2	44.7	1052.6	1.9	23.67
ZN	1120	41.83	0.0059	1.632	108.7	87.1	98.9	54.6	1072.7	1.9	58
ZO	1120	42.71	0.0021	1.210	84.4	242.5	99.2	62.8	1092.4	2.0	133.4
ZP	1120	43.49	0.0013	1.393	103.1	399.5	99.1	73.5	1106.3	1.9	238.1
ZQ	1200	44.84	0.0008	0.7180	101.6	670.4	99.5	84.9	1135.9	2.0	8.165
ZR	1300	47.56	0.0008	0.9410	114.7	629.9	99.4	98.9	1185.7	2.1	8.724
ZS	1400	54.70	0.0024	1.820	3.91	215.3	99.0	99.4	1308.4	3.5	8.767
ZT	1690	52.71	0.0010	5.530	4.48	520.6	96.9	100.0	1254.3	2.9	8.301
Total gas age ± 1σ			n=46		1138.6	74.8		K2O=9.83%	1024.7	1.6	

ID	Temp (°C)	$^{40}Ar/^{39}Ar$	$^{37}Ar/^{39}Ar$	$^{36}Ar/^{39}Ar$ (x 10^{-3})	$^{39}Ar_K$ (x 10^{-15} mol)	K/Ca	$^{40}Ar^*$ (%)	^{39}Ar (%)	Age (Ma)	±1σ (Ma)	Time (min)
RP-40B, K-feldspar, 1.34 mg, J=0.0153566±0.10%, D=1.00461±0.00118, NM-102, Lab#=50036-01											
AA	450	76.82	0.0210	72.96	2.84	24.3	71.9	0.5	1121.8	4.4	19.53
BB	450	20.01	-0.0090	10.10	1.91	-	85.1	0.8	423.6	2.8	26.47
CC	500	22.35	-0.0010	3.290	3.54	-	95.7	1.4	517.9	1.6	17.05
D	500	22.33	0.0007	1.790	4.96	728.9	97.6	2.3	526.8	1.4	27.23
E	550	30.46	0.0062	2.270	4.83	82.3	97.8	3.1	687.4	1.5	16.69
F	550	28.80	0.0070	1.471	7.39	72.9	98.5	4.4	659.7	1.2	26.89
G	600	33.98	0.0091	1.310	9.14	56.1	98.9	5.9	759.1	1.7	17.35
H	600	35.20	0.0119	0.9080	10.81	42.9	99.2	7.7	783.8	1.2	27.33
I	650	38.19	0.0118	0.7130	14.3	43.4	99.5	10.1	838.7	1.8	17.13
J	650	39.66	0.0110	0.7940	13.6	46.5	99.4	12.4	864.1	1.3	27.28
K	700	40.67	0.0116	0.5290	14.8	43.9	99.6	14.9	883.0	1.3	18.11
L	700	41.28	0.0091	0.9090	16.7	56.3	99.4	17.7	891.5	1.3	28.13
M	750	41.90	0.0119	0.4910	17.2	42.7	99.7	20.5	904.3	1.4	17.82
N	750	42.41	0.0127	0.6230	16.0	40.1	99.6	23.1	912.4	1.3	27.85
O	800	42.67	0.0170	0.3990	8.64	30.0	99.7	24.5	918.0	2.0	8.119
P	850	43.04	0.0171	0.2860	16.7	29.8	99.8	27.2	924.7	1.2	7.872
Q	900	43.37	0.0197	0.2670	21.1	25.9	99.8	30.6	930.4	1.6	7.754
R	950	42.98	0.0153	0.3430	23.1	33.4	99.8	34.3	923.3	1.2	7.627
S	1000	42.73	0.0137	0.3360	26.2	37.2	99.8	38.5	919.2	1.7	7.896
T	1050	42.58	0.0235	0.6130	27.7	21.7	99.6	42.8	915.3	1.8	7.512
U	1100	43.77	0.0356	1.146	23.1	14.3	99.2	46.4	932.8	1.4	8.223
V	1100	44.11	0.0325	1.009	45.6	15.7	99.3	53.4	939.2	2.1	28.03
W	1100	45.50	0.0212	1.067	52.6	24.1	99.3	61.4	962.0	1.4	57.67
X	1100	48.58	0.0074	0.9880	78.8	69.0	99.4	73.0	1012.6	5.8	118.1
Y	1100	51.35	0.0045	1.388	81.0	114.7	99.2	84.6	1055.0	5.4	237.7
Z	1100	52.84	0.0025	2.470	38.6	205.7	98.6	90.1	1073.2	1.8	16.56
ZA	1200	50.47	0.0033	0.9380	9.32	154.6	99.5	91.4	1043.1	2.0	4.893
ZB	1300	50.72	0.0022	0.9640	27.9	227.8	99.4	95.3	1046.9	1.9	5.736
ZC	1350	51.61	0.0013	1.623	8.69	392.5	99.1	96.4	1057.8	1.6	5.696
ZD	1400	53.38	0.0037	1.358	13.1	137.9	99.3	98.2	1086.7	1.6	5.658
ZE	1650	54.48	0.0013	18.23	12.8	408.2	90.1	100.0	1025.5	2.0	5.135
Total gas age ± 1σ			n=31		653.0	40.5		K2O=12.19%	948.0	1.5	

ID	Temp (°C)	$^{40}Ar/^{39}Ar$	$^{37}Ar/^{39}Ar$	$^{36}Ar/^{39}Ar$ (x 10^{-3})	$^{39}Ar_K$ (x 10^{-15} mol)	K/Ca	$^{40}Ar^*$ (%)	^{39}Ar (%)	Age (Ma)	±1σ (Ma)	Time (min)
PVBR02-18, K-feldspar, 1.65 mg, J=0.0190443±0.10%, D=1.0052±0.00172, NM-157, Lab#=53535-01											
A	450	39.31	0.0116	63.10	1.83	44.0	52.5	0.1	605.0	10.0	13.29
B	450	18.62	-0.0018	15.14	1.19	-	75.9	0.2	434.8	6.8	23.29
C	450	17.07	0.0004	12.93	1.10	######	77.6	0.3	410.2	6.1	31.74
D	450	16.38	0.0012	8.300	1.22	425.2	85.0	0.4	428.7	5.5	48.41
E	500	18.24	0.0014	14.44	1.46	364.4	76.6	0.5	430.1	6.7	13.15
F	500	16.30	0.0033	4.920	2.01	154.6	91.1	0.6	454.0	3.6	23.17
G	500	16.75	0.0022	3.210	2.02	231.9	94.3	0.8	479.6	4.0	31.58
H	500	17.37	0.0017	2.300	2.37	300.1	96.1	1.0	503.1	2.9	48.3
I	550	20.06	0.0020	6.380	2.74	255.1	90.6	1.2	541.8	3.0	13.05
J	550	19.88	0.0023	2.760	3.66	221.8	95.9	1.4	564.7	2.3	23.18
K	550	21.03	0.0014	1.520	3.78	364.4	97.9	1.7	603.2	2.2	31.34
L	550	22.20	-0.0003	2.470	4.63	-	96.7	2.1	625.1	2.0	48.15
M	600	24.53	0.0010	5.110	4.48	510.2	93.8	2.4	663.0	2.4	12.88
N	600	24.40	0.0022	0.9700	6.21	231.9	98.8	2.9	689.4	2.0	22.89
O	600	25.46	0.0020	1.340	7.2	257.7	98.5	3.4	711.9	2.1	31.26
P	600	26.30	0.0015	0.9200	9.1	351.9	99.0	4.1	734.5	1.9	48
Q	650	27.51	0.0012	1.380	8.5	432.4	98.5	4.7	759.1	1.8	13.24
R	650	28.07	0.0011	0.6800	11.1	476.8	99.3	5.6	776.8	1.9	23.4
S	650	28.90	0.0010	0.4170	12.7	490.6	99.6	6.6	797.3	1.3	31.7
T	700	29.81	0.0012	0.7910	15.2	418.2	99.2	7.8	815.1	1.6	13.01
U	700	30.72	0.0013	0.4690	20.8	395.5	99.6	9.4	837.3	1.6	23.32
V	700	31.67	0.0006	0.4850	18.4	809.8	99.6	10.9	858.1	1.9	31.62
W	750	32.59	0.0016	0.6650	21.1	316.9	99.4	12.6	876.8	1.7	13.48
X	750	33.13	0.0014	0.3150	23.2	361.8	99.7	14.5	890.5	1.5	23.55
Y	750	33.85	0.0016	0.3780	24.0	313.0	99.7	16.5	905.5	1.5	31.83
Z	800	33.99	0.0033	0.3750	21.2	157.0	99.7	18.2	908.5	1.6	13.38
ZA	800	34.44	0.0019	0.5930	21.3	275.8	99.5	20.1	916.6	2.0	23.46
ZB	850	34.53	0.0041	0.2810	27.2	124.1	99.8	22.4	920.5	1.7	13.69
ZC	850	34.75	0.0022	0.3420	27.4	228.8	99.7	24.9	924.8	1.8	23.67
ZD	900	34.75	0.0034	0.4840	29.7	150.9	99.6	27.5	923.9	1.6	13.6
ZE	900	34.69	0.0022	0.4720	30.5	233.0	99.6	30.3	922.6	1.9	23.64
ZF	950	34.41	0.0026	0.3870	22.8	197.0	99.7	32.5	917.2	1.7	13.78
ZG	950	34.36	0.0016	0.4480	19.3	316.9	99.6	34.3	915.9	1.7	23.8
ZH	1000	34.11	0.0036	0.7260	20.4	140.9	99.4	36.3	908.8	1.6	13.68
ZI	1000	34.19	0.0029	0.4190	24.4	179.0	99.6	38.7	912.5	1.5	23.59
ZJ	1050	34.12	0.0091	0.8740	24.7	55.8	99.2	41.2	908.2	1.9	13.73
ZK	1050	33.86	0.0056	0.6090	26.3	91.1	99.5	43.8	904.4	1.6	23.8
ZL	1110	33.12	0.0060	1.015	24.8	85.5	99.1	46.4	886.0	1.8	13.67
ZM	1110	33.25	0.0039	1.082	27.1	132.5	99.0	49.3	888.4	1.6	23.71
ZN	1110	33.50	0.0028	1.284	40.0	179.6	98.9	53.6	892.3	1.6	58.13
ZO	1110	32.65	0.0016	2.645	132.6	322.1	97.6	69.0	865.6	1.6	120.9
ZP	1120	33.71	0.0018	3.253	94.7	284.6	97.2	81.1	884.3	1.8	238.2
ZQ	1200	33.79	0.0018	2.154	38.2	283.4	98.1	86.2	893.1	1.5	8.218
ZR	1300	35.24	0.0016	2.952	95.0	322.9	97.5	99.7	918.8	1.6	8.755
ZS	1400	35.32	-0.0057	9.390	1.52	-	92.1	99.9	880.1	4.2	8.786
ZT	1690	69.48	0.0225	107.5	0.530	22.7	54.3	100.0	988.0	15.0	8.321
Total gas age ± 1σ			n=46		959.6	210.8		K2O=11.73%	865.8	1.4	

ID	Temp (°C)	$^{40}Ar/^{39}Ar$	$^{37}Ar/^{39}Ar$	$^{36}Ar/^{39}Ar$ (x 10^{-3})	$^{39}Ar_K$ (x 10^{-15} mol)	K/Ca	$^{40}Ar^*$ (%)	^{39}Ar (%)	Age (Ma)	±1σ (Ma)	Time (min)
H03PV004b, K-feldspar, 1.17 mg, J=0.018859±0.10%, D=1.0063±0.001, NM-171, Lab#=54329-01											
A	450	85.54	-0.0024	154.1	1.23	-	46.8	0.4	1026.0	12.0	12.59
B	450	19.85	-0.0690	12.80	0.512	-	80.9	0.6	483.0	18.0	22.7
C	450	17.64	-0.0720	14.50	0.383	-	75.6	0.7	409.0	27.0	31.25
D	450	18.25	-0.0710	24.00	0.436	-	61.0	0.9	347.0	22.0	47.99
E	500	14.65	-0.0390	-3.3000	0.623	-	106.6	1.1	470.0	14.0	12.72
F	500	15.33	-0.0210	1.900	0.79	-	96.4	1.4	448.0	11.0	22.74
G	500	16.66	-0.0336	3.100	0.75	-	94.4	1.7	474.0	11.0	31.2
H	500	17.43	-0.0278	3.200	0.84	-	94.6	2.0	494.0	10.0	47.62
I	550	19.38	-0.0077	-0.0500	1.04	-	100.1	2.3	568.5	8.7	12.55
J	550	18.92	-0.0129	0.2800	1.31	-	99.6	2.8	554.4	7.1	22.54
K	550	20.53	-0.0089	-2.0500	1.22	-	103.0	3.2	612.0	7.4	31.05
L	550	22.35	-0.0083	0.4400	1.40	-	99.4	3.7	638.5	6.6	47.73
M	600	25.97	-0.0029	1.660	1.67	-	98.1	4.3	715.9	5.9	12.51
N	600	24.00	0.0084	-0.4800	2.06	60.7	100.6	5.1	684.5	4.2	22.44
O	600	25.00	0.0049	-0.1100	2.07	104.1	100.1	5.8	705.5	4.1	30.8
P	600	26.36	0.0032	-0.0200	2.47	159.4	100.0	6.7	736.3	3.7	47.52
Q	650	28.02	0.0314	-1.1800	2.18	16.2	101.3	7.5	782.0	4.0	12.33
R	650	28.05	0.0204	-0.5800	3.06	25.0	100.6	8.7	778.7	3.3	22.44
S	650	29.00	0.0108	0.1500	3.01	47.2	99.9	9.8	795.1	3.2	30.66
T	700	29.35	0.0233	-1.0900	4.04	21.9	101.1	11.3	810.9	2.5	12.82
U	700	29.92	0.0082	-0.2000	4.95	62.2	100.2	13.1	817.8	2.7	22.77
V	700	30.27	0.0060	0.0400	4.40	85.0	100.0	14.8	823.7	2.7	31.24
W	750	31.02	0.0076	-0.9900	4.18	67.1	100.9	16.4	846.9	2.5	12.79
X	750	31.26	0.0056	-0.5500	5.43	91.1	100.5	18.5	849.2	2.3	22.76
Y	750	31.57	0.0064	-0.0900	4.72	79.7	100.1	20.3	853.0	2.2	31.24
Z	800	31.50	0.0131	-0.7200	4.55	38.9	100.7	22.0	855.6	2.3	13.18
ZA	800	31.97	0.0161	-0.3300	5.60	31.7	100.3	24.2	863.0	2.3	23.22
ZB	850	32.47	0.0351	0.2200	6.02	14.5	99.8	26.6	870.4	2.3	13.09
ZC	850	32.34	0.0273	-0.2900	5.98	18.7	100.3	29.0	870.8	2.7	23.09
ZD	900	32.36	0.0464	0.0000	6.03	11.0	100.0	31.5	869.4	2.0	13.37
ZE	900	31.85	0.0414	-0.5600	5.56	12.3	100.5	33.7	862.1	2.4	23.36
ZF	950	30.51	0.0719	-0.0600	5.17	7.1	100.1	35.9	830.0	2.3	13.26
ZG	950	30.35	0.0357	0.4600	5.02	14.3	99.6	38.0	823.0	2.3	23.34
ZH	1000	29.56	0.0403	0.0200	4.96	12.7	100.0	40.1	808.5	2.2	13.48
ZI	1000	30.32	0.0297	1.380	5.28	17.2	98.7	42.3	816.2	2.3	23.51
ZJ	1050	30.18	0.0525	1.690	7.18	9.7	98.4	45.4	811.2	2.0	13.4
ZK	1050	31.31	0.0512	2.380	9.0	10.0	97.8	49.3	831.7	1.9	23.37
ZL	1100	31.57	0.0923	3.090	8.4	5.5	97.1	53.0	832.8	1.9	13.48
ZM	1100	32.88	0.0558	3.330	10.4	9.2	97.0	57.6	859.5	1.7	23.61
ZN	1100	33.99	0.0452	3.851	17.8	11.3	96.7	65.8	880.1	1.7	58.61
ZO	1100	35.35	0.0494	5.170	20.3	10.3	95.7	75.4	900.7	1.6	118.6
ZP	1100	38.07	0.0688	8.420	22.9	7.4	93.5	86.7	937.2	1.8	238.5
ZQ	1200	40.77	0.0866	4.420	13.3	5.9	96.8	93.5	1015.7	1.7	8.408
ZR	1250	39.43	0.0437	3.190	8.3	11.7	97.6	97.8	996.1	2.3	8.58
ZS	1350	40.87	0.0715	2.680	1.49	7.1	98.1	98.6	1027.6	5.7	8.57
ZT	1700	50.17	0.2204	22.85	2.62	2.3	86.6	100.0	1092.6	4.5	8.197
Total gas age ± 1σ			n=46		230.5	11.9		K2O=4.01%	852.7	1.1	

ID	Temp (°C)	$^{40}Ar/^{39}Ar$	$^{37}Ar/^{39}Ar$	$^{36}Ar/^{39}Ar$ (x 10^{-3})	$^{39}Ar_K$ (x 10^{-15} mol)	K/Ca	$^{40}Ar^*$ (%)	^{39}Ar (%)	Age (Ma)	±1σ (Ma)	Time (min)
PVBR02-17, K-feldspar, 1.99 mg, J=0.0194493±0.10%, D=1.0052±0.00172, NM-157, Lab#=53539-01											
A	450	42.45	0.0581	55.19	3.96	8.8	61.6	0.2	750.3	5.4	13.11
B	450	16.12	0.0216	10.53	2.18	23.7	80.7	0.4	411.1	5.2	23.25
C	450	15.34	0.0177	9.840	1.95	28.8	81.0	0.5	394.5	5.6	31.66
D	450	15.24	0.0128	6.560	2.16	39.8	87.3	0.6	419.4	3.5	48.23
E	500	15.03	0.0201	4.080	3.02	25.4	92.0	0.8	434.0	3.3	13.1
F	500	15.78	0.0114	3.390	3.70	44.8	93.7	1.1	460.4	2.7	23.12
G	500	16.84	0.0106	2.590	3.54	48.1	95.5	1.3	496.0	2.7	31.47
H	500	17.97	0.0079	2.840	4.22	64.3	95.3	1.5	524.4	2.6	48.12
I	550	19.65	0.0070	2.600	4.99	73.3	96.1	1.8	570.3	2.1	12.93
J	550	20.43	0.0045	1.720	6.41	112.4	97.5	2.2	597.1	1.8	22.95
K	550	21.60	0.0046	1.400	6.61	110.7	98.1	2.7	629.3	1.8	31.36
L	550	22.66	0.0047	1.410	7.6	108.1	98.2	3.1	655.6	1.7	47.95
M	600	24.16	0.0061	1.360	8.2	83.2	98.3	3.7	693.0	1.8	12.83
N	600	24.62	0.0059	0.9000	10.1	86.2	98.9	4.3	707.4	1.6	22.95
O	600	25.46	0.0057	0.9900	10.6	89.2	98.9	5.0	726.9	1.6	31.18
P	600	26.08	0.0053	0.7790	12.0	95.5	99.1	5.8	743.1	1.6	47.95
Q	650	27.35	0.0082	0.9350	9.7	62.3	99.0	6.4	771.7	1.8	13.3
R	650	27.89	0.0070	0.7370	12.5	72.8	99.2	7.2	785.6	1.7	23.25
S	650	28.33	0.0077	0.6020	12.0	66.7	99.4	8.0	796.7	1.9	31.68
T	700	29.03	0.0081	0.8180	13.7	62.7	99.2	8.9	811.2	1.5	13.15
U	700	29.62	0.0077	0.4970	15.7	66.3	99.5	10.0	826.9	2.2	23.1
V	700	30.36	0.0070	0.6560	14.1	72.5	99.4	10.9	842.4	1.9	31.51
W	750	30.67	0.0079	0.6590	13.9	64.6	99.4	11.9	849.4	1.8	13.38
X	750	30.98	0.0063	0.6060	16.0	80.9	99.4	13.0	856.5	1.8	23.52
Y	750	31.36	0.0058	0.3380	14.1	88.3	99.7	14.0	866.6	1.7	31.82
Z	800	31.21	0.0065	0.5220	13.3	78.1	99.5	14.9	862.2	1.9	13.3
ZA	800	31.45	0.0054	0.3720	15.0	94.7	99.7	15.9	868.5	1.8	23.44
ZB	850	31.28	0.0107	0.6360	17.0	47.9	99.4	17.2	863.1	1.6	13.61
ZC	850	31.42	0.0060	0.4500	17.9	85.3	99.6	18.5	867.2	1.9	23.66
ZD	900	31.27	0.0137	0.7080	17.3	37.2	99.3	19.7	862.3	1.8	13.52
ZE	900	30.79	0.0079	0.5110	17.4	65.0	99.5	21.0	852.9	1.4	23.58
ZF	950	30.41	0.0083	1.012	16.5	61.8	99.0	22.2	841.0	1.7	13.72
ZG	950	30.09	0.0061	1.017	17.8	83.9	99.0	23.6	834.0	1.9	23.75
ZH	1000	29.99	0.0077	1.712	18.2	65.9	98.3	25.0	827.1	1.7	13.51
ZI	1000	30.09	0.0087	1.806	20.5	58.6	98.2	26.5	828.7	1.8	23.63
ZJ	1050	30.19	0.0228	4.269	23.7	22.4	95.8	28.4	814.4	1.8	13.67
ZK	1050	30.82	0.0227	3.389	28.2	22.5	96.8	30.6	834.7	1.8	23.8
ZL	1120	29.95	0.0198	2.956	124.4	25.8	97.1	41.1	817.9	1.7	13.65
ZM	1120	30.52	0.0072	2.050	139.6	71.0	98.0	53.9	836.8	1.5	23.66
ZN	1120	31.81	0.0025	1.664	253.3	205.1	98.5	80.7	867.9	2.0	75.91
ZO	1120	33.68	0.0012	1.505	100.5	417.9	98.7	92.9	909.7	1.5	121.6
ZP	1120	35.31	0.0009	2.222	37.8	543.3	98.1	97.7	940.1	1.6	250.8
ZQ	1200	35.55	0.0018	1.167	14.2	278.8	99.0	99.6	951.8	1.8	8.216
ZR	1300	37.02	0.0029	1.900	3.14	175.9	98.5	100.0	978.1	3.6	8.711
ZS	1400	52.70	0.0750	27.00	0.037	6.8	85.0	100.0	1140.0	130.0	8.642
ZT	1690	62.19	0.1597	111.0	0.195	3.2	47.2	100.0	825.0	40.0	8.407
Total gas age ± 1σ			n=46		1108.7	65.4		K2O=11.00%	828.8	1.4	

ID	Temp (°C)	$^{40}Ar/^{39}Ar$	$^{37}Ar/^{39}Ar$	$^{36}Ar/^{39}Ar$ (x 10^{-3})	$^{39}Ar_K$ (x 10^{-15} mol)	K/Ca	$^{40}Ar^*$ (%)	^{39}Ar (%)	Age (Ma)	±1σ (Ma)	Time (min)
PVBR02-17B, K-feldspar, 2.35 mg, J=0.0113314±0.17%, D=1.0052±0.00172, NM-158, Lab#=53630-01											
A	450	80.30	0.0561	154.1	1.13	9.1	43.3	0.2	605.9	9.7	13.46
B	450	33.65	0.0084	54.00	0.75	60.7	52.5	0.4	333.2	9.3	23.38
C	450	29.35	0.0011	32.30	0.623	463.8	67.5	0.5	369.0	11.0	31.69
D	450	29.17	-0.0096	31.90	0.558	-	67.6	0.6	368.0	11.0	48.33
E	500	24.00	0.0085	7.200	0.76	60.0	91.2	0.7	404.1	7.5	13.04
F	500	24.72	0.0103	9.350	1.15	49.5	88.8	0.9	405.3	5.0	23.27
G	500	24.60	0.0082	8.610	1.21	62.2	89.6	1.2	406.9	5.2	31.46
H	500	26.61	0.0113	9.110	1.43	45.2	89.9	1.4	437.5	4.4	48.22
I	550	29.62	0.0066	3.560	1.58	77.3	96.5	1.7	511.7	3.5	12.97
J	550	28.89	0.0108	2.060	1.92	47.2	97.9	2.1	507.1	3.2	23.05
K	550	31.78	0.0096	3.350	2.25	53.1	96.9	2.5	546.1	3.1	31.46
L	550	33.17	0.0089	3.360	2.78	57.6	97.0	3.0	567.3	2.8	48.09
M	600	38.65	0.0149	4.720	2.46	34.2	96.4	3.5	642.8	3.0	12.88
N	600	37.18	0.0131	1.070	3.79	39.0	99.2	4.2	637.0	2.1	23.02
O	600	39.16	0.0121	1.050	3.89	42.0	99.2	5.0	665.8	2.1	31.28
P	600	41.13	0.0118	1.350	4.59	43.2	99.0	5.9	692.5	2.1	47.9
Q	650	43.89	0.0177	1.560	3.75	28.8	99.0	6.6	730.5	2.3	13.32
R	650	43.73	0.0161	0.5200	5.35	31.7	99.7	7.7	732.5	1.8	23.4
S	650	45.50	0.0163	0.4800	5.06	31.4	99.7	8.7	757.0	2.4	31.64
T	700	47.09	0.0207	1.220	5.04	24.7	99.2	9.7	775.7	2.1	13.16
U	700	47.52	0.0185	0.1000	5.52	27.5	99.9	10.8	785.9	2.0	23.26
V	700	48.56	0.0185	-0.4400	6.52	27.6	100.3	12.1	802.1	2.1	31.64
W	750	49.37	0.0206	0.3300	4.93	24.8	99.8	13.1	809.8	2.2	13.4
X	750	50.46	0.0190	0.0500	6.63	26.9	100.0	14.5	825.2	1.8	23.53
Y	750	51.12	0.0148	-0.5300	5.63	34.5	100.3	15.7	836.2	1.9	31.91
Z	800	51.41	0.0172	0.2100	4.55	29.7	99.9	16.6	837.1	2.5	13.42
ZA	800	51.33	0.0168	-0.0500	5.65	30.3	100.0	17.8	837.1	2.0	23.42
ZB	850	51.70	0.0325	0.3700	6.07	15.7	99.8	19.1	840.3	1.9	13.65
ZC	850	51.81	0.0290	-0.4500	6.55	17.6	100.3	20.6	844.9	1.8	23.66
ZD	900	52.37	0.0972	0.4000	6.31	5.2	99.8	21.9	849.0	2.0	13.57
ZE	900	52.29	0.0643	0.0300	6.90	7.9	100.0	23.5	849.4	2.0	23.6
ZF	950	52.35	0.2136	0.6600	6.73	2.4	99.7	25.0	847.9	2.2	13.65
ZG	950	51.55	0.1566	0.4200	7.03	3.3	99.8	26.5	838.4	2.0	23.91
ZH	1000	50.18	0.2227	0.8600	6.56	2.3	99.5	28.0	818.7	2.4	13.69
ZI	1000	50.42	0.0505	1.160	7.3	10.1	99.3	29.7	820.4	2.0	23.66
ZJ	1050	49.67	0.0500	1.390	7.4	10.2	99.2	31.5	809.7	2.0	13.73
ZK	1050	50.09	0.0356	1.650	8.9	14.3	99.0	33.6	814.1	3.3	23.73
ZL	1120	49.56	0.1040	5.430	16.2	4.9	96.8	37.5	792.3	3.2	13.64
ZM	1120	52.55	0.0728	5.710	17.2	7.0	96.8	41.7	830.8	2.3	23.69
ZN	1120	53.26	0.0704	6.156	29.5	7.2	96.6	49.3	838.5	1.7	58.18
ZO	1120	53.79	0.0717	6.497	36.2	7.1	96.4	59.2	844.1	1.7	118.2
ZP	1120	53.06	0.0495	5.849	43.1	10.3	96.8	71.7	836.9	1.9	238.2
ZQ	1200	51.74	0.0271	4.562	35.5	18.8	97.4	82.8	824.6	1.8	8.286
ZR	1300	56.86	0.0170	3.370	29.8	30.0	98.3	92.7	895.3	1.8	8.692
ZS	1400	53.94	0.0250	3.440	4.80	20.4	98.1	94.4	857.6	4.0	8.693
ZT	1690	55.32	0.0449	5.710	16.1	11.4	97.0	100.0	866.7	1.8	8.326
Total gas age ± 1σ			n=46		387.8	9.9		K2O=5.59%	804.2	1.7	

ID	Temp (°C)	$^{40}Ar/^{39}Ar$	$^{37}Ar/^{39}Ar$	$^{36}Ar/^{39}Ar$ (x 10^{-3})	$^{39}Ar_K$ (x 10^{-15} mol)	K/Ca	$^{40}Ar^*$ (%)	^{39}Ar (%)	Age (Ma)	±1σ (Ma)	Time (min)
H03PV007c, K-feldspar, 2.62 mg, J=0.0189074±0.10%, D=1.007±0.001, NM-171, Lab#=54330-01											
A	450	219.2	0.0655	692.4	1.34	7.8	6.7	0.3	445.0	42.0	12.56
B	450	46.05	0.0010	103.5	0.484	510.2	33.5	0.3	467.0	26.0	22.7
C	450	37.93	-0.0100	69.50	0.348	-	45.8	0.4	519.0	35.0	31.13
D	450	35.68	-0.0340	63.30	0.341	-	47.6	0.5	508.0	29.0	47.69
E	500	22.41	0.0090	17.90	0.434	56.7	76.3	0.6	511.0	20.0	12.44
F	500	21.30	0.0310	17.90	0.537	16.5	75.2	0.7	482.0	19.0	22.54
G	500	23.21	0.0170	16.60	0.506	30.0	78.9	0.8	542.0	18.0	30.86
H	500	25.16	0.0363	25.40	0.546	14.1	70.1	0.9	525.0	17.0	47.51
I	550	28.55	0.0460	35.10	0.659	11.1	63.6	1.0	539.0	16.0	12.24
J	550	20.64	0.0676	2.800	0.80	7.5	96.0	1.1	580.6	10.0	22.33
K	550	21.91	0.0589	2.900	0.72	8.7	96.1	1.3	611.0	11.0	30.72
L	550	24.60	0.0783	6.600	0.81	6.5	92.0	1.4	650.0	10.0	47.31
M	600	41.10	0.1008	60.40	0.92	5.1	56.6	1.6	665.0	14.0	11.99
N	600	31.12	0.1296	24.40	1.13	3.9	76.9	1.8	680.9	9.2	22.03
O	600	30.56	0.1304	15.00	1.04	3.9	85.5	2.0	732.9	8.5	30.33
P	600	27.10	0.1275	2.010	1.13	4.0	97.8	2.2	741.6	7.1	47.05
Q	650	46.69	0.2439	64.50	1.30	2.1	59.2	2.5	767.3	7.9	11.65
R	650	29.71	0.1561	0.6500	1.46	3.3	99.4	2.8	809.5	5.6	21.68
S	650	30.40	0.1244	0.6400	1.42	4.1	99.4	3.1	824.8	6.0	30.1
T	700	53.22	0.1811	77.93	2.43	2.8	56.7	3.5	824.5	6.8	12.31
U	700	34.04	0.1202	8.450	2.57	4.2	92.7	4.0	853.8	4.2	22.3
V	700	32.20	0.1091	0.4000	2.44	4.7	99.7	4.5	865.5	3.4	30.83
W	750	43.45	0.1249	41.55	3.91	4.1	71.7	5.3	845.7	4.8	12.21
X	750	35.35	0.1042	12.78	4.71	4.9	89.3	6.2	854.5	3.0	22.33
Y	750	32.80	0.1016	2.800	4.31	5.0	97.5	7.0	863.0	2.7	30.64
Z	800	35.91	0.1211	15.03	5.51	4.2	87.7	8.1	852.2	3.1	12.62
ZA	800	36.46	0.1259	15.85	6.28	4.1	87.2	9.4	858.9	2.8	22.78
ZB	850	44.86	0.1190	48.33	19.4	4.3	68.2	13.3	832.8	3.1	12.54
ZC	850	34.31	0.1535	9.270	12.8	3.3	92.1	15.9	854.5	1.8	22.56
ZD	900	33.86	0.1510	10.10	55.5	3.4	91.2	27.6	839.5	1.4	12.87
ZE	900	32.75	0.3717	3.450	19.8	1.4	97.0	32.0	858.4	1.6	22.89
ZF	950	32.82	0.7450	4.187	24.5	0.68	96.4	37.4	856.2	1.8	12.73
ZG	950	31.53	0.2128	3.594	22.5	2.4	96.7	42.6	830.6	1.6	23.18
ZH	1000	31.25	0.1825	3.624	29.7	2.8	96.6	49.6	824.3	1.5	13.19
ZI	1000	30.94	0.1451	3.702	35.8	3.5	96.5	58.4	816.8	1.4	23.33
ZJ	1050	30.80	0.1744	4.266	35.0	2.9	96.0	67.3	810.1	1.4	13.34
ZK	1050	30.94	0.1959	5.317	34.5	2.6	95.0	76.3	806.3	1.3	23.26
ZL	1100	31.08	0.4338	5.810	16.3	1.2	94.6	80.8	806.8	1.5	13.54
ZM	1100	31.36	0.4806	7.360	14.4	1.1	93.2	84.7	803.0	1.7	23.55
ZN	1100	32.27	0.5794	8.330	13.6	0.88	92.5	88.6	817.1	2.0	58.52
ZO	1100	33.96	0.9274	11.62	9.4	0.55	90.1	91.3	833.6	2.0	118.5
ZP	1100	37.24	1.252	17.87	6.86	0.41	86.1	93.2	865.6	2.9	238.5
ZQ	1200	46.93	1.913	16.24	1.86	0.27	90.2	93.8	1074.0	5.9	8.437
ZR	1250	39.62	1.812	7.230	1.14	0.28	95.0	94.1	982.1	7.2	8.432
ZS	1350	35.80	0.8430	8.180	6.72	0.61	93.5	96.1	895.0	2.6	8.614
ZT	1700	36.63	1.312	10.49	13.3	0.39	91.9	100.0	899.3	1.6	8.258
Total gas age ± 1σ			n=46		421.1	1.5		K2O=3.27%	818.7	1.2	

ID	Temp (°C)	$^{40}Ar/^{39}Ar$	$^{37}Ar/^{39}Ar$	$^{36}Ar/^{39}Ar$ (x 10^{-3})	$^{39}Ar_K$ (x 10^{-15} mol)	K/Ca	$^{40}Ar^*$ (%)	^{39}Ar (%)	Age (Ma)	±1σ (Ma)	Time (min)
PVBR02-31, K-feldspar, 1.98 mg, J=0.0190443±0.10%, D=1.0052±0.00172, NM-157, Lab#=53536-01											
A	450	73.78	0.0133	74.94	2.47	38.3	70.0	0.2	1250.1	6.5	13.31
B	450	20.06	0.0049	15.68	1.36	104.1	76.9	0.3	469.6	6.9	23.33
C	450	17.77	0.0052	11.18	1.91	98.7	81.4	0.4	443.4	4.6	31.69
D	450	17.59	-0.0005	8.870	1.38	-	85.1	0.5	457.1	5.4	48.39
E	500	19.09	0.0036	5.610	2.30	141.7	91.3	0.7	522.7	3.7	13.06
F	500	18.29	0.0050	4.870	3.72	102.0	92.1	1.0	507.5	2.5	23.29
G	500	18.70	0.0036	3.800	2.84	141.3	94.0	1.2	526.6	3.1	31.54
H	500	19.67	0.0036	3.890	3.27	142.9	94.2	1.5	550.8	2.8	48.24
I	550	23.61	0.0031	4.710	4.13	163.0	94.1	1.8	643.6	2.4	11.9
J	550	21.59	0.0043	1.960	5.70	120.0	97.3	2.2	614.0	1.9	22.88
K	550	22.85	0.0026	1.790	5.16	200.1	97.7	2.6	646.2	1.9	31.45
L	550	23.91	0.0038	1.910	4.89	136.1	97.6	3.0	670.8	2.2	47.95
M	600	26.93	0.0041	4.210	6.77	126.0	95.4	3.5	726.5	2.2	12.84
N	600	25.59	0.0031	1.123	7.6	164.6	98.7	4.1	716.4	2.0	22.91
O	600	26.53	0.0032	1.290	5.64	158.9	98.6	4.6	737.3	2.0	31.24
P	600	26.92	0.0030	0.9800	6.61	173.0	98.9	5.1	748.3	2.1	47.93
Q	650	28.33	0.0032	2.570	6.98	162.0	97.3	5.6	770.0	2.2	13.32
R	650	27.95	0.0027	0.6210	8.4	191.1	99.3	6.3	774.4	1.9	23.3
S	650	28.71	0.0028	0.6910	7.5	182.9	99.3	6.9	791.2	2.0	31.69
T	700	29.32	0.0038	0.8700	8.2	134.3	99.1	7.6	803.8	2.3	13.21
U	700	29.37	0.0034	0.7600	8.9	152.3	99.2	8.3	805.5	1.9	23.21
V	700	29.54	0.0032	0.6300	8.7	162.0	99.4	9.0	810.2	2.2	31.62
W	750	29.86	0.0052	0.7500	9.8	98.9	99.3	9.8	816.5	1.7	13.48
X	750	29.95	0.0043	0.1650	10.7	119.5	99.8	10.7	822.3	1.6	23.54
Y	750	30.04	0.0045	0.4860	11.1	113.1	99.5	11.6	822.2	1.7	31.9
Z	800	30.02	0.0091	0.6000	10.5	56.2	99.4	12.5	821.1	1.7	13.42
ZA	800	30.13	0.0057	0.6470	12.1	88.9	99.4	13.5	823.2	1.6	23.48
ZB	850	29.96	0.0133	0.5060	16.0	38.2	99.5	14.8	820.4	1.7	13.65
ZC	850	29.90	0.0071	0.3360	16.0	72.3	99.7	16.2	820.2	1.7	23.66
ZD	900	29.70	0.0233	0.6410	15.0	21.9	99.4	17.5	813.7	1.5	13.56
ZE	900	29.52	0.0102	0.6290	13.6	49.9	99.4	18.7	809.9	1.6	23.58
ZF	950	29.10	0.0141	0.7590	16.4	36.3	99.2	20.2	799.4	1.6	13.73
ZG	950	28.83	0.0050	0.7730	17.0	102.2	99.2	21.7	793.3	1.7	23.63
ZH	1000	28.59	0.0074	1.080	15.7	69.1	98.9	23.1	785.8	1.5	13.65
ZI	1000	28.50	0.0056	0.8630	16.3	90.6	99.1	24.6	785.4	1.6	23.68
ZJ	1050	29.02	0.0171	1.773	15.3	29.9	98.2	26.0	791.1	1.7	13.79
ZK	1050	29.13	0.0146	1.383	18.3	34.9	98.6	27.7	796.2	1.6	23.78
ZL	1110	28.83	0.0354	1.902	20.7	14.4	98.1	29.7	785.8	1.6	13.71
ZM	1110	28.52	0.0179	2.225	31.3	28.5	97.7	32.8	776.6	1.5	23.64
ZN	1110	28.11	0.0088	2.445	83.8	58.2	97.4	41.2	765.7	1.6	61.48
ZO	1110	29.01	0.0078	2.806	142.0	65.7	97.1	56.9	783.9	1.7	136.4
ZP	1110	30.22	0.0083	3.176	118.6	61.6	96.9	71.4	808.6	1.8	248.5
ZQ	1200	32.61	0.0039	2.454	136.2	130.0	97.8	89.9	865.7	1.8	8.281
ZR	1300	34.54	0.0077	3.395	68.0	65.9	97.1	100.0	901.2	1.8	8.78
Total gas age ± 1σ			n=44		928.9	61.1		K2O=9.46%	794.6	1.4	

ID	Temp (°C)	$^{40}Ar/^{39}Ar$	$^{37}Ar/^{39}Ar$	$^{36}Ar/^{39}Ar$ (x 10^{-3})	$^{39}Ar_K$ (x 10^{-15} mol)	K/Ca	$^{40}Ar^*$ (%)	^{39}Ar (%)	Age (Ma)	±1σ (Ma)	Time (min)
RP-90A, K-feldspar, 1.3 mg, J=0.0153813±0.10%, D=1.00461±0.00118, NM-102, Lab#=50035-01											
A	450	42.98	0.0069	77.60	1.31	73.9	46.6	0.3	490.3	7.8	18.57
B	450	18.28	-0.0260	16.31	0.972	-	73.6	0.6	343.1	4.7	26.67
C	500	16.83	-0.0206	6.870	1.64	-	87.9	1.0	373.8	2.6	17.16
D	500	17.35	-0.0129	4.480	2.36	-	92.4	1.7	401.7	2.0	27.52
E	550	21.45	0.0043	2.540	4.43	118.7	96.5	2.8	504.2	1.3	17.1
F	550	24.17	0.0013	2.130	5.15	392.5	97.4	4.2	563.7	1.2	27.25
G	600	28.26	0.0074	1.581	7.59	68.9	98.4	6.2	649.5	1.2	17.59
H	600	30.20	0.0048	1.655	6.51	106.3	98.4	7.9	686.8	1.3	27.7
I	650	32.65	0.0066	1.561	7.54	77.3	98.6	9.9	733.9	1.2	17.38
J	650	32.92	0.0051	1.720	4.46	100.0	98.5	11.0	738.2	1.4	27.38
K	700	33.56	0.0163	1.685	5.65	31.3	98.5	12.5	750.3	1.4	18.19
L	700	33.50	0.0080	2.430	4.09	63.8	97.9	13.6	745.0	1.6	28.22
M	750	33.08	0.0136	2.120	4.32	37.5	98.1	14.7	738.9	1.3	18.05
N	750	33.33	0.0112	2.710	3.61	45.6	97.6	15.6	740.4	2.0	28.1
O	800	32.97	0.0123	3.070	1.86	41.5	97.3	16.1	731.7	2.6	8.039
P	850	33.00	0.0491	3.010	4.77	10.4	97.3	17.3	732.5	1.4	8.079
Q	900	32.69	0.0775	1.831	7.55	6.6	98.4	19.2	733.4	1.2	7.986
R	950	32.00	0.0505	1.602	9.64	10.1	98.5	21.7	721.7	1.1	7.84
S	1000	31.43	0.0218	1.793	12.8	23.4	98.3	24.9	709.6	1.2	7.843
T	1050	30.75	0.0241	2.784	24.6	21.1	97.3	31.1	691.1	1.2	7.858
U	1100	31.98	0.0370	3.741	23.2	13.8	96.6	36.8	709.2	1.6	8.23
V	1100	32.86	0.0351	3.144	61.8	14.5	97.2	51.8	729.2	1.7	28.01
W	1100	33.65	0.0188	1.804	81.7	27.2	98.4	70.7	751.5	3.8	57.71
X	1100	34.47	0.0085	1.816	70.9	60.0	98.5	86.5	766.6	1.5	117.9
Y	1100	36.38	0.0060	3.141	41.6	84.8	97.5	95.5	794.3	1.6	237.7
Z	1100	41.16	1.100	14.84	12.0	0.46	89.6	98.1	820.4	2.6	16.56
ZA	1200	36.60	-0.0053	3.550	2.38	-	97.1	98.6	796.1	2.4	8.16
ZB	1300	35.58	-0.0037	3.570	3.20	-	97.0	99.3	777.3	2.0	8.493
ZC	1350	35.97	-0.0226	6.920	1.61	-	94.3	99.6	766.4	2.8	8.732
ZD	1400	38.88	-0.0071	13.35	1.37	-	89.9	99.9	784.8	3.7	8.505
ZE	1650	796.1	-0.0560	2551.0	0.309	-	5.3	100.0	916.0	81.0	7.871
Total gas age ± 1σ			n=31		421.0	10.4		K2O=8.09%	727.7	1.3	

ID	Temp (°C)	$^{40}Ar/^{39}Ar$	$^{37}Ar/^{39}Ar$	$^{36}Ar/^{39}Ar$ (x 10^{-3})	$^{39}Ar_K$ (x 10^{-15} mol)	K/Ca	$^{40}Ar^*$ (%)	^{39}Ar (%)	Age (Ma)	±1σ (Ma)	Time (min)
PVSDC02-6B, K-feldspar, 2.51 mg, J=0.0185198±0.10%, D=1.0052±0.00172, NM-157, Lab#=53541-01											
A	450	37.20	0.0671	86.28	2.03	7.6	31.4	0.2	357.7	9.2	13.27
B	450	19.92	0.0334	16.17	1.19	15.3	76.0	0.3	450.6	6.4	23.22
C	450	18.86	0.0339	11.12	1.14	15.1	82.6	0.3	462.0	5.9	31.59
D	450	18.81	0.0259	8.010	1.31	19.7	87.4	0.4	484.8	4.1	48.29
E	500	19.20	0.0281	2.720	1.52	18.2	95.8	0.6	534.7	2.9	13.08
F	500	19.28	0.0259	3.060	2.16	19.7	95.3	0.7	534.1	3.3	23.19
G	500	20.43	0.0244	2.360	2.06	20.9	96.6	0.9	568.1	2.7	31.37
H	500	21.65	0.0167	1.960	2.32	30.6	97.3	1.1	600.8	2.9	48.23
I	550	23.40	0.0314	3.560	2.48	16.3	95.5	1.3	631.8	2.7	12.92
J	550	23.98	0.0397	1.700	2.94	12.8	97.9	1.5	658.6	2.4	23.07
K	550	25.14	0.0551	1.830	2.69	9.3	97.9	1.7	684.8	2.4	31.19
L	550	25.81	0.0446	1.560	2.89	11.4	98.2	1.9	702.3	2.8	48.06
M	600	27.37	0.0517	4.510	2.68	9.9	95.1	2.2	718.0	2.7	12.71
N	600	27.44	0.0376	0.8800	3.16	13.6	99.1	2.4	743.8	2.4	22.88
O	600	28.27	0.0362	0.2900	3.09	14.1	99.7	2.6	766.4	2.5	31.15
P	600	28.87	0.0278	1.260	2.98	18.4	98.7	2.9	773.2	2.8	47.8
Q	650	28.97	0.0445	4.350	2.63	11.5	95.6	3.1	755.2	3.2	13.24
R	650	29.28	0.0355	0.9200	2.84	14.4	99.1	3.3	784.7	2.3	23.36
S	650	29.57	0.0290	0.3800	2.49	17.6	99.6	3.5	794.4	2.8	31.62
T	700	28.93	0.0435	2.540	3.08	11.7	97.4	3.8	766.3	2.8	13.21
U	700	29.50	0.0363	0.4900	2.89	14.0	99.5	4.0	792.2	2.5	23.19
V	700	29.77	0.0360	0.9200	2.49	14.2	99.1	4.2	795.4	3.1	31.54
W	750	28.82	0.0409	2.070	2.81	12.5	97.9	4.4	766.9	2.7	13.5
X	750	29.45	0.0391	0.1800	2.87	13.0	99.8	4.7	793.2	2.5	23.53
Y	750	29.05	0.0348	0.7900	2.60	14.7	99.2	4.9	780.3	2.6	31.83
Z	800	28.72	0.0627	1.490	2.62	8.1	98.5	5.1	768.7	2.7	13.29
ZA	800	29.17	0.0549	0.6600	3.09	9.3	99.4	5.3	783.8	3.0	23.38
ZB	850	28.92	0.1004	2.180	3.65	5.1	97.8	5.6	768.6	2.4	13.51
ZC	850	29.06	0.0725	1.350	4.11	7.0	98.6	6.0	777.1	2.3	23.57
ZD	900	28.85	0.1425	2.500	6.30	3.6	97.5	6.5	765.0	2.1	13.49
ZE	900	29.04	0.1340	1.050	6.41	3.8	99.0	7.0	778.8	1.9	23.54
ZF	950	27.78	0.3190	2.466	10.0	1.6	97.5	7.9	741.7	1.8	13.67
ZG	950	27.76	0.1178	0.9380	8.7	4.3	99.0	8.6	750.9	1.7	23.72
ZH	1000	25.80	0.0718	1.549	13.3	7.1	98.3	9.7	702.0	1.6	13.62
ZI	1000	26.27	0.0458	1.321	13.6	11.1	98.5	10.9	714.5	1.5	23.66
ZJ	1050	24.98	0.0535	1.633	23.5	9.5	98.1	12.9	682.6	1.5	13.77
ZK	1050	25.94	0.0490	1.556	20.4	10.4	98.2	14.8	705.4	1.5	23.67
ZL	1120	25.61	0.1048	2.268	65.4	4.9	97.4	20.8	693.0	1.5	13.63
ZM	1120	25.96	0.0707	1.840	56.0	7.2	97.9	26.2	703.9	1.4	23.65
ZN	1120	26.44	0.0480	1.560	79.9	10.6	98.3	34.4	716.8	1.8	58.17
ZO	1120	26.66	0.0335	1.292	131.9	15.3	98.6	49.2	723.6	1.9	118.1
ZP	1120	27.12	0.0209	1.222	167.1	24.4	98.7	71.0	734.4	1.9	238.1
ZQ	1200	27.64	0.0063	0.8460	78.7	81.4	99.1	82.6	748.5	1.8	8.256
ZR	1300	28.08	0.0132	0.7140	55.1	38.7	99.3	91.3	759.2	1.6	8.536
ZS	1400	28.01	0.0237	0.6790	19.2	21.5	99.3	94.4	758.0	1.4	8.783
ZT	1690	28.12	0.0264	1.430	32.9	19.3	98.5	100.0	755.5	1.4	8.289
Total gas age ± 1σ			n=46		863.2	11.5		K2O=7.13%	717.4	1.3	

ID	Temp (°C)	$^{40}Ar/^{39}Ar$	$^{37}Ar/^{39}Ar$	$^{36}Ar/^{39}Ar$ (x 10^{-3})	$^{39}Ar_K$ (x 10^{-15} mol)	K/Ca	$^{40}Ar^*$ (%)	^{39}Ar (%)	Age (Ma)	±1σ (Ma)	Time (min)
PVBR02-7, K-feldspar, 2.34 mg, J=0.0185266±0.10%, D=1.0052±0.00172, NM-157, Lab#=53542-01											
A	450	64.28	0.0039	141.0	5.10	129.5	35.2	0.2	638.4	9.5	13.22
B	450	19.13	0.0044	33.65	4.00	114.9	47.9	0.4	286.0	5.1	23.24
C	450	15.55	0.0028	20.51	3.28	183.5	61.0	0.5	295.0	3.6	31.64
D	450	14.43	0.0024	16.27	3.68	212.6	66.6	0.7	298.6	3.3	48.3
E	500	12.78	0.0034	5.410	4.10	150.1	87.5	0.8	343.1	2.2	13.06
F	500	13.46	0.0015	4.780	5.84	349.5	89.5	1.1	367.1	2.2	23.09
G	500	14.53	0.0026	5.340	5.99	194.7	89.1	1.3	391.8	1.7	31.52
H	500	15.59	0.0024	3.810	8.0	209.1	92.8	1.7	432.8	1.6	48.24
I	550	26.98	0.0024	12.27	7.9	215.3	86.6	2.0	655.8	2.5	12.87
J	550	18.59	0.0024	2.563	11.2	215.3	95.9	2.5	520.6	1.4	22.97
K	550	19.72	0.0020	1.966	10.8	259.0	97.1	2.9	553.5	1.4	31.25
L	550	21.12	0.0009	2.623	11.9	586.4	96.3	3.4	583.3	1.4	48.03
M	600	24.32	0.0020	4.470	8.8	256.4	94.6	3.8	647.4	2.0	12.78
N	600	23.00	0.0015	0.9500	10.2	347.1	98.8	4.3	640.8	2.0	22.95
O	600	24.05	0.0012	1.650	9.0	411.5	98.0	4.6	660.8	1.5	31.24
P	600	24.47	0.0011	1.801	11.0	468.1	97.8	5.1	669.5	1.6	47.88
Q	650	25.87	0.0014	3.950	8.6	377.9	95.5	5.5	687.3	1.8	13.35
R	650	25.33	0.0014	1.770	7.9	369.7	97.9	5.8	689.8	1.8	23.28
S	650	25.25	0.0014	0.9460	8.4	364.4	98.9	6.2	693.7	1.6	31.62
T	700	28.71	0.0023	8.900	8.8	221.8	90.8	6.6	719.2	2.3	13.15
U	700	24.97	0.0018	0.7440	8.2	289.9	99.1	7.0	688.6	1.6	23.27
V	700	24.94	0.0011	0.5180	6.8	451.5	99.4	7.3	689.4	1.9	31.52
W	750	31.14	0.0041	15.23	11.1	123.5	85.5	7.7	731.8	2.4	13.39
X	750	24.54	0.0018	0.7000	8.2	278.8	99.2	8.1	678.8	1.6	23.45
Y	750	24.55	0.0018	0.6250	7.7	283.4	99.3	8.5	679.6	1.5	31.82
Z	800	24.68	0.0038	1.527	7.1	134.3	98.2	8.8	676.4	1.7	13.39
ZA	800	24.64	0.0038	0.7600	8.7	135.7	99.1	9.2	680.8	1.6	21.91
ZB	850	25.48	0.0097	3.034	9.9	52.5	96.5	9.6	684.7	1.6	13.51
ZC	850	25.18	0.0081	0.9070	11.2	62.8	98.9	10.1	692.3	1.7	23.68
ZD	900	26.02	0.0206	5.020	12.3	24.8	94.3	10.7	683.6	1.7	13.41
ZE	900	25.06	0.0383	1.134	14.5	13.3	98.7	11.4	688.1	1.5	23.61
ZF	950	26.12	0.2194	5.860	18.3	2.3	93.4	12.2	680.7	1.8	13.64
ZG	950	25.32	0.0950	2.766	15.8	5.4	96.8	12.9	683.1	1.7	23.67
ZH	1000	25.75	0.0456	5.910	21.1	11.2	93.2	13.9	671.2	1.8	13.6
ZI	1000	25.44	0.0074	3.438	21.1	69.2	96.0	14.9	680.9	1.7	23.6
ZJ	1050	25.60	0.0104	4.807	28.9	49.2	94.5	16.3	675.2	1.6	13.69
ZK	1050	25.96	0.0071	4.077	34.5	72.3	95.4	18.0	688.7	1.6	23.74
ZL	1120	25.56	0.0254	3.727	38.7	20.1	95.7	19.9	681.8	1.4	13.6
ZM	1120	26.15	0.0120	2.507	30.9	42.7	97.2	21.5	703.7	1.5	23.57
ZN	1120	26.19	0.0144	2.212	69.2	35.3	97.5	25.0	706.6	1.5	71.12
ZO	1120	26.61	0.0204	2.882	64.8	25.0	96.8	28.4	711.7	1.4	119.3
ZP	1120	27.03	0.0162	3.674	94.4	31.5	96.0	33.6	716.1	1.6	238.1
ZQ	1200	26.24	0.0202	3.918	45.2	25.3	95.6	36.2	696.3	1.7	8.257
ZR	1300	27.48	0.0019	5.017	582.4	262.2	94.6	74.9	717.3	2.0	8.751
ZS	1400	27.72	0.0016	7.096	116.4	317.5	92.4	84.2	708.7	1.6	8.686
ZT	1690	28.45	0.0014	6.811	181.3	356.8	92.9	100.0	727.2	1.6	8.347
Total gas age ± 1σ			n=46		1623.1	50.7		K2O=14.38%	689.3	1.5	

ID	Temp (°C)	$^{40}Ar/^{39}Ar$	$^{37}Ar/^{39}Ar$	$^{36}Ar/^{39}Ar$ (x 10^{-3})	$^{39}Ar_K$ (x 10^{-15} mol)	K/Ca	$^{40}Ar^*$ (%)	^{39}Ar (%)	Age (Ma)	±1σ (Ma)	Time (min)
PVHD02-1, K-feldspar, 2.03 mg, J=0.0188467±0.10%, D=1.0052±0.00172, NM-157, Lab#=53534-01											
A	450	37.97	0.0373	102.6	5.40	13.7	20.1	0.5	245.4	9.9	13.26
B	450	14.18	0.0110	22.78	3.41	46.4	52.5	0.8	239.1	4.4	23.2
C	450	12.91	0.0071	15.91	3.38	71.9	63.5	1.1	261.8	4.1	31.66
D	450	12.75	0.0061	12.95	4.01	83.2	69.9	1.4	282.8	2.9	48.31
E	500	12.70	0.0166	6.160	4.67	30.7	85.7	1.8	339.8	2.3	13.12
F	500	12.74	0.0101	4.200	6.54	50.5	90.2	2.4	357.2	2.0	23.05
G	500	13.16	0.0085	3.640	6.64	59.8	91.8	3.0	373.8	2.2	31.51
H	500	13.77	0.0073	3.350	7.5	69.9	92.8	3.6	393.2	1.9	47.98
I	550	14.95	0.0096	3.150	6.52	53.1	93.8	4.2	427.3	1.8	12.6
J	550	15.08	0.0071	1.977	8.6	72.2	96.1	5.0	440.2	1.7	22.87
K	550	15.27	0.0056	1.890	7.8	91.4	96.3	5.7	446.0	1.5	31.3
L	550	15.73	0.0050	2.070	8.2	101.6	96.1	6.4	456.9	1.5	47.97
M	600	17.06	0.0072	3.000	6.45	70.8	94.8	7.0	485.0	1.9	12.72
N	600	16.98	0.0082	1.827	8.0	62.3	96.8	7.8	491.9	1.5	22.79
O	600	17.37	0.0070	1.610	7.3	73.1	97.3	8.4	504.1	1.9	31.21
P	600	17.72	0.0071	1.790	7.7	72.3	97.0	9.1	511.6	1.5	47.86
Q	650	18.78	0.0080	2.220	5.72	63.7	96.5	9.7	535.8	1.9	13.16
R	650	18.64	0.0080	1.380	6.9	64.1	97.8	10.3	538.6	1.7	23.32
S	650	19.02	0.0069	1.310	6.33	73.5	98.0	10.9	548.9	1.8	31.68
T	700	19.68	0.0096	2.140	6.49	53.0	96.8	11.5	559.3	1.9	13.22
U	700	19.58	0.0072	1.250	6.80	71.1	98.1	12.2	563.5	1.7	23.18
V	700	19.69	0.0072	1.540	5.73	71.2	97.7	12.7	564.2	1.6	31.6
W	750	19.97	0.0075	2.850	5.64	68.2	95.8	13.3	561.3	2.0	13.45
X	750	20.16	0.0063	1.630	5.83	80.7	97.6	13.8	575.4	2.0	23.56
Y	750	20.29	0.0081	1.590	5.07	63.0	97.7	14.3	578.9	2.0	31.79
Z	800	20.63	0.0107	4.080	5.46	47.6	94.2	14.9	569.0	2.1	13.39
ZA	800	20.63	0.0099	1.920	6.01	51.4	97.3	15.5	584.9	2.0	23.46
ZB	850	20.85	0.0236	4.420	9.0	21.6	93.7	16.4	571.9	1.9	13.6
ZC	850	21.32	0.0197	2.490	8.8	25.9	96.6	17.2	598.0	1.6	23.56
ZD	900	21.01	0.0287	5.368	13.8	17.8	92.5	18.6	569.0	1.6	13.48
ZE	900	21.21	0.0231	3.218	14.2	22.1	95.5	20.1	589.9	1.5	23.47
ZF	950	20.69	0.0334	5.230	23.6	15.3	92.5	22.5	561.8	1.6	13.72
ZG	950	21.08	0.0123	3.667	24.2	41.6	94.9	25.1	583.3	1.4	23.69
ZH	1000	20.69	0.0098	4.262	35.0	52.2	93.9	28.9	569.0	1.3	13.63
ZI	1000	21.36	0.0084	3.195	33.2	60.7	95.6	32.6	593.7	1.4	23.48
ZJ	1050	21.19	0.0129	3.880	45.9	39.5	94.6	38.0	584.5	1.4	13.77
ZK	1050	22.25	0.0128	3.049	33.9	39.7	96.0	42.1	616.7	1.3	23.69
ZL	1120	22.59	0.0259	3.499	104.2	19.7	95.5	55.5	622.0	1.5	13.61
ZM	1120	22.85	0.0133	2.970	107.1	38.4	96.2	70.9	632.1	1.2	23.64
ZN	1120	23.82	0.0101	2.580	107.1	50.4	96.8	88.1	658.3	1.4	70.94
ZO	1120	25.35	0.0072	2.558	50.5	71.1	97.0	97.0	694.8	1.6	136.1
ZP	1120	28.00	0.0052	4.060	14.8	97.9	95.7	99.7	745.8	1.6	238.2
ZQ	1200	28.78	-0.0013	2.150	1.96	-	97.8	100.0	776.5	3.5	8.145
Total gas age ± 1σ			n=43		795.3	36.9		K2O=7.99%	587.0	1.2	

ID	Temp (°C)	$^{40}Ar/^{39}Ar$	$^{37}Ar/^{39}Ar$	$^{36}Ar/^{39}Ar$ (x 10^{-3})	$^{39}Ar_K$ (x 10^{-15} mol)	K/Ca	$^{40}Ar^*$ (%)	^{39}Ar (%)	Age (Ma)	±1σ (Ma)	Time (min)
PV03-01 ksp, L4:164, K-Feldspar, 1.58 mg, J=0.0162956±0.09%, D=1.00484±0.00092, NM-164, Lab#=54025-01											
A	450	9.790	0.0839	10.17	8.7	6.1	69.3	1.7	191.1	1.7	13.03
B	450	11.48	0.0552	8.360	3.48	9.2	78.5	2.4	249.6	3.0	23.16
C	450	12.21	0.0425	9.280	2.84	12.0	77.5	3.0	261.5	3.1	31.48
D	450	12.46	0.0464	7.770	3.04	11.0	81.6	3.6	279.3	3.6	48.13
E	500	14.19	0.0506	10.20	2.82	10.1	78.7	4.1	304.9	3.0	12.98
F	500	12.06	0.0489	3.320	3.67	10.4	91.9	4.9	302.4	2.5	23.09
G	500	12.68	0.0478	3.060	3.22	10.7	92.9	5.5	320.0	2.5	31.37
H	500	13.41	0.0506	4.190	3.39	10.1	90.8	6.2	329.9	2.4	48.1
I	550	13.58	0.0651	3.270	2.86	7.8	92.9	6.8	340.8	2.5	12.84
J	550	13.86	0.0610	1.940	3.44	8.4	95.9	7.5	357.5	2.4	22.98
K	550	14.36	0.0694	2.280	2.97	7.4	95.3	8.1	367.1	2.4	31.23
L	550	14.69	0.0686	2.440	3.09	7.4	95.1	8.8	373.9	2.6	48.03
M	600	14.92	0.2847	2.850	2.42	1.8	94.5	9.3	377.1	2.8	12.64
N	600	15.04	0.6740	4.490	3.38	0.76	91.5	10.0	369.2	2.5	22.86
O	600	15.61	0.8858	3.760	2.99	0.58	93.3	10.6	388.7	2.4	31.14
P	600	15.81	0.8080	3.160	3.01	0.63	94.5	11.2	397.5	2.2	47.71
Q	650	15.32	2.149	2.900	2.45	0.24	95.5	11.8	390.5	2.8	13.18
R	650	15.77	0.4744	1.550	2.58	1.1	97.3	12.3	407.2	2.5	23.22
S	650	15.97	0.1821	1.590	2.44	2.8	97.1	12.8	411.0	3.0	31.65
T	700	15.79	1.139	2.230	2.51	0.45	96.4	13.4	404.3	2.7	13.09
U	700	15.95	0.1931	1.020	3.01	2.6	98.2	14.0	414.5	2.3	23.12
V	700	16.23	0.1704	2.020	2.87	3.0	96.4	14.6	414.2	2.3	31.53
W	750	15.75	0.7328	0.9800	3.18	0.70	98.5	15.3	411.2	2.2	13.44
X	750	16.04	0.2576	1.160	3.69	2.0	98.0	16.1	416.0	2.0	23.25
Y	750	16.12	0.2400	1.250	3.55	2.1	97.8	16.9	417.2	1.8	31.69
Z	800	15.76	0.3740	0.7200	4.07	1.4	98.8	17.8	412.5	1.6	13.31
ZA	800	15.99	0.2661	1.280	4.59	1.9	97.8	18.8	413.9	1.7	23.37
ZB	850	15.63	0.2304	1.100	8.1	2.2	98.0	20.6	406.5	1.4	13.42
ZC	850	15.82	0.1062	0.4100	9.2	4.8	99.3	22.7	415.5	1.1	23.59
ZD	900	15.87	0.1125	0.5610	16.2	4.5	99.0	26.5	415.83	0.88	13.4
ZE	900	15.90	0.0740	0.4580	18.2	6.9	99.2	30.8	416.97	0.84	23.44
ZF	950	15.90	0.0787	0.5420	28.6	6.5	99.0	37.8	416.52	0.70	13.47
ZG	950	15.92	0.0513	0.5330	28.8	9.9	99.0	45.2	417.00	0.74	23.62
ZH	1000	15.87	0.0586	0.5740	31.6	8.7	99.0	53.7	415.56	0.63	13.41
ZI	1000	16.04	0.0623	0.6340	28.9	8.2	98.9	61.8	419.13	0.55	23.51
ZJ	1050	16.10	0.1160	0.7640	28.1	4.4	98.7	70.2	419.79	0.74	13.69
ZK	1050	16.44	0.1544	0.8860	21.0	3.3	98.5	76.7	427.00	0.81	23.6
ZL	1100	16.50	0.4535	1.125	19.6	1.1	98.2	82.9	427.4	1.3	13.46
ZM	1100	16.50	0.3080	1.259	15.9	1.7	97.9	88.2	426.31	0.97	23.59
ZN	1100	16.44	0.3341	1.687	16.5	1.5	97.1	93.8	421.8	1.0	58.07
ZO	1100	18.73	0.4581	4.840	8.1	1.1	92.6	96.7	453.8	1.5	118
ZP	1100	21.65	0.3151	12.69	5.24	1.6	82.8	98.5	467.6	2.4	238
ZQ	1200	15.33	0.1985	-0.1000	1.87	2.6	100.3	99.2	407.8	3.1	8.098
ZR	1250	17.24	0.4635	-1.5000	0.397	1.1	102.8	99.4	463.0	12.0	8.759
ZS	1350	18.73	0.4879	1.740	1.66	1.0	97.5	100.0	475.1	3.4	8.805
Total gas age ± 1σ			n=45		378.3	2.6		K2O=5.64%	400.00	0.53	

ID	Temp (°C)	$^{40}Ar/^{39}Ar$	$^{37}Ar/^{39}Ar$	$^{36}Ar/^{39}Ar$ (x 10^{-3})	$^{39}Ar_K$ (x 10^{-15} mol)	K/Ca	$^{40}Ar^*$ (%)	^{39}Ar (%)	Age (Ma)	±1σ (Ma)	Time (min)
H03PV007b, K-feldspar, 1.86 mg, J=0.0190268±0.10%, D=1.007±0.001, NM-171, Lab#=54327-01											
A	450	83.91	0.0353	271.5	3.88	14.5	4.4	0.6	123.0	20.0	11.8
B	450	22.50	0.0139	60.30	1.91	36.7	20.7	0.9	155.0	11.0	22.42
C	450	16.24	0.0103	37.70	1.61	49.5	31.3	1.2	169.0	10.0	30.64
D	450	14.47	0.0088	26.87	1.75	58.0	45.0	1.4	212.8	9.1	47.32
E	500	11.59	0.0181	13.98	2.10	28.2	64.3	1.8	241.3	6.5	11.78
F	500	10.65	0.0204	9.990	2.79	25.0	72.2	2.2	248.8	4.4	22.08
G	500	10.08	0.0036	7.540	2.57	141.7	77.8	2.6	253.2	4.3	30.62
H	500	10.81	0.0178	6.950	2.48	28.7	81.0	3.0	280.6	5.3	46.64
I	550	12.20	0.0233	7.970	2.35	21.9	80.7	3.4	312.8	5.3	11.13
J	550	11.29	0.0249	3.930	2.78	20.5	89.7	3.8	321.1	4.2	21.22
K	550	11.92	0.0228	3.540	2.36	22.4	91.2	4.2	342.5	4.1	29.59
L	550	12.61	0.0180	5.090	2.44	28.3	88.1	4.6	349.3	4.7	46.29
M	600	14.54	0.0394	10.55	2.28	12.9	78.5	5.0	358.5	5.1	10.78
N	600	12.89	0.0371	2.390	2.72	13.8	94.5	5.4	380.0	3.7	20.87
O	600	13.23	0.0353	2.350	2.46	14.5	94.8	5.8	390.0	4.2	29.31
P	600	13.86	0.0373	2.740	2.55	13.7	94.2	6.2	404.2	3.8	45.82
Q	650	14.95	0.1083	6.980	1.99	4.7	86.2	6.5	399.8	5.6	10.47
R	650	13.78	0.0485	-0.0800	2.34	10.5	100.2	6.9	425.2	4.4	20.55
S	650	14.09	0.0259	1.540	2.16	19.7	96.8	7.3	420.4	4.4	28.93
T	700	16.24	0.0424	10.63	2.87	12.0	80.7	7.8	405.8	4.2	11.63
U	700	14.91	0.0196	1.540	2.73	26.0	97.0	8.2	442.8	3.7	21.63
V	700	14.65	0.0188	0.2500	2.41	27.1	99.5	8.6	446.1	4.2	29.95
W	750	15.48	0.0336	7.570	2.97	15.2	85.5	9.1	409.7	3.7	11.26
X	750	15.00	0.0383	1.960	2.99	13.3	96.2	9.6	442.0	3.2	21.32
Y	750	15.11	0.0382	2.690	2.78	13.4	94.8	10.0	439.2	3.3	29.76
Z	800	15.44	0.0953	7.820	4.43	5.4	85.1	10.8	406.7	2.9	12.04
ZA	800	15.14	0.0887	3.290	4.35	5.8	93.6	11.5	435.3	2.5	22.07
ZB	850	15.69	0.1755	8.730	9.4	2.9	83.6	13.1	406.3	2.1	11.79
ZC	850	15.31	0.1583	3.890	8.8	3.2	92.6	14.6	435.3	1.6	21.83
ZD	900	15.65	0.4247	8.439	22.4	1.2	84.3	18.4	408.3	1.4	12.15
ZE	900	14.94	0.4592	6.072	22.8	1.1	88.2	22.3	408.0	1.1	22.3
ZF	950	14.42	0.5036	7.325	38.5	1.0	85.3	29.2	383.33	0.94	12.12
ZG	950	13.96	0.0786	5.212	32.7	6.5	89.0	35.2	386.79	0.88	22.14
ZH	1000	13.78	0.0505	6.705	42.5	10.1	85.6	43.2	369.0	1.1	12.36
ZI	1000	13.72	0.0401	6.321	39.8	12.7	86.4	50.9	370.61	0.92	22.76
ZJ	1050	13.72	0.0941	7.244	47.1	5.4	84.4	60.5	362.96	0.94	12.58
ZK	1050	13.69	0.0987	7.374	37.7	5.2	84.1	68.4	360.9	1.0	22.58
ZL	1100	13.89	0.2618	8.220	20.7	1.9	82.6	72.9	360.2	1.3	12.7
ZM	1100	14.20	0.3303	9.572	25.4	1.5	80.2	78.4	357.7	1.0	22.71
ZN	1200	14.19	0.3699	8.787	38.8	1.4	81.9	87.2	364.2	1.2	8.124
ZO	1240	18.17	0.3262	21.61	3.23	1.6	65.0	88.0	369.5	4.3	7.853
ZP	1280	17.45	0.3685	22.69	3.02	1.4	61.7	88.7	339.8	5.4	8.251
ZQ	1320	15.53	0.3005	11.55	2.39	1.7	78.1	89.3	378.8	5.0	8.247
ZR	1380	14.80	0.2990	10.42	1.61	1.7	79.3	89.7	367.7	6.3	8.503
ZS	1460	13.94	0.3447	11.14	25.0	1.5	76.6	95.6	337.1	1.4	8.446
ZT	1700	15.18	0.3822	13.47	18.3	1.3	74.0	100.0	352.9	1.6	8.233
Total gas age ± 1σ			n=46		511.3	2.4		K2O=5.55%	364.95	0.78	

ID	Temp (°C)	$^{40}Ar/^{39}Ar$	$^{37}Ar/^{39}Ar$	$^{36}Ar/^{39}Ar$ (x 10^{-3})	$^{39}Ar_K$ (x 10^{-15} mol)	K/Ca	$^{40}Ar^*$ (%)	^{39}Ar (%)	Age (Ma)	±1σ (Ma)	Time (min)
H06-WB-01, K-Feldspar, 2 mg, J=0.0036118±0.19%, D=1.002±0.001, NM-194J, Lab#=56189-01											
B	440	251.5	0.2575	456.0	0.463	2.0	46.4	0.5	642.9	5.7	3
C	440	64.85	0.2132	17.43	0.284	2.4	92.1	0.7	356.6	5.6	7
D	490	70.66	0.3683	5.311	0.163	1.4	97.8	0.9	407.0	8.6	3
E	490	69.87	0.3924	-9.9789	0.146	1.3	104.3	1.0	426.6	9.9	4
F	540	109.4	0.1628	40.76	0.84	3.1	89.0	1.9	550.4	2.3	5
G	540	104.6	0.1987	0.2994	0.365	2.6	99.9	2.2	585.1	4.3	8
H	590	124.8	0.2061	18.23	0.592	2.5	95.7	2.8	654.8	3.4	5
I	590	133.6	0.2964	0.8129	0.366	1.7	99.8	3.1	718.0	5.2	8
J	640	139.3	0.3970	18.08	0.72	1.3	96.2	3.8	721.1	3.4	5
K	640	145.8	0.6252	3.197	0.488	0.82	99.4	4.3	768.9	4.1	8
L	690	143.1	1.009	13.79	1.01	0.51	97.2	5.3	743.9	2.6	5
M	690	151.2	0.4748	-0.7134	0.622	1.1	100.2	5.9	797.2	3.4	8
N	740	146.4	0.7624	9.696	1.26	0.67	98.1	7.2	763.2	2.1	5
O	740	150.1	0.2155	0.9492	0.89	2.4	99.8	8.0	789.9	2.9	8
P	790	144.4	0.4259	7.343	1.56	1.2	98.5	9.6	757.4	1.9	5
Q	790	147.6	0.1431	0.3270	1.24	3.6	99.9	10.8	779.9	2.0	8
R	840	145.6	0.1754	6.003	3.23	2.9	98.8	13.9	764.0	1.5	6
S	840	149.2	0.1760	5.640	3.13	2.9	98.9	17.0	780.3	1.5	9
T	890	143.4	0.5588	10.04	8.4	0.91	98.0	25.2	749.42	0.97	6
U	890	137.6	0.2039	4.534	3.92	2.5	99.0	29.1	731.1	1.3	9
V	940	119.9	0.1632	5.809	5.38	3.1	98.6	34.3	649.4	1.2	6
W	940	114.5	0.0829	4.874	3.45	6.2	98.7	37.7	625.1	1.4	6
X	990	104.6	0.0772	5.801	8.2	6.6	98.4	45.8	577.28	0.83	6
Y	1040	104.5	0.1838	6.725	12.5	2.8	98.1	58.0	575.16	0.86	6
Z	1090	112.6	0.2129	4.745	12.3	2.4	98.8	70.0	616.86	0.86	6
AA	1190	132.2	0.0943	3.349	12.2	5.4	99.3	82.0	708.36	0.96	6
AB	1240	129.2	0.2791	6.867	3.13	1.8	98.4	85.0	690.3	1.3	6
AC	1340	122.0	0.3177	5.623	14.8	1.6	98.7	99.5	659.16	0.93	6
AD	1640	142.0	2.791	100.8	0.526	0.18	79.2	100.0	623.3	4.0	6
Total gas age ± 1σ			n=29		102.1	2.0		K2O=5.43%	658.1	1.2	

Notes:
Isotopic ratios corrected for blank, radioactive decay, and mass discrimination, not corrected for interfering reactions.
Errors quoted for individual analyses include analytical error only, without interfering reaction or J uncertainties.
Total gas age calculated by summing isotopic measurements of all steps.
Total gas age error calculated by quadratically combining errors of isotopic measurements of all steps.
Decay constants and isotopic abundances after Steiger and Jäger (1977).
symbol preceding sample ID denotes analyses excluded from plateau age calculations.
Weight percent K_2O calculated from ^{39}Ar signal, sample weight, and instrument sensitivity.
Ages calculated relative to FC-2 Fish Canyon Tuff sanidine interlaboratory standard at 28.27 Ma
Decay Constant (LambdaK (total)) = 5.476e-10/a
Correction factors:
NM-84: $(^{39}Ar/^{37}Ar)_{Ca}$ = 0.00065 ± 5e-05, $(^{36}Ar/^{37}Ar)_{Ca}$ = 0.00026 ± 2e-05, $(^{38}Ar/^{39}Ar)_K$ = 0.0119, $(^{40}Ar/^{39}Ar)_K$ = 0.02615 ± 0.00006
NM-102: $(^{39}Ar/^{37}Ar)_{Ca}$ = 0.00077 ± 2e-05, $(^{36}Ar/^{37}Ar)_{Ca}$ = 0.00028 ± 5e-06, $(^{38}Ar/^{39}Ar)_K$ = 0.0119, $(^{40}Ar/^{39}Ar)_K$ = 0.0262 ± 0.0001
NM-145: $(^{39}Ar/^{37}Ar)_{Ca}$ = 0.0007 ± 2e-05, $(^{36}Ar/^{37}Ar)_{Ca}$ = 0.00028 ± 5e-06, $(^{38}Ar/^{39}Ar)_K$ = 0.01077, $(^{40}Ar/^{39}Ar)_K$ = 0.0002 ± 0.0003
NM-157: $(^{39}Ar/^{37}Ar)_{Ca}$ = 0.0007 ± 2e-05, $(^{36}Ar/^{37}Ar)_{Ca}$ = 0.00027 ± 5e-06, $(^{38}Ar/^{39}Ar)_K$ = 0.01077, $(^{40}Ar/^{39}Ar)_K$ = 0.0316 ± 0.0002
NM-158: $(^{39}Ar/^{37}Ar)_{Ca}$ = 0.00075 ± 3e-05, $(^{36}Ar/^{37}Ar)_{Ca}$ = 0.000292 ± 6e-06, $(^{38}Ar/^{39}Ar)_K$ = 0.01077, $(^{40}Ar/^{39}Ar)_K$ = 0.0296 ± 0.0005
NM-164: $(^{39}Ar/^{37}Ar)_{Ca}$ = 0.0007 ± 5e-05 , $(^{36}Ar/^{37}Ar)_{Ca}$ = 0.00027 ± 1e-05, $(^{38}Ar/^{39}Ar)_K$ = 0.01077, $(^{40}Ar/^{39}Ar)_K$ = 0.02559 ± 0.001487
NM-171: $(^{39}Ar/^{37}Ar)_{Ca}$ = 0.0007 ± 2e-05, $(^{36}Ar/^{37}Ar)_{Ca}$ = 0.000284 ± 5e-06, $(^{38}Ar/^{39}Ar)_K$ = 0.0122, $(^{40}Ar/^{39}Ar)_K$ = 0.0295 ± 0.0002

TABLE A2.5: $^{40}Ar/^{39}Ar$ analytical data for single-grain K-feldspar analyses.

ID	Temp (°C)	$^{40}Ar/^{39}Ar$	$^{37}Ar/^{39}Ar$	$^{36}Ar/^{39}Ar$ (x 10^{-3})	$^{39}Ar_K$ (x 10^{-15} mol)	K/Ca	$^{40}Ar^*$ (%)	^{39}Ar (%)	Age (Ma)	±1σ (Ma)	Time (min)
PVBR02-28-05, K-Feldspar, 0.054 mg, J=0.010266±0.05%, D=1.0032±0.0005, NM-201J, Lab#=56662-01											
B	600	58.46	0.0015	1.688	3.10	343.3	99.1	13.4	852.5	1.8	8
C	700	66.01	0.0020	1.609	5.07	261.5	99.3	35.2	939.4	1.5	8
D	800	67.82	0.0048	1.469	3.92	107.3	99.4	52.1	960.0	2.0	8
E	900	66.63	0.0029	1.948	1.87	177.1	99.1	60.2	945.3	2.7	8
F	975	66.57	-0.0020	1.770	1.232	-	99.2	65.5	945.2	3.9	8
G	1050	68.35	0.0071	6.009	1.089	71.6	97.4	70.1	951.1	4.0	8
H	1100	70.64	-0.0033	5.595	1.34	-	97.7	75.9	977.7	3.7	8
I	1150	74.26	-0.0029	2.266	3.16	-	99.1	89.5	1027.6	2.2	8
J	1200	79.85	-0.0002	4.214	2.41	-	98.4	99.9	1080.4	2.7	8
K	1225	157.4	0.0777	228.7	0.035	6.6	57.1	100.0	1193.0	106.6	8
Total gas age ± 1σ		n=10			23.2	365.6	K2O=16.10%		951.22	0.93	

ID	Temp (°C)	$^{40}Ar/^{39}Ar$	$^{37}Ar/^{39}Ar$	$^{36}Ar/^{39}Ar$ (x 10^{-3})	$^{39}Ar_K$ (x 10^{-15} mol)	K/Ca	$^{40}Ar^*$ (%)	^{39}Ar (%)	Age (Ma)	±1σ (Ma)	Time (min)
PVBR02-28-07, K-Feldspar, 0.13 mg, J=0.010266±0.05%, D=1.0032±0.0005, NM-201J, Lab#=56661-01											
B	450	334.6	-0.3194	304.9	0.021	-	73.1	0.1	2292.4	151.1	8
C	450	546.1	-3.0558	935.3	0.006	-	49.3	0.1	2418.9	432.8	13
D	450	546.9	-2.5043	1257.1	0.008	-	32.0	0.1	1877.3	447.4	18
E	500	122.5	-1.0656	96.05	0.021	-	76.7	0.2	1232.8	150.3	8
F	500	142.2	-0.4546	276.9	0.029	-	42.4	0.3	880.0	137.8	13
G	500	154.3	-0.8826	309.5	0.031	-	40.7	0.4	907.4	137.3	18
H	550	66.45	-0.1109	23.02	0.098	-	89.7	0.7	872.0	41.9	8
I	550	79.98	-0.0989	73.95	0.101	-	72.7	1.0	854.3	42.7	13
J	550	87.49	-0.0684	110.7	0.101	-	62.6	1.3	814.5	43.3	18
K	600	64.85	-0.0500	8.734	0.216	-	96.0	2.0	902.3	19.2	8
L	600	70.13	-0.0317	27.07	0.245	-	88.6	2.8	900.8	16.9	13
M	600	76.64	-0.0977	42.70	0.241	-	83.5	3.5	922.2	17.2	18
N	650	67.99	-0.0132	10.97	0.361	-	95.2	4.7	930.5	11.4	8
O	650	72.20	-0.0349	19.41	0.408	-	92.1	5.9	949.8	9.4	13
P	650	73.82	-0.0274	34.83	0.421	-	86.1	7.3	916.7	11.0	18
Q	700	67.74	-0.0420	2.877	0.588	-	98.7	9.1	954.5	7.3	8
R	700	69.32	-0.0289	11.28	0.596	-	95.2	11.0	944.5	7.3	13
S	750	68.10	-0.0215	3.588	0.805	-	98.4	13.5	956.2	5.7	8
T	750	70.51	-0.0045	10.79	0.641	-	95.5	15.5	959.3	6.9	13
U	800	69.15	-0.0069	6.279	0.698	-	97.3	17.7	959.0	6.7	8
V	800	71.21	-0.0071	13.35	0.540	-	94.5	19.4	958.7	7.9	13
W	850	70.87	-0.0201	13.79	0.557	-	94.2	21.2	953.5	7.6	8
X	850	72.52	-0.0261	18.89	0.428	-	92.3	22.5	955.0	10.2	13
Y	900	70.42	-0.0332	9.033	0.432	-	96.2	23.9	964.0	9.9	8
Z	900	73.18	-0.0506	11.52	0.373	-	95.3	25.1	986.3	11.4	13
AA	950	70.82	-0.0276	7.801	0.412	-	96.7	26.4	972.5	9.9	8
AB	950	72.64	-0.0088	23.14	0.421	-	90.6	27.7	942.4	9.2	13
AC	1000	71.32	-0.0200	13.83	0.512	-	94.3	29.3	958.3	8.4	8
AD	1000	74.24	-0.0017	20.45	0.546	-	91.9	31.0	969.0	8.0	13
AE	1050	69.71	-0.0043	6.326	0.749	-	97.3	33.4	965.1	6.1	8
AF	1050	71.68	-0.0058	17.16	0.858	-	92.9	36.1	951.4	5.6	13
AG	1100	71.98	0.0026	9.262	1.47	198.5	96.2	40.7	980.5	3.6	8
AH	1100	71.41	-0.0097	8.783	1.95	-	96.4	46.9	975.8	3.1	13
AI	1100	72.77	-0.0028	10.97	1.60	-	95.5	51.9	983.7	3.4	18
AJ	1100	75.55	-0.0032	18.36	1.55	-	92.8	56.8	990.1	3.5	28
AK	1100	85.24	-0.0074	48.54	2.27	-	83.2	63.9	998.5	2.9	58
AL	1100	111.6	0.0005	141.0	2.74	######	62.7	72.5	988.2	3.8	118
AM	1200	71.54	-0.0037	4.930	4.35	-	98.0	86.2	989.7	1.8	8
AN	1300	75.96	0.0027	6.114	3.25	188.1	97.6	96.5	1033.5	1.9	8
AO	1400	87.25	0.0103	47.62	0.356	49.5	83.9	97.6	1023.2	12.9	8
AP	1550	86.60	0.0030	75.25	0.770	168.0	74.3	100.0	926.3	6.9	8
Total gas age ± 1σ			n=41		31.8	-39.508	K2O=9.15%		968.1	1.2	

ID	Temp (°C)	$^{40}Ar/^{39}Ar$	$^{37}Ar/^{39}Ar$	$^{36}Ar/^{39}Ar$ (x 10^{-3})	$^{39}Ar_K$ (x 10^{-15} mol)	K/Ca	$^{40}Ar^*$ (%)	^{39}Ar (%)	Age (Ma)	±1σ (Ma)	Time (min)
PVBR02-28-13, K-Feldspar, 0.11 mg, J=0.0102959±0.05%, D=1.0032±0.0005, NM-201H, Lab#=56658-01											
B	600	43.12	-0.0008	2.010	2.63	-	98.6	5.3	663.0	2.1	8
C	700	54.25	0.0029	2.202	2.68	173.7	98.8	10.6	802.4	2.1	8
D	800	54.83	0.0011	1.695	1.94	477.4	99.1	14.5	811.2	2.8	8
E	900	54.03	0.0004	3.429	1.94	######	98.1	18.4	795.3	2.9	8
F	975	53.43	0.0102	4.504	1.78	50.3	97.5	21.9	784.1	2.8	8
G	1050	52.54	0.0066	4.670	2.20	77.3	97.4	26.3	772.5	2.7	8
H	1100	51.46	0.0044	5.925	2.45	116.8	96.6	31.2	754.6	2.3	8
I	1150	48.97	0.0051	5.149	6.21	100.6	96.9	43.6	726.3	1.4	8
J	1200	53.33	0.0019	5.412	22.0	273.5	97.0	87.6	779.65	0.71	8
K	1225	57.67	-0.0007	7.215	3.12	-	96.3	93.8	825.8	2.2	8
L	1250	61.65	0.0291	20.99	0.438	17.5	89.9	94.7	824.7	10.3	8
M	1275	67.27	-0.0328	62.85	0.225	-	72.4	95.1	742.0	20.2	8
N	1300	65.52	-0.0172	30.90	0.266	-	86.1	95.7	835.9	15.0	8
O	1350	65.19	-0.0105	28.53	0.324	-	87.1	96.3	840.2	13.0	8
P	1400	62.61	-0.0052	20.01	0.613	-	90.6	97.5	839.6	7.4	8
Q	1700	63.15	0.1033	90.49	1.232	4.9	57.7	100.0	581.3	5.7	8
Total gas age ± 1σ			n=16		50.1	104.9	K2O=16.99%		759.51	0.69	

ID	Temp (°C)	$^{40}Ar/^{39}Ar$	$^{37}Ar/^{39}Ar$	$^{36}Ar/^{39}Ar$ (x 10^{-3})	$^{39}Ar_K$ (x 10^{-15} mol)	K/Ca	$^{40}Ar^*$ (%)	^{39}Ar (%)	Age (Ma)	±1σ (Ma)	Time (min)
PVBR02-28-15, K-Feldspar, 0.36 mg, J=0.0102959±0.05%, D=1.0032±0.0005, NM-201H, Lab#=56657-01											
B	450	217.5	-0.0029	131.7	0.327	-	82.1	0.2	1905.5	14.1	8
C	450	59.92	0.0303	95.78	0.152	16.9	52.8	0.2	514.6	32.4	13
D	450	60.80	-0.0321	96.58	0.146	-	53.0	0.3	523.6	36.7	18
E	500	35.85	-0.0110	18.90	0.355	-	84.4	0.5	495.2	13.8	8
F	500	36.73	-0.0362	22.42	0.411	-	82.0	0.7	492.9	12.2	13
G	500	40.28	-0.0165	33.82	0.444	-	75.2	0.9	495.4	11.4	18
H	550	45.41	-0.0024	7.193	1.191	-	95.3	1.5	672.9	4.4	8
I	550	39.41	-0.0066	12.81	1.038	-	90.4	2.0	570.5	4.6	13
J	550	43.55	-0.0095	18.78	0.930	-	87.3	2.5	602.9	5.9	18
K	600	45.05	0.0052	6.039	1.73	98.4	96.0	3.4	672.7	3.0	8
L	600	48.09	-0.0007	8.536	1.48	-	94.8	4.1	702.4	3.3	13
M	600	51.93	0.0050	15.64	1.214	101.3	91.1	4.7	724.5	4.3	18
N	650	51.98	-0.0005	4.459	1.74	-	97.5	5.6	766.5	3.2	8
O	650	54.80	-0.0027	8.263	1.66	-	95.5	6.4	787.2	2.9	13
P	650	57.61	0.0038	12.66	1.41	135.0	93.5	7.1	805.6	3.6	18
Q	700	57.40	-0.0022	6.418	1.78	-	96.7	8.0	825.3	3.0	8
R	700	58.40	-0.0010	8.543	1.57	-	95.7	8.8	829.7	3.2	13
S	750	56.57	0.0035	4.828	2.11	146.2	97.5	9.8	821.0	2.8	8
T	750	57.76	0.0029	9.303	1.68	175.4	95.2	10.7	819.4	3.3	13
U	800	56.79	0.0021	3.987	1.95	246.0	97.9	11.6	826.6	2.8	8
V	800	57.58	-0.0047	11.96	1.66	-	93.9	12.5	807.8	3.4	13
W	850	56.64	-0.0060	5.076	1.92	-	97.4	13.4	821.0	2.9	8
X	850	57.49	0.0029	7.470	1.65	176.1	96.2	14.2	822.6	3.8	13
Y	900	57.33	-0.0005	7.486	2.00	-	96.1	15.2	820.7	2.6	8
Z	900	57.97	0.0006	8.487	1.92	902.5	95.7	16.2	824.8	3.1	13
AA	950	57.35	0.0023	5.246	2.62	218.3	97.3	17.5	828.9	2.2	8
AB	950	57.52	0.0013	7.428	2.18	398.1	96.2	18.6	823.2	2.7	13
AC	1000	56.93	-0.0036	7.327	2.45	-	96.2	19.8	816.5	2.4	8
AD	1000	57.06	0.0010	9.973	2.41	515.3	94.8	21.0	808.6	2.4	13
AE	1050	57.16	0.0007	6.399	3.73	758.6	96.7	22.9	822.5	1.6	8
AF	1050	57.23	0.0017	7.420	3.48	298.9	96.2	24.6	819.7	1.9	13
AG	1100	58.28	0.0027	8.276	4.42	189.3	95.8	26.8	829.3	1.7	8
AH	1100	57.42	0.0045	7.920	4.67	112.6	95.9	29.1	820.3	1.9	13
AI	1100	57.53	-0.0011	8.635	4.54	-	95.6	31.4	819.1	1.7	18
AJ	1100	58.72	0.0015	12.21	4.36	349.6	93.9	33.6	820.6	1.7	28
AK	1100	60.14	0.0030	16.49	6.05	167.5	91.9	36.6	822.5	1.4	58
AL	1100	63.08	-0.0001	23.47	7.85	-	89.0	40.5	832.9	1.5	118
AM	1200	54.42	0.0017	5.068	23.1	299.1	97.2	52.0	794.14	0.79	8
AN	1300	56.93	0.0017	5.138	61.5	295.0	97.3	82.6	824.16	0.67	8
AO	1400	56.87	0.0024	6.089	26.8	210.4	96.8	96.0	820.16	0.91	8
AP	1600	58.76	0.0049	17.12	8.03	104.5	91.4	100.0	803.6	1.3	8
Total gas age ± 1σ			n=41		200.7	368.9	K2O=20.80%		802.59	0.57	

ID	Temp (°C)	$^{40}Ar/^{39}Ar$	$^{37}Ar/^{39}Ar$	$^{36}Ar/^{39}Ar$ (x 10^{-3})	$^{39}Ar_K$ (x 10^{-15} mol)	K/Ca	$^{40}Ar^*$ (%)	^{39}Ar (%)	Age (Ma)	±1σ (Ma)	Time (min)
PVBR06-20-12, K-Feldspar, 0.27 mg, J=0.0102959±0.05%, D=1.0032±0.0005, NM-201H, Lab#=56650-01											
B	600	54.44	0.0039	14.17	2.26	132.3	92.3	2.0	761.3	3.2	8
C	700	53.97	0.0075	3.684	2.45	68.4	98.0	4.1	793.7	2.4	8
D	800	58.69	0.0007	2.173	3.05	724.5	98.9	6.8	855.5	1.8	8
E	900	58.43	0.0036	2.303	3.20	140.6	98.8	9.6	852.0	2.0	8
F	975	56.49	0.0053	3.107	3.06	96.7	98.4	12.2	826.2	2.1	8
G	1050	54.54	0.0139	2.966	5.30	36.6	98.4	16.9	803.2	1.5	8
H	1100	53.54	0.0051	2.916	9.20	99.9	98.4	24.9	791.2	1.0	8
I	1150	55.73	0.0027	2.496	35.3	190.1	98.7	55.8	819.17	0.79	8
J	1200	60.14	0.0018	1.897	37.4	284.2	99.1	88.4	873.41	0.75	8
K	1225	61.90	0.0024	3.167	7.31	216.1	98.5	94.8	889.5	1.4	8
L	1250	64.08	-0.0055	8.457	1.000	-	96.1	95.6	896.6	5.3	8
M	1275	64.74	0.0007	7.602	1.143	763.3	96.5	96.6	907.1	5.0	8
N	1300	74.85	-0.0877	36.70	0.192	-	85.5	96.8	924.2	21.7	8
O	1350	64.04	0.0000	5.434	3.39	-	97.5	99.8	906.4	2.0	8
P	1400	108.7	-0.1394	126.9	0.077	-	65.5	99.8	1004.3	51.6	8
Q	1700	184.4	0.0406	422.0	0.190	12.6	32.4	100.0	875.0	31.0	8
Total gas age ± 1σ			n=16		114.5	175.9	K2O=15.83%		833.45	0.61	

ID	Temp (°C)	$^{40}Ar/^{39}Ar$	$^{37}Ar/^{39}Ar$	$^{36}Ar/^{39}Ar$ (x 10^{-3})	$^{39}Ar_K$ (x 10^{-15} mol)	K/Ca	$^{40}Ar^*$ (%)	^{39}Ar (%)	Age (Ma)	±1σ (Ma)	Time (min)
PVBR06-20-22, K-Feldspar, 0.22 mg, J=0.0102959±0.05%, D=1.0032±0.0005, NM-201H, Lab#=56643-01											
A	400	1154.7	0.0310	515.1	0.100	16.5	86.8	0.1	4431.6	47.0	5
B	450	298.7	0.0116	170.8	0.107	43.9	83.1	0.2	2316.4	34.9	8
C	450	127.1	-0.0577	320.5	0.066	-	25.5	0.3	524.9	75.4	13
D	450	164.9	-0.3634	420.1	0.058	-	24.7	0.4	639.5	86.1	18
E	500	65.01	-0.1159	101.8	0.119	-	53.7	0.5	560.7	39.7	8
F	500	76.89	-0.1066	175.8	0.121	-	32.4	0.6	417.2	45.6	13
G	500	96.99	-0.1046	212.4	0.112	-	35.3	0.8	551.2	49.1	18
H	550	57.94	-0.0322	40.20	0.287	-	79.5	1.1	708.6	16.4	8
I	550	61.58	-0.0160	74.01	0.272	-	64.5	1.4	625.7	17.8	13
J	550	71.29	-0.0736	95.75	0.242	-	60.3	1.6	669.0	20.3	18
K	600	56.51	-0.0155	26.88	0.472	-	85.9	2.2	740.3	9.8	8
L	600	57.00	-0.0167	39.64	0.512	-	79.4	2.7	698.8	8.9	13
M	600	64.65	-0.0511	59.76	0.495	-	72.7	3.3	720.4	10.9	18
N	650	59.37	-0.0039	22.47	0.737	-	88.8	4.1	791.8	7.3	8
O	650	64.82	-0.0217	25.80	0.773	-	88.2	5.0	845.4	6.4	13
P	650	70.19	-0.0311	38.86	0.723	-	83.6	5.8	863.2	7.0	18
Q	700	66.89	-0.0059	13.72	0.981	-	93.9	6.9	911.0	5.4	8
R	700	70.19	-0.0038	21.25	0.938	-	91.1	7.9	923.2	5.2	13
S	750	69.48	-0.0103	9.866	1.37	-	95.8	9.4	953.0	3.7	8
T	750	71.77	-0.0080	18.88	1.077	-	92.2	10.6	948.9	5.0	13
U	800	70.87	-0.0077	11.46	1.280	-	95.2	12.0	963.3	3.9	8
V	800	73.53	-0.0012	22.87	0.983	-	90.8	13.1	955.3	5.0	13
W	850	73.08	-0.0204	14.19	1.081	-	94.3	14.3	978.8	5.0	8
X	850	77.18	-0.0246	29.12	0.830	-	88.8	15.3	975.4	5.8	13
Y	900	76.08	-0.0157	16.24	0.952	-	93.7	16.3	1004.9	5.4	8
Z	900	79.30	-0.0176	28.70	0.844	-	89.3	17.2	999.9	5.7	13
AA	950	78.86	0.0035	19.16	1.071	147.5	92.8	18.4	1025.6	4.7	8
AB	950	80.20	-0.0037	22.45	1.053	-	91.7	19.6	1029.6	4.6	13
AC	1000	85.93	0.0024	13.00	1.53	213.2	95.5	21.3	1118.5	3.6	8
AD	1000	79.06	-0.0057	16.71	1.54	-	93.8	23.0	1035.5	3.5	13
AE	1050	84.05	-0.0039	7.818	2.91	-	97.3	26.2	1115.0	2.5	8
AF	1050	80.70	-0.0038	11.06	2.76	-	96.0	29.3	1070.5	2.4	13
AG	1100	81.58	-0.0005	5.035	6.07	-	98.2	36.1	1098.1	1.7	8
AH	1100	80.11	0.0006	8.949	4.23	887.9	96.7	40.7	1070.8	2.0	13
AI	1100	81.27	0.0025	16.80	2.69	202.0	93.9	43.7	1058.7	2.7	18
AJ	1100	83.03	-0.0026	24.62	2.59	-	91.2	46.6	1052.8	2.8	28
AK	1100	87.51	-0.0009	38.04	3.33	-	87.2	50.3	1058.3	2.7	58
AL	1100	96.39	0.0008	69.71	3.95	671.9	78.6	54.7	1053.2	3.3	118
AM	1200	77.58	0.0006	3.008	16.6	823.4	98.9	73.1	1062.8	1.0	8
AN	1300	75.16	0.0014	2.915	20.9	359.6	98.9	96.4	1037.35	0.76	8
AO	1400	80.36	0.0061	30.22	1.91	84.0	88.9	98.5	1006.6	3.3	8
AP	1600	100.2	0.0010	184.0	1.37	490.3	45.7	100.0	705.6	6.9	8
Total gas age ± 1σ			n=42		90.0	-174.122	K2O=15.27%		1026.94	0.78	

ID	Temp (°C)	$^{40}Ar/^{39}Ar$	$^{37}Ar/^{39}Ar$	$^{36}Ar/^{39}Ar$ (x 10^{-3})	$^{39}Ar_K$ (x 10^{-15} mol)	K/Ca	$^{40}Ar^*$ (%)	^{39}Ar (%)	Age (Ma)	±1σ (Ma)	Time (min)
PVBR06-20-33, K-Feldspar, .21 mg, J=0.0102959±0.05%, D=1.0032±0.0005, NM-201H, Lab#=56647-01											
B	450	109.8	-0.0568	-9.7850	0.131	-	102.6	0.2	1406.1	30.6	8
C	450	69.99	0.0964	17.16	0.064	5.3	92.8	0.2	934.8	64.2	13
D	450	80.06	0.0345	50.93	0.153	14.8	81.2	0.4	935.7	29.2	18
E	500	90.08	0.0997	15.90	0.453	5.1	94.8	1.0	1152.0	9.8	8
F	500	57.65	0.0457	14.47	0.313	11.2	92.6	1.4	799.8	13.9	13
G	550	58.92	0.0458	9.444	0.630	11.1	95.3	2.2	832.8	7.4	8
H	550	58.79	0.0314	8.010	0.557	16.3	96.0	2.9	836.3	8.6	13
I	600	68.88	0.0135	4.599	0.972	37.8	98.0	4.2	963.7	4.9	8
J	600	60.29	0.0404	8.774	0.844	12.6	95.7	5.2	851.4	5.4	13
K	650	69.19	0.0274	5.029	1.46	18.6	97.9	7.1	965.8	3.3	8
L	650	64.55	0.0364	10.32	1.048	14.0	95.3	8.4	895.8	4.5	13
M	650	66.60	0.0655	14.30	0.679	7.8	93.7	9.3	905.9	7.0	18
N	700	63.44	0.0328	1.805	0.742	15.6	99.2	10.2	911.9	6.5	8
O	700	65.94	0.0530	10.000	0.669	9.6	95.5	11.1	912.7	7.3	13
P	750	64.00	0.0333	3.386	0.823	15.3	98.4	12.1	912.9	5.6	8
Q	750	64.95	0.0601	14.74	0.641	8.5	93.3	12.9	885.3	6.9	13
R	800	63.45	0.0470	6.264	0.733	10.9	97.1	13.8	896.9	7.0	8
S	800	66.30	0.0548	8.368	0.560	9.3	96.3	14.5	922.3	7.8	13
T	850	65.26	0.0274	3.345	0.736	18.6	98.5	15.5	927.4	5.7	8
U	850	67.37	0.1403	11.30	0.608	3.6	95.1	16.2	924.7	8.1	13
V	900	68.89	0.0417	6.249	0.831	12.2	97.3	17.3	958.5	5.9	8
W	900	69.01	0.0619	8.363	0.729	8.2	96.4	18.2	952.9	6.1	13
X	950	75.67	0.0555	3.854	1.008	9.2	98.5	19.5	1039.9	5.6	8
Y	950	71.44	0.0326	6.158	1.083	15.7	97.5	20.8	986.9	4.7	13
Z	1000	75.16	0.0172	3.900	1.314	29.7	98.5	22.5	1034.4	3.7	8
AA	1000	74.80	0.0367	6.060	1.200	13.9	97.6	24.0	1023.6	4.5	13
AB	1050	78.49	0.0069	1.618	2.80	73.8	99.4	27.5	1076.6	2.4	8
AC	1050	78.05	0.0180	2.361	2.24	28.4	99.1	30.3	1069.7	2.5	13
AD	1100	78.56	0.0075	2.139	4.22	68.1	99.2	35.6	1075.7	2.1	8
AE	1100	78.34	0.0067	2.755	3.90	76.5	99.0	40.4	1071.5	1.9	13
AF	1100	79.81	0.0226	4.379	3.79	22.6	98.4	45.1	1081.8	1.9	18
AG	1100	81.15	0.0190	5.936	4.58	26.8	97.8	50.8	1090.9	1.9	28
AH	1100	81.39	0.0225	7.483	7.80	22.7	97.3	60.3	1088.7	1.4	58
AI	1100	84.76	0.0221	11.21	10.41	23.1	96.1	73.0	1112.0	1.3	118
AJ	1200	84.71	0.0035	1.193	12.07	145.8	99.6	87.6	1141.5	1.2	8
AK	1600	83.18	0.2933	9.712	10.34	1.7	96.6	100.0	1100.8	1.3	8
Total gas age ± 1σ			n=36		81.1	9.0	K2O=14.41%		1054.22	0.74	

ID	Temp (°C)	$^{40}Ar/^{39}Ar$	$^{37}Ar/^{39}Ar$	$^{36}Ar/^{39}Ar$ (x 10^{-3})	$^{39}Ar_K$ (x 10^{-15} mol)	K/Ca	$^{40}Ar^*$ (%)	^{39}Ar (%)	Age (Ma)	±1σ (Ma)	Time (min)
PVBR06-20-40, K-Feldspar, 0.34 mg, J=0.0102959±0.05%, D=1.0032±0.0005, NM-201H, Lab#=56648-01											
B	450	1197.2	-0.0026	63.82	0.618	-	98.4	0.4	4702.5	14.3	6
C	450	70.86	0.0135	26.07	0.362	37.9	89.1	0.7	914.7	12.5	13
D	450	55.30	0.0230	53.36	0.211	22.1	71.5	0.8	623.5	23.2	18
E	500	55.36	-0.0382	3.099	0.459	-	98.3	1.1	812.6	9.5	8
F	500	46.46	-0.0289	16.89	0.427	-	89.3	1.4	649.2	10.9	13
G	500	52.11	-0.0288	22.29	0.420	-	87.4	1.7	701.8	11.8	18
H	550	44.18	-0.0207	2.552	0.722	-	98.3	2.2	674.7	6.4	8
I	550	48.95	-0.0158	10.99	0.793	-	93.4	2.7	704.1	5.7	13
J	550	55.73	-0.0155	20.66	0.653	-	89.0	3.2	753.5	8.2	18
K	600	54.38	-0.0028	7.071	0.882	-	96.2	3.8	786.5	4.7	8
L	600	58.38	-0.0159	7.755	0.949	-	96.1	4.4	832.2	5.3	13
M	600	63.36	0.0060	14.43	0.878	85.3	93.3	5.0	867.8	5.5	18
N	650	64.44	0.0099	4.579	1.140	51.5	97.9	5.8	913.9	4.4	8
O	650	66.12	-0.0154	6.156	1.208	-	97.2	6.6	927.7	4.2	13
P	650	68.81	-0.0093	11.70	1.075	-	95.0	7.3	939.5	4.5	18
Q	700	66.65	-0.0205	2.470	1.36	-	98.9	8.2	945.8	3.8	8
R	700	68.81	-0.0042	8.240	1.37	-	96.5	9.2	950.9	3.6	13
S	750	68.20	0.0010	2.478	1.88	494.8	98.9	10.4	963.1	2.9	8
T	750	68.74	-0.0054	5.501	1.60	-	97.6	11.5	959.2	3.1	13
U	800	71.52	-0.0007	2.045	2.12	-	99.2	12.9	1001.0	2.6	8
V	800	68.97	-0.0092	5.690	1.56	-	97.6	14.0	961.2	3.1	13
W	850	70.11	-0.0042	4.009	2.00	-	98.3	15.4	979.3	3.0	8
X	850	69.51	-0.0171	8.105	1.54	-	96.6	16.4	959.2	3.2	13
Y	900	71.22	0.0011	4.093	2.17	474.9	98.3	17.9	991.1	2.6	8
Z	900	71.09	-0.0118	8.134	1.85	-	96.6	19.1	976.6	3.1	13
AA	950	74.89	-0.0054	3.325	3.03	-	98.7	21.2	1033.2	2.4	8
AB	950	72.53	-0.0051	4.953	2.61	-	98.0	22.9	1002.6	2.4	13
AC	1000	75.74	-0.0012	2.211	6.17	-	99.1	27.1	1045.8	1.4	8
AD	1000	74.67	0.0012	3.555	5.57	409.2	98.6	30.9	1030.1	1.4	13
AE	1050	75.32	0.0000	1.623	6.32	-	99.4	35.2	1043.1	1.6	8
AF	1050	75.89	-0.0025	4.524	5.50	-	98.2	38.9	1040.2	1.5	13
AG	1100	75.30	0.0035	1.980	10.27	146.0	99.2	45.8	1041.8	1.0	8
AH	1100	74.50	0.0005	3.496	6.41	######	98.6	50.2	1028.5	1.4	13
AI	1100	75.96	0.0002	6.090	5.14	######	97.6	53.7	1035.9	1.6	18
AJ	1100	76.94	-0.0014	8.122	5.00	-	96.9	57.0	1040.0	1.9	28
AK	1100	80.06	-0.0023	15.26	6.42	-	94.4	61.4	1050.6	1.5	58
AL	1100	85.22	0.0006	28.78	7.37	882.4	90.0	66.4	1063.0	1.5	118
AM	1200	76.52	0.0017	2.150	9.70	302.9	99.2	72.9	1054.2	1.1	8
AN	1300	77.92	0.0021	1.068	36.7	240.2	99.6	97.8	1072.28	0.97	8
AO	1400	80.17	0.0072	8.399	2.58	71.0	96.9	99.5	1073.2	2.5	8
AP	1600	95.50	-0.0037	67.78	0.714	-	79.0	100.0	1049.8	7.9	8
Total gas age ± 1σ			n=41		147.7	-613.972	K2O=16.21%		1063.72	0.68	

ID	Temp (°C)	$^{40}Ar/^{39}Ar$	$^{37}Ar/^{39}Ar$	$^{36}Ar/^{39}Ar$ (x 10^{-3})	$^{39}Ar_K$ (x 10^{-15} mol)	K/Ca	$^{40}Ar^*$ (%)	^{39}Ar (%)	Age (Ma)	±1σ (Ma)	Time (min)
PVBR06-20-44, K-Feldspar, 0.31 mg, J=0.0102959±0.05%, D=1.0032±0.0005, NM-201H, Lab#=56655-01											
B	450	222.6	0.1029	109.5	0.123	5.0	85.5	0.1	1981.3	31.8	8
C	450	141.4	0.0135	148.3	0.069	37.7	69.0	0.1	1269.9	54.3	13
D	450	117.9	-0.1041	197.6	0.061	-	50.5	0.2	872.7	71.4	18
E	500	104.5	-0.0765	31.03	0.138	-	91.2	0.3	1248.3	27.4	8
F	500	65.28	-0.0342	59.63	0.132	-	73.0	0.4	728.9	34.9	13
G	500	62.50	-0.0568	73.70	0.132	-	65.1	0.5	639.2	34.4	18
H	550	103.9	-0.0198	23.31	0.425	-	93.4	0.8	1264.3	10.6	8
I	550	42.99	-0.0361	18.39	0.333	-	87.3	1.0	596.7	13.3	13
J	550	49.28	-0.0330	38.87	0.256	-	76.7	1.2	600.1	20.3	18
K	600	129.5	0.0014	31.74	0.570	376.8	92.8	1.6	1470.4	7.8	8
L	600	48.43	-0.0108	13.44	0.418	-	91.8	1.9	688.1	10.8	13
M	600	51.32	-0.0314	23.67	0.384	-	86.4	2.2	686.4	12.3	18
N	650	75.33	-0.0260	13.63	0.569	-	94.6	2.6	1005.2	7.9	8
O	650	53.40	-0.0023	22.33	0.519	-	87.6	2.9	718.2	9.3	13
P	650	56.20	-0.0224	29.09	0.406	-	84.7	3.2	728.2	11.4	18
Q	700	180.9	0.0106	52.32	2.71	48.3	91.5	5.1	1815.7	3.1	8
R	700	55.22	0.0036	15.79	0.767	141.2	91.5	5.7	765.0	6.2	13
S	750	55.48	-0.0090	5.270	1.070	-	97.2	6.5	806.2	4.7	8
T	750	53.25	-0.0129	10.43	0.964	-	94.2	7.1	760.3	5.0	13
U	800	54.77	-0.0013	4.668	1.267	-	97.5	8.0	799.8	4.1	8
V	800	51.89	0.0023	7.019	1.101	221.0	96.0	8.8	755.9	4.6	13
W	850	55.55	-0.0030	3.926	1.36	-	97.9	9.8	811.9	3.8	8
X	850	53.02	-0.0010	7.058	1.171	-	96.1	10.6	769.8	4.1	13
Y	900	85.01	0.0059	17.78	2.73	86.8	93.8	12.6	1094.6	2.3	8
Z	900	55.12	-0.0090	6.874	1.41	-	96.3	13.6	796.1	3.8	13
AA	950	60.42	0.0163	5.966	1.69	31.2	97.1	14.8	862.6	3.2	8
AB	950	57.87	0.0006	8.236	1.45	808.3	95.8	15.8	824.5	3.4	13
AC	1000	77.08	0.0200	8.024	2.08	25.6	96.9	17.3	1041.8	2.7	8
AD	1000	61.89	-0.0004	9.380	1.68	-	95.5	18.5	868.0	2.9	13
AE	1050	80.25	0.0220	7.729	3.28	23.2	97.2	20.8	1076.1	2.1	8
AF	1050	70.19	0.0102	9.635	2.35	50.0	95.9	22.5	961.7	2.8	13
AG	1100	84.06	0.0171	10.70	3.16	29.9	96.2	24.7	1106.4	2.1	8
AH	1100	83.30	0.0127	10.17	2.65	40.0	96.4	26.6	1100.2	2.4	13
AI	1100	87.04	0.0122	11.82	2.61	41.7	96.0	28.5	1133.4	2.5	18
AJ	1100	90.69	0.0063	14.00	3.13	81.4	95.4	30.7	1163.5	2.5	28
AK	1100	90.00	0.0096	18.15	5.08	53.3	94.0	34.3	1144.3	1.7	58
AL	1100	89.57	0.0061	23.67	7.98	83.4	92.2	40.0	1123.5	1.7	118
AM	1200	84.99	0.0037	6.258	26.5	137.3	97.8	58.8	1129.24	0.99	8
AN	1300	89.58	0.0022	7.063	53.8	231.7	97.7	97.1	1172.77	0.96	8
AO	1400	94.40	0.0067	14.93	3.01	76.5	95.3	99.2	1197.4	3.1	8
AP	1600	91.44	0.0015	69.56	1.106	349.8	77.5	100.0	1000.6	5.4	8
Total gas age ± 1σ			n=41		140.6	127.2	K2O=16.93%		1109.38	0.76	

ID	Temp (°C)	$^{40}Ar/^{39}Ar$	$^{37}Ar/^{39}Ar$	$^{36}Ar/^{39}Ar$ (x 10^{-3})	$^{39}Ar_K$ (x 10^{-15} mol)	K/Ca	$^{40}Ar^*$ (%)	^{39}Ar (%)	Age (Ma)	±1σ (Ma)	Time (min)
PVBR04-2-03, K-feldspar, 0.18 mg, J=0.013604±0.10%, D=1.004±0.001, NM-206B, Lab#=57045-03											
B	465	67.87	0.0039	201.1	0.166	129.9	12.4	0.3	198.1	49.4	5
C	465	26.81	0.0100	92.00	0.139	51.0	-1.4	0.5	-9.7	63.7	15
D	465	16.44	0.0024	46.47	0.129	216.9	16.4	0.7	65.8	64.9	21
E	515	8.972	0.0090	12.96	0.225	56.9	57.3	1.0	123.2	35.0	11
F	515	8.968	0.0027	7.560	0.264	191.2	75.1	1.4	159.8	29.4	16
G	515	10.17	-0.0038	10.13	0.144	-	70.5	1.6	169.8	52.9	18
H	565	11.04	0.0046	2.654	0.366	110.0	92.9	2.2	238.2	20.4	11
I	565	12.59	0.0044	0.6770	0.315	115.0	98.4	2.7	284.1	23.1	14
J	565	15.11	-0.0007	5.543	0.263	-	89.1	3.1	307.0	27.6	19
K	615	21.15	0.0061	2.537	0.718	83.7	96.5	4.1	447.1	9.5	11
L	615	24.18	0.0057	2.555	0.408	89.0	96.9	4.8	505.0	16.0	16
M	615	26.90	-0.0053	7.175	0.268	-	92.1	5.2	530.2	24.1	21
N	665	29.72	0.0026	2.565	0.445	198.9	97.4	5.8	606.5	14.0	11
O	665	31.41	0.0027	3.056	0.293	186.2	97.1	6.3	633.8	20.8	16
P	665	32.58	0.0052	5.295	0.225	98.7	95.2	6.6	642.7	27.0	21
Q	715	32.88	-0.0037	2.961	0.297	-	97.3	7.1	659.8	20.5	10
R	715	33.48	0.0049	6.635	0.304	104.5	94.1	7.5	651.4	20.1	16
S	765	34.89	0.0066	6.536	0.438	77.7	94.5	8.2	676.3	13.7	11
T	765	39.21	0.0068	22.32	0.239	74.8	83.2	8.6	670.3	24.8	15
U	815	38.69	0.0088	22.36	0.505	58.2	82.9	9.3	661.1	12.5	11
V	815	56.86	0.0008	81.05	0.336	663.7	57.9	9.8	675.4	20.2	16
W	865	56.40	0.0105	82.93	0.393	48.6	56.5	10.4	657.9	17.1	10
X	865	46.14	0.0125	50.70	0.354	40.7	67.5	11.0	645.1	18.4	16
Y	915	36.88	0.0055	15.68	0.471	92.1	87.4	11.7	664.0	12.8	11
Z	915	37.57	0.0055	16.20	0.352	92.3	87.3	12.2	673.3	17.2	16
AA	965	35.86	0.0062	9.732	0.438	81.8	92.0	12.9	676.8	13.7	11
AB	965	37.43	0.0107	14.01	0.406	47.8	88.9	13.5	682.1	14.9	16
AC	1015	36.15	0.0086	6.949	0.520	59.0	94.3	14.3	695.8	11.7	11
AD	1015	40.09	0.0065	19.56	0.500	78.9	85.6	15.1	699.3	12.4	16
AE	1065	36.53	0.0058	8.134	0.711	88.1	93.4	16.1	696.3	8.7	11
AF	1065	37.88	0.0098	9.624	0.608	52.2	92.5	17.1	711.7	9.9	16
AG	1115	35.46	0.0096	5.504	1.05	53.0	95.4	18.7	691.3	6.0	11
AH	1115	36.34	0.0051	7.782	1.03	99.2	93.7	20.2	694.7	6.2	16
AI	1115	36.17	0.0081	9.400	1.06	63.0	92.3	21.8	683.8	5.9	21
AJ	1115	36.29	0.0124	12.87	1.46	41.3	89.5	24.0	668.1	4.5	31
AK	1115	36.26	0.0050	13.30	2.57	103.0	89.2	27.9	665.5	3.0	61
AL	1115	37.22	0.0093	19.27	4.01	54.7	84.7	34.0	651.5	2.1	119
AM	1215	29.91	0.0027	2.677	5.89	186.7	97.4	43.0	609.2	1.4	11
AN	1315	28.85	0.0021	3.549	23.9	247.5	96.4	79.3	585.53	0.88	11
AO	1415	31.23	0.0118	6.433	13.7	43.3	93.9	100.0	613.0	1.1	11
Total gas age ± 1σ			n=40		65.9	88.0	K2O=10.33%		605.2	1.1	

ID	Temp (°C)	$^{40}Ar/^{39}Ar$	$^{37}Ar/^{39}Ar$	$^{36}Ar/^{39}Ar$ (x 10^{-3})	$^{39}Ar_K$ (x 10^{-15} mol)	K/Ca	$^{40}Ar^*$ (%)	^{39}Ar (%)	Age (Ma)	±1σ (Ma)	Time (min)
PVBR04-2-04, K-feldspar, 0.09 mg, J=0.013604±0.10%, D=1.004±0.001, NM-206B, Lab#=57045-04											
B	515	17.04	0.0147	4.095	0.101	34.8	92.9	0.3	356.0	85.3	11
C	565	18.41	0.0076	-0.3594	0.201	67.2	100.6	0.9	410.1	42.2	11
D	615	22.73	0.0060	-0.5854	0.695	85.1	100.8	3.1	495.0	12.1	11
E	665	27.55	0.0087	0.3921	0.574	58.9	99.6	4.9	578.9	14.3	9
F	715	30.76	0.0079	-0.0332	0.806	64.4	100.0	7.4	638.3	9.9	11
G	765	32.80	0.0100	-0.7372	0.684	51.1	100.7	9.5	677.4	11.7	10
H	815	33.14	0.0310	0.9266	0.632	16.5	99.2	11.4	674.8	12.5	11
I	865	33.02	0.0882	-0.3683	0.563	5.8	100.4	13.2	679.4	13.8	11
J	915	33.27	0.1317	2.184	0.706	3.9	98.1	15.4	670.8	11.3	11
K	965	33.81	0.3295	1.256	0.894	1.5	99.0	18.2	685.1	9.0	11
L	1015	34.55	0.0351	4.353	1.10	14.6	96.3	21.6	681.6	7.4	11
M	1040	35.36	0.0173	6.635	0.920	29.5	94.5	24.4	684.0	8.8	11
N	1065	33.43	0.0257	1.741	0.890	19.8	98.5	27.2	675.6	8.9	11
O	1090	33.37	0.0476	2.573	0.967	10.7	97.7	30.2	670.4	8.3	11
P	1115	32.54	0.0516	3.291	1.14	9.9	97.0	33.7	652.3	7.0	11
Q	1215	31.13	0.0278	2.065	12.1	18.3	98.0	71.2	634.1	1.1	11
R	1315	36.98	0.0821	4.496	8.20	6.2	96.4	96.6	722.0	1.4	11
S	1415	44.83	0.0748	33.33	1.09	6.8	78.0	100.0	710.9	7.6	11
Total gas age ± 1σ			n=18		32.3	9.4	K2O=10.12%		664.3	1.4	
PVBR04-2-05, K-feldspar, 0.07 mg, J=0.013604±0.10%, D=1.004±0.001, NM-206B, Lab#=57045-05											
B	515	31.73	0.0149	79.44	0.212	34.3	26.0	0.9	194.3	48.4	11
C	565	21.70	0.0087	36.61	0.381	58.9	50.1	2.6	251.9	24.3	11
D	615	16.68	0.0074	-0.6436	0.545	68.7	101.1	5.1	377.0	16.0	11
E	665	23.48	0.0118	-0.1907	0.553	43.4	100.2	7.6	507.0	14.9	11
F	715	29.92	0.0111	1.058	0.516	46.1	99.0	9.9	617.8	15.6	11
G	765	32.38	0.0028	-1.3871	0.471	181.3	101.3	12.0	673.4	16.6	10
H	815	34.13	0.0149	-3.6667	0.414	34.3	103.2	13.8	714.7	18.5	10
I	865	34.13	0.0670	-0.9289	0.574	7.6	100.8	16.4	701.1	13.6	11
J	915	34.61	0.1744	1.186	0.471	2.9	99.0	18.5	698.8	16.5	10
K	965	33.71	0.2653	0.3764	0.587	1.9	99.7	21.1	687.7	13.2	11
L	1015	34.13	0.0290	1.993	0.499	17.6	98.3	23.3	686.3	15.6	11
M	1040	34.27	0.0284	9.160	0.427	17.9	92.1	25.2	652.3	18.7	11
N	1065	32.33	0.0399	0.8241	0.368	12.8	99.3	26.9	661.4	21.2	11
O	1090	31.96	0.0654	0.8844	0.381	7.8	99.2	28.6	654.7	20.7	11
P	1115	31.12	0.0799	-0.5804	0.357	6.4	100.6	30.2	647.6	22.2	11
Q	1215	27.96	0.0553	2.698	3.81	9.2	97.2	47.2	574.2	2.4	11
R	1315	30.30	0.0486	3.105	10.2	10.5	97.0	92.8	614.0	1.2	11
S	1415	36.19	0.1142	15.37	1.60	4.5	87.5	100.0	653.9	5.3	11
Integrated age ± 1σ			n=18		22.4	8.8	K2O=9.03%		606.8	1.8	
PVBR04-2-06, K-feldspar, 0.13 mg, J=0.013604±0.10%, D=1.004±0.001, NM-206B, Lab#=57045-06											
B	515	43.98	0.0035	25.20	0.031	144.5	83.1	0.1	736.6	247.0	11
C	565	56.05	0.0058	117.4	0.087	88.2	38.1	0.2	465.7	98.2	10
D	615	23.87	0.0059	1.020	0.307	86.7	98.7	0.8	507.7	28.5	11
E	665	27.62	0.0222	-4.3098	0.240	23.0	104.6	1.3	605.3	33.1	8
F	715	35.84	0.0109	-0.5701	0.497	47.0	100.5	2.3	727.9	15.7	11
G	765	40.76	0.0090	1.003	0.577	56.7	99.3	3.4	800.8	13.1	11
H	815	42.37	0.0032	0.4954	0.584	160.4	99.7	4.5	828.7	12.9	11
I	865	40.94	0.0043	-0.1223	0.596	119.6	100.1	5.7	808.9	12.8	11
J	915	40.14	0.0070	3.641	0.735	72.9	97.3	7.1	778.1	10.4	11
K	965	37.83	0.0004	1.969	0.603	1303.2	98.5	8.3	748.4	12.8	10
L	1015	36.91	0.0051	2.262	0.757	99.1	98.2	9.8	731.7	10.3	11
M	1040	37.08	0.0027	2.666	0.582	186.4	97.9	10.9	732.6	13.3	11
N	1065	38.34	0.0041	6.053	0.722	123.6	95.3	12.3	737.0	10.7	11
O	1090	36.90	0.0080	2.359	0.910	64.1	98.1	14.1	731.1	8.6	11
P	1115	37.33	0.0058	1.582	1.74	88.3	98.7	17.5	742.1	4.7	11
Q	1215	36.85	0.0017	1.509	8.90	304.3	98.8	34.8	734.4	1.3	11
R	1315	39.43	0.0010	1.490	17.6	523.7	98.9	69.1	777.0	1.0	11
S	1415	41.49	0.0034	2.332	15.9	151.6	98.3	100.0	806.2	1.3	11
Total gas age ± 1σ			n=18		51.3	188.0	K2O=11.15%		772.8	1.2	

ID	Temp (°C)	$^{40}Ar/^{39}Ar$	$^{37}Ar/^{39}Ar$	$^{36}Ar/^{39}Ar$ (x 10^{-3})	$^{39}Ar_K$ (x 10^{-15} mol)	K/Ca	$^{40}Ar^*$ (%)	^{39}Ar (%)	Age (Ma)	±1σ (Ma)	Time (min)
PVBR04-2-07, K-feldspar, 0.06 mg, J=0.013604±0.10%, D=1.004±0.001, NM-206B, Lab#=57045-07											
B	515	50.26	-0.0712	129.1	0.021	-	24.1	0.2	278.0	341.6	11
C	565	19.58	0.0127	11.48	0.054	40.2	82.6	0.5	363.1	126.0	11
D	615	18.87	0.0054	-2.6499	0.084	95.3	104.1	1.1	432.4	79.6	9
E	665	29.35	0.0079	4.870	0.241	64.5	95.1	2.8	587.5	25.6	11
F	715	37.09	-0.0004	5.415	0.251	-	95.7	4.6	719.2	23.2	10
G	765	41.71	0.0106	1.894	0.364	48.2	98.7	7.2	811.6	15.4	10
H	815	43.67	0.0019	1.779	0.348	275.7	98.8	9.7	843.1	15.8	11
I	865	44.62	0.0043	4.996	0.268	119.8	96.7	11.6	843.2	20.2	11
J	915	43.81	-0.0025	6.311	0.216	-	95.7	13.1	824.3	25.1	11
K	965	42.36	0.0138	6.999	0.196	36.9	95.1	14.5	798.0	28.2	11
L	1015	41.86	-0.0021	4.242	0.266	-	97.0	16.4	803.0	21.1	11
M	1040	40.31	0.0177	12.48	0.229	28.8	90.8	18.0	738.1	25.4	11
N	1065	40.45	0.0044	5.348	0.276	116.5	96.1	19.9	775.0	20.8	11
O	1090	39.96	0.0121	3.679	0.142	42.0	97.3	21.0	775.1	38.9	11
P	1115	39.98	0.0019	3.649	0.400	266.9	97.3	23.8	775.6	14.4	11
Q	1165	38.82	0.0028	3.348	1.36	183.4	97.5	33.4	758.0	4.5	11
R	1215	42.71	0.0012	2.228	5.17	435.8	98.5	70.1	825.9	1.7	11
S	1265	46.63	0.0012	3.046	2.36	422.2	98.1	86.8	883.2	2.8	11
T	1315	47.67	0.0037	7.752	1.86	138.3	95.2	100.0	877.9	3.3	11
Total gas age ± 1σ			n=19		14.1	200.1	K2O=6.64%		821.4	2.0	
PVBR04-2-08, K-feldspar, 0.04 mg, J=0.013604±0.10%, D=1.004±0.001, NM-206B, Lab#=57045-08											
B	515	64.83	0.0589	130.7	0.039	8.7	40.4	0.3	557.1	210.7	11
C	565	34.93	0.0257	32.65	0.049	19.8	72.4	0.6	539.7	165.7	11
D	615	21.88	0.0098	-6.3816	0.169	52.3	108.6	1.8	511.4	48.1	11
E	665	28.86	0.0201	-3.8764	0.288	25.4	104.0	3.7	625.0	27.3	11
F	715	35.42	-0.0002	-2.6278	0.405	-	102.2	6.5	731.1	19.1	11
G	765	40.03	0.0040	-0.3515	0.578	126.5	100.3	10.4	795.4	13.4	11
H	815	42.99	0.0041	-2.0380	0.491	125.6	101.4	13.8	850.1	15.1	9
I	865	44.11	0.0039	1.049	0.427	130.6	99.3	16.7	853.4	17.6	11
J	915	43.64	0.0098	-0.7623	0.315	51.9	100.5	18.9	854.5	23.6	11
K	965	42.85	0.0072	-3.9220	0.317	70.6	102.7	21.0	856.6	23.5	11
L	1015	43.07	0.0128	-0.4850	0.355	39.9	100.3	23.4	844.3	21.2	11
M	1040	45.17	0.0066	10.03	0.297	77.6	93.4	25.5	828.3	25.4	11
N	1065	44.74	0.0112	1.090	0.266	45.7	99.3	27.3	863.1	27.6	11
O	1090	42.58	-0.0028	-2.9722	0.232	-	102.1	28.9	848.1	32.0	11
P	1115	45.17	0.0067	-2.1675	0.166	75.9	101.4	30.0	884.5	44.3	11
Q	1215	37.46	0.0016	2.855	2.91	311.7	97.7	49.9	738.0	3.0	11
R	1315	42.71	0.0021	2.333	5.29	243.7	98.4	86.0	825.5	1.8	11
S	1415	47.29	0.0090	15.81	2.05	56.5	90.1	100.0	834.9	4.1	11
Total gas age ± 1σ			n=18		14.6	112.3	K2O=10.33%		802.5	2.4	

Notes:

Isotopic ratios corrected for blank, radioactive decay, and mass discrimination, not corrected for interfering reactions.
Errors quoted for individual analyses include analytical error only, without interfering reaction or J uncertainties.
Total gas age calculated by summing isotopic measurements of all steps.
Total gas age error calculated by quadratically combining errors of isotopic measurements of all steps.
Decay constants and isotopic abundances after Steiger and Jäger (1977).
Weight percent K_2O calculated from ^{39}Ar signal, sample weight, and instrument sensitivity.
K_2O values reflect inacurracy in weight measurements due to small sample size.
Ages calculated relative to FC-2 Fish Canyon Tuff sanidine interlaboratory standard at 28.27 Ma
Decay Constant (LambdaK (total)) = 5.476e-10/a

Correction factors:

NM-201: $(^{39}Ar/^{37}Ar)_{Ca} = 0.0007 \pm 2e\text{-}05$, $(^{36}Ar/^{37}Ar)_{Ca} = 0.00028 \pm 2e\text{-}05$, $(^{38}Ar/^{39}Ar)_K = 0.013$, $(^{40}Ar/^{39}Ar)_K = 0.01 \pm 0.002$

NM-206: $(^{39}Ar/^{37}Ar)_{Ca} = 0.0007 \pm 5e\text{-}05$, $(^{36}Ar/^{37}Ar)_{Ca} = 0.00028 \pm 2e\text{-}05$, $(^{38}Ar/^{39}Ar)_K = 0.013$, $(^{40}Ar/^{39}Ar)_K = 0.01 \pm 0.002$

APPENDIX 2.6: ARRHENIUS AND LOG R/Ro PLOTS FOR MULTIPLE AND SINGLE-GRAIN K-FELDSPAR.

Arrhenius diagrams for step-heating data from bulk and single-grain analyses are presented in Figures A2.2 to A2.9. Data are plotted as the inverse of the furnace temperature against the diffusion coefficient for a given heating step. Isothermal heating schedules are critical to identifying a shift in diffusion coefficient values at a single temperature interpreted as gas evolution from a mixture of different size diffusion domains (cf. Lovera et al., 1989). In practice an Arrhenius law, or reference line, is calculated from the slope or slopes of low temperature isothermal heating step data, the slope of which reflects the activation energy (E) of a sample. Although this method is highly sensitive to furnace calibration, the small percentage of total gas released during low temperature heating steps, and small sample weights with consequently small ^{39}Ar signals for single grain analyses, it is a method to establish the kinetic parameters of a given sample, particularly between contrasting microtextures within the same hand sample. Complete details and methods for both Arrhenius and log r/r_o calculations see Sanders et al. (2006) DR3.

Log r/r_o plots are a different graphical way of portraying Arrhenius data with the benefit of more visually identifying the distribution of diffusion domain sizes in a given sample. This is a plot of the log of the deviation of the measured data from r_o versus the cumulative % ^{39}Ar released. A sample with a single diffusion domain would be represented by a single line with a given slope on an Arrhenius diagram and a horizontal line through 0 on a log r/r_o plot. As K-feldspar contain a distribution of different size diffusion domains, these plots are more complicated, and $\log(r/r_o)$ values increase as the

measured frequency factors fall below r_o on the Arrhenius diagram. A $\log(r/r_o)$ value of 1 indicates a relative increase in diffusion domain size of 10 whereas a value of 2 means a domain size that is 100 times larger than the reference value. The nondiffusive loss of ^{39}Ar that stems from sample melting is quite apparent on the $\log(r/r_o)$ plot as noted by a sudden drop of the $\log(r/r_o)$ value near the end of an analysis.

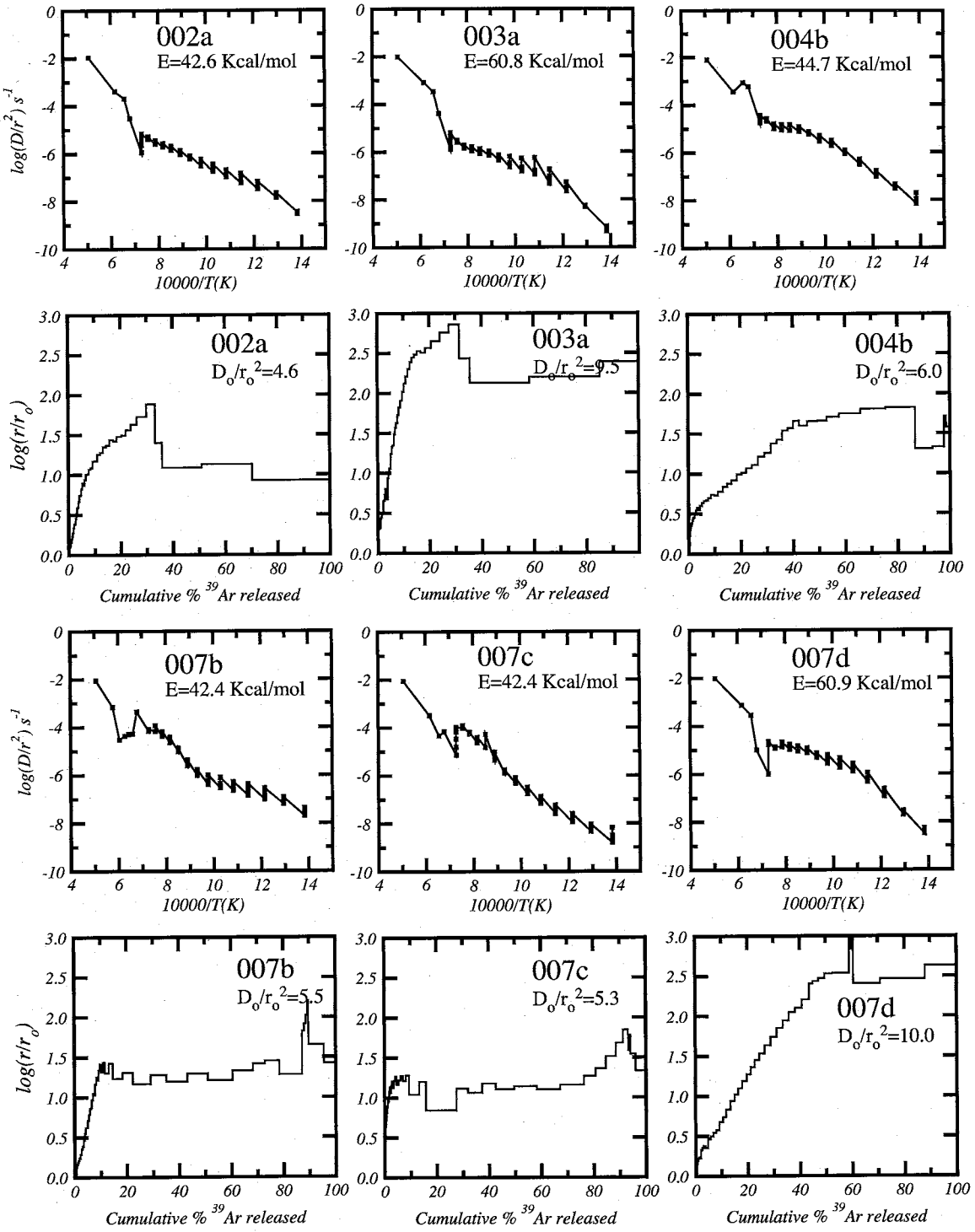

Figure A2.2: Arrhenius and log r/r_o plots calculated from K-feldspar step heating data.

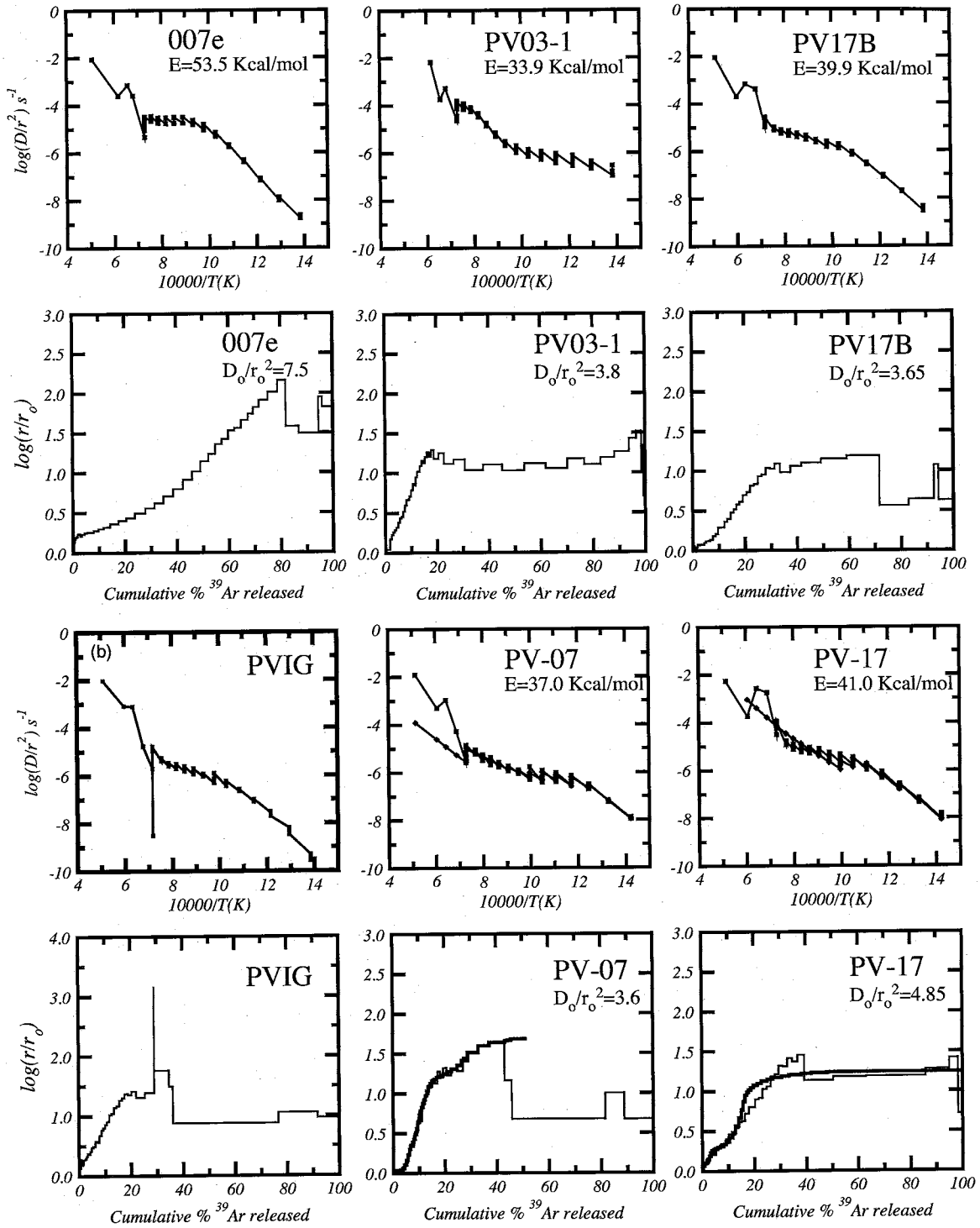

Figure A2.3: Arrhenius and log r/r_o plots calculated from K-feldspar step heating data.

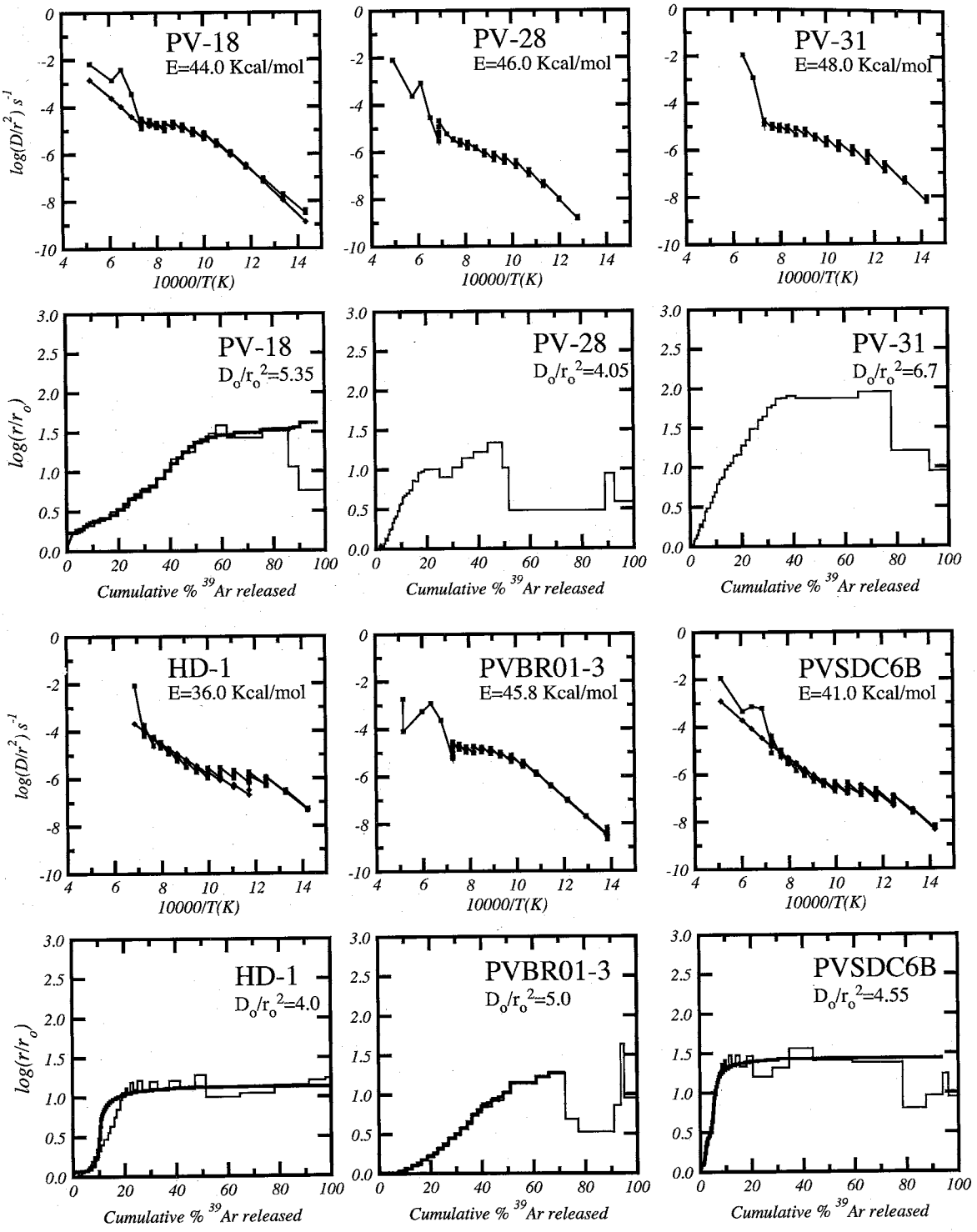

Figure A2.4: Arrhenius and log r/r_o plots calculated from K-feldspar step heating data.

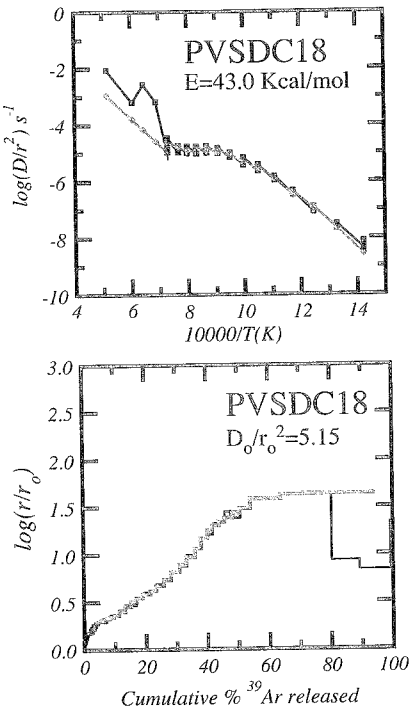

Figure A2.5: Arrhenius and log r/r_o plots calculated from K-feldspar step heating data.

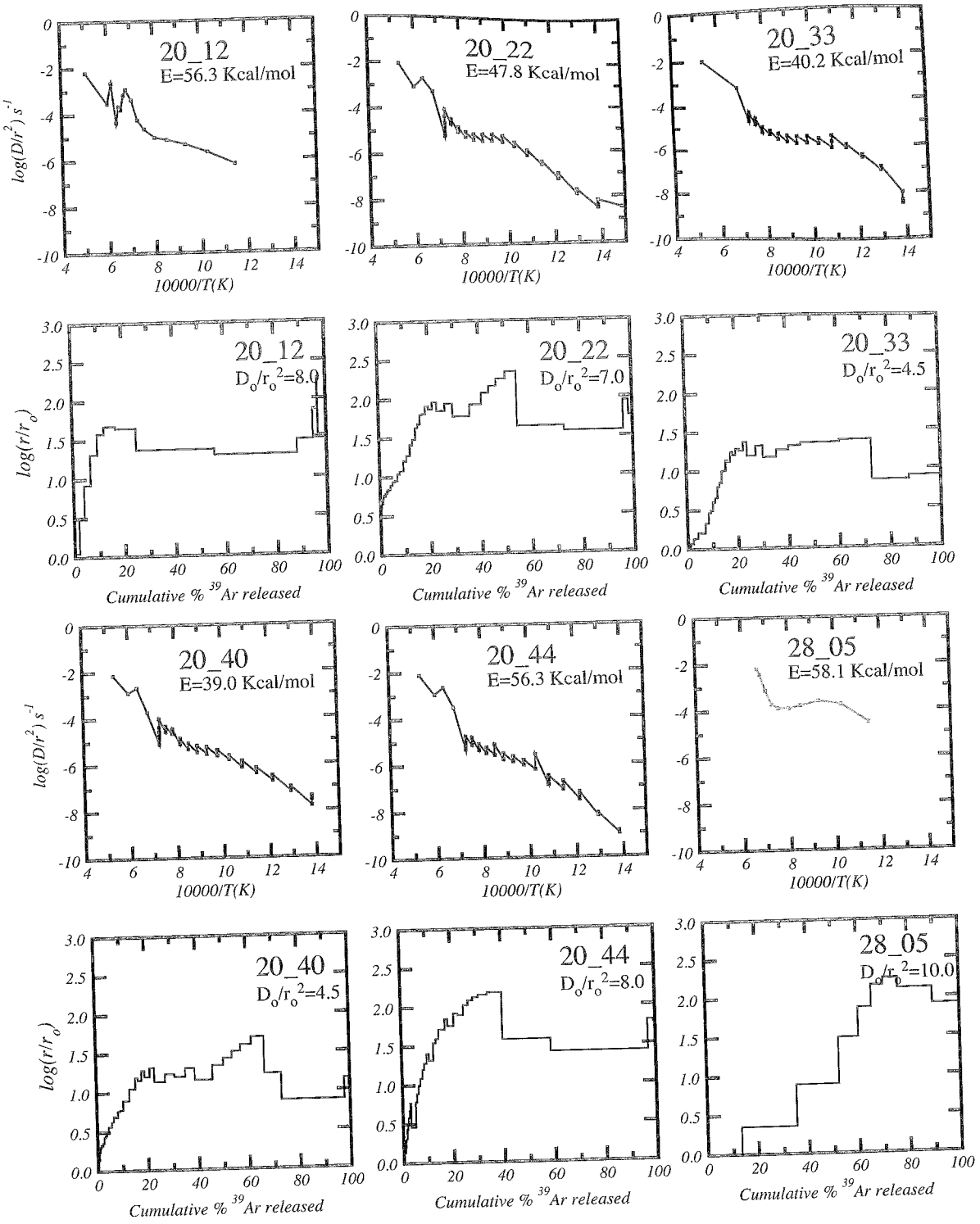

Figure A2.6: Arrhenius and log r/r_o plots calculated from K-feldspar step heating data.

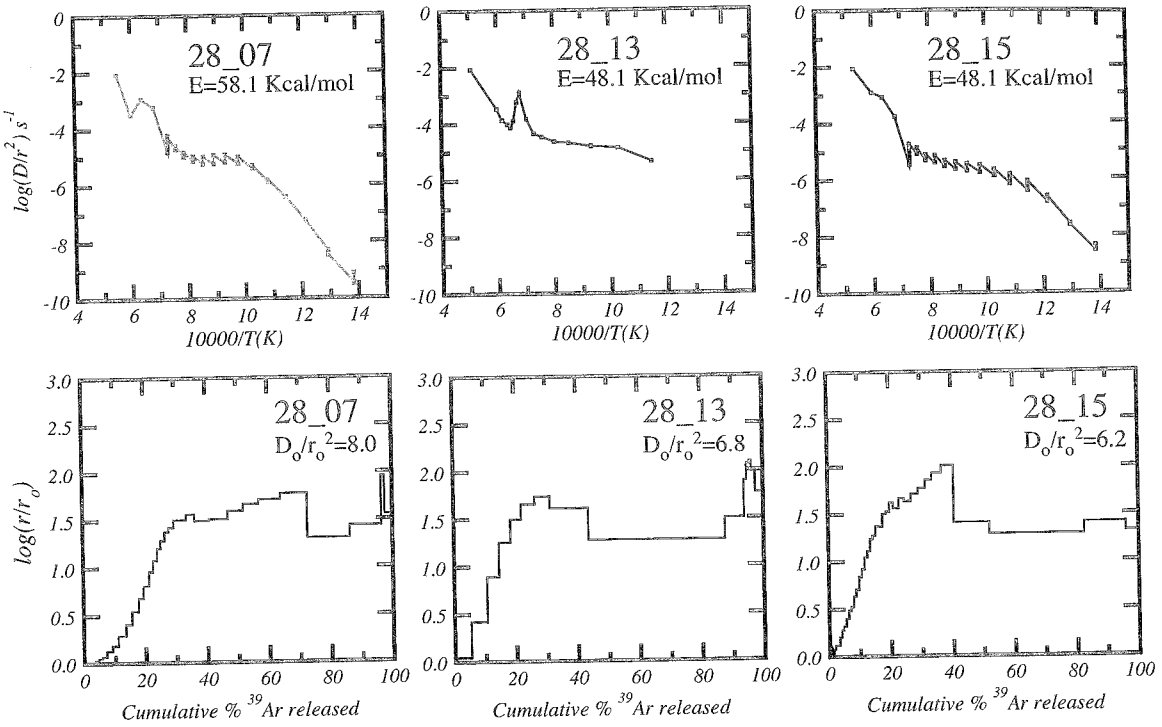

Figure A2.7: Arrhenius and log r/r_o plots calculated from K-feldspar step heating data.

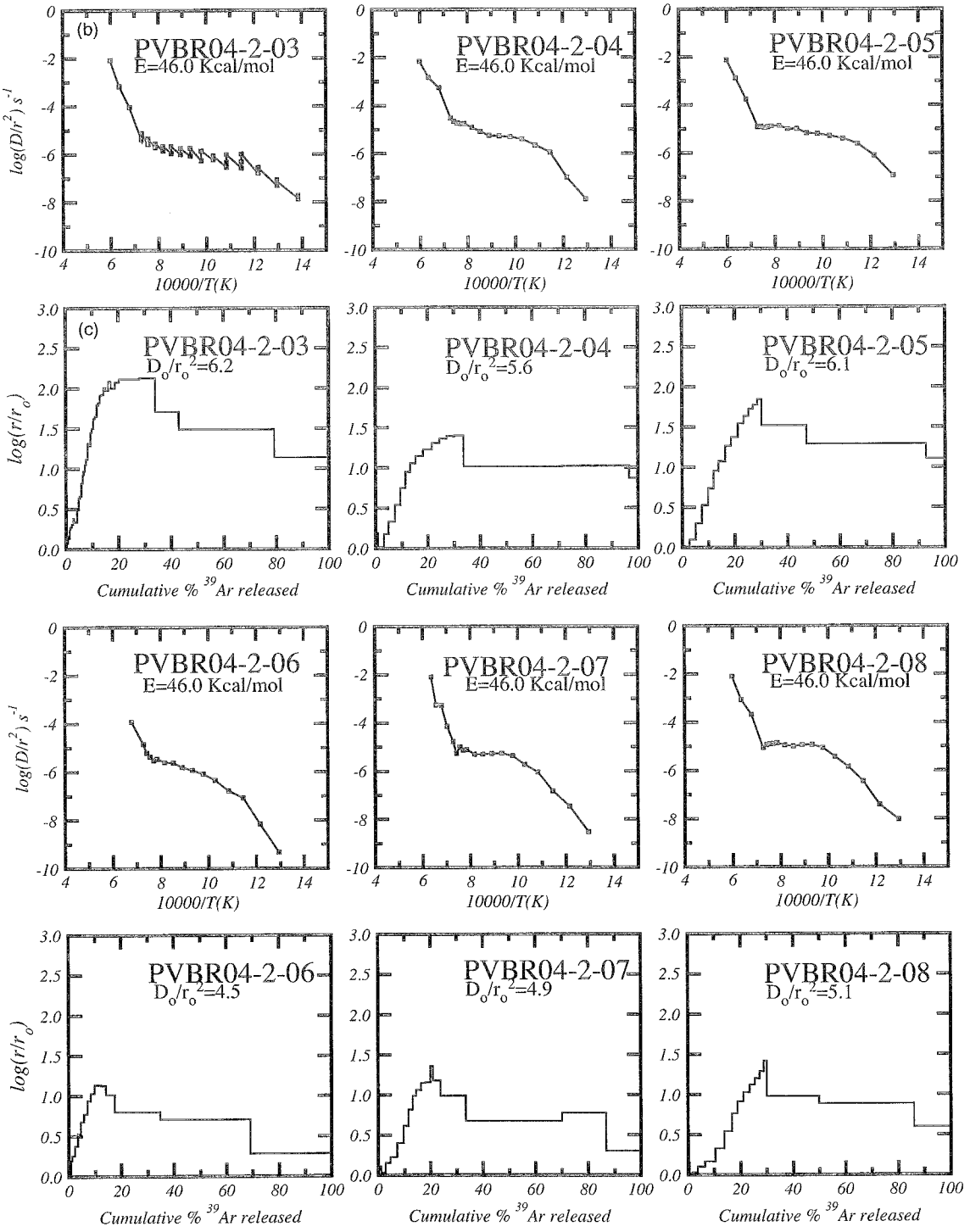

Figure A2.8: Arrhenius and log r/r_o plots calculated from K-feldspar step heating data.

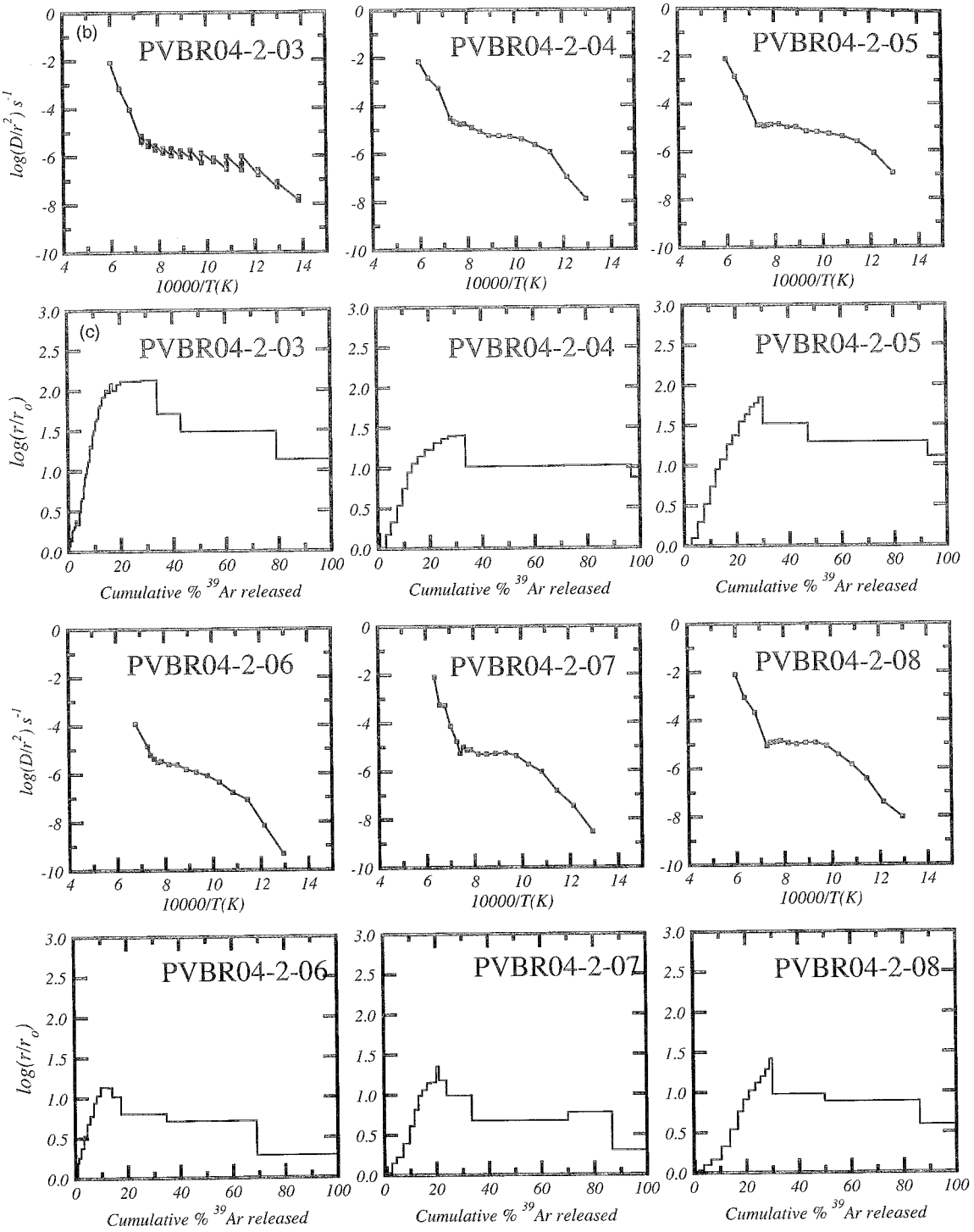

Figure A2.9: Arrhenius and log r/r_o plots calculated from K-feldspar step heating data.

Table A3.1: $^{40}Ar/^{39}Ar$ analytical data for biotite and hornblende from the Klokken intrusion.

	ID	Temp (°C)	$^{40}Ar/^{39}Ar$	$^{37}Ar/^{39}Ar$	$^{36}Ar/^{39}Ar$ (x 10^{-3})	$^{39}Ar_K$ (x 10^{-15} mol)	K/Ca	$^{40}Ar^*$ (%)	^{39}Ar (%)	Age (Ma)	±1σ (Ma)
	Klokken 140025, Biotite, 1.35 mg, J=0.010409±0.16%, D=1.002±0.001, NM-201F, Lab#=56630-01										
X	A	650	71.53	0.0376	14.81	12.9	13.6	93.9	6.8	956.2	1.2
	B	750	89.36	0.0157	2.167	18.7	32.5	99.3	16.6	1180.0	1.2
	C	850	90.09	0.0079	1.209	20.2	64.8	99.6	27.2	1189.9	1.2
	D	920	89.55	0.0132	0.7328	22.1	38.5	99.8	38.8	1186.0	1.2
	E	1000	88.25	0.0051	0.3129	57.6	99.9	99.9	69.0	1174.6	1.1
	F	1075	87.27	0.0080	0.3517	41.8	64.1	99.9	91.0	1164.8	1.1
	G	1110	87.53	0.0375	1.000	5.61	13.6	99.7	93.9	1165.6	1.4
	H	1180	87.72	0.1181	2.290	2.97	4.3	99.2	95.5	1163.7	1.6
	I	1210	87.81	0.0362	0.9338	4.58	14.1	99.7	97.9	1168.5	1.4
	J	1250	87.95	0.0061	0.5690	3.10	83.5	99.8	99.5	1170.9	1.6
	K	1300	87.05	0.0974	4.867	0.698	5.2	98.4	99.9	1149.5	3.9
X	L	1680	63.78	0.5583	83.03	0.254	0.91	61.6	100.0	618.6	11.1
	Integrated age ± 1σ			n=12		190.6	34.5	K2O=5.21%		1160.5	1.6
	Plateau ± 1σ	steps B-K		n=10	MSWD=54.84	177.421	65.510±34.230		93.1	1174.35	3.436
	Klokken 140025, Hornblende, 1.81 mg, J=0.010413±0.17%, D=1.002±0.001, NM-201F, Lab#=56632-01										
	A	800	90.28	1.304	9.790	7.58	0.39	96.9	14.0	1169.2	1.4
	B	900	91.04	0.7056	2.165	8.48	0.72	99.4	29.6	1197.7	1.4
	C	1000	87.56	1.932	1.234	20.6	0.26	99.8	67.6	1168.1	1.3
	D	1030	85.11	1.338	2.547	3.15	0.38	99.2	73.4	1139.1	1.9
	E	1060	85.44	1.559	2.097	2.73	0.33	99.4	78.4	1144.1	1.8
	F	1090	86.15	1.911	1.691	4.00	0.27	99.6	85.8	1152.8	1.5
	G	1120	85.42	2.035	1.907	3.75	0.25	99.5	92.7	1145.2	1.7
	H	1170	84.13	2.021	2.741	3.96	0.25	99.2	100.0	1129.7	1.6
	Integrated age ± 1σ			n=8		54.2	0.32	K2O=1.11%		1164.6	1.8
	Plateau ± 1σ	steps A-H		n=8	MSWD=212.74	54.224	0.362±0.158		100.0	1159.87	8.067
	Klokken 43738, Hornblende, 3.51 mg, J=0.01041±0.13%, D=1.002±0.001, NM-201F, Lab#=56634-01										
X	A	800	162.7	1.236	199.9	0.887	0.41	63.8	4.1	1322.0	6.0
	B	900	95.03	2.755	20.89	0.372	0.19	93.8	5.8	1185.5	6.2
	C	1000	88.07	3.155	3.276	3.74	0.16	99.2	23.0	1168.9	1.9
	D	1030	86.12	2.926	1.308	9.10	0.17	99.8	65.0	1155.0	1.2
	E	1060	84.52	3.109	1.768	1.90	0.16	99.7	73.7	1137.9	2.0
	F	1090	82.21	3.981	2.810	1.79	0.13	99.4	82.0	1112.8	2.5
	G	1120	83.46	4.973	2.753	3.91	0.10	99.5	100.0	1127.0	1.8
	Integrated age ± 1σ			n=7		21.7	0.15	K2O=0.23%		1155.0	1.6
	Plateau ± 1σ	steps B-G		n=6	MSWD=110.98	20.802	0.154±0.031		95.9	1145.97	8.145

Notes:

Isotopic ratios corrected for blank, radioactive decay, and mass discrimination, not corrected for interfering reactions.
Errors quoted for individual analyses include analytical error only, without interfering reaction or J uncertainties.
Integrated age calculated by summing isotopic measurements of all steps.
Integrated age error calculated by quadratically combining errors of isotopic measurements of all steps.
Plateau age is inverse-variance-weighted mean of selected steps.
Plateau age error is inverse-variance-weighted mean error (Taylor, 1982) times root MSWD where MSWD>1.
Plateau error is weighted error of Taylor (1982).
Decay constants and isotopic abundances after Steiger and Jäger (1977).
symbol preceding sample ID denotes analyses excluded from plateau age calculations.
Weight percent K_2O calculated from ^{39}Ar signal, sample weight, and instrument sensitivity.
Ages calculated relative to FC-2 Fish Canyon Tuff sanidine interlaboratory standard at 28.02 Ma
Decay Constant (LambdaK (total)) = 5.543e-10/a
Correction factors:
$(^{39}Ar/^{37}Ar)_{Ca}$ = 0.0007 ± 5e-05
$(^{36}Ar/^{37}Ar)_{Ca}$ = 0.00028 ± 2e-05
$(^{38}Ar/^{39}Ar)_K$ = 0.013
$(^{40}Ar/^{39}Ar)_K$ = 0.01 ± 0.002

Table A3.2. $^{40}Ar/^{39}Ar$ analytical data for unheated and heat-treated Klokken sample 140182.

ID	Temp (°C)	$^{40}Ar/^{39}Ar$	$^{37}Ar/^{39}Ar$	$^{36}Ar/^{39}Ar$ (x 10^{-3})	$^{39}Ar_K$ (x 10^{-15} mol)	K/Ca	$^{40}Ar^*$ (%)	^{39}Ar (%)	Age (Ma)	±1σ (Ma)	Time (min)
Klokken 140182, K-Feldspar, 1.2 mg, J=0.01037±0.48%, D=1.005±0.001, NM-201K, Lab#=56693-01											
X B	450	244.2	-0.1957	97.72	0.147	-	88.2	0.2	2142.2	14.0	9
X C	450	61.48	-3.0156	34.81	0.062	-	82.9	0.2	773.1	42.5	16
X D	450	63.29	-1.0806	57.41	0.053	-	73.1	0.3	714.7	52.4	21
X E	500	56.27	0.6638	23.66	0.093	0.77	87.7	0.4	754.7	29.4	6
X F	500	51.19	-0.2057	22.15	0.142	-	87.2	0.5	694.4	19.8	19
X G	500	56.33	-0.1811	32.78	0.117	-	82.8	0.6	720.0	23.9	24
X H	550	53.32	-0.4311	4.771	0.207	-	97.3	0.9	785.7	13.2	9
X I	550	58.31	0.6254	15.04	0.264	0.82	92.5	1.1	811.2	10.5	19
X J	550	67.43	-0.3654	18.83	0.235	-	91.7	1.4	904.4	11.6	24
X K	600	62.98	0.2090	1.368	0.229	2.4	99.4	1.6	913.5	11.6	9
X L	600	70.76	0.2521	11.72	0.316	2.0	95.1	1.9	967.0	8.8	19
X M	600	74.80	-0.0828	15.24	0.321	-	94.0	2.3	999.6	8.5	24
X N	650	75.95	-0.0094	3.057	0.775	-	98.8	3.1	1051.1	3.8	9
X O	650	79.11	-0.2373	5.518	0.713	-	97.9	3.8	1076.4	4.1	19
X P	650	82.14	-0.0507	5.718	1.15	-	97.9	5.0	1107.7	3.2	24
X Q	700	82.70	0.1399	1.607	1.89	3.6	99.4	7.0	1126.1	2.7	9
X R	700	84.41	0.0395	2.430	2.29	12.9	99.2	9.4	1141.0	2.0	19
X S	750	84.89	0.0618	1.327	2.60	8.2	99.5	12.1	1149.2	2.0	9
X T	750	85.43	-0.0084	1.892	3.34	-	99.3	15.6	1152.8	2.2	17
X U	800	85.38	0.0007	0.4636	3.66	700.2	99.8	19.4	1156.6	1.6	9
X V	800	86.21	0.0611	1.179	4.65	8.4	99.6	24.3	1162.9	1.5	19
X W	850	86.13	-0.0408	0.7694	4.30	-	99.7	28.7	1163.1	1.8	9
X X	850	86.28	0.1210	1.389	5.16	4.2	99.5	34.1	1163.1	1.6	19
X Y	900	86.43	0.0712	0.9915	4.39	7.2	99.7	38.7	1165.6	1.5	9
X Z	900	86.92	-0.0098	1.599	5.05	-	99.5	44.0	1168.6	1.4	18
X AA	950	86.55	0.0542	0.6638	3.79	9.4	99.8	47.9	1167.7	1.6	9
X AB	950	86.30	-0.0349	1.760	3.64	-	99.4	51.7	1161.9	1.7	19
X AC	1000	86.03	0.0548	1.178	3.27	9.3	99.6	55.1	1161.1	1.8	9
X AD	1000	86.43	0.0921	2.190	3.41	5.5	99.3	58.7	1162.1	1.8	19
X AE	1050	85.40	0.0528	1.270	3.84	9.7	99.6	62.7	1154.5	1.8	9
X AF	1050	87.36	0.0751	2.510	6.46	6.8	99.2	69.4	1170.4	1.6	29
X AG	1050	88.36	0.0615	2.965	11.7	8.3	99.0	81.6	1179.1	1.6	59
X AH	1050	88.59	0.0320	5.555	10.4	16.0	98.2	92.4	1173.7	1.4	119
X AI	1050	93.80	0.0417	21.95	4.71	12.2	93.1	97.4	1177.3	1.7	239
X AJ	1100	88.09	-0.6665	7.328	0.241	-	97.5	97.6	1162.4	10.3	9
X AK	1200	89.29	0.7927	8.462	0.313	0.64	97.3	97.9	1173.1	8.0	9
X AL	1250	89.21	-0.0541	8.476	0.337	-	97.2	98.3	1171.1	7.9	9
X AM	1300	91.07	0.5426	13.81	0.402	0.94	95.6	98.7	1174.8	6.3	9
X AN	1500	92.34	-0.0867	21.15	0.919	-	93.2	99.7	1165.0	3.8	9
X AO	1650	137.6	0.1420	206.8	0.324	3.6	55.6	100.0	1066.7	10.7	9
Total gas age ± 1σ			n=40		95.9	12.7	K2O=2.96%		1159.1	4.3	

Klokken 140182-650, Kspar, 1.84 mg, J=0.013537±0.11%, D=1.005±0.001, NM-206B, Lab#=57030-01

X	B	450	57.08	0.0260	190.1	0.099	19.7	1.6	0.1	22.3	52.6	9
X	C	450	14.20	-0.0296	21.67	0.038	-	54.9	0.1	182.9	120.1	19
X	D	450	19.28	-0.0882	34.42	0.029	-	47.2	0.1	211.9	147.0	24
X	E	500	-3.9507	0.1538	-17.1821	0.048	3.3	-28.5	0.1	27.7	102.8	9
X	F	500	4.640	0.1376	7.686	0.068	3.7	51.2	0.2	57.7	66.3	19
X	G	500	8.381	0.0287	24.15	0.060	17.8	14.8	0.2	30.3	80.1	24
X	H	550	-1.0150	-0.0659	-15.1159	0.113	-	-335.3	0.3	83.0	39.8	9
X	I	550	3.006	0.0262	0.3906	0.160	19.5	96.2	0.3	69.9	27.8	19
X	J	550	4.972	0.0626	12.39	0.135	8.1	26.3	0.4	32.0	34.9	24
X	K	600	0.8242	-0.0043	-4.7724	0.220	-	273.2	0.5	54.2	21.3	9
X	L	600	3.262	0.0206	-1.0200	0.320	24.8	109.3	0.7	85.8	14.3	19
X	M	600	4.924	0.0360	3.653	0.307	14.2	78.1	0.9	92.5	15.8	24
X	N	650	3.410	0.0170	-1.7561	0.426	29.9	115.3	1.1	94.4	10.5	9
X	O	650	6.708	0.0315	1.697	0.704	16.2	92.6	1.5	147.2	6.2	19
X	P	650	9.346	0.0398	2.506	0.631	12.8	92.1	1.9	201.1	7.2	24
X	Q	700	10.59	0.0337	0.0727	0.839	15.1	99.8	2.4	244.0	5.3	9
X	R	700	14.79	0.0391	1.165	1.50	13.1	97.7	3.2	326.0	3.0	19
X	S	750	18.48	0.0359	0.0894	3.53	14.2	99.9	5.2	407.0	1.3	9
X	T	750	21.96	0.0303	0.5370	3.78	16.8	99.3	7.4	472.2	1.3	19
X	U	800	26.47	0.0329	0.2658	6.42	15.5	99.7	11.0	557.72	0.97	9
X	V	800	32.01	0.0331	0.3994	8.09	15.4	99.6	15.5	655.3	1.1	19
X	W	850	37.24	0.0332	0.2019	7.20	15.4	99.8	19.6	744.3	1.1	9
X	X	850	42.16	0.0316	0.5134	9.60	16.2	99.6	25.0	822.1	1.5	19
X	Y	900	46.95	0.0316	0.3430	8.29	16.1	99.8	29.7	896.8	1.3	9
X	Z	900	51.02	0.0335	0.4207	10.5	15.2	99.8	35.6	957.0	1.3	19
X	AA	950	54.98	0.0310	0.3512	8.60	16.5	99.8	40.5	1014.4	1.4	9
X	AB	950	57.22	0.0316	0.4772	9.54	16.1	99.8	45.9	1045.3	1.5	19
X	AC	1000	59.10	0.0326	0.4339	7.79	15.7	99.8	50.3	1071.5	1.6	9
X	AD	1000	60.51	0.0303	0.4444	9.05	16.8	99.8	55.4	1090.8	1.5	19
X	AE	1050	61.44	0.0319	0.4786	9.29	16.0	99.8	60.6	1103.3	1.6	9
X	AF	1050	62.56	0.0326	1.047	10.5	15.7	99.5	66.6	1116.1	1.4	29
X	AG	1050	63.59	0.0322	2.247	8.24	15.9	99.0	71.2	1125.2	1.8	59
X	AH	1050	64.66	0.0319	3.832	9.82	16.0	98.3	76.7	1133.2	1.8	119
X	AI	1050	66.38	0.0358	6.597	11.7	14.2	97.1	83.4	1145.2	1.8	239
X	AJ	1100	65.49	0.0359	0.7025	6.09	14.2	99.7	86.8	1156.4	1.2	9
X	AK	1200	65.47	0.0330	0.5465	13.4	15.5	99.8	94.4	1156.7	1.7	9
X	AL	1250	65.13	0.0474	1.156	2.10	10.8	99.5	95.6	1149.9	2.4	9
X	AM	1300	65.38	0.0424	1.190	2.67	12.0	99.5	97.1	1153.0	2.1	9
X	AN	1500	66.51	0.0384	2.990	3.65	13.3	98.7	99.1	1160.8	1.8	9
X	AO	1650	72.82	0.0355	25.14	1.52	14.4	89.8	100.0	1157.8	3.2	9
Total gas age ± 1σ				n=40		177.1	15.4	K2O=2.73%		978.8	1.2	

Klokken 140182-700, Kspar, 0.72 mg, J=0.01352±0.10%, D=1.005±0.001, NM-206B, Lab#=57034-01

X	B	450	59.30	0.0885	182.4	0.050	5.8	9.1	0.1	128.5	95.5	9
X	C	450	24.43	0.0724	102.2	0.024	7.1	-23.6	0.1	-148.3	232.3	16
X	D	450	44.72	0.1296	131.9	0.017	3.9	12.9	0.1	136.6	281.0	24
X	E	500	-3.7530	-0.1396	7.309	0.026	-	157.7	0.2	-152.7	206.9	9
X	G	500	8.857	-0.0078	33.89	0.031	-	-13.2	0.2	-29.1	163.2	16
X	H	500	19.08	-0.3855	46.44	0.031	-	27.9	0.3	126.8	152.5	24
X	I	550	-0.4630	0.0566	-14.0162	0.061	9.0	-776.7	0.4	88.5	76.9	9
X	J	550	9.208	-0.0838	22.38	0.057	-	28.0	0.5	62.6	84.9	19
X	K	550	11.60	0.0533	32.49	0.065	9.6	17.2	0.6	48.5	73.8	21
X	L	600	2.373	0.0191	2.232	0.132	26.8	72.2	0.8	41.6	34.7	9
X	M	600	6.618	0.0300	6.642	0.173	17.0	70.3	1.1	111.3	26.4	19
X	N	600	9.280	0.0049	4.382	0.188	104.2	86.0	1.4	187.0	23.2	24
X	O	650	7.140	0.0276	-3.6087	0.317	18.5	115.0	1.9	192.0	13.8	9
X	P	650	11.26	0.0353	3.048	0.475	14.4	92.0	2.7	239.2	9.2	19
X	Q	650	14.53	0.0455	3.905	0.449	11.2	92.1	3.4	303.5	9.2	24
X	R	700	14.69	0.0296	-0.7282	0.616	17.2	101.5	4.4	335.1	7.0	9
X	S	700	17.58	0.0323	2.151	0.972	15.8	96.4	6.0	376.5	4.4	19
X	T	750	19.53	0.0288	0.0355	1.36	17.7	100.0	8.2	427.5	3.1	9
X	U	750	23.10	0.0379	1.259	1.96	13.5	98.4	11.4	489.3	2.4	19
X	V	800	27.02	0.0325	0.4499	2.15	15.7	99.5	15.0	566.1	2.0	9
X	W	800	31.47	0.0326	1.349	2.60	15.7	98.7	19.2	640.4	1.9	19
X	X	850	35.92	0.0329	0.4578	2.57	15.5	99.6	23.4	720.6	1.8	9
X	Y	850	40.49	0.0357	1.177	3.37	14.3	99.1	28.9	791.6	1.6	19
X	Z	900	44.91	0.0336	0.3593	3.11	15.2	99.8	34.0	864.7	1.8	8
X	AA	900	48.90	0.0345	1.159	4.08	14.8	99.3	40.6	921.5	1.6	19
X	AB	950	52.87	0.0321	0.4549	3.07	15.9	99.8	45.7	982.9	2.0	9
X	AC	950	55.25	0.0295	1.413	3.95	17.3	99.2	52.1	1012.9	1.8	19
X	AD	1000	57.66	0.0360	1.109	3.01	14.2	99.4	57.0	1048.0	1.8	9
X	AE	1000	59.13	0.0332	2.112	3.63	15.4	98.9	63.0	1064.1	1.8	19
X	AF	1050	60.61	0.0303	1.357	2.86	16.8	99.3	67.6	1087.4	2.0	9
X	AG	1050	63.19	0.0365	2.616	4.62	14.0	98.8	75.2	1117.3	1.6	29
X	AH	1050	64.45	0.0367	3.401	6.30	13.9	98.4	85.5	1130.9	1.5	59
X	AI	1050	66.39	0.0366	7.896	5.62	13.9	96.5	94.6	1139.1	1.6	119
X	AJ	1050	75.31	0.0350	39.41	2.35	14.6	84.5	98.5	1134.0	3.0	239
X	AK	1100	65.34	0.0444	12.37	0.058	11.5	94.4	98.6	1107.5	47.2	9
X	AL	1200	68.06	0.0742	5.695	0.087	6.9	97.5	98.7	1169.7	31.5	9
X	AM	1250	68.26	0.0250	12.65	0.076	20.4	94.5	98.8	1145.3	34.9	9
X	AN	1300	75.70	-0.0415	48.57	0.070	-	81.0	99.0	1102.8	39.9	9
X	AO	1500	73.82	0.0474	31.87	0.583	10.8	87.2	99.9	1143.7	6.3	9
X	AP	1650	343.3	-0.1025	945.6	0.053	-	18.6	100.0	1136.3	66.1	9
	Total gas age ± 1σ			n=40		61.2	15.1	K2O=2.42%		930.5	1.2	

Klokken 140182-900, Kspar, 0.63 mg, J=0.013506±0.11%, D=1.005±0.001, NM-206B, Lab#=57037-01

X B	450	64.44	-0.0033	206.2	0.043	-	5.4	0.1	84.5	125.5	9
X C	450	22.09	0.4863	25.42	0.014	1.0	66.2	0.1	328.9	282.6	19
X D	450	40.06	0.2141	144.4	0.011	2.4	-6.5	0.1	-65.7	470.7	24
X E	500	-15.5953	-0.4944	-76.0948	0.019	-	-43.8	0.1	161.3	226.6	9
X F	500	5.848	-0.1613	22.80	0.027	-	-15.6	0.2	-22.6	182.8	19
X G	500	15.89	-0.2635	49.33	0.022	-	8.1	0.2	31.4	210.7	24
X H	550	-6.8127	-0.1245	-21.8762	0.040	-	5.4	0.3	-9.1	120.4	9
X I	550	4.509	-0.0565	12.37	0.056	-	18.6	0.4	20.5	82.5	19
X J	550	6.995	-0.1106	5.537	0.050	-	76.4	0.4	127.2	94.7	24
X K	600	-4.6359	0.0066	-32.7863	0.062	77.6	-108.5	0.5	120.3	70.6	6
X L	600	1.891	-0.0155	3.862	0.132	-	39.3	0.7	18.1	35.3	19
X M	600	4.089	0.0365	12.96	0.115	14.0	6.2	0.9	6.2	40.7	24
X N	650	-1.2130	-0.0014	-9.4397	0.161	-	-128.1	1.2	38.2	28.5	9
X O	650	1.487	0.0420	-0.6699	0.248	12.2	113.6	1.5	40.9	18.8	19
X P	650	2.546	0.0300	5.978	0.232	17.0	30.5	1.9	18.9	20.2	24
X Q	700	-0.1627	0.0299	-2.5856	0.295	17.1	-343.9	2.4	14.6	16.1	9
X R	700	1.436	0.0213	0.3531	0.464	24.0	92.8	3.1	32.3	10.3	19
X S	750	0.6736	0.0371	-1.9211	0.650	13.8	186.0	4.1	30.2	7.1	9
X T	750	1.621	0.0318	1.113	0.996	16.0	79.8	5.6	31.4	4.9	19
X U	800	1.134	0.0299	-1.0491	1.15	17.0	127.8	7.4	35.1	4.2	7
X V	800	1.963	0.0304	0.4038	1.96	16.8	94.0	10.4	44.7	2.4	17
X W	850	2.136	0.0337	-0.0146	2.17	15.2	100.3	13.7	51.9	2.2	9
X X	850	3.499	0.0362	0.4324	2.94	14.1	96.4	18.3	81.2	1.7	18
X Y	900	4.649	0.0375	-0.1986	2.55	13.6	101.3	22.2	112.4	1.9	9
X Z	900	6.909	0.0370	0.6316	3.50	13.8	97.3	27.6	158.5	1.3	19
X AA	950	9.555	0.0379	0.0364	2.86	13.5	99.9	32.0	221.3	1.6	9
X AB	950	12.99	0.0339	0.8466	3.84	15.1	98.1	37.9	289.8	1.2	19
X AC	1000	18.35	0.0384	0.2643	3.07	13.3	99.6	42.7	402.7	1.5	9
X AD	1000	22.67	0.0369	0.8660	3.69	13.8	98.9	48.4	482.7	1.4	19
X AE	1050	33.33	0.0437	0.6351	3.79	11.7	99.4	54.2	675.5	1.4	9
X AF	1050	37.52	0.0396	1.523	5.75	12.9	98.8	63.1	741.2	1.2	29
X AH	1050	45.90	0.0366	3.028	5.12	13.9	98.1	71.0	867.2	1.3	59
X AI	1050	54.22	0.0378	7.027	5.27	13.5	96.2	79.1	973.5	1.6	119
X AJ	1050	60.68	0.0430	14.08	5.29	11.9	93.1	87.3	1035.8	1.7	239
X AK	1100	62.48	0.0441	1.945	1.47	11.6	99.1	89.5	1109.5	2.8	9
X AL	1200	61.69	0.0507	0.9885	2.81	10.1	99.5	93.9	1102.8	2.1	9
X AM	1250	60.59	0.0621	1.244	1.63	8.2	99.4	96.4	1086.8	2.6	9
X AN	1300	61.16	0.0771	1.572	1.33	6.6	99.3	98.4	1093.3	3.0	9
X AO	1500	64.85	0.1804	16.66	0.444	2.8	92.4	99.1	1083.0	8.0	9
X AP	1650	75.68	0.0463	45.05	0.566	11.0	82.4	100.0	1115.8	6.8	9
Total gas age ± 1σ			n=40		64.8	12.8	K2O=2.93%		614.83	0.91	

Klokken 140182-1000, Kspar, 0.69 mg, J=0.01368±0.13%, D=1.005±0.001, NM-206B, Lab#=57040-01

X B	450	19.69	0.0028	73.01	0.092	184.9	-9.6	0.1	-47.8	56.1	9
X C	450	4.097	0.1355	41.27	0.030	3.8	-198.1	0.2	-214.4	181.0	19
X D	450	14.13	-0.5129	59.80	0.015	-	-25.4	0.2	-92.0	363.2	24
X E	500	-13.0187	-0.4691	-52.6461	0.016	-	-19.1	0.2	61.1	290.1	8
X F	500	2.198	-0.1450	3.533	0.022	-	51.8	0.3	28.1	217.1	19
X G	500	13.21	-0.1487	18.63	0.016	-	58.2	0.3	182.6	272.4	24
X H	550	-9.4191	0.2199	11.09	0.020	2.3	134.6	0.3	-348.2	289.2	6
X I	550	2.250	-0.1457	-3.4666	0.038	-	145.2	0.4	79.5	134.1	19
X J	550	9.899	-0.0391	32.78	0.029	-	2.0	0.4	4.9	167.7	21
X K	600	-3.2290	0.0044	-11.4584	0.050	115.1	-4.6	0.5	3.7	94.9	9
X L	600	1.606	0.0577	3.502	0.066	8.8	35.4	0.6	14.1	74.3	19
X M	600	4.000	-0.1133	9.979	0.064	-	25.8	0.7	25.6	74.4	24
X N	650	-2.3722	0.0330	-2.1666	0.086	15.5	73.0	0.8	-44.0	54.9	8
X O	650	1.096	0.0352	4.502	0.141	14.5	-22.2	1.1	-6.0	36.1	19
X P	650	2.072	-0.0077	3.359	0.133	-	51.8	1.3	26.5	35.6	24
X Q	700	-0.9557	0.0033	-4.7484	0.173	153.0	-45.3	1.5	10.9	27.6	9
X R	700	0.8805	0.0398	2.516	0.275	12.8	15.0	2.0	3.3	17.8	19
X S	750	-0.2131	0.0097	-1.0538	0.387	52.4	-40.0	2.6	2.2	12.7	9
X T	750	0.4785	0.0167	0.5724	0.549	30.6	64.2	3.4	7.5	9.3	19
X U	800	-0.0435	0.0096	-0.9398	0.685	53.0	-420.8	4.5	5.6	7.1	9
X V	800	0.3522	0.0338	0.5566	1.01	15.1	52.8	6.0	4.5	4.8	19
X W	850	0.0348	0.0372	-0.5359	1.12	13.7	751.6	7.7	4.6	4.3	9
X X	850	0.3519	0.0346	1.009	1.58	14.7	13.6	10.2	1.2	3.1	19
X Y	900	0.1654	0.0296	-0.4284	1.40	17.2	183.1	12.3	7.1	3.4	8
X Z	900	0.5081	0.0262	1.016	1.77	19.5	40.1	15.1	5.0	2.7	18
X AA	950	0.4261	0.0320	0.1932	1.40	15.9	86.9	17.2	9.0	3.5	9
X AB	950	0.8191	0.0361	0.6141	1.88	14.1	77.9	20.1	15.7	2.5	19
X AC	1000	0.9200	0.0267	0.0707	1.58	19.1	97.9	22.6	22.1	3.0	9
X AD	1000	1.558	0.0310	0.4096	2.16	16.5	92.3	25.9	35.4	2.2	19
X AE	1050	3.258	0.0330	-0.1576	2.80	15.5	101.5	30.2	80.6	1.7	9
X AF	1050	8.696	0.0314	0.8962	5.51	16.2	97.0	38.7	199.19	0.89	29
X AG	1050	15.40	0.0330	1.809	6.10	15.4	96.5	48.1	337.85	0.94	59
X AH	1050	23.31	0.0315	3.415	6.89	16.2	95.7	58.7	486.1	1.1	119
X AI	1050	31.60	0.0330	8.589	5.49	15.5	92.0	67.2	611.1	1.3	239
X AJ	1100	35.30	0.0372	0.6422	5.48	13.7	99.5	75.6	716.3	1.3	9
X AK	1200	43.80	0.0347	0.3794	10.7	14.7	99.8	92.2	855.5	1.1	9
X AL	1250	46.35	0.0455	0.7450	1.76	11.2	99.5	94.9	893.4	2.3	9
X AM	1300	44.51	0.0568	3.058	0.702	9.0	98.0	96.0	854.3	5.4	9
X AN	1500	49.46	0.0541	2.187	2.39	9.4	98.7	99.7	934.0	2.0	9
X AO	1650	64.15	0.0688	66.59	0.218	7.4	69.3	100.0	867.9	16.5	9
Total gas age ± 1σ			n=40		64.9	15.3	K2O=2.64%		462.31	0.81	

Klokken 140182, Kspar, 0.38 mg, J=0.013645±0.10%, D=1.005±0.001, NM-206B, Lab#=57043-01

B	450	10.52	-0.0289	24.55	0.203	-	31.0	1.5	79.4	24.6	6
C	450	2.223	-0.0425	4.176	0.169	-	44.1	2.8	24.1	29.0	19
D	450	3.014	-0.0393	3.792	0.120	-	62.6	3.7	46.3	40.8	24
E	500	0.4103	-0.0256	-5.0403	0.110	-	471.4	4.5	46.5	42.3	9
F	500	1.498	0.0101	-1.5214	0.155	50.5	130.3	5.7	47.7	31.7	19
G	500	2.476	-0.0157	-2.1699	0.134	-	125.9	6.7	75.9	35.5	24
H	550	0.3161	-0.0164	-5.4742	0.131	-	628.0	7.6	47.3	35.9	9
I	550	1.336	-0.0069	0.0808	0.183	-	98.2	9.0	32.2	26.2	19
J	550	1.945	-0.0511	0.2934	0.164	-	95.3	10.2	45.4	29.4	24
K	600	0.4389	-0.0153	-8.4791	0.136	-	683.8	11.3	71.7	34.3	9
L	600	1.360	-0.0180	1.226	0.203	-	73.0	12.8	24.4	24.9	19
M	600	2.106	-0.0514	-0.1024	0.185	-	101.2	14.2	52.2	26.5	24
N	650	0.3663	0.0471	-3.0964	0.152	10.8	357.9	15.3	31.5	31.6	9
O	650	1.084	0.0645	0.6957	0.232	7.9	81.4	17.0	21.7	20.6	19
P	650	1.608	-0.0013	2.084	0.203	-	61.4	18.5	24.3	23.7	24
Q	700	0.0637	-0.0314	-6.3152	0.167	-	3569.9	19.8	47.2	28.4	9
R	700	0.9205	0.0547	0.0104	0.258	9.3	100.2	21.7	22.6	18.7	19
S	750	0.3068	0.0338	-2.2993	0.275	15.1	329.8	23.8	24.2	18.1	9
T	750	0.8811	0.0036	-1.6567	0.390	143.7	156.2	26.7	33.6	12.2	19
U	800	0.2906	0.0413	-0.6801	0.370	12.4	172.8	29.4	12.0	13.1	9
V	800	0.7529	0.0350	-0.4961	0.517	14.6	120.1	33.3	22.1	9.5	19
W	850	0.3675	0.0285	-1.1935	0.457	17.9	199.3	36.7	17.7	10.5	9
X	850	0.7731	0.0437	0.1445	0.707	11.7	94.9	42.0	18.0	7.0	18
Y	900	0.5780	0.0125	-1.5516	0.558	40.7	180.9	46.2	25.4	8.9	9
Z	900	1.032	0.0361	0.5284	0.707	14.1	85.0	51.5	21.5	7.0	19
AA	950	0.9025	0.0071	-2.0120	0.503	72.0	166.7	55.2	36.7	9.8	9
AB	950	1.507	0.0258	0.0843	0.649	19.8	98.5	60.1	36.4	7.6	19
AC	1000	1.352	0.0423	-0.5560	0.456	12.1	112.5	63.5	37.3	10.8	9
AD	1000	1.979	0.0313	1.477	0.594	16.3	78.0	67.9	37.9	8.5	19
AE	1050	1.635	0.0494	-1.8919	0.429	10.3	134.7	71.1	53.8	11.6	9
Xi AF	1050	3.087	0.0339	1.398	0.742	15.0	86.7	76.7	65.3	6.6	29
Xi AG	1050	5.426	0.0481	6.862	0.719	10.6	62.6	82.0	82.7	6.7	59
Xi AH	1050	10.68	0.0381	18.41	0.618	13.4	49.0	86.7	126.1	8.6	119
Xi AI	1050	20.81	0.0427	47.35	0.561	11.9	32.7	90.9	162.7	10.2	239
Xi AJ	1100	21.66	0.0566	-38.5699	0.020	9.0	152.7	91.0	685.1	183.5	9
Xi AK	1200	10.62	0.0018	-1.7680	0.220	290.4	104.9	92.6	259.0	20.2	9
Xi AL	1250	11.71	0.0562	-2.7825	0.190	9.1	107.1	94.1	289.2	22.8	9
Xi AM	1300	13.05	-0.0511	-6.5540	0.098	-	114.8	94.8	341.0	45.1	9
Xi AN	1500	11.69	0.0348	2.042	0.664	14.7	94.9	99.8	257.9	6.8	9
Xi AO	1650	56.30	-0.4106	111.1	0.033	-	41.6	100.0	509.4	118.3	9
Total gas age ± 1σ			n=40		13.4	22.3	K2O=1.04%		71.6	2.3	

Notes:
Isotopic ratios corrected for blank, radioactive decay, and mass discrimination, not corrected for interfering reactions.
Errors quoted for individual analyses include analytical error only, without interfering reaction or J uncertainties.
Integrated age calculated by summing isotopic measurements of all steps.
Integrated age error calculated by quadratically combining errors of isotopic measurements of all steps.
Plateau age is inverse-variance-weighted mean of selected steps.
Plateau age error is inverse-variance-weighted mean error (Taylor, 1982) times root MSWD where MSWD>1.
Plateau error is weighted error of Taylor (1982).
Decay constants and isotopic abundances after Steiger and Jäger (1977).
symbol preceding sample ID denotes analyses excluded from plateau age calculations.
Weight percent K_2O calculated from ^{39}Ar signal, sample weight, and instrument sensitivity.
Ages calculated relative to FC-2 Fish Canyon Tuff sanidine interlaboratory standard at 28.27 Ma
Decay Constant (LambdaK (total)) = 5.476e-10/a
Correction factors:
$(^{39}Ar/^{37}Ar)_{Ca}$ = 0.0007 ± 5e-05
$(^{36}Ar/^{37}Ar)_{Ca}$ = 0.00028 ± 2e-05
$(^{38}Ar/^{39}Ar)_{K}$ = 0.013
$(^{40}Ar/^{39}Ar)_{K}$ = 0.01 ± 0.002

Table A3.3: $^{40}Ar/^{39}Ar$ analytical data for multiple grain Klokken sample 140115.

ID	Temp (°C)	$^{40}Ar/^{39}Ar$	$^{37}Ar/^{39}Ar$	$^{36}Ar/^{39}Ar$ (x 10^{-3})	$^{39}Ar_K$ (x 10^{-15} mol)	K/Ca	$^{40}Ar^*$ (%)	^{39}Ar (%)	Age (Ma)	±1σ (Ma)	Time (min)
Klokken 140115, K-Feldspar, 1.7 mg, J=0.01037±0.48%, D=1.005±0.001, NM-201K, Lab#=56694-01											
X B	450	294.7	-0.3190	120.8	0.448	-	87.9	0.2	2381.8	12.4	9
X C	450	70.77	-8.0263	78.43	0.136	-	66.3	0.2	720.7	57.8	19
X D	450	66.14	-4.8597	117.8	0.120	-	46.7	0.2	506.2	67.0	24
X E	500	33.92	0.2899	14.31	0.189	1.8	87.6	0.3	490.5	45.5	9
X F	500	39.17	-1.0073	35.15	0.299	-	73.3	0.4	475.3	28.5	19
X G	500	41.46	-1.8914	50.71	0.281	-	63.5	0.5	440.1	31.5	24
X H	550	33.65	0.2857	14.26	0.365	1.8	87.5	0.6	486.7	22.5	6
X I	550	35.64	0.3979	19.57	0.604	1.3	83.9	0.8	493.1	14.7	19
X J	550	44.88	-0.6406	38.10	0.381	-	74.8	1.0	545.2	19.8	24
X K	600	44.85	-0.2597	10.64	0.651	-	92.9	1.2	655.9	12.0	9
X L	600	53.43	0.2622	21.81	0.681	1.9	88.0	1.4	725.1	10.9	16
X M	600	67.68	0.4111	29.14	0.648	1.2	87.3	1.6	873.1	11.1	24
X N	650	72.57	0.0290	6.134	0.748	17.6	97.5	1.9	1004.8	8.7	8
X O	650	80.30	-0.6812	16.96	0.956	-	93.7	2.2	1052.7	7.7	19
X P	650	86.12	0.1201	20.17	0.851	4.2	93.1	2.5	1104.9	8.8	24
X Q	700	86.90	0.0498	7.479	1.126	10.3	97.5	2.9	1151.1	6.0	9
X R	700	86.79	0.3671	10.31	1.680	1.4	96.5	3.5	1141.9	4.5	19
X S	750	85.87	0.0342	3.877	2.241	14.9	98.7	4.2	1151.4	4.0	9
X T	750	86.69	0.2738	6.569	3.08	1.9	97.8	5.3	1152.0	3.2	19
X U	800	86.31	-0.0189	2.314	3.63	-	99.2	6.5	1160.4	2.5	7
X V	800	86.31	0.0470	4.130	5.59	10.9	98.6	8.4	1155.1	2.6	19
X W	850	87.08	0.0093	1.810	6.01	54.8	99.4	10.5	1169.6	1.9	9
X X	850	86.34	-0.0160	2.921	8.33	-	99.0	13.3	1158.9	1.9	19
X Y	900	86.79	0.0852	1.209	6.97	6.0	99.6	15.7	1168.6	2.0	9
X Z	900	86.40	0.1077	2.615	9.48	4.7	99.1	18.9	1160.5	1.6	18
X AA	950	86.01	0.0778	1.961	8.47	6.6	99.3	21.8	1158.5	1.7	9
X AB	950	86.23	0.0299	2.173	10.99	17.1	99.3	25.5	1160.1	1.7	19
X AC	1000	86.36	-0.0383	1.589	9.81	-	99.5	28.9	1163.0	1.7	9
X AD	1000	86.30	0.0280	2.472	13.83	18.3	99.2	33.6	1159.9	1.6	19
X AE	1050	85.41	0.0243	1.028	14.84	21.0	99.6	38.6	1155.2	1.3	9
X AF	1050	85.87	0.0387	2.187	23.79	13.2	99.3	46.7	1156.4	2.0	29
X AG	1050	85.95	0.0173	3.865	24.6	29.4	98.7	55.1	1152.2	1.5	59
X AH	1050	87.07	0.0598	7.204	26.3	8.5	97.6	64.1	1153.6	1.7	119
X AI	1050	88.87	0.0150	12.19	28.1	34.0	95.9	73.6	1156.9	1.7	239
X AJ	1100	86.35	-0.1334	3.757	3.08	-	98.7	74.7	1156.3	2.8	9
X AK	1200	86.90	0.0210	0.2889	42.8	24.3	99.9	89.3	1172.3	1.5	9
X AL	1250	86.98	0.1043	2.115	9.93	4.9	99.3	92.6	1167.8	1.6	9
X AM	1300	87.38	0.1186	2.638	11.06	4.3	99.1	96.4	1170.3	1.7	9
X AN	1500	88.95	0.2356	9.919	9.09	2.2	96.7	99.5	1164.6	1.8	9
X AO	1650	110.0	1.029	177.0	1.447	0.50	52.5	100.0	857.4	7.7	9
Total gas age ± 1σ			n=40		293.7	12.7	K2O=6.40%		1140.1	4.2	

Notes:
Isotopic ratios corrected for blank, radioactive decay, and mass discrimination, not corrected for interfering reactions.
Errors quoted for individual analyses include analytical error only, without interfering reaction or J uncertainties.
Integrated age calculated by summing isotopic measurements of all steps.
Integrated age error calculated by quadratically combining errors of isotopic measurements of all steps.
Plateau age is inverse-variance-weighted mean of selected steps.
Plateau age error is inverse-variance-weighted mean error (Taylor, 1982) times root MSWD where MSWD>1.
Plateau error is weighted error of Taylor (1982).
Decay constants and isotopic abundances after Steiger and Jäger (1977).
symbol preceding sample ID denotes analyses excluded from plateau age calculations.
Weight percent K_2O calculated from ^{39}Ar signal, sample weight, and instrument sensitivity.
Ages calculated relative to FC-2 Fish Canyon Tuff sanidine interlaboratory standard at 28.27 Ma
Decay Constant (LambdaK (total)) = 5.476e-10/a
Correction factors:
$(^{39}Ar/^{37}Ar)_{Ca}$ = 0.0007 ± 5e-05
$(^{36}Ar/^{37}Ar)_{Ca}$ = 0.00028 ± 2e-05
$(^{38}Ar/^{39}Ar)_K$ = 0.013
$(^{40}Ar/^{39}Ar)_K$ = 0.01 ± 0.002

Table A3.4: $^{40}Ar/^{39}Ar$ analytical data for unheated and heated Klokken sample 140025.

ID	Temp (°C)	$^{40}Ar/^{39}Ar$	$^{37}Ar/^{39}Ar$	$^{36}Ar/^{39}Ar$ (x 10^{-3})	$^{39}Ar_K$ (x 10^{-15} mol)	K/Ca	$^{40}Ar^*$ (%)	^{39}Ar (%)	Age (Ma)	±1σ (Ma)	Time (min)
Klokken 140025, K-Feldspar, 0.82 mg, J=0.01037, D=1.005±0.001, NM-201K, Lab#=56692-01											
X R	450	101.7	1.005	103.1	0.602	0.51	70.1	0.5	1025.1	12.1	9
X S	450	21.23	-0.6796	1.622	0.306	-	97.5	0.8	356.5	27.6	16
X T	450	20.37	-0.9099	0.8957	0.280	-	98.3	1.1	346.0	30.0	24
X U	500	22.51	-0.6810	-4.6241	0.428	-	105.8	1.5	405.1	19.5	8
X V	500	18.52	-0.2866	-0.6474	0.472	-	100.9	1.9	324.7	18.3	19
X W	500	20.80	0.8333	0.3009	0.325	0.61	99.9	2.2	358.2	26.2	24
X X	550	29.71	0.4814	2.945	0.538	1.1	97.2	2.7	481.6	15.1	6
X Y	550	21.96	0.7922	-0.4300	0.546	0.64	100.9	3.2	379.6	15.8	19
X Z	550	24.17	0.7619	5.505	0.334	0.67	93.5	3.5	386.7	24.6	24
X AA	600	38.56	0.6412	5.113	0.831	0.80	96.2	4.3	599.5	9.2	9
X AB	600	28.76	-0.4349	-1.5217	0.408	-	101.4	4.6	485.6	19.8	16
X AC	600	31.18	0.1414	2.448	0.334	3.6	97.7	4.9	504.8	24.1	24
X AD	650	33.99	-0.8219	-0.2601	0.441	-	100.0	5.3	555.2	17.5	9
X AE	650	34.75	-0.5168	1.934	0.430	-	98.2	5.7	557.3	17.8	19
X AF	650	37.08	-1.9061	2.700	0.338	-	97.4	6.0	584.8	23.2	24
X AG	700	39.07	-0.0333	-2.4161	0.492	-	101.8	6.5	636.0	15.2	9
X AH	700	38.19	-0.5331	3.434	0.471	-	97.2	6.9	599.4	16.3	18
X AI	750	38.68	-0.4759	-3.0874	0.552	-	102.3	7.4	632.7	13.6	9
X AJ	750	39.49	-0.2249	0.5685	0.587	-	99.5	8.0	629.4	12.7	17
X AK	800	38.99	-0.8584	-5.0622	0.640	-	103.7	8.5	644.3	11.5	9
X AL	800	39.86	-0.4622	0.1277	0.714	-	99.8	9.2	635.8	10.6	19
X AM	850	39.68	1.192	-1.1343	0.728	0.43	101.1	9.9	641.0	10.5	9
X AN	850	40.94	0.3099	0.0950	0.884	1.6	100.0	10.7	651.8	8.8	19
X AO	900	38.91	0.1939	3.679	1.060	2.6	97.2	11.6	609.5	8.6	8
X AP	900	39.50	0.4614	3.555	1.515	1.1	97.4	13.0	618.4	5.8	19
X AQ	950	36.00	0.5711	2.754	1.949	0.89	97.9	14.8	573.2	5.5	9
X AR	950	35.98	0.5960	3.480	2.308	0.86	97.3	16.9	569.9	3.9	19
X AS	1000	32.63	0.0677	3.461	3.21	7.5	96.9	19.8	521.4	2.9	9
X AT	1000	32.82	0.3703	4.083	3.54	1.4	96.4	23.1	521.9	2.7	19
X AU	1050	30.73	-0.0199	3.237	5.35	-	96.9	27.9	494.6	2.0	9
X AV	1050	31.18	0.0460	3.884	8.24	11.1	96.3	35.5	498.4	1.5	29
X AW	1050	32.79	0.0193	4.864	9.09	26.5	95.6	43.7	517.6	1.4	59
X AX	1050	35.93	0.0521	6.017	11.20	9.8	95.1	54.0	557.9	1.3	119
X AY	1050	41.32	0.0260	9.601	11.85	19.6	93.1	64.8	618.2	1.5	239
X AZ	1100	46.80	0.0566	1.536	4.72	9.0	99.0	69.1	723.5	2.2	9
X AAA	1200	49.03	0.0706	1.192	21.19	7.2	99.3	88.4	753.7	1.3	9
X AAB	1250	46.01	0.0998	1.254	3.53	5.1	99.2	91.6	714.4	2.9	9
X AAC	1300	50.86	0.2133	1.228	6.49	2.4	99.3	97.5	777.0	2.0	9
X AAD	1500	41.77	0.5470	1.540	2.398	0.93	99.0	99.7	657.6	3.9	9
X AAE	1650	72.03	-0.7786	43.82	0.292	-	81.9	100.0	881.4	26.5	9
Total gas age ± 1σ			n=40		109.6	5.3	K2O=5.24%		610.2	0.8	

ID	Temp (°C)	$^{40}Ar/^{39}Ar$	$^{37}Ar/^{39}Ar$	$^{36}Ar/^{39}Ar$ (x 10^{-3})	$^{39}Ar_K$ (x 10^{-15} mol)	K/Ca	$^{40}Ar^*$ (%)	^{39}Ar (%)	Age (Ma)	±1σ (Ma)	Time (min)
Klokken 140025-650, Kspar, 3.34 mg, J=0.013551±0.10%, D=1.005±0.001, NM-206B, Lab#=57031-01											
X B	450	21.31	0.8222	69.83	3.49	0.62	3.5	0.4	18.2	5.8	9
X C	450	4.891	0.0319	16.62	1.512	16.0	-0.5	0.5	-0.7	8.2	19
X D	450	4.001	0.0028	13.20	1.074	184.2	2.3	0.7	2.3	12.3	21
X E	500	1.319	0.0070	3.873	2.188	72.5	12.6	0.9	4.1	5.4	9
X F	500	1.292	0.0126	4.115	2.98	40.4	5.2	1.2	1.7	3.9	19
X G	500	1.123	0.0052	3.798	2.67	97.5	-0.8	1.5	-0.2	4.5	24
X H	550	0.5158	0.0090	1.772	4.84	56.6	-3.4	2.1	-0.4	2.5	9
X I	550	0.4975	0.0044	1.359	6.26	116.0	17.7	2.7	2.1	2.0	19
X J	550	0.5832	0.0095	1.481	5.18	53.7	23.8	3.3	3.4	2.3	24
X K	600	0.3109	0.0144	0.4099	6.50	35.3	60.1	4.0	4.5	1.9	9
X L	600	0.4812	0.0111	0.8429	7.70	45.9	47.3	4.9	5.5	1.6	19
X M	600	0.7610	0.0107	1.334	4.94	47.5	47.7	5.4	8.8	2.6	24
X N	650	0.8493	0.0199	0.7291	4.82	25.6	74.5	5.9	15.4	2.6	9
X O	650	1.421	0.0168	1.076	5.64	30.3	77.6	6.6	26.9	2.1	19
X P	650	2.138	0.0193	1.190	4.07	26.4	83.6	7.0	43.5	3.2	24
X Q	700	3.057	0.0196	1.160	4.48	26.0	88.8	7.5	65.8	2.6	9
X R	700	4.031	0.0166	0.9791	5.93	30.7	92.8	8.2	90.1	2.0	19
X S	750	6.514	0.0239	1.842	6.63	21.3	91.7	8.9	141.9	1.8	9
X T	750	8.318	0.0176	1.339	8.40	29.0	95.3	9.8	186.0	1.4	19
X U	800	12.71	0.0198	2.233	9.01	25.7	94.8	10.8	276.1	1.3	9
X V	800	14.32	0.0162	1.329	10.11	31.4	97.3	11.9	315.6	1.2	19
X W	850	18.90	0.0210	3.351	11.10	24.3	94.8	13.1	396.7	1.2	9
X X	850	19.26	0.0106	2.303	12.77	48.1	96.5	14.5	409.8	1.1	19
X Y	900	22.26	0.0173	3.689	17.63	29.5	95.1	16.5	460.5	1.1	9
X Z	900	21.24	0.0090	2.299	21.82	56.5	96.8	18.9	448.57	0.92	19
X AA	950	22.45	0.0136	2.955	30.7	37.6	96.1	22.2	468.27	0.86	9
X AB	950	21.08	0.0075	1.862	33.0	67.8	97.4	25.9	448.09	0.73	19
X AC	1000	22.15	0.0096	2.370	44.4	53.2	96.8	30.7	465.74	0.73	9
X AD	1000	21.25	0.0059	1.952	40.0	86.4	97.3	35.1	450.85	0.75	19
X AE	1050	23.11	0.0075	2.406	58.1	68.4	96.9	41.5	483.83	0.63	9
X AF	1050	25.52	0.0080	2.239	106.4	64.1	97.4	53.2	530.08	0.74	29
X AG	1050	27.56	0.0069	1.949	103.7	73.9	97.9	64.6	568.88	0.78	59
X AH	1050	28.62	0.0058	2.152	87.9	88.6	97.8	74.3	587.02	0.94	119
X AI	1050	29.16	0.0057	4.225	50.2	89.4	95.7	79.8	585.6	1.0	239
X AJ	1100	30.71	0.0036	1.450	17.29	142.3	98.6	81.7	627.78	0.97	9
X AK	1200	28.73	0.0029	1.029	115.8	178.8	98.9	94.4	594.92	0.77	9
X AL	1250	25.09	0.0110	1.496	19.66	46.3	98.2	96.6	526.1	1.2	9
X AM	1300	27.09	0.0086	1.578	17.14	59.5	98.3	98.5	562.3	1.0	9
X AN	1500	29.40	0.0099	2.945	12.24	51.4	97.0	99.8	596.8	1.3	9
X AO	1650	45.75	-0.0009	32.68	1.786	-	78.9	100.0	727.0	5.9	9
Total gas age ± 1σ			n=40		910.2	45.0	K2O=7.72%		481.9	0.7	

ID	Temp (°C)	$^{40}Ar/^{39}Ar$	$^{37}Ar/^{39}Ar$	$^{36}Ar/^{39}Ar$ (x 10^{-3})	$^{39}Ar_K$ (x 10^{-15} mol)	K/Ca	$^{40}Ar^*$ (%)	^{39}Ar (%)	Age (Ma)	±1σ (Ma)	Time (min)
Klokken 140025-700, Kspar, 2.22 mg, J=0.013506±0.10%, D=1.005±0.001, NM-206B, Lab#=57035-01											
X C	450	22.83	0.3852	75.27	1.540	1.3	2.7	0.3	15.0	9.7	9
X D	450	6.380	0.0082	20.49	0.661	62.2	4.9	0.4	7.8	18.6	19
X E	450	4.632	-0.0471	13.99	0.471	-	10.5	0.4	11.9	25.0	21
X F	500	1.393	0.0170	7.221	0.922	30.0	-54.2	0.6	-18.6	13.0	9
X G	500	1.751	0.0031	4.928	1.275	163.8	16.4	0.8	7.0	9.4	19
X H	500	1.511	-0.0140	4.632	1.027	-	8.8	1.0	3.2	10.9	21
X I	550	0.4757	-0.0061	0.7237	2.235	-	54.0	1.4	6.2	5.4	9
X J	550	0.5839	-0.0009	1.320	2.51	-	32.0	1.8	4.5	4.9	16
X K	550	0.7283	0.0031	2.470	2.68	166.8	-1.6	2.2	-0.3	4.4	24
X L	600	0.2808	0.0053	1.219	2.79	96.9	-32.8	2.7	-2.2	4.3	6
X M	600	0.3587	0.0098	0.9571	5.19	52.0	19.1	3.6	1.6	2.3	19
X N	600	0.4604	0.0025	0.9788	3.26	200.8	35.8	4.1	4.0	3.7	21
X O	650	0.2504	0.0072	-0.0628	3.96	70.4	108.0	4.8	6.4	2.9	9
X P	650	0.4720	0.0066	0.8544	4.17	77.1	45.5	5.5	5.2	2.9	19
X Q	650	0.8282	0.0032	1.348	2.69	157.2	51.4	5.9	10.3	4.5	24
X R	700	0.8538	0.0111	1.028	2.52	45.8	64.1	6.3	13.3	4.6	9
X S	700	1.477	0.0080	1.333	2.99	64.1	73.2	6.8	26.3	4.0	19
X T	750	2.656	0.0228	1.390	3.31	22.4	84.6	7.4	54.4	3.5	9
X U	750	3.646	0.0058	2.314	3.65	87.4	81.2	8.0	71.4	3.2	19
X V	800	6.648	0.0188	1.872	4.05	27.2	91.7	8.7	144.3	2.8	9
X W	800	7.584	0.0105	1.583	4.40	48.4	93.8	9.4	167.4	2.6	17
X X	850	12.39	0.0263	2.931	4.91	19.4	93.0	10.2	263.9	2.2	9
X Y	850	13.06	0.0150	2.016	5.76	34.0	95.4	11.2	284.0	1.9	19
X Z	900	18.28	0.0248	3.831	7.12	20.6	93.8	12.4	380.2	1.7	9
X AA	900	17.59	0.0091	2.271	8.05	56.2	96.2	13.7	375.7	1.5	19
X AB	950	21.07	0.0146	3.537	10.83	34.9	95.0	15.5	436.9	1.3	9
X AC	950	19.84	0.0091	2.423	12.60	56.4	96.4	17.6	419.3	1.1	19
X AD	1000	22.00	0.0084	2.749	18.59	60.4	96.3	20.7	459.36	0.97	9
X AE	1000	20.41	0.0070	2.081	18.42	72.7	97.0	23.8	432.40	0.94	19
X AF	1050	22.54	0.0090	2.802	30.1	56.6	96.3	28.8	469.52	0.83	9
X AG	1050	22.47	0.0073	2.618	43.0	69.7	96.6	36.0	469.14	0.69	29
X AH	1050	24.28	0.0053	2.821	49.2	96.9	96.6	44.2	502.29	0.66	59
X AI	1050	25.67	0.0061	3.172	57.0	83.5	96.4	53.7	526.21	0.76	119
X AJ	1050	27.21	0.0056	3.938	51.2	91.1	95.7	62.2	550.36	0.91	239
X AK	1100	27.55	0.0072	2.321	5.65	71.3	97.5	63.2	565.2	1.9	9
X AL	1200	29.52	0.0024	1.265	176.3	212.9	98.7	92.6	605.97	0.84	9
X AM	1250	27.31	0.0044	1.988	15.29	117.1	97.9	95.1	562.5	1.1	9
X AN	1300	26.35	0.0048	1.632	20.16	106.5	98.2	98.5	547.1	1.1	9
X AO	1500	29.66	0.0047	2.716	8.61	108.0	97.3	99.9	600.8	1.5	9
X AP	1650	55.03	-0.0009	99.12	0.357	-	46.8	100.0	544.6	27.5	9
Total gas age ± 1σ			n=40		599.5	73.6	K2O=7.68%		483.61	0.67	

ID	Temp (°C)	$^{40}Ar/^{39}Ar$	$^{37}Ar/^{39}Ar$	$^{36}Ar/^{39}Ar$ (x 10^{-3})	$^{39}Ar_K$ (x 10^{-15} mol)	K/Ca	$^{40}Ar^*$ (%)	^{39}Ar (%)	Age (Ma)	±1σ (Ma)	Time (min)
Klokken 140025-900, Kspar, 3.49 mg, J=0.013671±0.07%, D=1.005±0.001, NM-206B, Lab#=57038-01											
X B	450	7.507	0.1317	23.63	4.53	3.9	7.0	0.5	13.0	3.6	9
X C	450	1.246	-0.0075	3.431	2.060	-	17.9	0.8	5.5	5.9	19
X D	450	1.096	-0.0002	2.233	1.394	-	39.2	1.0	10.6	8.3	21
X E	500	0.2181	0.0022	0.2253	3.13	233.0	68.1	1.3	3.5	3.9	9
X F	500	0.3220	0.0041	1.224	4.19	124.2	-15.8	1.8	-1.2	2.8	19
X G	500	0.4015	0.0009	1.375	3.67	587.4	-3.8	2.3	-0.4	3.3	24
X H	550	0.1174	0.0062	-0.0412	7.53	82.3	111.8	3.2	3.0	1.6	9
X I	550	0.1737	0.0083	0.2215	9.47	61.3	60.5	4.3	2.5	1.2	19
X J	550	0.2201	0.0042	0.4298	7.63	122.4	39.7	5.2	2.1	1.6	24
X K	600	0.0913	0.0071	0.1213	9.95	72.0	56.7	6.4	1.2	1.2	9
X L	600	0.1631	0.0089	0.1318	12.26	57.6	75.1	7.8	2.87	0.97	19
X M	600	0.2296	0.0091	0.5318	8.59	55.8	28.8	8.9	1.6	1.5	24
X N	650	0.1394	0.0068	-0.2128	7.98	74.6	149.1	9.8	4.8	1.5	8
X O	650	0.2705	0.0094	0.1505	9.65	54.3	83.2	11.0	5.4	1.3	19
X P	650	0.4318	0.0124	0.4135	6.14	41.1	71.3	11.7	7.5	2.0	24
X Q	700	0.3628	0.0107	0.2433	4.48	47.6	79.9	12.2	7.0	2.7	9
X R	700	0.5593	0.0123	0.4944	6.08	41.6	73.6	13.0	10.1	1.9	19
X S	750	0.6499	0.0191	-0.0449	7.44	26.7	102.3	13.8	16.3	1.6	9
X T	750	0.9048	0.0149	0.2490	8.38	34.3	91.9	14.8	20.4	1.4	19
X U	800	1.175	0.0215	0.3215	8.35	23.7	92.0	15.8	26.6	1.4	9
X V	800	1.664	0.0167	0.4176	10.63	30.5	92.6	17.1	37.9	1.1	19
X W	850	2.424	0.0204	0.4474	9.10	25.1	94.6	18.2	56.1	1.3	9
X X	850	3.241	0.0127	0.4399	12.44	40.3	96.0	19.7	75.84	0.95	19
X Y	900	5.799	0.0170	0.5415	13.05	30.1	97.3	21.2	135.42	0.90	9
X Z	900	6.617	0.0135	0.5979	15.94	37.7	97.3	23.1	153.90	0.75	19
X AA	950	11.52	0.0227	0.8452	19.08	22.5	97.8	25.4	261.53	0.75	9
X AB	950	11.87	0.0167	1.025	22.63	30.5	97.5	28.1	268.00	0.70	19
X AC	1000	16.65	0.0254	1.472	33.5	20.1	97.4	32.1	365.52	0.65	9
X AD	1000	17.34	0.0187	1.138	31.7	27.3	98.1	35.9	381.54	0.76	19
X AE	1050	21.44	0.0191	1.630	57.5	26.8	97.8	42.7	459.95	0.61	9
X AF	1050	24.01	0.0140	1.660	94.5	36.5	98.0	54.0	508.91	0.76	29
X AG	1050	27.13	0.0100	1.570	90.4	51.1	98.3	64.7	567.38	0.86	59
X AH	1050	29.47	0.0081	1.732	90.0	63.1	98.3	75.5	608.85	0.76	119
X AI	1050	30.99	0.0060	2.270	86.6	84.4	97.8	85.8	633.04	0.93	239
X AJ	1100	31.77	0.0076	1.678	5.83	67.2	98.4	86.5	649.9	1.9	9
X AK	1200	33.05	0.0031	0.9350	74.9	163.2	99.2	95.4	675.91	0.95	9
X AL	1250	30.01	0.0171	1.242	17.45	29.8	98.8	97.5	621.2	1.1	9
X AM	1300	29.23	0.0143	1.579	11.03	35.7	98.4	98.8	605.5	1.3	9
X AN	1500	29.10	0.0238	2.329	9.37	21.4	97.6	99.9	599.1	1.4	9
X AO	1650	42.31	0.0245	41.68	0.710	20.9	70.9	100.0	627.3	13.4	9
Total gas age ± 1σ			n=40		839.3	40.5	K2O=6.76%		433.44	0.53	

ID	Temp (°C)	$^{40}Ar/^{39}Ar$	$^{37}Ar/^{39}Ar$	$^{36}Ar/^{39}Ar$ (x 10^{-3})	$^{39}Ar_K$ (x 10^{-15} mol)	K/Ca	$^{40}Ar^*$ (%)	^{39}Ar (%)	Age (Ma)	±1σ (Ma)	Time (min)
Klokken 140025-1000, Kspar, 2.44 mg, J=0.013673, D=1.005±0.001, NM-206B, Lab#=57041-01											
X B	450	9.889	0.1195	31.35	1.468	4.3	6.3	0.2	15.6	8.7	9
X C	450	2.021	-0.0017	2.596	0.618	-	61.9	0.3	30.8	18.9	19
X D	450	2.744	-0.0102	6.147	0.425	-	33.5	0.4	22.8	27.6	24
X E	500	0.4598	0.0156	-2.2554	0.650	32.7	248.5	0.4	27.7	18.0	8
X F	500	0.9612	0.0057	3.087	0.999	89.0	4.2	0.6	1.0	12.6	19
X G	500	1.218	0.0173	5.163	0.873	29.5	-26.2	0.7	-7.9	13.6	24
X H	550	0.1955	0.0063	0.5328	1.561	80.7	15.4	0.9	0.7	7.8	9
X I	550	0.4246	0.0179	0.9958	1.952	28.5	29.4	1.2	3.0	6.1	16
X J	550	0.5362	0.0036	1.434	2.044	141.9	19.5	1.5	2.6	5.8	24
X K	600	0.1327	0.0042	-0.0276	3.00	121.1	107.0	1.9	3.3	4.0	9
X L	600	0.2824	0.0053	0.4194	4.41	97.0	54.7	2.6	3.7	2.7	19
X M	600	0.5235	0.0070	1.442	3.82	72.6	17.1	3.1	2.2	3.1	24
X N	650	0.1396	0.0057	0.4478	5.00	89.3	-1.7	3.8	-0.1	2.4	9
X O	650	0.2489	0.0099	0.4159	6.80	51.5	48.9	4.8	2.9	1.8	19
X P	650	0.3661	0.0096	0.5985	5.21	53.3	50.6	5.5	4.5	2.3	24
X Q	700	0.2011	0.0115	0.2690	5.14	44.4	58.9	6.2	2.8	2.3	9
X R	700	0.3752	0.0193	0.5569	6.37	26.5	55.4	7.1	5.0	1.9	19
X S	750	0.3304	0.0093	0.0259	5.49	54.7	97.9	7.9	7.8	2.2	9
X T	750	0.5900	0.0172	0.5398	5.41	29.7	72.7	8.7	10.5	2.2	19
X U	800	0.6274	0.0164	0.1466	4.22	31.2	93.2	9.3	14.3	2.8	9
X V	800	0.8981	0.0189	0.7429	4.68	27.0	75.5	10.0	16.7	2.6	19
X W	850	0.8393	0.0161	0.1712	3.98	31.6	94.1	10.5	19.4	3.1	9
X X	850	0.9186	0.0242	0.7159	5.16	21.1	76.9	11.3	17.4	2.4	19
X Y	900	0.7834	0.0202	0.1995	4.61	25.2	92.6	11.9	17.8	2.6	9
X Z	900	0.9752	0.0224	0.7574	6.01	22.7	77.0	12.8	18.5	2.0	19
X AA	950	1.303	0.0257	0.4672	5.22	19.9	89.5	13.5	28.7	2.3	9
X AB	950	1.569	0.0215	0.3051	6.79	23.7	94.3	14.5	36.4	1.8	19
X AC	1000	1.990	0.0224	0.3830	6.07	22.8	94.4	15.3	46.1	1.9	9
X AD	1000	2.902	0.0155	0.8964	8.49	32.9	90.9	16.5	64.5	1.5	19
X AE	1050	3.428	0.0175	0.3935	9.64	29.2	96.6	17.9	80.7	1.2	9
X AF	1050	5.385	0.0145	0.6100	19.31	35.3	96.7	20.6	125.54	0.66	29
X AH	1050	9.160	0.0126	1.159	44.9	40.4	96.3	27.0	208.24	0.42	119
X AI	1050	12.28	0.0136	1.735	74.6	37.6	95.8	37.6	273.23	0.45	239
X AJ	1100	14.17	0.0163	0.7424	34.1	31.3	98.5	42.4	319.91	0.65	9
X AK	1200	23.62	0.0083	0.7437	329.5	61.4	99.1	89.2	510.00	0.66	9
X AL	1250	20.81	0.0103	1.135	31.1	49.4	98.4	93.6	453.08	0.81	9
X AM	1300	24.13	0.0082	0.9269	19.27	62.4	98.9	96.4	518.59	1.02	9
X AN	1500	27.65	0.0098	1.083	23.85	52.1	98.8	99.8	583.68	0.91	9
X AO	1650	31.06	0.0091	13.95	1.728	56.3	86.7	100.0	576.6	5.8	9
Total gas age ± 1σ			n=39		704.5	45.2	K2O=8.53%		364.16	0.53	

ID	Temp (°C)	$^{40}Ar/^{39}Ar$	$^{37}Ar/^{39}Ar$	$^{36}Ar/^{39}Ar$ (x 10^{-3})	$^{39}Ar_K$ (x 10^{-15} mol)	K/Ca	$^{40}Ar^*$ (%)	^{39}Ar (%)	Age (Ma)	±1σ (Ma)	Time (min)
Klokken 140025-1100, Kspar, 3.01 mg, J=0.013644, D=1.005±0.001, NM-206B, Lab#=57044-01											
X B	450	4.129	0.0216	13.83	11.19	23.6	0.8	1.6	0.8	1.6	9
X C	450	0.2425	0.0183	0.4810	6.25	27.9	39.6	2.5	2.3	1.9	19
X D	450	0.2779	0.0195	0.3867	5.35	26.1	58.0	3.2	3.9	2.2	21
X E	500	0.1237	0.0261	0.3059	4.61	19.5	22.5	3.9	0.6	2.5	9
X F	500	0.2003	0.0172	0.4585	7.20	29.7	29.6	4.9	1.4	1.8	19
X G	500	0.2421	0.0197	0.2818	6.43	25.9	64.9	5.8	3.7	1.9	24
X H	550	0.1216	0.0144	-0.1820	4.66	35.4	149.3	6.5	4.1	2.5	9
X I	550	0.3629	0.0228	0.7903	8.70	22.4	34.4	7.7	3.0	1.4	19
X J	550	0.2468	0.0212	0.3929	7.49	24.0	51.8	8.8	3.1	1.6	24
X K	600	0.1388	0.0196	-0.1373	5.96	26.0	132.8	9.6	4.3	2.1	9
X L	600	0.1869	0.0185	0.2123	12.59	27.6	65.4	11.4	2.9	0.94	19
X M	600	0.2116	0.0196	0.3018	12.37	26.1	56.6	13.2	2.8	1.01	24
X N	650	0.1417	0.0148	0.2950	8.66	34.5	34.8	14.4	1.1	1.4	9
X O	650	0.2035	0.0140	0.1802	17.32	36.6	73.1	16.8	3.5	0.70	19
X P	650	0.2243	0.0148	0.2607	16.37	34.4	64.7	19.2	3.4	0.75	24
X Q	700	0.1789	0.0163	0.2127	10.41	31.3	63.6	20.6	2.7	1.2	9
X R	700	0.2472	0.0150	0.0999	19.00	33.9	88.1	23.3	5.2	0.67	19
X S	750	0.2359	0.0139	0.1522	14.23	36.6	80.6	25.4	4.5	0.85	9
X T	750	0.3360	0.0119	0.0965	21.56	42.8	91.6	28.4	7.4	0.57	19
X U	800	0.4039	0.0129	0.1836	13.57	39.5	86.5	30.3	8.5	0.86	9
X V	800	0.6224	0.0121	0.3523	19.10	42.3	83.2	33.1	12.6	0.62	19
X W	850	0.7921	0.0116	0.2566	11.56	43.9	90.4	34.7	17.5	1.04	9
X X	850	1.044	0.0122	0.3924	18.09	41.7	88.9	37.3	22.8	0.67	19
X Y	900	1.247	0.0119	0.0768	11.60	43.0	98.3	38.9	30.0	1.04	9
X Z	900	1.418	0.0114	0.2943	19.44	44.8	93.9	41.7	32.7	0.63	19
X AA	950	1.568	0.0092	0.2548	12.39	55.3	95.2	43.4	36.6	0.97	9
X AB	950	1.793	0.0123	0.3917	22.08	41.4	93.6	46.6	41.1	0.58	19
X AC	1000	2.036	0.0141	0.2453	13.55	36.1	96.5	48.5	48.1	0.89	9
X AD	1000	2.428	0.0110	0.3068	22.66	46.3	96.3	51.7	57.2	0.54	19
X AE	1050	2.694	0.0110	0.0275	14.94	46.3	99.7	53.8	65.6	0.79	9
X AF	1050	2.955	0.0107	0.3837	35.9	47.5	96.2	58.9	69.3	0.38	29
X AG	1050	3.581	0.0099	0.5952	46.9	51.4	95.1	65.6	82.8	0.33	59
X AH	1050	4.263	0.0106	0.9693	52.9	48.0	93.3	73.1	96.4	0.33	119
X AI	1050	5.470	0.0111	1.721	59.2	46.1	90.7	81.5	119.6	0.35	239
X AJ	1100	7.163	0.0083	0.4031	2.220	61.6	98.3	81.8	167.7	5.0	9
X AK	1200	13.42	0.0112	0.4680	58.0	45.6	99.0	90.0	305.0	0.48	9
X AL	1250	11.31	0.0130	0.4001	27.0	39.3	99.0	93.8	260.1	0.67	9
X AM	1300	9.143	0.0299	0.5353	11.94	17.1	98.3	95.5	211.6	1.04	9
X AN	1500	7.817	0.0243	0.4269	29.1	21.0	98.4	99.7	182.5	0.51	9
X AO	1650	14.45	0.0161	8.542	2.411	31.6	82.5	100.0	276.0	4.9	9
Total gas age ± 1σ			n=40		704.9	37.2	K2O=6.92%		85.1	0.18	

Notes:
Isotopic ratios corrected for blank, radioactive decay, and mass discrimination, not corrected for interfering reactions.
Errors quoted for individual analyses include analytical error only, without interfering reaction or J uncertainties.
Integrated age calculated by summing isotopic measurements of all steps.
Integrated age error calculated by quadratically combining errors of isotopic measurements of all steps.
Plateau age is inverse-variance-weighted mean of selected steps.
Plateau age error is inverse-variance-weighted mean error (Taylor, 1982) times root MSWD where MSWD>1.
Plateau error is weighted error of Taylor (1982).
Decay constants and isotopic abundances after Steiger and Jäger (1977).
symbol preceding sample ID denotes analyses excluded from plateau age calculations.
Weight percent K_2O calculated from ^{39}Ar signal, sample weight, and instrument sensitivity.
Ages calculated relative to FC-2 Fish Canyon Tuff sanidine interlaboratory standard at 28.27 Ma
Decay Constant (LambdaK (total)) = 5.476e-10/a
Correction factors:
$(^{39}Ar/^{37}Ar)_{Ca}$ = 0.0007 ± 5e-05
$(^{36}Ar/^{37}Ar)_{Ca}$ = 0.00028 ± 2e-05
$(^{38}Ar/^{39}Ar)_{K}$ = 0.013
$(^{40}Ar/^{39}Ar)_{K}$ = 0.01 ± 0.002

Table A3.5: $^{40}Ar/^{39}Ar$ analytical data for multiple grain unheated and pre-heated Klokken sample 43738.

ID	Temp (°C)	$^{40}Ar/^{39}Ar$	$^{37}Ar/^{39}Ar$	$^{36}Ar/^{39}Ar$ (x 10^{-3})	$^{39}Ar_K$ (x 10^{-15} mol)	K/Ca	$^{40}Ar^*$ (%)	^{39}Ar (%)	Age (Ma)	±1σ (Ma)	Time (min)
Klokken 43738, K-Feldspar, 0.8 mg, J=0.01037, D=1.005±0.001, NM-201K, Lab#=56690-01											
B	450	935.9	-0.0428	74.91	1.004	-	97.6	0.7	4440.7	9.0	9
C	450	44.23	0.0152	5.036	0.471	33.5	96.6	1.0	675.9	13.4	19
D	450	38.26	0.3647	5.680	0.308	1.4	95.7	1.2	592.5	21.1	21
E	500	198.0	0.1421	7.610	2.424	3.6	98.9	2.9	2070.0	3.6	9
F	500	55.92	-0.8214	-1.2244	0.737	-	100.5	3.5	847.4	8.5	19
G	500	47.63	2.340	1.016	0.396	0.22	99.8	3.7	739.8	15.2	24
H	550	148.6	-0.0674	8.163	1.884	-	98.4	5.0	1717.8	5.1	9
I	550	38.53	0.7314	1.615	0.440	0.70	98.9	5.4	613.5	14.3	19
J	550	47.82	2.507	5.217	0.255	0.20	97.2	5.5	726.3	24.9	24
K	600	120.2	0.2618	14.02	0.741	1.9	96.6	6.0	1467.8	9.0	9
L	600	49.95	0.2250	6.753	0.362	2.3	96.0	6.3	744.6	16.3	19
M	600	46.29	0.5895	5.588	0.240	0.87	96.5	6.5	702.0	26.6	24
N	650	104.7	-1.0939	7.128	0.679	-	97.9	6.9	1343.1	9.8	8
O	650	56.18	-0.9419	1.771	0.450	-	98.9	7.3	839.7	13.1	19
P	650	59.66	1.274	0.4412	0.340	0.40	100.0	7.5	889.8	17.3	24
Q	700	89.66	-0.3513	8.206	0.673	-	97.3	8.0	1193.2	9.4	9
R	700	62.32	1.006	2.275	0.680	0.51	99.1	8.4	914.7	9.4	19
S	750	73.65	-0.9288	1.330	1.022	-	99.4	9.1	1044.2	6.7	9
T	750	61.71	-0.1599	2.910	1.159	-	98.6	10.0	903.5	5.3	19
U	800	63.79	-0.1291	1.236	1.309	-	99.4	10.9	933.8	5.3	9
V	800	58.98	-0.1216	0.9694	1.510	-	99.5	11.9	877.7	4.4	17
W	850	60.33	-0.1624	1.525	1.667	-	99.2	13.1	891.8	4.4	9
X	850	56.84	-0.0713	1.327	1.967	-	99.3	14.5	850.6	4.1	19
Y	900	61.87	0.3965	2.538	2.134	1.3	98.8	16.0	907.5	3.4	9
Z	900	57.60	0.0468	1.412	2.79	10.9	99.3	17.9	859.7	2.9	18
AA	950	66.23	0.0358	2.634	3.80	14.2	98.8	20.6	957.6	2.5	9
AB	950	60.15	0.0492	1.963	4.23	10.4	99.0	23.5	888.5	2.2	19
AC	1000	69.62	-0.0380	2.439	6.43	-	99.0	28.0	996.9	1.9	9
AD	1000	63.42	0.0632	2.468	6.48	8.1	98.9	32.5	925.5	1.7	19
AE	1050	71.07	0.1037	2.593	10.13	4.9	98.9	39.6	1012.8	1.7	9
AF	1050	67.32	0.0303	3.264	12.09	16.9	98.6	48.0	968.0	1.6	29
AG	1050	67.71	0.0729	4.258	10.98	7.0	98.2	55.7	969.1	1.6	59
AH	1050	69.92	0.0874	6.543	10.72	5.8	97.2	63.2	986.7	1.9	119
AI	1050	71.88	0.0680	10.04	9.16	7.5	95.9	69.6	997.2	1.7	239
AJ	1100	73.13	-0.0357	2.291	5.61	-	99.1	73.5	1036.6	1.9	9
AK	1200	74.97	0.1426	1.579	25.8	3.6	99.4	91.5	1059.4	1.4	9
AL	1250	79.67	0.1270	3.188	5.56	4.0	98.8	95.4	1105.2	2.6	9
AM	1300	77.44	-0.1662	3.168	4.40	-	98.8	98.4	1080.8	2.4	9
AN	1500	80.77	0.3008	3.917	2.176	1.7	98.6	99.9	1114.8	3.6	9
AO	1650	109.3	-10.9587	129.8	0.076	-	64.1	100.0	1048.7	76.0	9
Total gas age ± 1σ			n=40		143.2	8.7	K2O=6.63%		1068.0	1.0	
Klokken 43738-650, Kspar, 1.93 mg, J=0.013559±0.10%, D=1.005±0.001, NM-206B, Lab#=57032-01											
B	450	16.51	0.0479	55.13	0.512	10.7	1.3	0.2	5.2	11.3	9
C	450	4.042	0.0329	13.68	0.255	15.5	-0.2	0.4	-0.2	20.1	19
D	450	3.932	-0.0460	12.98	0.197	-	2.1	0.5	2.1	27.4	24
E	500	0.1291	0.0347	-0.9957	0.365	14.7	349.5	0.6	10.3	13.6	9
F	500	1.004	0.0166	1.839	0.513	30.8	45.5	0.9	11.2	9.6	19
G	500	1.282	0.0158	2.976	0.442	32.3	30.9	1.1	9.7	11.0	24
H	550	0.1870	0.0141	0.1196	0.834	36.1	80.7	1.5	3.5	5.9	9
I	550	0.5123	0.0286	0.5245	0.816	17.9	69.6	1.9	8.6	6.0	16
J	550	0.8624	0.0144	2.087	0.724	35.5	27.8	2.3	5.9	6.8	24
K	600	0.1402	0.0258	-1.4982	0.761	19.8	441.6	2.6	14.2	6.2	9
L	600	0.8039	0.0292	0.4024	0.757	17.5	85.3	3.0	16.7	6.5	19
M	600	1.227	0.0325	1.936	1.04	15.7	53.2	3.5	16.0	4.7	21
N	650	1.479	0.0716	-0.7754	1.18	7.1	116.0	4.1	41.7	3.9	9
O	650	3.216	0.1042	0.7913	1.31	4.9	93.0	4.7	72.4	3.7	19
P	650	5.574	0.1734	1.678	0.913	2.9	91.3	5.1	121.7	5.3	24
Q	700	8.050	0.1621	1.597	0.932	3.1	94.3	5.6	178.7	4.8	8
R	700	10.81	0.1623	1.900	1.32	3.1	94.9	6.2	237.7	3.4	18
S	750	16.47	0.1456	2.966	1.46	3.5	94.8	6.9	350.3	2.8	7

ID	Temp (°C)	$^{40}Ar/^{39}Ar$	$^{37}Ar/^{39}Ar$	$^{36}Ar/^{39}Ar$ (x 10^{-3})	$^{39}Ar_K$ (x 10^{-15} mol)	K/Ca	$^{40}Ar^*$ (%)	^{39}Ar (%)	Age (Ma)	±1σ (Ma)	Time (min)
T	750	18.86	0.1182	1.238	2.06	4.3	98.1	7.9	408.6	2.2	19
U	800	26.32	0.0905	2.097	2.39	5.6	97.7	9.1	546.0	2.0	9
V	800	28.04	0.0782	1.506	2.70	6.5	98.4	10.4	580.5	1.7	19
W	850	36.45	0.0754	2.688	3.10	6.8	97.8	11.9	720.1	1.7	9
X	850	35.45	0.0684	2.229	3.55	7.5	98.2	13.6	705.7	1.5	19
Y	900	46.41	0.0541	3.377	4.75	9.4	97.9	15.9	876.1	1.5	9
Z	900	43.40	0.0505	2.320	5.56	10.1	98.4	18.6	834.2	1.2	19
AA	950	52.56	0.0413	2.413	9.35	12.3	98.7	23.1	972.2	1.4	9
AB	950	47.41	0.0316	1.911	10.7	16.2	98.8	28.2	897.8	1.3	19
AC	1000	52.87	0.0295	2.041	16.3	17.3	98.9	36.1	978.2	1.0	9
AD	1000	48.78	0.0320	1.811	14.2	15.9	98.9	43.0	919.0	1.3	19
AE	1050	53.13	0.0357	1.783	19.3	14.3	99.0	52.3	983.1	1.5	9
AF	1050	50.16	0.0523	1.946	21.0	9.8	98.9	62.4	938.9	1.3	29
AG	1050	49.02	0.0634	2.328	18.1	8.1	98.6	71.2	920.3	1.3	59
AH	1050	50.47	0.0595	3.286	15.4	8.6	98.1	78.7	937.8	1.2	119
AI	1050	53.38	0.0554	5.846	12.9	9.2	96.8	84.9	969.3	1.6	239
AJ	1100	54.66	0.0356	1.147	6.18	14.3	99.4	87.9	1007.8	1.4	9
AK	1200	55.37	0.0861	1.104	7.70	5.9	99.4	91.6	1018.2	1.6	9
AL	1250	54.99	0.0721	1.121	6.55	7.1	99.4	94.8	1012.7	1.3	9
AM	1300	55.36	0.0765	1.478	9.51	6.7	99.2	99.4	1016.4	1.7	9
AN	1500	58.69	0.0929	8.829	0.848	5.5	95.6	99.8	1032.8	4.4	9
AO	1650	67.64	0.0809	43.98	0.447	6.3	80.8	100.0	1012.4	7.8	9
Total Gas Age ± 1σ			n=40		207.0	9.4	K2O=3.04%		884.7	1.1	

ID	Temp (°C)	$^{40}Ar/^{39}Ar$	$^{37}Ar/^{39}Ar$	$^{36}Ar/^{39}Ar$ (x 10^{-3})	$^{39}Ar_K$ (x 10^{-15} mol)	K/Ca	$^{40}Ar^*$ (%)	^{39}Ar (%)	Age (Ma)	±1σ (Ma)	Time (min)
Klokken 43738-700, Kspar, 2.38 mg, J=0.01355±0.10%, D=1.005±0.001, NM-206B, Lab#=57033-01											
B	450	20.39	0.0752	70.31	0.409	6.8	-1.9	0.2	-9.7	15.9	9
C	450	5.766	0.0292	17.09	0.247	17.4	12.3	0.3	17.5	21.0	19
D	450	3.606	0.0273	11.98	0.204	18.7	1.6	0.3	1.4	23.2	24
E	500	0.3537	0.0395	0.0658	0.423	12.9	95.3	0.5	8.1	11.2	8
F	500	0.8267	0.0208	1.893	0.757	24.5	31.7	0.8	6.4	6.6	19
G	500	1.004	0.0248	2.530	0.620	20.5	25.0	1.1	6.2	7.8	24
H	550	0.1340	0.0214	-0.4221	0.832	23.8	202.0	1.4	6.2	5.7	9
I	550	0.4469	0.0252	0.9386	1.37	20.3	37.0	1.9	4.0	3.5	19
J	550	0.7329	0.0276	1.910	0.888	18.5	22.2	2.3	4.0	5.3	21
K	600	0.3019	0.0367	-0.2098	1.40	13.9	122.3	2.8	8.8	3.4	9
L	600	0.7628	0.0486	0.2525	1.34	10.5	90.6	3.4	16.8	3.5	16
M	600	1.423	0.0628	1.205	1.06	8.1	75.2	3.8	26.1	4.4	24
N	650	1.739	0.1083	-0.2171	1.04	4.7	104.2	4.2	44.1	4.5	9
O	650	3.193	0.1573	0.9003	1.27	3.2	92.1	4.7	71.1	3.8	19
P	650	4.927	0.1906	1.297	0.956	2.7	92.5	5.1	109.2	5.0	24
Q	700	7.456	0.2658	1.585	1.22	1.9	94.0	5.6	165.5	3.7	9
R	700	9.093	0.2690	2.029	1.65	1.9	93.6	6.2	199.2	2.7	18
S	750	13.95	0.2460	1.926	2.08	2.1	96.1	7.0	304.6	2.2	9
T	750	16.94	0.1568	1.635	2.72	3.3	97.2	8.1	367.7	1.7	19
U	800	24.76	0.1292	2.041	2.94	3.9	97.6	9.3	517.2	1.6	9
V	800	27.90	0.1078	1.403	3.56	4.7	98.5	10.7	578.2	1.5	19
W	850	36.68	0.0929	3.447	3.86	5.5	97.2	12.2	719.9	1.6	9
X	850	37.58	0.0846	1.895	4.54	6.0	98.5	14.0	742.3	1.3	19
Y	900	46.57	0.0694	3.147	5.54	7.4	98.0	16.2	879.1	1.3	9
Z	900	44.55	0.0575	2.488	6.59	8.9	98.4	18.8	851.0	1.2	18
AA	950	50.83	0.0533	3.023	8.93	9.6	98.3	22.4	943.8	1.7	9
AB	950	46.95	0.0455	2.056	10.1	11.2	98.7	26.4	889.8	1.3	19
AC	1000	51.47	0.0428	2.409	15.0	11.9	98.6	32.3	955.7	1.3	9
AD	1000	49.20	0.0437	2.047	14.6	11.7	98.8	38.1	923.7	1.4	19
AE	1050	53.59	0.0440	1.997	22.9	11.6	98.9	47.2	988.3	1.3	9
AF	1050	54.73	0.0580	1.958	31.1	8.8	99.0	59.6	1004.9	1.1	29
AG	1050	55.43	0.0632	2.392	23.8	8.1	98.7	69.0	1013.1	1.4	59
AH	1050	56.31	0.0666	2.594	26.3	7.7	98.6	79.4	1024.7	1.3	119
AI	1050	57.24	0.0615	3.378	26.7	8.3	98.3	90.0	1034.5	1.3	239
AJ	1100	55.85	0.0572	1.623	2.11	8.9	99.2	90.8	1022.1	2.3	9
AK	1200	59.40	0.0968	1.476	6.58	5.3	99.3	93.4	1072.3	1.3	9
AL	1250	59.90	0.1055	1.704	4.96	4.8	99.2	95.4	1078.4	1.5	9
AM	1300	59.42	0.0875	1.222	7.61	5.8	99.4	98.4	1073.7	1.7	9
AN	1500	63.35	0.1076	2.958	3.66	4.7	98.6	99.9	1120.0	2.0	9
AO	1650	79.58	0.1458	64.02	0.304	3.5	76.2	100.0	1095.6	11.2	9
Total Gas Age ± 1σ			n=40		252.1	7.5	K2O=3.00%		918.7	1.1	

ID	Temp (°C)	$^{40}Ar/^{39}Ar$	$^{37}Ar/^{39}Ar$	$^{36}Ar/^{39}Ar$ (x 10^{-3})	$^{39}Ar_K$ (x 10^{-15} mol)	K/Ca	$^{40}Ar^*$ (%)	^{39}Ar (%)	Age (Ma)	±1σ (Ma)	Time (min)
Klokken 43738-900, Kspar, 3.19 mg, J=0.013498±0.10%, D=1.005±0.001, NM-206B, Lab#=57036-01											
B	450	7.672	0.0309	20.61	1.83	16.5	20.5	0.6	38.4	3.5	9
C	450	1.675	0.0083	3.318	0.767	61.6	41.1	0.8	16.8	6.4	16
D	450	1.592	0.0100	3.434	0.609	51.3	35.9	1.0	13.9	7.9	21
E	500	0.3724	0.0189	-0.2152	0.986	27.0	118.0	1.3	10.5	4.8	6
F	500	0.6063	0.0177	0.9199	1.70	28.9	54.7	1.8	8.0	2.8	19
G	500	0.6643	0.0184	1.014	1.42	27.7	54.4	2.3	8.8	3.3	24
H	550	0.2022	0.0182	-0.2065	2.75	28.1	132.6	3.2	6.3	1.7	9
I	550	0.3151	0.0192	0.1344	3.36	26.6	87.5	4.2	6.6	1.4	19
J	550	0.4048	0.0210	0.7899	2.76	24.3	41.3	5.1	4.0	1.8	24
K	600	0.1832	0.0256	0.1313	3.94	19.9	78.8	6.3	3.4	1.2	9
L	600	0.3172	0.0252	0.1707	4.75	20.2	84.3	7.8	6.4	1.0	19
M	600	0.4531	0.0351	0.3775	3.74	14.5	75.5	9.0	8.2	1.3	24
N	650	0.3330	0.0483	0.1499	3.85	10.6	87.5	10.2	7.0	1.2	9
O	650	0.5955	0.0664	0.3010	4.37	7.7	85.8	11.5	12.3	1.1	19
P	650	0.9732	0.0752	0.7474	2.71	6.8	77.7	12.4	18.4	1.8	24
Q	700	0.7792	0.1154	-0.0486	3.53	4.4	103.1	13.5	19.4	1.3	9
R	700	1.275	0.1347	0.5257	2.84	3.8	88.6	14.4	27.4	1.7	19
S	750	1.262	0.1748	0.2436	4.83	2.9	95.4	15.9	29.22	1.00	9
T	750	1.939	0.1781	0.4534	6.56	2.9	93.8	18.0	44.08	0.73	19
U	800	2.622	0.1586	0.2909	4.90	3.2	97.2	19.5	61.6	1.0	9
V	800	3.786	0.1122	0.4894	6.41	4.5	96.4	21.5	87.61	0.82	19
W	850	5.536	0.0762	0.4679	5.50	6.7	97.6	23.2	128.34	0.83	8
X	850	7.559	0.0573	0.7176	7.62	8.9	97.3	25.6	172.55	0.66	19
Y	900	13.45	0.0537	0.7130	7.29	9.5	98.5	27.9	300.10	0.77	9
Z	900	16.05	0.0519	0.8979	9.89	9.8	98.4	31.0	352.55	0.82	19
AA	950	27.44	0.0514	1.227	10.8	9.9	98.7	34.4	568.76	0.95	9
AB	950	27.66	0.0490	1.237	12.6	10.4	98.7	38.3	572.62	0.86	19
AC	1000	40.02	0.0449	1.575	16.0	11.4	98.8	43.4	781.2	1.1	9
AD	1000	38.72	0.0522	1.649	15.9	9.8	98.8	48.4	759.85	0.98	19
AE	1050	48.31	0.0496	1.742	25.5	10.3	98.9	56.4	909.0	1.2	9
AF	1050	49.89	0.0638	1.874	35.3	8.0	98.9	67.4	932.0	1.1	29
AG	1050	53.09	0.0730	2.315	31.0	7.0	98.7	77.2	976.9	1.3	59
AH	1050	56.23	0.0727	3.115	22.4	7.0	98.4	84.2	1018.4	1.3	119
AI	1050	60.68	0.0737	4.941	13.3	6.9	97.6	88.3	1072.8	1.5	239
AJ	1100	61.86	0.0631	2.254	1.27	8.1	98.9	88.7	1099.5	3.1	9
AK	1200	61.28	0.0622	1.809	20.9	8.2	99.1	95.3	1093.5	1.4	9
AL	1250	60.25	0.1345	2.853	3.61	3.8	98.6	96.4	1075.3	1.9	9
AM	1300	61.58	0.1223	3.500	6.66	4.2	98.3	98.5	1090.9	1.5	9
AN	1650	63.99	0.1117	6.387	4.68	4.6	97.1	100.0	1111.9	1.6	9
Total Gas Age ± 1σ			n=39		318.8	7.5	K2O=2.84%		706.51	0.89	

ID	Temp (°C)	$^{40}Ar/^{39}Ar$	$^{37}Ar/^{39}Ar$	$^{36}Ar/^{39}Ar$ (x 10^{-3})	$^{39}Ar_K$ (x 10^{-15} mol)	K/Ca	$^{40}Ar^*$ (%)	^{39}Ar (%)	Age (Ma)	±1σ (Ma)	Time (min)
Klokken 43738-1000, Kspar, 3 mg, J=0.013679, D=1.005±0.001, NM-206B, Lab#=57039-01											
B	450	5.507	0.0483	17.10	1.30	10.6	8.1	0.4	11.1	4.1	9
C	450	1.056	0.0314	2.211	0.645	16.3	37.8	0.7	9.9	8.2	19
D	450	1.199	0.0150	2.402	0.493	33.9	40.4	0.8	12.0	10.0	24
E	500	0.1943	0.0197	0.6294	0.752	25.9	0.0	1.1	0.0	6.4	8
F	500	0.4254	0.0198	0.8523	1.16	25.8	39.8	1.5	4.1	4.3	19
G	500	0.5874	0.0163	1.416	1.03	31.3	27.8	1.8	4.0	4.8	24
H	550	0.1662	0.0226	0.1776	1.89	22.6	67.6	2.5	2.6	2.5	9
I	550	0.3075	0.0240	0.6210	2.08	21.3	39.0	3.2	2.9	2.4	16
J	550	0.4016	0.0218	0.7445	1.86	23.4	44.3	3.8	4.3	2.6	21
K	600	0.1434	0.0269	0.0771	3.23	19.0	84.6	4.9	2.8	1.5	9
L	600	0.2458	0.0275	0.4319	4.21	18.6	46.9	6.3	2.8	1.2	19
M	600	0.3595	0.0348	0.4744	3.19	14.7	60.7	7.4	5.3	1.6	24
N	650	0.1949	0.0395	0.1402	3.49	12.9	79.4	8.6	3.7	1.4	9
O	650	0.3714	0.0489	0.2980	4.12	10.4	76.8	10.0	6.9	1.2	19
P	650	0.4903	0.0492	0.3622	3.27	10.4	78.6	11.1	9.4	1.5	24
Q	700	0.3376	0.0668	-0.1916	2.90	7.6	119.0	12.1	9.7	1.7	9
R	700	0.5361	0.0858	0.1726	4.04	5.9	91.7	13.4	12.0	1.2	18
S	750	0.4865	0.1117	0.1148	4.69	4.6	94.8	15.0	11.25	1.04	9
T	750	0.7816	0.1336	0.2819	5.39	3.8	90.6	16.9	17.40	0.90	19
U	800	0.7981	0.1572	0.1293	4.56	3.2	96.8	18.4	19.0	1.1	9
V	800	1.140	0.1451	0.3375	5.67	3.5	92.2	20.3	25.85	0.85	19
W	850	1.158	0.1224	0.2513	4.73	4.2	94.4	21.9	26.88	1.03	9
X	850	1.518	0.0854	0.4699	6.23	6.0	91.3	24.0	34.09	0.80	19
Y	900	1.633	0.0684	0.2966	5.03	7.5	95.0	25.7	38.12	0.98	9
Z	900	2.137	0.0633	0.5378	7.08	8.1	92.8	28.1	48.68	0.69	19
AA	950	2.655	0.0600	0.2235	5.73	8.5	97.7	30.1	63.48	0.84	9
AB	950	3.611	0.0622	0.5335	8.08	8.2	95.8	32.8	84.27	0.64	19
AC	1000	4.881	0.0594	0.3918	6.40	8.6	97.7	35.0	115.37	0.76	9
AD	1000	6.643	0.0545	0.5624	9.20	9.4	97.6	38.1	155.21	0.61	19
AE	1050	10.17	0.0590	0.4874	9.27	8.7	98.6	41.3	235.37	0.64	9
AF	1050	15.83	0.0594	0.8713	23.7	8.6	98.4	49.3	354.05	0.51	29
AG	1050	26.68	0.0564	1.065	44.2	9.0	98.8	64.3	566.28	0.69	59
AH	1050	39.71	0.0618	1.749	52.1	8.3	98.7	81.9	791.28	1.01	119
AI	1050	49.32	0.0685	3.620	22.0	7.5	97.8	89.4	935.5	1.4	239
AJ	1100	61.59	0.0524	1.861	1.95	9.7	99.1	90.0	1122.5	2.6	9
AK	1200	59.08	0.0618	1.859	17.4	8.3	99.1	96.0	1087.3	1.6	9
AL	1250	52.93	0.1269	2.990	2.60	4.0	98.4	96.8	993.1	2.1	9
AM	1300	53.58	0.1261	2.937	2.63	4.0	98.4	97.7	1002.9	2.2	9
AN	1500	56.85	0.1292	3.037	6.12	4.0	98.4	99.8	1050.4	1.4	9
AO	1650	62.57	0.1006	18.46	0.582	5.1	91.3	100.0	1067.0	6.1	9
Total Gas Age ± 1σ			n=40		295.0	7.6		K2O=2.91%	497.8	0.7	

ID	Temp (°C)	$^{40}Ar/^{39}Ar$	$^{37}Ar/^{39}Ar$	$^{36}Ar/^{39}Ar$ (x 10^{-3})	$^{39}Ar_K$ (x 10^{-15} mol)	K/Ca	$^{40}Ar^*$ (%)	^{39}Ar (%)	Age (Ma)	±1σ (Ma)	Time (min)
Klokken 43738-1100, Kspar, 2.44 mg, J=0.013653, D=1.005±0.001, NM-206B, Lab#=57042-01											
B	450	2.016	0.0327	6.335	2.28	15.6	6.8	1.0	3.4	2.6	6
C	450	0.5137	0.0251	0.7113	0.925	20.3	58.7	1.4	7.4	5.4	19
D	450	0.8152	0.0242	2.502	0.586	21.1	8.5	1.6	1.7	8.5	24
E	500	0.2248	0.0173	-0.0154	0.552	29.6	102.8	1.9	5.5	8.8	9
F	500	0.5402	0.0266	0.6466	0.838	19.2	64.4	2.2	8.5	5.9	19
G	500	0.7658	0.0393	1.503	0.741	13.0	41.7	2.6	7.8	6.5	24
H	550	0.2973	0.0145	-0.9933	0.898	35.3	202.6	2.9	14.5	5.4	9
I	550	0.5184	0.0372	1.207	1.35	13.7	30.5	3.5	3.9	3.6	19
J	550	0.6495	0.0196	0.7581	1.20	26.1	65.2	4.0	10.4	4.1	24
K	600	0.3046	0.0261	0.2887	1.39	19.6	71.8	4.6	5.3	3.5	9
L	600	0.4589	0.0320	0.2288	1.91	15.9	85.5	5.5	9.5	2.5	16
M	600	0.5682	0.0278	0.9926	2.11	18.4	47.9	6.4	6.7	2.4	24
N	650	0.3042	0.0359	0.2252	2.20	14.2	78.4	7.3	5.7	2.2	9
O	650	0.4289	0.0323	0.1594	3.51	15.8	89.4	8.8	9.3	1.4	19
P	650	0.5749	0.0398	0.3376	3.04	12.8	82.9	10.1	11.6	1.6	24
Q	700	0.3784	0.0434	0.1146	2.73	11.8	91.8	11.3	8.4	1.8	9
R	700	0.5256	0.0524	0.2840	4.10	9.7	84.6	13.1	10.8	1.2	19
S	750	0.4419	0.0602	0.1134	3.66	8.5	93.4	14.7	10.0	1.3	7
T	750	0.6427	0.0709	0.3340	5.73	7.2	85.3	17.1	13.4	0.88	19
U	800	0.5963	0.0887	0.0192	4.89	5.8	100.3	19.2	14.6	1.00	9
V	800	0.8300	0.0870	0.2518	6.97	5.9	91.8	22.2	18.7	0.68	19
W	850	0.8514	0.0970	0.2569	5.46	5.3	91.9	24.6	19.2	0.89	8
X	850	1.107	0.0983	0.2391	8.29	5.2	94.3	28.2	25.6	0.60	19
Y	900	1.173	0.1016	0.2304	6.13	5.0	94.9	30.8	27.3	0.81	9
Z	900	1.480	0.0834	0.3331	9.61	6.1	93.8	35.0	34.1	0.52	19
AA	950	1.531	0.0796	0.2242	6.92	6.4	96.1	37.9	36.1	0.69	9
AB	950	1.799	0.0676	0.2611	10.7	7.5	96.0	42.6	42.4	0.46	19
AC	1000	1.957	0.0633	0.2009	7.22	8.1	97.2	45.7	46.6	0.67	9
AD	1000	2.296	0.0689	0.3590	10.5	7.4	95.6	50.2	53.7	0.48	19
AE	1050	2.580	0.0725	0.3322	6.30	7.0	96.4	52.9	60.8	0.79	9
AF	1050	3.353	0.0771	0.4936	12.5	6.6	95.8	58.4	78.3	0.41	29
AH	1050	5.911	0.0868	1.143	17.1	5.9	94.4	65.7	134.1	0.38	119
AI	1050	12.39	0.0961	4.095	10.5	5.3	90.3	70.2	260.3	0.77	239
AJ	1100	15.63	0.0446	2.385	0.435	11.4	95.5	70.4	339.9	9.5	9
AK	1200	25.45	0.0503	0.6922	29.7	10.1	99.2	83.2	544.2	0.74	9
AL	1250	17.29	0.0824	0.7031	8.21	6.2	98.8	86.8	384.5	0.84	9
AM	1300	14.86	0.0821	0.6028	9.91	6.2	98.8	91.0	334.9	0.69	9
AN	1500	19.17	0.0718	0.6014	18.8	7.1	99.1	99.2	423.2	0.65	9
AO	1650	20.32	0.0677	4.741	1.95	7.5	93.1	100.0	421.7	2.4	9
Total Gas Age ± 1σ			n=39		232.0	7.2	K2O=2.81%		186.8	0.3	

Notes:

Isotopic ratios corrected for blank, radioactive decay, and mass discrimination, not corrected for interfering reactions.

Errors quoted for individual analyses include analytical error only, without interfering reaction or J uncertainties.

Integrated age calculated by summing isotopic measurements of all steps.

Integrated age error calculated by quadratically combining errors of isotopic measurements of all steps.

Plateau age is inverse-variance-weighted mean of selected steps.

Plateau age error is inverse-variance-weighted mean error (Taylor, 1982) times root MSWD where MSWD>1.

Plateau error is weighted error of Taylor (1982).

Decay constants and isotopic abundances after Steiger and Jäger (1977).

symbol preceding sample ID denotes analyses excluded from plateau age calculations.

Weight percent K_2O calculated from ^{39}Ar signal, sample weight, and instrument sensitivity.

Ages calculated relative to FC-2 Fish Canyon Tuff sanidine interlaboratory standard at 28.27 Ma

Decay Constant (LambdaK (total)) = 5.476e-10/a

Correction factors:

$(^{39}Ar/^{37}Ar)_{Ca}$ = 0.0007 ± 5e-05

$(^{36}Ar/^{37}Ar)_{Ca}$ = 0.00028 ± 2e-05

Table A3.6: $^{40}Ar/^{39}Ar$ analytical data for single grain Klokken analyses.

ID	Temp (°C)	$^{40}Ar/^{39}Ar$	$^{37}Ar/^{39}Ar$	$^{36}Ar/^{39}Ar$ (x 10^{-3})	$^{39}Ar_K$ (x 10^{-15} mol)	K/Ca	$^{40}Ar^*$ (%)	^{39}Ar (%)	Age (Ma)	±1σ (Ma)	Time (min)
Klokken 140115-02, K-Feldspar, 0.06 mg, J=0.0103±0.49%, D=1.002±0.001, NM-201J, Lab#=56669-01											
B	700	49.59	-0.0189	9.906	0.217	-	94.1	1.8	716.5	10.3	9
C	800	72.74	0.0050	1.930	0.285	101.7	99.2	4.1	1014.9	7.1	9
D	900	88.80	0.0140	3.986	0.647	36.5	98.7	9.3	1174.4	3.9	9
E	1000	88.46	0.0196	1.818	1.25	26.0	99.4	19.5	1177.4	2.8	9
F	1075	88.47	0.0216	2.124	1.35	23.6	99.3	30.5	1176.6	2.4	9
G	1150	86.45	0.0168	1.463	1.84	30.4	99.5	45.4	1158.5	2.4	9
H	1200	85.93	0.0196	2.275	1.66	26.1	99.2	59.0	1151.0	2.1	9
I	1250	87.83	0.0194	1.475	3.79	26.3	99.5	89.8	1172.2	1.6	9
J	1300	89.54	0.0178	5.378	0.845	28.7	98.2	96.7	1177.7	3.2	9
K	1325	99.70	-0.0251	34.92	0.146	-	89.6	97.9	1191.7	12.9	9
L	1350	94.39	-0.0403	26.35	0.180	-	91.7	99.3	1164.2	11.5	9
M	1375	111.6	-0.1355	59.44	0.065	-	84.3	99.9	1236.7	29.8	9
N	1400	336.9	-1.6345	593.0	0.008	-	47.9	99.9	1788.0	202.0	9
O	1450	326.4	-1.0154	634.3	0.008	-	42.6	100.0	1621.4	189.9	9
Total gas age ± 1σ			n=14		12.3	36.6	K2O=7.64%		1159.5	4.3	
Klokken 140182-07, K-Feldspar, 0.49 mg, J=0.01037±0.48%, D=1.002±0.001, NM-201K, Lab#=56682-02											
B	550	871.5	-0.5791	642.9	0.021	-	78.2	0.0	3812.1	66.4	7
C	550	92.78	-0.6730	-14.5256	0.017	-	104.6	0.1	1270.8	91.9	14
D	550	218.8	-2.4265	168.2	0.005	-	77.2	0.1	1845.9	240.4	19
E	600	53.60	-0.3589	-147.2759	0.015	-	181.1	0.1	1271.7	106.7	9
F	600	111.2	-1.4073	-136.2090	0.009	-	136.1	0.1	1721.9	165.2	11
G	600	77.13	-0.4277	67.68	0.029	-	74.0	0.2	848.9	63.9	19
H	650	55.50	-0.2676	-10.7423	0.044	-	105.7	0.3	867.4	43.5	9
I	650	59.78	-0.1174	3.501	0.053	-	98.3	0.4	868.4	36.1	14
J	650	79.91	-0.0752	82.25	0.058	-	69.6	0.5	831.2	33.3	19
K	700	63.04	0.0265	-3.2181	0.103	19.3	101.5	0.7	929.4	19.2	9
L	700	67.91	-0.0222	29.42	0.113	-	87.2	0.9	874.2	17.8	14
M	750	73.19	0.0348	7.626	0.226	14.7	96.9	1.3	1006.8	8.9	9
N	750	83.92	-0.0008	15.10	0.184	-	94.7	1.6	1097.5	11.1	14
O	800	84.09	0.0225	3.894	0.387	22.7	98.6	2.4	1133.3	6.0	9
P	800	89.32	0.0299	9.631	0.300	17.1	96.8	2.9	1168.9	6.7	14
Q	850	88.47	0.0365	4.429	0.499	14.0	98.5	3.9	1175.8	5.0	9
R	850	89.82	0.0202	9.614	0.519	25.2	96.8	4.9	1174.0	4.3	14
S	900	87.02	0.0256	2.176	0.815	19.9	99.3	6.4	1168.0	3.4	9
T	900	87.66	0.0250	5.037	0.931	20.4	98.3	8.1	1165.9	3.4	14
U	950	86.80	0.0238	1.148	1.42	21.4	99.6	10.8	1168.8	2.6	9
V	950	88.15	0.0321	4.998	2.31	15.9	98.3	15.2	1170.9	2.2	13
W	1000	87.36	0.0326	1.772	2.46	15.6	99.4	19.8	1172.5	1.7	9
X	1000	88.19	0.0315	3.604	1.69	16.2	98.8	23.0	1175.4	2.2	14
Y	1050	87.79	0.0260	2.226	1.83	19.6	99.3	26.4	1175.5	2.0	9
Z	1050	87.65	0.0323	3.331	1.63	15.8	98.9	29.5	1170.9	2.3	14
AA	1100	86.97	0.0336	1.927	1.88	15.2	99.3	33.0	1168.2	1.9	9
AB	1100	87.30	0.0268	2.944	1.71	19.1	99.0	36.2	1168.4	2.1	14
AC	1150	87.56	0.0287	1.380	2.11	17.8	99.5	40.2	1175.7	1.7	9
AD	1150	88.33	0.0333	4.295	1.48	15.3	98.6	43.0	1174.8	2.3	14
AE	1200	86.71	0.0288	1.123	11.7	17.7	99.6	65.0	1168.0	1.5	9
AF	1200	86.93	0.0287	1.593	5.76	17.8	99.5	75.9	1168.8	1.4	14
AG	1200	87.42	0.0282	1.812	4.95	18.1	99.4	85.2	1173.0	1.4	19
AH	1200	88.02	0.0280	2.705	4.84	18.2	99.1	94.3	1176.3	1.4	29
AI	1300	88.12	0.0292	2.331	1.10	17.5	99.2	96.4	1178.5	2.8	9
AJ	1400	88.33	0.0246	4.443	0.787	20.7	98.5	97.9	1174.3	3.2	9
AK	1700	90.73	0.0295	10.63	1.14	17.3	96.5	100.0	1180.0	2.5	9
Total gas age ± 1σ			n=36		53.1	18.9	K2O=4.02%		1170.8	4.3	

ID	Temp (°C)	$^{40}Ar/^{39}Ar$	$^{37}Ar/^{39}Ar$	$^{36}Ar/^{39}Ar$ (x 10^{-3})	$^{39}Ar_K$ (x 10^{-15} mol)	K/Ca	$^{40}Ar^*$ (%)	^{39}Ar (%)	Age (Ma)	(Ma)	
Klokken 43738-01, K-Feldspar, 0.037 mg, J=0.01037, D=1.004±0.001, NM-201K, Lab#=56687-01											
B	630	173.0	0.3432	27.29	0.227	1.5	95.4	4.8	1859.1	65.9	9
C	730	55.95	0.6454	-12.6527	0.118	0.79	106.8	7.3	890.8	208.1	9
D	830	67.22	0.5710	-5.3359	0.150	0.89	102.4	10.5	996.6	154.7	9
E	930	73.11	0.3749	1.451	0.207	1.4	99.5	14.9	1039.8	109.9	9
F	1005	64.88	0.3895	-0.6313	0.253	1.3	100.3	20.2	953.6	93.8	9
G	1080	70.62	0.1305	5.432	0.963	3.9	97.7	40.7	998.4	24.3	9
H	1130	68.25	0.1950	3.142	0.608	2.6	98.7	53.6	979.2	38.8	9
I	1180	65.47	0.1103	1.030	0.937	4.6	99.5	73.5	954.3	25.5	9
J	1230	67.66	0.1462	2.872	0.686	3.5	98.8	88.0	973.3	34.4	9
K	1255	67.52	3.571	-55.6279	0.028	0.14	124.8	88.6	1165.4	771.5	9
L	1280	64.42	0.3050	2.095	0.537	1.7	99.1	100.0	938.8	44.8	9
Total gas age ± 1σ			n=11		4.71	2.1	K2O=5.0%		1001.0	16.0	
Klokken 43738-02, K-Feldspar, 0.01 mg, J=0.01037±0.48%, D=1.004±0.001, NM-201K, Lab#=56686-01											
B	630	146.7	1.021	3.858	0.061	0.50	99.3	4.9	1681.4	80.6	9
C	730	75.38	1.074	-25.2159	0.051	0.48	110.0	9.0	1133.7	129.3	9
D	830	81.36	0.5816	-25.1216	0.078	0.88	109.2	15.3	1192.7	81.2	9
E	930	87.06	0.9076	-13.7257	0.110	0.56	104.7	24.2	1216.0	57.5	9
F	1005	88.97	0.4442	-12.6063	0.127	1.1	104.2	34.4	1230.6	49.7	9
G	1080	94.24	0.3286	-2.8550	0.231	1.6	100.9	53.0	1253.3	27.1	9
H	1130	87.57	0.6272	-5.7650	0.167	0.81	102.0	66.5	1197.6	38.4	9
I	1180	91.01	0.3932	-7.7209	0.133	1.3	102.5	77.2	1236.3	46.8	9
J	1230	82.82	3.113	-126.4611	0.023	0.16	145.4	79.1	1482.3	233.3	9
K	1255	87.63	0.5133	-4.8354	0.174	0.99	101.7	93.1	1195.3	37.1	9
L	1280	56.12	8.008	-151.1230	0.010	0.064	180.8	94.0	1318.0	564.9	9
M	1305	66.83	6.102	-199.3090	0.013	0.084	188.9	95.0	1532.7	412.3	9
N	1330	78.32	4.754	-67.6369	0.029	0.11	126.0	97.4	1290.2	206.2	9
O	1380	62.77	10.69	-91.2431	0.015	0.048	144.4	98.6	1216.6	422.1	9
P	1430	66.69	13.97	-54.2522	0.018	0.037	125.8	100.0	1151.3	367.8	9
Total gas age ± 1σ			n=15		1.24	0.44	K2O=4.59%		1238.0	20.0	
Klokken 43738, K-Feldspar, 0.267 mg, J=0.01037±0.48%, D=1.004±0.001, NM-201K, Lab#=56691-01											
B	630	61.96	0.0495	5.960	0.599	10.3	97.2	1.7	885.7	13.2	9
C	730	41.02	0.2286	-3.5554	0.496	2.2	102.6	3.0	661.4	17.4	7
D	830	88.00	0.3822	1.609	0.808	1.3	99.5	5.3	1179.9	8.4	9
E	930	84.52	0.1876	0.8883	1.90	2.7	99.7	10.6	1146.9	4.1	9
F	1005	81.72	0.0861	0.2344	2.74	5.9	99.9	18.2	1120.2	3.2	9
G	1080	82.34	0.0661	1.472	5.15	7.7	99.5	32.6	1122.8	2.1	9
H	1130	83.64	0.0592	1.822	3.86	8.6	99.4	43.3	1134.9	2.5	8
I	1180	85.48	0.0709	2.016	6.21	7.2	99.3	60.6	1153.0	2.1	9
J	1230	86.38	0.0690	2.035	6.80	7.4	99.3	79.5	1162.0	1.8	9
K	1255	87.09	0.1641	-1.7650	0.312	3.1	100.6	80.3	1180.4	21.6	8
L	1280	87.28	0.0805	2.644	2.92	6.3	99.1	88.5	1169.3	3.1	9
M	1305	94.24	0.1527	-0.1452	0.184	3.3	100.1	89.0	1245.5	34.3	9
N	1330	94.13	0.1907	-0.9866	0.165	2.7	100.3	89.4	1246.9	39.2	9
O	1380	91.88	0.0689	3.039	0.287	7.4	99.0	90.2	1213.5	24.7	9
P	1430	88.55	0.0804	4.727	1.65	6.3	98.4	94.8	1175.8	4.5	9
Q	1730	91.53	0.0979	16.88	1.86	5.2	94.6	100.0	1169.7	5.1	9
Total gas age ± 1σ			n=16		35.9	5.7	K2O=5.0%		1141.1	4.3	

ID	Temp (°C)	$^{40}Ar/^{39}Ar$	$^{37}Ar/^{39}Ar$	$^{36}Ar/^{39}Ar$ (x 10^{-3})	$^{39}Ar_K$ (x 10^{-15} mol)	K/Ca	$^{40}Ar^*$ (%)	^{39}Ar (%)	Age (Ma)	(Ma)	(n)
Klokken 43738, K-Feldspar, 0.236 mg, J=0.01037±0.48%, D=1.004±0.001, NM-201K, Lab#=56691-10											
B	630	163.4	0.0321	328.6	0.655	15.9	40.6	2.1	956.0	19.7	9
C	730	50.40	0.1032	1.090	0.660	4.9	99.4	4.1	763.8	12.5	9
D	830	91.80	0.3223	-2.3417	0.538	1.6	100.8	5.8	1228.5	12.2	7
E	930	86.28	0.1555	0.8674	1.92	3.3	99.7	11.8	1164.6	3.9	9
F	1005	80.49	0.0699	-0.5925	2.15	7.3	100.2	18.6	1110.1	3.9	8
G	1080	77.83	0.0624	1.533	4.48	8.2	99.4	32.6	1075.8	2.0	9
H	1130	78.47	0.0438	0.8786	3.51	11.7	99.7	43.6	1084.5	2.5	8
I	1180	78.02	0.0456	1.582	8.49	11.2	99.4	70.3	1077.7	1.5	9
J	1230	80.79	0.0419	0.8319	4.20	12.2	99.7	83.4	1108.7	2.1	9
K	1255	83.23	0.0361	0.6407	2.15	14.1	99.8	90.2	1134.3	3.5	9
L	1280	87.78	0.0861	-4.4716	0.176	5.9	101.5	90.7	1195.0	36.9	9
M	1305	89.24	0.1080	-21.1160	0.113	4.7	107.0	91.1	1256.8	56.8	9
N	1330	85.63	0.0956	1.033	0.790	5.3	99.7	93.6	1157.5	8.7	9
O	1380	96.39	-0.2211	-7.8556	0.125	-	102.4	94.0	1286.9	49.0	9
P	1430	89.96	0.0712	3.223	0.471	7.2	98.9	95.4	1194.1	14.3	9
Q	1730	91.90	0.0215	16.52	1.46	23.7	94.7	100.0	1174.4	5.2	9
Total gas age ± 1σ			n=16		31.9	8.4	K2O=5.0%		1098.4	4.2	
Klokken 43738, K-Feldspar, 0.307 mg, J=0.01037±0.48%, D=1.004±0.001, NM-201K, Lab#=56691-03											
B	630	176.5	0.0535	12.02	1.37	9.5	98.0	3.3	1875.8	5.1	4
C	730	86.24	0.1455	1.094	1.08	3.5	99.6	5.9	1163.5	6.6	9
D	830	82.61	0.2469	-0.4945	0.926	2.1	100.2	8.1	1131.7	7.6	9
E	930	75.52	0.1542	-0.0858	2.06	3.3	100.1	13.1	1056.6	3.7	9
F	1005	71.01	0.0716	-0.0257	2.41	7.1	100.0	19.0	1007.8	3.3	9
G	1080	72.99	0.0582	1.103	6.44	8.8	99.6	34.5	1025.6	1.6	9
H	1130	75.44	0.0675	1.303	6.38	7.6	99.5	49.9	1051.2	1.7	9
I	1180	78.22	0.0686	1.232	7.77	7.4	99.5	68.7	1080.9	1.6	9
J	1230	80.40	0.0670	0.8413	4.69	7.6	99.7	80.1	1104.8	2.0	9
K	1255	80.88	0.0889	0.8112	5.89	5.7	99.7	94.3	1109.9	1.7	9
L	1280	82.72	0.1142	0.0689	0.347	4.5	100.0	95.2	1130.9	19.4	9
M	1305	83.75	0.0779	0.8756	0.891	6.6	99.7	97.3	1139.0	7.9	9
N	1330	82.46	0.1050	0.1700	0.281	4.9	99.9	98.0	1128.0	24.4	9
O	1380	84.89	0.1661	5.253	0.343	3.1	98.2	98.8	1137.5	19.9	9
P	1430	84.62	0.0932	2.709	0.490	5.5	99.1	100.0	1142.3	13.9	9
Total gas age ± 1σ			n=15		41.4	6.3	K2O=5.0%		1108.7	4.2	
Klokken 43738, K-Feldspar, 0.01 mg, J=0.01037±0.48%, D=1.004±0.001, NM-201K, Lab#=56691-04											
B	630	241.2	0.0144	10.89	1.17	35.5	98.7	4.6	2270.6	4.8	8
C	730	101.2	0.0584	4.334	1.04	8.7	98.7	8.7	1299.0	6.4	9
D	830	65.19	0.1876	-4.4192	0.503	2.7	102.0	10.7	957.9	14.8	7
E	930	65.60	0.0551	1.066	1.47	9.3	99.5	16.5	944.1	5.4	9
F	1005	52.85	0.0666	0.1937	1.28	7.7	99.9	21.5	797.3	6.4	9
G	1080	62.51	0.0388	2.338	3.92	13.1	98.9	36.9	904.6	2.4	9
H	1130	63.53	0.0320	2.067	4.32	15.9	99.0	54.0	917.2	2.1	9
I	1180	62.69	0.0434	1.625	5.09	11.8	99.2	74.1	909.0	2.0	9
J	1230	66.21	0.0513	1.081	4.44	10.0	99.5	91.6	950.9	2.1	8
K	1255	70.35	0.1430	-5.4752	0.217	3.6	102.3	92.4	1018.1	32.9	9
L	1280	68.45	0.0247	-0.9283	0.419	20.6	100.4	94.1	982.5	17.5	9
M	1305	70.40	0.0589	2.387	1.27	8.7	99.0	99.1	993.3	6.2	9
N	1330	83.92	-0.6772	-55.6980	0.036	-	119.5	99.2	1301.7	167.6	9
O	1380	71.84	0.1569	1.216	0.193	3.3	99.5	100.0	1012.9	37.0	9
Total gas age ± 1σ			n=14		25.4	10.8	K2O=5.0%		1029.9	4.0	

ID	Temp (°C)	$^{40}Ar/^{39}Ar$	$^{37}Ar/^{39}Ar$	$^{36}Ar/^{39}Ar$ (x 10^{-3})	$^{39}Ar_K$ (x 10^{-15} mol)	K/Ca	$^{40}Ar^*$ (%)	^{39}Ar (%)	Age (Ma)	± 1σ (Ma)	(n=n)
Klokken 43738, K-Feldspar, 0.188 mg, J=0.01037±0.48%, D=1.004±0.001, NM-201K, Lab#=56691-05											
B	630	104.6	0.0116	6.135	0.524	43.8	98.3	1.6	1324.7	**11.9**	**6**
C	730	65.20	0.1542	-1.3537	0.675	3.3	100.6	3.7	947.8	**11.1**	**9**
D	830	82.94	0.3550	0.6780	0.654	1.4	99.8	5.7	1131.7	**12.8**	**9**
E	930	83.26	0.2075	-1.0611	1.22	2.5	100.4	9.4	1140.0	6.1	7
F	1005	79.87	0.0859	-0.5681	1.85	5.9	100.2	15.0	1103.6	4.2	8
G	1080	78.33	0.0766	1.211	4.47	6.7	99.6	28.7	1082.1	2.3	9
H	1130	78.68	0.0799	1.594	3.72	6.4	99.4	40.1	1084.5	2.4	8
I	1180	80.61	0.0645	1.166	7.20	7.9	99.6	62.1	1105.9	1.5	9
J	1230	83.18	0.0730	0.3403	2.04	7.0	99.9	68.3	1134.8	4.0	8
K	1255	82.49	0.0530	0.8288	4.73	9.6	99.7	82.7	1126.2	1.9	9
L	1280	88.04	-0.1539	-10.3668	0.132	-	103.5	83.2	1214.3	48.4	9
M	1305	95.24	-0.5326	-34.4336	0.063	-	110.6	83.3	1348.0	94.0	9
N	1330	101.3	-0.9930	-46.6099	0.033	-	113.5	83.4	1432.9	171.6	9
O	1380	92.61	-0.3814	-7.3646	0.072	-	102.3	83.7	1249.5	86.2	9
P	1430	89.45	-0.0026	0.4870	0.299	-	99.8	84.6	1197.0	22.0	9
Q	1730	86.07	0.0624	5.466	5.05	8.2	98.1	100.0	1148.7	2.1	9
Total gas age ± 1σ			n=16		32.7	6.8	K2O=121.20%		1116.4	4.2	
Klokken 43738, K-Feldspar, 0.21 mg, J=0.01037±0.48%, D=1.004±0.001, NM-201K, Lab#=56691-06											
B	630	242.5	0.0481	13.72	1.75	10.6	98.3	6.0	2273.2	4.9	9
C	730	100.1	0.2446	5.989	0.726	2.1	98.3	8.5	1283.8	9.2	9
D	830	85.63	0.3404	3.610	0.816	1.5	98.8	11.4	1150.2	8.3	9
E	930	68.07	0.2812	2.757	1.48	1.8	98.8	16.4	966.5	5.4	9
F	1005	54.02	0.1717	1.545	1.42	3.0	99.2	21.3	806.8	5.9	8
G	1080	67.06	0.0935	2.971	4.00	5.5	98.7	35.1	954.3	2.4	8
H	1130	68.67	0.0814	3.049	4.42	6.3	98.7	50.4	972.0	2.3	9
I	1180	69.33	0.0931	2.646	5.10	5.5	98.9	68.0	980.7	2.1	9
J	1230	75.33	0.1467	2.825	3.17	3.5	98.9	78.9	1045.4	2.8	9
K	1255	73.18	0.1643	2.165	4.36	3.1	99.1	94.0	1024.5	2.3	9
L	1280	105.0	0.7539	-11.5982	0.052	0.68	103.3	94.2	1377.0	111.8	9
M	1305	97.97	0.8356	-37.9960	0.047	0.61	111.5	94.3	1383.9	123.4	9
N	1330	98.60	0.0434	-38.3964	0.042	11.8	111.5	94.5	1389.5	137.6	9
O	1380	111.5	1.242	12.52	0.151	0.41	96.8	95.0	1372.0	39.3	9
P	1430	87.53	0.6505	5.405	0.321	0.78	98.2	96.1	1164.4	20.6	9
Q	1730	80.09	0.2260	17.72	1.13	2.3	93.5	100.0	1049.4	6.7	9
Total gas age ± 1σ			n=16		29.0	3.4	K2O=5.0%		1112.0	4.3	
Klokken 43738, K-Feldspar, 0.198 mg, J=0.01037±0.48%, D=1.004±0.001, NM-201K, Lab#=56691-07											
B	630	165.7	0.0722	4.698	1.32	7.1	99.2	4.9	1816.2	5.3	9
C	730	70.75	0.1445	0.9760	0.514	3.5	99.6	6.9	1001.8	14.1	9
D	830	82.79	0.1908	-1.6761	0.782	2.7	100.6	9.8	1137.0	8.8	9
E	930	71.48	0.1233	-0.0258	1.54	4.1	100.0	15.6	1012.9	5.0	9
F	1005	67.17	0.0788	-0.3245	1.63	6.5	100.2	21.7	966.3	4.8	8
G	1080	73.46	0.0434	1.376	5.80	11.8	99.5	43.4	1029.8	1.7	9
H	1130	73.99	0.0482	1.217	4.41	10.6	99.5	59.9	1036.0	2.2	9
I	1180	75.39	0.0636	0.8560	4.40	8.0	99.7	76.4	1052.1	2.1	9
J	1230	79.86	0.0671	0.9346	1.26	7.6	99.7	81.1	1098.8	5.9	9
K	1255	74.97	0.1114	1.294	1.39	4.6	99.5	86.3	1046.3	5.3	9
L	1280	79.56	0.1161	1.489	2.61	4.4	99.5	96.1	1094.1	3.3	9
M	1305	95.22	1.327	-54.6094	0.030	0.38	117.1	96.2	1403.7	187.2	9
N	1330	84.28	-0.3760	-17.4773	0.075	-	106.1	96.5	1197.7	85.3	9
O	1380	88.89	0.0562	-1.6545	0.164	9.1	100.6	97.1	1197.8	39.3	9
P	1430	83.22	0.1787	2.932	0.491	2.9	99.0	99.0	1127.6	13.9	9
Q	1730	98.09	0.0404	63.73	0.277	12.6	80.8	100.0	1095.5	25.6	9
Total gas age ± 1s			n=16		26.7	6.7	K2O=5.0%		1095.0	4.2	

ID	Temp (°C)	$^{40}Ar/^{39}Ar$	$^{37}Ar/^{39}Ar$	$^{36}Ar/^{39}Ar$ (x 10^{-3})	$^{39}Ar_K$ (x 10^{-15} mol)	K/Ca	$^{40}Ar^*$ (%)	^{39}Ar (%)	Age (Ma)	± (Ma)	
Klokken 43738, K-Feldspar, 0.281 mg, J=0.01037±0.48%, D=1.004±0.001, NM-201K, Lab#=56691-08											
B	630	215.6	0.0551	17.23	1.81	9.3	97.6	4.8	2114.5	**3.4**	**6**
C	730	126.9	0.1314	11.87	1.53	3.9	97.2	8.8	1505.0	**4.6**	**9**
D	830	75.26	0.2280	2.250	0.999	2.2	99.1	11.5	1046.6	**7.6**	**9**
E	930	57.23	0.1769	1.777	1.54	2.9	99.1	15.5	844.7	**5.6**	**7**
F	1005	57.58	0.0929	4.170	2.86	5.5	97.9	23.1	840.3	**3.2**	**9**
G	1080	61.34	0.0548	3.412	5.97	9.3	98.4	38.8	887.3	**1.8**	**9**
H	1130	63.13	0.0575	3.819	4.08	8.9	98.2	49.6	906.6	**2.3**	**9**
I	1180	65.47	0.0688	3.570	6.33	7.4	98.4	66.2	934.3	1.8	9
J	1230	69.93	0.0983	4.863	7.78	5.2	98.0	86.8	980.1	1.5	9
K	1255	69.83	0.1056	3.485	3.40	4.8	98.5	95.7	983.4	2.5	8
L	1280	70.33	0.0245	-9.6061	0.190	20.8	104.0	96.2	1031.0	36.7	9
M	1305	70.15	0.1154	3.370	1.43	4.4	98.6	100.0	987.4	5.3	9
Total gas age ± 1σ			n=12		37.9	5.8	K2O=5.0%		1036.5	4.0	
Klokken 43738-03, K-Feldspar, 0.18 mg, J=0.01025±0.49%, D=1.002±0.001, NM-201J, Lab#=56675-01											
B	550	313.6	-0.0136	33.65	0.149	-	96.8	1.9	2582.3	17.3	9
C	550	45.18	-0.0470	37.29	0.089	-	75.6	3.0	548.0	27.0	14
D	550	81.89	0.0100	114.8	0.058	50.9	58.6	3.7	730.2	36.6	19
E	600	104.7	-0.0260	8.759	0.124	-	97.5	5.2	1307.7	14.2	9
F	600	68.22	-0.2308	65.40	0.040	-	71.6	5.7	741.4	50.9	14
G	600	87.90	-0.1010	146.5	0.028	-	50.7	6.1	687.3	76.3	19
H	650	80.57	0.1029	24.22	0.053	5.0	91.1	6.7	1024.6	35.6	9
I	650	77.06	-0.1077	50.33	0.028	-	80.7	7.1	900.2	64.9	14
J	650	121.2	-0.4583	165.8	0.022	-	59.6	7.4	1011.1	88.4	19
K	700	96.93	-0.0568	25.97	0.049	-	92.1	8.0	1186.2	34.1	9
L	700	85.69	-0.1145	68.09	0.027	-	76.5	8.3	938.5	67.2	14
M	700	114.7	-0.0609	150.5	0.024	-	61.2	8.6	990.6	76.6	19
N	750	84.61	-0.0455	34.92	0.031	-	87.8	9.0	1033.7	58.7	9
O	750	92.87	-0.0700	70.24	0.035	-	77.6	9.4	1010.4	54.2	14
P	750	113.9	0.1164	164.6	0.033	4.4	57.3	9.8	935.2	57.6	19
Q	800	75.18	0.1160	4.032	0.046	4.4	98.4	10.4	1030.7	41.2	9
R	800	78.86	0.0686	50.79	0.045	7.4	81.0	11.0	919.5	42.2	14
S	850	66.09	0.0567	11.13	0.065	9.0	95.0	11.8	907.4	31.7	9
T	850	77.21	0.0076	62.09	0.061	67.3	76.2	12.5	862.0	30.9	14
U	900	64.78	0.1022	23.63	0.078	5.0	89.2	13.5	849.7	26.5	9
V	900	69.07	0.0187	37.57	0.079	27.3	83.9	14.5	851.6	25.9	14
W	950	65.22	-0.0422	10.31	0.108	-	95.3	15.8	900.2	17.9	9
X	950	66.46	-0.0348	32.42	0.095	-	85.6	17.0	838.7	21.9	14
Y	1000	67.94	0.0320	10.44	0.173	15.9	95.5	19.2	930.7	11.4	9
Z	1000	68.15	-0.1081	35.01	0.106	-	84.8	20.5	849.5	19.3	14
AA	1050	71.79	0.0180	9.166	0.278	28.4	96.2	23.9	977.6	7.2	9
AB	1050	67.40	-0.0200	22.81	0.225	-	90.0	26.8	882.9	9.4	14
AC	1100	70.61	0.0210	11.30	0.550	24.3	95.3	33.6	957.6	4.4	9
AD	1100	66.87	0.0313	17.93	0.332	16.3	92.1	37.7	893.4	7.0	14
AE	1150	70.16	0.0359	6.930	0.710	14.2	97.1	46.6	966.9	3.8	9
AF	1150	71.37	0.0518	14.62	0.481	9.9	94.0	52.6	955.2	5.0	14
AG	1200	67.44	0.0408	4.468	1.20	12.5	98.0	67.5	944.9	2.7	9
AH	1200	67.39	0.0201	5.460	1.38	25.4	97.6	84.7	941.0	2.3	14
AI	1200	70.69	0.0275	14.04	0.710	18.5	94.1	93.6	949.6	3.7	19
AJ	1200	94.42	0.0151	81.93	0.149	33.8	74.4	95.4	989.9	14.8	29
AK	1200	121.0	-0.0023	176.0	0.168	-	57.0	97.5	976.6	14.8	59
AL	1200	278.7	-0.0944	690.8	0.082	-	26.7	98.5	1036.5	31.9	119
AM	1300	240.3	-1.1073	354.4	0.006	-	56.4	98.6	1589.4	241.6	9
AN	1400	79.68	-0.0587	21.41	0.099	-	92.1	99.9	1023.8	18.3	9
AO	1500	443.8	-3.9472	592.4	0.004	-	60.5	99.9	2410.6	345.9	9
AP	1700	516.9	-1.4259	1241.6	0.008	-	29.0	100.0	1698.7	206.8	9
Total gas age ± 1σ			n=41		8.03	42.3	K2O=1.67%		996.2	4.3	

ID	Temp (°C)	$^{40}Ar/^{39}Ar$	$^{37}Ar/^{39}Ar$	$^{36}Ar/^{39}Ar$ (x 10^{-3})	$^{39}Ar_K$ (x 10^{-15} mol)	K/Ca	$^{40}Ar^*$ (%)	^{39}Ar (%)	Age (Ma)	± 1σ (Ma)	
Klokken 43738-05, K-Feldspar, 0.048 mg, J=0.01025±0.49%, D=1.002±0.001, NM-201J, Lab#=56676-01											
B	700	263.0	0.0367	25.58	0.581	13.9	97.1	9.1	2348.5	7.7	9
C	800	65.77	0.1777	17.05	0.249	2.9	92.4	13.0	884.0	8.6	9
D	900	54.82	0.1529	13.91	0.248	3.3	92.5	16.9	764.5	8.8	9
E	1000	49.52	0.0743	13.02	0.339	6.9	92.2	22.2	701.2	6.7	9
F	1075	55.43	0.0533	10.32	0.528	9.6	94.5	30.5	784.8	4.6	9
G	1150	60.82	0.0448	5.367	1.12	11.4	97.4	48.1	866.4	2.4	9
H	1200	59.22	0.0378	4.578	1.63	13.5	97.7	73.7	850.3	2.0	9
I	1250	61.22	0.0505	8.478	0.981	10.1	95.9	89.0	860.3	2.7	9
J	1300	68.05	0.1618	37.96	0.155	3.2	83.5	91.5	838.4	12.9	9
K	1325	73.97	0.0622	71.74	0.078	8.2	71.3	92.7	789.6	24.4	9
L	1350	80.70	0.0968	76.51	0.053	5.3	72.0	93.5	853.1	31.3	9
M	1375	107.9	-0.2174	149.4	0.027	-	59.1	93.9	918.2	64.6	9
N	1400	138.8	0.0030	305.3	0.014	169.7	35.0	94.2	738.0	144.4	9
O	1450	144.9	-0.4176	329.5	0.019	-	32.8	94.5	724.4	108.6	9
P	1500	135.2	0.0149	348.7	0.025	34.2	23.8	94.9	519.8	84.8	9
Q	1800	105.0	0.0648	257.3	0.328	7.9	27.6	100.0	474.8	12.6	9
Total gas age ± 1σ			n=16		6.38	9.0	K2O=5.0%		1023.0	4.2	
Klokken 140025-04, K-Feldspar, 0.01 mg, J=0.01025±0.49%, D=1.002±0.001, NM-201J, Lab#=56674-01											
B	700	61.95	0.0985	27.08	0.094	5.2	87.1	2.2	803.8	19.7	9
C	800	74.11	-0.0071	14.83	0.186	-	94.1	6.5	984.7	10.4	9
D	900	84.61	0.0653	15.08	0.169	7.8	94.7	10.4	1095.1	11.3	9
E	1000	86.78	0.0420	11.55	0.227	12.2	96.1	15.7	1127.8	8.0	9
F	1075	85.82	0.0327	14.40	0.251	15.6	95.0	21.5	1109.5	8.1	9
G	1150	82.98	0.0304	15.67	0.270	16.8	94.4	27.8	1076.5	7.6	9
H	1200	82.48	0.0064	5.936	0.780	80.1	97.9	46.0	1100.9	3.4	9
I	1250	87.25	0.0076	3.167	2.04	66.8	98.9	93.5	1157.3	1.8	9
J	1300	99.10	-0.0182	56.05	0.076	-	83.3	95.2	1119.3	22.1	9
K	1325	125.4	-0.0355	168.6	0.028	-	60.3	95.9	1047.1	60.8	9
L	1350	153.2	-0.2917	237.9	0.017	-	54.1	96.3	1122.6	99.5	9
M	1375	163.1	-0.0683	214.4	0.015	-	61.2	96.6	1285.9	104.5	9
N	1400	211.4	0.1617	314.3	0.012	3.2	56.1	96.9	1452.5	125.5	9
O	1450	157.9	0.0352	278.1	0.019	14.5	47.9	97.3	1048.3	81.6	9
P	1500	192.5	-0.1004	477.6	0.015	-	26.7	97.7	772.0	129.4	9
Q	1800	214.2	-0.0298	592.2	0.100	-	18.3	100.0	616.2	34.7	9
Total gas age ± 1σ			n=16		4.30	39.7	K2O=16.12%		1108.1	4.6	
Klokken 140025-05, K-Feldspar, 0.01 mg, J=0.01037±0.48%, D=1.002±0.001, NM-201K, Lab#=56688-01											
B	700	36.66	-0.0086	27.03	0.146	-	78.2	3.8	475.3	15.7	9
C	800	35.24	0.0394	10.04	0.084	13.0	91.6	6.0	527.1	25.1	9
D	900	33.14	-0.0037	3.109	0.072	-	97.2	7.8	526.2	26.3	9
E	1000	31.92	0.0726	16.00	0.102	7.0	85.2	10.5	453.5	19.6	9
F	1075	29.00	-0.0324	9.230	0.172	-	90.6	14.9	439.7	13.6	9
G	1150	26.40	0.0048	4.897	0.633	107.4	94.5	31.3	420.1	3.7	9
H	1200	28.15	0.0025	3.624	1.28	203.6	96.2	64.6	451.8	1.8	9
I	1250	29.88	-0.0003	3.858	0.506	-	96.2	77.7	476.2	4.2	9
J	1300	34.82	-0.0544	10.85	0.106	-	90.8	80.5	517.6	19.9	9
K	1325	33.98	-0.0018	5.150	0.622	-	95.5	96.6	529.7	3.6	9
L	1350	48.17	-0.1968	19.71	0.047	-	87.9	97.8	664.3	42.9	9
M	1375	103.5	0.0317	211.5	0.012	16.1	39.6	98.1	646.9	156.0	9
N	1400	168.3	-1.0518	406.3	0.008	-	28.6	98.3	738.5	207.0	9
O	1450	402.8	-0.0067	1003.7	0.005	-	26.4	98.4	1356.0	318.4	9
P	1500	238.0	-0.3233	570.1	0.006	-	29.2	98.6	991.3	296.0	9
Q	1800	265.7	0.1694	792.6	0.054	3.0	11.9	100.0	516.1	66.2	9
Total gas age ± 1σ			n=16		3.86	-259.686	K2O=14.28%		475.3	3.2	

ID	Temp (°C)	$^{40}Ar/^{39}Ar$	$^{37}Ar/^{39}Ar$	$^{36}Ar/^{39}Ar$ (x 10^{-3})	$^{39}Ar_K$ (x 10^{-15} mol)	K/Ca	$^{40}Ar^*$ (%)	^{39}Ar (%)	Age (Ma)	±1σ (Ma)	Time (min)
Klokken 140025, K-Feldspar, .182 mg, J=0.01037±0.48%, D=1.004±0.001, NM-201K, Lab#=56692-01											
B	630	62.19	0.0200	6.725	1.46	25.5	96.8	5.9	885.8	5.6	9
C	730	25.77	0.0281	-3.2342	0.436	18.2	103.7	7.7	446.6	22.0	9
D	830	24.12	0.0669	0.1082	0.582	7.6	99.9	10.1	407.1	16.9	9
E	930	20.15	0.0994	-0.7293	0.584	5.1	101.1	12.4	349.8	17.4	7
F	1005	23.09	0.0383	0.3284	0.837	13.3	99.6	15.8	390.4	12.0	8
G	1080	27.38	0.0069	2.362	2.66	73.5	97.5	26.6	445.9	3.7	9
H	1130	29.60	0.0127	2.753	2.35	40.2	97.3	36.2	476.8	4.1	8
I	1180	31.95	0.0037	1.383	4.99	137.0	98.7	56.4	516.6	2.0	9
J	1230	32.41	0.0100	1.570	5.79	51.2	98.6	80.0	522.4	1.8	8
K	1255	31.10	0.0188	2.617	2.76	27.2	97.5	91.1	499.3	3.5	9
L	1280	54.91	0.1836	55.95	0.139	2.8	69.9	91.7	611.9	62.9	8
M	1305	61.73	0.0657	90.05	0.334	7.8	56.9	93.1	567.1	27.7	9
N	1330	310.9	0.2574	930.5	0.101	2.0	11.6	93.5	578.5	96.7	9
O	1380	461.8	0.3855	1398.9	0.117	1.3	10.5	94.0	743.8	81.6	9
P	1430	93.30	0.0170	202.1	1.47	30.0	36.0	99.9	545.8	8.5	9
Q	1730	16409.8	5.740	54762.2	0.017	0.089	1.4	100.0	2221.0	525.0	9
Total gas age ± 1σ			n=16		24.6	21.3	K2O=5.0%		523.8	3.2	
Klokken 140025, K-Feldspar, 0.075 mg, J=0.01037±0.48%, D=1.004±0.001, NM-201K, Lab#=56692-02											
B	630	63.24	0.0269	-1.3827	0.115	19.0	100.6	1.1	925.5	64.8	6
C	730	35.92	0.0461	-7.4767	0.216	11.1	106.2	3.3	608.4	40.6	9
D	830	49.29	0.1639	-1.6598	0.320	3.1	101.0	6.4	760.2	25.5	9
E	930	64.05	0.1163	0.9234	0.328	4.4	99.6	9.7	927.0	22.7	9
F	1005	73.63	0.0785	-0.6781	0.394	6.5	100.3	13.5	1038.1	18.0	9
G	1080	83.15	0.0431	0.7001	0.651	11.8	99.8	20.0	1133.3	10.7	9
H	1130	82.45	0.0530	3.118	0.620	9.6	98.9	26.1	1118.9	11.1	9
I	1180	81.11	0.0238	1.086	2.33	21.4	99.6	49.0	1111.3	3.5	9
J	1230	81.62	0.0313	1.334	1.85	16.3	99.5	67.2	1115.7	4.5	9
K	1255	85.09	0.0678	3.559	0.685	7.5	98.8	74.0	1144.5	10.1	8
L	1280	98.48	-0.0284	25.11	0.091	-	92.5	74.9	1214.0	70.1	8
M	1305	135.7	0.1738	120.5	0.052	2.9	73.8	75.4	1299.9	115.7	9
N	1330	111.6	-0.0989	67.34	0.103	-	82.2	76.4	1220.4	61.8	9
O	1380	100.7	0.2440	45.97	0.236	2.1	86.5	78.8	1176.0	27.9	9
P	1430	108.1	0.0945	70.66	0.299	5.4	80.7	81.7	1176.6	22.4	9
Q	1730	104.3	0.0581	64.14	1.85	8.8	81.8	100.0	1157.2	4.5	9
Total gas age ± 1σ			n=16		10.1	9.5	K2O=5.0%		1101.4	5.0	
Klokken 140025, K-Feldspar, 0.17 mg, J=0.01037±0.48%, D=1.004±0.001, NM-201K, Lab#=56692-03											
B	630	57.93	0.1211	2.923	1.23	4.2	98.5	5.3	849.0	6.6	9
C	730	28.97	0.5003	-0.2585	0.541	1.0	100.4	7.7	481.4	17.4	7
D	830	27.04	0.3903	-0.0777	0.481	1.3	100.2	9.8	452.1	19.9	7
E	930	28.29	-0.0174	-1.0648	0.514	-	101.1	12.0	474.2	18.3	7
F	1005	36.36	0.0281	-0.1508	0.876	18.2	100.1	15.8	584.8	10.3	9
G	1080	40.03	0.0095	2.268	2.41	53.6	98.3	26.3	625.0	3.8	9
H	1130	39.16	0.0259	2.497	2.05	19.7	98.1	35.2	612.3	4.5	9
I	1180	42.28	0.0163	1.244	4.27	31.3	99.1	53.8	659.0	2.4	9
J	1230	45.64	0.0088	1.209	8.99	57.8	99.2	92.8	702.9	1.4	9
K	1255	39.48	0.0213	2.055	1.26	23.9	98.5	98.3	618.4	7.1	8
L	1280	35.52	0.0167	7.109	0.388	30.6	94.1	100.0	543.3	23.5	8
Total gas age ± 1σ			n=11		23.0	13.3	K2O=5.0%		660.5	3.0	

ID	Temp (°C)	$^{40}Ar/^{39}Ar$	$^{37}Ar/^{39}Ar$	$^{36}Ar/^{39}Ar$ ($\times 10^{-3}$)	$^{39}Ar_K$ ($\times 10^{-15}$ mol)	K/Ca	$^{40}Ar^*$ (%)	^{39}Ar (%)		
Klokken 140025, K-Feldspar, 0.094 mg, J=0.01037±0.48%, D=1.004±0.001, NM-201K, Lab#=56692-04										
B	630	40.71	0.0893	1.537	0.724	5.7	98.9	5.7	637.0	
C	730	25.31	0.2702	-2.2775	0.353	1.9	102.7	8.4	435.9	
D	830	35.85	0.1500	0.4177	0.547	3.4	99.7	12.7	575.7	
E	930	29.93	0.0318	-3.0440	0.452	16.0	103.0	16.3	506.4	
F	1005	30.11	0.0498	-0.4753	0.603	10.2	100.5	21.0	498.1	
G	1080	32.18	0.0219	2.967	1.46	23.3	97.3	32.5	513.3	
H	1130	35.03	0.0352	2.080	1.42	14.5	98.3	43.6	557.2	
I	1180	39.80	0.0181	1.955	2.39	28.2	98.6	62.3	623.1	
J	1230	36.14	0.0100	1.632	3.68	50.9	98.7	91.2	574.5	
K	1255	40.25	-0.1377	-2.0238	0.181	-	101.5	92.6	644.7	
L	1280	39.57	-0.2008	-5.7235	0.180	-	104.2	94.0	650.0	
M	1305	41.73	0.3124	1.381	0.139	1.6	99.1	95.1	651.7	
N	1330	44.35	-0.2801	18.83	0.152	-	87.4	96.3	616.7	
O	1380	46.87	0.0142	14.24	0.165	35.9	91.0	97.6	668.8	
P	1430	48.37	0.0520	18.72	0.308	9.8	88.6	100.0	671.2	
Total gas age ± 1σ			n=15		12.8	16.0	K2O=5.0%		576.1	

Klokken 140025, K-Feldspar, 0.132 mg, J=0.01037±0.48%, D=1.004±0.001, NM-201K, Lab#=56692-05											
B	630	42.05	0.0492	3.853	0.974	10.4	97.3	5.5	645.7	9.1	9
C	730	27.83	0.1483	0.4791	0.419	3.4	99.5	7.8	461.0	22.9	9
D	830	32.65	0.0136	-0.7661	0.495	37.4	100.7	10.6	535.6	18.4	9
E	930	30.20	0.0762	-1.2166	0.484	6.7	101.2	13.3	502.7	19.2	7
F	1005	28.59	0.0093	-0.3414	0.669	54.7	100.4	17.1	475.5	14.2	9
G	1080	28.35	0.0042	1.934	1.92	121.0	98.0	27.9	462.1	5.1	9
H	1130	30.79	0.0073	1.987	2.31	70.0	98.1	40.9	497.5	4.1	9
I	1180	33.44	0.0014	1.267	5.13	360.1	98.9	69.7	538.2	2.0	9
J	1230	34.08	-0.0005	1.565	1.78	-	98.6	79.7	546.0	5.3	9
K	1255	33.85	0.0188	1.454	2.38	27.2	98.7	93.0	543.3	4.0	9
L	1280	36.42	0.0683	3.192	0.482	7.5	97.4	95.7	572.1	18.7	8
M	1305	38.17	0.0348	7.801	0.412	14.7	94.0	98.0	577.4	21.7	9
N	1330	41.94	0.0004	6.107	0.168	1222.6	95.7	99.0	635.3	51.8	9
O	1380	41.17	0.1131	12.80	0.180	4.5	90.8	100.0	598.4	48.9	9
Total gas age ± 1σ			n=14		17.8	29.9	K2O=5.0%		530.7	3.0	

Klokken 140025, K-Feldspar, 0.132 mg, J=0.01037±0.48%, D=1.004±0.001, NM-201K, Lab#=56692-06											
B	630	36.20	0.0547	6.635	1.00	9.3	94.6	5.6	554.8	9.2	9
C	730	27.25	-0.0044	-0.5454	0.402	-	100.6	7.9	456.7	24.0	9
D	830	29.34	0.0315	1.627	0.494	16.2	98.4	10.6	478.0	19.1	9
E	930	27.67	-0.0019	0.0617	0.579	-	99.9	13.9	460.2	16.5	9
F	1005	26.08	0.0323	2.115	0.741	15.8	97.6	18.0	427.8	13.1	9
G	1080	25.70	-0.0086	3.159	2.37	-	96.4	31.3	417.3	4.3	9
H	1130	27.58	0.0053	3.465	2.63	95.4	96.3	46.0	444.1	3.8	9
I	1180	29.72	0.0029	1.765	4.88	174.3	98.2	73.3	482.9	2.1	9
J	1230	30.02	0.0069	2.881	1.30	73.4	97.2	80.6	482.5	7.4	9
K	1255	38.99	0.0020	4.322	0.191	256.7	96.7	81.6	602.6	46.5	8
M	1305	33.11	0.0071	2.630	2.43	72.1	97.7	95.2	527.9	4.0	9
N	1330	126.1	-0.8005	223.7	0.026	-	47.5	95.4	882.5	295.9	9
O	1380	82.44	-0.5577	109.9	0.059	-	60.6	95.7	761.5	137.6	9
P	1430	34.89	0.0116	18.25	0.764	44.1	84.5	100.0	487.2	12.5	9
Total gas age ± 1σ			n=14		17.9	112.1	K2O=5.0%		478.4	2.9	

ID	Temp (°C)	$^{40}Ar/^{39}Ar$	$^{37}Ar/^{39}Ar$	$^{36}Ar/^{39}Ar$ (x 10^{-3})	$^{39}Ar_K$ (x 10^{-15} mol)	K/Ca	$^{40}Ar^*$ (%)	^{39}Ar (%)			
Klokken 140025, K-Feldspar, 0.071 mg, J=0.01037±0.48%, D=1.004±0.001, NM-201K, Lab#=56692-08											
B	630	46.41	0.4403	-3.2380	0.220	1.2	102.1	2.3	730.2		
C	730	32.91	0.5074	8.472	0.164	1.0	92.5	4.0	501.1		
D	830	49.93	0.1269	1.010	0.288	4.0	99.4	7.0	758.3		
E	930	62.38	-0.0250	-0.4292	0.292	-	100.2	10.0	912.4		
F	1005	63.29	0.0502	0.4038	0.404	10.2	99.8	14.2	920.1		
G	1080	55.79	0.0250	2.977	0.724	20.4	98.4	21.7	823.0		
H	1130	54.45	0.0265	2.778	0.754	19.2	98.5	29.5	807.4		
I	1180	69.93	0.0426	1.555	2.06	12.0	99.3	50.9	990.8		
J	1230	72.82	0.0310	1.407	1.66	16.5	99.4	68.1	1022.8		
K	1255	74.00	0.0277	3.172	1.44	18.4	98.7	83.0	1029.9		
L	1280	89.89	-0.1120	-5.7955	0.103	-	101.9	84.1	1219.2		
M	1305	118.9	-0.8358	-31.7728	0.031	-	107.8	84.4	1543.7		
N	1330	100.5	-0.0701	46.42	0.088	-	86.3	85.3	1171.9		
O	1380	96.17	-0.3428	28.45	0.122	-	91.2	86.6	1181.2		
P	1430	83.62	0.0181	10.89	1.29	28.1	96.2	100.0	1107.2		
Q	1730	5685.3	2.947	17440.6	0.002	0.17	9.4	100.0	3426.2		
Total gas age ± 1σ			n=16		9.65	12.6	K2O=5.0%		978.1		

									5.7	1064.4	9
									4.9		

Notes:
Isotopic ratios corrected for blank, radioactive decay, and mass discrimination, not corrected for interfering reactions.
Errors quoted for individual analyses include analytical error only, without interfering reaction or J uncertainties.
Total gas age calculated by summing isotopic measurements of all steps.
Total gas age error calculated by quadratically combining errors of isotopic measurements of all steps.
Plateau age is inverse-variance-weighted mean of selected steps.
Plateau age error is inverse-variance-weighted mean error (Taylor, 1982) times root MSWD where MSWD>1.
Plateau error is weighted error of Taylor (1982).
Decay constants and isotopic abundances after Steiger and Jäger (1977).
symbol preceding sample ID denotes analyses excluded from plateau age calculations.
Weight percent K_2O calculated from ^{39}Ar signal, sample weight, and instrument sensitivity.
Ages calculated relative to FC-2 Fish Canyon Tuff sanidine interlaboratory standard at 28.27 Ma
Decay Constant (LambdaK (total)) = 5.476e-10/a
Correction factors:
$(^{39}Ar/^{37}Ar)_{Ca}$ = 0.0007 ± 5e-05
$(^{36}Ar/^{37}Ar)_{Ca}$ = 0.00028 ± 2e-05
$(^{38}Ar/^{39}Ar)_K$ = 0.013
$(^{40}Ar/^{39}Ar)_K$ = 0.01 ± 0.002